INDIAN JOURNAL OF PHYSICS

VOL. XVI

AND

PROCEEDINGS

OF THE

Indian Association for the Cultivation of Science, Vol. XXV

(Published in Collaboration with the Indian Physical Society)

BOARD OF EDITORS

M. N. Saha, D.Sc., F.R.S., I. R. Rao, Ph.D., D.Sc.,
S. K. Mitra, D.Sc.

P. N. Ghosh, Ph.D., Sc.D., *Secretary*

(With Eleven Plates)

Printed at the Calcutta University Press, 48, Hazra Road, Calcutta,
By Bhupendralal Banerjee and Published by the Secretary,
Indian Association for the Cultivation of Science,
210, Bowbazar Street, Calcutta.

1942

Price Rs. 12 or £1-2-6

AUTHOR INDEX

		PAGE
Ahmed, Waquar	On the Effect of Resistance Component in wave Filter Elements and Performance of non-ideal Filter Section.	229
Ali, Md. Innas ...	See Khastgir, S. R.	
Ananthasubrahmanyam, C. R.	See Rao, V. Paramasiva.	
Banerjee, B.	On Voltage Stabiliser Circuits ...	87
Banerjee, S. S. and Neogi, G. C.	Polar diagrams of Ultra-shortwave Horizontal Transmitting Aerials.	211
Banerjee, S. S. and Tiwari S. V.	Shunt excited Broadcasting Antenna ...	337
Basu-Mallik, J. K.	See Niyogi, K. C.	
Bhatnagar, P. L. and Kothari, D. S.	A Note on the Principle of Adiabatic Invariance	271
Bhattacharya, G. N. ...	On the Volume and Surface Resistivities of Shellacmoulded Materials.	147
	The thermal Conductivity of Lac and Lac moulded Compositions.	240
	The Effect of surrounding Medium on the Dielectric Strength of Lac and Lacmoulded Materials.	261
	Dipole moments of Palmitic acid, Aleuritic acid and Alkyl esters of Aleuritic acid.	360
Chakrabarty, S. K ...	Production of Burst by Meson and its dependence on the Meson Spin	377
Chakravarty, S. and Mahanti, P. C.	The Dielectric Strength of Indian Vegetable Oils.	82
Chatterjee, L. M.	A New Audio-frequency Bridge ...	130
Das, A. K. and Rao, V. P.	The Motion of Gases in the Sun's Atmosphere, Part IV.—On the occurrence of highly stripped Atoms in the Corona.	77
Khastgir, S. R. and Ali, Md. Innas	Investigations on Atmospherics in High Frequency channels.	300
Kar, K. C. ...	Proton-Proton Interaction and Yukawa Particle	187
Kothari, D. S. ...	See Bhatnagar, P. L.	
Krishnan, K. G ...	Effect of Depth of Liquid on damping of a Quartz Oscillator.	43

		PAGE
Kundu, D. N.	On the Identification of Lines on the Solar Corona.	317
Mahanti, P. C.	See Chakravarty, S.	
Mukherjee, J. N.	The velocity gradient method for the Measurement of Viscous Properties of Non-Newtonian Liquids.	40
	Methods of Measuring Yield Value, Viscosity and Thixotropy.	54
	A simple Rotary Viscometer for the Study of anomalous Viscous Properties.	66
Neogi, G. C. ..	See Banerjee, S. S.	
Niyogi, K. C. and Basu-Mallik, J. R.	On the Thermal Conductivity of Indigenous Insulating Substances.	241
Parshad, Ram ...	Propagation of Supersonic Waves in Liquid Mixtures and Intermolecular Forces—Ether and Acetone in Chloroform.	307
Prasad, Ram ...	Propagation of Ultra-sonic Waves in Liquid Mixtures and Intermolecular Forces, II.	1
Ramakrishnan, M. V. Siva	On a Comparative Study of the Reflectivities of Aluminium and Silver Films.	12
Rao, A. L. Sundar .	Visible Absorption Bands of Mercury halides HgCl, HgBr and HgI	393
Rao, A. S. ...	Overall Voltage gain of Low-frequency Amplifier with Negative Resistance.	111
Rao, C. V. H. ...	See Seth, J. B.	
Rao, M. Rama .	Thermal conductivity of Liquid Metals ...	155
	Thermal conductivity of Liquids. ...	161
Rao, M. R ...	Measurement of the Angle of arrival of Down-coming waves from Indian Regional short-wave Stations.	347
Rao, N. Rajeswara .	Study of Electrolytic Dissociation in Iodic Acid by Raman Effect.	71
Rao, V. V. L.	On the Theory of Q-meter and its corrections ...	107
Rao, V. P. .	See Das, A. K.	
Rao, V. Paramasiva .	Raman Frequencies of HDO. ..	205
Rao, V. Paramasiva and Anantasubrahmanyam, C. K.	Photometric Study of the Profiles of Fraunhofer Lines in the Solar Spectrum, Part I, Mg. b Group.	177
Ray, Santikumar .	Band Spectrum of Bismuth Monochloride ...	35
Sastry, M. G.	Structure of the Electronic Bands of the OD molecule, Part IV (Spin Doubling).	27
	Structure of Electronic Bands of the OD Molecule, Part V (Λ-Doubling).	169
	Structure of the Electronic Bands of OD Molecule, Part VI (Isotopic Shift).	343

Author Index

		PAGE
Sen, B. K ...	Volume Rectification of Crystals ...	320
Sen Gupta, N. C. and Thein Nyun, M. G.	Fluid Flow through Media, Part I. On the use of Gases for the measurement of true Permeability.	110
Sen Gupta, R. L. ...	See Sinha, M. S.	
Seth, J. B. and Rao, C. V. H.	The Linearity of the Mass-scale of Aston's Mass-Spectrograph.	210
Sinha, M. S. and Sen Gupta, R. L.	Evidence for the Existence of Associated Mesons in Cosmic Ray Showers.	120
Soonawala, M. F. ...	The Structure of Atomic Nuclei .	291
Suryan, G. ...	Propagation of Sound in Liquids and Viscosity	
Thaxton, H. Mack ...	Note on the Low Energy Scattering of Protons by Protons.	133
Thein Nyun, M. G. ...	See Sengupta, N. C.	
Tiwari, S. Y. ...	See Banerjee, S. S.	

SUBJECT INDEX

PAGE

Acoustics

Propagation of Sound in Liquids and Viscosity—by G. Suryan ... 77

Adiabatic Invariance— A Note on the Principle of—By P. L. Bhatnagar and D. S. Kothari 271

Astrophysics

The Motion of Gases in the Sun's Atmosphere, Part IV. On the Occurrence of highly stripped Atoms in the Corona—By A. K. Das and V. P. Rao 277

On the Identification of Lines in the Solar Corona—By D. N. Kundu 317

Cosmic Rays

Evidence for the Existence of Associated Mesons in Cosmic Rays—By M. S. Sinha and R. L. Sen Gupta 120

Production of Burst by Meson and its Dependence on the Meson Spin By S. K. Chakrabarty 377

Dielectrics

Dielectric Strength of Indian Vegetable Oils—The—By S. Chakravarty and P. C. Mahanti 84

The Effect of Surrounding Medium on the Dielectric Strength of Lac and Lac moulded Materials—By G. N. Bhattacharya ... 201

Dipole Moments

Dipole Moments of Palmitic acid, Aleuritic acid and Alkyl esters of Aleuritic acid—By G. N. Bhattacharya 369

Errata

Study of Electrolytic Dissociation in Iodic acid by Raman effect—By N. Rajeswara Rao 218

Effect of Resistance Component in Wave Filter Elements and Performance of Non-Ideal Filter Sections—By Waquar Ahmed ... 336

Fluid Flow through Media, Part I. On the Use of Gases for the Measurement of True Permeability—By N. C. Sengupta and M. G. Thein Nyun 119

Nuclear Physics

Note on the Low Energy Scattering of Protons by Protons—By H. Mack Thaxton 133

Proton-Proton Interaction and Yukawa Particle—By K. C. Kar ... 187

The Linearity of the Mass-scale of Aston's Mass-Spectrograph—By J. B. Seth and C. V. H. Rao 219

The Structure of Atomic Nuclei—By M. F. Soonawala 201

Raman Effect

Study of Electrolytic Dissociation in Iodic Acid by Raman effect—By N. Rajeswara Rao 71

Raman Frequencies of HDO—By V. Paramasiva Rao 205

PAGE

Reflectivities of Aluminium on Silver Films—On a Comparative Study of the—By M. V. Ramakrishnan 12
Resistivities of Shellacmoulded Materials—On the Volume and Surface—By G. N. Bhattacharya 147

Spectroscopy:
Structure of the Electronic Bands of the OD Molecule, Part IV (Spin Doubling)—By M. G. Sastry 27
Band Spectrum of Bismuth Monochloride—By Santikumar Ray .. 35
Structure of the Electronic Bands of the OD Molecule, Part V (Λ-Doubling)—By M. G. Sastry 100
Photometric Study of the Profiles of the Fraunhofer Lines in the Solar Spectrum, Part I, Mg b Group—By V. Paramasiva Rao and C. K. Anantasubrahmanyam 177
Structure of the Electronic Bands of the OD Molecule, Part VI (Isotopic Shift)—By M. G. Sastry 343
Visible Absorption Bands of Mercury Halides, HgCl, HgBr and HgI—By A. L. Sundara Rao 393

Supersonic Waves
Propagation of Ultrasonic Waves in Liquid Mixtures and Intermolecular Forces, II—By Ram Prasad 1
Propagation of Supersonic Waves in Liquid Mixtures and Intermolecular Forces—Ether and Acetone in Chloroform—By Ram Parshad .. 307

Thermal Conductivity:
Thermal Conductivity of Liquid Metals—By M. Rama Rao ... 155
Thermal Conductivity of Liquids—By M. Rama Rao 161
Thermal Conductivity of Indigenous Insulating Substances—On the—By K. C. Niyogi and J. R. Basu-Mallik 241
Thermal Conductivity of Lac and Lacmoulding Compositions—The—By G. N. Bhattacharya 249

Viscosity:
The Velocity Gradient Method for the Measurement of Viscous Properties of non-Newtonian Liquids—By J. N. Mukherjee ... 10
Methods of Measuring Yield Value, Viscosity and Thixotropy—By J. N. Mukherjee 54
A Simple Rotary Viscometer for the Study of Anomalous Viscous Properties—By J. N. Mukherjee . 66
Propagation of Sound in Liquids and Viscosity—By G. Suryan 77

Wireless and Electric Oscillations:
Effect of Depth of Liquid on Damping of a Quartz Oscillator—By K. G. Krishnan 23
On Voltage Stabiliser Circuits—By B. Banerjee 87
Overall Voltage Gain of Low-frequency Amplifiers with Negative Resistance—By A. S. Rao 111

PAGE
- A New Audio-frequency Bridge—By L. M. Chatterjee 139
- On the Theory of "Q"-meter and its Corrections—By V. V. L. Rao ... 197
- Polar Diagrams of Ultra-shortwave Horizontal Transmitting Aerials By S. S. Banerjee and G. C. Neogi 211
- On the Effect of Resistance Component in Wave Filter Elements and Performance of non-Ideal Filter Section—By Waquar Ahmed ... 229
- Volume Rectification of Crystals—By B. K. Sen 329
- Shunt excited Broadcasting Antenna—By S. S. Banerjee and S. Y. Tiwari 337
- Measurement of the Angle of Arrival of Down-coming Waves from Indian Regional Shortwave Stations—By M. R. Rao 347
- Investigations on Atmospherics in High frequency Channels—By S. R. Khastgir and Md. Innas Ali 399

Yield Value, Viscosity and Thixotropy—Methods of Measuring—By J. N. Mukherjee 54

PROPAGATION OF ULTRASONIC WAVES IN LIQUID MIXTURES AND INTERMOLECULAR FORCES II

By RAM PRASAD, M Sc.

(Received for publication, July 28, 1941)

ABSTRACT. This paper considers the compressibility-concentration curves of the liquids on the basis of intermolecular action.

The following mixtures have been studied here :-

(1) Ethyl alcohol and benzene, (2) Butyl alcohol and heptane, (3) Benzene and carbon tetrachloride, (4) Ether and benzene, (5) Ethyl acetate and carbon tetrachloride

The most interesting case is of alcohol and benzene, the compressibility curve being inflected. It is shown how the high polarisability of benzene and the association-forming tendency of alcohol determines the nature of the curve In butyl alcohol-heptane, the inertness of heptane as contrasted to the activity of benzene is very significant.

The analysis made in this series of papers is an approach to intermolecular action from a new angle In view of the approximate nature of the molecular fields, the treatment is necessarily qualitative.

INTRODUCTION

This paper is the second of the series on liquid mixtures, the first of which dealt with alcohols and water.[1] Herein are treated the following mixtures :—

(1) Ethyl alcohol and benzene ;
(2) Butyl alcohol and heptane ;
(3) Benzene and carbon tetrachloride ;
(4) Benzene and ether ;
(5) Ethyl acetate and carbon tetrachoride.

The data for velocities and compressibilities for mixtures (1) and (4) were taken by the author, for (2) by Wilson and Richards,[2] for (3) and (5) by Parthasarathy.[3] A qualitative explanation of the compressibility-concentration curves is attempted on the basis of intermolecular action.

EXPERIMENTAL RESULTS

The experimental technique and details employed for mixtures (1) and (4) haves been described in the first paper and will not be repeated here. In the following tables the collected results of all the mixtues are given.

---

* Communicated by the Indian Physical Society.

MIXTURE 1

Ethyl alcohol and benzene

Temp. = 29°.7C

No	Mole fraction of alcohol	Density gm./c.c.	Velocity m./s.	Compressibility (adiabatic) × 10⁻⁶
1	0	.869	1286	69.5
2	[illegible]	.855	1244	75.5
3	[illegible]	.8455	1225	78.3
4	·400	.8355	1214	81.2
5	[illegible]	.8295	1204	83.[illegible]
6	[illegible]	.812	1190	86.0
7	[illegible]	.802	1177	90.0
8	1.000	.784	1147	97.0

There are points of inflection in the curves of velocities and compressibilities (Fig. 1).

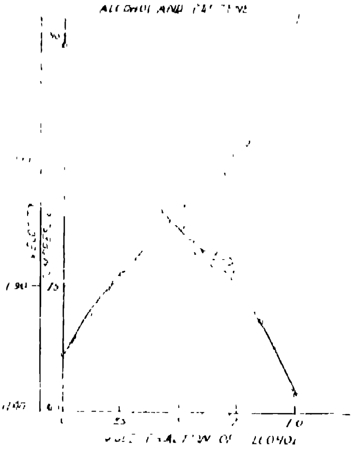

FIG. 1

MIXTURE 2

Butyl alcohol and heptane

Temp. = 25 C

No	Mole fraction of alcohol	Density gm c c	Velocity m /s.	Compressibility (adiabatic) × 10⁻⁶
1	0	·6793	1130	115.3
2	·2570	·7004	1136	110.0
3	·4843	·[illegible]52	1155	103.4
4	·7457	·7603	1190	92.0
5	·8241	·7735	1205	89.0
6	1	·8061	1245	80.0

In the compressibility-concentration graph the curve always remains above the straight line joining the points representing the pure liquids. It means that the compressibility is always more than that expected for ideal mixtures. The velocity-concentration curve always remains below the straight line corresponding to ideal cases (Fig. 2).

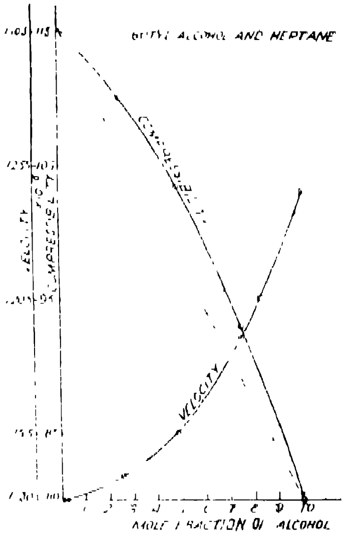

FIG. 2

MIXTURE 3

Benzene and carbon tetrachloride

Temp. = 23°C

No.	Mole fraction of benzene	Density gm./c.c.	Velocity m./s.	Compressibility (adiabatic) × 10⁻⁶
1	1	.8725	1312	66.4
2	.8362	1.001	1201	69.2
3	.7207	1.086	1130	71.0
4	.5175	1.237	1048	73.5
5	.3710	1.340	1018	72.0
6	0	1.596	927.2	72.0

The velocity-concentration curve lies below and the compressibility-concentration curve above their respective straight lines (Fig. 3).

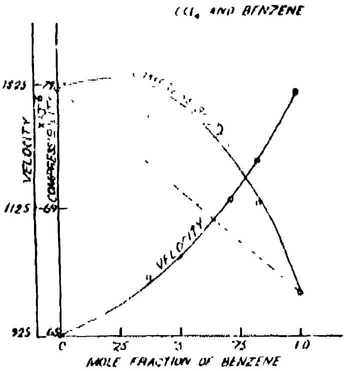

FIG. 3

MIXTURE 4

Benzene and ethyl ether

Temp. = 28°.54C

No.	Mole fraction of ether	Density gm./c.c.	Velocity m./s.	Compressibility (adiabatic) × 10^{-6}
1	0	.870	1290	69.1
2	·1748	.840	1234	78.1
3	·3609	.811	1180	88.5
4	·5598	·7755	1117	103.4
5	·7941	·7305	1032	128.4
6	1	699	972	151.5

The velocity-concentration curve is linear and the compressibility-concentration curve slightly concave (Fig. 4).

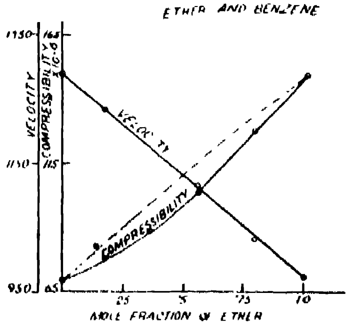

FIG. 4

MIXTURE 5

Ethyl acetate and carbon tetrachloride

Temp. = 23°C

No.	Mole fraction of ethyl acetate	Density gm./c.c	Velocity m./s.	Compressibility (adiabatic) × 10^{-6}
1	1	8989	1184	79·3
2	.8002	1 034	1119	77·3
3	.5476	1.200	1051	75·5
4	.3626	1 313	1003	75 7
5	.2555	1.404	984·2	73·5
6	0	1 596	927·2	72·9

The velocity-concentration curve lies below and the compressibility-concentration curve is irregular (Fig. 5).

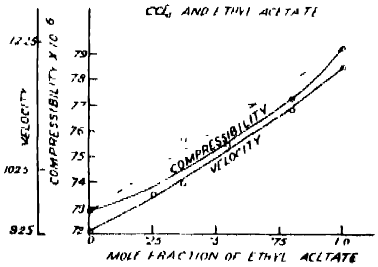

FIG. 5

DISCUSSION

The basic considerations relating the compressibility with molecular forces has been discussed in the first paper and will not be repeated here. Attempts will be made here to explain the nature of variation of the compressibility with concentration of the different mixtures on those basic considerations.

MIXTURE (1) ETHYL ALCOHOL AND BENZENE

Before discussing the curve proper let us review the structure of the pure liquids.

Alcohol :—It has been well established from many branches of investigation, *viz.*, infrared absorption spectra, Raman effect, dielectric polarisation, and directly by X-ray diffraction experiments that alcohols are highly associated liquids. This association is due to the nature of the hydroxyl dipole OH and its position with respect to the rest of the molecule.

It has been shown that associations detract from the cohesive energy between different associated groups and thus increase the compressibility. Again even allowing for the associations, the cohesive energy is mainly dipolar due to the dominating effect of the OH dipoles in molecular interaction.

Benzene :—Benzene has the well-known planar structure and has a high value of polarisability. Due to its high polarisability, it has a strong dissociating effect on the associated groups of any liquid that may be introduced in it and may be shown to be so as follows :—

(1) Benzene molecules will develop induced dipoles due to their polarisability, and these induced dipoles will so interact with the associations that they will be dissociated.

(2) Due to high polarisability, benzene molecules can exert high dispersion forces on the molecules of the associations as given by the formula,[1]

$$E = -\frac{3h}{2} \cdot \frac{\alpha_\beta . \alpha_2}{(\nu_\beta + \nu_2)} \cdot \frac{\nu_\beta . \nu_2}{R^6}$$

and so dissociate them.

(α_β is polarisability of benzene, α_2 of the other liquid, $\nu_\beta . \nu_2$ the main molecular frequencies, *h* Planck's Constant, and R the distance between the molecules).

(3) The dissociating effect of benzene due to its polarisability is enhanced by the nature of the planar structure of its molecules. Molecules tend to come in contact along their axes of polarisability. In benzene, the axis is at right angles to the plane of its molecule and so when benzene will approach the associated molecules, all the atoms of the plane will also come in close contact with the associations. These atoms of the plane will exert dispersion forces and so tend to dissociate the associations.

The dissociating effect of Benzene may be seen from the following experiments :—

(1) In Wolf's paper,[4] it is shown how the dielectric polarisation curves of alcohol in benzene are flattened out as compared to the steep curves in cyclohexane. In cyclohexane, the concentrations at which double and triple molecules only are formed are sharply defined, but not so in benzene and in fact there seems indication of only little or no double molecules being formed at all. Benzene is, thus, able to dissociate the association while cyclohexane cannot.

(2) From heat of mixing[4] it is seen that dissociation of alcohol into monomolecules is complete at .01 mol of alcohol in benzene, while it is complete at .001 mol. of alcohol in cyclohexane. The above points to the dissociating effect of benzene.

(3) Arkel and Snock[5] found that benzonitrile is unassociated in benzene, but associated in hexane. This was rightly attributed by them to benzene molecules having higher external fields than those of hexane, which were instrumental in giving benzene its high dissociating power.

The mixture :—Now we are in a position to discuss the interactions in the mixture with respect to its compressibility. We shall analyse the compressibility curve starting from the benzene side.

(1) Very little alcohol in benzene :—All the alcohol molecules will be in the monomolecular form and will be separated widely from one another. Now, since the interaction energy has an extremely short range (falling inversely as sixth power of the distance) and the cohesive energy of pure alcohol is mainly dipolar, it is clear that due to the great distance among the alcohol molecules, the cohesive energy of the mixture will be less than that in the ideal case. This means to say that the compressibility curve will rise above the straight line.

Now, all along, benzene molecules will interact with alcohol molecules, due to the induced dipoles developed in them in virtue of their polarisability. The cohesive energy will increase on this account, bringing the compressibility curve down In the case of inert liquids this influence will be negligible. There are thus two opposing influences in Benzene and the resulting curve will depend on the magnitudes of the two influences In our actual case, the interpolated curve goes very slightly above the straight line.

(2) More alcohol in benzene :—As more and more alcohol is introduced, the distance among the alcohol molecules decreases, the interaction becomes more effective, and so, the curve begins to come down towards the straight line.

After a large concentration of alcohol a stage comes when associations would have occurred, if there had been no dissociating influence of benzene. This non-formation of associations will enhance the cohesive energy in the way dealt with before[1] and thus decrease the compressibility further.

(3) Little benzene in alcohol .—Now the curve after going below the straight line must, near the alcohol-end, begin to rise due to the following reasons :-

With very little benzene, the dissociating power is decreased, while at the same time due to the high concentration of alcohol, the association-forming tendency is increased. Cohesive energy is therefore not so much more than that of the ideal case, as when there was more of benzene. Hence the curve rises and meets the point representing the pure alcohol

MIXTURE (2) BUTYL ALCOHOL AND HEPTANE

Heptane:—It is very inert. It has a very small value of polarisability and so cannot interact as benzene can. Also its axis of maximum polarisability is along the chain length[6] while the maximum numbers of points of contact of its molecule with another will be at right angles to the chain. The two requirements are mutually exclusive as contrasted to the case in benzene where they are mutually additive. This fact adds all the more to its inertness for the purpose of dissociation.

Butyl alcohol :—Its nature may be taken on the whole to be the same as that of ethyl alcohol.

The mixture :—Now, when some hexane is added to alcohol, it will not be able to dissociate the alcohol polymers, due to its inertness, the different polymers will only separate to a greater distance from one another. As more and more hexane is added, the different polymers will reduce in size from a high complex to triple, double and eventually monomolecules, at a very great dilution of .001. As seen from Wolf's paper on dielectric polarisation of ethyl alcohol in hexane, the associations rather persist, till they form into triple and double molecules rather suddenly. Also it is seen from Wolf's graphs, that the triple, then double and finally monomolecules of alcohol are formed at a very great dilution of alcohol, the mono-form being at about .001 mole fraction. So we see that nearly all along the different ranges of compositions, the alcohol molecules are in the form of associations.

Now because, all through the different compositions of the mixture, the alcohol molecules, mainly associated, are at a greater distance from one another than in the pure alcohol itself, and because the mutual energy of alcohol molecules is in all forms greater than the mutual energy of alcohol and hexane, the cohesive energy of the mixture will always be less than that expected for the ideal case. The compressibility curve will therefore be always above the straight line concerned.

MIXTURE (3) BENZENE AND CARBON TETRACHLORIDE

Pure liquids :—Benzene is planar and carbon tetrachloride symmetrically spherical, both being non-polar. In carbon tetrachloride the cohesive energy is predominantly due to dispersion forces between Cl atoms. Due to the widely different shapes of the molecules, there is not expected to be much interaction between the unlike molecules and so the cohesive energy of the mixture will be less than that of the ideal case and the compressibility curve in these conditions will lie above the straight line concerned. Side lights may be thrown on this mixture from the following :—

London[6] showed theoretically that, in approximate cases, energy of cohesion between two unlike atoms is equal to or less than the geometrical mean of the energies among the pure molecules separately. Hildebrand[7] has derived an approximate equation for solubility applicable to regular solutions *viz.*,

$$4{\cdot}575\text{T} \log\left(\frac{a_2}{\text{N}_2}\right) = \text{V}_1\text{V}_2^2\text{D}^2$$

where D is the difference between the square-roots of energies of vaporisation per c.c., *i.e.*, the internal pressures or energy densities. The equation has been deduced on the assumption that the potential between two unlike molecules is the geometrical mean of the two. Now D has been calculated on this assumption and also determined experimentally from solubility. The difference in the two values for the mixture in question being considerable (the values being .6 and 1), Hildebrand concludes that this may be interpreted as indicating that dispersion energy between the unlike molecules is less than the geometric mean. This fact will make the compressibility curve lie above the straight line of the ideal case.

2. Again Hildebrand and Wood[8] have obtained, for the energy of transfer of a molecule from its pure liquid to a given solution, the equation

$$\mathrm{RT} \log \mathrm{f} = \mathrm{V}_2 \left\{ \left(\frac{\mathrm{E}_2}{\mathrm{V}_2} \right)^{\frac{1}{2}} - \left(\frac{\mathrm{E}_1}{\mathrm{V}_1} \right)^{\frac{1}{2}} \right\}^2 \mathrm{U}_1^2,$$

where V_2 is the moleculer volume of the solvent, V_1 that of the solute ; E_1, E_2 their respective energies of vaporisations from the pure liquids, *i.e.*, the volume fraction of the solvent in the solution and 'f' the activity. There is systematic disparity between calculated and observed values in the case of benzene-carbon-tetrachloride mixture. The source of disagreement may be ascribed fully or partly to the assumption that the dispersion energy between benzene and carbon-tetrachloride molecules is equal to the mean of the separate molecules, in their pure liquids. Actually it must be less.

More considerations :—The tetrachloride-benzene mixture is rather anomalous in its behaviour which may be shown below :

(*a*) There is negative heat of mixing (heat absorbed), the value being 20.0 calories only for .44 mole fraction of benzene (Vold[9]).

(*b*) The viscosity curve is linear with concentration in mole fraction, while the fluidity curve lies below the straight line for ideal mixtures (Emel[10]).

(*c*) There is volume concentration on mixing.

(*d*) There is a small positive vapour pressure deviation, *i.e.*, the actual vapour pressure is more than required for ideal cases.[10]

Properties (*b*) and (*c*) indicate more intermolecular action than in the ideal case and require that the compressibility curve lie below the straight line concerned. Properties (*a*) and (*d*) indicate just the reverse.

Numerical estimate of the maximum deviation from ideality :—Now it may be argued, *a priori*, that the maximum deviation from ideal value of compressibility will be when the two unlike molecules have to come in for the maximum of interaction, *i.e.*, when they are present in the 1:1 ratio. The actual ratio obtained from the graph is roughly also 1:1, the exact ratio being ill defined, due to the nature of the curve.

MIXTURE (4) ETHYL ETHER AND BENZENE

Pure liquids :—Ether is polar but its positive end is embedded inside the molecule as is evident from the structural formula

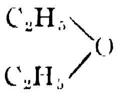

and only the negative end 'O' of the dipole is open to the surface. Consequently, the rôle of the dipole in intermolecular action is small, but still it is there, since with increasing length of the alkyl groups in the homologous ethers, the velocity goes on increasing, *i.e.*, compressibility goes on decreasing. This is due to more and more screening of the dipole, and also because the moment of the dipole itself becomes less and less.

Mixture :—In the mixture ether will exert effective polarising action on benzene. The inconspicuous position of the positive end of the dipole in ether and its great distance from the surface of the molecule, which is the cause for only little dipole energy in pure ether, becomes the very cause for great polarising action in benzene. The negative pole 'O' of ether can induce dipole in a benzene molecule without much counter-influence from the positive end and cause great intermolecular action between the unlike molecules.

Due to the separation of the ether molecules on the introduction of benzene, the dipole action among them is reduced more than proportionately due to the distance effect, and so, on this account alone, the compressibility curves should lie above the straight line for the ideal case, *i.e.*, be convex, but this convex curvature would be very small indeed, due to the minor rôle played by the dipoles in the pure liquid. From what we have considered above, however, there will be greater dipole action between ether and benzene molecules than between ether molecules themselves. Due to this cause the intermoleculer energy of the mixture is expected to be greater, rather than less, than that required for the ideal case. Hence the compressibility curve shall be concave, *i.e.*, lie below the straight line of the ideal case.

MIXTURE (5) ETHYL ACETATE AND CARBON TETRACHLORIDE

Pure liquids :—Ethyl acetate is an ester, having a dipole, but as in the ether molecule and for similar reasons the dipole plays a minor rôle in intermolecular action.

Mixture :—Due to the slightly polar character of ethyl acetate, and the non-polar and non-polarisable nature of carbon tetrachloride, the intermolecular energy is expected to be less than that for the ideal case, due to the separation of the dipoles in the mixtures. The compressibility curve is therefore expected to be slightly convex.

Now, Glasstone[11] has shown that the mixture shows abnormal dielectric polarisation. This shows roughly that there is some sort of dipole bond between the unlike molecules. We won't go into the discussion of the nature of the bond, etc., since it is highly controversial yet and also is not relevant. All we can say is that there is, therefore, a new source of molecular interaction between the unlike molecules which will tend to lower the compressibility curve.

The treatment of this mixture however, at the present stage, lacs precision.

In conclusion, it is my great pleasure to thank Dr. A. K. Dutta for discussions and helpful suggestions. I thank Prof. D. M. Bose for his keen interest in the work.

Bose Research Institute,
Calcutta.

REFERENCES

[1] R. Parshad, *In. J. Phys.*, **15**, 323 (1941).
[2] Wilson and Richards, *J. Phys. Chem.*, **36**, 1268 (1932).
[3] Parthasarathy, *Proc. Ind. Acad. Sci.*, **3**, 297 (1936).
[4] Wolf, *Trans. Farad. Soc.*, **33**, 179 (1937).
[5] Arkel and Snoek, *Trans. Farad. Soc.*, **30**, 707, (1934.)
[6] London, *Trans. Farad. Soc.*, **33**, 8 (1937.)
[7] Hildebrand, *Trans. Farad. Soc.*, **33**, 144 (1937.)
[8] Hildebrand and Wood, *J. Am. Chem. Soc.*, **57**, 866 (1935).
[9] Vold, *J. Am. Chem. Soc.*, **59**, 1515 (1937).
[10] Ewell, *J. Chem. Phys.*, **5**, 967 (1937).
[11] Glasstone, *Trans. Farad. Soc.*, **33**, 200 (1937).

2

ON A COMPARATIVE STUDY OF THE REFLECTIVITIES OF ALUMINIUM AND SILVER FILMS

By M. V. SIVA RAMAKRISHNAN

(Received for publication, August 2, 1941)

Plates I, II

ABSTRACT. A comparative study of evaporated aluminium films with that of chemically deposited and sputtered silver films is given. The reflectivity of the films in the visible, near infra-red and ultra-violet part of the spectrum is discussed at length and the deterioration of silver films with time is shown. Methods of preparing the respective films are also given.

INTRODUCTION

A study of metallic reflecting surfaces is engaging the attention of many physicists in recent years in view of its importance to various optical instruments, such as Reflectors in Telescopes, Interferometers, Coeleostats, etc. There are three well-known methods of obtaining thin films of metals on to surfaces namely, chemical deposition, cathode sputtering and evaporation.

Each of these is characterised by certain restrictions and advantages. Chemical deposition cannot be applied to surfaces like rock-salt which are attacked by water; sputtering is particularly suitable for preparing films of the platinum metals, and the evaporation process is suited to the application of aluminium films.

Of the metals useful for reflection of light in the visible spectrum, the three most important are aluminium, speculum and silver. The mirrors in astronomical reflecting telescopes were formerly made of speculum metal—a hard alloy of copper and tin capable of taking a fine polish and having a fairly high reflecting power. But on account of the low reflecting power of speculum[1] they have been entirely replaced by glass mirrors coated on the figured surface with a thin film of silver. The silvered surface, when fresh, has a high reflecting power for wavelengths greater than 3750 A.U. But the reflecting power diminishes with time, owing to the gradual oxidation or to tarnishing due to the action of sulphur dioxide in the atmosphere. Where such atmospheric contamination is intense, the reflecting power falls rapidly, and, even under the most favourable conditions, there is a gradual fall in the reflecting power. Hence the mirrors have to be periodically dismounted and resilvered. Mirrors coated with aluminium, on the other hand, have been found to have the remarkable property of withstanding the deleterious effect of atmospheric contamination for long periods of time. A

SIVA RAMKRISHNAN

PLATE I

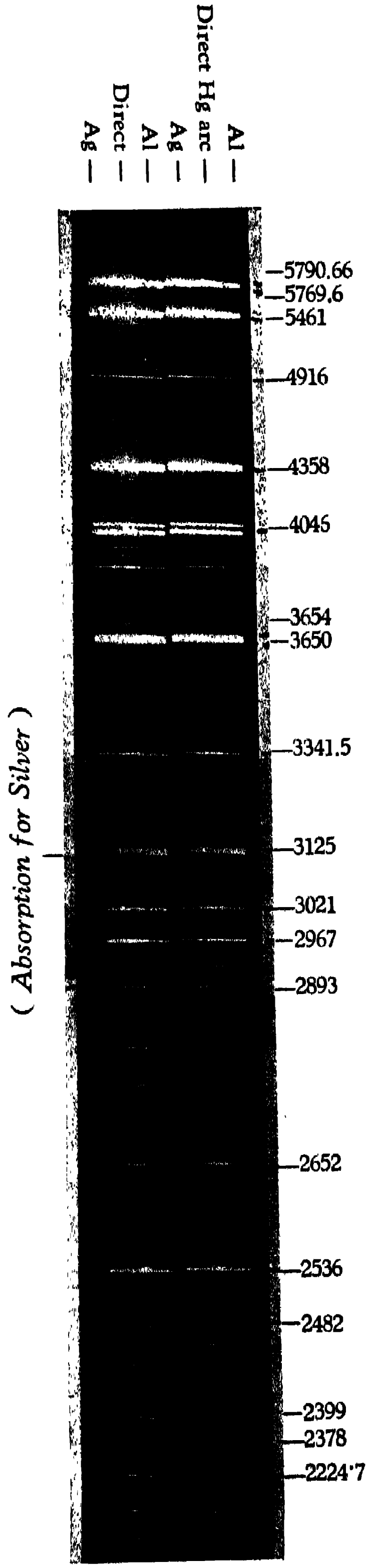

freshly deposited film on exposure to the air immediately oxidises, and the oxide coating forms a protective layer which prevents the film from tarnishing. Sulphur dioxide in the atmosphere does not tarnish an aluminium film, or if at all, it does at a very slow rate.[2] This observation is based on an experiment[3] conducted in Greenwich with a small mirror partly coated with silver and partly with aluminium. By the time the silver film had completely become yellow, the aluminium film was found unchanged. Dr. Strong mentions that the mirrors of a telescope aluminized in October, 1932, and in constant use since then, show no signs of tarnish.[4] In addition, aluminized surfaces have been reported to have higher reflectivity in the ultra-violet than silvered surfaces, and this paper deals with a comparative study of the reflectivities of aluminium films with those of silver obtained by sputtering and chemical deposition.

EXPERIMENTAL ARRANGEMENT

Previous Work.[5]—Dr. Strong has described an apparatus for measuring the reflectivities of metal films for small angles of incidence. His apparatus is shown in fig. 1(*a*). Light from a powerful source falls on one of the comparison mirrors B and the light is made to fall on a photometer and the reading is recorded. As shown in fig. 1(*b*) the mirror to be tested is placed between the two comparison mirrors so that light is reflected from that and then falls on the photometer. The apparatus therefore measures the square of the reflectivity. Measurements are made with monochromatic light obtained with a Müller-Hilger double quartz monochromator. A Nernst-filament as well as the Sun is used as light sources and quartz sodium or potassium cells as receivers. The photo-current is measured by an electrometer by a null method as well as with an amplifier and galvanometer.

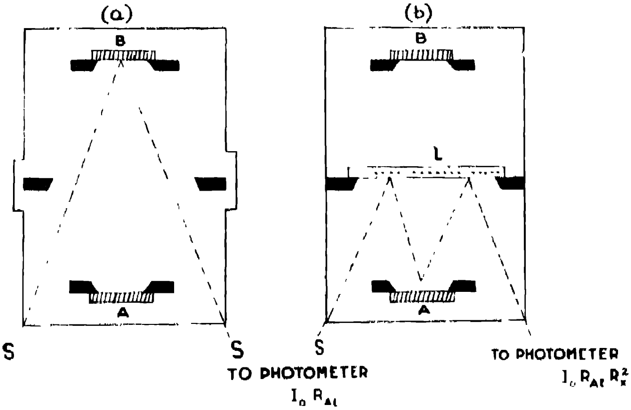

FIG. 1

The author has used a simple apparatus as described below for the visible and the near infra-red region of the spectrum. The method of procedure has been to measure the intensity of a light beam falling on a photo-cell directly, and after reflection from the test surface, and the ratio of these intensities, as measured by the respective photo-electric currents, gives a measure of the reflectivity of the surface.

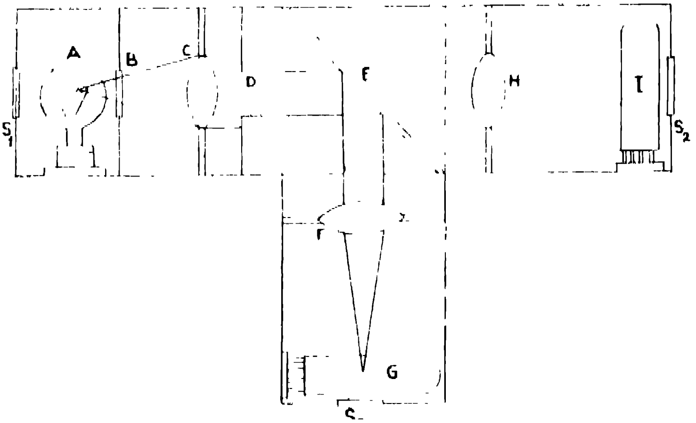

FIG. 2

Description. The apparatus as shown in fig. 2 consists of a T-shaped box. An incandescent 100-watts *frosted* tungsten-filament lamp A is used as the light source for the reflectivity measurements. For selecting various spectral ranges for the measurements, Wallace colour filters are used. The transmission band of the colour filter is determined using Hilger's constant-deviation spectrograph. Sunlight is used as a source and the drumhead of the spectrograph is adjusted by reference to the Fraunhofer's lines. The various colour filters are introduced in front of the slit of the spectrograph and the transmission band in the visible region of the spectrum is obtained for the different filters from the drumhead.

The blue filter transmits a band from	4000 to 5200 A.U.
The green filter transmits a band from	4800 to 6000 A.U.
The red filter transmits a band from	5800 to 7000 A.U.

The lamp is mounted on a holder fixed to the box and the switch for the lamp is also provided in the box. Light from the lamp passes through a 2″ square diaphragm B, and then falls on the colour filter which can be slid in the groove cut on the other side of the same plank carrying the diaphragm.

A convex lens of 6″ focus is placed 6″ from the lamp so that the rays from the filter after emerging from the lens are rendered parallel. A 2″ square diaphragm D is placed behind the lens so as to limit the beam falling on the test surface. The holder carrying the test surface is placed at 45° as shown in the diagram so that the angle of incidence of the beam is 45°. The reflected light falls on another convex lens of 6″ focus placed at 2″ from the T-joint as shown in the figure. The photo-cell used for the measurement is placed at 6″ from the centre of the lens, so that all the light is brought to a focus at the concave cathode of the cell. The cell used is a vacuum cell, R.C.A. 917 and measurements are taken with a sensitive galvanometer using a lamp and scale arrangement. The experiment is so conducted, that the same identical conditions prevail both for direct light and reflected light measurements. So the same photo-cell is used for both positions.

For direct incidence on the photo-electric cell, the plate-holder can be removed easily so that light is allowed to pass directly and fall on a similar convex lens of 6″ focus placed at 2″ from the T-joint as shown in the figure. The photo-cell is placed at 6″ from the centre of the lens in a 4-pin base already fixed there.

PREPARATION OF THE FILMS

Chemical Deposition.—The well-known Brashear process and the Rochelle salt process are used for obtaining the desired films. The first is used to obtain thick coats on front-silvered mirrors. The Rochelle salt method, because its action is slower, is used for partially silvered mirrors such as interferometer plates, which require a uniform thin film with a specified ratio of reflection and transmission.

Evaporation Process.—The process of obtaining evaporated films is described in the author's paper on "A Simple Method of Coating Optical Surfaces with Aluminium."[6] The high vacuum equipment necessary for the process is given in figure 3.

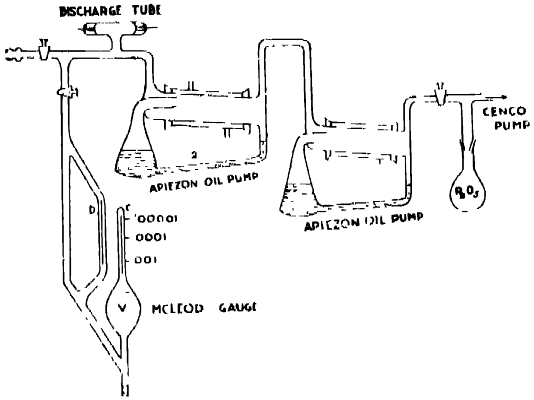

FIG. 3

Cathode Sputtering.—The sputtering chamber is the same bell jar used for the evaporation process with a hole in the top for the cathode connection. A cast-iron plate which is carefully machined in the lathe and lapped well with the bell jar is used as the base plate, so that it forms the anode. A terminal is provided in the base plate for connection to the secondary of the transformer.

The cathode is a rectangular silver plate 5″ × 4″ which is suspended from the top. The glow discharge is produced with an alternating potential of 25,000 volts from a Transformer working from 110 volts A.C. A milliammeter is used to measure the discharge current. The pressure is adjusted to be about .01 mm. The cathode is placed 5 cms. from the plate to be sputtered so that the boundary of the dark space is parallel to the surface to be coated. The same vacuum equipment as for aluminizing purposes is used but only the Cenco-Hyvac pump is worked. The pressure is indicated by the McLeod Gauge placed in the circuit.

EXPERIMENTAL PROCEDURE

The experiment consists in taking readings with the photo-cell and galvanometer for direct light and reflected light from the coated plate for a particular wavelength, using the proper filter. The reflection coefficients are calculated in each case and tabulated as shown in tables I to VII below.

Two 4-pin American bases are fixed one at G and another at I, so that the cell alone needs to be shifted from one position to another. The cell is worked with an anode voltage of 60 volts.

Readings are taken for the coated plates for different spectral regions choosing the proper filter and tabulated as shown in tables below.

The reflectivities of the following plates are compared :—

(1)	Chemically silvered (polished)	Table I
(2)	Chemically silvered (unpolished) ...	Table II
(3)	Sputtered (polished)	Table III
(4)	Sputtered (unpolished)	Table IV
(5)	Chemically silvered (after 15 days' exposure in Laboratory)	Table V
(6)	Chemically silvered (after 30 days' exposure in Laboratory)	Table VI
(7)	Aluminized plate	Table VII

TABLE I

Silver Plate (polished)

Filter used	Wave-length in A.U.	Deflection for direct light	Deflection for reflected light	Reflection coefficient
Blue	4000—5200	25 mm	23.5 mm	94 %
Green	4800—6000	15 mm	14.5 mm.	96 %
Red	5800—7000	155 mm.	147.5 mm.	95 %

TABLE II

Silver plate (unpolished)

Filter used	Wave-length in A.U.	Deflection for direct light	Deflection for reflected light	Reflection coefficient
Blue	4000—5200	25 mm	20.5 mm.	82 %
Green	4800—6000	15 mm	13.0 mm	87 %
Red	5800—7000	155 mm.	139.5 mm	90 %

TABLE III

Sputtered plate

Filter used	Wave-length in A.U.	Deflection for direct light	Deflection for reflected light	Reflection coefficient
Blue	4000—5200	25 mm	22.5 mm.	90 %
Green	4800—6000	15 mm.	14.0 mm.	93 %
Red	5800—7000	155 mm	147.5 mm.	95 %

TABLE IV

Sputtered plate (polished)

Filter used	Wave-length in A.U.	Deflection for direct light	Deflection for reflected light	Reflection coefficient
Blue	4000—5200	25 mm	23.5 mm.	94 %
Green	4800—6000	15 mm	14.5 mm.	96 %
Red	5800—7000	155 mm.	147.5 mm	95 %

TABLE V

Silver plate (after 15 days' exposure in laboratory)

Filter used	Wave-length in A.U.	Deflection for direct light	Deflection for reflected light	Reflection coefficient
Blue	4000—5200	24 mm	18 mm	75 %
Green	4800—6000	16 mm	13.5 mm.	84.4 %
Red	5800—7000	155 mm.	136.5 mm	89.8 %

TABLE VI

Silver plate (after 30 days' exposure in laboratory)

Filter used	Wave-length in A U.	Deflection for direct light	Deflection for reflected light	Reflection coefficient
Blue	4000- 5200	25 mm	17.5 mm.	70 %
Green	4800—6000	16 mm.	12.5 mm	83 %
Red	5800 -7000	155 mm.	136 5 mm.	88 %

TABLE VII

Aluminised plate

Filter used	Wave-length in A.U	Deflection for direct light	Deflection for reflected light	Reflection coefficient
Blue	4000—5200	25 mm	22 5 mm	90 %
Green	4800- 6000	15 mm.	13.5 mm.	90 %
Red	5800—7000	155 mm.	139 5 mm.	90 %

TABLE VIII

Wave-length in A U	Reflection Coefficient						
	Silvered polished	Silvered not polished	Sputtered Plate	Sputtered Plate (polished)	Ag, 15 days in the laboratory	Ag, 30 days in the laboratory	Al Plate
4000—5200	94 %	82 %	90 %	94 %	75 %	70 %	90 %
4800—6000	96 %	87 %	93 %	97 %	84 %	83 %	90 %
5800- 7000	95 %	90 %	95 %	95 %	90 %	88 %	90 %

DISCUSSION OF THE RESULT

Taking the case of silvered plate, the reflectivity of a polished plate is superior to that of an unpolished plate (Tables I to IV). The reflectivity of silver decreases with time (Tables V and VI). The reflectivity of evaporated and sputtered films are less than that of polished chemical silver, but the films on polishing give a better reflection. It is probable that chemical silver, sputtered and evaporated films require burnishing to form the metal into a compact film which exhibits a higher reflection coefficient.

We find aluminium films are inferior to freshly deposited silver for reflectivity in the visible region, but they have more or less uniform reflectivity from 4000 A.U. to 7000 A.U. which is very useful from the point of view of photography.

Reflectivity in the red and near infra-red.—For taking measurements in the red and near infra-red, Zeiss Ikon Infra-red filters, R-10, R-15, R-20 are used.

EXPERIMENTAL ARRANGEMENT

The same apparatus as used for the visible region is used for the measurements as the glass can transmit up to 2.2μ in the infra-red. The same photo-cell which is very sensitive in the infra-red, as shown in the special chart given by the makers, is used for the readings. Measurements are taken as before, first for direct light and then for reflected light, in the case of the chemically silvered plate and aluminized plate respectively.

TABLE IX

Aluminium (near Infra-red)

Filter used (Zeiss Ikon)	Deflection for direct light	Deflection for reflected light	Reflection coefficient
R—10	155 mm.	139.5 mm.	90 %
R—15	177 mm	101.0 mm.	86 %
R—20	122 mm	95.0 mm.	84 %

TABLE X

Silvered (polished) Plate

Filter used (Zeiss Ikon)	Deflection for direct light	Deflection for reflected light	Reflection coefficient
R—10	155 mm.	147.5 mm.	95 %
R—15	177 mm.	111.5 mm.	95 %
R—20	112 mm	107.5 mm.	96 %

Inference :—From the Tables IX and X one can easily see how the aluminium films are inferior to silver in reflectivity in the red and near infra-red.

The following table reveals to us a comparative percentage reflection in the visible and near infra-red region of the spectrum for the chemically silvered and aluminized plates.

TABLE XI

Wave-length in A.U.	Visible			Near infra-red	
	4000–5300 Blue	4800–6000 Green	5800–7000 Red	R-15 Zeiss Ikon filter	R-20 Zeiss Ikon filter
Percentage of reflection (Al)	90	90	90	86	84
Percentage of reflection (Ag)	94	97	95	95	96

On the superiority of Aluminium over Silver Films in the ultra-violet region of the spectrum.—For investigating the reflectivity of aluminium films in the ultra-violet region of the spectrum, a quartz spectrograph and quartz mercury-arc are used. Following, in the main, the method of Ben Johnson[7] and Sabine,[8] the attempt has been to take photographs of the spectrum of mercury arc for direct light first and then after reflection from the test surface, the surface being placed here at 45° angle of incidence. The spectrograms show clearly the relative "density" of the lines

(*a*) when photographed directly,

(*b*) when photographed after reflection from the test surface.

Micro-photometer records are taken for wave-lengths below 2500 A.U. and the records clearly show how aluminium is superior to silver in that region of spectrum. The exact experimental details are given below.

EXPERIMENTAL PROCEDURE

The same 'T' Box (Fig. 2) as previously used for finding the reflection coefficient in the visible region of the spectrum is used with all the lenses removed leaving the plate-holder alone. As shown in photograph the box is provided with slits at the three corners of the 'T' Box, so that light can pass through them freely. After making the preliminary adjustments of the quartz spectrograph such as the width of the slit, focus, tilt motion, the quartz arc is placed in a vertical position, so that a photograph of the spectrum of the direct light can be

MICROPHOTOMETER RECORDS FOR WAVE LENGTHS 2482, 2399, 2378
OF MERCURY ARC

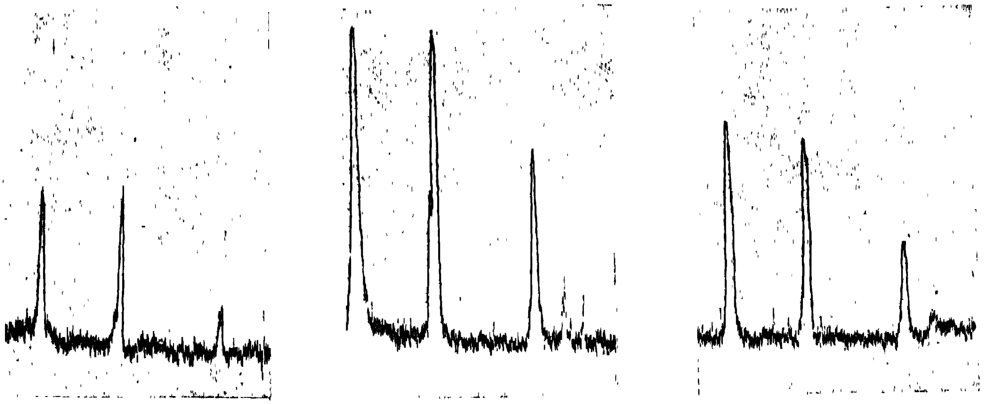

REFLECTED LIGHT
(Silver)

DIRECT LIGHT

REFLECTED LIGHT
(Aluminium)

taken. Then the quartz arc is placed for the reflected light position, so that a photograph of the spectrum of the reflected light from the test surface can be taken. In order to get a comparison photograph of the direct light and reflected light for aluminium and silver films respectively, a wedge is used. The middle aperture is used for direct light, the top and bottom ones are used for aluminium and silver films respectively

The plates used for the spectrograms are "Ilford special rapid panchromatic H.D. 700." Everything being kept at identical conditions, 3 minutes' exposures are given both for direct light and reflected light. The plates are developed and the photographs thus obtained are shown in the left page.

DISCUSSION OF THE RESULT

1. From the photograph we can easily see how the reflection is strong with the aluminized plate even down to $\lambda = 2200$. The lines do not suffer much in intensity by reflection from the aluminized surface.

Below 3340 A.U. the lines of the mercury are reflected from aluminium are definitely more intense than from silvered surfaces.

2. Silver as can be seen from the spectrograms shows clearly a strong absorption at 3123 A.U. unlike aluminium. That is, on the short wave-length side of 3750, the reflecting power of silver falls off rapidly owing to selective absorption. This is a serious disadvantage when observations are required in the ultra-violet region. In a reflecting telescope where the image is normally produced by reflection at two silvered mirrors this loss by the selective absorption is a serious handicap for photographic work. It has been decided therefore to coat the Presidency College 24″ Reflector which has been correctly figured, polished and parabolised with aluminium instead of silver.

3. Below 2500 A.U. the microphotometer records taken show clearly how aluminium is superior to silver in that region of the spectrum. The microphotometer records are given in the left page.

4. For wave-lengths greater than 4000 the lines of mercury are for silver are more intense than for aluminium, showing the superiority of silver in the red region.

SUMMARY OF RESULTS

1. Chemical silver has better reflectivity when polished (Tables I to V).

2. Silver films get tarnished soon and so lose in reflectivity with time (Tables V and VI).

3 Sputtered films when polished have better reflectivity and they are very nearly equal in this respect to polished chemical silver (Tables III and IV).

4. Aluminium has uniform reflectivity in the visible region (Table VII).

5. Aluminium films are inferior to silver films in the red and near infra-red region of the spectrum (Tables IX and X).

6. Aluminium is found to be superior to silver in the ultra-violet region of the spectrum.

7. A freshly deposited film of aluminium on exposure to the air immediately oxidises and the oxide coating forms a protective layer which protects the film from tarnishing. Nevertheless the film can be dissolved by alkali or dilute Hydrochloric acid to which a trace of copper salt is added.

8. Aluminium films are more strongly adherent to glass than silver films. This tenacity makes it possible to clean the surface of dust or other contamination by washing with soap and water.

9. Aluminized mirror scatters less light than silver mirrors as the latter have to be polished and this process leaves many small scratches upon the silver.

I wish to express my thanks to Professor G. P. Krishnamoorthi Iyer for his interest in my work and to Sir C. V. Raman for allowing me facilities to take the microphotometer records in his Department at the Institute of Science, Bangalore.

PHYSICS DEPARTMENT,
PRESIDENCY COLLEGE, MADRAS

REFERENCES

[1] Kaye and Laby's Table, pp. 84 (1932).

[2] R. C Williams, *Astro. Phys. Jour.* **89**,611 (1939).

[3] Spencer Jones, *Nature* **133**, 552 (1934).

[4] Strong, *Astro. Phys. Jour.*, **83**, 422 (1936).

[5] Edwards, *Phys. Rev.*, **50**, 871 (1936) . B. K. Johnson, *Nature* **134**, 216 (1934), Sabine, *Phys. Rev.* **55**, 1064 (1939); Strong, *Procedures in Experimental Physics*, pp. 376; Baxter, *Jour. Sci. Inst* **14**, 303 (1937); Amateur Telescope making (Advanced), pp. 467-476.

[6] M. V. Sivaramakrishnan, *Ind. Jour. Phys.*, Vol. XIII, Part IV, August (1939.)

[7] Ben Johnson, *Nature* **134**, 216 (1934).

[8] Sabine, *Phys. Rev.*, **55**, 1064 (1939).

EFFECT OF DEPTH OF LIQUID ON DAMPING OF A QUARTZ OSCILLATOR

BY K. G. KRISHNAN

(*Received for publication, August 19, 1941*)

Plate III

ABSTRACT. The paper describes the results obtained in the investigations of damping of high frequency sound waves at different depths of liquids. The result obtained for these liquids suggests that there is no definite dependence of the damping effect either on the hydrostatic pressure of the liquid or viscosity, but it is found to have closer agreement with the order of the absorption values recently determined by others.

INTRODUCTION

Measurements made at a high frequency of several millions per second in liquid show damping. Damping produces (1) a change in the frequency and (2) a lowering of the amplitude.

Parthasarathy[1] has detected a change of frequency of a quartz oscillator in liquids due to damping. This change in frequency with depth may be attributed to the hydrostatic pressure of the liquid, viscosity or the absorption of the sound waves.

The experiments of Lucas[2] and Biquard[3] in absorption showed serious disagreement with the classical theory, according to which the absorption is entirely due to viscosity and thermal conductivity. Recently E. G. Richardson,[4] by using a hot wire detector in a few liquids has shown that though the absorption values were higher than those required by the classical theory, they were very much lower than those obtained by Claeys[5] and others The serious difference is that while Claeys has shown the value of CS_2 to be 2000 times that of its calculated one, Richardson has shown it to be only about 4 times greater An attempt is made in this paper to examine the dependence of damping on the density and viscosity of a few liquids which show considerable absorption of ultrasonic waves.

EXPERIMENTAL ARRANGEMENT

A single valve oscillator circuit of Hartley type was employed. The quartz crystal used was an x-cut of dimension 20 × 20 × 2 mm. The frequency of the oscillation was about 4.3 m c., *i.e.*, the third harmonic of the crystal. The quartz crystal was held between two metal contacts.

The container used was a tall rectangular vessel one foot in height and 2″ × 2″ in sectional area. The vessel was placed on a rising table with a fine screw arrangement by which it was possible to raise the table gradually and the stem of which was graduated in mms. to denote the distance through which the vessel has been raised. The quartz crystal was mounted on an independent stand.

The frequency of the oscillator was measured at different depths with a precision wavemeter of the General Radio Co. A suitable optical system was set up to get the diffraction spectra at different depths on a photographic plate. A constant wave-length of light of mercury spectrum isolated by a wratten filter No. 77 was used.

EXPERIMENTAL PRECAUTIONS

It is important to check that there is no fluctuation in the frequency at the same depth. The H. T. and L. T. voltages should be maintained without variation during the time of measurement. Care was taken to prevent evaporation which would cause a change in the level of the liquid.

A constant distance of 1.50 cm. between the base of the crystal and the beam of light was maintained when the diffraction photographs at varying depths were taken. The quartz crystal was kept undisturbed throughout the investigation. The liquids used were all pure and redistilled.

RESULTS

The damping coefficient k can be calculated from the usual formula

$$k = \sqrt{n^2 - n_1^2}$$

where n is the undamped frequency and n_1 the damped frequency. Table I gives the frequency at different depths and the corresponding coefficient of damping.

TABLE I

Damping Co-efficient

Depth of incident beam from liquid level *	Benzene		Xylol		Carbon Tetrachloride		Carbon Bisulphide	
	Frequency in m.c.	Damping Coefficient	Frequency in m.c.	Damping Coefficient	Frequency in m.c.	Damping Coefficient	Frequency in m.c.	Damping Coefficient
1.5 cm.	4.3381	Standard	4.2401	Standard	4.2053	Standard	4.2959	Standard
2.5 cm.	4.3034	0.5491 × 10^6	4.2190	0.5000 × 10	4.2248	0.5917 × 10^6.	4.2491	0.6403 × 10^6
3.5 cm.	4.2959	0.6001 × ,,	4.2086	0.5917 × ,,	4.2168	0.5403 × ,,	5.2375	0.7142 × ,,
4.0 cm.	4.2896	0.6403 × ,,	4.2058	0.6082 × ,,	4.2011	0.7416 × ,,	4.2306	0.7551 × ,,
5.5 cm.	4.2774	0.7211 × ,,	4.1673	0.8307 × ,,	4.1641	0.9219 × ,,	4.2162	0.8307 × ,,
7.5 cm.	4.2030	0.8000 × ,,	4.1538	0.8945 × ,,	4.1527	0.9747 × ,,	4.1722	1.0290 × ,,
8.0 cm.	4.2595	0.8307 × ,,	4.1405	0.9164 × ,,	4.1500	0.9849 × ,,	4.1700	1.0350 × ,,
8.5 cm.	4.2572	0.8368 × ,,	4.1441	0.9383 × ,,	4.1479	0.9949 × ,,	4.1662	1.0490 × ,,

* The depth of the crystal will be 1.50 cms. less than the values shown in this column.

Depth

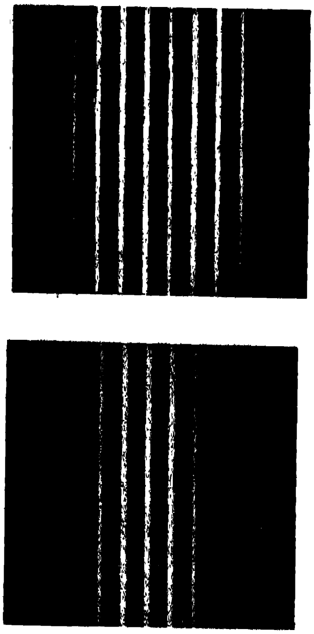

4·0 cms

8·5 cms

BENZENE

Depth

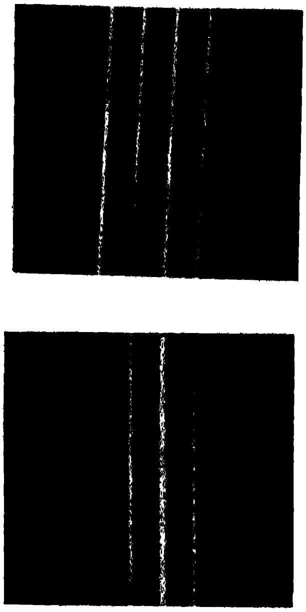

1·5 cms

8·5 cms

ccl$_4$

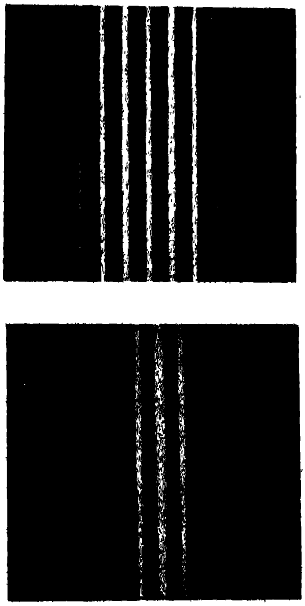

1·5 cms

8·5 cms

XYLOL

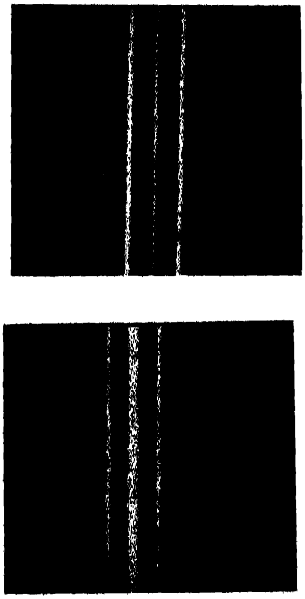

1·5 cms

8·5 cms

cs$_2$

The frequency of the oscillator when the crystal was just immersed in the liquid was taken as the standard in each case. It is evident from the table that the damping is considerable at a depth of about 8.0 cms. for all the liquids investigated.

TABLE II

Liquid	Damped frequency of the crystal at a depth of 6.5 cms.	Density (Hand-Book of Chemistry and Physics)	Viscosity (Hand-Book of Ch. and Ph.)
Benzene	0.0786 m.c. =1.8%	0.8784 at 20°C.	0.00649 at 20°C.
Xylol	0.0996 ,, =2.3%	0.8641 ,,	0.00615 ,,
CCl_4	0.1153 ,, =2.7%	1.5950 ,,	0.00969 ,,
CS_2	0.1259 ,, =2.9%	1.2628 ,,	0.00367 ,,

Table II gives the percentage damping of frequency in each liquid at a constant depth of 8.0 cms. of the beam of light from the surface of the liquid or 6.5 cms. of the crystal from the surface.

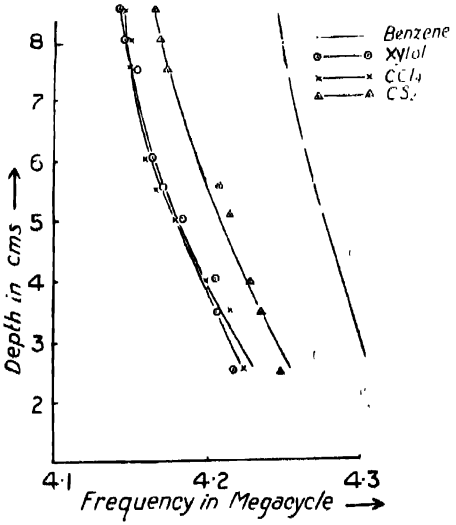

FIG. 1

Fig. I shows the relation between the depth of the crystal, rather the beam of light, below the surface of the liquid and the corresponding frequency of oscillation. The experimental points for all liquids are in straight lines. Near the bottom (where $d > 6$ cms.) there is a slight deviation.

DISCUSSION

The energy of the oscillation is lost through the crystal holders and by damping of the liquid. Now, if this damping effect is due to the hydrostatic pressure $h\rho g$ of the liquid, then it must depend on the density of the liquid. But from table II it is seen that the damped frequencies do not increase with the liquids of higher density. It is also seen that there is no increase of damped frequencies with viscosity. It is observed that the change in the magnitude of the damping effect in the liquids investigated follows more closely the order of their absorption values of ultrasonic waves in them.

The photographs also depict the decrease of orders with depth, which suggests that the supersonic intensity decreases with the increase of damping.

The author wishes to thank Prof. J. West, D.Sc., F. Inst. P., for his constant interest and kind encouragement.

Department of Physics,
University College, Rangoon

REFERENCES

[1] Parthasarathy, S., *Proc. Ind. Acad. Sci.* (A), **3**, 551 (1936).

[2] Lucas, R., and Biquard, P., *Trans. Farad. Soc.*, **33**, 130 (1937).

[3] Biquard, P., *Ann. de Phys.*, **6**, 195 (1936).

[4] Richardson, E. G., *Proc. Phys. Soc.* (*Lond.*) **52**, 487 (1940).

[5] Claeys, J., Errera, J., and Sack, H., *Trans. Farad. Soc.*, **33**, 136 (1937).

STRUCTURE OF THE ELECTRONIC BANDS OF THE OD MOLECULE. PART IV (SPIN DOUBLING)

By M. G. SASTRY

(*Received for publication, August 10, 1941*)

ABSTRACT. The theoretical formula derived by Hill and Van Vleck for the energy difference (ignoring the magnetic effect of molecular rotation) between the components of a doublet π-state, representing any intermediate stage of coupling, has been verified by application to the observed data of the spin-doublet widths of the OD molecule. Contrary to the observations of Johnston, the agreement between the experimental and calculated values is shown to be fairly satisfactory, considering the approximation made in the theoretical derivation. Incidentally, type value of the spin-coupling constant for the upper electronic state, $^2\Sigma^+$ of the OD molecule, is believed to have been determined as equal to 0.2, which cannot otherwise be estimated unless the satellite branches are also identified.

The spin-doublet widths for the OH and OD molecules are compared and, as observed by Johnston and by Shaw and Gibbs, the latter are found to be larger, although the OD molecule is heavier. The variation of the difference between these widths with K indicates a maxim at K=6. This is shown to be in complete agreement with the theoretical value derived from Hill and Van Vleck's formula.

INTRODUCTION

Using the method of the old quantum theory, Kemble[1] first derived energy formulae for diatomic molecules which are applicable over portions of the transition range between Hund's Case (*a*) and Case (*b*). Hill and Van Vleck[2] later treated the problem by the new quantum mechanics and obtained for doublet electronic states, representing any stage of coupling, the following closed formula for the rotational energy,

$$W = B_v[(J+\tfrac{1}{2})^2 - \Lambda^2 \pm \tfrac{1}{2}\{4(J+\tfrac{1}{2})^2 + \lambda(\lambda-4)\Lambda^2\}^{\frac{1}{2}} \quad \ldots \quad (1)$$

where $\lambda = A/B_v$ and $\Lambda = 1$ for the π-state; the upper and lower signs refer to the two component states $^2\pi_{\frac{1}{2}}$ and $^2\pi_{1\frac{1}{2}}$ respectively. The above equation gives the combined effects of the rotational and spin energy in a given state. The energy difference between the two doublet components due to spin effects alone could not be separated out ; but Hill and Van Vleck obtained from (1), by simplification, the doublet energy difference approximately as

$$\delta = B_v[\{4(J+\tfrac{1}{2})^2+\lambda(\lambda-4)\Lambda^2\}^{\frac{1}{2}}-(2J+1)] \qquad (2)$$

The equation was tested by them, by reference to the spin doublets of the (1, 0) band of OH at λ2811. Except for a small discrepancy, the observed and calculated values were found to agree well and better than was shown earlier by Kemble. The discrepancy was ascribed to the neglect of the contribution towards the doublet interval arising from the magnetic field developed by molecular rotation.

In a recent paper Dawson and Johnston[3] applied the formula to the various OH bands and concluded that it failed to reproduce accurately the spin-doubling spacing obtained from experimental data. The failure of the equation when applied to the spin doublets of the OD molecule was also briefly reported by Johnston[4] but the detailed data have not so far been published.

The recent work of the author[5] on the structure of the OD bands has enabled a detailed study of the validity of Van Vleck's equation, which forms the subject of this paper.

RESULTS AND DISCUSSION

To obtain the experimental values of the electronic spin width the usual method is adopted. We have[6]

$$Q_1(K) = F_1'(K) - F_1''_c(K)$$

and

$$Q_2(K) = F_2'(K) - F_2''_c(K).$$

Hence

$$\begin{aligned} F_2''_c(K) - F_1''_c(K) &= [Q_1(K) - Q_2(K)] - [F_1'(K) - F_2'(K)] \\ &- [Q_1(K) - Q_2(K)] - \gamma.K \end{aligned}$$

where γ is a small constant representing the spin doubling in the upper state $^2\Sigma^+$ Similarly,

$$\begin{aligned} F_2''_d(K) - F_1''_d(K) &= [R_1(K) - R_2(K)] - \gamma(K+1) \\ &= [P_1(K) - P_2(K)] - \gamma(K-1). \end{aligned}$$

In Van Vleck's theoretical equation the difference between the terms $F_c''(K)$ and $F_d''(K)$ was ignored so that when the mean of these terms is taken, the experimental value should agree with the theoretical value if the equation is correct. We therefore write

$$\begin{aligned} \delta &= \tfrac{1}{2}[\{F_2''_d(K) - F_1''_d(K)\} + \{F_2''_c(K) - F_1''_c(K)\}]. \\ &= \tfrac{1}{2}[\{Q_1(K) - Q_2(K)\} + \tfrac{1}{2}\{(P_1(K) - P_{.}(K)) + (R_1(K) - (R_2(K))\}] - \gamma K \quad \ldots \quad (3) \end{aligned}$$

TABLE I

Spin-doublet widths in the OD molecule for $v'' = 1$

K	R doublets			Q doublets			P doublets			Mean	
	(1,1)	(2,1)	(3,1)	(1,1)	(2,1)	(3,1)	(1,1)	(2,1)	(3,1)	R and P	Q
1	(125.5)		130.9	131.2	132.7	132.0	126.9	128.4	132.8	128.9	132.0
2	115.8	116.4	117.5	116.2	116.6	118.8	115.7	116.2	116.9	116.4	117.2
3	102.8	103.0	105.6	103.7	103.9	104.1	101.0	105.3	104.0	104.1	103.9
4	92.9	94.4	94.5	92.7	91.8	93.5	93.1	93.9	93.9	93.8	92.7
5	84.9	85.4	85.5	83.3	84.1	84.4	84.2	84.1	84.8	84.8	83.9
6	78.0	76.6	77.3	76.7	77.3	76.7	77.1	77.4	77.0	77.2	76.9
7	69.6	71.2	70.8	70.6	70.0	69.5	70.4	70.3	70.9	70.5	70.2
8	64.9	65.3	65.0	64.3	64.2	62.6	65.3	65.8	65.4	65.4	63.7
9	61.4	61.2	60.8	60.5	60.3	59.5	62.3	61.1	60.6	61.2	60.1
10	56.6	57.9	56.9	55.3	55.6	55.6	56.5	56.8	56.8	56.9	55.5
11	52.6	(47.2)	54.1	51.9	51.6	52.2	52.7	53.3	53.6	53.3	51.9
12	51.9	—	49.1	49.0	48.9	46.4	52.0	50.0	50.2	50.6	48.1
13	48.3	—	48.3	46.0	46.4	44.0	47.7	47.7	47.8	48.0	45.5
14	(41.0)	—	43.6	42.6	43.4	—	44.0	45.5	45.2	44.6	43.0
15	(45.5)	—	—	40.5	40.9	—	44.3	43.1	—	44.3	40.7
16	40.2	—	—	39.7	38.9	—	42.3	40.9	—	41.1	39.3
17	40.4	—	—	37.8	37.6	—	39.7	39.3	—	39.8	37.7
18	37.5	—	—	35.1	36.4	—	38.2	38.4	—	38.0	35.8
19	35.9	—	—	34.3	35.1	—	36.1	36.9	—	36.3	34.7
20	33.1	—	—	33.6	32.9	—	34.1	35.7	—	34.3	33.3
21	33.6	—	—	31.9	32.0	—	34.9	34.8	—	34.4	32.0
22	32.6	—	—	30.6	31.0	—	33.8	33.7	—	33.4	30.8
23	(34.3)	—	—	29.6	30.9	—	32.7	32.6	—	32.7	30.3
24	30.0	—	—	32.0	29.8	—	(26.8)	31.2	—	(30.6)	30.9
25	(35.2)	—	—	28.2	27.6	—	31.9	31.3	—	31.6	27.9
26	31.6	—	—	27.3	—	—	31.0	30.2	—	30.9	27.3
27	28.4	—	—	26.0	—	—	30.4	—	—	29.4	26.0
28	28.3	—	—	25.8	—	—	30.4	—	—	29.3	25.8
29	30.1	—	—	24.8	—	—	30.0	—	—	30.1	24.8
30	31.4	—	—	25.2	—	—	29.1	—	—	30.2	25.2
31	30.2	—	—	27.8	—	—	28.4	—	—	29.3	27.8

TABLE II

Spin-Doublet Widths

K	$v''=0$					$v''=1$				
	OD		OII		Diff. $(\delta_d-\delta_h)$	OD		OII		Diff. $(\delta_d-\delta_h)$
	Obs.	Calc.	Obs	Calc.	Obs.	Obs.	Calc.	Obs.	Calc.	Obs.
1	131.1	130.7	126.22	—	4.9	130.5	131.4	126.5	—	4.0
2	116.1	—	103.45	—	12.6	116.8	—	104.7	—	12.1
3	103.8	102.0	86.72	—	17.1	104.0	104.1	87.0	—	17.0
4	92.7	—	74.21	—	18.5	93.3	—	74.9	—	18.4
5	83.7	82.8	63.83	63.60	19.9	81.4	81.2	65.3	65.14	19.1
6	76.4	-	56.30	—	20.0	77.1	—	57.5	—	19.6
7	69.7	68.1	50.40	—	19.3	70.4	69.6	51.7	—	18.7
8	64.0	—	44.82	—	19.2	64.6	-	47.0	—	17.6
9	59.3	57.4	41.52	—	17.8	60.7	58.8	43.4	—	17.3
10	55.4	—	38.22	36.75	17.2	56.2	—	39.9	37.85	16.5
11	51.8	49.3	35.40	-	16.4	52.6	50.6	36.2	—	16.4
12	48.7	—	32.81	—	15.9	49.4	—	34.1	—	15.3
13	45.9	43.0	30.88	—	15.0	46.8	44.2	31.7	—	15.1
14	43.5	-	29.25	—	14.2	43.8	—	30.0	—	13.8
15	41.7	38.1	27.79	25.50	13.9	42.5	39.2	28.7	26.31	13.8
16	39.7	-	26.39	-	13.3	40.2	—	27.7	—	12.5
17	37.9	34.2	25.36	-	12.5	38.8	35.4	25.6	—	13.2
18	36.7	—	24.11	—	12.6	36.9	—	24.8	—	12.1
19	35.7	30.9	23.50	—	12.2	35.5	31.9	23.9	—	11.6
20	33.2	—	22.38	19.46	10.8	33.8	—	23.1	20.08	10.7
21	33.0	28.2	22.17	-	10.8	33.2	29.2	22.0	—	11.2
22	31.9	—	20.97	—	10.9	32.1	—	20.8	—	11.3
23	31.2	26.0	20.44	—	10.8	31.5	26.8	19.8	—	11.7
24	30.5	—	19.90	—	10.6	30.8	—	20.3	—	10.5
25	30.4	24.1	19.55	15.71	10.9	29.8	24.8	19.2	16.23	10.6
26	—	—	18.72	—	—	29.1	—	19.1	—	10.0
27	—	—	18.34	—	—	27.7	23.1	17.7	—	10.0
28	—	—	17.61	—	—	27.6	—	—	—	—
29	—	—	17.47	—	—	27.5	21.5	—	—	—
30	-	—	17.16	13.17	-	27.7	—	—	—	—

TABLE II (*contd.*)

	$v''=2$					$v''=3$	
K	OD		OH		Diff. $(\delta_d - \delta_h)$	OD	
	Obs.	Calc.	Obs.	Calc.	Obs	Obs.	Calc
1	131.5	131.2	126.2	—	5.3	132.0	132.4
2	117.2	—	106.2	—	11.0	118.0	—
3	105.0	104.2	89.1	—	15.9	105.0	105.9
4	94.5	—	76.2	—	18.3	95.5	—
5	86.2	84.5	66.6	66.58	19.6	86.4	86.3
6	78.7	—	58.8	—	19.9	79.0	—
7	72.0	70.0	52.4	—	19.6	72.4	71.7
8	66.1	—	47.3	—	18.8	69.3	—
9	61.4	59.1	44.6		16.8	62.3	60.7
10	56.7	—	39.8	38.91	16.0	60.6	—
11	53.8	50.8	37.6	—	16.2	53.8	52.5
12	50.5	—	34.6	—	15.9	48.8	—
13	47.3	44.6	32.0	—	15.3	—	—
14	46.4	—	31.7	—	14.7	—	—
15	44.5	39.5	29.8	27.09	14.7	—	—
16	39.9	—	28.5	—	11.4		—
17	39.2	35.5	—	—	—	—	—
18	38.8	—	—	—	—	—	—
19	36.6	32.2	—	—	—	—	—
20	34.2	—	—	—	—	—	—
21	31.5	29.4	—	—	—	—	—

In Table I the doublet intervals derived according to the above equation are shown in detail for the bands having the final state $v''=1$. For the remaining bands the observed average values only are given in Table II.[7] It should be noted that the correction term γK is ignored, as the value of γ has not been determined for the OD bands. The tables also give the calculated values of δ in each case, in determining which from equation (2) the following mean values of the constants have been adopted (they are in cms.$^{-1}$):

$$B_0''=9.89, \qquad B_3''=9.08$$

$$B_1''=9.57, \qquad A=-139.4.$$

$$B_2''=9.40$$

The agreement between the observed and the calculated values is close for small rotational quantum numbers, but for large values of K there are markedly increasing divergencies. The difference (obs. - calc.), however, varies linearly with K. The representative curves drawn for $v''=0$ in fig. 1 bring out these features clearly; the linear relation from curve (3) may be expressed as

$$\delta(\text{obs.}) - \delta(\text{calc.}) = 0.2\,K.$$

The constant 0.2 obviously represents the small factor γ of equation (3). It is of the right order of magnitude that should be expected for the OD molecule, for which the spin-coupling constant A is -130.4, nearly the same as that for OH. If this correction, depending on γK is made in each of the observed values, according to equation (3), the agreement becomes very close even for large rotational quantum numbers. The outstanding differences after this correction are to be ascribed to the approximation made in deriving equation (2) and perhaps partly to observational errors.

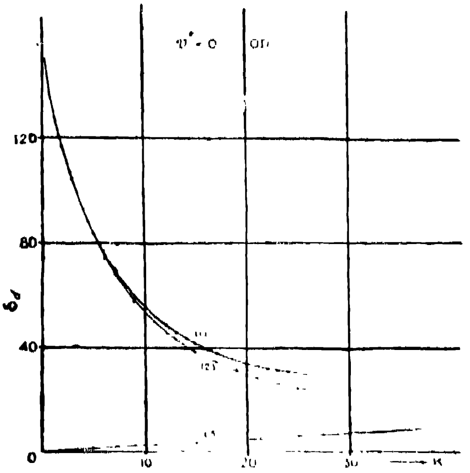

FIG. 1

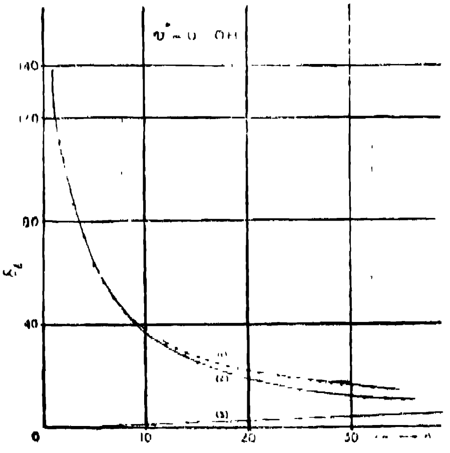

FIG. 2

Explanation of figures:—In these, curve (1) represents the observed, curve (2) the calculated values and curve (3) the differences plotted against K.

The author therefore considers, contrary to what Johnston had observed, that Van Vleck's theoretical equation represents the electronic spin doubling in the doublet π-state of the OD molecule fairly accurately. In the light of the above view, the data for the OH molecule given by Johnston and Dawson are re-examined. The curves in Fig. (2) are drawn for $v''=0$ for OH, similar to those in Fig. (1) for OD. The linear curve (3) in this figure gives the value of $\gamma_{OH}=0.2$ which agrees very well with that determined otherwise by Almy[8] as equal to 0.216. Dawson and Johnston appear to have omitted the correction factor γK, in estimating the observed values of the spin-doublet spacing. If this correction is applied, the agreement becomes very satisfactory even for the larger values of K as well.

Incidentally, it is desirable to point out that the above discussion provides perhaps a new method for obtaining the spin doubling constant γ of the upper state $^2\Sigma^+$ of the OD molecule, which cannot otherwise be determined from observational data alone, unless the satellite branches are also identified.

COMPARISON OF THE SPIN-DOUBLET INTERVALS IN OH AND OD

It was reported by Johnston[4] and also by Shaw and Gibbs,[9] from as yet unpublished data, that the spin-doublet spacing is larger for the OD than for the OH molecule, though the former is the heavier of the two. Johnston also observed that the difference in the spin-doublet widths for the two isotopic molecules is zero at the origin and increases rapidly with K up to a maximum and then approaches zero asymptotically. The present detailed data confirm the above observations as is evident from Table II. It is possible from these data further to verify the validity of Van Vleck's theoretical equation, as is shown below.

Equation (2) for the spin-doublet interval may be written as

$$\delta_h = B_h\{(y^2+M)^{\frac{1}{2}}-y\}$$

$$\delta_d = B_d\{(y^2+N)^{\frac{1}{2}}-y\}$$

where δ_h and δ_d are the spin doublet widths for the OH and the OD molecules, B_h and B_d are the respective constants and

$$y = 2K+1$$

$$M = (A/B_h)[(A/B_h)-4]$$

$$N = (A/B_d)[(A/B_d)-4].$$

If the value of $(\delta_d-\delta_h)$ is plotted against K, the value of K for which the curve shows a maximum is given by the condition,

$$\frac{d(\delta_d-\delta_h)}{dy} = B_h\left[\frac{y}{\sqrt{y^2+M}}-1\right]-B_d\left[\frac{y}{\sqrt{y^2+N}}-1\right]=0.$$

Taking the first three terms in the expansion of

$$\left[1+\frac{\text{M or N}}{y^2}\right]^{-\frac{1}{2}}$$

the value of y when the above condition is satisfied is given by

$$y^2 = \frac{\frac{3}{4}(N^2B_d - M^2B_h)}{NB_d - MB_h}.$$

Substituting the values of the constants given above for the OD molecule and the corresponding constants for the OH molecule,[10] we obtain that the maximum occurs at

$K = 5.7$ for $v'' = 0$, $K = 6.0$ for $v'' = 1$, $K = 6.2$ for $v'' = 2$.

Fig. 3 shows a curve for $v'' = 1$ between $\delta_d - \delta_h$ and K similar to that shown by Johnston[4] for $v'' = 0$. It indicates a maximum at $K = 6$, in beautiful agreement with the theoretical value.

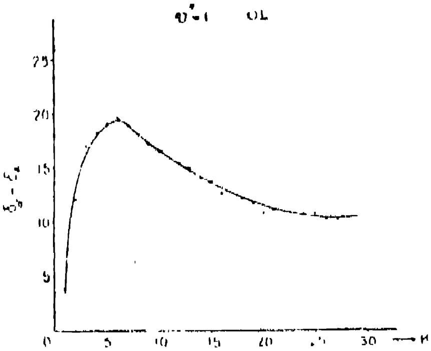

FIG. 3

The author is indebted to Dr. K. R. Rao for his interest in the work and to the Andhra University for the award of a Fellowship.

REFERENCES

[1] Kemble, *Phy. Rev.*, **30**, 387 (1927).

[2] Hill and Van Vleck, *Phy. Rev.*, **32**, 250 (1928).

[3] Dawson and Johnston, *Phy. Rev.*, **43**, 980 (1933).

[4] Johnston, *Phy. Rev.*, **46**, 80 (1934).

[5] Sastry and Rao, (Part I), *Ind. Jour. Phy.*, **15**, 27 (1941); Sastry, (Part II), *Ind. Jour. Phy.* In press); Sastry, (Part III), *Ind. Jour. Phy.* (In press).

[6] Jevons, *Report on Band Spectra*, 171.

[7] The data quoted in these tables are taken from the author's papers referred to above for all the bands except for (0, 0), (2, 0) and (3, 1) which are from Ishaq, *Proc. Nat. Inst. Sci. Ind.*, **3**, 389 (1939) and *Proc Roy. Soc.*, **A 159**, 110 (1937).

[8] Almy, *Phy. Rev.*, **35**, 1495 (1930).

[9] Shaw and Gibbs, *Phy. Rev.*, **45**, 124 (1934).

[10] Johnston, Dawson and Walker, *Phy. Rev.*, **43**, 478 (1933).

BAND SPECTRUM OF BISMUTH MONOCHLORIDE

By SANTI KUMAR RAY

(Received for publication, August 21, 1941)

Plate IV

ABSTRACT. The band spectrum of bismuth chloride has been photographed both in emission and in absorption. A number of new bands has been discovered and is found to form a part of the existing less refrangible system of BiCl. The correctness of the vibrational analysis of Morgan for the two band systems of BiCl is confirmed.

INTRODUCTION

It is now well known from the recent work of Morgan[1] that bismuth monochloride has two band systems with a common lower state. One of them lies in the blue-green region between λ4300-λ5400 and consists of bands degraded towards the longer wave-lengths. The other system comprises bands in the violet region between λ3600-λ4000 and shows perturbations in the upper state. The direction in which these bands degrade is uncertain but they look somewhat diffuse on the red side. The two systems have been designated by Morgan as the less refrangible and the more refrangible system respectively.

In the course of an investigation conducted with the object of identifying the bands of bismuth monoxide, a number of new bands due to bismuth monochloride has been observed in the region λ4300-λ5700. They are quite distinct in appearance from the oxide bands which lie in the longer wavelength side of λ5400 and are partially resolved even with the dispersion of Hilger E.1 quartz spectrograph in this region. Like the bands of the less refrangible system of BiCl, they are entirely absent in the spectrum of the flaming arc fed with pure metallic bismuth, but appear intense when the arc is fed with solid bismuth trichloride. It may, however, be noted that sometimes they are weakly developed in the spectrum of the flaming arc fed with metallic bismuth, evidently due to the presence of the subchloride as an impurity in the metal. That these new bands are due to bismuth monochloride is further evidenced from the fact that several of them show isotopic heads due to $BiCl^{35}$ and $BiCl^{37}$ in their expected positions. This alone is sufficient to prove the identity of their emitter beyond any doubt. The object of the present paper is to report the vibrational quantum analysis of these bands.

EXPERIMENTAL

For source of emission of the BiCl bands, the flame surrounding a carbon arc running from 220V. d.c. mains and taking a current of about 3A was used. The lower electrode (+) of the arc had a cavity which was filled with solid $BiCl_3$ and fed with it at regular intervals during exposure.

To obtain these bands in absorption, light from a Philips 500-watt projection lamp was passed through the vapour obtained by heating solid $BiCl_3$ in an open iron tube contained in an electric resistance furnace and then focussed on the slit of the spectrograph. The iron tube had a length of 70 cms., an internal diameter of 1.6 cms., and a wall thickness of 0.25 cm. It was held coaxially inside the furnace whose ends were properly insulated to minimise the loss of heat. When the temperature inside the furnace was about 800°C., only the bands of the more refrangible system began to appear while when the temperature was more than about 1000°C., bands of both the systems made their appearance. At about 1100°C., they were very excellently developed.

A Fuess quartz prism spectrograph of large light-gathering power was used for preliminary observations. Hilger E.1 quartz spectrograph and E. 52 glass spectrograph as well as a 6-ft. concave grating spectrograph on a Paschen mounting were used for obtaining plates for measurements Ilford Hypersensitive (HP 2) and Empress plates were used. For comparison, iron arc lines were photographed.

Measurements were done on a Precision type Gaertner comparator (M101). Several sets of measurements were taken. In no case the individual wave-length of a band head differed from the average value by more than ±0.01A.

THE LESS REFRANGIBLE BAND SYSTEM

The bands of this system were known to the early investigators, but until recently there existed considerable doubt regarding their emitter. Eder and Valenta,[2] who had photographed the flame spectrum of various bismuth compounds, recorded as many as twenty-two of these band heads in the region λ4350-λ4935, but attributed them to the oxide of the metal Mecke and Guillery[3] were also of the same opinion. Using the data of the above authors they attempted at a vibrational quantum analysis of these bands and ascribed them to the diatomic molecule of bismuth monoxide. A different view was, however, put forward by Saper[4] who excited them by introducing vapour from heated $BiCl_3$ into active nitrogen and attributed the band system to the diatomic molecule of bismuth monochloride. Saper substantiated his assignment from observations of a vibrational isotope shift in agreement with the expected shift for Cl=35 and Cl=37 in some of the bands. In 1933 Ghosh,[5] who had not evidently taken notice of Saper's work, photographed these bands in the spectrum of a flaming

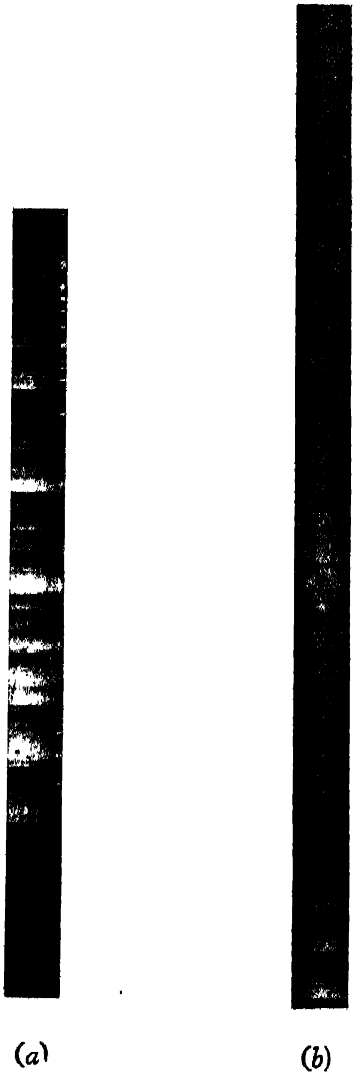

Fig. I.

(a) A portion of the less refrangible system
(b) A portion of the more refrangible system

are fed with either metallic bismuth or bismuth trichloride and attributed them to bismuth monoxide. These conflicting views regarding the identity of their emitter led Morgan to investigate the spectrum of bismuth trichloride in absorption. For the source of absorption, he used the vapour from solid $BiCl_3$ heated at a temperature sufficiently high to vaporise bismuth trichloride and dissociate it to form BiCl. The spectrum was also developed when chlorine gas was passed over the molten metal. Using spectrographs of different dispersions, Morgan measured about eighty-two band heads in the region λ4300-λ5400 and carried out their vibrational analysis. Besides obtaining a satisfactory conformation of isotope theory, he noticed marked similarity of this band system to the corresponding band system of BiF and BiBr and confirmed Saper's view that its emitter is the diatomic molecule of bismuth monochloride.

In the present investigation, in addition to the bands recorded by Morgan, a large number of new bands has been added to the system, a portion of which is reproduced in Fig. 1(a). It is found from an analysis of their vibrational structure that some of these bands belong to the higher members of the different sequences observed by Morgan while others form new negative sequences of the system in question.

The band head data for the complete system are given in Table I which includes observed wave-length and wave-number data of heads together with their estimated relative intensities (given in parentheses) and vibrational quantum assignments. The last column of the table contains the wave-number data of band heads recorded by Morgan and his estimated intensities. The v', v''-values of band heads due to the less abundant isotopic molecule, $BiCl^{37}$, are marked with asterisks. The differences between wave-numbers observed and those calculated from Morgan's equations are also given. It may be noted here that the deviations in the case of the new bands are well within the limits of experimental error. This shows evidently the correctness of not only the vibrational quantum assignments to the new bands but also of the vibrational constants in the band head equations evaluated by Morgan. His equations are as follows :

$$BiCl^{35}: \quad \nu = 21801.8 + \{220.3(v'+\tfrac{1}{2}) - 2.50(v'+\tfrac{1}{2})^2\} - \{308.4(v''+\tfrac{1}{2}) - 0.96(v''+\tfrac{1}{2})^2\}$$

$$BiCl^{37}: \quad \nu = 21801.8 + \{215.1(v'+\tfrac{1}{2}) - 2.38(v'+\tfrac{1}{2})^2\} - \{301.2(v''+\tfrac{1}{2}) - 0.92(v''+\tfrac{1}{2})^2\}$$

It is only for the band head at 20283.5v that the present assignment of v', v''-values is different from that of Morgan. Although the observed wave-number is equally close to the calculated wave-number of the band heads, (6, 9) and (3, 7), it is assigned to the latter from a consideration of the intensity distribution among the band heads of the system.

The intensities of the band heads have been estimated on a 0 to 8 scale. They lie on a well-defined and wide Franck-Condon parabola (Fig. 2).

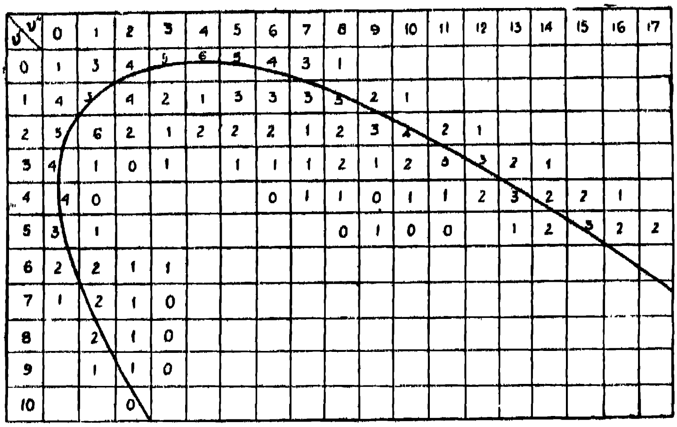

$v' \backslash v''$	0	1	2	3	4	5	6	7	8	9	10	11	12	13	14	15	16	17
0	1	3	4	5	6	5	4	3	1									
1	4	5	4	2	1	3	3	3	3	2	1							
2	5	6	2	1	2	2	2	1	2	3	2	2	1					
3	4	1	0	1		1	1	1	2	1	2	6	3	2	1			
4	4	0					0	1	1	0	1	1	2	3	2	2	1	
5	3	1							0	1	0	0		1	2	3	2	2
6	2	2	1	1														
7	1	2	1	0														
8		2	1	0														
9		1	1	0														
10			0															

FIG. 2

It may be noted here that the band head, (9, 0), recorded by Morgan on the shorter wave-length side of this system has not been observed although there are a number of fairly intense bands, due presumably to BiO, present in the region λ4000-λ4300.

TABLE I

Band head data of the less refrangible system

v', v''	λ (I.A.)	$\nu_{vac.}$ (cm.$^{-1}$)	O—C (cm^{-1})	Morgan's wave-number data
9,1	4308.00(1)	23206.1	−2.5	...
7,0	16.70(1)	159.4	−0.1	23158.3(1)
*7,0	22.11(0)	130.4	−0.4	125.1(0)
10,2	32.19(0)	076.5	2.2	071.3(1)
8,1	40.19(2)	034.0	0.7	031.0(2)
*8,1	45.06(0)	008.2	−0.3	005.7(0)
6,0	51.79(2)	22972.6	−1.6	22971.1(3)
*6,0	56.64(1)	947.0	−2.0	946.0(1)
9,2	64.80(1)	904.1	0.1	906.0(1)
*9,2	69.08(0)	881.7	−1.5	882.1(0)
7,1	74.44(2)	853.7	0.7	849.6(3)
*7,1	78.25(1)	833.8	2.3	828.1(1)
5,0	87.85(3)	783.9	0.0	783.4(4)

TABLE I (*contd.*)

v', v''	λ (I.A.)	$\nu_{vac.}$ (cm.$^{-1}$)	O—C (cm.$^{-1}$)	Morgan's wave-number data
$\overset{*}{5,0}$	4392.30(1)	22760.7	−1.8	22760.1(1)
8,2	99.08(1)	725.8	−2.9	727.0(1)
$\overset{*}{8,2}$	4402.56(0)	707.7	−3.3	706.6(0)
6,1	10.38(2)	667.4	−0.3	665.2(2)
$\overset{*}{6,1}$	13.79(1)	649.9	0.2	647.1(1)
9,3	23.50(0)	600.2	−1.2	
4,0	25.89(4)	588.0	−0.6	588.4(8)
$\overset{*}{4,0}$	29.20(2)	571.1	−0.1	571.5(3)
7,2	33.46(1)	549.4	1.0	
5,1	47.71(1)	477.2	−0.2	476.0(2)
8,3	57.70(0)	426.8	0.7	...
3,0	65.26(4)	388.9	0.6	388.1(10)
$\overset{*}{3,0}$	68.12(2)	374.5	−0.6	374.5(4)
6,2	70.38(1)	363.2	0.1	...
4,1	86.90(0)	280.9	−1.2	...
7,3	94.14(0)	245.0	−0.8	...
2,0	4506.72(5)	182.9	−0.1	182.8(7)
$\overset{*}{2,0}$	$\overset{*}{08}$.44(2)	174.4	0.1	176.7(2)
5,2			1.6	
3,1	27.35(1)	081.8	0.0	081.7(1)
$\overset{*}{3,1}$	28.77(0)	074.9	−0.9	071.4(0)
6,3	31.72(1)	060.5	0.0	...
1,0	49.92(4)	21972.3	−0.4	21972.3(5)
2,1	69.91(6)	876.2	−0.3	876.4(10)
3,2	90.68(0)	877.2	0.0	...
0,0	95.06(1)	756.4	−1.0	756.2(1)
$\overset{*}{1,1}$	4613.43(3)	669.8	0.4	670.4(3)
1,1	14.38(8)	665.3	−0.9	666.0(10)
$\overset{*}{2,2}$	33.20(1)	577.3	−0.1	576.2(0)

TABLE I (*contd.*)

v', v''	λ (I.A.)	$\nu_{vac.}$ (cm.$^{-1}$)	O—C (cm.$^{-1}$)	Morgan's wave-number data
2,2	4634.30(2)	21572.2	0.3	21572.1(0)
3,3	55.25(1)	475.1	0.4	475.4(4)
$0,\overset{*}{1}$	58.64(1)	459.5	0.5	459.5(2)
0,1	60.35(3)	451.6	0.7	450.8(5)
$1,\overset{*}{2}$	77.83(2)	371.6	−0.3	372.1(3)
1,2	80.07(4)	361.2	−0.4	361.5(7)
$2,\overset{*}{3}$	97.95(0)	279.9	−1.9	...
2,3	4700.40(1)	268.9	−0.4	...
$0,\overset{*}{2}$	24.40(1)	160.8	−0.7	162.2(3)
0,2	27.62(4)	146.1	0.1	146.7(8)
$1,\overset{*}{3}$	43.58(1)	075.2	−1.0	074.6(1)
1,3	47.51(2)	057.8	−1.6	058.3(2)
$2,\overset{*}{4}$	62.67(1)	990.8	2.9	...
2,4	67.80(2)	968.2	−0.4	20969.8(1)
$3,\overset{*}{5}$	4783.69(0)	898.5	1.8	...
3,5	88.50(1)	877.5	2.4	...
$0,\overset{*}{3}$	91.22(2)	865.7	−0.1	866.0(3)
0,3	96.34(5)	843.4	0.0	843.9(9)
4,6	4810.81(0)	780.7	2.2	...
1,4	16.30(1)	757.0	−1.3	...
$2,\overset{*}{5}$	30.57(1)	695.7	−0.2	...
2,5	36.62(2)	669.8	0.0	669.6(1)
$3,\overset{*}{6}$	51.62(0)	606.0	−0.7	...
3,6	58.25(1)	577.8	−0.4	578.3(0)
$0,\overset{*}{4}$	59.58(3)	572.2	0.2	572.2(3)
0,4	66.42(6)	543.2	0.2	543.1(7)
$4,\overset{*}{7}$	73.26(0)	514.4	0.1	...
$1,\overset{*}{5}$	79.00(1)	490.3	0.0	...
4,7	80.63(1)	483.5	0.0	...

TABLE I (*contd.*)

v', v''	λ (I.A.)	$\nu_{vac.}$ (cm.$^{-1}$)	O—C (cm.$^{-1}$)	Morgan's wave-number data
1,5	4886.35(3)	20459.5	0.0	...
5,8*	96.02(0)	419.1	0.0	...
2,6*	99.53(0)	404.4	−1.4	...
5,8	4903.98(0)	385.9	0.1	...
2,6	07.20(2)	372.5	−0.4	...
3,7*	20.46(0)	317.6	−0.7	...
3,7	28.74(1)	283.5	0.3	20284.3(0)
0,5*	29.70(3)	279.6	−0.4	280.6(3)
0,5	38.40(5)	243.8	0.6	244.5(6)
1,6*	49.10(1)	200.1	−0.1	...
4,8	51.65(1)	189.7	−0.8	190.0(1)
1,6	58.18(3)	163.1	0.5	163.5(2)
5,9*	64.67(0)	136.7	2.2	...
2,7*	69.60(0)	116.7	−0.7	...
5,9	4974.63(1)	096.4	1.7	095.0(1)
2,7	79.58(1)	076.4	−1.5	...
3,8*	90.95(0)	030.7	−1.1	...
3,8	5000.76(2)	19991.4	1.2	19991.1(1)
0,6*			1.6	
0,6	11.64(4)	948.0	0.7	948.2(4)
1,7*	20.72(2)	911.9	0.0	911.2(1)
4,9	23.85(0)	899.5	0.1	898.0(0)
1,7	32.07(3)	867.0	−0.6	868.3(3)
2,8*	41.25(1)	830.8	−0.1	...
5,10	47.68(0)	805.6	0.1	805.0(1)
2,8	52.96(2)	784.9	0.0	785.0(0)
0,7*	74.29(1)	701.7	0.2	702.2(1)
3,9			2.6	
4,10*	84.39(0)	662.6	2.2	...

TABLE I (*contd.*)

v', v''	λ (I.A.)	$\nu_{vac.}$ (cm.$^{-1}$)	O—C (cm^{-1})	Morgan's wave-number data
0,7	5087.12(3)	19652.0	−0.3	19653.5(2)
$1,\overset{*}{8}$	93.64(2)	626.9	1.5	...
4,10	97.92(1)	610.4	0.2	...
1,8	510 .38(5)	574.1	−0.5	575.0(2)
$2,\overset{*}{9}$	14.53(1)	546.7	0.4	548.0(1)
5,11	21.82(0)	518.9	0.7	...
2,9	28.37(3)	494.0	0.2	494.0(2)
$3,\overset{*}{10}$	36.00(0)	465.0	0.7	...
3,10	50.58(2)	409.9	0.0	410.0(2)
0,8	64.23(1)	358.6	−0.7	360.0(1)
$1,\overset{*}{9}$	69.40(1)	339.2	−1.5	...
4,11	73.78(1)	322.9	0.0	322.0(0)
1,9	84.15(2)	284.2	0.7	284.0(2)
$2,\overset{*}{10}$	5189.59(1)	264.0	0.5	262.0(1)
2,10	5205.72(4)	204.3	−0.3	204.0(2)
$3,\overset{*}{11}$	11.77(1)	182.0	−1.4	...
3,11	27.80(3)	123.2	0.6	124.0(0)
4,12	51.32(2)	037.5	0.0	037.0(1)
1,10	63.36(1)	18994.0	−0.3	18994.0(1)
$2,\overset{*}{11}$	66.56(1)	982.4	−0.2	...
5,13	75.96(1)	948.6	−0.8	947.0(1)
2,11	84.85(2)	916.8	−0.5	917.0(1)
$3,\overset{*}{12}$	88.33(1)	904.3	0.0	...
6,14	5301.40(0)	857.7	−0.1	...
3,12	07.20(3)	837.1	−0.1	837.0(1)
$4,\overset{*}{13}$	11.40(1)	822.2	−0.8	...
4,13	30.69(3)	754.1	0.0	754.0(0)
$2,\overset{*}{12}$	45.14(0)	703.4	0.0	...
51,4	55.23(2)	668.2	0.4	...

TABLE I (*contd.*)

v', v''	λ (I.A.)	$\nu_{vac.}$ (cm.$^{-1}$)	O—C (cm.$^{-1}$)	Morgan's wave-number data
2,12	5365.41(1)	18632.7	0.8	...
6,15	81.22(1)	578.0	−0.5	...
3,13	88.34(2)	553.4	−0.4	18552.0(0)
4,14	5411.80(2)	473.0	0.4	...
5,15	36.70(3)	388.4	0.1	...
* 3,14	47.92(0)	350.5	−1.0	...
6,16	63.00(2)	299.9	−1.0	...
3,14	71.20(1)	272.5	0.2	...
7,17	90.20(1)	209.2	−1.2	...
4,15	94.90(2)	193.7	0.7	...
5,16	5520.10(2)	110.6	0.0	...
6,17	46.38(2)	024.8	−0.3	...
7,18	74.18(2)	17934.9	−1.7	...
4,16	5580.06(1)	916.0	−0.7	...
5,17	5605.47(2)	834.8	0.0	...
6,18	32.55(2)	749.0	−2.3	...
7,19	60.52(1)	661.3	−3.4	...

THE MORE REFRANGIBLE BAND SYSTEM

The bands of this system have been for the first time investigated in detail by Morgan[1] in absorption. He has measured and analysed about one hundred band heads in the region λ3600-λ4000. Previously Eder and Valenta[2] had recorded only the approximate measurements of a group of five line-like heads in the neighbourhood of λ3900 in the flame spectrum of a bismuth compound. This group represents the sequence, $\Delta v = 0$. Morgan has also identified the isotopic heads due to $BiCl^{35}$ and $BiCl^{37}$, thereby confirming the identity of their emitter beyond any doubt.

In the present investigation, a few new bands due to the less abundant molecule $BiCl^{37}$ have been measured at the longer wave-length side of this band system. On the other hand, the band heads, which Morgan recorded on the shorter wave-length side of λ3654, could not be detected on the plates taken by the present author.

When the bands are arranged in a Deslandres scheme, it is found that while the interval between the successive vibrational levels in the lower state decreases practically at a constant rate, that in the upper state does not. This shows that a third power term in $(v'+\frac{1}{2})$ is necessary to represent the vibrational levels in the upper state. Hence the equations of Morgan have been modified to represent the observed data of band heads for this system. These equations are as follows :

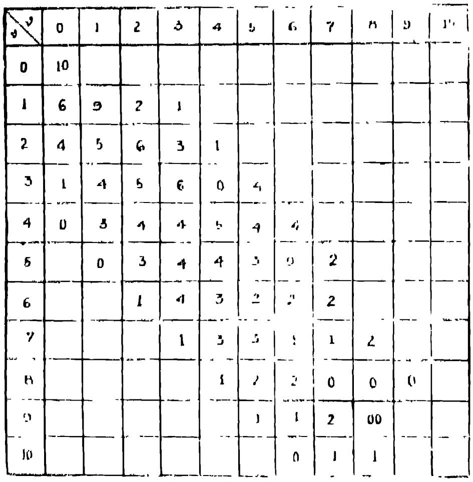

v' / v''	0	1	2	3	4	5	6	7	8	9	10
0	10										
1	6	9	2	1							
2	4	5	6	3	1						
3	1	4	5	6	0	4					
4	0	3	4	4	5	4	4				
5		0	3	4	4	3	0	2			
6			1	4	3	2	2	2			
7				1	3	3	1	1	2		
8					1	2	2	0	0	0	
9						1	1	2	00		
10							0	1	1		

FIG. 3

$$\text{BiCl}^{35}: \quad \nu = 25492{\cdot}7 + \{403.50(v'+\tfrac{1}{2}) - 3{\cdot}768(v'+\tfrac{1}{2})^2 + 0.0016(v'+\tfrac{1}{2})^3\}$$
$$- \{307.66(v''+\tfrac{1}{2}) - 0.954(v''+\tfrac{1}{2})^2\}$$

$$\text{BiCl}^{37}: \quad \nu = 25492.7 + \{394.02(v'+\tfrac{1}{2}) - 3{\cdot}593(v'+\tfrac{1}{2})^2 + 0.0015(v'+\tfrac{1}{2})^3\}$$
$$- \{300.45(v''+\tfrac{1}{2}) - 0.910(v''+\tfrac{1}{2})^2\}.$$

The band head data for the complete system are given in Table II and are arranged in a way similar to that in Table I for the less refrangible system. It will be seen that the O-C values are in most cases within the limits of experimental error.

The intensities of the band heads for this system have been estimated on a 0 to 10 scale. As in the case of the less refrangible system, there is a divergence of the intensity data of Morgan from those given here. The intensity distribution is similar to that obtained by Morgan for the more refrangible band system of BiBr and lies on a well-defined narrow Condon parabola.

TABLE II

Band head data of the more refrangible system

v', v''	λ (I.A.)	$\nu_{vac.}$ (cm.$^{-1}$)	O−C (cm.$^{-1}$)	Morgan's wave-number data
10, 6	3654.28 (0)	27357.4	1.1	27358.0 (1)
9, 5	58.56 (1)	325.4	1.4	325.4 (2)
9, $\overset{*}{5}$	63.53 (0)	288.3	0.0	288.3 (0)
8, 4	63.83 (1)	286.1	0.1	285.7 (1)
8, $\overset{*}{4}$	68.89 (0)	248.5	−1.4	248.3 (0)
7, 3	69.63 (1)	243.0	0.5	240.8 (1)
7, $\overset{*}{3}$	74.65 (0)	205.8	−0.3	203.8 (0)
6, 2	76.43 (1)	192.6	−0.9	191.6 (1)
6, $\overset{*}{2}$	81.41 (0)	155.8	−1.3	154.4 (0)
5, 1	83.85 (0)	137.8	−1.0	137.3 (1)
5, $\overset{*}{1}$	88.72 (00)	102.0	−0.8	100.7 (00)
4, 0	92.03 (0)	077.7	−1.0	077.7 (00)
10, 7	94.18 (1)	061.9	−0.1	063.2 (1)
10, $\overset{*}{7}$	98.00 (0)	034.0	−0.1	034.0 (0)
9, 6	98.82 (1)	028.0	0.3	028.7 (2)
9, $\overset{*}{6}$	3702.86 (0)	26998.5	−0.4	26998.5 (1)
8, 5	04.43 (2)	987.4	−0.5	987.2 (2)
8, $\overset{*}{5}$	08.28 (1)	959.0	0.4	956.7 (1)
7, 4	10.58 (3)	942.3	−0.2	940.6 (2)
7, $\overset{*}{4}$	14.93 (1)	910.8	−2.2	910.3 (1)
6, 3	17.62 (4)	891.3	−0.2	889.2 (2)
6, $\overset{*}{3}$	21.95 (1)	860.0	−2.2	859.2 (1)
5, 2	25.43 (3)	834.9	−0.1	833.1 (2)
5, $\overset{*}{2}$	29.58 (1)	805.1	−0.9	803.6 (1)
4, 1	33.98 (3)	773.5	0.6	772.1 (2)
10, 8	34.46 (0)	770.0	0.4	770.5 (1)
10, $\overset{*}{8}$	37.58 (0)	747.7	−0.6	747.5 (0)
4, $\overset{*}{1}$	37.99 (0)	744.8	0.2	743.3 (1)

TABLE II (*contd.*)

v', v''	λ (I.A.)	$\nu_{vac.}$ (cm.$^{-1}$)	O−C (cm.$^{-1}$)	Morgan's wave-number data
9, 7	3739.54 (2)	26733.7	0.3	26733.8 (2)
9, $\overset{*}{7}$	42.77 (0)	710.6	−0.8	710.4 (1)
3, 0	43.57 (1)	704.9	−0.4	705.9 (2)
8, 6	45.49 (2)	691.2	−0.4	690.7 (3)
3, $\overset{*}{0}$	47.35 (0)	678.0	0.2	678.0 (0)
8, $\overset{*}{6}$	48.72 (1)	668.2	−0.4	666.8 (1)
7, 5	52.10 (3)	644.2	−0.2	642.1 (3)
7, $\overset{*}{5}$	55.54 (1)	619.8	−1.9	618.4 (1)
6, 4	59.61 (3)	591.0	−0.5	588.7 (3)
6, $\overset{*}{4}$	62.97 (1)	567.2	−1.9	565.6 (1)
5, 3	67.85 (4)	532.8	−0.2	530.9 (4)
5, $\overset{*}{3}$	71.14 (2)	509.7	−1.4	508.3 (2)
4, 2	76.96 (4)	468.8	−0.3	467.9 (4)
4, $\overset{*}{2}$	80.10 (2)	446.8	−1.0	446.2 (1)
9, 8	81.00 (00)	440.5	−0.5	441.5 (00)
3, 1	86.85 (4)	399.7	0.2	399.7 (3)
8, 7	87.28 (0)	396.7	−0.6	396.6 (0)
3, $\overset{*}{1}$	89.84 (2)	378.9	−0.3	379.0 (2)
7, 6	94.38 (1)	347.3	−0.8	345.7 (2)
7, $\overset{*}{6}$	96.80 (0)	330.5	−1.8	328.9 (1)
2, 0	97.54 (4)	325.4	1.1	325.7 (4)
2, $\overset{*}{0}$	3800.34 (1)	306.0	0.7	306.3 (2)
6, 5	02.42 (2)	291.6	−1.8	290.5 (3)
6, $\overset{*}{5}$	04.74 (0)	275.6	−2.2	274.2 (1)
5, 4	11.09 (4)	231.8	−1.2	230.7 (3)
5, $\overset{*}{4}$	13.45 (1)	215.6	−2.4	215.0 (2)
4, 3	20.56 (4)	166.8	−0.3	166.0 (4)
4, $\overset{*}{3}$	22.78 (3)	152.6	−0.3	151.2 (2)
8, 8	29.78 (0)	103.8	−1.1	103.8 (1)
3, 2	30.92 (5)	096.0	0.3	096.0 (5)

TABLE II (*contd.*)

v', v''	λ (I.A.)	$\nu_{vac.}$ (cm.$^{-1}$)	O − C (cm.$^{-1}$)	Morgan's wave-number data
3, 2*	3832.95 (3)	26082.2	−0.2	26082.2 (2)
7, 7	37.05 (1)	054.3	0.5	051.5 (3)
7, 7*	38.85 (0)	042.1	−2.7	041.1 (1)
2, 1	42.10 (5)	020.0	1.5	020.0 (5)
2, 1*	44.00 (3)	007.2	0.5	007.6 (2)
6, 6	45.53 (2)	25996.9	−0.2	25993.8 (1)
6, 6*	47.08 (0)	986.4	−2.0	984.1 (0)
1, 0	54.41 (6)	937.0	1.1	937.0 (6)
5, 5	54.90 (3)	933.7	−1.2	932.4 (2)
1, 0*	56.01 (3)	926.2	0.5	926.2 (3)
4, 4	65.00 (5)	865.9	−1.2	865.8 (6)
4, 4*	66.03 (4)	859.0	−0.8	858.0 (3)
8, 9	72.89 (0)	813.2	−1.1	812.9 (0)
8, 9*	73.25 (2)	810.8	−1.2	808.4 (0)
3, 3	75.77 (6)	794.0	0.3	794.0 (7)
3, 3*	76.80 (5)	787.2	−0.3	787.2 (4)
7, 8	80.86 (2)	760.2	−1.2	759.1 (0)
7, 8*	81.31 (0)	757.2	−1.8	755.4 (0)
2, 2	87.53 (6)	716.0	1.3	716.4 (8)
2, 2*	88.38 (7)	710.4	0.5	710.9 (4)
6, 7	89.54 (2)	702.7	−0.1	702.7 (1)
6, 7*	89.92 (1)	700.2	−0.7	700.2 (1)
5, 6	99.36 (0)	638.0	−0.6	636.6 (0)
1, 1	3900.27 (9)	632.0	1.9	632.0 (2)
1, 1*	00.96 (2)	627.5	0.4	628.1 (4)
4, 5	09.94 (4)	568.6	−0.4	568.5 (1)
0, 0	14.26 (10)	540.4	−0.5	539.9 (10)
3, 4	21.38 (0)	494.0	0.3	494.9 (0)
2, 3*	33.57 (0)	415.0	0.0	417.2 (0)
2, 3	34.01 (3)	412.2	−0.5	415.7 (1)

TABLE II (*contd.*)

v', v''	λ (I.A.)	$\nu_{vac.}$ (cm.$^{-1}$)	O−C (cm.$^{-1}$)	Morgan's wave-number data
5, 7*	3943·75 (0)	25349·4	−0.4	—
5, 7	44·53 (2)	344·4	0.1	25344·4 (0)
1, 2	47.08 (2)	328.0	1.7	328.6 (0)
4, 6*	54·58 (0)	280.0	0.9	—
4, 6	55.64 (4)	273.2	0.5	273.8 (0)
3, 5*	66.57 (0)	203.6	0.5	—
3, 5	67.61 (4)	197.0	1.4	197.5 (0)
2, 4*	79.26 (0)	123.2	1.3	—
2, 4	80.85 (1)	113.2	0.5	113.5 (0)
1, 3*	93.18 (1)	035.6	0.2	—
1, 3	94.96 (1)	024.5	0.2	024.9 (0)

ACKNOWLEDGEMENT

The author begs to acknowledge his best thanks to Prof. P. N. Ghosh for giving all facilities to carry out the investigation and to Dr. P. C. Mahanti for helpful discussions and guidance. The author also wishes to express his appreciation to Mr. D. C. Ray for placing at his disposal some of the plates and measurements which the latter had previously taken.

SPECTROSCOPIC LABORATORIES,
APPLIED PHYSICS DEPARTMENT

REFERENCES

[1] Morgan, *Phys. Rev.*, **49**, 41 (1936).
[2] Eder and Valenta, *Atlas Typischer Spektren* (1928).
[3] Mecke and Guillery, *Physik Zeits.*, **28**, 514 (1927).
[4] Saper, *Phys. Rev.*, **37**, 1710A (1931).
[5] Ghosh, *Zeits. f. Physik.*, **86**, 241 (1933).

THE VELOCITY GRADIENT METHOD FOR THE MEASUREMENT OF VISCOUS PROPERTIES OF NON-NEWTONIAN LIQUIDS*

By J. N MUKHERJEE

AND

N. C. SEN GUPTA

(Received for publication, September 1, 1941)

ABSTRACT A method has been described which admits of a direct measurement of velocities at different depths in a flowing liquid. The liquid is contained in a rectangular cell of depth of the order of 1 mm. and the velocities measured with a microscope using an objective with a large working distance. Velocity distribution curves have been obtained with a sugar solution, two gelatin sols and a bentonite suspension. The advantages of the method are discussed.

A large number of liquids, especially concentrated colloids, do not obey Newton's linear relation between shearing stress and rate of shear. They are designated as non-Newtonian liquids. A systematic study of the viscous properties of such liquids has both theoretical and practical interest. The earlier work of Hess,[1] Hatschek,[2] Bingham,[3] Ostwald[4] and others has been considerably extended in recent years[5,6,7,8] and several accounts are available.[9] Newton's equation for viscous fluids is :

$$dv/dz = F/\eta \qquad \dots \quad (1)$$

where dv/dz is the rate of shear (velocity gradient) in cm./sec./cm., F the shearing stress in dynes/sq. cm. and η the coefficient of viscosity in dynes.sec./sq. cm.

Ostwald[4] assumed that in colloids like gelatin sols a structure exists in the undisturbed sol which is progressively broken down as the rate of shear is increased so that the apparent fluidity (reciprocal of viscosity) of the system gradually rises.

Ostwald's relation is :

$$dv/dz = F^n/\eta' \qquad \dots \quad (2)$$

where n is a constant greater than unity and has been called the "coefficient of structure " and η' is a constant whose dimensions are different from that of η the coefficient of viscosity.

---

* Communicated by the Indian Physical Society.

According to Bingham[8] a minimum shearing stress is necessary to start flow in " plastic " systems beyond which the rate of shear is proportional to the shearing stress. Bingham proposed for them an equation of the form :

$$dv/dz = (F - f)/\eta. \qquad (3)$$

He called, *f*, the yield value[9] of the system.

Many examples of both ' structure-viscous ' and ' plastic ' systems have been found in the literature while some show intermediate behaviour.[9]

In viscometric measurements, especially by the capillary method, the rate of shear varies from layer to layer over wide limits. While this variation can be easily taken into account in Newtonian liquids where the coefficient η is constant and has a definite significance, it is not easy to do so in the case of non-Newtonian liquids where the values given by different viscometers of such quantities as the yield value, apparent viscosity or mobility depend on the method and also on the dimensions of the apparatus where the same method is used. It is obviously desirable to measure the rate of shear (velocity gradient) at different layers in the viscometer. Pichot[10] and Philippoff[11] have described methods which permit observations of the velocity gradient, but these methods do not give the velocity gradient in absolute units. Kroepelin[12] uses a pitot tube for this purpose but his method is applicable for rather high rates of shear whereas measurements at low rates of shear are of especial interest, *e.g.*, in distinguishing between equations (2) and (3). His method also involves the use of fairly wide tubes which may complicate the conditions of flow. A flat cell of the type used in the microscopic measurement of cataphoretic velocities of colloids is a convenient form of apparatus which has been used by us at low rates of shear.

The flat cell used had the following dimensions : length—8.0 cm., breadth—1.0 cm., height—0.0644 cm.

For Newtonian liquids in a rectangular flat cell,

$$dv/dz = -\pi z/\eta \qquad (4)$$

where π is the pressure gradient (negative in this case) and z the distance from the central plane.

From equations (2) and (3) we have for non-Newtonian liquids respectively :

$$dv/dz = -\pi^n z^n/\eta' \qquad (5)$$

and

$$dv/dz = -\pi(z - z_0)/\eta \qquad (6)$$

z_0 is the distance along the normal to the direction of flow measured from the central plane, up to which the fluid flows as a solid plug,[9] $-\pi z_0$ gives a measure of, and is equal to, the lower yield value.[9]

Measurements have been made on the following systems :

(*a*) a saturated sugar solution (67%),

(*b*) two gelatin sols, and

(*c*) a hydrogen bentonite suspension.†

Finely powdered pure sugar charcoal was suspended and the speeds of the particles at different depths were measured.

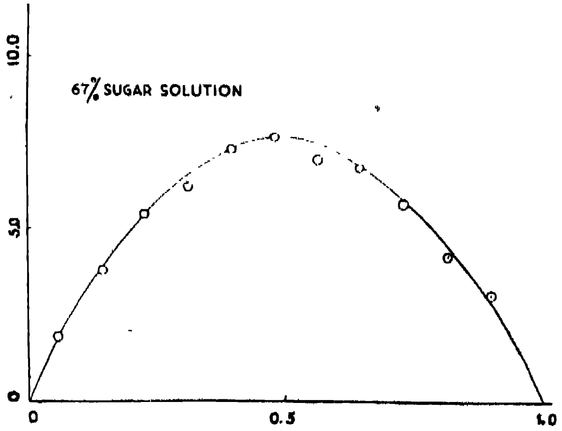

FIG. 1

(*a*) As is to be expected, the sugar solution (Fig. 1) gives a perfect parabolic distribution of velocities which is characteristic of Newtonian liquids. The pressure gradient was, however, very small and in the present form of the

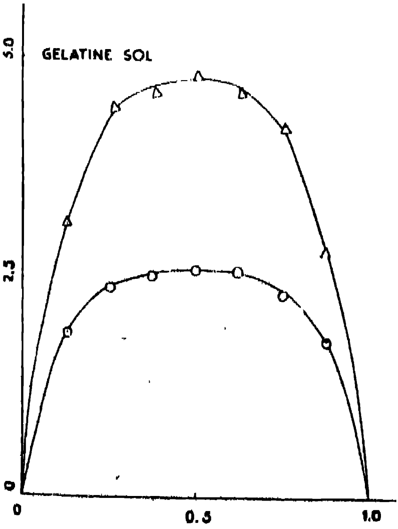

FIG. 2

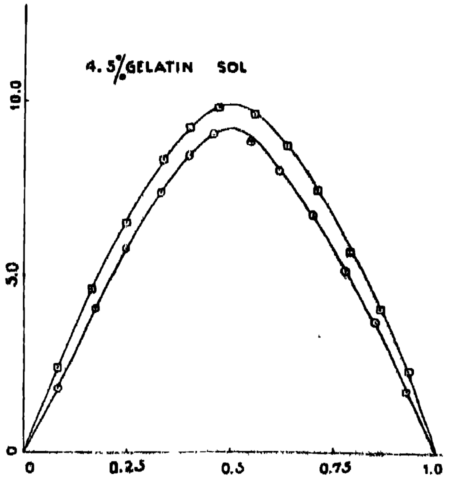

FIG. 3

---

† A very fine suspension of a bentonite, obtained by means of a Sharples supercentrifuge, was electrodialysed to give the hydrogen bentonite. The methods of preparation and other experimental details will be described elsewhere.

apparatus could not be measured very accurately. The coefficient of viscosity obtained from the approximate pressure gradient is about 2 poise. The viscosity of the same solution measured by means of a rotary viscometer is 1.7 poise which agrees with the value given in International Critical Tables.[13]

(*b*) The velocity distribution in concentrated gelatin sols gives curves of a higher degree than the parabola. The value of '*n*' in equation (5) calculated from the curves in Fig. 2 is about 2.8. Curves given in Fig. 3 are however parabolic in nature, and the behaviour of gelatin sols depends on concentration and other factors.

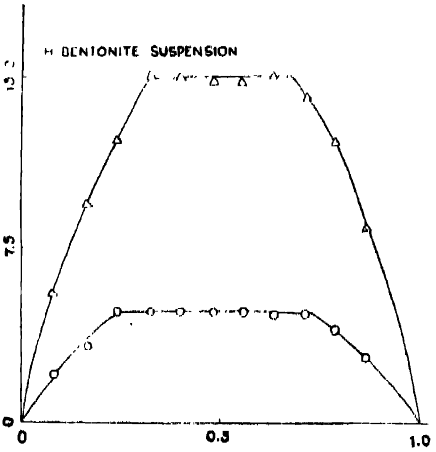

FIG. 4

(*c*) The bentonite suspension (Fig. 4, curves i and ii) shows a parabolic distribution of velocities with a central flat region whose depth diminishes with increase in the pressure gradient. z_0 is evidently equal to half the depth of the flat region. The yield values calculated from the two curves are 27 and 30 dynes/sq.cm. respectively. The yield value of the same suspension obtained by means of a capillary viscometer is 86 dynes/sq.cm. which is more than three times the value obtained from Fig. 4 while a rotary viscometer gives values nearly equal to those obtained by the flat cell.

It is evident that the method described here gives curves which are significantly characteristic of the variation of the velocity gradient with shearing stress. These curves are capable of yielding on mathematical analysis very useful information not obtainable by the usual viscometric methods. The apparatus is being modified for more accurate measurements at low rates of shear and at constant temperature.

PHYSICAL CHEMISTRY LABORATORY,
UNIVERSITY COLLEGE OF SCIENCE
& TECHNOLOGY,
92, UPPER CIRCULAR ROAD,
CALCUTTA.

REFERENCES

[1] Hess, see for references *Kolloid-Z.*, **27**, 154 (1920).

[2] See Hatschek, " The Viscosity of Liquids," *Bell and Sons* (1928).

[3] See Bingham, " Fluidity and Plasticity," *McGraw-Hill Co.* (1922).

[4] Ostwald, *Kolloid-Z.*, **36**, 99, 157, 248 (1925); and a series of papers afterwards; see also de Waale, *J. Amer. Chem. Soc.*

[5] Buckingham, *J. Amer. Soc. Test Mats.*, **21** (*II*), 1154 (1921).

[6] Scott Blair and Crowther, *J. Phys. Chem.*, **33**, 321 (1929); Schofield and Scott Blair, *J. Phys. Chem.*, **34**, 248, 1505 (1930); **35**, 1212 (1931); **39**, 973 (1935); Schofield, *Physics*, **4**, 122 (1933).

[7] Reiner, *Kolloid-Z.*, **39**, 80 (1926); Reiner and Riwilin, *Kolloid-Z.*, **43**, 1 (1927); Reiner and Reiner, *Kolloid-Z.*, **65**, 44 (1933); Reiner, *Physics*, **5**, 321, 342 (1934).

[8] Philippoff, *Physik. Zeit.*, **22**, 884, 900 (1934); *Kolloid-Z.*, **71**, 1 (1935); **75**, 142, 155 (1936); **83**, 163 (1938).

[9] First Report on Viscosity and Plasticity, *Academy of Sciences, Amsterdam* (1935); Second Report on Viscosity and Plasticity, *Academy of Sciences, Amsterdam* (1938); Evans and Reid, *Drilling Mud*; Its Manufacture and Testing, *Trans. Min. Geol. Inst. India*, **32** (1936); Houwink, Elasticity, Plasticity and Structure of Matter, *Cambridge* (1937); Scott Blair, Introduction to Industrial Rheology, *Churchill* (1938); Goodeve, The Viscosity of non-Newtonian Liquids, *Reports on Progress of Physics*, **5**, 20 (1938).

[10] Pichot, *Physics*, **5**, 200 (1934).

[11] Philippoff, *Kolloid-Z.*, **83**, 163 (1938).

[12] Kroepelin, *Z. Physik. Chem.*, **149**, 291 (1930).

[13] *Int. Crit. Tables*, **V**, 23 (1929).

METHODS OF MEASURING YIELD VALUE, VISCOSITY AND THIXOTROPY*

By J. N. MUKHERJEE, N. C. SEN GUPTA

AND

K. C. SEN

(Received for publication, September 1, 1941)

ABSTRACT. The capillary and the rotary viscometer do not give the same Bingham yield value and viscosity for bentonite suspensions. A direct method using a rectangular flat cell for measuring the velocity gradient along the normal during flow has been developed which is expected to give yield value and viscosity in absolute units. Values obtained by the velocity gradient method are more in accord with those obtained by the rotary viscometer than those obtained by the capillary viscometer. Variations in both the lower yield value and the apparent viscosity of thixotropic suspensions with time have been observed. Compared with the apparent viscosity the lower yield value appears to give a better measure of the rate of thixotropic gelation.

Bentonite is a typical colloid system which shows most of the known anomalous viscous properties depending on the colloid content and on the p_H of the system.[1] Dilute suspensions of bentonite obey Newton's equation for viscosity. Beyond a certain concentration, which depends on the nature of the suspension, yield value appears and the suspensions cease to behave as Newtonian liquids. Thixotropy appears at a somewhat higher concentration. The purpose of the present investigation has been to evolve a suitable method for the measurement of properties such as yield value, viscosity and thixotropy in absolute units.

A large number of liquids especially concentrated colloids possess a variable viscosity[2] which changes in a complicated manner with the rate of shear or the shearing stress. The pioneering investigations on non-Newtonian liquids of Hess,[3] Hatschek,[4] Bingham,[5] Ostwald[6] and others have recently been extended by a large number of workers.[7] A new type of non-Newtonian behaviour namely thixotropy was discovered by Miss Schalek and Szegvari[8] in 1923. In thixotropic systems the coefficient of viscosity besides being a function of the rate of shear is also a function of time.

---

* Communicated by the Indian Physical Society. Figs. 5, 6 and 7 have been taken from the previous paper by the same authors.

A mathematical expression for the flow of liquids possessing yield value was first developed by Bingham[5] in the following form .

$$\frac{dv}{dz}=\mu(F-f) \qquad (1)$$

where dv/dz is the rate of shear, F the shearing stress, f the yield value and μ the coefficient of mobility, its inverse being called the coefficient of true viscosity η. The relation is obeyed[9] by bentonite suspensions excepting at very low rates of shear.

The form of a complete consistency curve obtained with bentonite suspensions is shown in figure 1. The intercepts f_l, f_B and f_m on the shearing stress axis are respectively the lower yield value, the Bingham yield value and the maximum yield value. The lower yield value is the minimum shearing stress at which the flow of a suspension begins in a viscometer. The Bingham yield value, f_B, equals the intercept on the shearing stress axis made by the straight portion of the consistency curve on extrapolation. The maximum yield value is the shearing stress above which the consistency curve becomes straight. At very low rates of shear the curve is convex towards the axis representing shearing stress and this form has been ascribed to plug flow.[10]

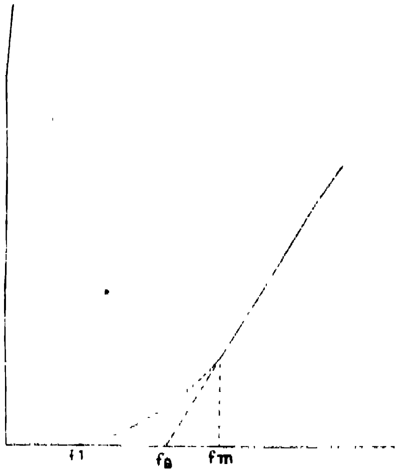

FIG 1

Ostwald[6] assumed that in the case of colloids like gelatin a structure exists in the undisturbed sol which is progressively broken down as the rate of shear is increased, so that the fluidity of the system gradually increases, *i.e.*, the viscosity decreases.

According to Ostwald,[6]

$$dv/dz=F^n/\eta' \qquad \ldots \quad (2)$$

where n is a constant greater than unity and has been called the 'coefficient of structure' and η' is a constant whose dimensions are different from those of η.

Systems possessing a yield value have been called 'plastic' and those which obey Ostwald's relation 'structure-viscous.' Many examples of both structure-viscous and plastic systems will be found in the literature while some systems show more complex behaviour.

In the usual viscometric measurements, especially by the capillary method, the rate of shear varies over a wide limit from zero at the axis to a maximum at the walls and the quantities observed represent a summation of these variations. This makes it often difficult to interpret the results since in the case of non-Newtonian liquids the ratio, shearing stress/rate of shear, is not a constant quantity and it appears that this difficulty has been the source of some controversies.[11] In view of this it is desirable that viscous properties in such systems should be estimated by direct measurements of the velocity gradient.

Complete consistency curves cannot be obtained with thixotropic systems, especially quick-gelling ones. It is, however, possible to measure the variations in apparent viscosity*[12] or lower yield value with time during thixotropic gelation. In order that the results of apparent viscosity measurements can be interpreted it is desirable that the measurements should be made at constant rates of shear. The variation of the lower yield value which gives some measure of the 'gel strength' seems to give a better estimate of the rate of thixotropic gelation.

EXPERIMENTAL

Methods of preparing samples have been described elsewhere.[1] Fine subfractions of bentonites have been obtained by means of a Sharple's supercentrifuge. Hydrogen bentonites have been prepared by electrodialysis.

Consistency curves have been obtained with a capillary viscometer of the Ubbelohde type and a rotary viscometer of the Couette type which was made in

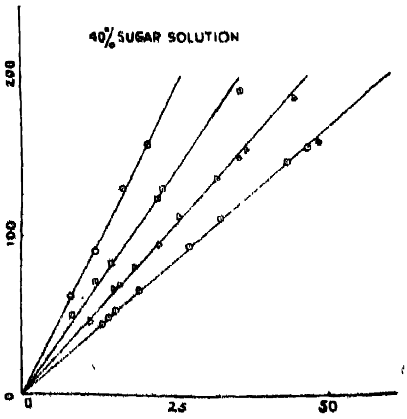

FIG. 2

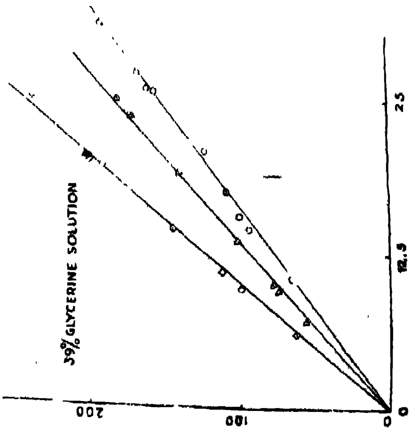

FIG. 3

---

* Apparent viscosity is the ratio of any shearing stress and the corresponding rate of shear.

our workshop and has been described elsewhere.[13] The end correction of the viscometer has been estimated by the method of Searle.[14] Results are given in figures 2, 3 and 4. The viscosity of 40% sugar solution, corrected for end effect, is given in Table I. The corrected value agrees within 2 p.c. with the standard data. No thermostat was used and a better agreement could not be expected.

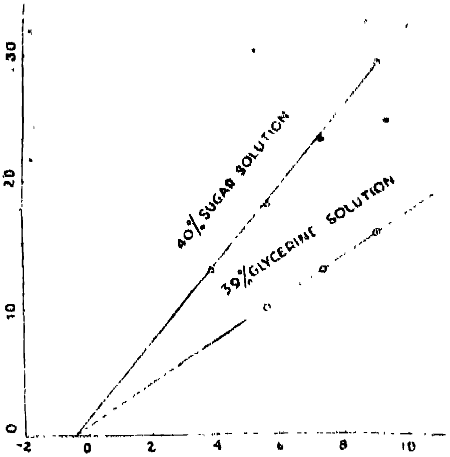

FIG. 4

TABLE I

Length of the inner cylinder dipping into the solution	40% sugar soution η (centipoise)	
	obs.	corr.
3.85 cms.	5·14	4·55
5·6 ,,	4·96	4·55
7·35 ,,	4·85	4·54
9·1 ,,	4·90	4·75
		Mean 4·60 From standard data 4·56*

* Barr, A Monograph on Viscometry, 1931, p. 308

The capillary viscometer has also been calibrated with the 40% sugar solution. Lower yield values of thixotropic suspensions were measured by means of cylinders of different radii and also by a Stormer viscometer.

The procedure used in measuring the velocity gradient during flow has been described elsewhere.[15] A flat cell is used for the purpose.

Velocity gradients have been measured recently by Kroepelin,[16] Pichot[17] and Philippoff[18] for the purpose of studying viscous properties of non-Newtonian liquids. The methods used by Pichot and Philippoff do not give yield values or consistencies in absolute units. Further, as Richardson[19] has pointed out, from the two photographs published by Pichot it is difficult to distinguish between the two types of flow found in water and gelatin. The method of Kroepelin requires that the velocities should be measured at high rates of shear, at which non-Newtonian behaviour in the majority of cases is known to disappear.

In the present investigation velocities at different depths have been measured in absolute units by means of a microscope. Finely ground pure sugar charcoal has been suspended in the systems and the speeds of these particles have been measured by means of a microscope. The following systems have been used for the preliminary measurements : (*a*) a saturated sugar solution, (*b*) a gelatin sol and (*c*) a 2.34% hydrogen bentonite suspension consisting of very fine particles (diameter of particles 0.05—0.025μ).

RESULTS AND DISCUSSIONS

(*a*) *Velocity gradient method*

Results of velocity gradient measurements are given in figures 5, 6 and 7.

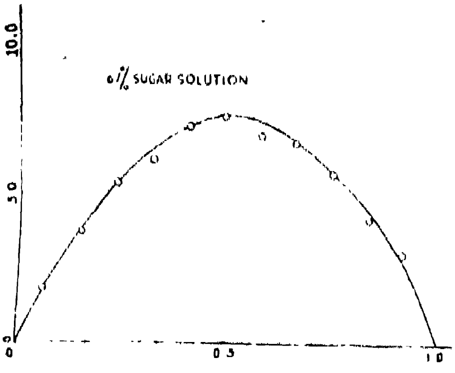

FIG. 5

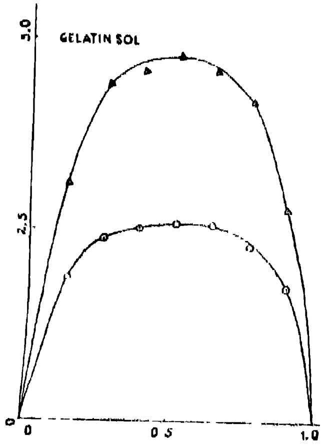

FIG. 6

Figure 5 is a typical parabola. This is expected of Newtonian liquids. The pressure gradient was very small and consequently could not be measured very accurately with the present arrangement. The coefficient of viscosity obtained from the approximate pressure gradient is about 2 poise. The viscosity of the same solution measured by the rotary viscometer is 1.7 poise.

Figure 6 gives curves which are of a higher degree than the parabola. The system appears to follow Ostwald's relation (equation 2) and the value of '*n*' calculated from the two curves is approximately 2.8.

The bentonite suspensions give a parabolic curve of distribution of velocities with depth excepting the central portion which is straight and whose length diminishes at higher rates of shear. The flat portion gives a measure of the yield value of the suspension. The two curves show that the yield values are 27 and 30 dynes/sq.cm. respectively. The yield value of the same suspension obtained by the capillary viscometer is about 88 dynes/sq.cm. or about three times the value obtained by the velocity gradient method.

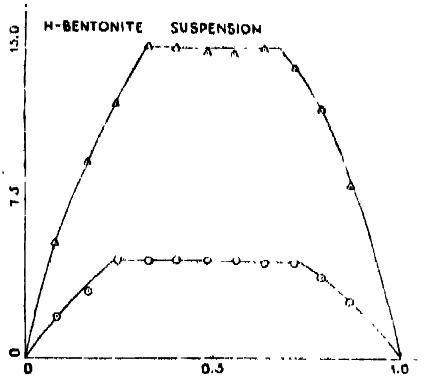

FIG. 7

Further measurements by the velocity gradient method are under way.

(b) Comparative study of the rotary viscometer and the capillary viscometer

Consistency curves of suspensions of natural bentonites No. D_5' at concentrations of 5.0, 4.5, 4.0, 3.5 and 3.0 gms. per 100 c.c. have been obtained by the rotary and the capillary viscometers (figures 8 and 9). The curves obtained by both methods are similar in form. At the lowest concentration studied the

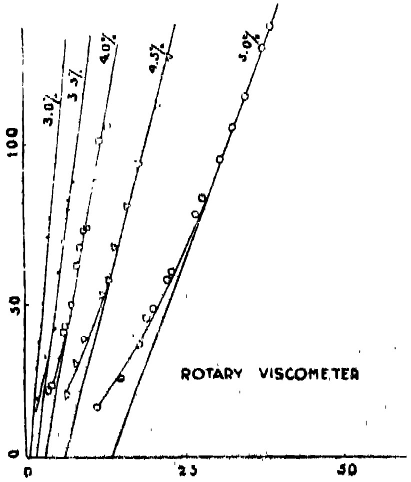

FIG. 8

curves are straight and on extrapolation pass almost through the origin. At higher concentrations the curves have a shape similar to that given in figure 1,

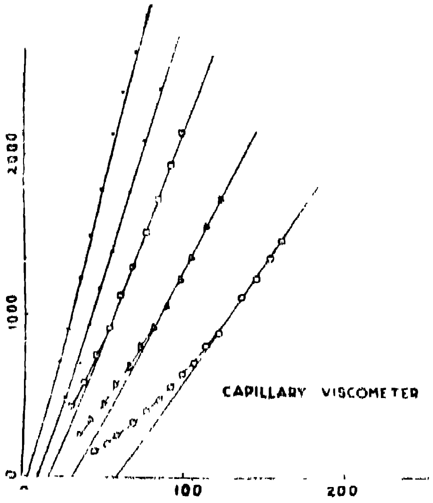

FIG. 9

The yield value and true viscosity obtained by the two methods (Table II) are different.

TABLE II

D_5' (Natural)

Concentration gms. per 100 c.c.	Yield value (dynes/sq cm)		η (centipoise)	
	Rotary	Capillary	Rotary	Capillary
5.0	13.5	58	22.2	9.0
4.5	6.0	30	11.3	6.6
4.0	2.5	16	10.6	4.6
3.5	1.0	8	7.6	3.5
3.0	0.2	1	5.1	2.6

The viscosities obtained by the capillary method are less than half the values obtained by the rotary method. This may be due to the wall effect in the capillary. Schofield and Scott-Blair[20] found that the mobility μ of clay suspensions diminishes with increase in the radius of the capillary. They estimated the true mobility from the consistency curves obtained by using capillaries of different radii. The mobility μ was plotted against $1/r$ where r is the radius of the capillary and the true mobility was noted from the graph by extrapolation to $1/r=0$. In one case μ was found to be about 20 rhe for $r=0.05$ cm. and μ_0 was about half being about 10 rhe. In other words the extrapolated value of the viscosity was approximately double that for $r=0.05$ cm. This observation possibly explains the discrepancy between the true viscosities observed by us when measured by the two methods discussed here.

The yield value obtained by the capillary viscometer is about four to five times as great as that obtained by the rotary viscometer. The reason for this discrepancy is not very clear. The velocity gradient method gives values in better agreement with the rotary viscometer and the latter appears to be preferable for ordinary measurements.

The yield value and the true viscosity obtained by the two methods have been plotted against concentration in figure 10. In spite of the differences in magnitudes, the relative variations of viscosity and yield value given by the two methods are more or less the same and both methods seem to be equally applicable for relative measurements. This is important in practice, especially in respect of drilling mud control.

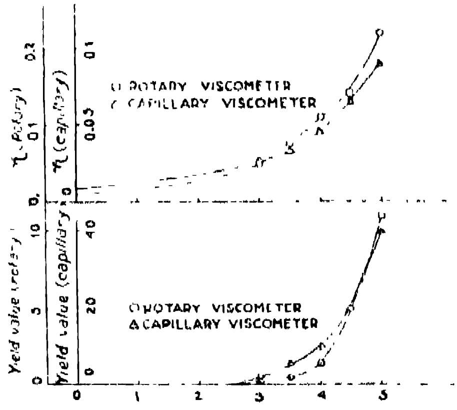

FIG. 10

(c) *Variation of lower yield value of thixotropic suspensions with time*

The wall stress F_w in a cylinder is given by the relation $F_w = g.\rho.r/2$. ... (3)

where ρ is the specific gravity of the suspension, g the acceleration due to gravity and r the radius of the cylinder in cms. It is difficult to measure ρ for quick-gelling systems. Approximate figures are, however, sufficient for present purposes.

If t_1 is the time in seconds required for a suspension to solidify in a cylinder of radius r_1 then the lower yield value at time t_1 is $g.\rho.r_1/2$.

Results are given in figures 11, 12 and 13 and in table III.

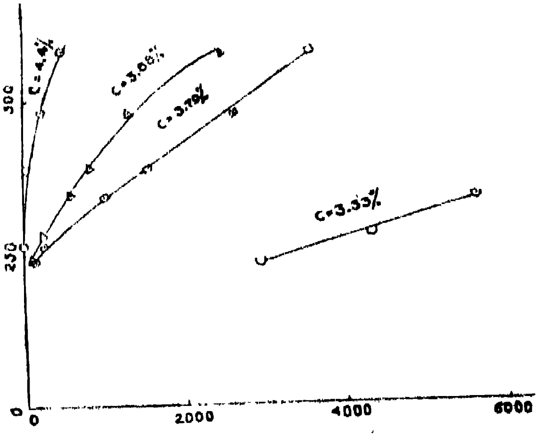

FIG. 11

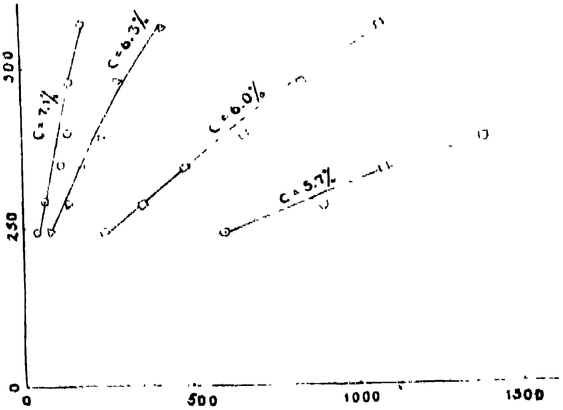

FIG. 12

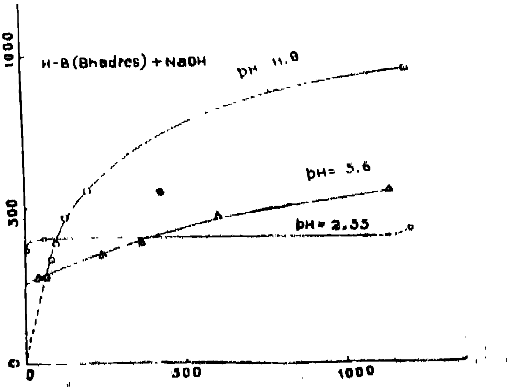

FIG. 13

TABLE III

H-B + NaOH p_H-11.8 Concentration-6.0% Temperature 23-24°C

Radius of the cylinder (cm.)	Time of solidification (seconds)	Yield value (dynes/sq.cm.)
0.48	10	242
0.56	65	283
0.68	80	343
0.77	90	389
0.94	120	474
1.11	195	560
1.83	1200	949

The lower yield value of the fine subfractions of natural bentonites (Figs. 11 and 12) increases almost linearly with time during the period of measurement. Figure 13 shows that hydrogen bentonite possesses a high initial f_t which increases only slowly with time In the case of bentonite treated with excess of caustic soda (p_H 11.8), however, initial f_t is very small but increases rapidly with time towards a constant limiting value. At p_H 5.6 an intermediate behaviour is observed. The suspension possesses a high f_t in the thoroughly stirred condition which also increases rapidly with the period of rest to a constant limiting value. The rate of thixotropic gelation is thus strongly influenced by the p_H, a fact which does not seem to have been observed by previous workers.

TABLE IV

H-B + NaOH p_H-11.8 Temperature 23-24°C

Concentration 6.3%		Concentration 5.3%	
Time of solidification (seconds)	Relative yield value (gms.)	Time of soldification (seconds)	Relative yield value (gms.)
90	39.4	1140	23.1
190	37.2	1440	26.2
300	52.5	1920	29.2
660	63.3	2 ·20	32.6
1560	75.2	5400	35.1
0 (graph)	4.2	0 (graph)	1.0

Variation in f_t with time observed with the Stormer viscometer has been given in table IV. The yield values are not expressed in absolute but in arbitrary units. They are given in grams. Yield values at zero time have been observed from the weight/speed curve measured after shaking the sol thoroughly (Fig. 14).

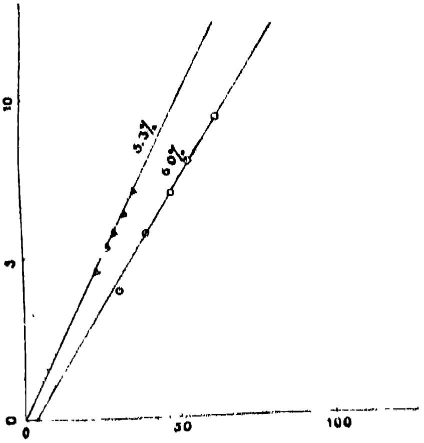

FIG. 14

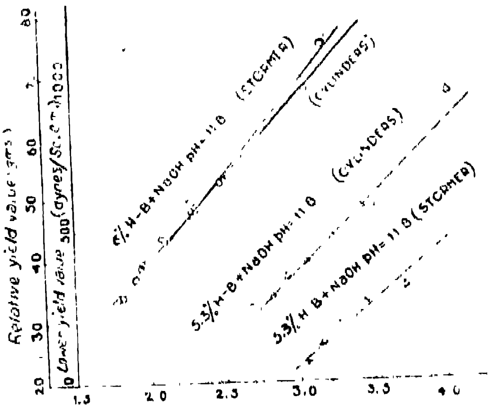

FIG. 15

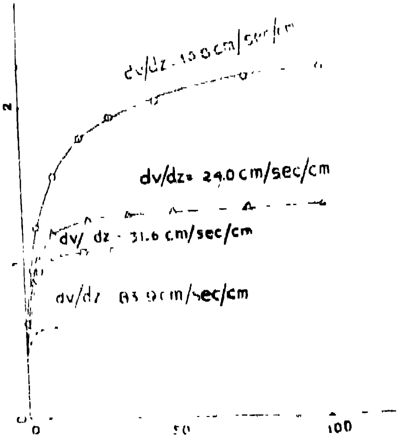

FIG. 16

Values of f_t are plotted against t, in figure 15. Both methods give straight lines within the range of experimental error for mixtures of different concentrations of H-B and NaOH having p_H 11.8.

(*d*) *Variation of the apparent viscosity* η_s *with time*

Variations in η_s of a thixotropic sodium bentonite suspension with time have been measured using the rotary viscometer. The rates of shear were maintained constant in each measurement. The sol was thoroughly stirred prior to each measurement. Results are given in figure 16.

η_A increases with time and finally attains a constant limiting value. This limiting value of η_A depends on the rate of shear. The higher the rate of shear the lower the limiting value of η_A and the more quickly is it reached.

REFERENCES

[1] Mukherjee, Sen Gupta and Indra, paper to be communicated shortly.

[2] Barr, "A Monograph of Viscometry," Oxford University Press, 1931.

[3] Hess, see for reference *Kolloid-Z.*, **27**, 154 (1920).

[4] Hatschek, " The Viscosity of Liquids," Bell and Sons (1928).

[5] Bingham, ' Fluidity and Plasticity." *MacGraw-Hill Co.* (1922).

[6] Ostwald, *Kolloid-Z.*, **36**, 99, 157, 248 (1925); and a series of papers afterwards; see also de Waale, *J. Amer. Chem. Soc.*

[7] Buckingham, *J. Amer. Soc. Test. Mats.*, **21** (ii), 11 (1921). Scott Blair and Crowther, *J. Phys. Chem.*, **33**, 321 (1929); Schofield and Scott Blair, *J. Phys. Chem.*, **34**, 248, 1505 (1930); **35**, 1212 (1931); **39**, 973 (1933); Schofield, *Physics*, **4**, 122 (1933); Reiner, *Kolloid-Z.*, **39**, 80 (1926); Reiner and Riwilin, *Kolloid-Z.*, **43**, 1 (1927); Reiner and Reiner, *Kolloid-Z.*, **56**, 44 (1933); Reiner, *Physics*, **5**, 321, 342 (1934).

[8] Miss Schalek and Szegvari, *Kolloid-Z.*, **32**, 318 (1923); *Ibid.*, **33**, 326 (1923).

[9] Houwink, " Elasticity, Plasticity and Structure of Matter," 345 (1937).

[10] *Ibid.*, 347 (1937).

[11] Ostwald, *Kolloid-Z.*, **47**, 176 (1929); Scott Blair, *Kolloid-Z.*, **47**, 76 (1929); Ostwald and Auerbach, *Kolloid-Z.*, **88**, 273 (1926). The phenomenon of structure viscosity has been termed *flow elasticity* by Freundlich.

[12] Pryce Jones, *J. Oil and Colour Chem. Assoc.*, **17**, 305 (1934); *ibid.*, **19**, 295 (1936).

[13] Mukherjee and Sen Gupta, paper communicated to *Indian Journal of Physics.*

[14] Searle, *Proc. Cambridge Phil. Soc.*, **16**, 600 (1912).

[15] Mukherjee and Sen Gupta, paper communicated to *Indian Journal of Physics.*

[16] Kroepelin, *Z. physik. Chem.*, **149**, 291 (1930).

[17] Pichot, *Physics*, **5**, 200 (1934).

[18] Philippoff, *Kolloid-Z.*, **83**, 163 (1938).

[19] Richardson, *Physics*, **6**, 273 (1935).

[20] Schofield and Scott Blair, *J. Phys. Chem.*, **34**, 248 (1930).

A SIMPLE ROTARY VISCOMETER FOR THE STUDY OF ANOMALOUS VISCOUS PROPERTIES*

BY J. N. MUKHERJEE

AND

N. C. SEN GUPTA

(Received for publication, September 1, 1941)

ABSTRACT. A simple rotary viscometer suitable for the study of 'anomalous' viscous properties is described. It admits of easy end correction and there is no slip at the metal walls with sugar and glycerine solutions. Consistency curves of bentonite suspension, gelatin sol and starch paste representing respectively plastic, structure viscous and dilatant systems have been obtained.

In investigations on anomalous viscous properties, the shearing stresses corresponding to different rates of shear have to be measured. Rotary viscometers have the advantage over capillary viscometers that the annular space can be made small compared to the diameter of the cylinders and the velocity gradient can be made to vary over a comparatively smaller range. Further it appears from direct measurements of the velocity gradient by us that the capillary viscometer does not give true estimates of the yield value whereas the rotary viscometer does. In the simple rotary viscometer[1] described in this note the outer cylinder rotates and the torque on the inner cylinder is measured.

The new viscometer has the following features (Fig. 1):

(*a*) The speed of an outer cylinder, A, which can be varied from 10 to 1000 rotations per minute is measured by a revolution counter, C.

(*b*) The inner cylinder, I, is suspended from a graduated torsion head, H fitted with a vernier. The position at rest of the inner cylinder is indicated by a lamp and scale arrangement (not shown in the figure). The torsion head is rotated in the opposite direction until the cylinder comes to its original

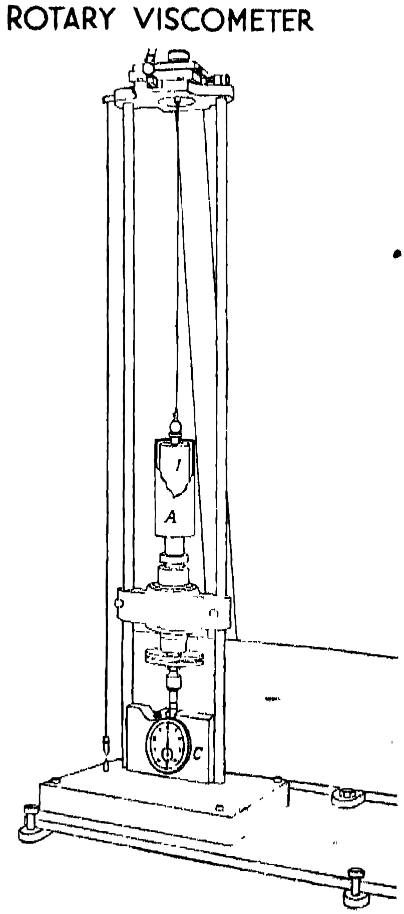

FIG.

---

* Communicated by the Indian Physical Society.

position of rest. The torque is read directly on the torsion head and can be measured up to 360° whereas if the deflection of light on the graduated scale[2] alone were utilised only a small torque could be measured.

(*c*) The torsion head, H, is fitted with a centering device and a plumb line and levelling screws ensure a vertical setting of the apparatus.

(*d*) The inner cylinder is about 9 cm. long and the end effect is small. The correction for this with simple liquids is of the order of 5%. Guard rings[3] have not been used as they might cause complications for non-Newtonian liquids.

(*e*) The radius of the outer cylinder is 2.017 cm. and those of the inner cylinders are 1.886, 1.792, 1.650 and 1.495 cms. The width of the annular space is thus small compared to the radii of the cylinders. This consideration is of importance in liquids where the rate of shear does not change linearly with the shearing stress.

(*f*) The apparatus has been made heavy enough to minimise vibrations.

The shearing stress, F, and the rate of shear, *dv*/*dz*, are given by the following relations :

$$F = \frac{M}{2\pi L R_1^2} \quad \cdots \quad (1)$$

$$dv/dz = \frac{2\Omega R_2^2}{R_2^2 - R_1^2} \quad \cdots \quad (2)$$

where Ω is the angular velocity ; R_2 and R_1 the radii of the outer and inner cylinders ; L the length of the latter immersed in the liquid ; $M = \tau\theta$ where θ is the torque and τ the moment of torsional couple. τ is as usual determined by the method of oscillation.

End effect is equivalent to a virtual increase in the length, L, of the inner cylinder and equation (1) can be written in the form

$$F = \frac{M}{2\pi(L + l) R_1^2}. \quad \cdots \quad (3)$$

l has been determined by the method of Searle[4] with a 40% sugar solution and a 39% glycerine solution. Results are given in figures 2, 3 and 4 and in table I.

The viscosity of a 56% glycerine solution obtained with the different inner cylinders was found to be 5·5, 5·6, 5·7 and 5.6 centipoises respectively.

Liquids showing anomalous viscous properties are often classified in four groups,[6] namely (*i*) plastic, (*ii*) structure viscous, (*iii*) dilatant and (*iv*) thixotropic. Some systems show a behaviour which combines the features of more than one of the above typical classes. Plastic systems are characterised by a yield value and straight consistency curves at sufficiently high rates of shear. Structure viscous bodies have a constant viscosity at low rates of shear but at higher rates the ratio between the shearing stress and the rate of shear gradually decreases. Dilatant suspensions have also a constant viscosity at low rates of shear but in contrast to the structure viscous system the ratio between the shearing stress and the rate of shear gradually increases at higher rates of shear. In thixotropic systems shearing stress at a particular rate of shear changes with time. Consistency curves which show the relationship between the rate of shear and shearing stress of the first three types of systems are represented respectively by a bentonite suspension, a gelatin sol[7] and a starch paste.[7] These have been obtained by

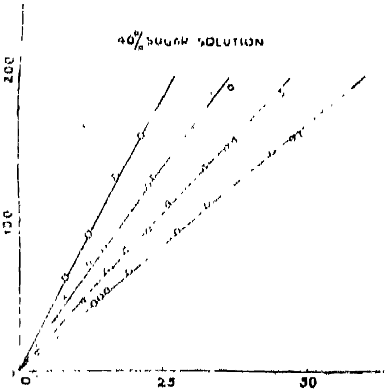

FIG. 2

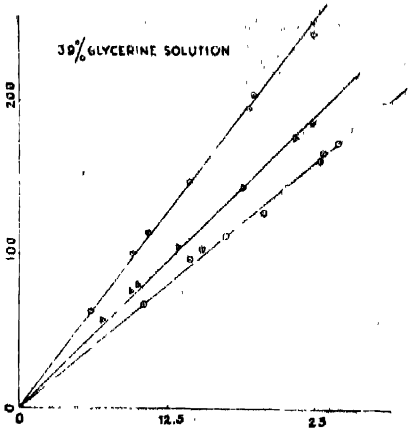

FIG. 3

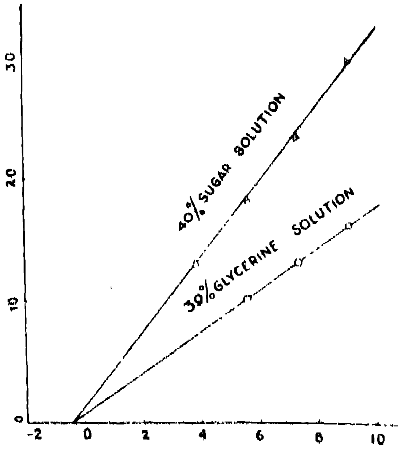

FIG. 4

the rotary viscometer described above and are shown in figs. 5, 6 and 7. Curves for thixotropic systems obtained by this viscometer will be described elsewhere.

TABLE I

End correction for the Rotary Viscometer

$R_1 = 1.792$ cm.; $R_2 = 2.017$ cm.; l (from fig. 4) $= 0.5$ cm.

Length of the inner cylinder immersed in the solution (cm.)	40 per cent. sugar solution η (centipoise) Temp. 29°C.		39 per cent. glycerine solution η (centipoise) Temp 31°C.	
	obs	corr	obs.	corr.
3·85	5·14	4·55	—	—
5·6	4·96	4·65	2·72	2·50
7·35	4·85	4·54	2·69	2·52
9·1	4·90	4·75	2·66	2·52
		mean 4·60		mean 2·51
		from standard data 4·56		2·55

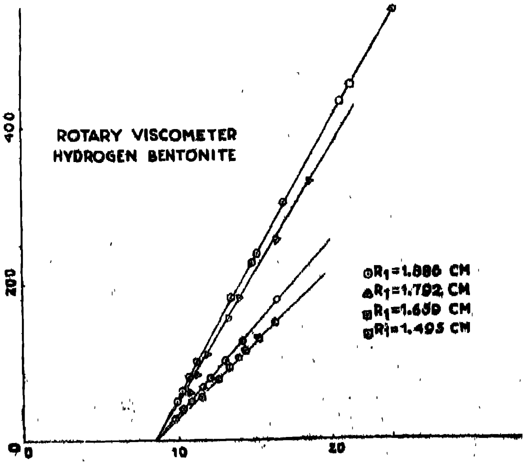

FIG. 5

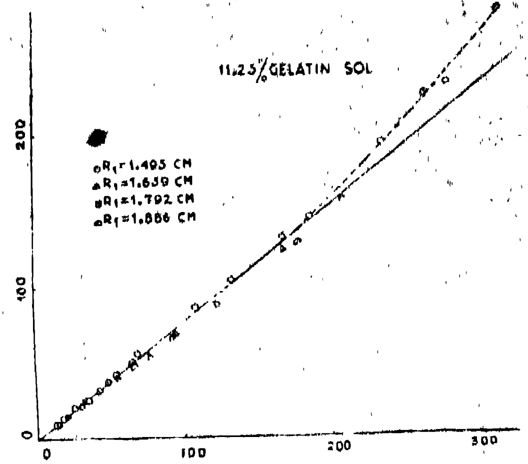

Fig. 6

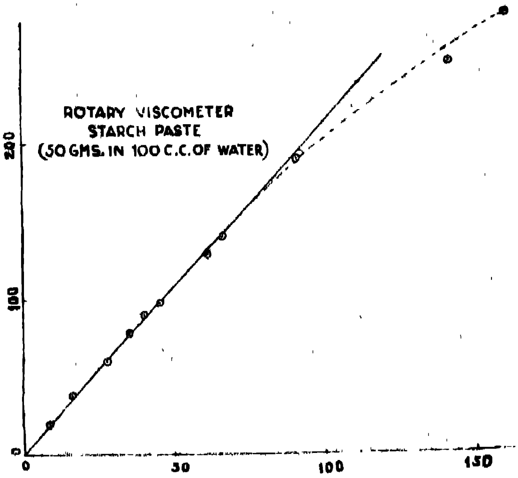

Fig. 7

The rotary viscometer described in this note has been found convenient for rapid measurements with non-Newtonian liquids.

Physical Chemistry Laboratory,
University College of Science and Technology.
92, Upper Circular Road, Calcutta.

REFERENCES

1 Barr, *Monograph of Viscometry*, 229 (1931).
2 See reference 1, p. 231.
3 Hatschek, *The Viscosity of Liquids*, 53 (1928)
4 Searle, *Proc. Cambridge Phil. Soc.*, **16**, 600 (1912).
5 *Int. Crit. Tables*, 23 (1929); Sheely, *Ind. Eng. Chem.*, **24**, 1063 (1932).
6 Houwink, *Elasticity, Plasticity and Structure of Matter*, 10 (1937).
7 Measurements by Mr. R. P. Pal.

9

STUDY OF ELECTROLYTIC DISSOCIATION IN IODIC ACID BY RAMAN EFFECT *

By N. RAJESWARA RAO, M.Sc.

(Received for publication, September 10, 1941)

ABSTRACT The present work is an attempt at studying the electrolytic dissociation in iodic acid by Raman Effect on the same lines as is done in the case of nitric acid and sulphuric acid by the author. Iodic acid is found to contain polymerised molecules of the type $(HIO_3)_2$ in concentrated solutions. As the acid is diluted, the polymers are found to dissociate into HIO_3 molecules which again dissociate into IO_3 ions at still lower concentrations. On comparing 0.1N solutions of KIO_3 and HIO_3, it is found that the intensity of IO_3 line in KIO_3 solution is much larger than in HIO_3 solution. It is concluded that the acid is not completely dissociated even in such a dilute solution.

INTRODUCTION

In a previous communication,[1] the author made a quantitative study of electrolytic dissociation in sulphuric acid. The present work is an attempt at a similar study in iodic acid. Iodic acid has been studied both in crystalline state and in solution by many workers including Krishnamurty,[2] Nayar and Sharma,[3] Nayar and Gairola,[4] and Woodward.[5] The latest work is that of Venkateswaran[6] who made a study of the acid in many of its aspects. The interpretation of the results by various authors are conflicting. Woodward thinks that the acid is highly dissociated even in concentrated solutions and in fact Krishnamurty[2] and Shen, Yao and Wu[7] discussed the structure of IO_3 ions by assuming that a solution of iodic acid of 5N concentration is completely dissociated. On the other hand, Venkateswaran [6] maintains that the acid is very weak and undissociated molecules are found even in dilute solutions. Venkateswaran's observations are based on visual estimate of the structure and positions of the maxima of the wide bands of the acid at various concentrations. The author, from a study of the microphotometric records of the spectra, found discrepancies between the Raman frequencies of the maxima of the bands reported by Venkateswaran and those observed by the author. Also, the structures of the bands observed by

---

Communicated by Indian Physical Society.

Venkateswaran and those revealed by the microphotometric records were found to be different.

EXPERIMENTAL

Pure crystals of Iodic acid supplied by Merck are taken and dissolved in double-distilled conductivity water and filtered through a cintered glass crucible avoiding the use of any filter paper, lest the filter paper should be acted upon by the acid thereby contaminating it. Aqueous solutions of concentrations 18N, 15N, 12N, 6N, 3N, 1N, 1.6N, 0.8N, 0.4N are made. A solution of KIO_3 is made by dissolving pure crystals in pure water. This solution is treated with pure carbon while hot and filtered through a cintered glass crucible using a quantitative filter paper. This method is found to be very effective in purifying the solution from fluorescent and colloidal impurities.

The arrangement used to photograph the Raman spectra is the same as in the case of sulphuric acid by the author. In the case of very dilute solutions where very long exposures are needed to bring out the weak Raman lines with sufficient intensity the problem of the superposed continuous spectrum becomes very acute. Therefore, a double-jacketed Wood's tube is employed, so that two filters—iodine in carbon-tetrachloride and a saturated solution of $NaNO_2$—could be used to isolate the 4358 line of the mercury arc for exciting the Raman lines. The solution of $NaNO_2$ is replaced, every time the solution in the Wood's tube is replaced, so that the filter may not, owing to photochemical decomposition and development of colour, diminish the intensity of the exciting radiation. In the case of concentrated solutions, *viz.*, 18N, 15N, 12N, and 6N, equal exposures of one hour each are given. Solutions of concentrations 6N, 3N and 1N and 1.6N, 0.8N and 0.4N are exposed for periods proportional to dilution in two sets of three concentrations each.

An exposure of one hour was sufficient to bring out the Raman spectra of crystalline HIO_3 and KIO_3. To study the solution of iodic acid at higher temperature, the Wood's tube was sealed and enclosed in a steel tube with a slot cut on its side to allow the light from the mercury arc condensed by a large double condenser to fall on the Wood's tube. A current of about 2 amperes was sent through the heating coil wound on the steel tube to heat the tube inside. Thus a temperature of 130°C. could be attained. The spectra at 30°C. and 130°C. are compared.

RESULTS

The Raman frequencies of the maxima, in the crystals and in solutions of iodic acid and KIO_3, are given in the following table. Besides the frequencies reported in this table many low frequencies are found in the spectra of the crystals. But they are very feeble and are found to be absent in solutions.

TABLE I

HIO₃-crystal		18N		15N		12N		6N		3N		1N		0 5N	
1	2	1	2	1	2	1	2	1	2	1	2	1	2	1	2
328	331	334	326	—	324	334	324	330	324	328	324	—	324	328	—
377	376	463	—	—	—	463	—	—	—	—	—	—	—	—	—
633	636	644	640	—	640	644	636	644	636	644	—	—	—	644	—
713	728	779	772	—	770	796	796	796	796	798, 796	803	—	810	802	—
782	788	—	—	—	—	—	—	789	—	—	—	—	—	800	—
—	—	823	—	—	—	823	—	823	—	823	—	—	825	819	—

TABLE II

HIO₃ 1.6N	0 8N	0.4N	KIO₃ 0.4N	KIO₃ 1N	LiIO₃ 3.4N	LiIO₃ 2.3N	LiIO₃.HIO₃ 1.15N	KIO₃-crystal	
2	2	2	2	1	1	2	2	1	2
324	324	324	324	333	320	324	324	132 308 335 341 737 753 789 808	— — — — 742 761 795 812
—	—	—	—	—	423	—	—		
—	—	—	—	—	603	636	636		
810	810	810	810	803	794	810	810		
825	825	825	—	—	—	—	—		

In the above Tables the frequencies given under the column 1 are due to Venkateswaran and those under the column 2 are due to the author.

From the above tables, it is clear that there are large differences in the frequencies of the maxima of the Raman lines between those reported by Venkateswaran and the author. This should be attributed to the errors in visual judgement in the location of the maxima in Venkateswaran's pictures. The band at 636 is found in all the spectra, but in dilute solutions it is very weak and diffuse and therefore its maximum could not be correctly located.

STRUCTURE OF THE BANDS

The sharp lines 331 and 376 of crystalline iodic acid shift to a lower frequency and broaden out (see the photometric records) to form a band with its maximum at 324. This band appears with medium intensity in all the spectra, with varying structure and gets diffuse in the intermediate concentrations. But in the dilute solutions again, the band becomes narrower.

The line at 636 in the crystalline iodic acid gives rise to a diffuse band in the solution. This band appears with medium intensity in concentrated solutions but rapidly gets feebler and diffuse, but continues to persist even in very dilute solutions. This is found to be present even in solutions of iodates, especially in the solution of $LiIO_3$ of concentration 2.3N.

Venkateswaran reported a feeble band 463 which fades off with dilution. It is found in the pictures taken by the author.

The bright and sharp lines 728 and 788 of the crystal shift to higher frequency and diffuse out to give a bright diffuse band with its maximum at 772 in the 18N solution. It undergoes conspicuous changes with dilution. Venkateswaran describes that this band has a high-frequency component which gets feeble and gradually dies out with dilution, while the main band gets weaker and diffuse on dilution and in the solution of 6N it is superposed upon by a sharp line. This line becomes stronger at the expense of the band as the concentration is further decreased still at very low concentrations, the band disappears leaving a strong sharp line. He found a line 823 corresponding to the high-frequency component of the main band in the spectrum of crystalline $KIO_3.HIO_3$ and therefore attributed this to the I_2O_6 ions. He suggested that the strong line is due to the IO_3 ions formed due to the dissociation of the HIO_3 molecules represented by the main band.

But the photometric curves of the author reproduced in Fig. 1 give a different result. The main band has an unsymmetrical structure in the concentrated solutions, and its maximum gradually shifts to higher frequency from 15N. In the 3N solution, the band is shifted to 803 and assumes a symmetrical structure. At still lower concentrations it splits up into 2 lines, 810 and 825, of which 825 gets feebler and feebler and 810 gets more and more intense with dilution. This behaviour of the band can be looked upon as due to the superposition of 2 components, with their maxima at about 770 and 825 of the crystal corresponding to the lines 728 and 788 which shift to higher frequency from crystal to solution. As the concentration is decreased, the component 770 gets feeble until at 1N it is practically absent, while the component 825 gets brighter at the expense of its neighbour. As a result of blending of these bands into each other, the maximum of the resultant appears to shift to higher frequency. At still lower concentrations 1N, another line at 810 makes its appearance, while the band 125 is reduced to a feeble line at 825, which goes on diminishing in intensity on dilution while 810 is getting brighter, as is already described.

Effect of Temperature. Spectra of the acid of concentration 18N taken at the laboratory temperature and at a temperature 130°C. are compared to see if there are any changes in the structure, which would help to study its properties better. But the changes are found to be very slight and cannot be described accurately, though the range of temperatures is large. It could not be studied at still higher temperatures as the acid is found to decompose slightly.

DISCUSSION

The changes in the structure of the bands with dilution can be interpreted on assuming the presence of three kinds of molecules $(HIO_3)_2$, HIO_3 and IO_3, $(HIO_3)_2$ and HIO_3 being predominent in the concentrated solutions and HIO_3 and IO_3 in the dilute solutions. The band at 324 is the result of superposition of three bands excited by the three types of molecules. They are very close to each other and therefore the changes that each component undergoes on dilution cannot be traced.

Nayar and Sharma, attribute the band 636 to the $(HIO_3)_2$ molecules as the band gets feebler on dilution and could not be photographed by them in the dilute solutions. Venkateswaran [6] refuted the above contention as he found it in his spectra of dilute solutions also. The two conflicting views can be explained if it is assumed that this band is the resultant of the bands excited by $(HIO_3)_2$, HIO_3 and IO_3, and that the contribution to the intensity of this band due to $(HIO_3)_2$ is large compared to that due to HIO_3 or IO_3. With decreasing concentration $(HIO_3)_2$ molecules dissociate into HIO_3 and therefore the intensity of the band falls off more than in proportion to dilution.

The behaviour of the band 770, which is the most intense of all, also can be ragarded as due to the superposition of the bands excited by $(HIO_3)_2$ and HIO_3 and in dilute solutions by IO_3 ions. The component with the maximum at 770 is due to $(HIO_3)_2$ molecules and that at 825 to HIO_3 molecules. With decreasing concentration $(HIO_3)_2$ molecules dissociate to HIO_3 molecules and hence the 770 band is decreasing in intensity while 825 is increasing in intensity on dilution, the resultant of the band thus appearing to shift towards 825. 3N downwards, $(HIO_3)_2$ molecules are absent and HIO_3 molecules, which are predominent, begin to dissociate to IO_3 and H and the line at 810, due to IO_3 ions, becomes progressively intense on further dilution.

In this connection, one point requires elucidation. Venkateswaran attributes the component 825 to I_2O_6 ions as this line is found in the spectrum of crystalline $KIO_3.HIO_3$. This view warrants a large dissociation of the acid even in high concentrations where the intensity of this line is large, which means a high electrical conductivity of the acid at those concentration. But the acid is considered to be very weak. Therefore the above contention is untenable.

It is possible to calculate roughly the degree of dissociation of the acid in the lower concentrations by comparing the intensity of the 810 line in the solutions of the acid and KIO_3, on the same lines as was done for H_2SO_4 studied by the author. The following table gives the intensities of the lines in solutions of the acid and KIO_3.

Solution	Intensity of IO_3 line 810	Degree of dissoc.
KIO_3 0.4N	353	100%
HIO_3 0.4N	199	56%
HIO_3 0.8N	140	40%

Concentrations of only those solutions for which the lines 810 and 825 are sufficiently resolved are taken. At higher concentrations the lines are diffuse and the intensities of the two components cannot be accurately determined. At still lower concentrations the lines are superposed by the background and therefore their intensities could not be accurately determined.

From the above table it is clear that, even at such concentrations as 0.4N, the degree of dissociation is only 56%. Even in dilutions of 0.1N of HIO_3 the intensity of the 810 line of HIO_3 is found to be smaller than that in 0.1N KIO_3 which indicates that the dissociation is incomplete even at that dilution. Therefore iodic acid should be regarded as a weak acid compared with nitric acid or sulphuric acid.

In conclusion, the author wishes to record his grateful thanks to Dr. I. Ramakrishna Rao under whose direction the above work is done.

DEPARTMENT OF PHYSICS,
ANDHRA UNIVERSITY, WALTAIR.

REFERENCES

N. R. Rao, *Ind. Jour. Phys.*, **14**, 143 (1940).
[2] P. Krishnamurty, *Ind. Jour. Phys.*, **5**, 633 (1930).
[3] Nayar and Sharma, *Z. Anorg. Allgem. Chem.*, **220**, 169 (1934).
[4] Nayar and Gairola, ,, ,, ,, **220**, 163 (1934).
[5] Woodward, L., *Nature*, **32**, 212 (1931).
[6] Venkateswaran, C. S., *Proc. Ind. Acad. Sci.*, **2A**, 119 (1935).
[7] Shen, Yao, and Wu, *Phys. Rev.*, **51**, 235 (1937).

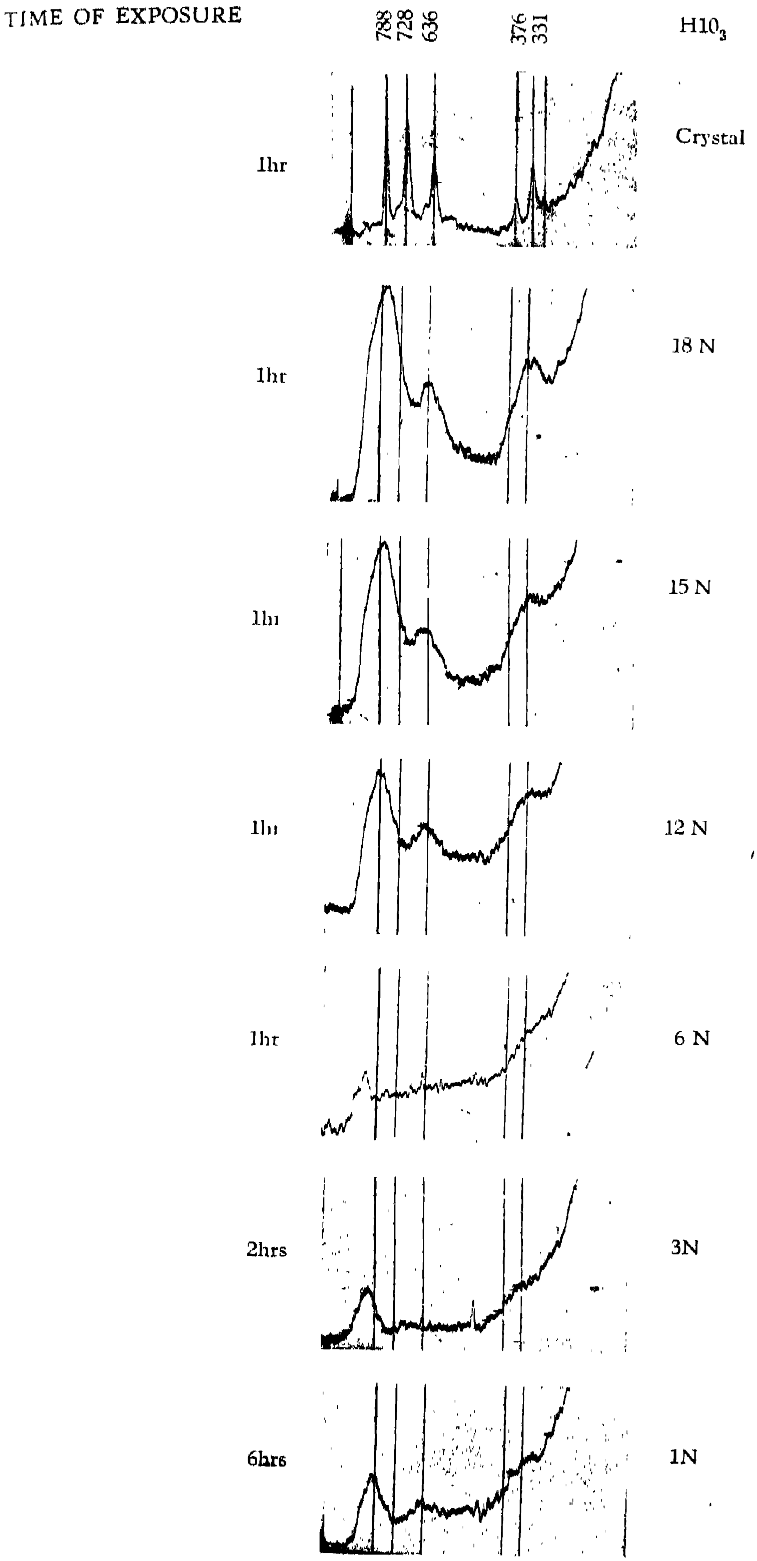
TIME OF EXPOSURE
788
728
636
376
331
HIO_3
Crystal
1hr
18 N
1hr
15 N
1hr
12 N
1hr
6 N
2hrs
3N
6hrs
1N

PROPAGATION OF SOUND IN LIQUIDS AND VISCOSITY

By G. SURYAN

(Received for publication, September 7, 1941)

ABSTRACT. An empirical relation $v = G\eta^{\frac{11}{10}}$ is given between sound velocity (v) and viscosity (η) of liquids The propagation of sound in liquids is discussed on the basis of energy transference between molecules The relation $v \propto \frac{1}{\sigma^9}$ between sound velocity and molecular diameter (σ) is also deduced theoretically therefrom. The relation $\eta \propto \frac{1}{\sigma^9}$ follows from above. Dispersion of acoustic velocity with frequency is shown to be true from the theory. The frequency range for dispersion is also discussed.

§ 1

It is well-known fact that the velocity of sound in a liquid varies with temperature and the viscosity of the liquid also varies rapidly with temperature. It is known that the velocity of sound depends upon the nature of movement of the molecules in a liquid and the viscosity of the liquid is dependent upon the nature of movement of the molecules under consideration. Both (sound velocity and viscosity) are known to be functions of the frequency of the molecules and their size. Then a relation may be expected between the two. The relation at first might seem too complicated but a closer investigation results in a simple relation.

It is seen that the ratio $\frac{\log v}{\log(\eta \times 10^5)}$ (where v is the velocity of sound in the liquid and η the viscosity of the liquid at that temperature) works out to be a constant independent of the liquid and independent of the temperature. This is shown by table I. The constant has a mean value of 1.2, where instead of using directly the value of η we use $\eta \times 10^5$, as η is a small quantity generally.

Therefore we have

$$\frac{\log_{10} v}{\log_{10}(\eta \times 10^5)} = 1.2. \tag{1}$$

From this we get the relation

$$\log_{10} = [\log_{10}(\eta \times 10^5)]1.2$$

or

$$v = (\eta \times 10^5)^{1 \cdot 2}, \text{ independent of temperature.} \tag{2}$$

TABLE I

Liquid	Temperature °C.	Velocity Metres/sec.	Viscosity × 10⁵	$\frac{\log v}{\log(\eta \times 10^6)}$
Acetone	0	1273	395.0	1.212
	20	1190	300.0	1.240
	40	1100	280.0	1.242
Aniline	0	1712	805.0	1.104
	20	1659	440.0	1.218
	30	1616	319.0	1.282
	40	1579.5	241.0	1.343
	50	1540	189.0	1.401
Benzene	20	1324	649.0	1.111
	40	1231	492.0	1.149
Ether	0	1095	300.0	1.226
	10	1054	258.0	1.253
	20	1006	234.0	1.267
	30	949	212.0	1.277
Heptane	0	1235	519.0	1.139
	20	1154	410.0	1.171
	40	1070	344.0	1.196
Hexane	20	113(2, 3)	320.0	1.215
Chloroform	23	1000	550.0	1.096
Methylene iodide	24	977.7	475.0	1.124
Methyl alcohol	0	1187	813.0	1'056
	20	1121	591.0	1.117
	40	1056	450.0	1.139
Octane	0	1277	703.0	1.091
	20	1192	538.0	1.127
	40	1108	428.0	1.157
Toluene	0	1414	768.0	1.091
	20	1327.5	586.0	1.128
	40	1242	466.0	1.157
Carbon disulphide	23	1149	360.0	1.198

To make equivalence between dimensions of both sides of the relation there must be on one side of the equation a constant with the required dimensions. Thus

$$v = G_1[\eta \times 10^5]^{1\cdot 22} \qquad \dots \quad (3)$$

where G_1 is a constant dependent on the nature of the liquid under consideration. Taking logarithms on both sides of (3) we get

$$\frac{\log_{10} v}{\log_{10}[\eta \times 10^5]} = \frac{\log_{10} G_1}{\log_{10}[\eta \times 10^5]} + \frac{11}{9}. \qquad \dots \quad (4)$$

The above equation (4) will explain the small variation of the results in the last column of table I. In getting the results of table I, we have neglected and have not considered the effect of $\frac{\log_{10} G_1}{\log_{10}[\eta \times 10^5]}$. For ordinary liquids considered in Table I, the constant G_1 is very nearly equal to 1. Therefore the term containing G_1 will vanish and very nearly equals zero.

But for liquids having a high viscosity and relatively low velocity of sound the ratio $\frac{\log_{10} v}{\log_{10}[\eta \times 10^5]}$ will not be in line with those of the other liquids like those of table I. In such a case the constant G_1 will no more be nearly 1 but will be less than 1 and small. Therefore the term containing in (4) will be negative and the resulting value of the ratio will be small.

In the case of liquids of small viscosity and a relatively large velocity of sound the constant G_1 will be large and the term containing G_1 in (4) will have large positive value thereby increasing the value of the ratio $\frac{\log_{10} v}{\log_{10}(\eta \times 10^5)}$.
For ordinary liquids the constant being very nearly 1, the effect of it is neglected and the value 1.22 or 11/9 is evaluated.

The following table II shows the case of highly viscous liquids like glycerine.

It will be seen from table II that for highly viscous substances the ratio attains a very low value.

Therefore we can write the equation in the final form as

$$v = G\eta^{\frac{11}{9}} \qquad (5)$$

where G is a constant.

Liquid	Temperature °C.	Velocity Metres/sec.	Viscosity	$\frac{\log v}{\log (\eta \times 10^6)}$
Glycerine	20	1923	8 5	·5526
Carbon tetrachloride	20	935	.0096	·9963
Butyl alcohol	23	1315	.0294	.8914

§2 PROPAGATION OF SOUND IN LIQUIDS

We can consider the propagation of sound in a liquid as due to a series of collisions between molecules initiated by the impinging wave. Let the sound wave in a liquid be divided into a number of parts each proportional to the intermolecular distance and let the total energy on the wave be divided into the same number of parts each proportional to the amplitude of the part ; then each part of the sound wave will have its associated energy proportional to its amplitude. If the wave reaches a molecule and the energy is absorbed by the molecule, the molecule will have an increased velocity to account for this increased energy. Then there will be an increase of the frequency of the molecule. Now assuming that at each vibration the molecule of higher energy gives its excess of energy to the neighbouring molecule, it will be seen that one part of the sound wave will travel the intermolecular distance (σ) in $1/\nu$ sec. If the sound wave be divided into x parts then x parts or one wave will travel through $kx\sigma$ in $1/n$ seconds, where n is the frequency of the wave, which is the same as x/ν seconds.

Now the velocity of sound is given by

$$v = n\lambda \qquad \ldots \quad (6)$$

and

$$\frac{1}{n} = \frac{x}{\nu} \quad \text{or} \quad n = \frac{\nu}{x} \qquad \ldots \quad (7)$$

and from our assumption

$$kx\sigma = \lambda \qquad \ldots \quad (8)$$

where k is the proportionality constant dependent on the liquid. Then we get

$$v = kx\sigma . \frac{\nu}{x} \qquad \ldots \quad (9)$$

$$v = k\nu\sigma . \qquad \ldots \quad (10)$$

Assuming that

$$\nu \propto \frac{1}{\sigma^m} \qquad \ldots \quad (11)$$

we get

$$v = k . \frac{1}{\sigma^{m-1}} \qquad \ldots \quad (12)$$

Now putting

$$m = 10$$

we get

$$v \propto \frac{1}{\sigma^9} . \qquad \ldots \quad (13)$$

Combining this with (5), we get $\eta \propto \frac{1}{\sigma^7}$ $\qquad \ldots \quad (14)$

The *theoretical* relation (13) above is seen to be true empirically also [1] such that the assumptions made in deriving (13) are essentially correct.

In deriving (13) it is assumed that the frequency of a molecule is not changed very much. This changed frequency (which frequency must be used instead of the normal frequency in deriving (13)) will not vary much from the normal frequency of the molecules at that temperature. This change of frequency and its magnitude will be dependent upon the frequency of the sound wave. Therefore there will be dispersion of acoustic velocity at very high frequencies. The acoustic dispersion in the range we are considering will be very small and is neglected in deriving (13). The dispersion will be larger when the acoustic frequency is comparable with the molecular frequency. The theory *outlined* above is still in its earlier stages and has to be perfected to give quantitative results about dispersion and acoustic frequency.

From the above relations it is seen that much interesting facts can be deduced. It is possible to derive an equation for the temperature change of velocity of sound in liquids from (5). By advancing the theory proposed in §2 to solids the author hopes to get valuable information.

In this connection the author thanks Prof. A. V. Telang of Central College for permitting him to make use of the Physics Library at the Central College, Bangalore. He also thanks Dr. B.V. Raghavendra Rao and Mr. D. S. Subbaramiah of Central College, Bangalore, for going through the paper.

129 URIOPET,
BANGALORE CITY.

REFERENCE

[1] *Ind. Jour. Phy.* XIV, 109 (1940)

11

THE DIELECTRIC STRENGTH OF INDIAN VEGETABLE OILS

By S. CHAKRAVARTY

AND

P. C. MAHANTI

(*Received for publication, September 17, 1931*)

INTRODUCTION

India is rich in vegetable oils. It is being felt that their physical and electrical properties should be carefully investigated with a view to ascertain whether they can be suitably substituted in place of mineral oils, which are used as insulants for various electrical purposes, especially in transformers, oil switches and oil-filled condensers and cables.

Their physical properties such as viscosity and gas absorption at different temperatures, their electrical properties such as d.c. conductivity and dielectric constant are being studied in this laboratory by other workers. The present authors have, however, begun a series of investigations on their dielectric strength (or electric breakdown), dielectric loss and power factor measurements.

In the present paper are reported the preliminary results obtained on the electric breakdown of as many as fourteen samples of Indian vegetable oils and the influence of moisture content on their breakdown voltages.

EXPERIMENTAL

For preliminary investigations it was thought fit to test the breakdown voltages of the oils according to the method prescribed in the B.S. Specification No 148, 1927. Tests have been performed with both a.c. and d.c. voltages impressed on the oils. The a.c. voltage was obtained from the secondary of a G.E.C. step-up voltage (220V/20,000V) transformer, the primary circuit being controlled by an auto-transformer. The control of the high-voltage circuits is shown in the circuit diagram, Fig. 1.

For tests with d.c. voltage a Kenetron rectifier was used in the secondary circuit of the H.T. transformer. A resistance of about 40,000 ohms was used in the high-tension circuit during the tests. The voltage across the cell containing the oil under test was measured with the help of an electrostatic voltmeter (0—25/50/100 KV). The frequency of the a.c. supply was maintained constant at 50 cycles per second. The wave-form of the supply voltage was sinu-

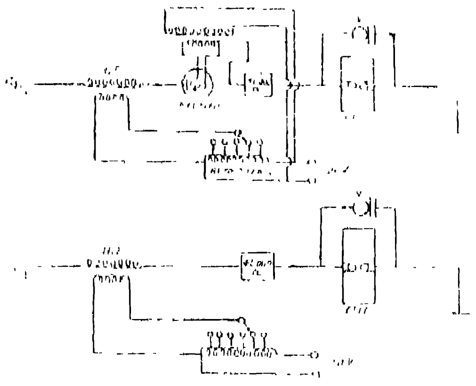

FIG. 1

soidal, the crest value being therefore 1.45 times the R.M.S. value as measured by the electrostatic voltmeter.

The oil container is made of a thick-walled glass vessel of internal dimensions 55 mm. × 90 mm. × 100 mm., according to specification. Two circular holes are made on the two opposite walls of the vessel to allow the spherical electrodes to pass through them. The electrodes are brass spheres of 13 mm. diameter, each being screwed up to a small stainless steel shaft with a terminal screw outside and held in position by means of collars such that the spherical electrodes remained perfectly horizontal. One of the electrodes is fixed while the other is made movable by a sliding adjustment of the shaft through a guide. The guide is provided with two slots having an interval of exactly 4 mm. (or 0.157 in.). When the fixing pin on the movable shaft is put in the first slot, the two spheres just touch each other, but when it is removed to the second slot, they are separated exactly by 4 mm.

The electrodes and the cell were thoroughly cleaned and dried before test on each oil was carried out.

The oil under test was initially heated slightly above the room temperature (to about 40°C.) and stirred in a vacuum chamber for several hours to remove the moisture already present in the oil and to drive out the dissolved air in it. It was then cooled down to the room temperature in the same chamber. A volume of about 300 c.c. was introduced into the previously cleaned cell. The final purification, *i.e.*, removal of dust and fibres, which might be present as suspended impurities, inspite of its being filtered by means of a stream-line filter, was done electrically. The cell was filled with the oil under test and a voltage of 10 KV across the electrodes was applied for thirty seconds, thus subjecting the oil to a voltage gradient of 25 KV per cm., so that all the dust particles and fibres might be attracted by the electrodes. The electrodes were washed clean by pouring over them some fresh oil. This operation was repeated several times at the beginning of each test.

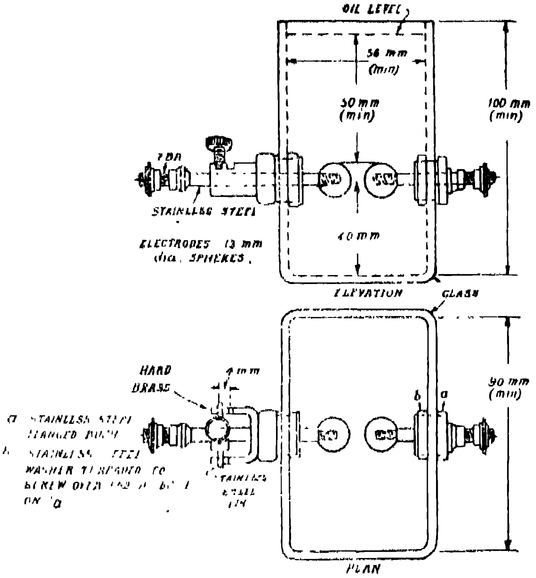

FIG. 2

TABLE I

Temperature = 30°C. Barometric Pressure = 75.32 cm.

Name of oil tested	Preliminary arcing formed at KV/cm. (R.M.S.)	Max. a.c voltage applied per cm (R.M.S.)	Remark
Castor oil		47·50 KV	No breakdown
Cocoanut oil	—	47·50 ,,	,,
Mohua oil	--	46.50 ,,	,,
Cotton Seed oil	--	46.50 ,,	,,
Rape oil	40.00	47·50 ,,	,,
Rayona oil	42.80	47·50 ,,	,,
Arachis oil	37·50	46.50 ,,	,,
Wood oil	30.00	16.50 ,,	Breakdown
Kapok oil	15.00	18.75 ,,	No breakdown
Punag oil	---	46.50 ,,	,,
Neem oil	37·50	18.75 ,,	,,
Chalmugra oil	—	48.75 ,,	,,
Linseed oil	--	47·75 ,,	,,
Sesame oil	40.15	48.75 ,,	,,

Voltage was then applied in gradual steps to the cell containing the purified oil. At each step the impressed voltage was sustained for at least one minute. Similar tests were performed with d.c. voltage of the same range. The results of these observations are given in Tables I and II.

TABLE II

Temperature = 31°.5 C. Barometric Pressure = 75.50 cm.

Name of oil tested	Preliminary arcing formed at KV/cm (d.c.)	Max. d.c. voltage applied per cm.	Remark
Castor oil	-	48.50 KV	No breakdown
Cocoanut oil	45.00	46.50 ,,	,,
Mohua oil	—	46.50 ,,	,,
Cotton Seed oil	—	47.50 ,,	,,
Rape oil	40.00	47.80 ,,	,,
Ravona oil	37.50	48.50 ,,	,,
Arachis oil	42.80	46.50 ,,	,,
Wood oil	30.00	45.00 ,,	Breakdown
Kapok oil	45.00	47.50 ,,	No breakdown
Punag oil	—	47.50 ,,	,,
Neem oil	37.50	48.75 ,,	,,
Chalmugra oil	—	48.75 ,,	,,
Linseed oil	—	47.50 ,,	,,
Sesame oil	40.00	48.75 ,,	,,

To study the effect of moisture on the breakdown voltage, the oil was dried and purified electrically as before. A known quantity of distilled water was added to a measured volume of the oil and shaken vigorously and stirred before being filled in the cell. Sufficient time was allowed for the air-bubbles to clear out from the oil adjacent to the electrodes. The test voltage was then gradually applied, carefully noting the effects produced thereby. The moisture content was gradually increased. The breakdown voltage was noted at each step. A few typical curves showing the relation between breakdown voltage and the percentage of moisture content for two of the oils studied are given in Fig. 3. The data for these curves are included in Table III.

It was further observed that when any impurity is introduced into the oil under test, the breakdown voltage diminishes. Such observations have already been made by several authors in the case of mineral oils.

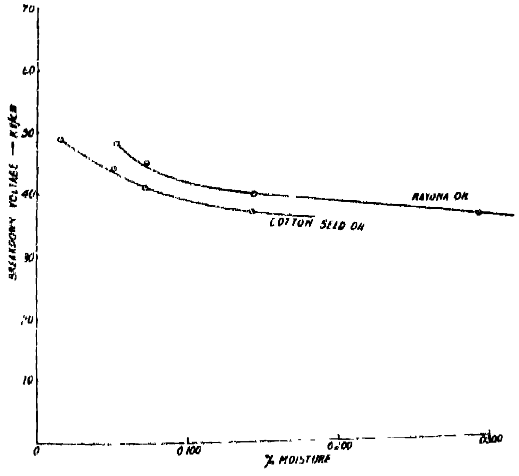

FIG. 3(a)

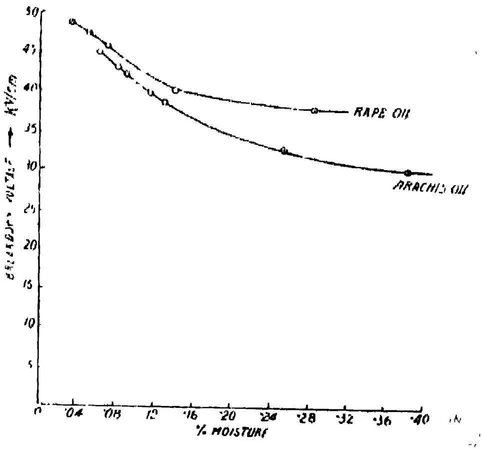

FIG. 3(b)

TABLE III

Temperature = 30°.5 C. Barometric Pressure = 78.5 cm.

Cotton Seed Oil			Rayona Oil		
% of Moisture	Arcing voltage in KV per cm. (R.M.S.)	Breakdown voltage in KV per cm. (R.M.S.)	% of Moisture	Arcing voltage in KV per cm. (R.M.S.)	Breakdown voltage in KV per cm. (R.M.S.)
0.0000	—	—	0.0000	37.50	—
0.0055	—	—	0.0071	32.75	—
0.0150	37.50	—	0.0143	30.00	—
0.0200	37.50	—	0.0214	30.00	—
0.0250	35.00	48.75	0.0280	30.00	—
0.0550	32.25	47.50	0.0357	30.00	48.75
0.0724	30.00	46.50	0.0500	30.00	46.50
0.1428	20.00	37.50	0.0714	25.00	45.25
—	—	—	0.1428	20.00	40.00
—	—	—	0.2856	12.50	37.75

Our conclusion regarding the suitability of these oils as insulants is reserved till our study of their physical and other electrical properties is complete.

MEASUREMENT LABORATORY,
DEPARTMENT OF APPLIED PHYSICS,
UNIVERSITY COLLEGE OF SCIENCE AND TECHNOLOGY,
92, UPPER CIRCULAR ROAD, CALCUTTA.

12

ON VOLTAGE STABILIZER CIRCUITS*

By BINDUMADHAB BANERJEE, M.Sc.

(Received for publication, November 4, 1941)

ABSTRACT The paper describes several improved forms of voltage stabilizer circuits. The single-valve and the two-valve Neher Pickering circuits have been improved by reducing the number of dry batteries used, without in any way sacrificing the performance. New principles are applied to the usual two-valve stabilizer circuit by which it is possible to have "perfect" stabilization and "zero" or negative internal resistance. A circuit is described which is suitable for supplying a stabilized current to the heaters of the thermionic tubes used in sensitive valve voltmeters. The performance of the circuit is very much superior to that of the stabilizing transformers and baretter tubes as regards the stabilization.

The effect of source resistance on the performance of stabilizers has been studied. The analysis has the advantage of being not only more general but also more simple and straightforward.

CONTENTS

1. Introduction.

2. Modifications on the Neher Pickering circuits.
   (a) Single-valve circuit—experimental arrangement for testing the performance.
   (b) Two-valve circuit.

3. Improvements on two-valve stabilizers
   (a) A circuit giving perfect stabilization
   (b) A circuit for high currents
   (c) A circuit having negative internal resistance
   (d) Mathematical theory of two-valve stabilizers
   (e) General considerations on the design of two-valve stabilizers.

4. Effect of Source Resistance in modifying the performance of a voltage stabilizer.
   (a) Nature of the problem
   (b) Overall stabilization factor
   (c) Overall internal resistance.

5. Conclusion.

---

* Communicated to the Indian Physical Society.

1. INTRODUCTION

A source of constant voltage is necessary for various physical and technological experiments and measurements. Ordinarily, storage or dry batteries are used for this purpose. They are, however, inconvenient and expensive and very much so when high voltages are required.

Stabilizer circuits of various types have therefore been developed to perform the function of the battery of dry or storage cells. The circuits employ only a few low voltage dry batteries, one or a few thermionic valves and some resistances. The voltage of the primary source, from which power is taken, may be fluctuating over a wide range but the output voltage V_0 from the stabilizer remains more or less constant ; its variation, with the variation of the input voltage V_i, is reduced very much in proportion. If the current I_0 drawn from such a stabilizer is changed, the output voltage V_0 changes even when the input voltage is held constant. The variational performance of the stabilizer circuit can thus be represented by the values of $\left(\frac{dV_i}{dV_0}\right)$ and of $\left(\frac{\partial V_0}{\partial I_0}\right)_{V_i}$. $\left(\frac{dV_i}{dV_0}\right)$ is called the stabilization factor and is designated by S_0, while the negative of $\left(\frac{\partial V_0}{\partial I_0}\right)_{V_i}$ gives the internal resistance R_0 of the stabilizer in analogy with that of a battery.

The stabilizer circuits can be classified into four groups according to their derivation from :[1]

(*a*) the amplification factor bridge (μ circuits),
(*b*) the transconductance bridge (S circuits),
(*c*) the degenerative amplifier (D circuit),
and (*d*) combination circuits involving two or more of the foregoing classes.

The most notable of these circuits are the one described by Evans[2] and two others described by Neher and Pickering.[3] These circuits are widely used but they suffer from certain defects. Thus the Evans circuit, which is a μ circuit employing a pentode, has a very high internal resistance. It is therefore not suitable for applications requiring a constant voltage under varying current drains. Also the output voltage can be varied only over a small range as otherwise the balance conditions will be upset.

Again, of the two Neher-Pickering circuits, the first one, which is an S circuit modified by the inclusion of a series resistance, though capable of giving excellent performance, particularly with systems requiring negligible current drains at high voltage (G. M. counters, etc.), suffer from the disadvantage of having two dry batteries, and also have a relatively high internal loss of voltage.

The second circuit of Neher and Pickering is also very good in the sense that it is capable of giving very high stabilization ratios and is suitable for large current drains; but its most serious obstacle to general use is that it employs four dry batteries, one of which has to be very thoroughly insulated and shielded.

In the present investigation the author has first effected certain improvements on the Neher-Pickering circuits removing some of their common defects. These are described in § 2. He has further introduced modifications to the usual two-valve stabilizer circuits by which it has been possible to have "perfect" stabilization and "zero" or negative internal resistance. These, along with a circuit suitable for supplying a stabilized current to the heaters of thermionic tubes as are used in sensitive valve voltmeters, are described in § 3. The effect of source resistance on the performance of stabilizers is investigated in § 4.

2 MODIFICATIONS ON THE NEHER-PICKERING CIRCUITS

(*a*) *Single valve circuit.* The first circuit of Neher and Pickering is modified to the form shown in Fig. 1. The improvement consists in eliminating the screen battery. The screen grid is supplied from a potentiometer connected across the input voltage terminals. But, as will be seen presently, in spite of this, the screen voltage remain constant, independent of fluctuations of the input voltage.

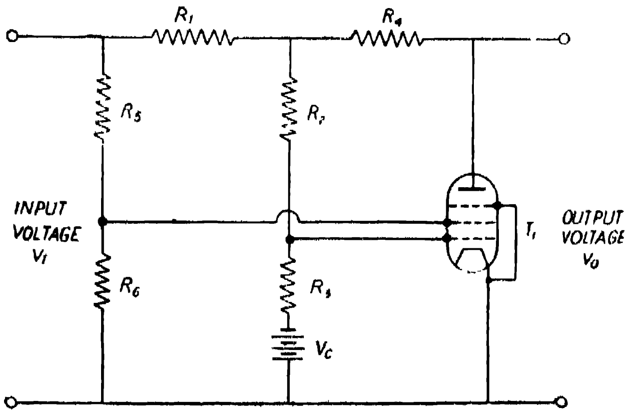

FIG. 1

Modified form of the single-valve Neher-Pickering circuit The screen battery is replaced by a potentiometer connected across the input terminals.

The action of the circuit is as follows. As the input voltage is increased from a very low value, the output voltage continually increases, until at a value

$$V_i' = \left[V_0 + (V_0 + V_c) \frac{R_1}{R_2 + R_3} \right]. \qquad \dots \quad (1)$$

The output voltage becomes equal to V_0, the stabilized voltage required, given by the relation *

$$V_0 = \left[\frac{R_2}{R_3} \,.\, (V_c - \epsilon) - \epsilon \right]. \qquad \dots \quad (2)$$

ϵ is the negative grid voltage at which the tube just begins to take current. Before this, none of the positive electrodes—the screen grid or the anode—takes any current. When the input voltage is equal to V_i', the screen voltage becomes equal to

$$V_s = \frac{R_6}{R_5 + R_6} \,.\, V_i'. \qquad \dots \quad (3)$$

As the input voltage is increased still further, the tube takes current simultaneously through the anode and the screen. The anode current is given by the relation

$$I_a = \frac{V_i - V_i'}{R_1}.$$

Assuming the screen current to be a constant fraction of the anode current, we have

$$I_s = \frac{V_i - V_i'}{R_1}. \qquad \dots \quad (4)$$

If no screen current were taken by the tube, the voltage across R_6 would increase to the value $V_i . \frac{R_6}{R_5 + R_6}$. But due to the screen current, the actual voltage will be smaller and may, by suitable choice of R_5 and R_6, be made exactly the same as it was previously, *viz.*, that given by (3). The method of calculation of the proper values of R_5 and R_6 is indicated below.

By Thevanin's theorem, the screen supply system may be replaced by the simple circuit having the constants as shown in Fig. 2. The condition to be satisfied is, therefore,

---

* The relation $V_0 = \frac{R_2 + R_3}{R_3} . (V_c - \epsilon)$ holds in the case when the battery is connected between the junction of R_2 and R_3 and the grid of the tube T_1.

$$\frac{R_6}{R_5+R_6} \cdot V_i - R_s I_s = V_s. \quad \dots \quad (5)$$

Next we are to prove that if equation (5) is satisfied at one value of V_i, it will hold for other values as well.

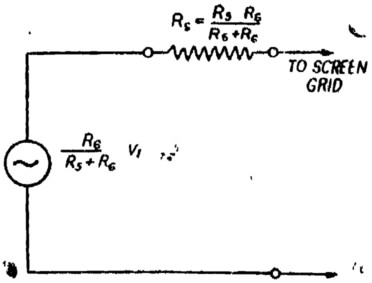

FIG. 2

Equivalent electrical circuit of the screen supply system

In other words, eq. (5) should be independent of V_i. Let us substitute eq. (4) in eq. (5). We get, after simplification,

$$\frac{R_6}{R_5+R_6} \cdot V_i - \frac{R_s a}{R} V_i + \frac{R_s a}{R_1} V'_i = V_s. \quad \dots \quad (6)$$

It is clear that the above equation will be independent of V_i, if

$$\frac{R_6}{R_5+R_6} = \frac{R_s a}{R_1}. \quad \dots \quad (7)$$

The other equality which equation (6) leads to is also satisfied by Equation (3).

The appropriate values of R_5 and R_6 can be calculated with the help of equations (3) and (7). They are

$$R_5 = \frac{R_1}{a} \quad \text{and} \quad R_6 = \frac{R_1}{a\left(\frac{V_i'}{V_s} - 1\right)} \quad \dots \quad (8)$$

It will be observed that the value of R_5 is independent of the voltages V_i or V_0. So that if the output voltage is changed by changing either R_3 or V_c, the value of R_5 need not be changed. But the value of R_6 will have to be changed so as to make a the same as before, as a depends on the screen and the anode voltages.*

For the sake of comparison, a circuit was set up, using nearly the same component values as were used by Neher and Pickering. The performance of the circuit, with a screen battery of 53 volts and with a potentiometer holding the screen voltage constant at 51 volts, is shown in the curves of Fig. 3. The effectiveness of the circuit in stabilizing its own screen voltage will be appreciated if a comparison is made between the screen voltage—input voltage curves depicted in Fig. 4.

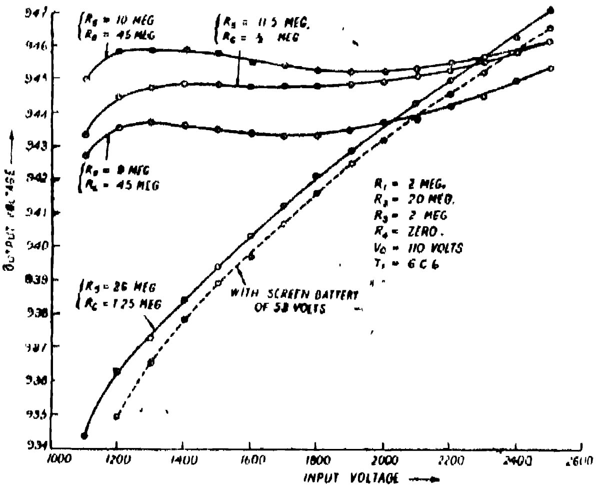

FIG. 3

Stabilization characteristics of the circuit of Fig. 1 for different values of the screen supply resistance. The curves for R_5 = 11·5 Meg. and R_6 = ½ Meg. shows that the output voltage variation is less than 0.1 volts over the input voltage range of 1400—1900.

The performance of the circuit can be considerably improved by utilising the screen grid as another control element of the stabilizer as described below.

The values of R_5 and R_6 may be so chosen that the screen voltage, instead of remaining constant, increases steadily with the input voltage. Under such condition the control applied to the screen grid forms a *transconductance* type stabilizer circuit and stabilizes the voltage at the output terminals even when no control is applied to the grid. A transconductance circuit gives perfect stabilization when the relation

---

* The screen current is not merely the primary electron current but may be greatly modified by secondary electrons ejected from the screen grid. These are drawn through the suppressor grid when a sufficiently high voltage is on the anode. The primary electron current, however, bears a constant ratio with the anode current, whatever may be the anode and screen voltages.

$$C S_m = \frac{1}{R_1} \qquad \dots \quad (9)$$

is satisfied. C gives the rate at which the voltage on the grid of the tube (in our case the screen grid) changes with change of the input voltage. Thus

$$C = \frac{dV_s}{dV_i} ;$$

S_m is the transconductance between the electrodes, being, in our case, the screen grid to anode transconductance.

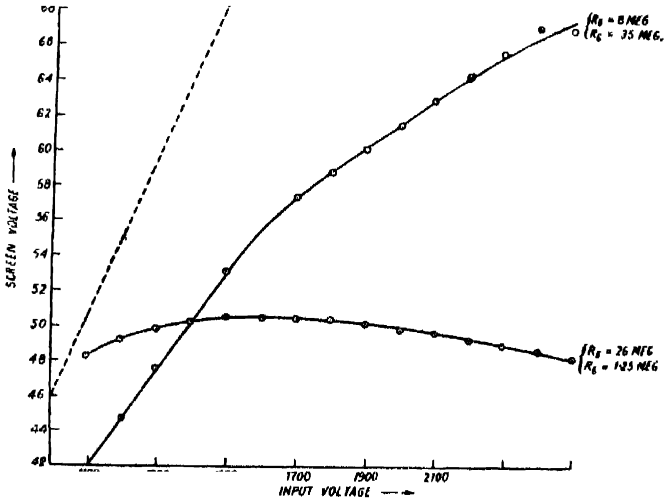

FIG. 4

Variation of screen voltage of the stabilizer tube with input voltage. It is to be noted how the variation of the screen voltage can be reduced by using suitable values (R_5=26 Meg. and R_6=1.25 Meg.) of the screen supply resistances. The dotted curve shows the variation of voltage across a potentiometer of 26 Meg. and 1.25 Meg

In the usual type of transconductance circuit where the control is applied to the grid maintained at a negative potential, the value of C is constant. In such a circuit the condition of perfect stabilization is satisfied at one value of the input voltage, *viz.*, where S_m has the value given by equation (9). At other values of the input voltage, the current through the tube being different, the transconductance is also different. As a result, such a circuit gives a high stabilization factor only over a small range on both sides of the input voltage where the condition given by the equation (9) is satisfied. In a screen grid anode transconductance so as to make a the same as before, as a depends on the screen and the anode voltages.*

For the sake of comparison, a circuit was set up, using nearly the same component values as were used by Neher and Pickering. The performance of the circuit, with a screen battery of 53 volts and with a potentiometer holding the screen voltage constant at 51 volts, is shown in the curves of Fig. 3. The effectiveness of the circuit in stabilizing its own screen voltage will be appreciated if a comparison is made between the screen voltage—input voltage curves depicted in Fig. 4.

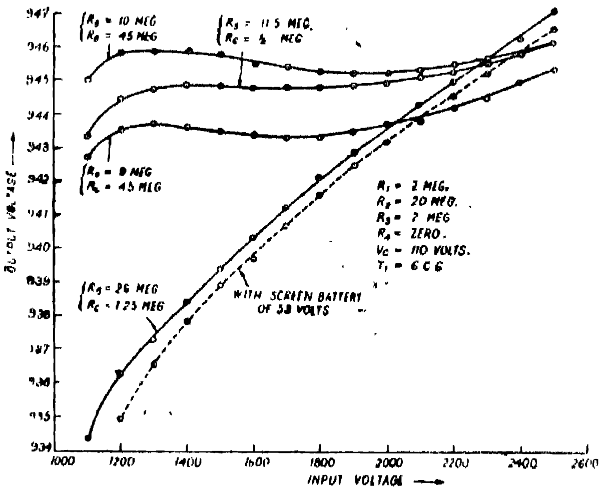

FIG. 3

Stabilization characteristics of the circuit of Fig. 1 for different values of the screen supply resistance. The curves for $R_5 = 11{\cdot}5$ Meg. and $R_6 = \frac{1}{2}$ Meg. shows that the output voltage variation is less than 0.1 volts over the input voltage range of 1400—1900.

The performance of the circuit can be considerably improved by utilising the screen grid as another control element of the stabilizer as described below.

The values of R_5 and R_6 may be so chosen that the screen voltage, instead of remaining constant, increases steadily with the input voltage. Under such condition the control applied to the screen grid forms a *transconductance* type stabilizer circuit and stabilizes the voltage at the output terminals even when no control is applied to the grid. A transconductance circuit gives perfect stabilization when the relation

---

* The screen current is not merely the primary electron current but may be greatly modified by secondary electrons ejected from the screen grid. These are drawn through the suppressor grid when a sufficiently high voltage is on the anode. The primary electron current, however, bears a constant ratio with the anode current, whatever may be the anode and screen voltages.

$$C\,S_m = \frac{1}{R_1} \tag{9}$$

is satisfied. C gives the rate at which the voltage on the grid of the tube (in our case the screen grid) changes with change of the input voltage. Thus

$$C = \frac{dV_s}{dV_i}\,;$$

S_m is the transconductance between the electrodes, being, in our case, the screen grid to anode transconductance.

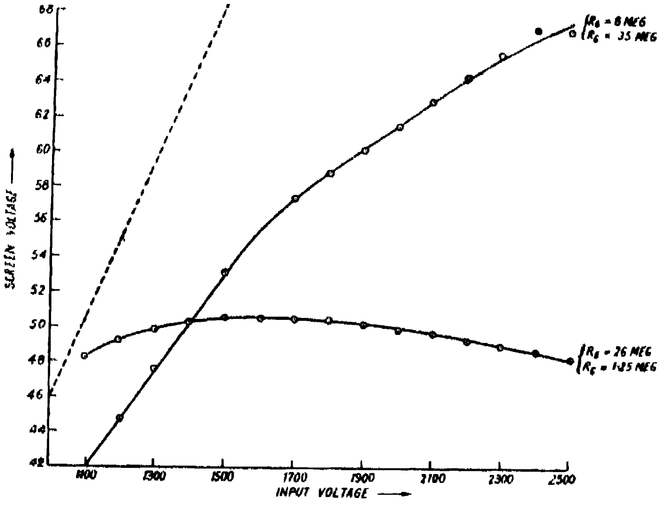

FIG. 4

Variation of screen voltage of the stabilizer tube with input voltage. It is to be noted how the variation of the screen voltage can be reduced by using suitable values ($R_5 = 26$ Meg. and $R_6 = 1.25$ Meg.) of the screen supply resistances. The dotted curve shows the variation of voltage across a potentiometer of 26 Meg. and 1.25 Meg

In the usual type of transconductance circuit where the control is applied to the grid maintained at a negative potential, the value of C is constant. In such a circuit the condition of perfect stabilization is satisfied at one value of the input voltage, *viz*., where S_m has the value given by equation (9). At other values of the input voltage, the current through the tube being different, the transconductance is also different. As a result, such a circuit gives a high stabilization factor only over a small range on both sides of the input voltage where the condition given by the equation (9) is satisfied. In a screen grid anode transconductance circuit, however, the value of C is not constant, being dependent on the rate of rise of screen current with input voltage. When the screen voltage is held constant, the magnitude of this quantity $\left(\frac{\partial I_s}{\partial V_i}\right)$ does not increase so much with the

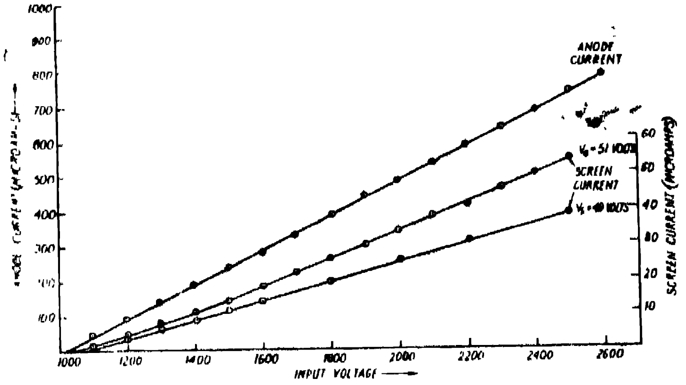

FIG. 5

Variation of the anode and screen currents of the stabilizer tube with input voltage.

input voltage V_i as will be seen from the two screen current curves in fig. 5, although it is still appreciable. If, however, the screen voltage increases with the input voltage, the increase in magnitude of $\frac{\partial I_s}{\partial V_i}$ becomes considerable as may be judged by comparing the two curves of Fig. 5. The result of this is to diminish the value of C as the input voltage increases. (See the screen voltage—input voltage curve for $R_5 = 8$ Meg. and $R_6 = .35$ Meg. in fig. 4.) This diminution of C with the input voltage may cause eq. (9) to be satisfied again at a higher value of input voltage giving perfect stabilization at another point on the higher voltage side as is depicted by the curves in Fig. 6. With a suitable choice of the values of R_5 and R_6 these two regions can be brought sufficiently close together giving high stabilization over a considerably wide range of voltages. Thus in the curve of $R_5 = 11.5$ Meg. and $R_6 = \frac{1}{2}$ Meg. where this condition is obtained, the output voltage varies by only 2 volts over a range of 300 volts. The dotted curve shows the nature of the stabilization characteristic if there were no screen current.

When control is applied both to the grid and to the screen grid, the stabilization curves become, as may be expected, very much better. This is shown in fig. 3. The curve for the circuit in which $R_5 = 11.5$ Meg. and $R_6 = \frac{1}{2}$ Meg. keeps the output voltage constant within 0.1 volt over the range of 1,400-1,900 volts. The resistance R_4 of the original Neher-Pickering circuit gives no advantage and is unnecessary. Better performance can be obtained even without it,

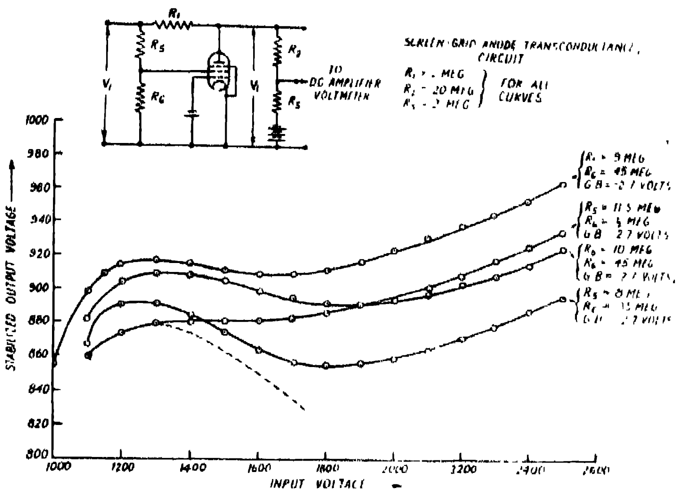

Fig. 6

Stabilization curves of the transconductance circuit which is formed when the screen voltage is supplied by a potentiometer

Experimental arrangement for testing the performance. The stabilizer circuit described above is ordinarily called upon to deliver small currents. Further, since the stabilization characteristics of the circuit are dependent on the value of the current drawn, it is necessary that the measuring instrument employed should consume little or no current. Accordingly a valve voltmeter may be used to measure the variations while the steady component is balanced out. Since the output voltage is high, it is convenient to make the measurements on a known fraction of the output voltage across a high resistance potential divider. A suitable arrangement is in the stabilizer circuit itself, *viz.*, the resistance R_2, R_3 and the battery V_c (Fig. 1). The voltage variations across the grid cathode of the stabilizer tube may therefore be measured for testing the performance. A specially designed valve voltmeter was used for this purpose. The circuit was similar to that of the one described by Roberts[4] and incorporated a variable degeneration resistance which was used as a sensitivity control.

(*b*) *Two-Valve Circuit.* The two-valve circuit of Neher and Pickering gives much better performance than the single-valve circuit. It has a higher stabilization ratio, lower internal resistance and is also capable of delivering large currents. The circuit, however, has the disadvantage that it requires as many as four dry batteries of which one has to be insulated very thoroughly.

The modified form uses only two batteries none of which demand very thorough insulation. The performance of the modified circuit, instead of deteriorating, is actually somewhat improved. The circuit is shown in Fig. 7.

It will be observed that the screen battery E_{s_2} and the grid battery E_{g_1} of the Neher-Pickering circuit have been eliminated. The arrangement for the screen supply of T_2 as used here is more convenient than a tap across R_2 as suggested by Neher and Pickering in the sense that it is now possible to change the output voltage by changing R_2, without affecting the screen voltage. The screen voltage is equal to $(V_1 - \epsilon)$, where ϵ is the grid voltage at which the tube T_2 operates. Not only does this method of connection save one battery, but actually it improves the performance although only by a small amount. Here the control is applied both to the grid and the screen grid as a result of which the effective gain G of the tube T_2 increases by about 5 to 6 per cent and with it the stabilization ratio.*

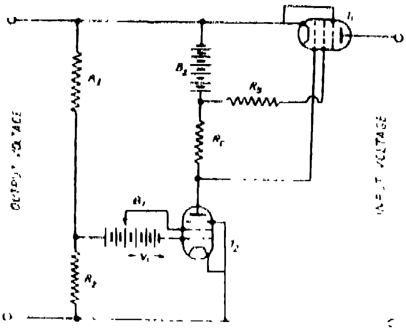

FIG. 7

Modified two-valve Neher-Pickering circuit. The two batteries in the circuit perform the duties of the four used in the original one.

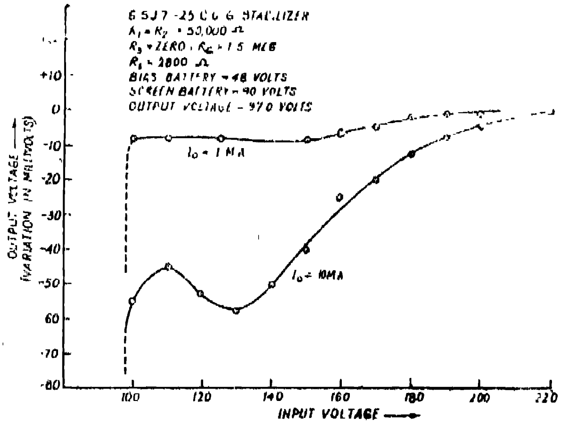

FIG. 8

Stabilization curves of the modified two-valve Neher-Pickering circuit

---

* The stabilization factor can be easily shown to be equal to $\frac{R_2}{R_1+R_2} \cdot G \cdot \mu$ to a very near approximation, where μ is the amplification factor of the tube T_1.

In the circuit described above the battery B_2 performs both the functions of the screen battery Es_1 and the grid battery Eg_1. The function of Eg_1 has been to increase the gain of T_2 by making the voltage drop across R_c and so the current through T_2 greater than what is otherwise possible. This battery has to be very carefully insulated and shielded. In the circuit by the author the battery B_2, which replaces this, requires only normal insulation. A leakage from B_2 to the negative line will affect the performance only in that it will place an extra load on the stabilizer.

The results on circuits of this type are shown by the curves in Fig. 8. All the measurements were carried out at low voltages but there is no reason why the circuit should not operate efficiently at high voltages.*

3. IMPROVEMENTS ON TWO-VALVE STABILIZERS

In this section two-valve stabilizer circuits embodying certain new principles are described. The circuits give considerably improved performance and have an extended range of usefulness. They are described under three heads, *viz.*, (*a*) A circuit giving "perfect" stabilization ; (*b*) A circuit for stabilizing the heater currents of vacuum tubes in valve voltmeters, etc. ; and (*c*) A circuit having negative internal resistance.

The mathematical analysis of a circuit embodying all these principles is given. The design of these stabilizers as regards the choice of suitable valves and their operating conditions is also discussed.

(*a*) *A circuit giving "Perfect" stabilization.* The usual two-valve stabilizer circuit like those shown in figs. 7 and 13 cannot give perfect stabilization, *i.e.*, the change in output voltage dV_0 can never become zero for a change dV_i in the input voltage although it may be very small in comparison. The very nature of operation of these circuits demand the presence of some control voltage at the grid of the tube T_2. This control voltage is furnished by the change in the output voltage dV_0 in the usual two-tube circuits. However the necessary control voltage may be easily supplied from the varying input voltage. In that case, no additional change in output voltage will be necessary to provide extra control and in this sense the circuit may be said to give perfect stabilization. A circuit embodying this principle is shown in fig. 9.

---

* It is necessary to mention here certain important precautions. When voltage changes of the order of millivolts are encountered, it was found absolutely necessary to use fixed resistances, preferably the wire-wound type for R_1 and R_2. Otherwise the spontaneous changes of voltage resulting from the fluctuations of the variable resistance completely swamp the changes which are to be measured. Further it may also be necessary to supply the heater voltage of T_2 from batteries. With two 6SJ7 tubes for T_1 and T_2, it was found necessary to short-circuit the resistance R_1, to use a heater battery and further to take the readings very quickly in order to get a proper measure of the stabilization. The stabilization factor of the circuit was of the order of a million.

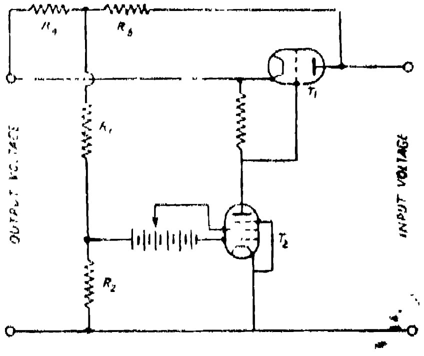

FIG. 9
A circuit capable of "perfect" stabilization

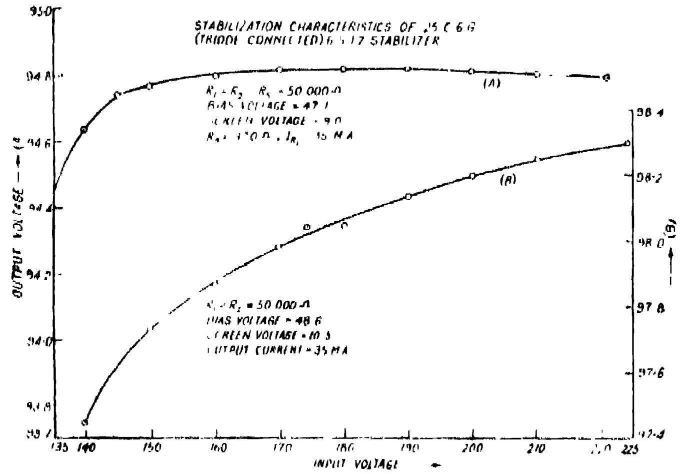

FIG. 10
Performance of the circuit of Fig. 9 compared with that of a straightforward two-valve circuit

The improvement in performance over the usual circuit will be evident from the curves in fig. 10. It will be seen that the stabilization characteristic of the single-battery two-tube circuit of this type is comparable to that of two-battery circuits shown in fig. 7. Circuits of this type are therefore strongly recommended for all classes of voltage stabilizer work.

(b) *A stabilizer for high currents.* A stabilized supply capable of giving currents much higher than can be carried by the tube or tubes in the position T_1 is sometimes necessary. A circuit has been developed from the usual two-tube circuit for this purpose. The most useful form is shown in fig. 11.

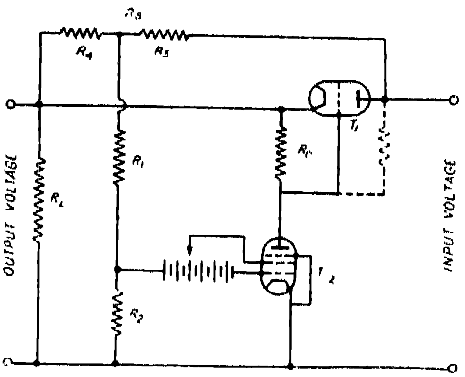

FIG. 11

A stabilizer circuit suitable for large current drains.

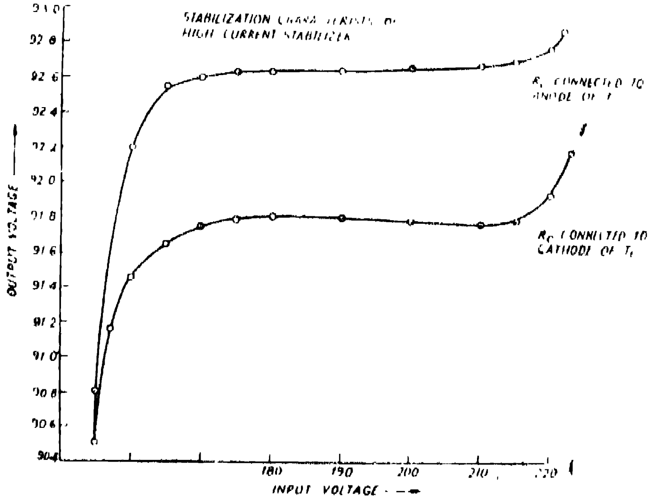

FIG. 12

Stabilization characteristics of a high current stabilizer. The curves are for a circuit using a 25 C6 G for T_1 and 6SJ7 for T_2 delivering an output current of 150 milliamps. R_1 and R_2 were both equal to 50,000 Ω and R_4 was adjusted for perfet stabilization.

From the curves in fig.12 it will be evident that stabilization occurs only over a range of input voltage, that from V_l to V_h. This is because the tubes T_1 and T_2 operate only over this range. At the high voltage end V_h, the whole of the current I_0 that the stablizer has to supply flows through R_s so that the tube T_1 is biased to the non-conducting condition. Hence we have the relation

$$\frac{V_h - V_0}{R_s} = I_0 . \quad \cdots \quad (10)$$

At the low voltage end V_l, the grid bias of tube T_1 approaches the zero value and cannot change any further, due to the fact that the current through T_2 is zero. In case R_c is connected to the anode of T_1 as shown dotted in Fig. 11, the grid of T_1 goes positive only by the amount that is necessary for it to draw the whole of current that comes through R_c, leaving nothing for T_2. If the current through T_1 at this point be I_m, then we have

$$\frac{V_l - V_a}{R_s} + I_m = I_a. \qquad \ldots \quad (10b)$$

The two equations (10*a*) and (10*b*) locate the points V_h and V_l.

Subtracting equation (10*b*) from equation (10*a*) and simplifying, we get

$$V_h - V_l = I_m . R_c. \qquad \ldots \quad (11)$$

If the mean value of the supply voltage be V_s and if R_c be adjusted such that it falls at the middle point of the horizontal part of the stabilization characteristic, then we can also write

$$\frac{V_s - V_a}{R_c} + \frac{I_m}{2} = I_a.$$

Combining with equation (11) and putting $\frac{V_h - V_l}{V_s} = R$ — the range of stabilization, we get finally

$$R = \frac{I_m}{I_a - I_m/2} \cdot \frac{V_s - V_a}{V_s} \cdot 100 \text{ per cent.} \qquad \ldots \quad (12)$$

It will be seen that the range increases as the ratio $\frac{I_m}{I_a - I_m/2}$ increases. The value of $\frac{V_s - V_a}{V_s}$ cannot exceed unity and should peferably be not lower than half. The heater supply of 0.3 ampere tubes may be stabilized over a range of 12% (±6%) using a 25C6G tube for T_1. This is somewhat small compared to that of a commercial " stabilizing transformer " which has a range of about ±15%. However, the stabilizer described here has the advantage of giving much better stabilization than any stabilizing transformer. Also if a wider range is necessary, one may use two 25C6G tubes in parallel for T_1.

(*c*) *A circuit having negative internal resistance.* Stabilizer circuits so far described* all have positive internal resistance, *i.e.*, the voltage at their output terminals decreased with increase in current drain. But in various applications it is highly desirable to have a voltage source capable of maintaining a constant voltage across its terminals even under varying current drains, *i.e.*, a source having zero internal resistance. It may even be desirable to have a source whose terminal voltage should increase with increase in current drain, in order that this increase may compensate for the increased voltage drop across some other circuit element through which the current may be flowing. In such cases, a voltage source with negative internal resistance is required.

---

* For discussion and reference see *Science and Culture*, **6**, 552 (1941).

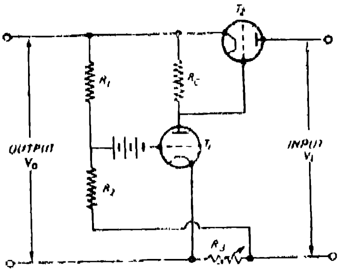

FIG. 13

Typical stabilizer circuit having negative internal resistance.

The resistance R_3 between the cathode of T_2 and the negative line in Fig. 13 brings about this property in two-valve voltage stabilizer circuits. A simple analysis gives the internal resistance R_0 defined by the relation $R_0 = -\left(\frac{\partial V_o}{\partial I_o}\right)_{V_i}$ as, $R_0 = \left[\frac{1}{G.A.b} - R_3\left(\frac{1}{b} - 1\right)\right]$ approximately, ... (13)
where G is the mutual conductance of the tube T_1, A, the amplification given by T_2 and $b = \frac{R_2}{R_1 + R_2}$

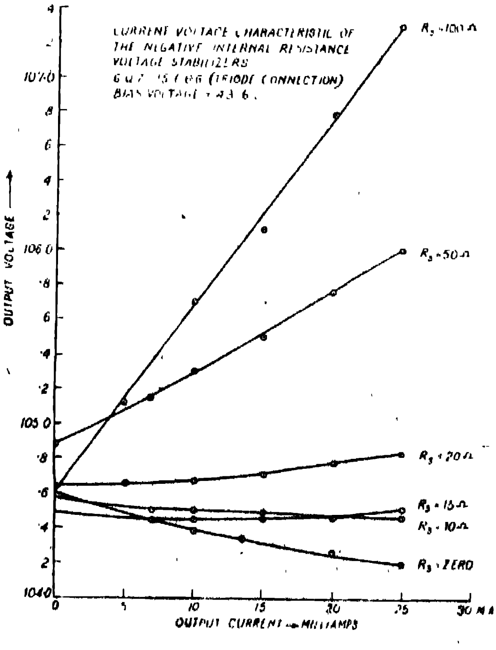

FIG 14

Current voltage curves of the circuit of Fig. 13 using 25C6G and 6Q7 tubes for T_1 d T_2

It will be seen that by a suitable choice of the value of R_3, one can make the internal resistance zero or negative. A negative value of several hundred ohms is not difficult to attain.

The stabilization factor of the circuit remains practically unaffected by the inclusion of R_3 and is approximately given by

$$S_0 = b.A.\mu$$

where μ is the amplification factor of the tube T_1.

A number of voltage current curves using two triodes for T_1 and T_2 in the circuit of fig. 13 is shown in fig. 14.

A voltage stabilizer with zero or negative internal resistance has great possibilities as a bias supply system of high power class B audio amplifiers. The grid current which flows in these systems when the grid swing is positive increases the negative bias. This increase of negative grid bias with the grid swing increases the distortion in the audio output. As a result the bias supply system has to be so designed that they present a very low internal resistance in order that the rise in the negative bias may be very small. Such a design is expensive. The problem can better be solved using a voltage stabilizer with zero internal resistance. It may be supplied by an ordinarily designed transformer-rectifier-filter system. The stabilizer will also smooth out the residual ripple in the bias voltage to a very low value.

The average anode current of a class B audio amplifier increases with the grid swing. This reduces the D.C. anode voltage and brings about further distortion in the audio output. This distortion due to anode circuit regulation can be minimized by making the grid bias diminish as the average anode current increases. It has been observed by Rockweli and Platts[5] that the distortion is also prevented

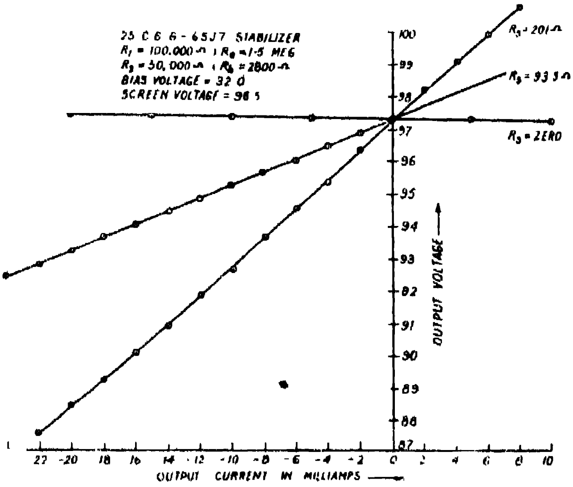

FIG. 15

Current-voltage characteristics of the circuit proposed for use as a bias supply system of class B amplifiers in a great measure if the grid bias is made to diminish with the grid current instead of the anode current. A voltage stabilizer having negative internal resistance, such as that shown in fig. 13 may be expected to perform this function. The circuit, however, has got to be modified by the inclusion of a bleeder resistance R_b across R_1 and R_2 or across the output terminals. For as the current that is forced into the system exceeds the value

$$I_m = \frac{v_o}{R_b} \qquad \ldots \quad (14)$$

the current I_t through the tube T_1 becomes equal to zero and the circuit ceases to function as 'G' and 'a' both are zero in this condition. It is evident that the internal resistance in this condition, of the two circuits, becomes equal to $(R_b + R_3)$ and R_b respectively. (See eq. 20.) For bias supply systems of class B amplifiers, I_m must exceed the maximum grid current

$$I_m \geqq I_g \qquad \ldots \quad (15)$$

and the tube or tubes for T_1 should be chosen keeping this in mind. The bias voltage v_o being known R_b should be calculated from (14) and (15).

(*d*) *Mathematical theory of the two-valve stabilizers.* The mathematical theory of the most general form of two-valve stabilizer circuit as shown in Fig. 16 is worked out below.

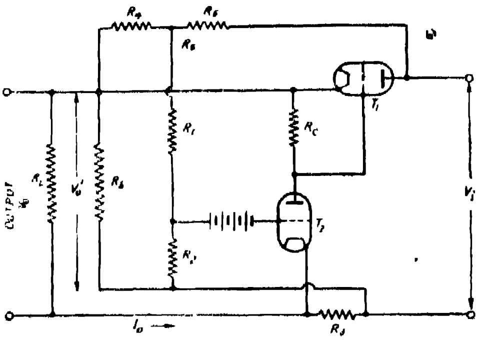

FIG. 16

Illustrating the general form of two-valve stabilizer circuit

The stabilization factor "*S*". Let the input voltage V_i change by an amount δV_i and let the resulting change in output voltage be δV_o. Let V_o', the voltage across R_b, change by an amount $\delta V_o'$. Then we can write for the grid voltage of T_2

$$\delta v_2 = b\{\delta V_o' + \rho(\delta V_i - \delta V_o')\} - R_3 \delta I_o$$

---

v_o is the output voltage when the current forced into the system is equal to I_m.

where $b=\frac{R_2}{R_1+R_2}$ and $\rho=\frac{R_4}{R_4+R_5}$; δI_0 the change in current through R_L is equal to $\frac{\delta V_0'}{R_L+R_3}$. Hence $\delta v_2 = b\left\{\delta V_0'\left(1-\rho-\frac{R_3/b}{R_L+R_3}\right)+\rho\delta V_i\right\}$.

The change in grid voltage of T_1 is, therefore,

$$\delta v_1 = -gR_c\left[b\left(1-\rho-\frac{R_3/b}{R_L+R_3}\right)\delta V_0'+b\rho\delta V_i\right]-\frac{R_c}{R_c+R_r}\delta V_0'$$

$$= -k'\delta V_0'-k''\delta V_i$$

where
$$\left.\begin{aligned} k' &= gR_c b\left(1-\rho-\frac{R_3/b}{R_L+R_3}\right)+\frac{R_c}{R_c+R_r} \\ k'' &= gR_c b\rho. \end{aligned}\right\} \qquad \dots \quad (17)$$
and

The change in total current, since the change through R_s is equal to

$$\frac{1}{R_s}(\delta V_i-\delta V_0'),$$

$$\delta I = -Gk'\delta V_0'-Gk''\delta V_i+\left(a+\frac{1}{R_s}\right)\left(\delta V_i-\delta V_0'\right).$$

This produces a change of voltage $\delta V_0'$ across R_b which may be written as

$$\delta V_0' = \frac{R_b(R_L+R_3)}{(R_b+R_L+R_3)}.\ \delta I$$

$$= \frac{R_b(R_L+R_3)}{(R_b+R_L+R_3)}\left[-Gk'\delta V'_0-Gk''\delta V_i+\left(a+\frac{1}{R_s}\right)\left(\delta V_i-\delta V'_0\right)\right]$$

whence
$$\frac{\delta V_i}{\delta V'_0} = \frac{1+\frac{R_b(R_L+R_3)}{R_b+R_L+R_3}\left[Gk'+a+\frac{1}{R_3}\right]}{\frac{R_b(R_L+R_3)}{R_b+R_L+R_3}\left[a+\frac{1}{R_3}-Gk''\right]}.$$

Also
$$V_0 = (V'_0-R_3I_0)$$

so that $\delta V_0 = \delta V'_0-R_3\delta I_0, \quad = \frac{R_L}{R_L+R_3}\delta V_0'.$

Therefore the stabilization ratio S_0 is equal to

$$\frac{\delta V_i}{\delta V_0} = \frac{1+\frac{R_b(R_L+R_3)}{R_b+R_L+R_3}\left[Gk'+a+\frac{1}{R_s}\right]}{\frac{R_b(R_L+R_3)}{R_b+R_L+R_3}\left[a+\frac{1}{R_s}-Gk''\right]}\cdot\frac{R_L+R_3}{R_L} \qquad \dots \quad (18)$$

The value of ρ for perfect stabilization may thus be found. The stabilization ratio approaches infinity when

$$a+1/R_s \longrightarrow Gk'' \quad Gk'\rho \quad \text{or} \quad 1/\rho \longrightarrow \frac{Gk'+a+1/R_s}{a+1/R_s}-1. \qquad \ldots \quad (19)$$

Now $\dfrac{Gk'+a+1/R_s}{a+1/R_s}$ is very nearly equal to the stabilization factor when R_4 and R_5 are zero. This may be found out experimentally when equation (19) will give the value of ρ.

Internal Resistance R_0. When a current δI_0 is drawn, let the change in output voltage be δV_0 and the change in voltage across R_b be $\delta V_0'$. Then we have, for the change in grid voltage of T_2,

$$\delta v_2 = b\{\delta V_0' - \rho\delta V_0'\} - R_3\delta I_0.$$

The change in grid voltage of T_1 is, therefore,

$$\delta v_1 = -gR_c[b(1-\rho)\delta V_0' - R_3\delta I_0] - \frac{R_c}{R_c+R_r} \cdot \delta V_0'$$

$$= -A[b(1-\rho)\delta V_0' - R_3\delta I_0]$$

neglecting $\dfrac{R_c}{R_c+R_r} \cdot \delta V_0'$ and putting $g\,R_c = A$.

The change in anode current of T_1 is therefore equal to

$$\delta I_a = -AG[b(1-\rho)\delta V_0' - R_3\delta I_0] - a\delta V_0'.$$

The change in current through R_s is equal to $-\dfrac{\delta V_0'}{R_s}$. The change in current through R_b is equal to $\dfrac{\delta V_0'}{R_b}$. Hence the change in output current

$$\delta I_0 = -\left[AGb(1-\rho) + a + \frac{1}{R_s} + \frac{1}{R_b}\right]\delta V_0' + AGR_3\delta I_0$$

or

$$\delta V_0' = -\frac{[1-AGR_3]}{\left[AGb(1-\rho) + \left(a + \dfrac{1}{R_s} + \dfrac{1}{R_b}\right)\right]}\,\delta I_0$$

Now

$$\delta V_0 = \delta V_0' - R_3\delta I_0$$

Hence

$$R_0 = -\left(\frac{\delta V_0}{\delta I_0}\right)_{v_i} = \frac{[1-AGR_3]}{\left[AGb(1-\rho) + \left(a + \dfrac{1}{R_s} + \dfrac{1}{R_b}\right)\right]} + R_3 \qquad (20)$$

(c) *General consideration on the design of two-valve Stabilizers.* It is possible to obtain zero internal resistance and infinite stabilization ratio by using any combination of tubes for T_1 and T_2 in the circuit of Fig. 16. These conditions will, however, be satisfied only over a narrow range of input voltages unless the tubes are properly selected and operated. The performance of the stabilizer under actual operating conditions is better described by the stabilization and current-voltage characteristics rather than by the stabilization ratio and internal resistance at certain points.

Good stabilization and current-voltage characteristics can be secured only if these characteristics are inherently good, *i.e.*, if the characteristics without R_4 and R_3 are linear and have a small slope. The function of R_4 and R_3 is only to change the slope of the curves so as to make them horizontal. If the slope is not small so that the correction required is large and if the curve is not linear initially, the final characteristic, although it may be made horizontal at certain points, will not be so over a wide range.

The inherent characteristics will be good if the tubes T_1 and T_2 are so selected and operated that the quantity G.A.b is large and has as constant a value as possible over the whole range of plate currents of the tube T_1. $b = R_2/(R_1 + R_2)$ has a constant value which cannot exceed unity. It is also usually limited to a small fraction inasmuch as it is also equal to V_c/V_0 and the battery voltage V_c cannot conveniently and economically have a value much greater than 100 volts. The tube T_1 should be selected as one having a high, and as far as possible a constant, value of the mutual conductance G. Beam tubes, because of their uniform electrode structure and high mutual conductance are most suited for this purpose. These may be used with the screen grid connected to the anode so as to make them virtually a triode. The tube T_2 should be a sharp-cut-off pentode. A sharp-cut-off pentode gives much greater amplification than any triode or pentode of the remote-cut-off type. The amplification 'A' however decreases as the voltage drop across R_c, *i.e.*, the grid bias of T_1, diminishes. But the mutual conductance G of the tube T_1 increases as the plate current increases due to the reduction of the grid bias. As a result of this, the product GA tends to be more constant over a range of plate currents of the tube T_1. This makes the current-voltage characteristic of stabilizers of both types and the stabilization characteristic of the high current stabilizer more linear than is otherwise possible.

The tube T_2 should be operated with a low screen voltage,* of the order of 10-20 volts, and a high value of the coupling resister R_6. This enables it to give a greater and more constant amplification.

---

* With a stabilizer using 25C6G and 6SJ7 tubes for T_1 and T_2 respectively a screen voltage of 4.5 volts gave the best stabilization curve. The stabilization characteristic deteriorated rapidly below this optimum and relatively slowly above this.

Although R_r forms in effect the grid leak of the tube T_1, its value need not be limited to the usual ¼MΩ or ½MΩ recommended by tube manufacturers and may with advantage be considerably exceeded. Any tendency towards the diminution of grid voltage due to collection of positive ions, etc., by the grid and the resulting increase in anode current, increases the output voltage, a fraction of which is applied to the grid of T_2. The anode current of T_2 rises in consequence and takes away the major part of the positive ion current. As a result of this self-adjusting action a much higher value than is recommended by tube makers may be tolerated for R_r. Higher values of R_r are advantageous in that they enable the tube T_2 to give a greater amplification.

The battery voltage V_r and so the value of "b" should be as large as is economically and conveniently possible. This not only gives a better inherent stabilization and current-voltage characteristic but also makes the output voltage less dependent on the filament voltage of T_2.

4. EFFECT OF SOURCE RESISTANCE IN MODIFYING THE PERFORMANCE OF A VOLTAGE STABILIZER

(*a*) *Nature of the problem.* The performance of voltage stabilizers is modified if the primary source has appreciable internal resistance. This effect has been studied by Hunt and Hickman.[1] We are presenting here a more general analysis which is also more simple and straightforward.

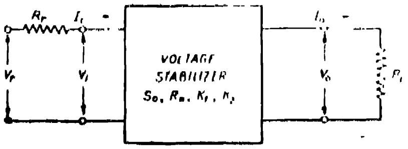

FIG. 17

Equivalent circuit of the stabilizer together with the primary source

The overall stabilization ratio S and internal resistance R of the stabilizer system, when the primary source has an internal resistance R_r, may be defined as

$$S = \frac{dV_r}{dV_0} \qquad \dots (21)$$

and

$$R = -\left(\frac{\partial V_0}{\partial I_0}\right)_{v_r}, \qquad \dots (22)$$

whereas the corresponding ratios for the voltage stabilizer alone are

$$S_0 = \frac{dV_i}{dV_0} \qquad \dots (23)$$

and

$$R_0 = -\left(\frac{\partial V_0}{\partial I_0}\right)_{v_i}, \qquad \dots (24)$$

v_r denoting the e.m.f. of the source.

Our problem is to express the values of S and R in terms of the constants of the voltage stabilizer, the source resistance R_r and the load resistance R_l.

(*b*) *Overall Stabilization Ratio.* We have the overall stabilization ratio

$$S = \frac{dV_r}{dV_0},$$

which may be written with the help of equation (23) as

$$\left(\frac{dV_r}{dV_i}\right).S_0. \qquad \ldots \quad (25)$$

Now we have,

$$V_r = V_i + R_r I_i \qquad \ldots \quad (26)$$

where I_i is the current taken in by the voltage stabilizer. This can be written as

$$I_i = I_0 + K_1 V_i + K_2 V_0, \qquad \ldots \quad (27)$$

where K_1 and K_2 are the leakage conductances present across the input and output terminals of the voltage stabilizer.

Hence, substituting in (26) we get after simplification

$$V_r = V_i(1 + R_r K_1) + \left(\frac{R_r}{R_L} + R_r K_2\right)V_0,$$

whence

$$\frac{dV_r}{dV_i} = 1 + R_r K_1 + \left(\frac{R_r}{R_L} + R_r K_2\right)\frac{1}{S_0}. \qquad \ldots \quad (28)$$

Substituting this in (25), we get

$$S = S_0(1 + R_r K_1) + \frac{R_r}{R_L} + R_r K_2. \qquad \ldots \quad (29)$$

This gives the overall stabilization factor "S" in terms of the constants of the stabilizer S_0, K_1, K_2, the source resistance R_r and the load resistance R_L.

(*c*) *Overall Internal Resistance.* When an excess current δI_o is drawn, the change in output voltage δV_o may be written as

$$\delta V_o = \left(\frac{\partial V_o}{\partial I_o}\right)_{V_i} \delta I_o + \left(\frac{\partial V_o}{\partial V_i}\right)_{I_o} \delta V_i$$

or

$$\left(\frac{\partial V_o}{\partial I_o}\right)_{V_r} = \left(\frac{\partial V_o}{\partial I_o}\right)_{V_i} + \left(\frac{\partial V_o}{\partial V_i}\right)_{I_o} \cdot \left(\frac{\partial V_i}{\partial I_o}\right)_{V_r}. \qquad \ldots \quad (30)$$

We are to find the value of $\left(\frac{\partial V_o}{\partial V_i}\right)_{I_o}$. For this we note

$$\frac{dV_o}{dV_i} = \left(\frac{\partial V_o}{\partial V_i}\right)_{I_o} + \left(\frac{\partial V_o}{\partial I_o}\right)_{V_i} \cdot \left(\frac{\partial I_o}{\partial V_i}\right),$$

whence
$$\left(\frac{\partial V_o}{\partial V_i}\right)_{I_o}=\left(\frac{dV_o}{dV_i}\right)-\left(\frac{\partial V_i}{\partial I_o}\right)_{V_i}\cdot\left(\frac{\partial I_o}{dV_i}\right)=\frac{1+R_o/R_L}{S_o}. \qquad \ldots \quad (31)$$

The change in voltage δV_i, V_r remaining constant due to a change of output current δI_o may be obtained as follows :

We have, $\delta V_i = -R_r\,\delta I_i$

Now $I_i = I_o + K_1 V_i + K_2 V_o = I_o + K_1(V_r - R_r I_i) + K_2 I_o R_L$,

whence
$$\left(\frac{\partial I_i}{\partial I_o}\right)_{V_r}=\frac{1+K_2R_L}{1+K_1R_r}$$

and
$$\left(\frac{\partial V_i}{\partial I_o}\right)_{V_r}=\left(\frac{\partial V_i}{\partial I_i}\right)\cdot\left(\frac{\partial I_i}{\partial I_o}\right)_{V_r}=-R_r.\frac{1+K_2R_L}{1+K_1R_r}. \qquad \ldots \quad (32)$$

Substituting (31) and (32) in (30) the overall internal resistance comes out as
$$R=-\left(\frac{\partial V_o}{\partial I_o}\right)_{V_r}=R_o+\frac{(1+R_o/R_L)(1+K_2R_L)}{(1+K_1R_r)}\cdot\frac{R_r}{S_o}. \qquad \ldots \quad (33)$$

It will be observed from equations (28) and (33) that the source resistance has only very slight effect on the performance of stabilizers having high stabilization ratios.

CONCLUSION

In the single-valve circuit described by Neher and Pickering, the screen grid may be conveniently supplied from a potential divider across the input terminals instead of from the usual dry battery. The fluctuations of the screen voltage with the input voltage may then be greatly reduced because the screen grid current fluctuates with the input voltage and this produces a voltage fluctuation in the opposite sense. Further, the performance is considerably improved if the screen grid potential fluctuates in a prescribed manner. In fact, the performance is better than that of a circuit using a dry battery for the screen supply.

It is possible to eliminate two of the four dry batteries in the two-valve circuit described by Neher and Pickering by an improved method of connection, whereby each battery is made to perform the function of two batteries simultaneously.

The two-valve degenerative amplifier type of stabilizer can be made to give "perfect" stabilization and "zero" or negative internal resistance. This is achieved by applying to the grid of the amplifier tube, over and above the usual control derived solely from the output voltage, small voltages which are proportional to the input voltage as also to the output current. The performance of the resulting circuits is superior in almost every respect to other types of stabilizer circuits. Such a circuit, with negative internal resistance is very useful in reducing distortion of class B power amplifiers.

The high current stabilizer which has been developed from the two-valve stabilizer circuit gives better stabilization than any "stabilizing transformer" or "baretter" tube and may be used for supplying the heaters of thermionic tubes employed in sensitive valve voltmeters.

ACKNOWLEDGMENTS

The author wishes to express his sincere gratitude to Professor S. K. Mitra for his kind interest and to Dr. H. Rakshit for his constant advice during the progress of the work.

Wireless Laboratory,
University College of Science,
92, Upper Circular Road,
Calcutta.

REFERENCES

1 Hunt and Hickman, *Rev. Sci. Instr.*, **10**, 9 (1939).
2 Evans, *Rev. Sci. Instr.*, **5**, 371 (1934).
3 Neher and Pickering, *Rev. Sci. Instr.*, **10**, 53 (1939).
4 Roberts, *Rev. Sci. Instr.*, **10**, 181 (1939).
5 Rockwell and Platts, *Proc. I. R. E.*, **24**, 553 (1936).

OVERALL VOLTAGE GAIN OF LOW FREQUENCY AMPLIFIERS WITH NEGATIVE RESISTANCE*

BY A. S. RAO, M.Sc.

(Received for publication, November 7, 1941)

ABSTRACT. A detailed study of the low-frequency amplifiers has been made to investigate the loss of amplified voltage while it is transferred from one stage to the other. An equivalent circuit of a resistance-capacity-coupled amplifier has been analysed and it is found that the loss of voltage will be minimum with a negative grid resistance the value of which depends on the circuit elements. It is also pointed out that the maximum value of the gain increases for high values of the coupling condenser. The above conclusions are verified by using the negative resistance of a dynatron valve in the grid circuit of the valve in the second stage of the amplifier.

INTRODUCTION

The overall voltage gain of a low-frequency valve amplifier of more than one stage is generally found to be sensibly less than that calculated theoretically from the constants of the valves used and the circuit components connected with them. This disagreement has often been attributed partly to the stray and fixed capacities and inductances involved in the circuit, and partly to the behaviour of the valve under the circumstances.[1,2,3]

In the present communication a detailed study has been made of low-frequency amplifiers investigating the cause of the loss of amplified voltage when the energy is transferred from one valve to the next following it. A preliminary note on this has already been published.[4] A two-stage low-frequency resistance-capacity-coupled amplifier was employed for the present investigation and it has been found after analysis of such circuit that the primary seat of attenuation of voltage transferred from one stage to the other lies in the intervalve coupling components. Out of all the components the grid resistance of the second valve only can be varied at will for compensating the loss of voltage incurred without causing any serious alteration in the circuit or valve parameters. The minimum loss of voltage is, however, obtained only by a negative resistance in the grid circuit of the second valve, the exact value of which has been calculated mathematically as shown subsequently. The condition of minimum loss has been verified experimentally by applying a negative resistance with a dynatron valve along

---

Communicated by the Indian Physical Society.

with a fixed positive resistance in parallel with it in the grid circuit of the second valve. The resistance of the dynatron was varied from positive to negative values by changing the grid and plate potentials applied, and the gradual change of the overall amplification passing through the maximum value has been recorded.

THEORY

The equivalent circuit diagram of a resistance-capacity-coupled low-frequency amplifier is shown in fig. 1. R_1 represents the plate resistance of the first valve

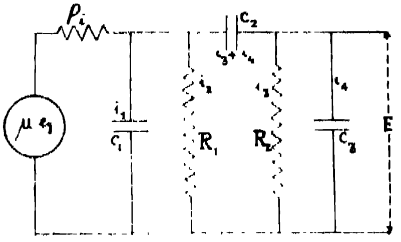

FIG. 1

and R_2 represents the grid resistance of the second valve. C_1 and C_3 are the inter-electrode capacities of the valves. C_2 is the coupling condenser. ρ· represents the internal resistance of the first value V_1. Let i_1, i_2, i_3 and i_4 be the currents flowing through different branches of the circuit and i the total current as shown in fig. 1.

If w be the angular frequency of the input e.m.f., the following circuit equations can be obtained from fig. 1.

$$i = i_1 + i_2 + i_3 + i_4 \qquad \ldots \quad (1)$$

$$\mu e_g = \rho i + \frac{i_1}{jwC_1} \qquad \ldots \quad (2)$$

$$R_1 i_2 = \frac{i_1}{jwC_1} \qquad \ldots \quad (3)$$

$$R_2 i_3 : \qquad \ldots \quad (4)$$

$$R_1 i_2 = \frac{i_3 + i_4}{jwC_2} + R_2 i_3. \qquad \ldots \quad (5)$$

If the value of i_2 obtained from equation (5) be substituted in equation (3) and i_4 be expressed in terms of i_3, we will get

$$i_1 = \frac{C_1}{C_2}(i_3 + jwC_3R_2i_3) + jwC_1R_2i_3. \qquad \ldots \quad (6)$$

From equations (1) and (2) we get after some simplifications

$$\mu e_g = \rho\left\{ \frac{C_1}{C_2}\,(i_3 + jwC_3R_2i_2) + jwC_1R_2i_3 \right\}$$

$$+ \frac{\rho}{R_1}\left\{ \frac{1}{jwC_2}\,(i_3 + jwC_3R_2i_3) + R_2i_3 \right\}$$

$$+ \rho i_3 + jwC_3\rho R_2 i_3 + \frac{1}{jwC_2}\,(i_3 + jwC_3R_2i_3) + R_2i_3. \quad \dots \quad (7)$$

Taking the output voltage E to be equal to R_2i_3 and eliminating the currents we can rewrite the above equation (7) as

$$\mu e_g = E\left[\left\{ 1 + \frac{\rho C_1}{R_2C_2} + \frac{\rho C_3}{R_1C_2} + \frac{\rho}{R_1} + \frac{\rho}{R_2} + \frac{C_3}{C_2} \right\} \right.$$

$$\left. + j\left\{ \frac{w\rho C_1C_3}{C_2} + w\rho C_1 - \frac{\rho}{wC_2R_1R_2} + \rho wC_3 - \frac{1}{wC_2R_2} \right\} \right]. \quad \dots \quad (8)$$

From equation (8) the absolute value of E will be given by

$$|E| = \frac{\mu e_g}{\sqrt{\left(A + \dfrac{B}{R_2}\right)^2 + \left(C - \dfrac{D}{R_2}\right)^2}} \quad \dots \quad (9)$$

where

$$A = 1 + \frac{C_3}{C_2} + \frac{\rho}{R_1} + \frac{\rho C_3}{R_1C_2}$$

$$B = \frac{\rho C_1}{C_2} + \rho$$

$$C = \frac{w\rho C_1C_3}{C_2} + wC_1\rho + wC_3\rho$$

$$D = \frac{\rho}{wR_1C_2} + \frac{1}{wC_2}.$$

It may be pointed out that in order to obtain the maximum value of E, the voltage developed across the grid and the filament of the second valve, the plate resistance R_1 cannot be changed to a large extent as it will alter the working conditions of the valve. The loss of transferred voltage decreases with the increase of the capacity of the coupling condenser C_2 and it will be minimum when the capacity reaches infinity. But this is not practicable as it will make the grid of the second valve highly positive and the valve will cease to function.

Therefore in order to get the maximum value of $|E|$ we differentiate the equation (9) with respect to grid resistance R_2 and get

$$\frac{d|E|}{dR_2} = -\mu c_u \left\{ \left(A + B/R_2 \right)^2 + \left(C - D/R_2 \right)^2 \right\}^{-3/2}$$

$$\left\{ \frac{D}{R_2^2} \left(C - D/R_2 \right) - \frac{B}{R_2^2} \left(A + B/R_2 \right) \right\}. \quad \ldots \quad (10)$$

Equating the expression for $\frac{d|E|}{dR_2}$ to zero, we get the condition for maximum or minimum value of transferred voltage given by

$$R_2 = \frac{B^2 + D^2}{DC - AB}$$

$$= \frac{\rho_2 + \frac{\rho^2 C_1^2}{C_2^2} + \frac{2\rho^2 C_1}{C_2} + \frac{\rho^2}{w^2 R_1^2 C_2^2} + \frac{1}{w^2 C_2^2} + \frac{2\rho}{w^2 R_1 C_2^2}}{-\left(\rho + \frac{\rho^2}{R_1} \right)}. \quad \ldots \quad (11)$$

Differentiating $|E|$ once more with respect to R_2 we have

$$\frac{d^2|E|}{dR_2^2} = \mu c_u \left\{ \left(A + B/R_2 \right)^2 + \left(C - D/R_2 \right)^2 \right\}^{-5/2}$$

$$\left[3 \left\{ \frac{D}{R_2^2} \left(C - D/R_2 \right) - \frac{B}{R_2^2} \left(A + B/R_2 \right) \right\}^2 \right.$$

$$\left. - \left(\frac{3B^2}{R_2^4} - \frac{2DC}{R_2^3} + \frac{2AB}{R_2^3} + \frac{3D^2}{R_2^4} \right) \left\{ (C - D/R_2)^2 + (A + B/R_2)^2 \right\} \right]. \quad (12)$$

Substituting, the value of R_2 from equation (11) in the above equation and simplifying, we get

$$\frac{d^2|E|}{dR_2^2} = -\mu c_u \left\{ \left(A + B/R_2 \right)^2 + \left(C - D/R_2 \right)^2 \right\}^{-3/2}$$

$$\frac{1}{R_2^4 (B^2 + D^2)} \left(2AB^3CD + A^2B^2D^2 + 2ABCD^3 \right.$$

$$\left. + A^2D^4 + B^4C^2 + B^2C^2D^2 \right). \quad \ldots \quad (13)$$

From the above equation it will be observed that the value of $\frac{d^2|E|}{dR_2^2}$ is negative. Thus the expression for R_2 given in equation (11) corresponds to the maximum value of the transferred voltage.

From equation (11) it will be observed that the resistance required for minimum loss of voltage will be always negative and the magnitude of this will depend on the constants of the valve used and the values of other associated components. This condition for maximum transfer of voltage has been verified by applying the negative resistance of a dynatron valve between the grid and the filament circuit of the second valve of the amplifier as shown in the next section.

Two typical curves have been drawn in fig. 2, to indicate the variation of the voltage gain in decibels when the grid resistance is altered from positive to negative values. The voltage gain is calculated from equation (9). Curve A in fig. 2 has been drawn for high value of coupling condensers and B for low value of the same. From these curves it will be observed that the magnitude of the negative resistance for maximum transfer of voltage decreases as the capacity of the coupling condenser is increased. It will finally reach a limit of about 10,000 ohms with very large value of coupling condensers. It will be further observed that the maximum value of the voltage gain increases very rapidly as the capacity of the coupling condenser is increased. This is shown by the peak of the curve A at P. It may be noted that under suitable circumstances voltage gain with negative resistance may be substantially higher than that with positive resistance. The portions of the curves for negative voltage gain have not been shown in fig. 2, but they can be easily computed from equation (11).

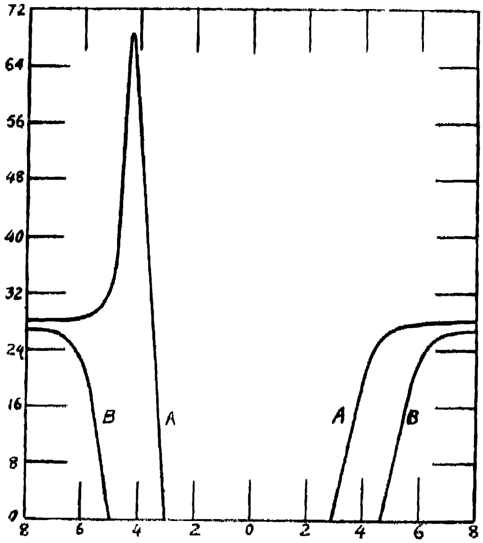

FIG. 2

Experimental Arrangement and Observations

The connections were made as shown in fig. 3 above. V_1 and V_2 represent the two valves of different stages of the amplifier. Other notations for different components are retained the same as in fig. 1. The overall amplification is obtained by measuring the amplified voltage E across the grid of the second valve by a thermionic voltmeter. A small input voltage was applied between the grid and the filament of the first valve from an audio-frequency valve oscillator through an attenuator. Different values of positive and negative resistances were applied in the grid circuit by a dynatron valve V_3 of internal resistance r_1 along with two other resistances r_2 and r_3. Thus the combination of r_1, r_2 and r_3 is equivalent to R_2 in fig. 1. The values of the positive and negative resistances of the valve were obtained from its characteristics drawn under similar conditions.

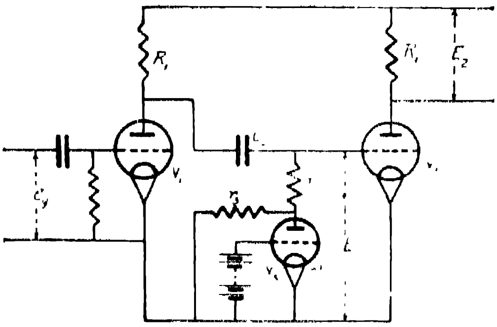

FIG. 3

Table I below gives the observed and calculated values of $|E|/e_g$ for different negative grid leak resistances R_2 of the second valve, with the following circuit constants :

$\rho = 3,25,000$ ohms,

$\mu = 25$,

$C_2 = .002$ microfarad,

$C_1 = C_3 = 10$ micro-microfarads,

$R_1 = 2,50,000$ ohms,

R_2 for minimum loss of voltage $= -1.87 \times 10^5$ ohms.

TABLE 1

Negative grid leak resistance (R_2) in ohms	Voltage gain (calculated) in decibels	Voltage gain (observed) in decibels
7.1	22.5	21.7
6.0	22.8	22.1
5.0	23.3	22.7
4.1	23.9	23.5
3.5	24.5	24.7
3.0	25.1	25.5
2.8	25.4	25.6
2.1	26.5	26.1
1.9	26.6	26.4
1.5	24.9	26.0
0.5	8.9	11.1

Fig. 4 is drawn to show the variation of voltage gain with negative values of R_2. The continuous curve is drawn from the theoretically calculated values and dotted one from experimentally observed values.

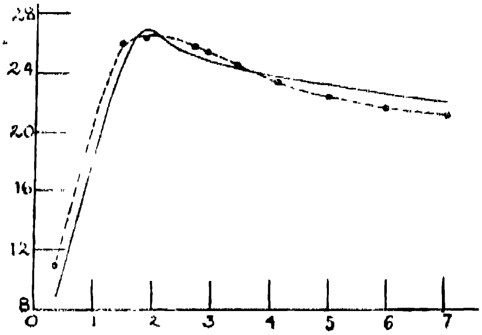

FIG. 4

SUMMARY

Analysis of the circuit of a low-frequency resistance-capacity-coupled amplifier has shown that the loss of voltage incurred in transferring the energy from one stage to the other is minimum with negative resistance in the grid circuit of the second stage of the amplifier. The value of the negative resistance required for minimum loss has been calculated theoretically from the equations derived for the purpose and it has been experimentally verified by inserting a dynatron valve in the grid circuit. It has been shown that the maximum voltage gain with negative resistance is always higher than the gain with positive resistance.

ACKNOWLEDGMENT

In conclusion, I express my deep sense of gratitude to Dr. S. S. Banerjee for suggesting the problem and constant help during the progress of the above work.

Wireless Section,
Physics Laboratory,
Benares Hindu University.

REFERENCES

1 F. W. Schor, *Proc. Inst. Rad. Eng.*, **20**, 87 (1932).
2 D. G. C. Luck, *Proc. Inst. Rad. Eng.*, **20**, 1401 (1932).
3 W. F. Curtis, *Proc. Inst. Rad. Eng.*, **24**, 1230 (1936).
4 S. S. Banerjee and E. S. Rao, *Science and Culture*, **6**, 070 (1941).

FLUID FLOW THROUGH POROUS MEDIA

PART I. ON THE USE OF GASES FOR THE MEASUREMENT OF TRUE PERMEABILITY *

By N. C. SENGUPTA

AND

MG. THEIN NYUN

(Received for publication, November 4, 1951)

ABSTRACT. The rate of flow of hydrogen and oxygen at various pressure gradients through two cores, one of high permeability the other of low permeability, was studied. The permeability calculated from the data for the core of lower permeability was more or less constant up to the highest pressure gradient studied, namely, 0.39 atm./cm with hydrogen and 0.45 atm./cm. with oxygen. With the other core the permeability appeared to decrease with increase in the pressure gradient. This decrease could not be accounted for by a turbulence effect since the Reynolds number was in all cases considerably below unity For both cores permeabilities calculated using data from the rate of flow of oxygen were less than those obtained from similar calculations with hydrogen. This appeared to be due to slip effect and the true permeabilities obtained after correction for slip were less than the observed permeabilities obtained by direct measurement with gases.

INTRODUCTION

The permeability of a porous medium has been defined as the rate of flow through unit cross-section of the medium of a fluid of unit viscosity under unit pressure gradient. When the rate of flow is measured in c.c. per second, the cross-section in sq. cm., the viscosity in centipoise and the pressure gradient in atm./cm., the unit of permeability is called a darcy.[1] A knowledge of the permeability has many applications especially in the production of oil and gas from underground reservoirs.

Both liquids and gases have been used for permeability measurements,[2] but gases offer certain advantages over liquids. Unlike liquids they do not produce any swelling of the medium and a measurable flow with gases is obtained at a moderate pressure gradient so that the experimental technique becomes simple especially with media of low permeabilities. The main objection against the use of a gas is that its volume changes with pressure and the change under certain conditions becomes adiabatic. Again, gases like carbon dioxide do not even approximately obey Boyle's law at ordinary temperatures.

The following relation connecting the permeability, K_a, with the rate of flow and the pressure gradient can be obtained assuming that the gas obeys

---

* Communicated by the Indian Physical Society.

Boyle's law, that the flow is isothermal and that turbulence, kinetic energy and slip effects are absent.

$$K_a = \frac{2V.p.\eta.L}{(p_2^2 - p_1^2)A} \qquad (1)$$

where "V" is the volume of gas flowing per unit time at atmospheric pressure p, p_2 is the pressure of the entering and p_1 that of the issuing gas, η is the viscosity of the gas at the temperature of measurement, L is the thickness and A is the cross-section of the cylindrical core. When $p_1 = p$* equation (1) reduces to

$$K_a = \frac{V.p.\eta.L}{\Delta p(p + \frac{1}{2}\Delta p)A} \qquad (2)$$

where Δp equals $p_2 - p$.

The permeability of any porous medium calculated by the above equation should be independent of the nature of the gas or of the magnitude of Δp within a certain range. It has, however, been observed in this laboratory that the measured permeabilities of consolidated sand samples depend on the gas used and with the same gas a decrease with increasing pressure gradient, even when the latter is very small, has been noted.

The purpose of the present paper is to discuss the possibility of calculating from permeability measurements a true permeability which would be independent of the gas used and from which the rate of flow of liquids under specific conditions could be found.

EXPERIMENTAL

The apparatus used for permeability measurements is shown in Figure 1.

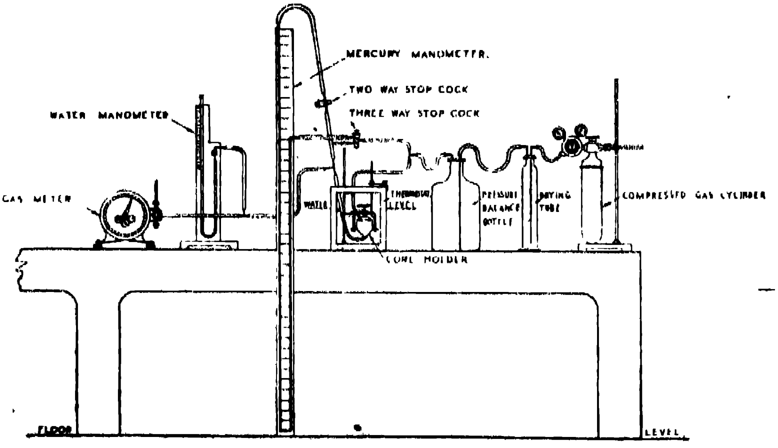

FIG. 1

The pressure was regulated by means of a needle valve and could be kept constant within 0.5 m.m. of mercury. The core holder and the empty bottle were both immersed in water baths. When the rate of flow was small a gas burette was used instead of the gas meter.

---

* In the experiments described below the pressure of the issuing gas was atmospheric.

Cores as received from the field in sealed tins were prepared for permeability measurements as follows :

A cylindrical piece was cut along a line parallel to the bedding plane in a suitable core-cutting machine. This core was then extracted with light spirits to remove oil and dried in an air-oven. When dried it was shaped as necessary with a carborundum wheel, placed in the core holder (see Fig. 1) and sealed on the sides with a special cement.

Particle size distribution curves for the two cores used in the present experiments were obtained by breaking down specimens of the cores under petrol, drying the grains in an air-oven and making triplicate runs in the Puri Siltometer.[3]

The porosities of the samples were found using the method of Melcher and Nutting.[4]

RESULTS AND DISCUSSION

The particle size distribution curves for the two cores are shown in Figure 2.

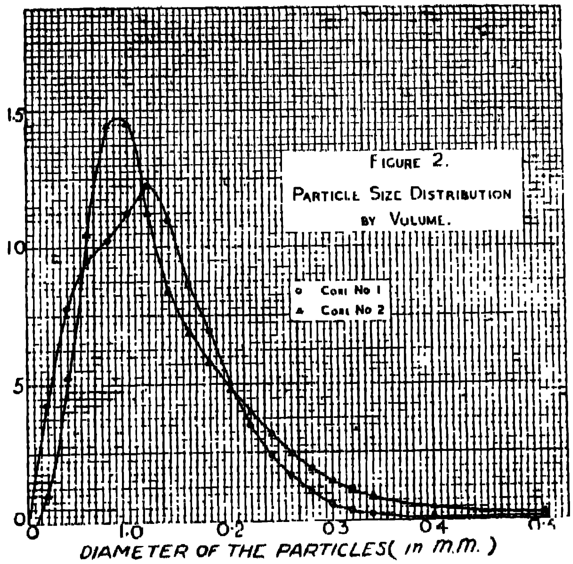

FIG. 2

Core No. 1 was of low permeability and the other core was highly permeable. Average particle radius, $\bar{r}$, of the sand grains has been calculated from the particle size distribution curve, using the formula :—

$$\bar{r} = \sqrt[3]{\frac{100}{\Sigma P_s / r_s}}$$

where P_s is the percentage in volume of particles having radius r_s.

The porosities and the average particle radii of the two cores are given in Table I.

TABLE I

Core No	Porosity (%)	$r \times 10$ cm.
1	21.0	1.7
2	35.5	3.7

It will be seen that the core which has the higher value for the average radius has also the higher porosity. In the course of this investigation some interesting relations between average radius, porosity and permeability of cores were observed. These will be described in a future communication.

Results of permeability measurements are given in Tables II-V.

TABLE II

Core No. 1 Hydrogen

Temperature = 29° C. Length of Core = 2.249 cm. Area of Cross-Section of Core = 4.382 sq. cm. Viscosity of Hydrogen at 29°C = 0.00907 centipoise. Atmospheric Pressure = 0.985 atmosphere.

Pressure difference Δp in atmospheres	Rate of flow (V) in c.c. per sec.	$\frac{\Delta p}{L}$	$\frac{V.p.}{(p+\frac{1}{2}\Delta p)A}$	K_a (millidarcy) *
0.151	1.121	0.0672	0.238	32.0
0.170	1.332	0.0796	0.279	31.8
0.204	1.532	0.0907	0.317	31.7
0.249	1.896	0.1108	0.384	31.5
0.313	2.403	0.1392	0.473	30.8
0.346	2.683	0.1539	0.521	30.7
0.384	3.039	0.1708	0.586	30.8
0.420	3.377	0.1867	0.628	30.8
0.433	3.488	0.1926	0.653	30.8
0.467	3.940	0.2077	0.727	30.7
0.547	4.625	0.2433	0.826	30.8
0.601	5.220	0.2673	0.913	31.9
0.686	6.163	0.3053	1.043	31.0
0.711	6.385	0.3162	1.070	30.8
0.782	7.263	0.3477	1.187	31.0
0.858	8.215	0.3816	1.306	30.3

TABLE III

Core No. 2 Hydrogen

Temperature = 29°C. Length of Core = 2.545 cm. Cross-Section of Core = 4.620 sq. cm. Viscosity of Hydrogen at 29°C = 0.00907 centipoise. Atmospheric Pressure = 0.985 atmosphere.

Pressure difference Δp in atmospheres	Rate of flow (V) in c.c. per sec.	$\frac{\Delta p}{L}$	$\frac{V.p.}{(p+\frac{1}{2}\Delta p)A}$	K_a (millidarcy)
0.114	7.71	0.0448	1.608	326
0.217	14.83	0.0853	2.881	306
0.329	22.84	0.1263	4.222	303
0.338	23.11	0.1328	4.309	291
0.352	24.39	0.1383	4.462	293
0.426	29.90	0.1674	5.303	287
0.433	30.26	0.1701	5.357	286
0.445	31.09	0.1749	5.450	284
0.459	32.18	0.1803	5.627	283
0.486	34.12	0.1909	5.912	281
0.584	42.65	0.2295	7.078	280
0.773	58.70	0.3037	9.101	272
0.818	62.37	0.3215	9.540	268

TABLE IV

Core No. 1 Oxygen

Temperature = 29°C. Length of the Core = 2.249 cm. Cross-Section of the Core = 4.382 sq. cm. Viscosity of Oxygen at 29°C = 0.02037 centipoise. Atmospheric Pressure = 0.980 atmosphere.

Pressure difference Δp in atmospheres	Rate of flow (V) in c.c. per sec.	$\frac{\Delta p}{L}$	$\frac{V.p.}{(p+\frac{1}{2}\Delta p)A}$	K_a (millidarcy)
0.066	0.183	0.0294	0.0404	28.1
0.126	0.358	0.0560	0.0768	27.1
0.177	0.514	0.0787	0.1076	27.9
0.245	0.732	0.1090	0.1485	27.8
0.363	1.148	0.1640	0.2210	27.9
0.434	1.417	0.1931	0.2646	27.9
0.497	1.654	0.2211	0.3011	27.7
0.584	1.980	0.2597	0.3481	27.3
0.651	2.271	0.2902	0.3890	27.4
0.721	2.584	0.3206	0.4310	27.4
0.778	2.815	0.3467	0.4598	27.1
0.849	3.141	0.3776	0.5000	27.0
0.906	3.443	0.4029	0.5374	27.2
0.949	3.671	0.4221	0.5643	27.2
1.016	4.030	0.4517	0.6054	27.3

TABLE V

Core No. 2 Oxygen

Temperature = 30°C. Length of the Core = 2.545 cm. Cross-Section of the Core = 4.620 sq. cm. Viscosity of Oxygen at 30°C = 0.02040 centipoise. Atmospheric Pressure = 0.9826 atmosphere.

Pressure difference Δp in atmospheres	Rate of flow in c.c. per sec.	$\frac{\Delta p}{L}$	$\frac{Vp}{(p+\frac{1}{2}\Delta p)A}$	K_a (millidarcy)
0.1	2.35	0.0393	0.484	251
0.2	4.81	0.0786	0.945	250
0.3	7.43	0.1179	1.332	242
0.4	10.14	0.1571	1.824	236
0.5	13.00	0.1964	2.244	233
0.6	15.07	0.2358	2.651	229
0.7	19.05	0.2751	3.041	226
0.8	22.50	0.3144	3.461	220
0.9	25.72	0.3536	3.810	220
1.0	29.53	0.3929	4.336	220

It is evident from the above Tables that permeability decreases with increase in the pressure gradient, especially in the case of core No. 2. In Figures 3 and 4

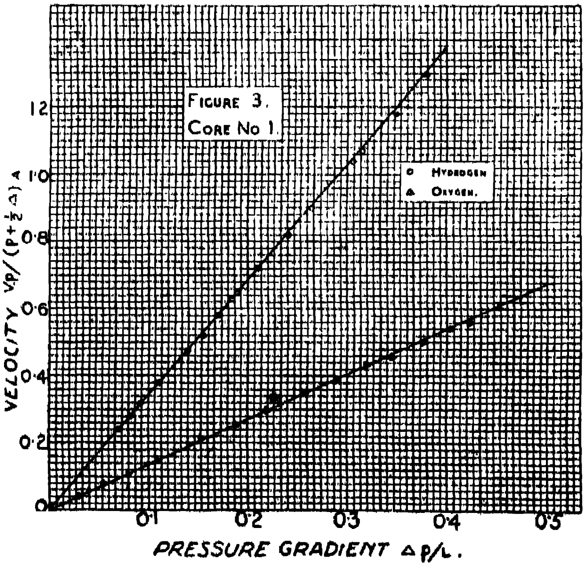

FIG. 3

the velocities, $V.p/A(p+\frac{1}{2}\Delta p)$, have been plotted against the corresponding pressure gradients $\Delta p/L$.

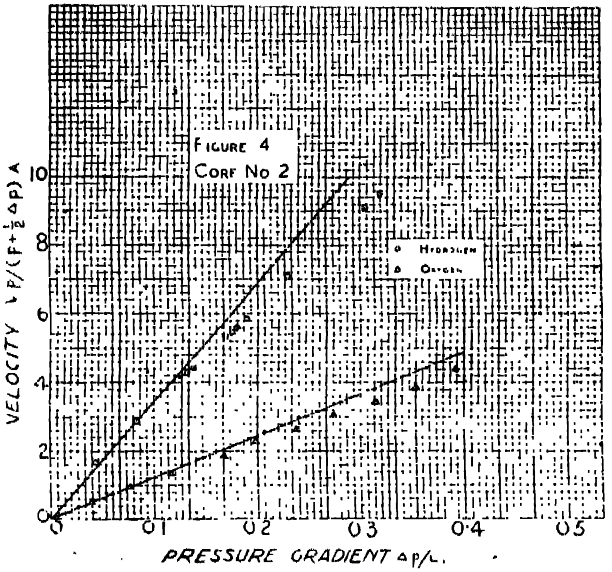

FIG. 4

The curves obtained with core No. 1 (Figure 3) are more or less straight lines within the range of experimental error while the curves obtained with core No. 2 (Figure 4) are concave to the pressure gradient axis. Muscat[5] has assumed that any deviation of the curve from linearity is due to turbulence. The Reynolds numbers have been calculated after Muscat from the relation[5]:—

$$R = \frac{d.V.p.\rho}{A(p+\frac{1}{2}\Delta p)\eta} \quad \cdots \quad (4)$$

where d is the average diameter of the grains and ρ the density of the gas at the temperature and mean pressure of measurements. Results are given in Table VI.

TABLE VI

Core No	'Gas used'	Highest pressure gradient atm /cm²./cm.	'Reynolds number'
1	Hydrogen	0.3816	0.0044
1	Oxygen	0.4517	0.014
2	Hydrogen	0.3215	0.069
2	Oxygen	0.3929	0.222

The highest Reynolds number is 0.222 while according to Muscat[5] the lowest Reynolds number for the appearance of turbulence is 1. Thus it appears that the variation of the permeability with pressure, observed in the range of low pressure gradients, is not due to turbulence. The alternative explanation is that this diminution of permeability is due to a kinetic energy effect which should be corrected for in order to calculate the true permeability. This can be done graphically by obtaining the slope of the velocity/pressure gradient curve at the origin which equals K_a/η where K_a is the permeability after the kinetic energy correction has been applied. The slope at the origin for the four curves and the corresponding calculated permeabilities are given in Table VII.

TABLE VII

Core No.	Gas used	Slope of the pressure gradient velocity curve	η (centipoise)	$\bar{K}_a$ (millidarcy)
1	Hydrogen	3.45	0.00907	31.3
1	Oxygen	1.35	0.02037	27.8
2	Hydrogen	34.60	0.00907	31.4
2	Oxygen	12.25	0.02040	25.0

The permeabilities obtained after kinetic energy corrections have been made are higher in the case of measurements with hydrogen than for those with oxygen. Although similar discrepancies have been noticed previously no explanation seems to have been put forward. This question cannot be settled unless an independent method of measuring permeability is developed. The following is a tentative explanation.

In the measurement of viscosity of gases by the method of capillary flow, it is necessary to apply a correction for slip[6] at the walls of the tube. The greater the slip the greater will be the volume of flow. Assuming that the flow becomes zero at a distance $r+\xi$* from the axis of a capillary of radius r, the volume of flow V is given by the relation

$$V=\frac{\pi(p_2^2-p_1^2)}{16\eta Lp}(r+\xi)^4 \quad \ldots \quad (5)$$

or

$$V=\frac{\pi(p_2^2-p_1^2)r^4(1+4\xi/r)}{16\eta Lp} \quad \ldots \quad (6)$$

where $r >> \xi$.

---

* For gases ξ is known to equal approximately the mean free path of the molecules (see Ref. 6).

The volume of flow $\bar{V}$ in absence of slip will be given by the formula

$$\bar{V} = \frac{\pi(p_2^2 - p_1^2)}{16\eta L p} r^4 \qquad \ldots \quad (7)$$

V and $\bar{V}$ are connected by the relation

$$V = V(1 + 4/_r). \qquad \ldots \quad (8)$$

Since $\bar{V}$ is the true volume of flow in absence of slip we should have used $\bar{V}$ instead of V in order to calulate the true permeability, $\bar{K}$, thus

$$\bar{K} = \frac{2\bar{V}p\eta L}{(p_2^2 - p_1^2)A} = \frac{2Vp\eta L}{(p_2^2 - p_1^2)A(1 + 4\xi/_r)} = \frac{\bar{K}_a}{(1 + 4\xi/_r)} \qquad \ldots \quad (9)$$

r cannot be experimentally determined but is likely to be of the order of $\frac{1}{10}$th of the average radius of grains in consolidated polydispersed sands. Values for $\bar{K}$ and r can be calculated from the measurements with two gases whose mean free paths are known. Results of such calculations are given in Table VIII.

TABLE VIII

Core No.	'Gas used'	Mean free path at the temp of measurement	r (average radius of pores)	$\bar{K}$ (millidarcy)
1	Hydrogen	19.2×10^{-6}cm.	3.0×10^{-4}cm.	23.6
1	Oxygen	10.8×10^{-6}cm.		
2	Hydrogen	19.2×10^{-6}cm.	0.88×10^{-4}cm.	16.8
2	Oxygen	10.8×10^{-6}cm.		

The calculated permeabilities in both cases are much lower than those obtained with either hydrogen or oxygen.

Further research on this topic is proceeding and results will be communicated in due course.

Our thanks are due to the Manager of the Burmah Oil Co. (Burmah Concessions), Ltd., for permission to publish this paper. The work was carried out under the general direction of Mr. A. Reid, Senior Fields Chemist.

BURMAH OIL CO. RESEARCH LABORATORIES
KHODAUNG (UPPER BURMA).

REFERENCES

[1] Wyckoff, R. D., *et al*, *Rev. Sci. Instr.*, **4**, 394 (1933).

[2] Muscat, M., *The Flow of Homogeneous fluids through Porous Media, McGraw-Hill Book Co., Ltd.*, p. 78 (1937).

[3] Puri, A. N., The Punjab Irrigation Research Inst., *Research Publication*, Vol. V, No. 1 (1933)

[4] Melcher, A. F., *T.I.M.E.*, **65**, 469, 1921; *Nutting, Amer. Assoc. Petrol Geol.*, **14**, 1337 (1930).

[5] See Reference 1, pp. 57-69.

[6] Barr, G., *A Monograph of Viscometry, Oxford University Press*, p. 157 (1931).

EVIDENCE FOR THE EXISTENCE OF ASSOCIATED MESONS IN COSMIC-RAY SHOWERS*

By M. S. SINHA, M.Sc., and R. L. SENGUPTA, M.Sc., Ph.D.

(Received for publication, February 17, 1942)

ABSTRACT Evidence has been obtained of the existence of associated mesons in cosmic-ray showers with a Counter-controlled Wilson Chamber arranged so as to record showers only. A 2.2 cm lead plate was placed inside the chamber and the nature of the particles photographed has been ascertained from the fact whether they have been absorbed or multiplied by this lead plate or have emerged out of it without producing secondaries

Investigations of Janossy and Ingleby,[1] Wataghin, de Souza Santos, etc,[2] with coincidence counters interposing large thicknesses of lead absorbers have indicated the existence of showers of penetrating particles. Cloud chamber evidence of associated penetrating particles have also been obtained by Braddick and Hensby[3] working under 30 metres of London clay and by Herzog and Bostick[4] in the substratosphere. The present work is an attempt to take a large number of photographs of penetrating cosmic-ray showers to furnish an adequate data for a complete investigation of their behaviour. We have been using a cloud chamber operated by a five-fold coincidence arrangement shown in Figure 1. The arrangement is practically a three-fold coincidence one, the extreme bottom counters being used to define the geometry more precisely and to make the number of accidentals very small.

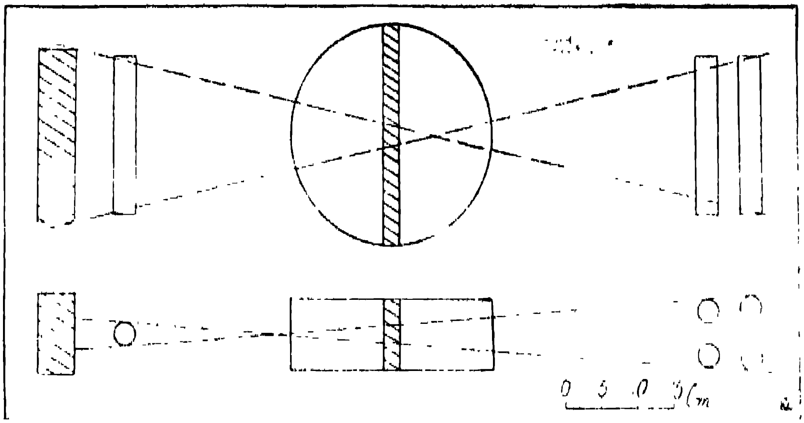

Fig. 1

---

* Communicated by the Indian Physical Society.

A lead plate of 2.2 cm. thickness has been inserted in the chamber. The nature of a particle traversing the lead plate can be ascertained from the rate of production of secondaries during the traversal. For an electron, for example, of energy 10^9 ev. it is very unlikely that it will emerge out of it without being accompanied by secondaries, whereas for a meson of the same energy the probability of emerging with a secondary is very small.

The preliminary experiment was carried out without any lead plate above the top counter and the photographs obtained were mostly of cascade showers, a typical and interesting case of which is shown in Figure 2, which shows both absorption and multiplication of an extensive air shower in the lead plate placed inside the chamber.

With the arrangement given in Figure 1, *i.e.*, with the top absorber 5 cm. thick, about thirty photographs have been taken, of which Figure 3 is an interesting case.

In Figure 4, we find two penetrating particles with a few electrons associated with them. The slight convergence between the tracks (*a*) and (*b*) is apparently due to scattering of the particles in the top lead absorber. The track (*a*) can be assigned to that of a meson as no secondary has been produced in the traversal of 2.2 cm. of lead. Although the particle (*b*) has emerged from the lead plate with a secondary it is very unlikely that the incident particle is an electron due to the following reasons :—

(1) The magnitude of scattering suffered by the incident particle sets a lower limit to its energy which is 10^9 ev.

(2) The probability that an electron of this energy will penetrate 2.2 cm. lead plate with a single secondary is of the order of 10^{-4}.

We therefore consider it to be the case of an associated meson pair accompanied with a few soft electrons which are observed on the photograph along with the penetrating particles.

Some photographs have also been taken by changing the thickness of the top absorber to 10 cms. The coincidence rate has not appreciably changed which is in agreement with Janossy and Ingleby's observation on penetrating showers where they find associated penetrating particles in groups of different numbers occurring almost with the same frequency even when the thickness of the absorber is gradually increased. With 5 cm. thick top absorber the majority of the photographs were of cascade showers either in the absorber or in the lead plate inside the chamber. The yield of penetrating showers has apparently increased on changing the thickness of the top absorber to 10 cm. Any attempt at interpretation regarding this is however premature until more data is available to make the indication statistically significant.

Two interesting cases with the top absorber 10 cms. are shown in Figures 4 and 5. Figure 4 shows clearly a pair of penetrating particles. No magnetic

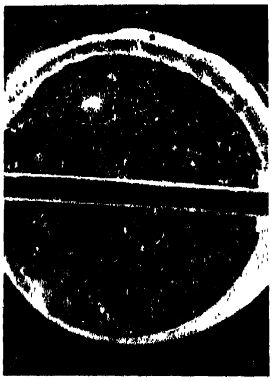

Fig. 2.

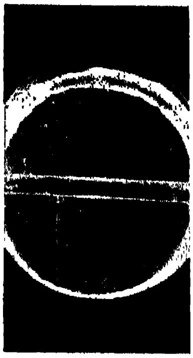

Fig. 3.

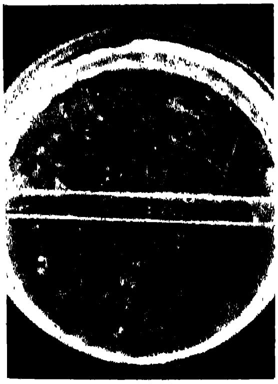

Fig. 4

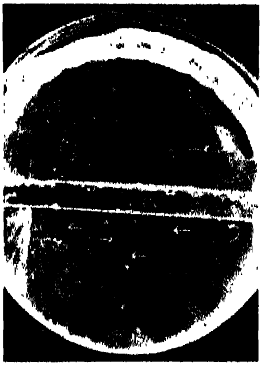

Fig. 5.

field has been applied so that the slight bending of the tracks is due to convection currents set up in the chamber. The pair appears to be generated within a few centimetres from the wall of the chamber and can be looked upon as an air shower. A similar photograph has been reported by Braddick and Hensby.[3]

Figure 5 is the most important of the series of photographs. It shows at least four penetrating mesons (shown by arrow heads) with a large number of fairly energetic electrons, one of which has produced a cascade shower in the lead plate. Janossy and Ingleby[1] have also observed, by means of counters, showers containing penetrating particles up to eight in number. From the geometry of the tracks it is evident that the lead absorber on the top cannot be the source of generation of the particles. We therefore presume that the rays constitute an air shower consisting of electrons and mesons in conformity with the general view on the structure of the extended air showers.

In conclusion, the authors wish to express their gratefulness to Dr. D. M. Bose, M.A., Ph.D., for his advice and encouragement throughout the work. The experiment is in progress and a detailed account of the complete work will be published later.

THE BOSE INSTITUTE,
UPPER CIRCULAR ROAD,
CALCUTTA

REFERENCES

[1] Janossy, L., and Ingleby, P., *Nature*, **145**, 511 (1940).

[2] Wataghin G., M. de Souza Santos, and Pompea, P. A., *Phys. Rev.*, **57**, 61 (1940).

[3] Braddick, H. J., and Hensby, G. S., *Nature*, **144**, 1012 (1939).

[4] Herzog, G. H., and Bostick, W. H., *Phys. Rev.*, **58**, 278 (1940)

16

NOTE ON THE LOW ENERGY SCATTERING OF PROTONS BY PROTONS

BY H. MACK THAXTON

(*Received for publication, November 5, 1941*)

ABSTRACT. The scattering of protons by protons has been investigated in the energy region .2 to .3 Mev by Ragan, Kanne and Taschek.[1] This note derives the necessary theoretical calculations for the analysis of the experimental data Phase shifts for the Gauss, Meson, Exponential, Morse and Square potential wells are determined Curves of the Mott ratio, including the effect of S-wave scattering for all potential wells, are given.

G. L. Ragan, W. R. Kanne and R. F. Taschek[1] have investigated the scattering of protons by protons in the energy region from 200 to 300 kev, experimentally. For purpose of comparison with theoretical results, a detailed investigation of this energy region has been made, theoretically, at energy intervals of 10 kev and for all the potential functions utilized thus far in the study of the problem. The analysis of proton scattering data [1,2,3] has shown that experimental data may be fitted almost exactly to theory by the assumption of a pure *s*-scattering alone; this is especially true in the region under consideration. It has been shown that the experimental data on proton-proton scattering can be fitted by a square well[2] of depth 10.5 Mev and range e^2/mc^2 and a Gaussian[2] type potential[3] well $Ae^{-r^{-}}$ with $A=51.44\ mc^2$ and $=21.50$ Mmc^2 cut off at $3\ e^2/mc^2$; a Meson potential well[4] $Ce^{-r/a}/(r/a)$ with $C=89.65\ mc^2$ and $a=0.42\ e^2/mc^2$; an exponential potential well[5] $Be^{-2r/b}$ with $B=137.6\ mc^2$, $b=0.193\ (Mmc^2)^{-\frac{1}{2}}$; a Morse potential well[6] $D(e^{-4r/a} - 2e^{-2r/a})$, with $D=119.36\ mc^2$, $a=e^2/2mc^2$. The agreement between theoretical and experimental results using these potentials confirms the existence of only an *s*-wave anomaly in the scattering and the equality of neutron-proton and proton-proton interactions.

The present theoretical calculations extend the region of investigation so as to cover the new experimental data. The method of calculation consists in solving numerically the differential equation $d^2F/dr^2 + (E - V(r))\ F = 0$ using the units and numerical values of the constants given above for each potential, cutting off the solutions at $3\ e^2/mc^2$ and joining to Coulomb functions. The Coulomb functions needed for these calculations were computed from series expansions.[7] Curves giving the variation of phase shift with energy over this region are given in Figure I for all potentials. The curve represented by crosses gives the variation of K_0 with energy for the Meson potential; the elliptical circles represent the square well potential; the circles represent the exponential and the dots and squares the Gauss and Morse potentials respectively. Figure II

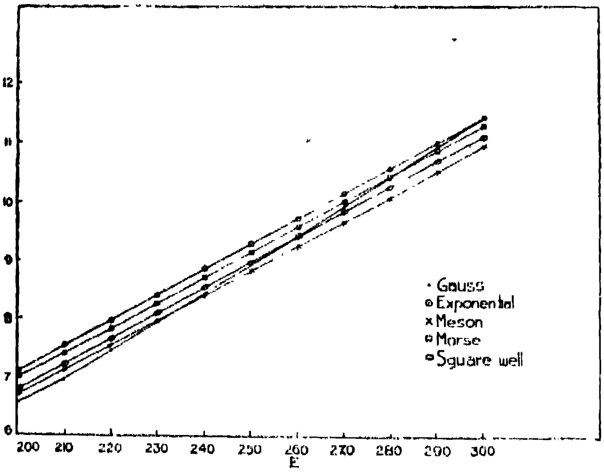

FIG. I
Variation of Phase shift with energy

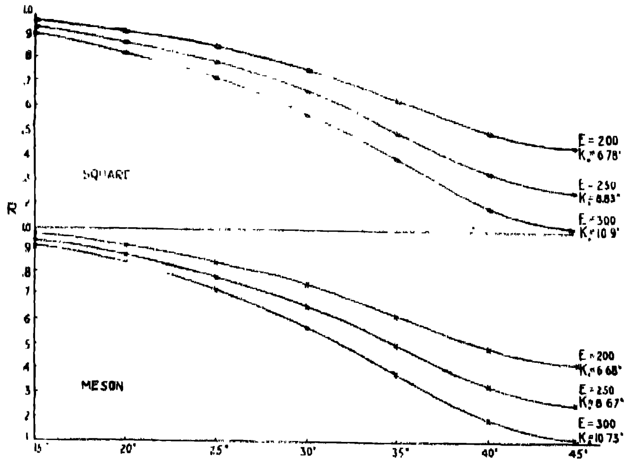

FIG. II
Mott ratio as a function of the angle of scattering

shows curves of the Mott ratio (R) plotted as ordinates with the scattering angle Θ as abscissae for the square well and the meson potentials. These curves are typical of the curves for R as a function of Θ for all potentials. The actual numerical values for the calculated phase shifts for all potentials are tabulated in Table I.

TABLE I

Theoretical Phase Shifts

—	Square	Gauss	Exponential	Meson	Morse
E_{kev}	K_0	K_0	K_0	K_0	K_0
200	6.78°	6.59°	7.05°	6.68°	6.97°
210	7.18°	6.93°	7.45°	7.08°	7.35°
220	7.60°	7.15°	7.87°	7.47°	7.77°
230	8.02°	7.90°	8.28°	7.87°	8.18°
240	8.43°	8.37°	8.68°	8.27°	8.59°
250	8.83°	8.82°	9.11°	8.67°	9.02°
260	9.25°	9.30°	9.53°	9.06°	9.43°
270	9.70°	9.78°	9.96°	9.48°	9.85°
280	10.08°	10.28°	10.38°	9.88°	10.28°
290	10.52°	10.78°	10.82°	10.31°	10.72°
300	10.90°	11.30°	11.25°	10.73°	11.15°

Figure III gives typical curves of the Mott ratio R as a function of energy

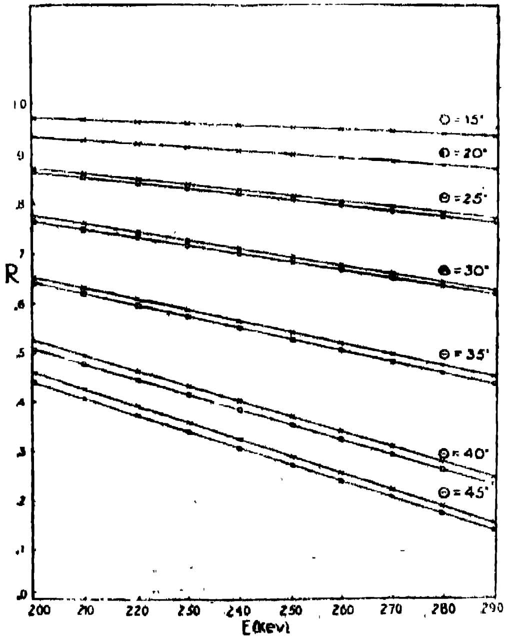

FIG. III
Mott ratio as a function of the energy

in Kev for the Meson potential (crosses) and the Morse type potential (squares). Figure IV shows the quantity $4cMR/sE^2$ plotted against energy for the

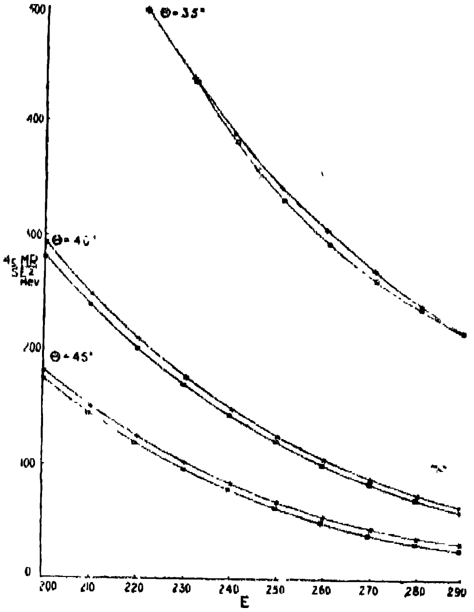

FIG. IV

The quantity $4cMR/sE^2$ as a function of energy

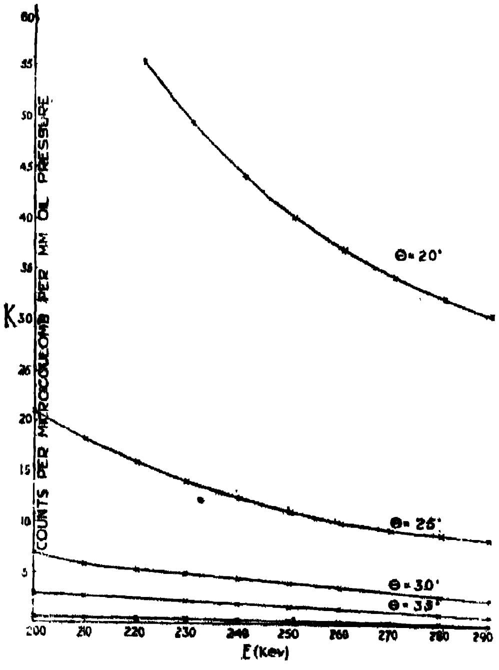

FIG. V

Counts per microcoulomb per millimetre oil pressure as a function of energy scattering angles $\Theta = 35°$, $40°$ and $45°$. Figure V are curves of the proton counts per microcoulomb per millimetre oil pressure against energy as calculated for the Meson potential.

The data given by these calculations may be used for direct comparison with the experimental data and such a comparison may lead to the choice of a potential well more closely satisfying the conditions in nuclear problems.

THE AGRICULTURAL AND TECHNICAL COLLEGE
OF NORTH CAROLINA.

REFERENCES

[1] G. Breit, H. M. Thaxton and L. E. Eisenbud, *Phys Rev*, **55**, 1018 (1939).
[2] E. Creutz, *Phys. Rev.*, **56**, 893 (1939).
[3] H. M. Thaxton and A. M Monroe, *Phys. Rev.*, **56**, 6 (1939). A. S. Eddington and H. M. Eddington, *Physica*, **6**, 12 (1940)
[4] L E. Hoisington, S. S Share and G. Breit, *Phys. Rev*, **56**, 884 (1939).
[5] W. Rarita and R D. Present, *Phys. Rev.*, **51**, 793 (1937).
[6] H. M. Thaxton and A. M. Monroe, *Phys. Rev.*, **57**, 246 (1940).
[7] F. L Yost, John A. Wheeler and G. Breit, *Phys. Rev.*, **49**, 174 (1936).

A NEW AUDIO-FREQUENCY BRIDGE

By L. M. CHATTERJEE, M.Sc.

(Received for publication, November 7, 1941)

ABSTRACT. A new bridge for the measurement of the frequency of an alternating current in the audio-frequency range has been devised, in which the null point is obtained virtually by the adjustment of the resistance in one of the arms; the adjustment characteristic is given by $l = a\sqrt{\lambda}$ which is a parabola The vector diagrams of the balanced bridge have been constructed and discussed.

INTRODUCTORY

The basic principles underlying the many available methods for measuring the frequency of an alternating current are very varied but they have been classified under six broad headings by A. Campbell and E. Childs[1]; the bridge method is one of these six groups. This group comprises those instruments in which an alternating voltage is applied between two points of an electrical network and by proper adjustment of the values of capacity, resistance and inductance (self or mutual) in the network, the potential difference between two other points in the circuit is reduced to zero, as indicated by a detecting instrument, such as a telephone or a vibration galvanometer, connected across these points. If one of the adjustments depends on the frequency of the alternating current then the bridge may be used as a measurer of frequency. It is desirable that no other adjustment should be necessary but this has not been really attained in most of the systems. Now these frequency bridges may be further subdivided into the following sections according to the nature of the elements used in the arms of the bridge :—

(*a*) Network containing R and L[2, 3]
(*b*) ,, ,, R and C[2, 3, 4, 5]
(*c*) ,, ,, R, L and C[2, 3, 6, 7, 8]
(*d*) ,, ,, R, L and M[9, 10, 11, 12, 13, 14, 15]
(*e*) ,, ,, R, L, M and C[16, 17, 18, 19, 20, 21, 22]

where R, L, M and C stand respectively for resistance, self-inductance, mutual-inductance and capacity. A useful summary of the methods is given by J. Kronert[23] and also by B. Hague.[24] H. Mukherjee[25] devised a Wheatstone network containing capacity and resistance, and put the moving coil of a dynamometer type A. C. galvanometer in one of diagonal arms and the fixed coils in the other in series with the current source ; the elements in the arms were adjusted till the galvanometer showed no deflection ; the value of the frequency was obtained in terms of resistance and capacity. On the other hand, the frequency bridges may be classified according to their adjustment characteristics. If x is the adjustment of the bridge entering into the frequency balance condition, we can write for the adjustment characteristic of the bridge, f=function (x). B. Hague[21] has graphically described eleven adjustment characteristics covering all the frequency bridges used in practice. The new bridge, a short account of which was published in *Current Science*,[26] has an adjustment characteristic given by $f=a\sqrt{x}$ which is a parabola.

THE THEORY AND DESCRIPTION OF THE BRIDGE

Fig. 1 is the circuit diagram of the new bridge. The branch AC of the bridge contains the primary coil of the mutual inductor M, the resistance and self-inductance L of the primary coil being known ; in series with it an adjustable non-inductive resistance box is connected ; P denotes the total resistance including that of the coil in the branch AC. The arms BC and AD contain adjustable non-inductive resistance boxes only ; K is a good mica condenser in the branch DB.

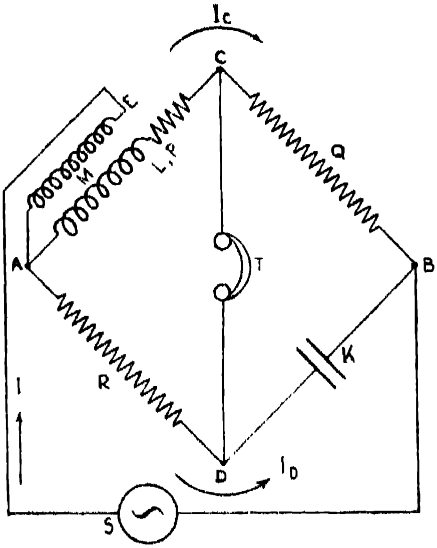

FIG. 1

Circuit diagram

One end of the secondary coil of the mutual inductor M is connected to that of the primary at A and the other end is connected to one terminal of the source S of the alternating current whose frequency has to be measured ; the other terminal of the source is connected to the point B, the junction of Q and K. T is a telephone used as a detector of the balanced state.

Let I_c be the vector representing the harmonically varying current of frequency f per sec., flowing along the branch ACB when the bridge is balanced, I_D that along ADB, and I that along BSEA ; no current flows along the branch CD at balanced state. Applying Kirchhoff's rules to the meshes of the impedance network carrying harmonic alternating current we get the following equations :—

At A
$$I = I_c + I_D ; \qquad \ldots \quad (1)$$
for the mesh ACD,
$$(P + j\omega L)I_c - RI_D + j\omega MI = 0, \qquad \ldots \quad (2)$$
where $\omega = 2\pi \times$ frequency, and $j = \sqrt{-1}$;
for the mesh CBD,
$$QI_c - \left(\frac{-j}{k\omega}\right)I_D = 0. \qquad \ldots \quad (3)$$

Substituting the equation (1) in (2) and rearranging the equations (2) and (3) we get
$$(P + j\omega L + j\omega M)I_c = (R - j\omega M)I_D ; \qquad \ldots \quad (4)$$
and
$$QI_c = \frac{-j}{k\omega} . I_D. \qquad \ldots \quad (5)$$

Dividing (4) by (5) we have
$$\frac{P + j\omega(L + M)}{Q} = \frac{R - j\omega M}{-\frac{j}{k\omega}}$$
or
$$-\frac{j}{k\omega}\{P + j\omega(L + M)\} = QR - j\omega MQ ,$$
or
$$-\frac{jP}{k\omega} + \frac{L + M}{k} = QR - j\omega MQ.$$

Equating the real quantities and likewise the unreal quantities we get
$$\frac{L + M}{k} = QR \qquad \ldots \quad (i)$$
and
$$\frac{P}{k\omega} = \omega MQ$$
or
$$\omega^2 = \frac{P}{kMQ}. \qquad \ldots \quad (ii)$$
$$\therefore \quad f = \sqrt{P}. \ (2\pi\sqrt{kMQ})^{-1}.$$

Hence the conditions (*i*) and (*ii*) are to be satisfied for no current in the telephone. The condition (*i*) may be secured by varying R, and the condition (*ii*) by varying P.

In practice, at first an audio-frequency alternating current is supplied to the bridge, and L, M, K and Q are maintained fixed; balance is obtained by successive adjustment of P and R. The process is easy and rapidly convergent since the two conditions of balance are mutually independent. When the proper values of P and R for balance at any frequency have been determined, the first condition, which is independent of frequency, remains satisfied for all frequencies, and the frequency bridge is thus brought to working order; we may now measure frequencies of alternating current sources by varying P alone so that virtually a single adjustment is all that is necessary in order to determine the frequency. The formula representing the frequency f may be written $f = a\sqrt{P}$, where $a = (2\pi\sqrt{KMQ})^{-1}$ = a constant; thus the adjustment characteristic is a parabola.

The vector diagram of the balanced bridge is constructed and discussed below. In Figs. 2a and 2b let the vector AB denote the voltage e across

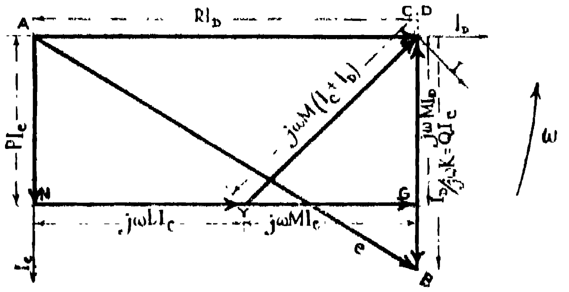

Fig. 2a

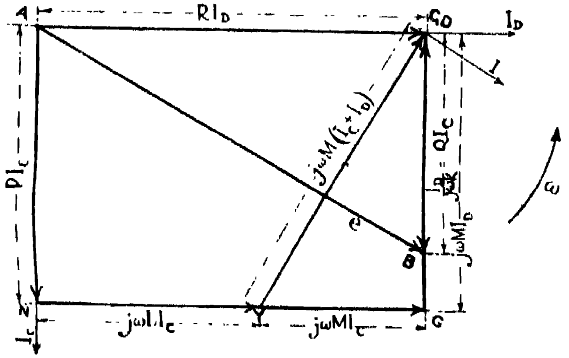

Fig. 2 b

the points A and B of the circuit diagram. The current I_C flowing along the inductive branch ACB lags behind e, while the current I_D flowing along the capacitative branch ADB leads e; RI_D is the potential drop across the resistance R and is represented by the vector AC or AD, since C and D are equipotential points when the bridge is balanced; the potential differences across the condenser K is $I_D/j\omega k$ and is represented by DB at right angles to AC, thus AC + CB = AB, that is, $RI_D + \frac{I_D}{j\omega k} = e$. Now the potential drop across the resistance Q is QI and is represented by CB or DB; therefore $QI_c = \frac{I_D}{j\omega k}$. The vector $AN = PI_c$ represents the potential drop in the resistance P of the arm AC of the circuit diagram; this vector is in phase with the current I_c; at right angles to this is the vector NY which represents the potential drop in the inductance L and is equal to $j\omega LI_c$; in phase with NY is the vector YG representing $j\omega MI_c$; the vector GD represents $j\omega MI_D$; thus $YD = YG + GD = j\omega M(I_c + I_D)$; and we notice that AD = AN + NY + YD; in other words, $RI_D = PI_c + j\omega LI + j\omega M(I_c + I_D)$; and finally AB = AN + NY + YD + DB or $e = PI_c + j\omega LI_c + j\omega M(I_c + I_D) + QI_c$; at right angles to YC is the vector of I, the total current drawn from the source. From the geometry of the vector diagrams it easily follows that

$$j\omega(L + M)I_c = RI_D \qquad \ldots \quad (\alpha)$$

$$PI_c = -j\omega MI_D \qquad \ldots \quad (\beta)$$

$$QI_c = \frac{I_D}{j\omega k}. \qquad \ldots \quad (\gamma)$$

Dividing (α) by (γ) we get

$$\frac{j\omega(L + M)}{Q} = R.\, j\omega k$$

$$\text{or} \quad \frac{L + M}{K} = QR,$$

which is the same as the equation (*i*) for the balanced condition.

Dividing (β) by (γ) we get

$$\frac{P}{Q} = \omega^2 MK$$

$$\text{or} \quad \omega^2 = \frac{P}{KMQ},$$

which is the same as the equation (*ii*) for the balanced condition.

Thus the two conditions for balance are deduced from the vector diagram. It may be noted that the currents I_c and I_D are at quadrature. It will be further observed from a study of the Figs. 2*a* and 2*b* that when P becomes equal to Q,

$$AN = CB = CG;$$

$$\therefore \frac{I_D}{j\omega k} = -j\omega MI_D \qquad \text{or} \quad \omega^2 = \frac{1}{MK};$$

that is, the second condition for balance is reduced to a simpler form $\omega^2 = \frac{1}{MK}$ when P = Q.

In deducing the balanced conditions it has been assumed that the resistances P, Q and R are perfect, *i.e.*, they contain no residual inductance and capacitance;

this is very nearly true in the case of resistances generally used in the alternating current experiments ; the small residuals may be ignored. Since there is no other coil offering self-inductance, excepting the primary of the mutual-inductor, in any arm of the bridge there is no necessity of arranging the elements in the arms with special precautions so as to avoid the stray mutual-inductance effect. It may be pointed out that the effects of the impurities in the mutual-inductor M and in the mica condenser K have been ignored all together in deducing the conditions for balance ; ordinarily these are very small and may be neglected ; it is desired to take into account these effects and their influence on the balance conditions later in a subsequent paper.

EXPERIMENTAL EXAMPLE AND REMARKS

The new frequency bridge was used to calibrate a triode oscillator meant to serve as a source for alternating current bridge measurements. The frequency could be varied by changing the capacity of the anode condenser. In the bridge set up, M was 80 5 milli-Henries from a Campbell mutual-inductometer, the fixed winding of which had an inductance $L = 98{\cdot}59$ milli-Henries , with $Q = 370$ ohms, $R = 487$ ohms, which were determined once for all in the beginning as explained above, and $K = 1$ micro farad, the balance was obtained by adjusting P with the following results ; the detector used was a telephone ; for the sake of comparison the corresponding values were also determined by the Campbell's frequency bridge and have been recorded in the last column of the table below.

Capacity of the Anode condenser		P		*f* in cycles per second	*f* in cycles/sec. as determined by Campbell's Bridge
2.1	micro-farad	190	ohms	402	398
1.6	,,	245	,,	456	452
1.1	,,	364	,,	556	552
0.9	,,	444	,,	614	609
0.7	,,	570	,,	696	692
0.5	,,	705	,,	822	827
0.3	,,	1330	,,	1064	1059
0.1	,,	2000	,,	1301	1293
0.06	,,	2470	,,	1449	1441
0.03	,,	3060	,,	1613	1616
0.01	,,	3640	,,	1750	1758
0.005	,,	3810	,,	1800	1802

If the alternating current is impure the harmonics may cause some trouble in securing a good balance, particularly if the experimenter has a bad ear for distinguishing one pitch from the other. This difficulty is common to all null methods for measuring frequency of an alternating current, but with a little practice most observers may learn to ignore harmonics. The difficulty does not arise at the lower frequencies if a vibration galvanometer is employed instead of a telephone. With telephones as detectors a good balance is often attained by earthing the point D (see Fig. 1) of the circuit thus bringing C and D at balance at the potential of the observer.

PHYSICS DEPARTMENT,
SCIENCE COLLEGE,
PATNA.

REFERENCES

[1] A. Campbell and E. Child, *Measurement of Inductance, Capacitance and Frequency*, (Macmillan & Co., 1935), page 378
[2] K. Kurokawa and T. Hoashi, *Journal I. E. E., Japan*, **437**, 1132 (1924)
[3] G. Sacerdote, *Alta Freq.*, **3**, 437 (1934)
[4] C. Robinson, *Journal P. O. E. E.*, **16**, 171 (1924).
[5] R. F. Field, *G. R. Exp.*, **6**, 1 (1931)
[6] E. Giebe and E. Alberti, *Zeits. f. Tech. Phys*, **6**, 92 and 135 (1925)
[7] G. D. Pegler, *Proc. Phys. Soc.*, **46**, 783 (1934).
[8] C. J. Soucy and B. de F. Baly, *Proc. Inst. Rad. Eng.*, **17**, 834 (1929)
[9] A. Campbell, *Proc. Phys. Soc.*, **38**, 97 (1925).
[10] A. Campbell, *Journal Sci. Instruments*, **2**, 381 (1925).
[11] S. Butterworth, *Proc. Phys. Soc.*, **24**, 86 (1912).
[12] A. Campbell, *Dictionary of Applied Physics*, Vol. 2, page 434 (1922)
[13] K. Kurokawa, *Journal Elect. Soc. Waseda*, **8**, 251 (1927).
[14] M. Sase and C. Muto, *Journal Elect. Soc. Waseda*, **8**, 170 (1927).
[15] Dunand, *Bull. Soc., Franc. des Elecns.*, 4th series, **7**, 222 (1928)
[16] A. Campbell, *Proc. Phys. Soc.*, **24**, 107 and 158 (1912).
[17] R. M. Davies, *Journal Sci. Instruments*, **10**, 274 (1933).
[18] A. Campbell, *Proc. Phys. Soc.*, **21**, 80 and 74 (1908).
[19] S. Butterworth, *Proc. Phys. Soc.*, **33**, 337 (1921).
[20] S. Chiba, *Journal I. E. E., Japan*, **405**, 294, (1922)
[21] E. Velander, *Journal Amer. I. E. E.*, **40**, 835 (1921).
[22] H. Schering and V. Engelhardt, *Zeits. f. Inst.*, **40**, 123 (1920).
[23] J. Kronert, "Frequenz Mess-brucken," *Arch. f. Tech. Mess. I.*, 921-8, Aug. (1932).
[24] B. Hague, *Alternating Current Bridge Methods* (Pitman, 1938), page 515
[25] H. Mukherjee, *Ind. Jour. Physics*, **12**, 195 (1938).
[26] L. M. Chatterjee, *Current Science*, **10**, 363, Aug. (1941).

ON THE VOLUME AND SURFACE RESISTIVITIES OF SHELLAC MOULDED MATERIALS

By G. N. BHATTACHARYA

(Received for publication, November 10, 1941)

ABSTRACT The volume and surface resistivities of a number of shellac moulded discs of different composition have been determined by the electron tube method using a Philips 4060 electrometer triode. Mercury electrodes were used and most of the determinations were made at a constant potential of 150 volts. The effects of humidity and temperature were also studied and the results have been shown in a number of diagrams. Shellac plastics may, as a result of this investigation, be safely classed among those materials which have a high value of volume and surface resistivity.

INTRODUCTION

The direct-current resistance of an insulating material is usually determined by applying a potential difference between two points on the material and measuring the feeble current by any suitable means. But this resistance is usually considered to be the resultant of two components, *viz.*, the volume resistance and the surface resistance. Curtis[1] devised an ingenious apparatus to measure these two resistances separately by means of guard rings and his method of test has been adopted by the British Standards Institution[2] for determining the surface resistivity of moulded insulating materials. The American Society for Testing Materials[3] has also adopted a similar apparatus for the determination of the two resistivities. But if the resistivities are very high, the measurement of the extremely small current in this method may sometimes involve some difficulty, since this current is often so small that it is difficult to measure it even with a sensitive galvanometer. The method of charging a condenser with the feeble current and discharging it through a ballistic galvanometer has been described by Brown[4] and others[5] in high-resistance circuits, but the limitations of this method, the most troublesome of which is the long time constant, have been fully discussed by Cherry.[6] An electrometer (Compton[7] or Lindemann[8]) may be used for this purpose, but this method has also several disadvantages which have been described by Müller[9] and Cherry.[6] At present the electron tube method[9] is perhaps the most sensitive method of measurement in such a case. For this purpose special vacuum tubes called electrometer tubes are being used now. Rose[10] has described a circuit which makes use of the pliotron FP-54 of the General Electric Company of America for the measurement of very high resistances. Other investigators[11] have also used this tube in different circuits but Müller[12] and Cherry[6] for simplicity used triodes and their circuits have been fully described. With the help of such a circuit the value of the unknown high resistance R_x may be obtained in terms of another known high resistance R_s, the applied voltage E and the potentiometer voltage e required for balance. The relation[13] is

$$R_x = R_s[(E/e) - 1].$$

PREVIOUS WORK

Dietrich[14] studied the effect of temperature, light and moisture on the resistivity of lac. Curtis[1] measured the volume and surface resistivities of shellac along with other insulating materials. Stäger[15] also studied the effect of temperature on lac, pure lac resin and shellac-wax. An excellent review of these results has been made by Verman,[16] who states that both Dietrich's and Stäger's results for lac samples could by a proper choice of constants be made to fit Koenigberger and Reichenheim[17] equation

$$\rho = \rho_0 \cdot e^{-qt/273\,(t-273)}$$

where ρ = resistivity at t°C., ρ_0 = resistivity at 0°C, q = a constant.

The object of this paper is to report the results of measurement of resistivities of a few shellac moulded discs of different compositions[18] which have been evolved at this Institute under different conditions of temperature and humidity.

EXPERIMENTAL

As the preliminary measurements revealed that the volume and surface resistivities of shellac moulded discs were too high to be measured simply with

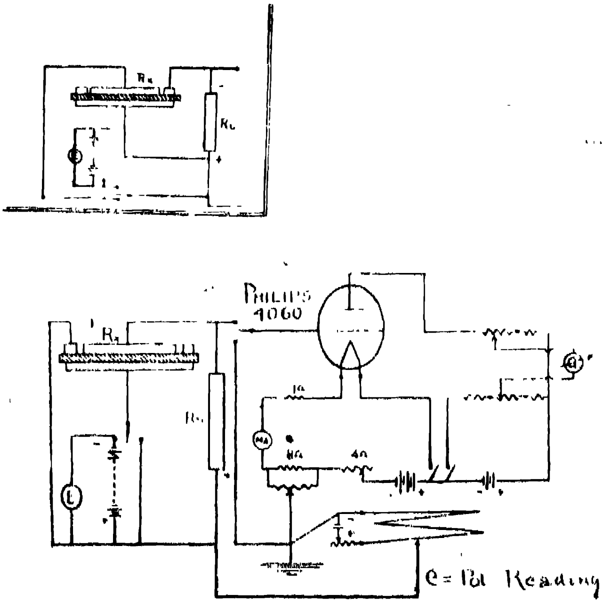

FIG. 1

a galvanometer, a circuit was constructed with a Philips 4060 electrometer triode. The particulars of this tube appeared in this journal [19] some time back and so these are not being given again. The circuit was similar in design to that described by Cherry[6] using the Westinghouse electrometer tube RH-507. The schematic diagram of the circuit used has been shown in Figure 1. The method of measurement and precautions regarding shielding and insulation have also been dealt by Müller[11] and other workers[20] and so these need not be repeated here.

Mercury electrodes as used by Curtis[1] were used in these investigations. Most of the measurements were done at a constant potential of 150 volts. The source of this voltage was a high-tension dry battery as used for radio sets. Humidity was controlled with solutions of different proportions of glycerine and water.[21] A big vacuum desiccator was used as the humidity chamber and tests were carried out inside this chamber. The leads were taken out through the top and holes made on the sides and closed with bushings made of beeswax-rosin. The voltage was applied across the dielectric together with a standard high resistance. A number of these standard high resistances of different values were made from liquid mixtures of alcohol, benzene, phenol and picric acid as described by Gemant.[22] These high resistances were kept in a chamber which was air tight and where some desiccating agent such as fused calcium chloride was kept in order to minimise surface leakage. The potential drop across the standard high resistance was measured by means of the electrometer triode on a potentiometer.

RESULTS AND DISCUSSIONS

The results of test have been shown in Tables I-III. They have also been shown in graphical form in Figures 2-4. Table IV shows the particulars of composition of shellač moulded discs. The variation of volume resistivity with temperature (Fig. 2) was found greater for kusum shellac than for shellac

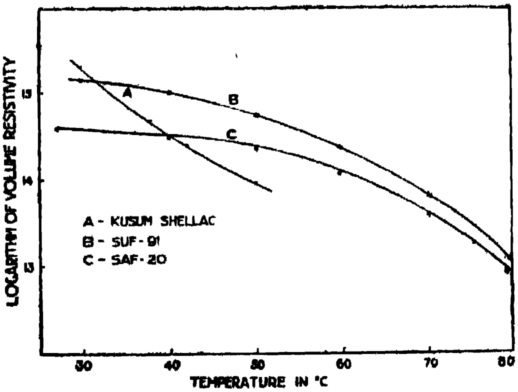

FIG. 2

moulding powders (Nos. SUF-91 and SAF-20) within the small range of temperatures through which it was possible to carry out measurements. At temperatures above 50°C. shellac discs began to soften slowly and it was not possible to make measurements. But shellac-urea-formaldehyde and shellac-aniline-furfural moulded discs withstood higher temperatures and measurements were carried out up to 80°C. After 65°C. the fall of resistivity of these discs however was somewhat rapid, probably owing to slight softening.

The effect of humidity on the volume resistivity of shellac discs has been shown in Fig. 3. Measurements were carried out when the discs were desiccated

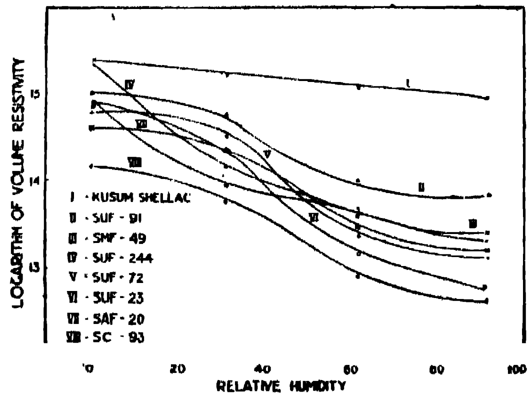

FIG. 3

and also under three different conditions of relative humidity, *viz.*, 30, 60 and 90 per cent. At each humidity the discs were kept for 72 hours before they were tested. The maximum slope of these curves seems to lie within 30 per cent and 60 per cent relative humidity indicating the maximum rate of fall. Similarly the variation of surface resistivity with humidity has been shown in Fig. 4. Here also the rate of fall is small up to 30 per cent humidity and thereafter it is more. A composition containing 10% rosin on the weight of lac (No. SUF-244; Curve IV, Fig. 4) shows a peculiarity in that the rate of decrease

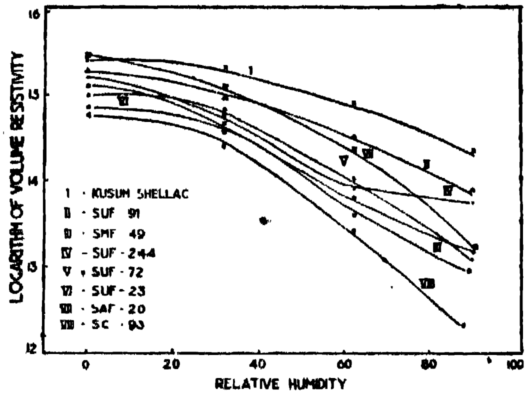

FIG. 4

of surface resistivity after 60% relative humidity is very small. This may be due to the presence of rosin which has been shown by Curtis[1] to have a very low rate of fall of resistivity with increasing humidity.

It may be mentioned in this connection that the current which flows through a solid insulating material as soon as the voltage is applied does not, as is well known, remain constant but changes with time. For some purposes[23] the current at the end of one minute is taken since the absorption current is usually negligible at the end of that period. In these tests, however, the current was measured at the end of 3 minutes since it was observed in a few cases that the effect of this absorption current could be noticed even after 2 minutes. At the end of three minutes, however, the current was more or less constant and hence that could be taken as the conductivity current. It should be noted, however, that the error of such hihh resistance measurements may be approximately 10% or even slightly more.

It may be said that the resistivity of shellac compositions generally is very high. At 50 per cent relative humidity and ordinary temperatures (25°C.-30°C.) the volume resistivity of these compositions usually lies within 3.5×10^{13} to 2.5×10^{14} ohm-cms. A comparison with the resistivity of other moulded materials is not feasible unless all the conditions of experiment are the same, *e.g.*, the method of measurement, the dimensions of the specimen, the applied voltage, the temperature, the humidity, etc. Nevertheless, on a scrutiny of the values of resistivity of most of the plastic materials,[24] shellac compositions may safely be classed among those plastics which have a very high resistivity.

TABLE I

Showing the variation of volume resistivity with temperature

ρ_v = volume resistivity.

Material	Temperature in °C	$\times 10^{13} - \rho_v$	Log ρ_v
Kusum shellac	28.4	262	15.41
	38.0	54.1	14.73
	42.6	28.0	14.44
	50.0	9.8	13.99
Shellac powder No. SUF-91	30.0	139	15.14
	40.0	95.7	14.98
	50.0	62.1	14.79
	60.0	28.9	14.46
	70.0	7.6	13.88
	80.0	1.4	13.14
Shellac powder No. SAF-20	27.0	42.2	14.62
	40.0	35.2	14.54
	50.0	21.4	14.32
	60.0	14.3	14.16
	70.0	5.1	13.7
	80.0	1.2	13.06

TABLE II

Showing the variation of volume resistivity with humidity

ρ_v = volume resistivity.

Material	$\times 10^{13} = \rho_v$, at relative humidity			
	0	30%	60%	90%
Kusum shellac	262	150	135	80
SUF—91	103	66	12.7	8.2
SMF—49	80	11	5.1	3.1
SUF—244	167	15.2	6.8	2.4
SUF—72	64	42	3.6	1.8
SUF—23	96	25	1.6	0.73
SAF—20	40	26	4.4	2.1
SC—93	16	7.6	1.3	0.51

TABLE III

Showing the variation of surface resistivity with humidity

ρ_s = surface resistivity.

Material	$\times 10^{13} = \rho_s$ at relative humidity			
	0	30%	60%	90%
Kusum Shellac	760	660	180	73
SUF—91	590	320	100	20
SMF—49	380	160	14	2.5
SUF—244	480	190	24	16
SUF—72	295	216	33	3.6
SUF—23	200	140	19.6	4.2
SAF—20	830	380	76	4.9
SC—93	175	113	10	0.42

TABLE IV

Showing the particulars of composition of shellac moulded discs used

Disc	Resin	Filler	Percentage of		
			Resin	Filler	Dye and lubricant
Kusum Shellac	Shellac	-	--	--	
SUF - 91	Shellac-urea-formaldehyde	Wood flour	48	49	3
SMF - 40	Shellac-melamine-formaldehyde	Wood flour	45	52	3
SUF - 44	Shellac-urea formaldehyde with resin and Phenol	Saw-dust	60	38	2
SUF—72	Shellac-urea-formaldehyde	Mica	30	69	1
SUF—25	,,	Asbestos	30	69	1
SAF—20	Shellac-aniline-furfural	Wood flour	49	49	2
SC 93	Shellac-casein	Wood flour	51	46	3

ACKNOWLEDGMENT

The author expresses his indebtedness to Dr. H. K. Sen, the Director of this Institute, for his kind interest and constant encouragement.

INDIAN LAC RESEARCH INSTITUTE,
RANCHI

REFERENCES

[1] Curtis, H. L., *Bull. Bur. Standards*, **11**, 359 (1914-15).

[2] B. S. Inst., *B S. Specifications for Moulded Insulation Materials suitable for Accessories for General Electrical Insulation*, No 488 (1933).

[3] *A. S. T. M. Standards, Part III*, 299 (1939)

[4] Brown, H., *J. Sci. Instr.*, **2**, 12 (1924).

[5*] Dole, M., *J. Am. Chem. Soc*, **53**, 620 (1931); Jones and Kaplan, *J. Am Chem. Soc.*, **50**, 1845 (1928).

[6] Cherry, R. H., *Trans. Electrochem. Soc.*, **72**, 33 (1937).

[7] MacInnes, A. and Belcher, D., *J. Am. Chem. Soc.*, **53**, 3315 (1931).

[8] Kenidge, B. M. T., *Biochem. J.*, **19**, 611 (1925); Müller, F., *Zeit. f. Elektrochem.*, **37**, 857 (1931).

[9] Müller, F., *Trans. Electrochem. Soc.*, **62**, 335 (1932).

[10] Rose, G. M., *Rev. Sci. Instr.*, **2**, 810 (1931).

[11] Du Bridge, L. A., *Phys. Rev.*, **37**, 392 (1931); Hill, *Science*, **73**, 529 (1931); Du Bridge, L. A., and Brown, H., *Rev. Sci. Instr.*, **4**, 532 (1931); Turner, L. A., and Siegelin, C. O., *Rev. Sci. Instr.*, **4**, 429 (1933).

[12] Müller, F., *Zeit. f. Elektrochem.*, **38**, 418 (1932).

[13] Littleton, J. T., and Morey, G. W., *The Electrical Properties of Glass (J. Wiley & Sons)*, 67 (1933).

[14] Dietrich, W., *Phys. Zeit.*, **11**, 187 (1910).

[15] Stager, H., *Elektrotechnische Isoliermaterialien* (*Wiss. Verlag. Stuttgart*), 210 (1931).

[16] Verman, L. C., *Lond. Shell Res. Bur. Tech.*, *Paper* No. 7, May (1936).

[17] Koenigberger and Reichenheim, *Phys. Zeit.*, **7**, 570 (1906), *ibid*, **8**, 833 (1907); *ibid*, **9**, 351, (1908); *Zeit. f. Elektrochem.* **15**, 7 (1909).

[18] Bhattacharya, G. N., *Paper under Publication.* Venugopalan, M., and Sen, H. K., *British Plastics & Moulded Products Trader*, **10**, 626 (1939); Sen, H. K., *J. Ind. Chem. Soc.*, **18**, 47 (1941).

[19] Thaes, J. A. N., *Ind. J. Phys.*, **13**, 199 (1939).

[20] Fosbinder and Schoonover, *J. Bio. Chem.*, **88**, 605 (1930); Janssen, *Chem. Weekbl.*, **28**, 218 (1931).

[21] Grover, D. W. and Nicol, J. M., *J. Soc. Chem. India*, **59**, 175 (1940).

[22] Gemant, A., *Liquid Dielectrics (J. Wiley & Sons)*, 66 (1933).

[23] *A. S. T. M. Standards, Part III*, 304 (1939), and *B. S. Specifications*, No. **488**, 14 (1933).

[24] Modern Plastics, **17**, *Plastics Properties Chart*, 1939-1940, *Oct.* (1939).

THERMAL CONDUCTIVITY OF LIQUID METALS

By M. RAMA RAO, M.Sc.

(Received for publication, November 26, 1941)

ABSTRACT. The abrupt decrease in the thermal conductivity of metals observed near the melting point is explained on the assumption that the frequency of vibration of molecules suffers a change near the melting point. The ratio of thermal conductivities in the solid and liquid phases near the melting point is shown to be given by $e^{\frac{2}{3}\frac{\lambda_m}{K_0T_m}}$ where K_0 is the Boltzman constant and $\frac{\lambda_m}{T_m}$ is the entropy of melting. This is found to be in good agreement with observed values. The slight decrease in the thermal conductivity in the liquid phase is ascribed to the disordered state in the liquid.

The thermal conductivity of normal metals in the liquid state just above the melting point is about half as great as that of the solid metal just below the melting point. Certain abnormal metals, however, such as bismuth and antimony which are poor conductors in the solid, increase their conductivity on melting. The abrupt change in thermal conductivity at the melting point has not been explained so far. An attempt is here made to explain such a change from the point of view of modern theory of electronic conduction based on wave mechanics.

From the standpoint of modern theory, the expression for the thermal conductivity of a metal should contain two additive terms, one due to the lattice and the other due to electron conductivity. A. H. Wilson[1] gives the equation as

$$K = \frac{1}{3}\rho c l u + \frac{\pi^2}{3}\frac{n_0 \tau K_0^2 T}{m}.$$

K is the thermal conductivity ; ρ the density, c the atomic heat, l the electron mean free path in the lattice ; u the velocity of elastic waves in the lattice (sound) ; n_0 the number of free electrons per unit volume ; τ the "relaxation time" (average time between collisions) ; K_0 the molecular gas constant ; T the absolute temperature. If we write the equation as

$$\frac{K}{\rho c} = \frac{1}{3} l u + \frac{\pi^2}{3}\frac{n_0 \tau K_0^2 T}{m \rho c}$$

it is in the form

$$\frac{K}{\rho c} = \frac{A}{T} + B.$$

This assumes that $\tau \propto T^{-1}$ and $lu \propto T^{-1}$ and that ρ and c compensate as to their temperature effects.

The equation in this latter form is experimentally verified by data on tin, lead and zinc.[2] Values of $\frac{K}{\rho c}$ plotted as ordinate against $\frac{1}{T}$ as abscissa give straight lines with intercepts on the y-axis and these intercepts turn out to be the values of $\frac{K}{\rho c}$ for the molten state. The conductivity for the molten state includes the residual atomic conductivity as well as that due to electrons. The conductivity of an insulating liquid is very small (1 per cent. or less than that of a conductor[1]. Hence the last term on the right is, very likely, almost entirely electron conductivity. The temperature effect for the solid is easily seen to be entirely due to the elastic lattice. The data indicate little or no temperature effect in the liquid state. The sharp decrease of thermal conductivity at the melting point from the solid to the liquid condition has not been explained.

In a solid each atom vibrates about a mean position (which is fixed) independently of the remaining atoms. In a liquid the atoms vibrate about mean positions which while not fixed move with velocities small compared with the velocity of the order of magnitude $\sqrt{\frac{KT}{m}}$ with which the atoms vibrate. This simple picture[3] of a liquid near its melting point has furnished valuable information regarding the physical properties of the liquid near the melting point.

Guggenheim and Fowler[4] have shown that if there are N positions of minimum potential energy in the quasi-crystalline liquid and that if each atom moves about a position of minimum potential energy in a field corresponding to an isotropic three-dimensional harmonic oscillator of frequency ν_l and if the corresponding frequency in the solid is denoted by ν_s, the entropy of melting is given by

$$\frac{\lambda_m}{T_m} = 3\,K_0 \log \frac{\nu_s}{\nu_l} + K_0$$

where λ_m is the molecular heat of melting, T_m the melting temperature, K_0 the Boltzman constant. The expression given above is based on the assumption amongst others that the vibrations are effectively classical, *i.e.*, that the temperature of melting T_m should be large compared with the characteristic temperature $\frac{h\nu}{K_0}$ Mott and Gurney have pointed out that it is only a rough approximation to retain the extra factor e in the partition function $\{\Omega(T)\}^N$ as has been done by Eyring. The true factor is not a constant but varies with temperature becoming more nearly unity near the melting point. In that case the term K_0 in the above equation will fall to a very small fraction of K_0 and the factor containing $\frac{\nu_s}{\nu_l}$ becomes more important. Mott[5] has applied these considerations to explain the change in electrical conductivity on melting according to the modern theory of electronic conduction in metals.

According to Bloch[6], in a pure metal the electrons move to a first approximation without resistance amongst the ions which are vibrating in an irregular fashion. It is only to a second approximation that there is any interaction between electrons and lattice vibrations so that the conduction of heat is a second-order effect. Further, it is shown by Bloch that a finite free path is caused by the heat motions of the lattice, so that the free path is reduced by raising the temperature. According to this view all the electrons in a metal are free but it does not follow that they are all conduction electrons. Actually the free electrons in a solid form open and closed groups in much the same way as do electrons in an atom and it is only when there are open groups that conduction electrons exist In this way it is possible to arrive at a theory of thermal conduction which embraces both metals and semi-conductors. The conductivity depends on the extent to which the electrons may be considered free, *i.e.*, to the ease with which they move from atom to atom under the influence of the temperature gradient.

According to Bethe[7] the thermal conductivity at fairly high temperatures is given by

$$K = \frac{\pi^2}{3}\left(\frac{K_0}{c}\right)^2 \frac{2n_0}{\pi^2}\,\frac{M}{m}\,\frac{K'}{C}\left(\frac{dE}{dK'}\right)^2 \frac{1}{hK'a_0}\,K_0\Theta^2.$$

Here n_0 denotes the number of free electrons per atom, M and m the mass of the vibrating atom and the electron respectively, a_0 the radius of the first Bohr orbit, K' denotes the wave number of an electron at the top of the Fermi-distribution, E the kinetic energy of such an electron, C is a constant depending on the interaction between the metallic ion and a free electron which is a property of the ion rather than the crystal structure. K' depends only on the specific volume and so will not alter appreciably on melting. Θ is the characteristic temperature. In the expression for the thermal conductivity the quantities which change when melting takes place are $K'\frac{dE}{dK'}$ and Θ. The change in $K'\frac{dE}{dK'}$ is comparatively small since the volume change is at most five per cent. for it can be shown that $K'\frac{dE}{dK'}$ is nearly twice the maximum energy of the Fermi-distribution and this depends only on the volume. Hence any change in the thermal conductivity from the solid to the liquid must be attributed to a change in Θ. Bidwell's experiments show that the conductivity at the melting point is almost entirely electronic. Hence we write for K at the melting point the expression

$$K = \frac{\pi^2}{3}\left(\frac{K_0}{e}\right)^2 \frac{2n_0M}{\pi^2 m} \frac{K'}{C}\left(\frac{dE}{dK'}\right)^2 \frac{1}{hK'a_0} K_0\Theta^2.$$

The change in thermal conductivity on melting is therefore given by

$$\frac{K_s}{K_l} = \left(\frac{\nu_s}{\nu_l}\right)^2 = \frac{2}{e^3} \frac{\lambda_m}{K_0T_m}.$$

Table I shows the extent to which the hypothesis is in agreement with experiment.

Element	$N\lambda_m$ (Cal./mole)	T_m °k	$\frac{T_m}{\Theta}$	$\frac{K_s}{K_l}$ (calc.)	$\frac{K_s}{K_l}$ (obs.)
Zinc	1700	692	2.9	2.23	2.01
Aluminium	1910	933	4.3	1.80	1.65
Lead	1120	590	6.6	1.88	1.78
Tin	(not accurate)	505	—	2.81	1.79
Sodium	630	370	1.85	1.58	1.33
Antimony	1660	903	—	5.65	1.14
Bismuth	2600	544	-	4.95	0.44

Aluminium, lead and sodium crystallize in the cubic form. Tin is tetragonal body-centered, zinc is hexagonal. Antiomony and bismuth are well known to be of complex crystalline structure and so do not invalidate the suggestion put forward. These metals are always exceptional as compared with others. For instance the ratio of electrical resistance of solid to that of the liquid is about 0.5 as compared to values in the neighbourhood of 2 for other metals. It is well known that bismuth contracts on melting in contradistinction to other metals. It is also found that the velocity of sound[8] in liquid bismuth is greater than the velocity in solid bismuth in the neighbourhood of the melting point in contradistinction to other metals. Excluding the case of antimony and bismuth the agreement between calculated and observed values is fair. The lower conductivity in the liquid is due to the greater amplitude of the atomic oscillations and not to any extent to the irregularity of the arrangement of the atoms as contrasted with regular arrangement in the crystalline solid. For sodium and aluminium, the assumptions on which the calculation is based, namely that T_m is greater than $\frac{h\nu}{K_0}$, is hardly justified and hence the more correct expression

$$\frac{e^{\frac{h\nu_s}{K_0T_m}}-1}{e^{\frac{h\nu_l}{K_0T_m}}-1}=e^{\frac{1}{3}\frac{\lambda_m}{K_0T_m}}$$

is used for the ratio of $\frac{\nu_s}{\nu_l}$ in the table. As regards the values of $\frac{k_s}{k_l}$, the values are taken from Konno's[9] paper (the only data found in the literature). The drop in conductivity at the melting point found by Bidwell in the case of zinc agrees with the data of Konno.

If the decrease of thermal conductivity in liquid metals is due entirely to the change in the value of ν, the thermal conductivity ought still to be independent of temperature. It is found that the values of thermal conductivity in the liquid state decrease slightly with temperature. While Konno's data suggested this, his results did not extend far enough to prove it. But recent experiments of Bidwell prove beyond doubt a slight decrease of thermal conductivity. The slight decrease in the liquid phase might be ascribed to the disordered state of the liquid.

In conclusion, it gives me very great pleasure to record my thanks to Professor A. Venkata Rao Telang for his guidance during the progress of this work.

DEPARTMENT OF PHYSICS,
UNIVERSITY OF MYSORE,
BANGALORE.

REFERENCES

[1] Wilson, A. H., *Semi conductors and Metals* (Macmillan, New York, 1939)

[2] Bidwell, *Phy. Rev.*, **56**, 594 (1939) and **58**, 561 (1940).

[3] Andrade, *Phil. Mag.*, **17**, 698 (1934); Sibaiya and Rama Rao, *Ind. Jour. Phy*, **13**, 293 (1939); Rama Rao, *Phy., Rev.*, **59**, 212 (1941); Rama Rao, *Jour. Chem. Phy*, **9**, 120 (1941).

[4] Guggenheim and Fowler, *Statistical Thermodynamics* (1939).

[5] Mott, *Proc. Roy. Soc.*, **146**, 465 (1934).

[6] Bloch, *Z. Physik*, **59**, 208 (1930).

[7] *Handb. Physik*, **24/11**, 507 (1933).

[8] Stierstadt, *Metallwirtschaft*, **11**, **18**, **32** (1932).

[9] Konno, *Phil. Mag.*, **40**, 542 (1920)

THERMAL CONDUCTIVITY OF LIQUIDS

By M. RAMA RAO, M.Sc.

(Received for publication, November 26, 1941)

ABSTRACT. Considering a liquid near its melting point as an assemblage of a large number of linear harmonic oscillators each vibrating with a frequency ν and assuming that communication of thermal energy takes place at each extreme vibration an expression for the thermal conductivity of the liquid at the melting point is deduced, *viz.*, $K = 2{\cdot}096 \times 10^5 \sqrt{\frac{\theta_s}{M V_s^{\frac{2}{3}}}}$, where θ_s is the melting point of the liquid on the absolute scale of temperature, M the molecular weight, V_s the molecular volume. A brief review of the subject is attempted and it is shown that the thermal conductivity K is intimately connected with the free volume of the liquid at the melting point. Calculated values of thermal conductivity according to the above expression are in agreement with observed values

The thermal conductivity of liquids is a subject which has been without any general theoretical basis. It has been recognised that the mechanism of conduction in liquids must be different from that in a gas. This is evinced for instance by the fact that the thermal conductivity of a liquid decreases with rise of temperature while the thermal conductivity of a gas increases with rise of temperature. In a gas there is transport of the individual atoms from one layer to another with a consequent transfer of energy. Between collisons the atoms are supposed to move freely over a distance large compared with the molecular size and it is essential for the theory that disparity between mean free path and molecular diameter should exist. In the case of liquids there is in the ordinary sense no free path at all, the motion being always in an intense field of intermolecular forces.

Leon Brillovin[1] has given a theory of liquid viscosity in which the fundamental idea is that the impact of molecules gives rise to elastic waves, the effect of which is that neighbouring molecules are successively disturbed from their positions. The theory is an attempt to transfer the general theory developed by Einstein and Debye for specific heats of solids and liquids to the field of liquid viscosity. The final formula which gives the temperature coefficient of viscosity in terms of the thermal conductivity and the velocity of sound fails by a factor of nearly 5,000. In 1923 Bridgman[2] put forward a theory of thermal conduction in liquids in which the energy difference between adjacent molecules in the direction of temperature gradient is to be conceived as handed down a row of molecules with the velocity of sound. He arrived at an expression for the thermal conductivity K in terms of the velocity of sound V and the mean molecular distance. Although this simple picture gives approximately the absolute value of the thermal conductivity at the ordinary temperatures, it does not explain quantitatively the variation of thermal conductivity with temperature. It does not account at all well for the phenomena of thermal conduction under pressure. In 1914 Debye[3] suggested a complicated equation for the conductivity of a solid which can readily be reduced to one exactly like Bridgman's by substituting the liquid values for the solid ones, with the exception that the constant 2 in Bridgman's expression is replaced by 1/2. Thus Debye's values are only one quarter of Bridgman's. Kardos[4] has modified Bridgman's theory by allowing for the diameter of the molecules. Kardos introduces in his expression a factor δ which is the mean distance between edges of molecules and suggests that as a first approximation δ be assumed constant and equal to 0.95×10^{-8} cm. Kardos gives expression to calculate δ, *viz.*, $\delta = \frac{C_1 \beta^{3}}{\sigma}$ where C_1 is the inner repelling force of molecules, β is the volume compressibility, σ the mean molecular distance. An examination of the above relation shows that the equation is dimensionally incorrect and does not seem to have any physical significance. Weber[5] in 1880 suggested an empirical relation connecting the thermal conductivity of liquids with their other properties, namely, $\frac{K}{\rho C}$ = constant and later modified to

$$\frac{K}{\rho C}\left(\frac{m}{\rho}\right)^{\frac{1}{3}} = \text{constant}.$$

Here ρ is the density of the liquid, C its specific heat, and m its molecular weight. The factor $\left(\frac{m}{\rho}\right)^{\frac{1}{3}}$ is seen to be proportional to the mean molecular distance. Weber's own data indicate a surprising constancy of the modified expression but later discussion by Aubel has disclosed considerably greater variations than supposed by Weber. Smith's[6] empirical equation for thermal conductivity involves a number of constants and is sufficiently complicated to merit any discussion.

It will be seen then that none of the older attempts have led to results which can withstand comparison with experimental results, in particular with the recent high pressure results of Bridgman which enable thermal conductivities at constant volume to be computed. As a result the study has hitherto consisted largely of a collection of more or less well-established empirical relations mostly of limited scope. In general, lack of agreement with experiment is the chief reproach that can be levelled against older theories. The theory of liquids should be approached not as has hitherto been done from the point of view of the kinetic theory of gases, which was constructed to deal with matter where the spaces between the molecules are large compared with the size of the molecules but from the point of view of the solid state, the density of which is not markedly different from that of the liquid state of the same substance. In a solid the atoms vibrate about mean positions which are fixed. In a liquid at temperatures near the melting point, it is now generally recognized that the atoms vibrate about mean positions which though not fixed move slowly compared with the velocity of the order of magnitude $\sqrt{\frac{KT}{m}}$ with which the atoms vibrate. The most direct evidence for this is afforded by the specific heat of substances which have within experimental error (7%) the same values (in the neighbourhood of 3R) for a given substance in the solid and liquid states near the melting point. Further evidence[7] is given by the rates of diffusion of gold in mercury or of thorium B in non-radio-active liquid lead. If one compares the numbers with the formula for the diffusion coefficient D in gases $D = \frac{1}{3}lc$ where l is the mean free path and c the mean molecular velocity, one finds on setting c equal to a quantity of the order of magnitude $\sqrt{\frac{KT}{m}}$ that l must be taken to be about 1/100 of the inter-atomic distance. A theory of viscosity of liquids has recently been given by Andrade[8] based on the same hypothesis. Based on the same hypothesis a theory of surface tension in liquids[9] at the melting point has been proposed by Sibaiya and Rama Rao.

Let us treat the atoms of the liquid as though they were vibrating about slowly displaced equilibrium positions. We shall also suppose that each atom vibrates with a frequency ν which is the same for each atom although it is probable that in a real liquid the frequencies will not all be exactly the same. The arrangement of molecules in the liquid state is not fundamentally dissimilar to the arrangement in the solid state—the difference in the two states being brought about by the large amplitude of vibration of the atoms in the liquid state. Hence a liquid at its melting point is regarded as an assemblage of a number of harmonic oscillators, each vibrating with a frequency ν about a slowly displaced equilibrium position and with an amplitude which is comparable with the mean molecular distance. In dealing with the problem of heat conduction in liquids we are concerned with the transport of thermal energy by the molecules. We shall treat the whole system as though there were merely a superimposed disturbance which is transmitted by the molecules, thus neglecting the effect of the superimposed disturbance on the original system. On the basis of the assumptions an estimate of thermal conductivity from other physical data such as can be found in tables can be made. A preliminary report[10] regarding this has already appeared in the "Physical Review." Such an estimate is a desirable feature of any theory of thermal conduction in liquids because the more complicated theories, based on considerations of partition functions, have failed not only to provide such an estimate, but have in general involved undetermined parameters in such a way that any experimental verification is difficult, except in the matter of generalities.

Let there be a thermal energy gradient $\frac{dE}{dZ}$ along the z-axis. Let us consider layers of molecules parallel to the direction of the thermal energy gradient and the molecules to be vibrating in random directions. We shall suppose that on an average 1/3 of the molecules are vibrating along each of three directions perpendicular to one another. The difference of energy between two layers is $\frac{dE}{dZ}\sigma$ where σ is the mean molecular distance. According to our assumption, since the amplitude of vibration is large at the melting point, molecules of one layer come into contact with the molecules of the neighbouring layers at every extreme vibration. When there is a contact (of very brief duration), we shall assume that the excess of thermal energy is communicated. A molecule of a given layer conveying thermal energy crosses a plane normal to the direction of drift twice in every complete vibration. A molecule of the adjacent layer also crosses this plane twice in every complete vibration. If ν is the frequency of vibration of the molecule, then the transfer of thermal energy per unit area per unit time is given by $\frac{4}{3}\nu\frac{1}{\sigma^2}\frac{dE}{dZ}\sigma$, where $\frac{1}{\sigma^2}$ refers to the number of molecules in unit area. This, by definition, is equal to the product of the coefficient of thermal conduction and the temperature gradient ; hence we have

$$K\frac{d\theta}{dZ} = \frac{4}{3}\nu\frac{1}{\sigma^2}\frac{dE}{dZ}\sigma,$$

i.e.,

$$K=\frac{4}{3}\frac{\nu}{\sigma}\frac{dE}{d\theta}.$$

The average energy (both kinetic and potential) of a vibrating molecule is $3k\theta$, where k is Boltzmann constant ; hence we have

$$K=\frac{4k\nu}{\sigma}.$$

For ν we substitute the Lindemann expression, *viz*.,

$$\nu=2.8\times 10^{12}\sqrt{\frac{\theta_s}{MV_s^{\frac{2}{3}}}}$$

where θ_s is the melting point on the absolute scale of temperture, V_s the molecular volume and M the molecular weight. Lindemann's theory is based upon Einstein's formula for the frequency of vibration of an individual atom in a regular array which implicitly assumes a single frequency ν. Lindemann assumes a simple harmonic vibration characterized by $m\frac{d^2x}{dt^2} = -ax$, and $\nu = \frac{1}{2\pi}\sqrt{\frac{a}{m}}$, which gives a maximum kinetic energy $\frac{1}{2}aA^2 = \frac{h\nu}{e^{\frac{h\nu}{k\theta_s}} - 1}$, where A is the amplitude of the vibration. Lindemann assumes that melting takes place when the vibration amplitude attains a value $1/2S\sigma$ where σ is the mean molecular distance and $S\sigma$ the distance between the peripheries of the atoms in their equilibrium positions. Then

$$\nu^2 = \frac{2}{\pi^2 S^2 \sigma^2 m} \cdot \frac{h\nu}{e^{\frac{h\nu}{k\theta_s}} - 1}.$$

Lindemann takes $\frac{h\nu}{k\theta_s}$ small, so that as a first approximation

$$\nu^2 = \frac{2}{\pi^2 S^2 \sigma^2 m} k\theta_s$$

$$\nu = \frac{1}{\pi S}\sqrt{\frac{2R\theta_s}{M\sigma^2}}$$

where M is the molecular weight, and R is the gas constant. This is further written in terms of the molecular volume V_s because σ^3 is proportional to V_s, hence we have finally

$$\nu = c\left(\frac{\theta_s}{MV_s^{\frac{2}{3}}}\right)^{\frac{1}{2}}.$$

The value of S being unknown, Lindemann found c by comparison with the best values for ν found by other methods for certain bodies. This naturally involves the assumption that S is the same for all substances or in other words that Gruneisen's rule is true, which states that for all simple solids increase in volume from absolute zero to melting point is about the same fraction of the volume, *viz.*, 7.5 per cent. Above all Lindemann's formula involves S which is a measure of the free volume so that ν involves this quantity.

For σ we substitute $\left(\frac{3V_s}{4\pi N}\right)^{\frac{1}{3}}$ where N is Avogadro number. It then follows that the thermal conductivity K at the melting point is given by

$$K = 2.096 \times 10^5 \left(\frac{\theta_s}{MV_s^{\frac{4}{3}}}\right)^{\frac{1}{2}}.$$

The constant $2.096 \times 10^{\text{[illegible]}}$ involves the factor S which has been assumed to be the same for all types of molecules. This is hardly justified when we consider different shapes of molecules. The constant may have to be modified when more precise methods of calculation are available. In Table I are given the calculated and the observed values of thermal conductivity. In some cases, where the variation of thermal conductivity with temperature has been studied, the extrapolated values at the melting point are recorded. As regards liquid metals they stand in a class by themselves because the contribution of the electrons in the metal in the process of thermal conduction has to be dealt with, which really forms the major contribution for thermal conduction in metals. In the present investigation only dielectric liquids are considered.

TABLE I

Substance	Melting point in °K	Thermal conductivity at melting point	
		Calculated	Observed
Carbon tetrachloride	243	1.315	1.124
Aniline	265	1.730	1.720
Chloroform	203	1.594	1.382
Diethyl ether	156	1.590	1.380
Benzene	278.4	2.012	1.677
Chloro-benzene	227.8	1.425	1.561
Fluoro-benzene	231.8	1.645	1.580
Bromo benzene	242.4	1.205	1.330
Iodo-benzene	241.6	1.014	1.230
Acetic acid	280	1.900	1.970
Liquid sulphur	388	1.350	1.810
,, oxygen	54	3.170	2.001
,, nitrogen	62.5	3.040	2.075

The calculated values are of the right order and places the conductivities of substances like liquid sulphur, oxygen and nitrogen in the right sequence of magnitude and gives their relative magnitudes.

The question of the variation of thermal conductivity with pressure and temperature will be dealt with separately. Also the relation between the liquid structure and the constant occurring in Lindemann's formula will be considered in a separate paper.

In conclusion, it gives me great pleasure to thank Prof. A. Venkat Rao Telang for his valuable guidance throughout the work.

DEPARTMENT OF PHYSICS,
UNIVERSITY OF MYSORE,
BANGALORE.

REFERENCES

[1] *Journal de Physique*, **3**, 326 (1922).
[2] Bridgmann, *The Physics of High Pressure* (London, 1931).
[3] Debye, *Vorträge über die kinetische Theorie der Materie* (Liepzig, 1914).
[4] Kardos, *Forschung auf dem Gebeite des Ingenieurwesens Ausgabe, A*. **5** 14 (1934).
[5] Weber, *Wied. Ann.*, **103**, 304, 472 (1880).
[6] Smith, *Trans. Am. Soc. Mech. Eng.*, **58**, 718 (1936).
[7] J. Groh and G. Von Hevesey, *Ann. der phys.*, **63**, 85 (1920).
[8] Andrade, *Phil. Mag.*, **17**, 497 (1934)
[9] Sibaiya and Rama Rao, *Ind. Journ. Phys.*, **13**, 293 (1934).
[10] Rama Rao, *Phy. Rev.*, **59**, 212 (1941), Dosida, *Proc. Phy. Math. Soc. of Japan*, **21**, 6 (1939).
[11] Lindemann, *Phy. Zeits.*, **11**, 609 (1910); *Blom Ann. d. Phys.* **42**, 1397 (1913).

STRUCTURE OF THE ELECTRONIC BANDS OF THE OD MOLECULE. PART V. Λ-DOUBLING

BY M. G. SASTRY

(Received for publication, December 5, 1941)

ABSTRACT. The Λ-doubling in the $^2\Pi$ states of the OD molecule has been examined in the light of Mulliken's deductions from Van Vleck's theoretical equations. The doublet difference $\delta\nu_{2dc}(K)-\delta\nu_{1dc}(K)$ is found to vary nearly linearly with K. Comparison of the Doubling in OH and OD molecules has confirmed the conclusion of Johnston that it is smaller for OD than for OH. The ratio is determined to be about 0·31 slightly higher than that obtained by Johnston.

INTRODUCTION

The theory of Λ-type doubling has been developed especially by Van Vleck[1] for $^1\Pi$, $^2\Pi$ and other states of diatomic molecules. Mulliken,[2] in a comprehensive paper, restated Van Vleck's equations in a convenient form for application to experimental data. The following expressions have been deduced for the doubling (in Mulliken's notation) :

$$\delta\nu_{2dc}=\left[\left(\tfrac{1}{2}p_0+q_0\right)\left(1+2X^{-1}-Y.X^{-1}\right)\quad+2q_0X^{-1}(J-\tfrac{1}{2})(J+1\tfrac{1}{2})\right](J+\tfrac{1}{2})\quad\ldots\ (1)$$

$$\delta\nu_{1dc}=\left[\left(\tfrac{1}{2}p_0+q_0\right)\left(-1+2X^{-1}-Y.X^{-1}\right)+2q_0X^{-1}(J-\tfrac{1}{2})(J+1\tfrac{1}{2})\right](J+\tfrac{1}{2}).\quad\ldots\ (2)$$

Hence
$$\delta\nu_{2dc}(J)-\delta\nu_{1dc}(J)=(p_0+2q_0)(J+\tfrac{1}{2})\quad\ldots\ (3)$$

$$\delta\nu_{2dc}(J)+\delta\nu_{1dc}(J)=\left[(p_0+2q_0)(2-Y)(J+\tfrac{1}{2})+4q_0(J-\tfrac{1}{2})(J+\tfrac{1}{2})(J+1\tfrac{1}{2})\right]X^{-1}.\quad\ldots\ (4)$$

Mulliken applied equations (3) and (4) to a number of molecules among which are the OH and others which correspond to intermediate coupling case between (*a*) and (*b*). It was emphasised that, for large values of J, the effect of "rotational stretching" of the molecules must be considered in evaluating the constants.

Dawson and Johnston[3] and later Johnston,[4] while investigating the structure of the OH bands, have examined the question of Λ-doubling. For $v''=0$, 1 and 2, they have shown that the difference $\delta_1(K)-\delta_2(K)$ which in Mulliken's notation is the same as $\delta\nu_{2dc}(J)-\delta\nu_{1dc}(J)$ varies directly with K and not with $(K+\tfrac{1}{2})^2$. They have concluded that Van Vleck's theoretical equation has thereby failed, to fit for OH, by quite a large factor. Mulliken's deduction [refer equation (3)] shows that the variation is in keeping with Van Vleck's theory.

In the light of data obtained by the writer of the Λ-doubling in the $^2\Pi$ states of the OD molecule an attempt is made to examine this question.

RESULTS

All the values* of the Λ-doubling for the two components of the $^2\Pi$ states corresponding to $v''=0$, 1, 2 and 3 have been collected in Tables I and II. For each state, the mean values are obtained utilising the data of different bands having the same final state. (The convention of 'signs' defined by Mulliken, *loc. cit.*, p. 103, has been adopted.)

TABLE I

Λ-doubling (δ) for $^2\Pi_{1\frac{1}{2}}$ levels)

K	$v''=0$				$v''=1$				$v''=2$			$v''=3$
	0,0	1,0	2,0	Mean	1,1	2,1	3,1	Mean	2,2	3,2	Mean	3,3
1	0	−.1	.7	.2	−1.2	.5	.5	−.4		.2	.2	
2	−.16	−.3	.5	0	−.6	−.2	−.3	−.4	−.9	−.3	−.6	
3	−.33	−.1	−.3	−.2	−.5	−.9	−.2	−.2	−.5	−1.0	−.8	−.3
4	+.49	−.2	−.6	−.4	−.3	−.5	−.1	−.1	−.4	−.1	−.7	.2
5	−.65	−.3	−.6	−.5	−.4	−.1	−.1	−.1	−1.5	−.1	−.8	−1.1
6	−.59	−.5	−.7	−.6	−.2	3	−.5	−.2	−.6	−.1	−.4	0
7	−.70	−.7	−.7	−.7	0	−.2	−.7	−.3	.3	−.2	.1	1.8
8	−1.08	−.6	−.8	−.8	−.7	−.8	−.9	−.8	−.6	−1.1	−.9	−.2
9	−1.40	−.8	−1.2	−1.1	−1.2	−1.3	−1.2	−1.2	−1.9	−1.3	−1.6	−1.4
10	−1.53	−.9	−1.3	−1.2	−1.8	−1.6	−1.3	−1.6	−3.7	−1.5	−2.6	−1.0
11	−1.90	−1.1	−1.9	−1.6	−2.3	−1.7	−1.7	−1.9	−2.6	−1.8	−2.2	−1.2
12	−2.01	−1.9	−2.0	−2.0	−2.9	−1.5	−2.1	−2.2	−3.8	−1.5	−2.7	—
13	−2.43	−2.4	−2.1	−2.3	−2.7	−1.8	−2.3	−2.3	−2.5	−2.1	−2.3	—
14	−2.82	−3.3	−2.8	−3.0	−3.2	−2.6	−2.6	−2.8	−2.5	—	−2.5	—
15	−3.35	−3.2	−3.0	−3.2	−3.5	−3.0	—	−3.3	−3.2	—	−3.2	—
16	—	−3.8	−3.7	−3.8	−3.0	−3.6	—	−3.3	−4.3	—	−4.3	—
17	—	−4.3	−3.8	−4.1	−4.4	−3.9	—	−4.2	−3.5	—	−3.5	—
18	—	−4.0	−3.9	−4.0	−3.8	−4.7	—	−4.3	−3.5	—	−3.5	—
19	—	−4.9	−1.2	−4.9	−4.8	—	—	−4.8	−3.6	—	−3.6	—
20	—	−4.8	—	−4.8	−4.8	—	—	−4.8	−5.4	—	−5.4	—
21	—	−5.7	—	−5.7	−5.8	—	—	−5.8	−5.8	—	−5.8	—
22	—	−5.8	—	−5.8	−6.2	—	—	−6.2	−7.1	—	−7.1	—
23	—	−6.1	—	−6.1	−4.6	—	—	−4.6	−8.3	—	−8.3	—
24	—	−6.6	—	−6.6	−6.2	—	—	−6.2	—	—	—	—
25	—	−7.7	—	−7.7	−8.6	—	—	−8.6	—	—	—	—
26	—	−9.7	—	−9.7	−8.1	—	—	−8.1	—	—	—	—
27	—	—	—	—	−7.3	—	—	−7.3	—	—	—	—
28	—	—	—	—	−8.8	—	—	−8.8	—	—	—	—
29	—	—	—	—	−10.0	—	—	−10.0	—	—	—	—
30	—	—	—	—	−11.9	—	—	−11.9	—	—	—	—
31	—	—	—	—	−12.6	—	—	−12.6	—	—	—	—
32	—	—	—	—	−11.2	—	—	−11.2	—	—	—	—
33	—	—	—	—	−8.7	—	—	−8.7	—	—	—	—
34	—	—	—	—	−9.3	—	—	−9.3	—	—	—	—

Taken from Parts I, II, and III of this series of papers.

TABLE II

Λ-doubling (δ_2 for $^2\Pi_{\frac{1}{2}}$ levels)

K	$v''=0$				$v''=1$				$v''=2$			$v''=3$
	0,0	1,0	2,0	Mean	1,1	2,1	3,1	Mean	2,2	3,2	Mean	3,3
1	.39	−7	.1	−.1			−1 5	−5				
2	.26	5	−.1	.2	−.6	4	.5	−.2		−.7	−7	
3	.15	.3	−.3	.1	.3	−.3	.8	.3	2.9	0	1.5	−1.0
4	.28	−.1	.3	.2	8	.7	.7	.7	2.8	.7	1.8	−.6
5	.27	.2	.3	.3	1 4	.5	.6	.8	1.9	.3	1.1	−.8
6	.39	−.2	5	2	−1	−.3	.5	0	−.2	.2	0	−.2
7	28	.2	.4	3	0	4	1.3	6	−1.6	7	1.2	.2
8	.08	.5	.3	.3	.6	2	9	.6	.6	.5	.6	1.1
9	.06	−.1	1	0	−.1	−2	.1	−1	−.2	1.0	−.1	.4
10	−.11	−.2	.3	0	−.7	4	.1	−.1	−1.4	.1	−.7	2
11	−26	−.2	−.2	−2	−.4	.3	1.1	.3	−2 6	—	−2 6	.9
12	−.29	−.4	−.2	−.3	−.6	—	1 3	1.3	−3 0	—	−3.0	—
13	−.73	−.1	−.5	−.4	.8	—	1.8	1 8	−1 7	—	1.7	—
14	−.90	−.7	—	−.8	−2 1	—	—	—	2 7	—	2.7	—
15	—	—	—	—	.3	—	—	—	.7	—	.7	—
16	—	—	—	—	−1.8	—	—	—	−2.1	—	−2.1	
17	—	—	—	—	−1 6	—	—	—	−2.6	—	−2.6	—
18	—	—	—	—	−1.7	—	—	—	−1.7	—	−1.7	—
19	—	—	—	—	−3.8	—	—	—	−3.2	—	−3 2	—
20	—	—	—	—	−3.5	—	—	—	−.3	—	−.3	—
21	—	—	—	—	−3 4	—	—	—	—		—	—
22	—	—	—	—	−3 6	—	—	—	—	—	—	—
23	—	—	—	—	−4.9	—	—	—	—	—	—	—
24	—	—	—	—	−5 3	—	—	—	—	—	—	—
25	—	—	—	—	−3.4	—	—	—	—	—	—	—
26	—	—	—	—	−5.0	—	—	—	—	—	—	—
27	—	—	—	—	−5.6	—	—	—	—	—	—	—
28	—	—	—	—	−6 1	—	—	—	—	—	—	—
29	—	—	—	—	−6 3	—	—	—	—	—	—	—
30	—	—	—	—	−7.3	—	—	—	—	—	—	—
31	—	—	—	—	−8.3	—	—	—	—	—	—	—

Table III gives the values of $\delta_2-\delta_1$, *i.e.*, of the difference $\delta\nu_{2dc}(K)-\delta\nu_{1dc}(K)$ for the OD bands corresponding to $v''=0$. The data for the other states, $v''=1$, 2, etc. (particularly the components due to $^2\Pi_{\frac{1}{2}}$ state of each level) are too meagre and too uncertain (as they are derived from the R_1 and R_2 branches) to be considered as a basis for this discussion and hence have not been shown in this Table.

Curve (*a*) shows the variation of the above difference with K. A general, almost linear, relation is obvious, consistent with Mulliken's equation (3). With higher K values, there appears to be a slight departure from linearity, indicating presumably the effect of "rotational stretching" referred to by Mulliken.

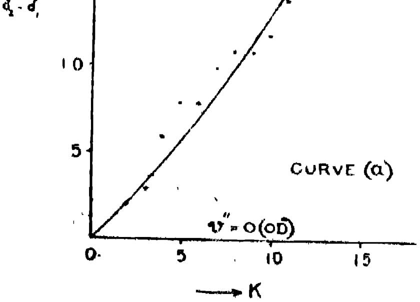

CURVE (*a*)

COMPARISON OF OH AND OD

Distinct from the conventional method of studying the isotope effect in band spectra, Johnston[4] referred to the isotope effect in Λ-doubling in the $^2\Pi$ states

TABLE III

Λ-doublet differences $(\delta_2-\delta_1)$ for $v''=0$, in OD bands

K	δ_1	δ_2	$(\delta_2-\delta_1)$
1	.2	−.1	−.3
2	0	.2	.2
3	−.2	.1	.3
4	.4	.2	.6
5	−.5	.3	.8
6	−.6	.2	.8
7	−.7	.3	1.0
8	−.8	.3	1.1
9	−1.1	0	1.1
10	−1.2	0	1.2
11	−1.6	−.2	1.4
12	−2.0	−.3	1.7
13	−2.3	−.4	1.9
14	−3.0	−.8	2.2
15	−3.2	—	—
16	−3.8	—	
17	−4.1	—	—
18	−4.0	—	—
19	−4.9	—	
20	−4.8	—	—
21	−5.7	—	—
22	−5.8	—	—
23	−6.1	—	—
24	−6.6	—	—
25	−7.7	—	—
26	−9.7	—	—

TABLE IV

Λ-doubling in $^2\Pi_{1\frac{1}{2}}$ states of OD and OH molecules

K	$v''=0$			$v''=1$			$v''=2$			$v''=3$
	OH	OD	Ratio	OH	OD	Ratio	OH	OD	Ratio	OD
1	− .33	.2	—	− .3	− .4	—	− .1	.2	—	—
2	− .40	0	—	− .4	− .4	—	—	− .6	—	—
3	− .59	− .2	.33	− .6	− .2	—	− .9	− .8	—	.3
4	− .99	− .4	.40	− .9	− .1	—	− .8	− .7	—	.2
5	− 1.40	− .5	.36	− 1.5	1	—	− 1.5	− .8	.53	− 1.1
6	− 2.07	− .6	.28	− 1.8	.2	.11	− 1.2	− .4	.33	0
7	− 2.61	− .7	.27	− 2.5	− .3	.12	− 2.1	− .1	—	1.8
8	− 3.34	− .8	.24	− 3.4	− .8	.23	− 2.9	− .9	.31	− .2
9	− 4.29	− 1.1	.26	− 4.2	− 1.2	.29	− 5.2	− 1.6	.30	− 1.4
10	− 5.13	− 1.2	.24	− 4.7	− 1.6	.34	− 6.2	− 2.6	42	− 1.0
11	− 6.18	− 1.6	.26	− 6.3	− 1.9	.30	—	− 2.2	—	− 1.2
12	− 7.03	− 2.0	.28	− 6.8	− 2.2	.32	—	− 2.7	—	—
13	− 7.74	− 2.3	.30	− 6.9	− 2.3	.33	—	− 2.3	—	—
14	− 8.94	− 3.0	.33	− 8.2	− 2.8	.34	—	− 2.5	—	—
15	− 10.03	− 3.2	.32	− 9.3	− 3.3	35	—	− 3.2	—	—
16	− 11.25	− 3.8	34	− 10.5	− 3.3	.31	—	− 4.3	—	—
17	− 12.27	− 4.1	33		− 4.2	—	—	− 3.5	—	—
18	− 13.36	− 4.0	30	—	− 4.3	—		− 3.5	—	
19	− 14.99	− 4.9	.33	—	− 4.8	—	—	− 5.6		
20	− 16.30	− 4.8	30	—	− 4.8	—		− 5.4	—	—
21	− 15.54	− 5.7	—	—	− 5.8	—	—	− 5.8	—	—
22	− 17.68	− 5.8	.33	—	− 6.2	—	—	− 7.1	—	
23	− 19.5	− 6.1	.31	—	− 4.6	—	—	− 8.3	—	
24	− 20.8	− 6.6	.31	—	− 6.2	—	—	—	—	
25	− 21.6	− 7.7	.36	—	− 8.6	—	—	—	—	—
26	− 25.1	− 9.7	—	—	—	—	—	—	—	—
			Mean .31			Mean .28			Mean .34	

of the OH and the OD molecules. Curves have been drawn by him (from as yet unpublished data) showing the variation of the doubling with K for the states $^2\Pi_{1\frac{1}{2}}$ and $^2\Pi_{\frac{1}{2}}$ for $v''=0$ in the case of the two molecules. The doubling in the OD molecule is found to be much smaller than for the OH molecule for the same value of K. The ratio of the spacings is stated to be 0.284.

Table IV presents the values of δ_{OD} and δ_{OH} for the $^2\Pi_{1\frac{1}{2}}$ state for $v''=0$, 1, 2 and 3. The data on the OD bands are due to the writer and those on the OH bands are quoted from Dawson and Johnston's paper,[3] with the signs changed. The results are presented in curves (*b*) and (*c*) for the two isotopic

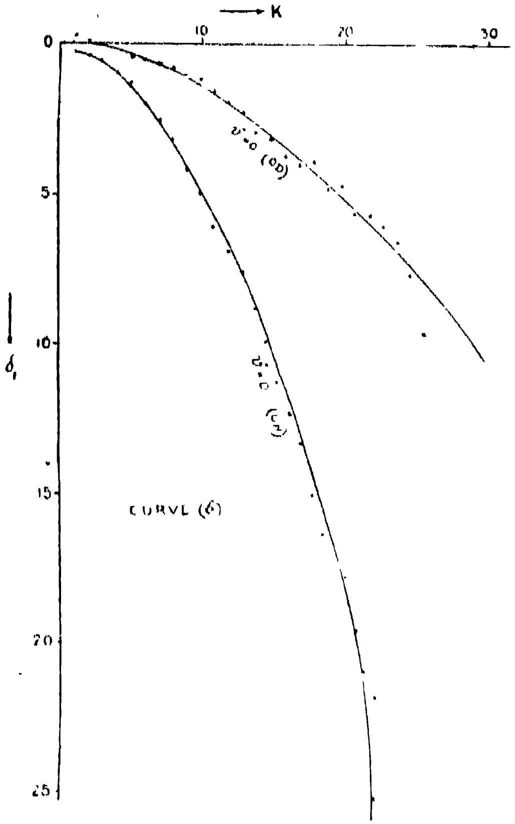

Curve (*b*)

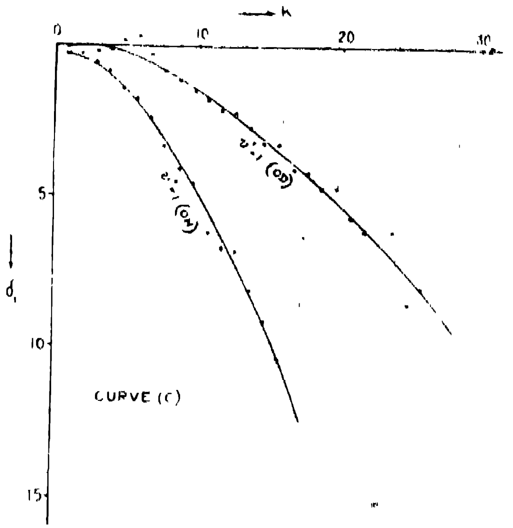

Curve (*c*)

molecules for $v''=0$ and 1. (These curves slope downwards and not upwards as indicated by Johnston if Mulliken's convention of signs referred to above is adopted.) The curves clearly indicate that, in magnitude, the Λ-doubling in the OD molecule is less than that in OH for the same value of K in all the vibrational states. The ratio between δ_{OD} and δ_{OH} is on an average about 0.31.

The author desires to express his grateful thanks to Dr. K. R. Rao for help and guidance in the course of the work and to the Andhra University for the award of a Fellowship which enabled him to pursue this investigation.

ANDHRA UNIVERSITY,
WALTAIR

REFERENCES

[1] Van Vleck, *Phy. Rev.*, **33**, 467 (1929)
[2] Mulliken, *Phy. Rev.*, **38**, 87 (1931).
[3] Dawson and Johnston, *Phy. Rev.*, **43**, 980 (1933)
[4] Johnston, *Phy Rev*, **45**, 80 (1934).

PHOTOMETRIC STUDY OF THE PROFILES OF THE FRAUNHOFER LINES IN THE SOLAR SPECTRUM

PART I. Mg b. GROUP

By Y. PARAMASIVA RAO
AND
C. K. ANANTHASUBRAHMANYAM

(Received for publication, January 9, 1952)

ABSTRACT The paper consists of the results of the photometric studies carried out by the authors during the last year. After a brief description of the improvements and refinements perfected in the Direct-Reading Photo-electric Spectrophotometer described by Narayan and Ananthasubrahmanyam, the use of the instrument in the study of the line contours is discussed. Contours obtained by photographic photometry and this instrument are given.

Accurate measurements of the intensity distribution in the absorption lines in the solar spectrum at various points across the sun's disc are necessary for a correct appreciation of the mechanism of absorption in the solar atmosphere. All the strong lines in the solar spectrum have been studied by more than one author ; but the results of the different workers do not show the necessary degree of agreement that it calls for further work. In continuation of the work carried out by Royds and Narayan[1] on the strong lines of hydrogen and ionised calcium, a study of the mg. b group lines was undertaken

All the measurements of the intensity distributions in the absorption lines have been made till now by the method of photographic photometry. This method yields accurate results if suitable precautions are adopted. But it is involved and laborious requiring separate callibration marks, etc. In recent years attempts have been made by some physicists to use a photo electric cell and an amplifier to measure the intensity distribution in spectral lines directly without recourse to photography. In a paper on "A Precision Reading Photo-electric Spectrophotometer" Narayan and Ananthasubrahmanyam[2] have described such a photo-electric photometer. The instrument was constructed by them at the Solar Physics Observatory and forms a permanent feature of the equipment of the Observatory. In the present paper the results obtained by the photographic method and with the direct-reading instrument are given. Since the instrument was set up, many improvements have been made in the light of experience. As this is the first paper reporting results with the improved instrument a short account is given of the modifications. The chief advantage of this method over photographic photometry lies in the saving of time.

DIRECT-READING PHOTO-ELECTRIC PHOTOMETER

The photo-electric current due to the light from any point in the spectral line is very minute and needs an amplification of many times. A single tube amplifier was first tried and found unsatisfactory. Fluctuations in the voltages of the filament and plate batteries cause a gradual drift in the zero reading of the galvanometer which measures the amplified current. Among the various amplification circuits tried, a two-tube balanced circuit described by Dubridge[3] has been found most satisfactory. When the circuit is properly balanced, variations of battery voltages do not affect the galvanometer and the measurements are thus more reliable. The circuit and the method of balancing are essentially the same as given by Dubridge and hence are not described here.

Osram electrometer triode tubes have been used in the amplifier circuit. They have a very high grid input resistance equal to 10^{16} ohms. On account of this very good grid insulation greater amplification can be achieved by using high grid leak resistances. Some difficulty was experienced in preparing suitable grid leak resistances high enough to take full advantage of the grid insulation of the valves. Resistances of the order of 10^{8} ohms are usually made with xylol-alcohol mixtures enclosed in soft glass tubes with sealed-in platinum electrodes or by drawing Indian ink or lead pencil lines on paper or unglazed porcelain. The authors have tried all these and found them unsuitable due to residual and variable polarisation. The material finally employed is colloidal graphite. It forms a tenacious coating on glass, the resistance of which depends on the density and the thickness of the film.

A piece of pyrex rod about 8 mm. in diameter and 6 cm. long is ground for a space of few millimetres at each end by holding a piece of emery paper against the rod as it is rotated and a narrow longitudinal grinding is then made along the length. Fairly concentrated aqueous solution of colloidal graphite is applied on the ground portions near each end of the rod. Brass caps with projecting wires for leads are then cast on the ends and a concentrated dispersion of colloidal graphite is then brushed on these caps and the rod down for a few millimetres. The fine longitudinal grinding is then brushed with a very dilute aqueous solution. In order to obtain adhesive and durable films the glass surface should first be carefully cleaned and dried in warm air. The colloidal graphite films function best after being baked at a sufficiently high temperature which ensures the removal of all moisture. The resistances are finally dipped in glyptal lacquer and allowed to dry. Tests made on these resistances indicate that they are free from polarisation, and have also a negligible temperature co-efficient.

As the amplification is very great it is necessary to screen the amplifier thoroughly. In this case the photo-electric cell with the amplifying valves and grid leak resistances is placed in a heavy cast-iron cylinder for the purpose of cutting out electrical and magnetic disturbances. The cylinder was then evacuated by means of Cenco HyVac pump. This evacuation removes any film of moisture from the valve surfaces and improves the insulation, resulting in a marked improvement in the performance and considerable increase in sensitivity. The amplification circuit so constructed was highly sensitive and steady.

The mechanical parts have been described in detail in the earlier paper. A scanning slit of adjustable width can be moved across the length of the spectrum by a micrometer screw worked by a divided drum head. The rotation of the drum head through each division displaces the slit through 0.005 cm. But the drum can be worked at smaller intervals. The light from the scanning slit is deflected by a right-angle prism and reaches the photo-cell. A sensitive galvanometer is fed with the amplified current and the deflection of the galvanometer is a measure of the current. If light from successive points in any absorption line is allowed to affect the photo-electric cell, the corresponding deflections of the galvanometer are proportional to the intensity at those points in the spectral line. The resolving power of the instrument depends on the width of the scanning slit which was kept sufficiently narrow.

EXPERIMENTAL

A 20-foot concave grating spectrograph in Eagle mount was employed in the photographic method. The photographs are made in the third order, giving a dispersion of 0.9 Å per mm. in the region 5100 to 5200 Å. Since stray radiations due to reflection and scattering by the optical parts are a troublesome source of error in this type of work, special precautions are taken to reduce it to a minimum. All the inner parts are painted dull black and several diaphragms are mounted inside so that there is no chance for any light to be reflected into the spectrum from the inner walls of the spectrograph. A double monochromator which allows only the small required region of wavelengths is used in front of a slit of the spectrograph. This device reduced the scattered light to the minimum. As the monochromator filtered out the other regions of the spectrum, overlapping of the different orders was also overcome by this device.

The Sun's image is formed by the 13-inch object glass of the Observatory fed from an 18-inch siderostat. The diameter of the image is about 60 mm. The Sun's image is formed on a plate in front of the vertical slit of the double monochromator. On this plate concentric circles were inscribed to facilitate accurate guiding of the Sun's image which was kept concentric with the circle. In order to obtain spectra from different points of the Sun's disc a series of small holes are drilled along a horizontal diameter of the circle and their positions are accurately measured. By displacing the slit plate horizontally so as to bring any of these holes exactly central on the slit of the monochromator, Sun's image also being displaced to be concentric with the inscribed circles, spectra would be obtained from different points on the Sun's disc.

A step wedge was used to record the standardising spectra in the photographic method. The wedge was always placed in front of the plate for which position it was also calibrated. All the spectra on any one plate had identically the same exposure. The necessary precautions have been adopted in the process of development. The plates were microphotometered with the Cambridge photo-electric microphotometer of the Observatory. The densities on the plate were converted into the intensities with the aid of the calibration marks.

In the measurements with the direct-reading instrument a glass littrow spectrograph giving a dispersion of 4.4 Å per mm. has been used. All precautions necessary to minimise scattered light were observed. But the monochromator was not employed with this method. The rest of the arrangement is the same as in the other method. The background in the neighbourhood of the b_1 line gives a galvanometer deflection of about 25 cm. with the scale at a distance of 1 metre. The drum head is set at successive intervals and the galvanometer deflection is noted in each position. 4 to 5 Angstroms on either side of the centre of absorption line, until the intensity reaches the background, are thus covered. Where faint absorption lines are present, observations are made at closer intervals. Knowing the dispersion of the spectrograph and the pitch of the screw, the drum readings can be converted into wavelengths. The galvanometer deflections plotted against the wavelengths give the intensity distribution in the spectral line.

By the photographic method four separate measurements are made and the mean values are reported. With the direct-reading instrument more observations (eight) could be made on account of the ease of operation ; the mean value is adopted. Observations were taken only under conditions of good sky. By the photographic method measurements were made upon the 3 lines at the centre of the sun's disc, equatorial and polar limbs and at other points across the disc. The studies by the second method were confined to the centre of the sun's disc.

RESULTS

(a) *Photographic Method.*—The intensity distributions in the b_1 line ($\lambda=5183.62$) of magnesium at the centre of the sun's disc and the equatorial and polar limbs are presented in Table I. The intensity at every point is expressed as a percentage of the background, which is chosen from a point free from absorption near the line. The absorption in the line is not symmetrical about the centre. The readings given in the table correspond to the mean of the intensities at equal distances on either side from the centre of the line. The distance from the centre is expressed in arbitrary units chosen for convenience. In the estimation of intensities faint absorption lines on the photometric trace are smoothed out.

TABLE I

Distance from the centre	Intensity at the centre of the sun's disc	Intensity at the equatorial limb	Intensity at the polar limb
0	15	21	23
10	25	35	36
20	35	46	46
30	43	53	54
40	51	60	60
50	57	65	65
60	63	68	69
70	67	73	74
80	71	76	78
90	75	79	81
100	78	81	84
110	81	84	86
120	83	86	88
130	85	88	90
140	87	90	92
150	89	92	94
160	91	94	95
170	94	96	95
180	96	97	97
190	96	98	98
200	98	98	98

The absorption is greater at the centre of the sun's disc than at the limbs. But it is evident that there is little difference between the equatorial and polar limbs. The distribution of intensity in the b_1 line at the limb and the centre is plotted in Fig. 1.

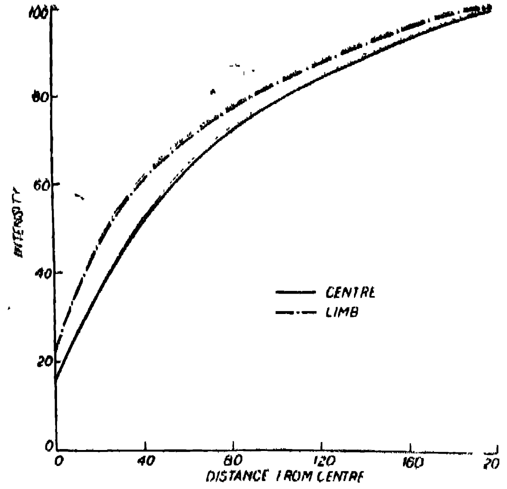

FIG. 1
Distribution of intensity in the b_1 line

The profiles of the lines, λ = 5183.62, 5172.70 and 5167.33 have been studied at the centre of the disc, the limbs and at four other points on the disc. Every line shows a progressive decrease in absorption as we proceed from the centre of the disc to the limb. The intensity distribution tables corresponding to different points on the sun's disc are not presented, as in the present state of the theoretical knowledge of absorption the equivalent width is more important than the actual profiles. The value obtained for the equivalent width of any line depends to a certain degree on the point to which the extreme extent of the line is judged to stretch. Care has been taken to estimate the extent of the wings as accurately as possible. Table II gives the equivalent width of $\lambda = 5183.62$ Å line at different points across the disc. The distance of the point from the centre is expressed as a fraction of the radius of the sun's image.

TABLE II

$\lambda = 5183.62$

Distance from the centre	Central intensity (% of background)	Equivalent width	NHf
0.00	15.5	1.46	4.90×10^{16}
0.36	18.7	1.45	4.84
0.55	19.0	1.40	4.51
0.70	18.9	1.42	4.64
0.96	20.6	1.31	4.13
0.98	24.2	1.17	3.20

TABLE III

$\lambda = 5172.70$

Distance from the centre	Central intensity (% of background)	Equivalent width	NHf
0.00	16.2	0.96	2.13×10^{16}
0.36	19.0	0.91	1.91
0.55	19.5	0.89	1.83
0.70	19.3	0.87	1.75
0.96	21.2	0.85	1.67
0.98	24.8	0.80	1.48

Tables III and IV are similar to Table II but correspond to the lines 5172.70 and 5167.33 Å. The equivalent width which may be considered to be a measure of the total absorption diminishes from the centre of the disc to the limb.

TABLE IV

$\lambda = 5167.33$

Distance from the centre	Central intensity (% of background)	Equivalent width	NHf
0.00	16.5	0.68	1.07×10^{16}
0.36	18.9	0.66	1.01
0.55	19.6	0.64	0.95
0.70	19.9	0.63	0.92
0.96	22.0	0.60	0.83
0.98	24.9	0.56	0.73

Unsold has derived the formula that in the case of absorption lines where the Doppler broadening is small the equivalent width is given by

$$W = \frac{\pi e^2}{mc^2} \lambda_0 \sqrt{\frac{2\pi}{2}} \sqrt{NHf} \tag{1}$$

where W is the equivalent width, λ_0 is the wavelength at the centre of the absorption line, N is the number of absorbing atoms per c.c., f is the oscillator strength for the particular line and H is the height of the atmosphere. If the Doppler broadening is large enough to predominate to such an extent that radiation damping may be neglected altogether, the equivalent width is given by

$$W = \frac{\pi}{mc^2} \lambda_0^2 \, NHf. \tag{2}$$

Neither of the equations correctly represents absorption lines in the solar spectrum where Doppler broadening is neither too large nor negligible. Where both types of effects are present, equation (1) gives the upper limit and (2) the lower limit of the number of atoms. The NHf values presented in Tables II, III and IV are calculated from equation (1) and hence represent the upper limit. From the equivalent width of any line at different points on the disc it is possible to calculate the density of atoms giving rise to the line at different heights in the sun's atmosphere, if f, the oscillator strength, is known. For the magnesium line, f has not been theoretically evaluated. So no attempt has been made to calculate the actual densities.

The sum rule of Burger and Dorgelo predicts for the intensity of the M_g-b lines, the ratio of 5 : 3 : 1. According to equation (1) there is direct proportionality between W and $\sqrt{NHf}$. For all the lines in a multiplet the thickness of the reversing layer, H, is the same. The value of Nf shall be proportional to the multiplet intensities. If, therefore, the square-root law is to hold, the observed total intensities (*i.e.*, the equivalent width) should be in the ratio of

$\sqrt{5} : \sqrt{3} : 1$. The ratio of the total intensities at the centre and the limb are shown in Table V. They do not correspond to the square-root law.

TABLE V

Ratio of Total Intensities

	b_1	b_2	b_3
Centre	1.15	1.41	1
Limb	2.09	1.43	1
Ratio of $\sqrt{5} : \sqrt{3} : 1$	2.24	1.73	1

(*b*) *Direct-Reading Method.*—The distribution of intensity in the b_1 line, as measured by the direct-reading method, is given in Table VI. The distances from the centre on each side (*i.e.*, increasing and decreasing wavelength) are expressed in terms of the drum readings.

TABLE VI

Increasing Wavelength		Decreasing Wavelength	
Distance from the Centre	Intensity	Distance from the Centre	Intensity
0	17·0	0	17·0
1	28.1	1	24·3
2	39·1	2	37·8
3	50.8	3	51·1
3½	54·2	4	66.5
4	59·2	5	78.2
4½	63·0	6	81.9
5	74·5	7	84·1
6	84·7	8	85.6
7	88.3	9	87·2
8	88.8	10	87·4
9	86.5	10½	85·1
10	84·7	11	88.5
10½	84·9	12	92·7
11	87·3	13	94·7
12	90·6	14	95·1
13	94·0	15	90.8
14	95·5	15½	86.5
15	97·4	16	90.1
16	98.9	17	96.1
—	—	18	99·7

The profile of the line is plotted in Fig. 2. The asymmetry of the line is seen clearly in the figure. For calculating the equivalent width the other absorption

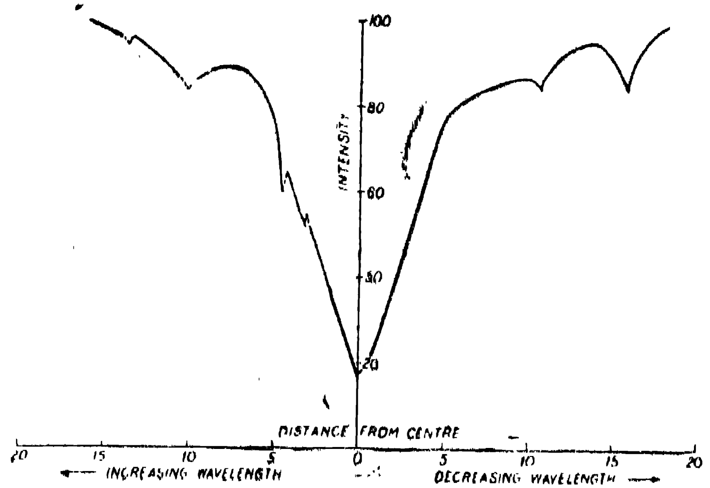

FIG. 2
The Profile of the line

lines seen in the graph are smoothed out and the area within that curve is computed. This gives an equivalent width of 1·63 which compares well with that obtained by the other method. The dispersion of the spectrograph used with the direct-reading instrument is smaller than that employed in the photographic method. Better agreement can be secured by using a spectrograph of higher dispersion with the direct-reading photometer. The detailed distribution in b_2 and b_3 lines is not given here but the equivalent widths calculated from the data are presented in Table VII.

A comparative table giving the equivalent width and central intensity obtained for the three lines by the authors and other workers is given below.

TABLE VII

Observer	5183.6		5172.7		5167.3	
	C. I.	E. W.	C. I.	E. W.	C. I.	E. W.
Kerll[4]	15	1.06	16	0.84	17	0.63
Plaskett[5]	16	1.54	16	1.08	—	—
Righini[6]	15	1.55	16	1.35	—	—
Allen[7]	11	1.60	12	1.20	16	0.75
Photographic method	16	1.46	16	0.96	17	0.68
Authors *(Direct-reading method)*	17	1.63	18	1.02	19	0.76

C. I. = Central Intensity expressed as percentage.
E. W. = Equivalent Width.

The authors have used a double monochromator besides adopting the other usual devices to minimise the scattered light. Spectrograph used in the photographic method is of a high dispersion. It can, therefore, be taken that the results of the authors are more accurate than those obtained by other workers.

The measurements by the direct-reading method illustrate the efficiency and dependability of the apparatus for studying the intensity distribution in the spectral lines. The use of the symmetrical balanced amplifier has overcome the tendency of zero drift and rendered the observations quite reliable. The accuracy of the measurements is as good as that by the method of photographic photometry. The labour involved in that method is saved and observations may be made with considerable ease and quickness. It is proposed to study the profiles of the strong Fraunhofer lines across the sun's disc and in sunspots with this instrument.

The authors take this opportunity to thank Dr. A L. Narayan, Director of the Observatory, under whose guidance the work was carried out.

SOLAR PHYSICS OBSERVATORY,
KODAIKANAL.

REFERENCES

[1] Royds and Narayan, *Kodaikanal Observatory Bulletin*, No. 109.
[2] Narayan and Ananthasubrahmanyam, *Ind. Jour. Phy.*, **14**, 393 (1940).
[3] Dubridge, *Phy. Rev.*, **37**, 392 (1931).
[4] Korff, *A. P. J.*, **76**, 291 (1932).
[5] Plaskett, *M. N. R. A. S.*, **91**, 870 (1931).
[6] Righini, *O. M. O. A. Arcetri*, **48**, 291 (1931).
[7] Allen, *Mem. Comm. Solar Obs.*, **5**, 47 (1934)

PROTON-PROTON INTERACTION AND YUKAWA PARTICLE*

By K. C. KAR

(Received for publication, January 26, 1942)

ABSTRACT. A rigorous formula is derived for proton-proton scattering taking the interaction potential to be of Yukawa type, *viz.*, $V(r) = \frac{A}{r} e^{-\alpha r}$. The formula agrees remarkably well with the experiment of Heydenburg, Tuve and Hafstad. It is shown that the fitting values of A and α give the values of the short range charge and mass of 'neutretto'. The charge and mass so obtained are found to be exactly same as those of mesotron previously determined by Heitler from the binding energy of deuteron

In a recent paper[1] I have developed the theory of proton-proton scattering taking the short range potential to be of the type $Ae^{-\alpha r}$. It may be mentioned that a similar short range potential was assumed in the case of neutron-proton interaction[2] in order to explain the spherical symmetry in scattering observed by many experimenters.[3] The point which appears to me to be in favour of taking such a potential is that it gives a constant value at $r = 0$. This is just what is found within the hard core in case of spontaneous and artificial disintegrations of atomic nuclei.[4]

In the present article I propose to study the problem of proton-proton scattering taking the short range interaction potential in the form

$$V = \frac{A}{r} e^{-\alpha r} , \qquad (1)$$

as suggested by Yukawa.[6] It gives, as before, spherical symmetry in neutron-proton scattering. Furthermore, as $\sqrt{A}$ has the dimension of electrical charge, its fitting value for proton-proton scatttering at a given angle and given incident velocity, gives the value of the electrical charge giving rise to the close range force during proton-proton interaction.

Before going into the details of these discussions I first proceed to derive the scattering formula with Yukawa potential and explain how the formula is verified experimentally. It should be noted at the outset that, as in electron scattering by nucleus,[7] I shall throughout take the solution to be bounded and shall use the wave-statistical idea of critical approach.

---

* Communicated by the Indian Physical Society.

It has been shown before [1, 2] that referring the motion to the centre of mass (C-system) we have for the first order scattering function

$$\lambda_1\chi_1(r_2, \theta_2) = -\frac{1}{4\pi\sqrt{v}} \cdot \frac{k^2}{E} \int V(r_1)\, e^{ikx_1} \frac{e^{ikr_{12}}}{r_{12}}\, d\tau_2 \qquad \dots \quad (2)$$

where $V(r_1)$ is the perturbing potential, v the velocity of the proton, $E = \frac{1}{2}Mv^2$, M being the proton mass and $k = \frac{\pi M v}{h}$. Now, on taking the solution to be bounded and on proceeding as before, formula (2) may be easily transformed to

$$\lambda_1\chi_1(r, \theta) = \frac{\operatorname{cosec}^2 \frac{\phi}{2}}{Mv^2} \cdot \frac{e^{ikr}}{\sqrt{v}\, r} F(r_0) \qquad \dots \quad (3)$$

where

$$F(r_0) = -k' \int_{r_0}^{\infty} \sin k'r\, V(r)\, r\, dr \qquad \dots \quad (3.1)$$

and

$$k' = 2k \sin \frac{\phi}{2}\, ; \; k = \frac{\pi M v}{h} \qquad \dots \quad (3.2)$$

and the critical approach (r_0), which must be always positive, is given by

$$r_0 = \frac{\operatorname{cosec}^2 \frac{\phi}{2}}{Mv^2} \cdot 2\rho \left(\sin \frac{\phi}{2} \pm \sin^2 \frac{\phi}{2} \right) G(r_0) \qquad \dots \quad (3.3)$$

where

$$G(r_0) = \pm k' \int_{r_0}^{\infty} \sin k'(r - r_0)\, V(r)\, r\, dr \qquad \dots \quad (3.4)$$

in which the + sign stands for repulsive force and − for attraction. Formulae (3)⟶(3.4) in the C-system are perfectly general, holding for any interaction potential $V(r)$ between two protons.

If the potential is Coulombian and repulsive $V = +\frac{e^2}{r}$ and so we have from (3)⟶(3.4)

$$\lambda_1\chi_1(r, \theta) = -\frac{e^2}{Mv^2} \operatorname{cosec}^2 \frac{\phi}{2} \cos k'r_0 \cdot \frac{e^{ikr}}{\sqrt{v}\, r} \qquad \dots \quad (4)$$

and

$$r_0 = 2\rho \frac{e^2}{Mv^2} \left(\operatorname{cosec} \frac{\phi}{2} + 1 \right); \; \rho = 1.35 \,. \qquad \dots \quad (4.1)$$

If, again, the short range interaction is attractive and of Yukawa type, we have for the scattering function and the critical approach

$$\lambda_1\chi_1(r, \theta) = \frac{4\pi^2 MA}{h^2} \cdot \frac{e^{-ar_0}\left\{ \cos k'r_0 + \frac{a}{k'} \sin k'r_0 \right\}}{a^2 + k'^2} \cdot \frac{e^{ikr}}{\sqrt{v}\, r} \qquad \dots \quad (5)$$

and $$r_0 = 2.7 \times \frac{\frac{4\pi^2 MA}{h^2} e^{-ar_0}}{a^2 + k'^2} \left\{ \sin\frac{\phi}{2} - \sin^2\frac{\phi}{2} \right\}. \qquad \ldots \quad (5.1)$$

As has been already noted, eqs. (4)⟶(5.1) are in C-system. For experimental verification we obviously require them to be referred to the laboratory coordinates. In a previous paper of mine[7] I have elaborately discussed this question and have shown that the above formulæ can easily be transformed into the laboratory co-ordinates by simply putting 2θ for ϕ, θ being the laboratory angle co-ordinate.

Now, in case of proton-proton interaction the potential is partly Coulombian repulsive and partly attractive of Yukawa type. Thus the total scattering function is obtained by adding (4) and (5) and we have in L-co-ordinates

$$\lambda_1 \chi_1(r, \theta) = -\frac{e^2}{Mv^2} \cdot \frac{e^{ikr}}{\sqrt{v}\, r} \left\{ \operatorname{cosec}^2\theta \cos k' r_0 - \frac{Mv^2}{e^2} g_1 f_1 \right\} \qquad \ldots \quad (6)$$

where $$g_1 = \frac{4\pi^2 MA}{h^2} \cdot \frac{e^{-ar_0'}}{a^2 + k'^2}, \qquad \ldots \quad (6.1)$$

$$f_1 = \cos k' r_0' + \frac{a}{k'} \sin k' r_0', \qquad \ldots \quad (6.2)$$

$$k' = 2k \sin\theta \;;\; k = \frac{\pi M v}{h}, \qquad \ldots \quad (6.3)$$

and the total value of the critical approach is

$$r_0' = 2.7 \times \frac{e^2}{Mv^2} (\operatorname{cosec}\theta + 1) + 2.7 \times (\sin\theta - \sin^2\theta) g_1. \qquad \ldots \quad (6.4)$$

In the case of proton-proton interaction it is not possible to distinguish between the scattering and the scattered proton ; so it is essential that the effect of exchange should be considered in calculating the intensity of scattering. The scattering function after exchange is obtained by simply putting $\left(\frac{\pi}{2} - \theta\right)$ for θ in eqs. (6)→(6.4). Thus we have after exchange

$$\lambda_1 \chi_1(r, \theta) = -\frac{e^2}{Mv^2} \cdot \frac{e^{ikr}}{\sqrt{v}\, r} \left(\sec^2\theta \cos k'' r_0'' - \frac{Mv^2}{e^2} g_2 f_2 \right) \qquad \ldots \quad (7)$$

where $$g_2 = \frac{4\pi^2 MA}{h^2} \cdot \frac{e^{-ar_0''}}{a^2 + k''^2}, \qquad \ldots \quad (7.1)$$

$$f_2 = \cos k'' r_0'' + \frac{a}{k''} \sin k'' r_0'', \qquad \ldots \quad (7.2)$$

$$k'' = 2k \cos\theta, \qquad \ldots \quad (7.3)$$

and
$$r_0''=2.7\times\frac{e^2}{Mv^2}(\sec\theta+1)+2.7\times(\cos\theta-\cos^2\theta)g_2\,. \quad \ldots \quad (7.4)$$

When the interacting protons have anti-parallel spin, an exchange of their positions would give a new configuration and consequently the total probability is obtained by adding the components. Or, in other words, the total space function is symmetrical. Hence, in this case, we have from (6) and (7) for the total scattering function

$$\lambda_1\chi_1(r,\theta)=-\frac{e^2}{Mv^2}\cdot\frac{e^{ikr}}{\sqrt{v}\,r}\left\{\operatorname{cosec}^2\theta\cos k'r_0'+\sec^2\theta\cos k''r_0''-\frac{Mv^2}{e^2}(g_1f_1+g_2f_2)\right\} \quad \ldots \quad (8)$$

In the case of parallel spin, no new configuration is obtained by exchange. So we have to take the difference of the components in getting the total probability. Or, in other words, the total space function should be taken antisymmetrical. Hence we have from (6) and (7)

$$\lambda_1\chi_1(r,\theta)=-\frac{e^2}{Mv^2}\cdot\frac{e^{ikr}}{\sqrt{v}\,r}\left\{\operatorname{cosec}^2\theta\cos k'r_0'-\sec^2\theta\cos k''r_0''-\frac{Mv^2}{e^2}(g_1f_1-g_2f_2)\right\}. \quad \ldots \quad (9)$$

The relative intensities in the two cases are respectively

$$I_1=\left(\frac{e^2}{Mv^2}\right)^2\left[\operatorname{cosec}^4\theta\cos^2k'r_0'+\sec^4\theta\cos^2k''r_0''+2\operatorname{cosec}^2\theta\sec^2\theta\cos k'r_0'\cos k''r_0''\right.$$
$$-2(g_1f_1+g_2f_2)\frac{Mv^2}{e^2}(\operatorname{cosec}^2\theta\cos k'r_0'+\sec^2\theta\cos k''r_0'')$$
$$\left.+\left\{\frac{Mv^2}{e^2}(g_1f_1+g_2f_2)\right\}^2\right]4\cos\theta \quad \ldots \quad (10)$$

and

$$I_2=\left(\frac{e^2}{Mv^2}\right)^2\left[\operatorname{cosec}^4\theta\cos^2k'r_0'+\sec^4\theta\cos^2k''r_0''-2\operatorname{cosec}^2\theta\sec^2\theta\cos k'r_0'\cos k''r_0''\right.$$
$$-2(g_1f_1-g_2f_2)\frac{Mv^2}{e^2}(\operatorname{cosec}^2\theta\cos k'r_0'-\sec^2\theta\cos k''r_0'')$$
$$\left.+\left\{\frac{Mv^2}{e^2}(g_1f_1-g_2f_2)\right\}^2\right]4\cos\theta. \quad \ldots \quad (11)$$

Now, as the weights of the two events are as 1 : 3, we have for the total intensity $I=\frac{1}{4}I_1+\frac{3}{4}I_2$. Or, we have

$$I=\left(\frac{e^2}{Mv^2}\right)^2\left[\operatorname{cosec}^4\theta\cos^2k'r_0'+\sec^4\theta\cos^2k''r_0''-\operatorname{cosec}^2\theta\sec^2\theta\cos k'r_0'\cos k''r_0''\right.$$
$$-2\frac{Mv^2}{e^2}\left\{(g_1f_1-\tfrac{1}{2}g_2f_2)\operatorname{cosec}^2\theta\cos k'r_0'+(g_2f_2-\tfrac{1}{2}g_1f_1)\sec^2\theta\cos k''r_0''\right\}$$
$$\left.+(g_1^2f_1^2+g_2^2f_2^2-g_1g_2f_1f_2)\left(\frac{Mv^2}{e^2}\right)^2\right]4\cos\theta. \quad \ldots \quad (12)$$

It is a perfectly general formula giving the relative intensity of proton scattering in the Laboratory System at any angle. It should be noted that for $\theta=45°$ the formula is considerably simplified, since at this angle $k'=k''$, $r_0'=r_0''$, $g_1=g_2$ and $f_1=f_2$.

It is evident that the corresponding formula, if the force is only Coulombian, is obtained from (12) by simply putting $g_1=g_2=0$. We have then

$$I_0=\left(\frac{e^2}{Mv^2}\right)^2\left[\operatorname{cosec}^4\theta\cos^2k'r_0'+\sec^4\theta\cos^2k''r_0''-\operatorname{cosec}^2\theta\sec^2\theta\cos k'r_0'\cos k''r_0''\right]\times 4\cos\theta. \qquad \ldots \quad (12.1)$$

Thus the departure from Coulomb scattering is obtained by taking the ratio, viz., $D=I/I_0$. This should give the correct value of the departure. But, unfortunately, the experimenters[8] often measure the departure from Mott's extension of Born-Rutherford formula which has been already shown to be wrong[9] in so far as it has neglected the effect of the critical approach. This extended Born-Rutherford formula for exchange derived by Mott[10] and also in a different way by Kar and Basu[11] is known as the MKB-formula. It may also be deduced from (12.1) by neglecting the critical approach, *i.e.*, by putting $r_0'=r_0''=0$. Thus we have

$$I_{MKB}=\left(\frac{e^2}{Mv^2}\right)^2\left[\operatorname{cosec}^4\theta+\sec^4\theta-\operatorname{cosec}^2\theta\sec^2\theta\right]4\cos\theta. \qquad \ldots \quad (12.2)$$

Hence the experimentally measured departure becomes

$$D=\frac{I}{I_{MKB}}=\frac{\begin{array}{l}\operatorname{cosec}^4\theta\cos^2k'r_0'+\sec^4\theta\cos^2k''r_0''-\operatorname{cosec}^2\theta\sec^2\theta\cos k'r_0'\cos k''r_0''\\ -2\dfrac{Mv^2}{e^2}\{(g_1f_1-\tfrac{1}{2}g_2f_2)\operatorname{cosec}^2\theta\cos k'r_0'+(g_2f_2-\tfrac{1}{2}g_1f_1)\sec^2\theta\cos k''r_0''\}\\ \qquad +(g_1^2f_1^2+g_2^2f_2^2-g_1g_2f_1f_2)\left(\dfrac{Mv^2}{e^2}\right)^2\end{array}}{\operatorname{cosec}^4\theta+\sec^4\theta-\operatorname{cosec}^2\theta\sec^2\theta}.$$

In order to calculate the value of D for any angle one must know the values of g_1, g_2, f_1, f_2, r_0' and r_0'' for that angle. These may be evaluated easily from (6.1)⟶(6.4) and (7.1)⟶(7.4), if the two unknown parameters A and α of Yukawa potential are known beforehand. The two unknowns may, however, be evaluated by solving the two equations obtained from (13) by substituting the experimental values of D for any two angles of scattering. But the method is very tedious. A much simpler method would be as follows :—

As already pointed out, formula (13) reduces to a very simple form at $\theta=45°$ and we have

$$D_{45°}=\frac{4\cos^2k'r_0'-4\cos k'r_0'\cdot\dfrac{Mv^2}{e^2}g_1f_1+\left(\dfrac{Mv^2}{e^2}\right)^2g_1^2f_1^2}{4} \qquad \ldots \quad (13.1)$$

$$=\frac{4\cos^2k'r_0'-4\cos k'r_0'\,x+x^2}{4}, \qquad \ldots \quad (13.2)$$

where $x=\frac{Mv^2}{e^2}g_1 f_1$. By judicious selection we take a trial value of g_1. On substituting this value in (6.4) we get the value of r_0' for a given incident velocity (v). Again from (6.3) k' is known Thus cos $k'r_0'$ and $\cos^2 k'r_0'$ are calculated. Also D_{45} is known from the experiment of Heydenburg and others. Hence on solving (13.2) we get the value of x Thus we calculate the corresponding value of f_1 and so from (6.2) the value of a the unknown parameter in the exponential. As a and g_1 are known, we are now in a position to calculate A from (6.1). Thus from one trial value of g_1 we are able to calculate a set of values of a and A. We next use the above known values of a and A to calculate D_{20} at $\theta=20°$. If the value of D_{20} so obtained does not agree with the experimental value, the trial value of g_1 is slightly changed. In this way two or three trials help us to find the exact values of g_1, a and A. Graphical method is extremely useful in getting at the above exact values. Now, having got the correct values of a and A we calculate the departure (D) for any angle.

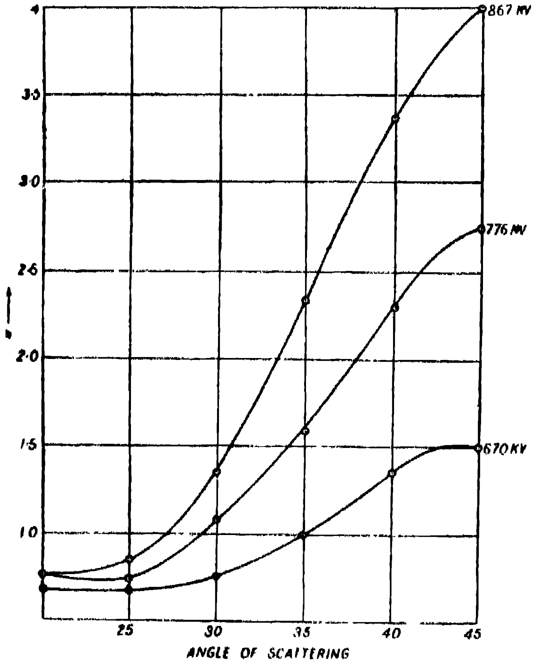

FIG. 1

Variation of D with the Angle Scattering

In Fig. 1 the theoretical curves are drawn giving the variation of D with the angle of scattering, for incident velocities 867 K.V., 776 K.V. and 670 K.V. The experimental points are indicated by solid circles. It is evident that the agreement is so close that no separate experimental curve need be drawn.

It has already been pointed out that $\sqrt{A}$ has the dimension of electrical charge. Therefore $\sqrt{A}/e$ is the charge in electronic unit which gives rise to the short range force. In the following table are given the values of a and $\sqrt{A}/e$ obtained from the curves in Fig. 1.

TABLE I

Incident Velocity	$a \times 10^{-13}$	$A^{\frac{1}{2}}/e$
867 K. V.	0.2839	6.013
776 K. V.	0.2966	6.542
670 K. V.	0.2794	6.190

Thus the charge causing the short range force is found to be ± 6e. This may be taken as the charge of the Yukawa particles inside the proton. It is interesting to note that the charge of the Yukawa particles as calculated by Heitler[12] from the mass defect of deuteron lies between 5e and 7e. Thus the present method of calculating the Yukawa charge is more reliable and accurate. Furthermore, according to Heitler, $^{1} - 3 \times 10^{-13}$ whereas from the above table the mean value of ^{1} is $3.5 \times 10^{-}$ The above striking agreement suggests that the present method when extended to other interactions may lead to a general method of determining the short range charge.

As, in the present wave-statistical method, the determination of the critical approach is very important, it is advisable to discuss the variation of the critical approach with angle and how it is affected by the presence of the short range attractive force. This variation, as calculated from formula (6.4), is shown in Fig. 2. The curves A, B and C indicate the variation of the total critical

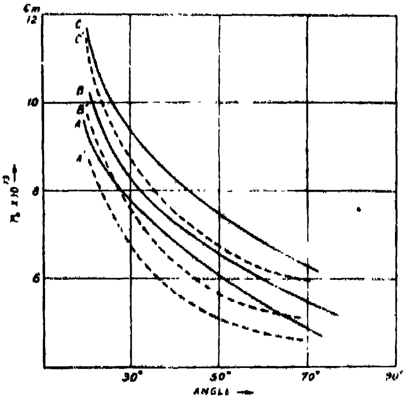

FIG. 2

Variation of Critical Approach with Angle approach for incident velocities 867 K V., 776 K.V. and 670 K.V. whereas the curves A′, B′ and C′ give the corresponding variation of the critical approach due to the repulsive force only. On comparing the corresponding curves A, A′, etc., it is evident that the effect of the short range attractive force is to slightly increase the value of the critical approach, which is, however, negligible at small angles.

Before concluding I would like to make a few remarks on the charge and mass of the Yukawa particles giving rise to the short range force between the protons. This force between neutron and proton or between two protons is found to be always attractive. It strongly suggests that the charges causing this short range force are opposite in nature and are developed temporarily through polarisation during the process of scattering, specially when the particles are at small distances apart. For, if the charges ± 6e permanently existed within the protons and neutrons, it would have been certainly possibie to observe cases of short range repulsion between neutron-proton and proton-proton. Now, the reason why the law of short range potential is different from Coulombian appears to me to be only due to the difference in the distribution of charge It is well known that for uniform distribution of charge on a sphere the potential is Coulombian. So it is quite likely that for some special distribution the potential may be of Yukawa type This is all the more plausible in view of the fact that the dimensions of the two charges are the same.

Now, as the short range charges associated with Yukawa particles in case of neutron-proton and proton-proton interactions are the same (± 6e), the masses of these particles must also be identical. It may be calculated in a very simple way. As the light quanta arising from the electromagnetic field satisfy the potential equation of the type

$$\Delta V - \frac{1}{c^2}\frac{d^2V}{dt^2} = 0, \quad \dots \quad (14)$$

the corresponding equation for the Yukawa potential will be of the type

$$\Delta V + \alpha^2 V - \frac{1}{c^2}\frac{d^2V}{dt^2} = 0. \quad \dots \quad (14.1)$$

Eq.(14.1) may be regarded as a wave equation for a particle with a rest mass

$$m = \frac{\alpha h}{2\pi c}. \quad \dots \quad (14.2)$$

Taking the mean value of α to be 0.2866×10^{13} (*vide* Table I), we find from (14.2), for the mass of Yukawa particles,

$$m \sim 110.8 \text{ electron mass.}$$

From the saturation properties of the nuclear forces, we know that the forces between a neutron and a proton are of exchange type. Thus the proton gives its long range positive charge to the neutron, thereby converting it into a proton, while becoming itself a neutron. A similar type of exchange cannot obviously take place in proton-proton interaction, since both the particles have the same long range charge. Therefore, the Yukawa particles giving rise to the short range force in proton-proton interaction should possess no long range electrical charge. These neutral particles are called 'neutrettos.' Thus there are two classes of Yukawa particles having the same mass (110.8 e.m.) and same short range charge ($\pm 6e$), *viz.*, (*i*) mesotrons, having long range charge e and taking part in neutron-proton interaction, and (*ii*) neutrettos, having no long range charge and taking part in proton-proton interaction.

PHYSICAL LABORATORY,
PRESIDENCY COLLEGE,
CALCUTTA.

REFERENCES

[1] K. C. Kar, *Phil. Mag.*, **29**, 200 (1940) ; *Ind. Jour. Phys* , **16**, 113 (1941).
[2] K. C. Kar and D. Basu, *Phil. Mag.*, **27**, 76 (1939).
[3] Chadwick, *Proc. Roy. Soc. A.*, **142**, 1, (1933) ; Kurie, *Phys Rev.*, **44**, 463 (1933) ; Monod-Herzen, *J. de Phys. et Rad.* **5**, 95 (1934).
[4] K. C. Kar, *Phil. Mag* , **16**, 1097 (1933) ; **21**, 1067 (1936).
[5] *Science and Culture*, **6**. 616 (1941).
[6] Yukawa, *Proc. Phys. Math. Soc. Japan*, **17**, 49 (1935) ; **19**, 1084 (1937)
[7] K. C Kar, *Ind. Jour. Phys.*, **15**, 113 (1941).
[8] N P. Heydenburg, M. A Tuve and L. R. Hafstad, *Phys. Rev.*, **50**, 806 (1936) ; *Phys. Rev.*, **56**, 1092 (1939).
[9] K. C. Kar, *Phil. Mag.*, **24**, 971 (1937)
[10] Mott and Massey, *Atomic Collisions*, 75-76 (Cambridge)
[11] K. C. Kar and D. Basu, *Phil. Mag.*, **29**, 200 (1940)
[12] Heitler, *Report in Progress of Physics*, **5** (1937)

ON THE THEORY OF 'Q'-METER AND ITS CORRECTIONS*

BY V. V. L. RAO

(*Received for publication, February 13, 1942*)

INTRODUCTION

In communication engineering, 'Q,' the ratio of effective reactance to resistance at any frequency has great significance as a figure of merit of a coil or a condenser.

$$Q \text{ for a coil is denoted by } Q_L = \frac{\omega L_e}{R_e}$$

and

$$Q \text{ for a condenser is denoted by } Q_c = \frac{1}{\omega C_e R_e}$$

where L_e, C_e, R_e are the effective values at the frequency $f(\omega = 2\pi f)$ considered.

In order to evaluate the 'Q' of a coil at different high frequencies, one has to measure carefully both L_e and R_e at each one of the frequencies concerned and then calculate the corresponding values of Q. To obviate this laborious process a few British and American firms have recently marketed a very ingenious and versatile meter called the circuit magnification or 'Q' meter, on which the values of Q between 10 and 500, and even up to 625, can be read off the meter directly in the frequency range 50 *kc/s* to 50 or even 75 *mc/s*. The accuracy of measurement of Q value in the Marconi Ekco 'Q' meter, Type TF 329D, is ±5% ±5 up to 10 *mc/s*. Its frequency range is 50 *kc/s* to 50 *mc/s*. The versatility of the meter will be seen from the following list of measurements that can be made with such a meter :

(1) Q of coils and condensers
(2) Self-capacity of coils
(3) Inductance of coils
(4) Capacity of condensers
(5) Power-factor of condensers
(6) Dielectrics and high resistances
(7) Low Impedances

---

* Communicated by Prof. P. N. Ghosh.

(8) Transmission-line Constants—

(*a*) Characteristic Impedance
(*b*) Attenuation Constant
(*c*) Wave velocity.

THEORY

A simple theory of this meter is worked out below.

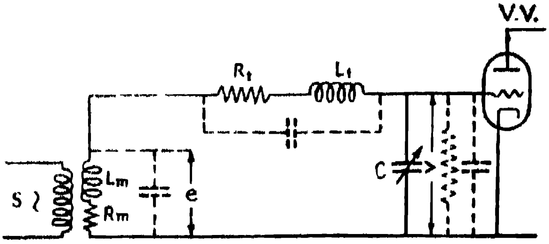

FIG. 1
Simplified circuit of a Q-meter

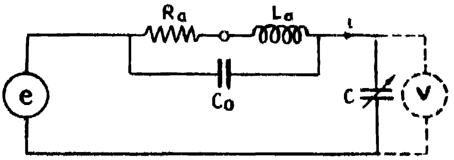

FIG. 2
Schematic-equivalent circuit of a Q-meter

Fig. 1 shows the simplified circuit of a Q-meter and Fig. 2 its equivalent circuit. S is an oscillator covering the desired frequency range and injecting a constant voltage 'e' into the tuned circuit by means of a small coil of inductance 'L_m' and resistance 'R_m' ($L_m = .05\mu h$ and $R_m = 0.04\Omega$ in the Marconi Ekco meter). V.V. is a valve-voltmeter, measuring the voltage across the condenser for convenience. Actually, at resonance, the voltage across the coil and that across the condenser are equal in magnitude. R_a and L_a represent the apparent values of resistance and inductance respectively, and C_0, the self-capacity of the coil, at the frequency in question. R_a and L_a are lumped so as to include R_m, the internal resistance, and L_m, the internal inductance of the source.

Then, the apparent Q of the coil is given approximately by the ratio $= V/e$, when the coil is tuned to resonance by the variable condenser C. When e is a known fixed value (say, 20 mv) the valve-voltmeter can be calibrated to read 'Q' directly as shown below :—

Let i be the current in the series circuit (*neglecting* C_0, the self-capacity).

Then
$$i = \frac{e}{R_a + j\omega L_a + \frac{1}{j\omega C}}$$

If $$Z_a = R_a + j\omega L_a, \quad i = \frac{e}{Z_a + \frac{1}{j\omega C}} \text{ or } \frac{je\omega C}{1 + jZ_a\omega C} \quad \ldots (1)$$

and $$V = i \cdot \frac{1}{j\omega C}. \quad \ldots (2)$$

On substituting in equation (2) the value of i obtained in equation (1) we get

$$V = \frac{e}{1 + jZ_a\omega C}. \quad \ldots (3)$$

But, by definition, $\text{magnification} = \frac{V}{e}$

$$\therefore \frac{V}{e} = \frac{1}{1 + jZ_a\omega C} = \frac{1}{1 + j\omega C(R_a + j\omega L_a)} = \frac{1}{(1 - \omega^2 L_a C) + j\omega R_a C}. \quad \ldots (4)$$

At resonance V is a maximum, and then, e being constant, $\frac{V}{e}$ is a maximum too.

But $$\left(\frac{V}{e}\right)^2 = \frac{1}{(1 - \omega^2 L_a C)^2 + (\omega R_a C)^2}. \quad \ldots (5)$$

Let $$D = (1 - \omega^2 L_a C)^2 + (\omega R_a C)^2. \quad \ldots (6)$$

Then $\left(\frac{V}{e}\right)^2$ is a maximum when $\frac{V}{e}$ is a maximum, and when $\left(\frac{V}{e}\right)^2$ is a maximum, D should be a minimum.

The condition for D to be a minimum is $\frac{d(D)}{dC} = 0$.

On differentiating expression (6), and equating to zero, we get

$$2(1 - \omega^2 L_a C)(-\omega^2 L_a) + 2\omega^2 C R_a^2 = 0. \quad \ldots (7)$$

This expression, on simplification, gives

$$C = \frac{L_a}{Z_a^2}. \quad \ldots (8)$$

Substituting this value of C in equation (5) and simplifying results ;

$$\left(\frac{V}{e}\right)^2 = \left(\frac{Z_a}{R_a}\right)^2 \text{ or } \frac{V}{e} = \frac{Z_a}{R_a}, \quad i.e., \frac{V}{e} = \frac{R_a + j\omega L_a}{R_a} \quad \ldots (9)$$

i.e., $$\frac{V}{e} = 1 + j\frac{\omega L_a}{R_a}. \quad \ldots (10)$$

Thus the valve-voltmeter deflection is proportional to

$$\sqrt{1 + Q^2} \doteqdot Q.$$

Hence the meter dial can be so calibrated that it gives $\frac{\omega L_a}{R_a}$, which is the apparent Q of the coil.

CORRECTIONS

As stated already, the 'Q' as read on the meter dial is not the true Q, but it is the apparent Q.

Foster and Newlon[1] state that the following corrections are required for the readings of a 'Q' meter above 9 Mc/s in the meter they worked with. These corrections will be discussed below as to how far they are really warranted.

The corrections are due to:

(1) the loading due to the valve-voltmeter,
(2) the internal impedance of the meter source,
(3) the self-capacity of the coil.

(1) This does not arise at all in the Marconi-Ekco or other similar meter, since the makers state that a special triode valve (Ac/HL/DD) having a very high input resistance is used.

(2) Internal impedance of the meter consists of two (principal) factors:

(*a*) R_m, the internal resistance

and (*b*) L_m, the internal inductance of the meter.

Then Q_t, the true Q of the coil is given by $\frac{\omega L_t}{R_t}$ (11)

and Q_a, the apparent Q of the coil by $\frac{\omega L_a}{R_a}$. (12)

But
$$L_t = L_a - L_m \tag{13}$$
and
$$R_t = R_a - R_m \tag{14}$$

$$\frac{Q_t}{Q_a} = \frac{\omega L_t}{R_t} \times \frac{R_a}{\omega L_a} = \frac{L_t}{L_a} \times \frac{R_a}{R_t}$$

or
$$Q_t = Q_a \frac{(L_a - L_m)}{L_a} \times \frac{R_a}{(R_a - R_m)}. \tag{15}$$

Evaluation of L_a *and* L_t :

L_a is obtained as follows from the meter readings.

Since at resonance
$$f = \frac{1}{2\pi\sqrt{L_a(C + C_0)}} \tag{16}$$

$$L_a = \frac{}{4\pi^2 f^2 (C + C_0)}, \tag{17}$$

where f is the frequency of the oscillator as read on the frequency calibration scale and C, the condenser reading on the meter, and C_0, the self capacity, which can be evaluated either by the negative intercept method (from the graph of $\frac{1}{f^2}$ *vs*. C or otherwise.

If f is in megacycles, C and C_0 in $\mu\mu f$, L_a in μh is obtained by

$$\frac{25330}{f^2(C+C_0)} \tag{18}$$

and the true inductance L_t (in μh) $= \dfrac{25330}{f^2(C+C_0)} - L_m$. ... (19)

$L_m = 0.05\mu h$ in the Marconi-Ekco meter the author used, and may even be neglected, when L_a is comparatively large as that 'Q' meter can measure the inductance of coils in the range $5\mu h$ to $25 mh$ approximately with an accuracy of ±3%:

Thus, if L_m is neglected, then equation (15) reduces to

$$Q_t = Q_a \frac{R_a}{R_a - R_m}. \quad \ldots \quad (20)$$

The need for the correction factor $\frac{R_a}{R_a - R_m}$ will solely depend on the relative values of R_a and R_m. If $R_m = 0.04\Omega$ and R_a even of the order of a few ohms, then $\frac{R_a}{R_a - R_m} \doteqdot 1$, when this correction also can be ignored without appreciable error.

(3) Correction for self-capacity of the coil is by far the most important correction, which need be applied below $15 mc/s$.

An expression for this correction is derived as follows :

If f_0 is the natural frequency of the coil, f the frequency at which Q is measured then

$$f_0 = \frac{1}{2\pi\sqrt{LC_0}} \quad \text{and} \quad f = \frac{1}{2\pi\sqrt{LC}}. \quad \ldots \quad (21)$$

$$\left.\begin{aligned} &\text{Let } k^2 \text{ denote the ratio } \frac{\omega^2}{\omega_0^2} = \left(\frac{f}{f_0}\right)^2 = \frac{C_0}{C} \\ &\text{Further,} \qquad \frac{1}{\omega_0^2} = LC_0 \\ &\therefore \qquad \frac{\omega^2}{\omega_0^2} = \omega^2 LC_0 = k^2. \end{aligned}\right\} \quad \ldots \quad (22)$$

It is well known that the effective inductance L_e and effective resistance R_e of a coil at a frequency $\omega = 2\pi f$ are approximately given by the following expressions[2] where L and R are the physical or absolute values of inductance and resistance of the coil, respectively. These apparent values at a frequency f are a consequence of the self-capacity C_0 of the coil.

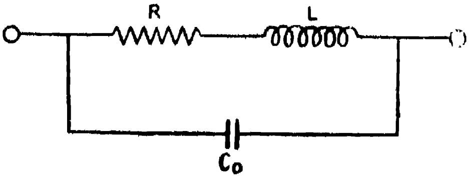

FIG. 3

Equivalent circuit of a coil at high frequencies

Fig. 3 shows the equivalent circuit at high frequencies of a coil having resistance and distributed or sellf-capacitance.

$$L_e \doteqdot \frac{L}{1-\omega^2 LC_0} \qquad (23)$$

and

$$R_e \doteqdot \frac{R}{(1-\omega^2 LC_0)^2}\,. \qquad \ldots\ (24)$$

Substituting these values of L_e and R_e in equation (12) for L_a and R_a respectively, we get $Q_a = \frac{\omega L(1-k^2)^2}{R(1-k^2)} = \frac{\omega L\,(1-k^2)}{(R)}$,

$$\text{i.e.,} \qquad Q_a = Q\,(1-k^2) \qquad \left(\because\ Q = \frac{\omega L}{R}\right)$$

$$\therefore \qquad \text{Actual } Q = \frac{Q_a}{1-k^2}\,. \qquad \ldots\ (25)$$

But $k^2 = \frac{C_0}{C}$ as proved in equation (22).

$$\therefore \qquad Q = \frac{Q_a}{1-\frac{C_0}{C}} = Q_a\left\{\frac{C}{C-C_0}\right\} \text{ or } Q_a\left\{1-\frac{C_0}{C}\right\}^{-1} \qquad \ldots\ (26)$$

Expanding $\left\{1-\frac{C_0}{C}\right\}^{-1}$ and neglecting the terms beyond the second, we get

$Q = Q_a\left(1+\frac{C_0}{C}\right)$, which is the only important correction below 15 Mc/s ... (27)

ORDER OF APPLYING CORRECTIONS

When more than one correction is required, they should be made in the following order, after having ruled out the necessity for correction as a result of the valve-voltmeter loading :

(1) Internal impedance of the meter

and (2) Self-capacitance of the coil.

At each stage the semi-corrected values of Q and L should be used for the pparent value of $Q(Q_a)$ and $L(L_a)$ in succeeding corrections.

Radio Engineer,
Government of Madras.

REFERENCES

[1] Dudley E. Foster and Arthur E Newlon, " Measurement of Iron Cores at Radi Frequencies," *Proc. I.R.E.*, **29**, 269, 274-75 ; May (1941).

[2] Bur. Standards Circ. C. **74** : Radio Instruments and Measurements, 133 (1937).

RAMAN FREQUENCIES OF HDO*

By Y. PARAMASIVA RAO

(Received for publication, November 7, 1951)

Plate VII

ABSTRACT. Mixtures of water and heavy water in two proportions 1 : 9 and 9 : 1—are studied. The Raman frequencies of HDO inferred from the spectra are 2523 and 3363. These results are compared with data available hitherto Changes in the structure of the H_2O and D_2O bands are also explained.

INTRODUCTION

In the study of the Raman spectrum of a mixture of water and heavy water by I. R. Rao and the author,[1] it was observed that the intensity of the D_2O band in the mixture increased by 50% from the pure liquid, while the H_2O band did not show any corresponding increase. This fact was explained as due to the formation of HDO molecule in the mixture. The Raman frequencies of HDO are not known with any certainty. Wood[2] who studied 18% and 80% mixtures concluded that HDO has two Raman frequencies of 2623 and 3445; but his studies with the vapour [2a] do not give any indication of the frequency of HDO corresponding to the OH oscillation. Rank, Larson and Bordner,[3] who also studied the Raman spectrum of the vapour of a mixture of water and heavy water, could report only a frequency of 2718 cm.$^{-1}$ for HDO in the vapour state. The results of these investigators regarding the absence of any OH oscillation for vapour are very interesting. Our results with the 50 : 50 mixture of H_2O and D_2O also showed a difference in the H_2O and D_2O bands in the mixture. We were hence led to investigate mixtures most suitable for recording the Raman frequencies of DOH, without the superposition of D_2O and H_2O bands.

Urey and Rittenberg[4] have calculated the equilibrium constant for the reversible reaction, $H_2O\ D_2O \rightleftharpoons 2HDO$ as 3·28. According to this the smaller the proportion of H_2O or D_2O in the mixture, the greater will be the percentage of HDO molecules compared to H_2O or D_2O respectively. If the proportion of HDO is very much greater compared to H_2O or D_2O, it will be possible to get the band due to HDO without the bands due to H_2O or D_2O overlapping it. But the proportion of H_2O or D_2O cannot be made too small. If the quantity of HDO in the mixture be small, unduly long exposures would be needed. Hence two mixtures of H_2O and D_2O in the ratios 1 : 9 and 9 : 1 (by volume) are chosen for study. Table I gives the proportion of H_2O, D_2O and

---

* Communicated by the Indian Physical Society

HDO molecules in these mixtures. The corresponding proportions for the mixtures studied by R. W. Wood[2] are also given there.

TABLE I

	Mixture		D_2O	H_2O	DOH
Author's	(*i*) $H_2O:D_2O$	1 : 9	81.9	1.1	17.8
	(*ii*) $H_2O:D_2O$	9 : 1	1.1	81.9	17.8
Wood's[2]	80% mixture		64.0	4.0	32.0
	18% mixture		3.4	66.0	39.0

It is evident that the mixtures used by the author are better suited for the study of HDO frequencies than those of R. W. Wood.

EXPERIMENTAL

The apparatus used is similar to that adopted in the studies of the 50 : 50 mixture. Only the Wood's tube used is of a smaller capacity of 50 c.c. Since it is our object to study the Raman spectrum of HDO, the spectra of the pure liquids are not recorded. The liquids are very carefully distilled in vacuum, so as to be free from dust. A close arc arrangement together with a glass spectrograph of high light-gathering power is used to photograph the spectra. With this arrangement an exposure of about 10 hours was enough to get fair records of the HDO bands. Longer exposures which would have given more intense pictures could not be availed of, on account of the unavoidable reflection of light from the sides of the Wood's tube, since it had a small cross section. The bands excited by the 4046 line of the mercury arc are chosen for study. The spectra are microphotometered and the frequencies of the HDO bands are measured by extrapolating from these curves, with the mercury lines as the standards.

RESULTS

The microphotometric curves corresponding to the two spectra taken with 9:1 and 1:9 proportions of D_2O and H_2O are reproduced in Fig. 1 (Plate VII). The band corresponding to the HDO oscillations excited by the 4046 line of the mercury arc are marked by arrows. The lower curve corresponds to the spectrum taken with the mixture containing excess of D_2O, and the upper curve to that with a mixture containing excess of H_2O. The curves clearly indicate that the band due to HDO appearing in the position of the pure D_2O band is much sharper than that in the position of the H_2O band. Only one of the frequencies due to HDO is recorded in either picture as the band due to the liquid in excess obscures the second HDO frequency lying in that region. In each case, the principal band due to the liquid in excess shows some minor changes which are to be expected from the presence of a second substance in the mixture. These changes are similar to those found in very dilute solutions.

DISCUSSION

The table given in the introduction shows that the number of HDO molecules in $H_2O : D_2O = 1 : 9$ mixture is nearly sixteen times the number of H_2O molecules. The proportion of H_2O molecules in the whole mixture is less than two per cent. Hence the band occurring in the region of the H_2O band must be mainly due to HDO and not to H_2O. Similarly the band in the position of the pure D_2O band in the mixture with excess of water cannot have its origin in D_2O, but must also be assigned to HDO. The frequencies of the maxima of these two bands are 3363 cm.$^{-1}$ and 2523 cm.$^{-1}$. The former frequency shows that HDO has a frequency corresponding to the OH oscillation and the failure of Wood[2] and Rank, Larson and Bordner[3] to get it in the vapour is perhaps accidental. The Raman frequencies assigned by the various workers to the HDO molecule are shown in Table II. The frequencies given by the author also refer to the liquid state. There is a large difference between the frequency given by Wood (2623) and the corresponding value of the author (2523). Wood did not measure from microphotometer records, and the proportion of HDO to D_2O is greater in the mixtures studied by the author, and these values are therefore more reliable.

TABLE II

Author	Frequencies in cm.$^{-1}$		
	(i)	*(ii)*	*(iii)*
R. W. Wood[2]	3445 (Liquid)	2623 (Liquid)	—
Rank, Larson, Bordner[3]	—	2718 (Vapour)	—
Van Vleck, Cross[5] (calculated)	3750	2720	1400
Author	3363	2523	—

The frequencies 2523 and 3363 cm.$^{-1}$ of the maxima of the Raman bands of HDO are smaller than those of D_2O and H_2O which are 2538 and 3443 cm.$^{-1}$ respectively. The decrease in the frequencies of both OH and OD oscillations in HDO from those in H_2O and D_2O respectively is difficult to explain. HDO results by substituting one of the hydrogen atoms in H_2O by a heavier isotope or one atom of heavy hydrogen in D_2O by the lighter isotope. That both these changes should result in a similar change (decrease) in the frequency is very interesting. Substitution of an atom by a heavier isotope in the molecule should diminish the frequency of any particular oscillation. The change in the frequency of the OH follows this rule, while the OD oscillation does not obey it, since it is expected that the frequency should increase when one of the atoms diminishes in mass. The frequency corresponding to the OH oscillation is much further away from that in H_2O than the corresponding OD oscillation from that in D_2O. The influence of the D atom on OH oscillation seems to be much more than that of the H atom upon the OD oscillation, as seen in the greater change of the OH frequency in DOH. This may be due to the heavier mass of the D atom.

In the discussion on the 50 : 50 mixture[1] it is pointed out that the HDO frequency in the region of the D_2O band is likely to be less than the frequency of D_2O band. The displacement of the D_2O band in the mixture towards the Rayleigh line must be due to the superposition of the DOH band. Though the HDO frequency in the region of H_2O band is also less than that of pure H_2O, in the 50 : 50 mixture the maximum of the H_2O band is not displaced in the direction of the HDO frequency.

The Raman frequencies of HDO, like those of D_2O and H_2O, are broad and diffuse. The extent of the 2523 cm.$^{-1}$ frequency is 200 cm.$^{-1}$ while that of the 3363 frequency is 490 cm.$^{-1}$. Thus the latter is broader by more than two times.* The width of the principal bands of pure D_2O is nearly 650 cm.$^{-1}$ and that of pure water 850 cm.$^{-1}$. These widths are in the ratio of their frequencies (maxima of the bands) as required by the isotopic substitution. In the case of DOH, however, the 2523 band is less broad (less than half) and sharper than the 3363 band. This cannot be explained merely on the basis of the difference in the reduced masses in the case of the two oscillations. It must be interrelated with the greater change in the frequency of the OH oscillation.

No band corresponding to the 1400 cm.$^{-1}$ is recorded. This band, if present, must be much less intense than the other two. The 1600 cm.$^{-1}$ band observed in water or the 1200 band in heavy water is much feebler than the principal bands. On this basis, it may be inferred that 1400 cm.$^{-1}$ of HDO is also very weak and much stronger impression than obtained here may be necessary to record it. The diffuseness and the breadth of the bands of HDO like those of water and heavy water indicate that they have a structure similar to that of H_2O or D_2O bands. Evidence about this can be obtained only by studying the temperature effect. A preliminary study with the $H_2O : D_2O = 9 : 1$ mixture indicates a shift in the maximum of the 2523 band to 2543 at 80°C. This is similar to the effect observed in water and heavy water by I. R. Rao[6] with increase of temperature.

The microphotometer record of the Raman spectrum of the mixture containing excess of water shows also the principal band of H_2O. It shows

---

* The limits of the 2523 and 3363 bands are respectively 2433 and 2643, and 3113 and 3603 cm.$^{-1}$.

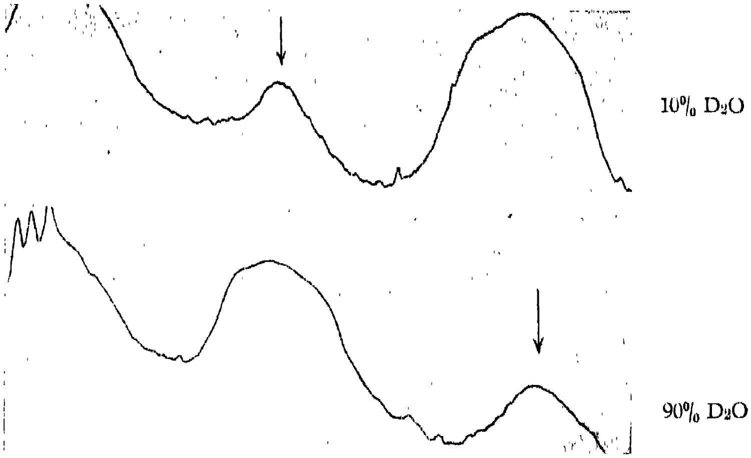

Microphotometric record of the Raman spectra of the mixture of H_2O and D_2O.

the diminution in the intensity of the shorter frequency component as compared to the pure liquid. The effect is not as pronounced as in the case of the 50 : 50 mixture. It is similar to the effect observed with increase of temperature or in solutions. This may be explained as due to a change in the equilibrium between the three types of structures responsible for the three components. According to I. R. Rao,[6] the shortest frequency component is due to triple polymers and in the mixture a fraction of the trihydrols is depolymerised. Similar changes in the heavy-water band in the mixture containing excess of heavy water are observed. They have a similar explanation based upon the splitting up of the triple polymers of heavy water. If the three structures proposed by Bernal and Fowler[7] are adopted, the structure of water or heavy-water in the mixtures containing them respectively in excess, must be reckoned as approximating less to type I (like tridymite) and more to type II (like quartz) than in the pure liquids. These changes are to be expected from the other components in each mixture. The mixture is only a solution and the changes found here are similar to the effect of dissolved substances upon the solvent.

The author expresses his gratefulness to Dr. I. Ramakrishna Rao for his helpful guidance during the course of this investigation.

DEPARTMENT OF PHYSICS,
ANDHRA UNIVERSITY,
WALTAIR.

REFERENCES

[1] I. R. Rao and Y. P. Rao., *Ind. Jour. Phys.*, **14**, 135 (1940).

[2] R. W. Wood, *Phys. Rev.*, **45**, 392 (1934).

[2a] „ „ „ 733 (1934).

[3] Rank, Larson and Bordner, *Jour. Chem. Phys.*, **2**, 484 (1934).

[4] Urey and Rittenberg, „ „ **1**, 137 (1933).

[5] Van Vleck and Cross, „ „ **1**, 357 (1933).

[6] I. R. Rao., *Proc. Roy. Soc.*, **A**, **145**, 489 (1934).

[7] Bernal and Fowler, *Jour. Chem. Phys.*, **1**, 515-548 (1933).

POLAR DIAGRAMS OF ULTRA-SHORT WAVE HORIZONTAL TRANSMITTING AERIALS*

By S. S. BANERJEE

AND

G. C. NEOGI

(Received for publication, February 17, 1942)

ABSTRACT Polar diagrams for various distances near horizontal transmitting aerials of different lengths have been obtained for ultra-short radio waves. A modulated valve oscillator was used for emitting waves from 3 to 8 metres in length. The field strengths were measured with the help of a calibrated ultra-short-wave receiver of the super regenerative type. The observed values of field strengths were compared with those deduced mathematically calculated on the theory of " induced e m.f." It has been noticed that aerials of different lengths radiate the energy along different channels and the polar diagrams for a particular length of the aerial depend on the distance at which the field strengths are measured.

INTRODUCTION

The importance of radio communication with short waves below hundred metres has been realized sufficiently long time back due to the numerous advantages which these waves possess. Recently, however, the necessity has been felt of going down to still shorter lengths of the waves specially for television, aircraft communications and upper-air weather observations. These waves which are below ten metres in length are known as ultra-short waves, and their applications are still in the early stages of development. Hence the study of these waves has been felt imperative and it has opened a great opportunity for further investigations. The application of the technology of ultra-short waves, as yet largely unexplored, has been proved to be most essential. The beacons and blind landing are well-known uses of these waves and they are also used for sending secret messages.

The guiding factor in designing a broadcast transmitter is that it should be able to produce good quality signals within a certain stipulated area around the transmitter. A definite knowledge of the field strength, near the transmitter, is therefore essential. The broadcast engineer tries to design the transmitter, so that most of the radiated energy is directed along the ground, in order to secure the largest possible service area.

---

* Communicated by the Indian Physical Society.

It is evident that the field strength will not only depend upon the power of the transmitter but will also depend upon the radiating system. Therefore it is necessary that the aerial must be carefully designed; and, in the case of ultra-short waves, special types of aerial have to be used due to their short lengths. On account of the limited range of the transmitter, one should be very careful that the waves may be travelling in the right direction. The directivity depends only upon the type of the aerial we use, and many investigators from time to time have tried to develop such directive aerials, and studied their polar diagrams, mostly with vertical aerials.

Though various investigations have been made in this direction, it appears that the study of single wire as directive aerial has not received adequate attention. In this communication, polar diagrams for ultra-short wave horizontal transmitting aerials of different lengths for various distances have been investigated. In order to draw the polar diagram the intensities of radiated field strengths were determined by an ultra-short wave calibrated receiver of super-regenerative type. For the purpose of radiation a modulated oscillator generating waves from 3 to 8 metres in length was employed in conjunction with horizontal aerials of different lengths varying from quarter wave to one wave in length. The plots for variation of field for different distances have been shown. Experimental polar diagrams for different wave-lengths have been drawn and verified by those obtained by calculation. Derivations of the necessary mathematical equations involved for calculating the field strength for multiples of quarter wave long aerial have been shown by the method of " induced e.m.f."

THEORETICAL

The method of calculating the field strengths for various lengths of aerial has been shown below.

If we take an aerial three-fourths of a wave long, a current antinode will be formed at the input end. The equation giving the current at any point in the aerial is represented by

$$i = \mathrm{I}e^{j\omega t} \cos my \qquad \ldots \quad (1)$$

where $m = 2\pi/\lambda$ and y = distance along the aerial from the input end O, in Fig. 1.

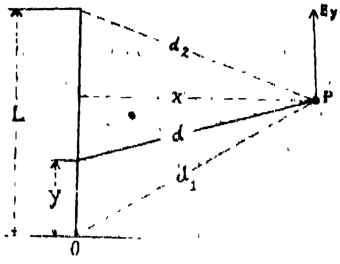

FIG.

Now the retarded scalar and vector potentials ψ and A may be denoted by

$$\psi=\int_0^l \frac{[\sigma]}{d}dy \qquad \ldots \quad (2)$$

and

$$A=\frac{K}{c}\int_0^l \frac{[i]}{d}\,dy \qquad \ldots \quad (3)$$

where $[\sigma]$ and $[\psi]$ denote the retarded instantaneous charge and current respectively ; K the unit vector in the direction parallel to the aerial, and c the velocity of light.

The relation between σ and i is given by

$$\frac{d\sigma}{dt}=-\frac{di}{dy}.$$

From equation (1) along with the above relation, we get

$$\sigma=\frac{I}{jc}\,e^{j\omega t}\sin my. \qquad \ldots \quad (4)$$

Thus from equations (1), (2), (3) and (4), we have

$$\psi=\frac{I}{jc}\int_0^l \frac{e^{-jmd}}{d}\quad \sin my \qquad \ldots \quad (5)$$

and

$$A=\frac{I}{c}\,e^{j\omega t}\int_0^l \frac{e^{-jmd}}{d}\quad \cos my\;dy. \qquad \ldots \quad (6)$$

The potential parallel to the aerial is given by

$$E_y=-\text{Grad}_y\psi-\frac{I}{c}\;\frac{dA}{dt}$$

$$=\frac{I}{jc}\,e^{j\omega t}\int_0^l \frac{e^{-jmd}}{d}\quad \cos my\;dy-\frac{jI\omega}{c^2}\,e^{j\omega t}\int_0^l \frac{e^{-jmd}}{d}\quad \cos my\;dy. \qquad (7)$$

Substituting $l=3\lambda/4$ in equation (7) we get

$$E_y=\frac{2I}{jc}e^{j\omega t}\left[\frac{e^{-jmd_2}}{d_2}\right] \qquad \ldots \quad (8)$$

Now, separating real and imaginary parts, we have

$$E_y=-60\;I\frac{\text{Sin }m\sqrt{l^2+d_1^2-2ld_1\cos\theta}}{\sqrt{l^2+d_1^2-2ld_1\cos\theta}}. \qquad \ldots \quad (9)$$

If the aerial is quarter wave long, a current node is formed at the input end. Therefore the current at any point Y (Fig. 1) along the wire is given by the relation

$$i=Ie^{j\omega t}\sin my. \qquad \ldots \quad (10)$$

Proceeding as above, it can be shown that

$$E_y = 2j\frac{I}{c}e^{j\omega t}\left[\frac{e^{-jmd_1}}{d_1} - \frac{e^{-jmd_2}}{d_2}\cos ml\right]. \qquad \cdots \quad (11)$$

Substituting $l=\lambda/4$ in equation (11) and taking real part only, we have

$$E_y = 60\ I\frac{\text{Sin}\ md_1}{d_1}. \qquad \cdots \quad (12)$$

The equations to calculate the field in the vicinity of half wave and one wave long aerials can be obtained from equation (11) by substituting the proper values of the lengths of the aerials. Thus it may be shown that the potential for half wave aerial will be given by

$$E_y = -30\ I\left\{\frac{\text{Sin}\ md_1}{d_1} + \frac{\text{Sin}\ m\sqrt{l^2+d_1^2-2ld_1\cos\theta}}{\sqrt{l^2+d_1^2-2ld_1\cos\theta}}\right\}. \qquad \cdots \quad (13)$$

Similarly the potential near full wave aerial will be given by

$$E_y = 30\ I\left\{\frac{\text{Sin}\ md_1}{d_1} - \frac{\text{Sin}\ m\sqrt{l^2+d_1^2-2ld_1\cos\theta}}{\sqrt{l^2+d_1^2-2ld_1\cos\theta}}\right\}. \qquad \cdots \quad (14)$$

It should be mentioned that the above relations shown in equations (13) and (14) for half wave and full wave aerials respectively have also been deduced by Carter.[6]

The polar diagrams for all the above lengths of aerial have been drawn for different distances from the aerial. Four typical diagrams have been shown below with an associated table showing the variation of field strength with angular direction in each case.

Table I shows the variation of field strength for an aerial $3\lambda/4$ long calculated from equation (9), for different angular directions at a distance of one wavelength from the input end. The corresponding polar diagram is shown in Fig. 2.

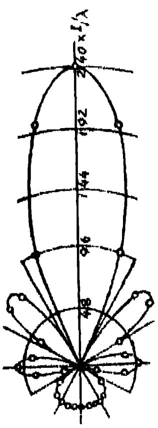

FIG. 2
Polar diagram of an aerial 3λ/4 long

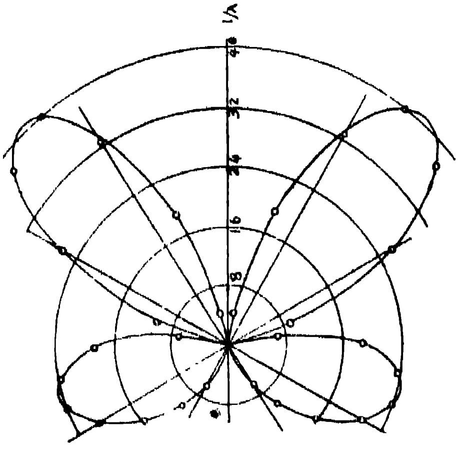

FIG. 3
Polar diagram of half wave aerial

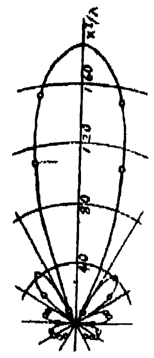

FIG. 4
Polar diagram of full wave aerial

Similar variations of field strength for half wave and full wave aerials are shown in Tables II and III respectively, while their polar diagrams are shown in Figs. 3 and 4.

TABLE I

Angular direction in degrees	Field strength in volts/metre × 1/λ	Angular direction in degrees	Field strength in volts/metre × 1/λ
0	−240.0	100	−36.0
10	−198.4	110	−14.8
20	− 97.1	120	5.1
30	9.7	130	21.3
40	73.0	140	29.0
50	76.7	150	33.1
60	38.6	160	34.4
70	− 9.0	170	34.3
80	− 40.8	180	34.3
90	− 48.0		

TABLE II

Angular direction in degrees	Field strength in volts/metre × 1/λ	Angular direction in degrees	Field strength in volts/metre × 1/λ
0	0	100	−23.6
10	5.4	110	−23.6
20	18.6	120	−20.3
30	33.0	130	−15.4
40	40.6	140	−10.2
50	41.0	150	− 5.7
60	25.6	160	− 2.5
70	9.2	170	− 1.6
80	0.6	180	0
90	− 18.2		

TABLE III

Angular direction in degrees	Field strength in volts/metre × 1/λ	Angular direction in degrees	Field strength in volts/metre × 1/λ
0	−186.0	100	3.9
10	−153.1	110	17.6
20	− 70.4	120	17.2
30	6.4	130	15.3
40	40.1	140	11.0
50	29.3	150	6.4
60	0	160	2.8
70	− 20.9	170	0.7
80	− 22.7	180	0
90	− 10.9		

It will be observed that the field strength will not show any change for different angular directions for a quarter-wave aerial at a fixed distance. The variation of field strength is, therefore, shown in Table IV as the distance from the input end is altered. The positions of maximum field strengths in the present case and the nature of the curve are shown in Fig. 5.

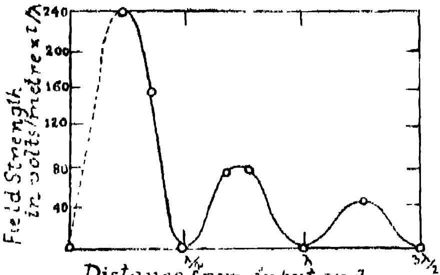

FIG. 5

Positions of maximum field strength

TABLE IV

Distance from input end	Field strength in volts/metre × 1/λ	Distance from input end	Field strength in volts/metre × 1/λ
λ/4	240	3λ/4	80
λ/3	156	λ	0
λ/2	0	5λ/4	48
2λ/3	78	3λ/2	0

EXPERIMENTAL

A modulated oscillator of the Hartley type was used for generating the ultra-short waves. A constant modulation was effected by a leak and a condenser. A super-regenerative receiver was built for measuring the field strengths. A milliammeter was put in the anode circuit of the detector stage for observing the change in its deflection due to the incoming signal. The receiver was calibrated by the same method as described by Banerjee and Parmanand,[7] in a previous paper published in this journal.

The ultra-short wave generator was connected with a horizontal aerial which was placed in a fixed direction and the receiver was moved along the circumference of a circle with the input end of the transmitting aerial as centre. The field strengths were measured at different angular directions with respect to the orientation of transmitting aerial. Special precautions have been taken, as far as possible, to avoid the reflection of the waves from the neighbouring walls of the laboratory. Most of the observations have been taken in clear open space on the terrace of the building, the reflection coefficient of which was actually found to be very small. This was evident from the absence of the formation of any interference pattern due to the direct and reflected rays. This pattern could always be found when such experiments were performed on the ground.

The wave-lengths used were between 3 to 7 metres and the lengths of the aerials were λ, 3λ/4, λ/2 and λ/4.

The observed values of field strengths in the neighbourhood of a horizontal transmitting aerial, λ/2 long, at a distance of λ from the input end, and for different angular directions, are shown in Table V below. The polar diagram for the same is depicted in Fig. 6.

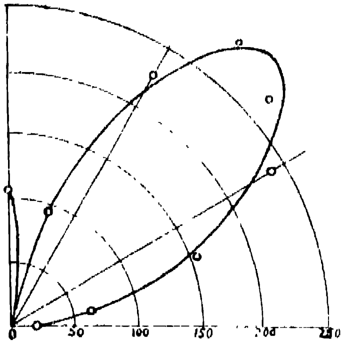

Field Strength in Milli-volts/metre

FIG. 6

Polar diagram of half-wave horizontal transmitting aerial

TABLE V

Angular distance in degrees	Field strength in milli-volts/metre	Angular distance in degrees	Field strength in milli-volts/metre
0	23	50	287
10	69	60	230
20	161	70	92
30	241	80	11.5
40	276	90	115

SUMMARY AND CONCLUSION

Field strengths have been measured at short distances in all directions from horizontal transmitting aerials of different lengths. Polar diagrams for the aerials have then been shown. In order to verify the results obtained experimentally, new equations have been derived based on the theory of "induced e.m.f." for each length of the aerial. Field strengths have been calculated from these equations, and theoretical polar diagrams have also been drawn. A modulated oscillator was used to energise the transmitting aerial and a calibrated super-regenerative receiver was employed for the purpose of measurements of the field.

It may be mentioned here that the equations derived in the present investigations could be applied for computing the fields, radiated from quarter-wave transmitting aerials and their odd multiples in addition to half-wave aerials and their multiples as generally used. It has been observed that the polar diagrams for such horizontal aerial will depend mainly on the length of the aerial and on the distances from the input end at which the field strengths are measured.

In conclusion, the authors have great pleasure to record their sincere thanks to Prof. Dr. B. Dasannacharya, Head of the Department of Physics, for giving facilities to carry out the above investigation.

WIRELESS SECTION,
PHYSICS DEPARTMENT,
BENARES HINDU UNIVERSITY.

REFERENCES

1 A. Miessner, *Proc. I. R. E.*, **15**, 928 (1927).
2 G. C. Southworth, *Proc. I. R. E.*, **18**, 1502 (1930).
3 H. Diamond, *Proc. I. R. E.*, **21**, 808 (1933).
4 F. G. Kear, *Proc. I. R. E.*, **22**, 847 (1934).
5 F. R. Stansel, *Proc. I. R. E.*, **24**, 802 (1936).
6 P. S. Carter, *Proc. I. R. E.*, **20**, 1004 (1932).
7 S. S. Banerjee and Parmanand, *Indian Journ. of Phys.*, **14**, 325 (1940)

THE LINEARITY OF THE MASS-SCALE OF ASTON'S MASS-SPECTROGRAPH

By J. B. SETH

AND

C. V. H. RAO

(Received for publication, February 2, 1932)

ABSTRACT. The portion of the mass-distance curve where it is most linear has been investigated, starting from the relationship between mass and distance as obtained by Aston and Fowler from considerations of pure geometry, and as obtained by Pidduck making use of co-ordinate geometry. Treatment of both the expressions leads to the same result, which is identical with that of Pidduck, but is different from that of Aston and Fowler. The mass-distance curve is also plotted and discussed.

STATEMENTS AND RESULTS

The mathematics of Aston's mass-spectrograph is not of much practical importance, since the results obtained by the use of the instrument must be regarded to be only of an empirical character. However, it must have been satisfactory to find that a mathematical analysis of the experimental arrangements did corroborate the empirically obtained results. The chief factor, mathematical or empirical, on which the success of the experiment and the importance and simplicity of its results depend, is that the relationship between the masses, or rather, the ratios of the mass to the charge, of the charged particles concerned, and the distances, from a fiducial point, of the "spectral" lines due to them on the photographic plate, is almost linear over quite a large range. It is the mathematical determination of the region over which the proportionality holds and in which the photographic plate must be placed that forms the subject-matter of this communication.

Aston and Fowler, in their paper[1] dealing with the mathematics of the experiment, show that the mass-scale is approximately linear in the neighbourhood of the region given by $\phi = 4\theta$, where θ and ϕ are deflections, in opposite directions, due to the electric and magnetic fields respectively. The relationship between masses and the distances of lines due to them was obtained by Aston and Fowler by geometrical considerations. An analytical solution of the problem is given in Pidduck's Treatise on Electricity,[2] which is much simpler than Aston and Fowler's geometrical treatment. Taking rectangular co-ordinates with the origin at the commencement of the electric field (A, Fig. 1), Pidduck finds that the curve

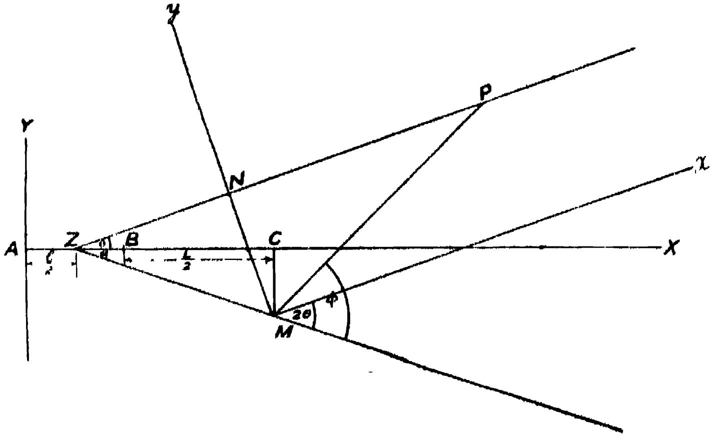

FIGURE 1

The geometry of the mass-spectrograph

AB, the length of the electric field; BC, half that of the magnetic field. Z, the centre of the electric field. AX, AY, the axes as taken in Pidduck's book, Mx, My, the axes as taken by Aston and in this paper.

obtained by plotting m, the mass, or rather, the specific mass, m/e, against x, the distance of the line due to this mass from the origin, has a point of inflexion in the region where the curve and, therefore, the mass-scale would, of course, be nearly linear. The point of inflexion comes out at $x=\frac{5}{4}l+\frac{3}{4}L$, where l and L are respectively the lengths over which the electric and magnetic fields act, the two fields being co-terminus at one of their ends. Then in the relationships

$$\theta=\frac{y}{x-\frac{1}{2}l}, \qquad \phi=\frac{2y}{x-l-\frac{1}{2}L},$$

which hold for focussing the particles having the same m/e, by substituting for x its inflexional value, one finds that the relationship between mass and distance is linear when $\phi=6\theta$.

Thus the value of ϕ as given in Pidduck's treatise namely "m in this region is nearly proportional to the distance of P from the fiducial point," and that as given in Aston's book,[3] near about which "the mass-scale is approximately linear," are very different. This difference is rather puzzling, for at first sight the two appear to refer to the same region. However, a deeper and closer scrutiny reveals that the two writers refer to different regions. Whereas Pidduck refers to the point of inflexion on the mass-distance curve, Aston, although attempting to find the position where the mass-scale is nearly linear, really determines the point where a straight line from the origin touches this curve. Evidently, the region referred to by Pidduck is the one which is relevant to the problem in hand and not the one found by Aston and Fowler. For, a curve will be approximately linear on either side of a point of inflexion, if there be such a point on the curve ; but round about the point of contact between a curve and the tangent from the origin, the curve need not at all be linear.

The mathematical determination of the position where the relationship between mass and distance may be linear is of no practical importance, as has already been remarked, for the result so obtained is not used in the calculation of the masses. Moreover, on plotting the curve it is found that between the region given by $\phi = 10\theta$ approximately, which is not very far from the origin and that given by $\phi = 2\theta$, which corresponds to the region of the curve at infinity, the curvature is nowhere very pronounced. Thus within comparatively large regions the curve, *i.e.*, the relationship between mass and distance, will be approximately linear, wherever the region may be situated within the limits given above The result, $\phi = 4\theta$, of Aston and Fowler conveys a sense of accuracy which is not true ; whereas the result, $\phi = 6\theta$, of Pidduck gives an impression of uniqueness of solution which is unnecessary.

ASTON AND FOWLER'S MATHEMATICAL EXPRESSION

The expression for r, the distance, measured from a suitable point of the spectral line due to a mass m, as obtained by Aston and Fowler,[3] is

$r = \mathrm{NF}/p$ (in Aston and Fowler's notation, p being a constant $=$ MN of Figure 1 ; also F of Aston and Fowler is P of this Figure 1)

$$= \frac{m - m_0 + 2 \tan 2\theta \sqrt{m m_0}}{2\sqrt{m m_0} - (m - m_0) \tan 2\theta}, \qquad \dots \quad (i)$$

where m_0 is another constant and $\sqrt{m m_0} = \cot \frac{\phi}{2}$, θ and ϕ being the electric and magnetic deflections respectively.

Writing $\sqrt{m m_0} = z$, one gets

$$\frac{r}{z^2} = \frac{z^2 - 1 + 2z \tan 2\theta}{z^2\{2z - (z^2 - 1)\tan 2\theta\}}.$$

Aston and Fowler find the region where the above relationship is approximately linear by determining where $\frac{d}{dz}\left(\frac{r}{z^2}\right)$ vanishes. This gives

$$(z \tan 2\theta - 1)\{(3z^2 - 1)\tan 2\theta + z(z^2 - 3)\} = 0.$$

The second factor equated to zero must be considered irrelevant to the problem in hand, for the exact roots of this cubic can be shown to be

$$\phi = \frac{\pi + 4\theta}{3}, \quad \frac{3\pi + 4\theta}{3}, \quad \frac{5\pi + 4\theta}{3},$$

where $$z = \cot\frac{\phi}{2}.$$

With $\theta = 5^\circ$, we are led to

$$\phi = 67^\circ,\ 187^\circ,\ 307^\circ \text{ approximately.}$$

All these values are clearly inapplicable for our purpose. Thus for the problem in hand, Aston and Fowler put

$$z \tan 2\theta - 1 = 0,$$

which gives, $\tan 2\theta = 1/z = \tan \phi/2$, so that for small values of θ and ϕ, $\phi = 4\theta$.

As already remarked, this merely determines where $d/dz(r/z^2) = 0$, which only gives the condition where the tangent from the origin touches the curve.*

To find whether the mass-scale is anywhere linear and, if so, where, we must first investigate whether the above curve has a point of inflexion. To do this, we put in the above relationship between r and m, $\tan 2\theta = a$, $\cot 2\theta = a'$, so that $aa' = 1$; and then determine $d^2 r/dm^2$. Thus

$$r = \frac{m - m_0 + 2a\sqrt{mm_0}}{2\sqrt{mm_0} - (m - m_0)a}.$$

$$\therefore \quad -ar = \frac{m + 2a\sqrt{mm_0} - m_0}{m - 2a'\sqrt{mm_0} - m_0} = 1 + \frac{2(a + a')\sqrt{mm_0}}{m - 2a'\sqrt{mm_0} - m_0}.$$

$$\therefore \quad \frac{-ar - 1}{2(a + a')\sqrt{m_0}} = \frac{\sqrt{m}}{m - 2a'\sqrt{mm_0} - m_0}$$

$$= \frac{A}{\sqrt{m} - k\sqrt{m_0}} + \frac{B}{\sqrt{m} + \frac{1}{k}\sqrt{m_0}} = \frac{A}{P} + \frac{B}{Q},$$

where $k - \frac{1}{k} = 2a'$; $A + B = 1$; $A = Bk^2$; P and Q are obvious.

---

* For the tangent at a point, (x,y), is given by

$$(Y - y) - (X - x\ dy/dx = 0$$

This will go through the origin, $X = Y = 0$, when

$$(y - x)\ dy/dx = 0. \qquad \dots (1)$$

And $d/dx(y/x) = (1/x)dy/dx - y/x^2$, and vanishes precisely when (1) holds.

Thus dr/dm is proportional to $\left(\frac{A}{P^2}+\frac{B}{Q^2}\right)m^{-\frac{1}{2}}$.

$$\therefore \quad d^2r/dm^2 : al \text{ to } \left(\frac{A}{P^3}+\frac{B}{Q^3}\right)\left(-m^{-1}\right)+\left(\frac{A}{P^2}+\frac{B}{Q^2}\right)\left(-\tfrac{1}{2}m^{-\frac{3}{2}}\right)$$

or
$$m^2\frac{d^2r}{dm^2} : al \text{ to } k^2\frac{3m-k\sqrt{mm_0}}{(\sqrt{m}-k\sqrt{m_0})^3}+\frac{3m+\frac{1}{k}\sqrt{mm_0}}{\left(\sqrt{m}+\frac{1}{k}\sqrt{m_0}\right)^3}.$$

This will be zero when

$$\left(\sqrt{m}-k\sqrt{m_0}\right)^3\left(3m+\frac{1}{k}\sqrt{mm_0}\right)$$
$$+k^3\left(\sqrt{m}+\frac{1}{k}\sqrt{m_0}\right)^3\left(3m-k\sqrt{mm_0}\right)=0,$$

i.e., $$3(m/m_0)^2+\frac{1-k^2}{k}(m/m_0)^{\frac{3}{2}}+6m/m_0+3\frac{1-k^2}{k}(m/m_0)^{\frac{1}{2}}-1=0.$$

Now $\quad m/m_0=\cot^2\phi/2,\quad$ and $(1-k^2)/k=-2a'=-2\cot 2\theta.$

$\therefore$ $\quad d^2r/dm^2$ vanishes when

$$3\cot^4\phi/2-2\cot^3\phi/2.\cot 2\theta+6\cot^2\phi/2-6\cot\phi/2.\cot 2\theta-1=0,$$

i.e., when $$\cot 2\theta=\frac{3\cot^4\phi/2+6\cot^2\phi/2-1}{2\cot^3\phi/2+6\cot\phi/2}$$

$$=\cot\phi+\frac{2}{(2-\cos\phi)\sin\phi}.$$

Thus for small values of θ and ϕ, $d^2r/dm^2=0$, when

$$\frac{1}{2\theta}=\frac{1}{\phi}+\frac{2}{\phi},$$

i.e., when $\phi\simeq 6\theta$.

It can be shown that for this value of ϕ, $d^3r/dm^3\neq 0$. This value of ϕ, therefore, gives the point of inflexion where the relationship between m and r will be linear.

THE ANALYTICAL TREATMENT OF THE PROBLEM

The relation between r and m given above, as found by Aston and Fowler using a pure geometrical method, is complicated and, as will be seen from the foregoing, the finding of d^2r/dm^2 from that expression involves some intricate analysis. By making use of analytical geometry (in the manner of Pidduck), one can obtain more easily a simpler relationship between r and m, and with the help of the new expression get all the information needed.

Thus, following the usual practice, we assume for the purpose in hand that the deflections due to the electric and magnetic fields take place at the respective centres (Z and M, Fig. 1) of the fields, the electric deflections being downwards and the magnetic upwards; and following Aston, take a straight line through M given by $\phi=2\theta$ as the axis of X. The foci lie on the straight line ZP parallel to MX (Fig. 1). The co-ordinates of a focal point, such as P, will be given by

$$x=\mathrm{NP}=r,$$

$$y=\mathrm{MN}=b.2\theta.$$

where b is the distance between Z and M, the centres of the two fields. It should be remembered that θ and ϕ are assumed to be small.

The co-ordinates of a focus being $(r, 2b\theta)$, we have

$$\theta=y/2b, \text{ and } \phi-2\theta=y/x=2b\theta/x.$$

$$\therefore \qquad \phi=2\theta(b/x+1).$$

In virtue of the fact that $\theta=k(e/m)(1/v^2)$ and $\phi=k'(e/m)(1/v)$, where e, m and v are respectively the charge, mass and velocity of the particle concerned and k and k' are geometric constants, we have

$$\frac{\phi^2}{\theta}=4\theta\left(\frac{b}{x}+1\right)^2=\frac{k'^2}{k}\cdot\frac{e}{m}$$

$$\therefore \qquad m=\frac{k'^2}{k}\cdot\frac{e}{4\theta}\cdot\left(\frac{x}{b+x}\right)^2$$

or

$$\frac{m}{\mathrm{R}}=\left(\frac{x}{b+x}\right)^2, \qquad \ldots \quad (ii)$$

where R is a constant for a given θ and for the same value of e for all the particles, *i.e.*, for all particles having the same charge.

From the above, it can be easily shown that

$$\frac{d^2m}{dx^2}=\mathrm{R}\frac{2b(b-2x)}{(b+x)^4},$$

and that the point of inflexion is at $x=b/2$.

Since $\phi=2\theta\left(\frac{b}{x}+1\right)$, we have, at the point of inflexion,

$$\phi=6\theta.$$

The above relationship between m and x is, allowing for a change of axes, the same as that derived by J. J. Thomson in the discussion on isotopes held in the Royal Society on March 3, 1921.[4]

THE CURVE

The complete curve connecting x and m in the equation (*ii*) above is given at A in Fig. 2. In the same figure the curve given by Aston's expression [eqation (*i*), Section 2] is also shown at B. The two curves are, as of course they should be, the same, except that the difference in notation gives rise to differences in the positions of the axes and in the values of the constants.

The two ends of the curve asymptotically meet a line parallel to the x-axis, the left end from above and the right end from below. The top of the curve is an exceedingly sharp cusp at infinity. At its lowest portion the curve circles sharply round and then very gradually changing the sign of curvature goes on to meet the asymptote from below.

The curvature at the lowest point is so small that the curve (Fig. 2, A or B) appears to have a cusp at this point as well. In order to exhibit the true nature of the curve in its lowest portion and round about the point of inflexion, the curve must be magnified very considerably, so much so that the resulting figure would be much too large for reproduction. To bring out the nature of the curve at this portion, it has been therefore magnified as well as distorted and shown at C in the right half of the same figure (Fig. 2).

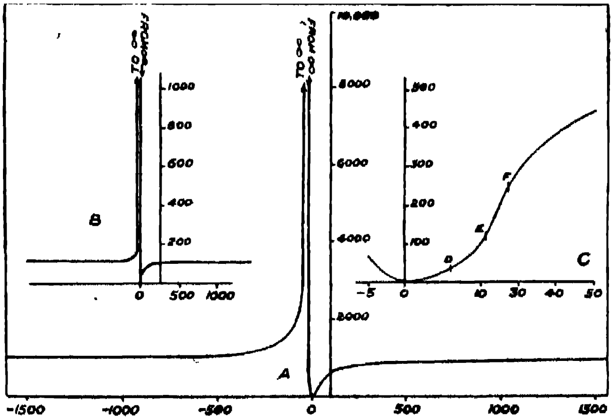

FIGURE 2

The mass-distance curves

In the middle, at A, is shown the plot of the equation,

$$\frac{m}{R}=y=\left(\frac{x}{b+x}\right)^2,$$

taking $b=25$.

On the left, at B, is the plot of the equation,

$$\frac{m}{m_0}=y=1+2\left(\frac{x-0.2}{1+0.2x}\right)^2+2\left(\frac{x-0.2}{1+0.2x}\right)\sqrt{\left(\frac{x-0.2}{1+0.2x}\right)}+1,$$

which is Aston's expression (equation *i*, Section 2) put in a form suitable for plotting (neglecting the negative value of the square root which is irrelevant for present purposes) taking $\tan 2\theta=0.2$. At C is shown the portion of the curve A near the origin, magnified but distorted.

The points marked as D, E, F, on the curve C, Fig. 2, correspond approximately to $\phi=10\theta$, $\phi=6\theta$, and $\phi=4\theta$, respectively. It will be seen that beyond D, the curvature is nowhere very marked, so that for small portions of the curve, the mass-scale would be approximately linear at all points. Beyond F, corresponding to $\phi=4\theta$, however, the change in mass (ordinate) for a given change in the distance from the origin (abscissa) or in other words the distance between two spectral lines due to a certain difference in masses, what may be called the 'dispersion' of the curve, becomes very small.

The deviation from linearity round about various points on the right half of the curve cannot, unfortunately, be shown unless the curve is drawn on an enormously magnified scale This departure from linearity can, however, be easily seen otherwise. Figures, given in Table I, show that the curve is most linear, and at the same time the 'dispersion' is greatest round about the point $\phi=6\theta$, the point of inflexion.

TABLE I

Dispersion and deviation from linearity at various points on the curve $m/\mathrm{R}=m'=\{x/(b+x)\}^2$, b being taken $=25$

ϕ/θ	x	M_x	for $dx=\frac{1}{2}$		for $dx=1$		for $dx=2$		for $dx=3$	
			D	d	D	d	D	d	D	d
11	50/9	33.06	9.7	20	9.7	41	9.6	84	9.4	133
10	6.25	40.00	10.2	16	10.2	32	10.1	66	10.0	104
9	50/7	49.38	10.7	12	10.7	24	10.6	48	10.5	75
8	25/3	62.50	11.2	7	11.2	16	11.2	31	11.1	48
7	10	61.61	11.7	3	11.6	7	11.6	15	11.6	16
6	12.5	111.111	11.8	0	11.8	0	11.8	0.2	11.8	1
5	50/3	160.00	11.5	3	11.5	6	11.5	12	11.5	18
4	25	250.00	10.0	5	10.0	10	10.0	18	10.0	33
3	50	444.44	5.9	3	5.9	9	5.9	20	5.9	30
2.5	100	640.00	2.6	0	2.6	8	2.6	14	2.6	21
2.2	250	826.45	0.6	0	0.6	8	0.6	8	0.6	3

Note (1) For $\phi=n\theta$, $x=50/(n-2)$.

,, (2) If $m'_x\times 1000=\mathrm{M}_x$, dispersion is taken to be $\mathrm{D}=(\mathrm{M}_{\quad dx}-\mathrm{M}_{x-dx})/2dx$.

,, (3) If $\mathrm{M}_{x+dx}-\mathrm{M}_x=d_1$, $\mathrm{M}_x-\mathrm{M}_{x-dx}=d_2$, then deviation from linearity is taken to be $(d_1-d_2)/(d_1+d_2)=d'$; $d'\times 1000=d$.

In practice, therefore, the photographic plate may be placed anywhere in the region from $\phi = 4\theta$ to $\phi =$ (say) 8θ. The 'fiducial' point will of course be different according to the region chosen, a fiducial point being given by the intersect of the tangent concerned with the axis of x. However, in actual determination of the masses, no use is made of the formula at all, and, therefore, the position of the fiducial point or that of the plate does not really matter. Approximate measurements made on the diagrams given in Aston's book[3] gave the following results:—

From Fig. 9, p. 42, Diagram of the First Mass-Spectrograph, $\theta = 3°$, $\phi = 21°$ for the middle of the photographic plate.

From Fig. 19, p. 72, Diagram of the Second Mass-Spectrograph, which is specifically indicated to have been given to scale, $\theta = 6°$, $\phi = 28°$, $33°$, $42°$, for the near end, the middle and the far end, respectively, of the plate.

Government College, Lahore.
Punjab University, Lahore.

REFERENCES

[1] Aston and Fowler, *Phil. Mag.*, **43**, 514 (1922).
[2] F. B. Pidduck, '*A Treatise on Electricity*,' *Camb. Univ. Press*, 2nd Ed., p 514 (1925).
[3] F. W. Aston, Arnold, *Mass Spectra and Isotopes*, 47 (1933).
[4] *Proc. Roy. Soc.*, *A.*, **99**, 94 (1921).

ON EFFECT OF RESISTANCE COMPONENT IN WAVE FILTER ELEMENTS AND PERFORMANCE OF NON-IDEAL FILTER SECTIONS *

By WAQUAR AHMED

(*Received for Publication, April 11, 1942*)

ABSTRACT. The paper relates to study of the effect of resistance component in wave-filter elements based on the theory and operation of " non-ideal " low-pass, high-pass and band-pass filter sections.

Characteristic impedance, attenuation and phase constants and cut-off frequency or frequencies of " non-ideal " sections have been deduced and measured. Comparison between characteristics of " non-ideal " and " ideal " sections has been made.

INTRODUCTION

The filter theory as given elsewhere relates to " ideal filter section," that is, those in which the filter elements are pure reactances; the characteristic impedances in transmission and attenuation bands are therefore pure resistances and pure reactances respectively. Such ideal filter sections, properly terminated should give zero and very large attenuations for frequency components in the transmission and attenuation bands respectively. The sharpness of cut-off at the edge or edges of the transmission band can be very great since the resistance in elements being negligible ' Q ' can be very large.

The wave-filter sections consisting of inductance and capacitance elements, designed and constructed in actual commercial practice for low- and high-frequency communication systems, cannot be regarded as " ideal " for reasons shown below. The resistance component in each *single* element (whether of inductance or capacitance type) is appreciable in majority of cases and cannot be regarded as zero. Further, since both series and shunt arms of a filter section may consist of several elements depending on the type of section chosen, the total effective resistance in series as well as in shunt arm will be large. It is therefore desirable to work out the exact performance of such " non-ideal sections " rather than apply the results developed for ideal filter sections to their cases.

The inductance elements consist of coils wound either on laminated iron, stalloy, silicon steel or on permalloy and mu-metal cores for audio-frequency range. They are wound on finely powdered iron[1] or permalloy[4] dust cores for higher frequencies up to 200 kc/s and on ferrocart[6] cores up to

---

Communicated by Prof. P. N. Ghosh

1500 kc/s and are air core coils[2,3] (screened) at high radio frequencies. In cases where the d.c. component circulates through the coil (forming an element of a filter section), the dust-core and air-core types (preferably the latter type) are the only ones which have to be used even for low-frequency range. Further, for broad-band linear systems, coils wound on laminated iron or stalloy cores or even on dust and ferrocart cores may not be so suitable as the air-core coils since the permeability of the core material in former types depends both on frequency as well as on amplitude of current through the coil. For a given inductance, the resistance component of coil wound on permalloy dust core is negligible, of coil wound on laminated iron, stalloy or iron dust core is small and that of coil with air core is sufficiently large.

The capacitance elements are invariably paper, mica or air condensers. Paper and mica condensers are generally used for audio-range, whereas mica and air condensers are used for carrier and high-frequency ranges. A condenser should be regarded in general as equivalent to a pure capacitance either connected in series with or shunted by a resistance. The equivalence of a condenser to a pure capacitance with a resistance in series may arise either due to the resistance of leads from plates to binding terminals and of plates, joints and contacts or to "equivalent resistance" due to dielectric absorption. The power-factor in this case = $r\omega C$ (where r = total resistance of leads etc. or "equivalent resistance" referred to above, C= capacitance and $\omega = 2\pi \times$ frequency) which increases with frequency. The equivalent resistance due to dielectric absorption varies as $\frac{1}{\omega < 1}$ at low frequencies and as $\frac{1}{\quad}$ at high frequencies. The equivalence of condenser to a pure capacitance shunted by a resistance may arise due to leakage of energy from one plate to another over the dielectric surface. The power-factor in this case is $\frac{1}{r\omega C}$ which decreases with frequency. The resistance component r varies as $\frac{1}{\omega}$

The piezo-electric crystal elements (mounted between two electrodes) used in h.f. filter sections are equivalent to series resonant circuits (consisting of inductance, effective resistance and capacitance in series) shunted by a capacitance. Having a negligible effective resistance and very high 'Q' value at high frequencies, these elements alone can be regarded as suitable for ideal filters and therefore will not be considered here.

The present paper relates to study of the effect of resistance component in inductance and capacitance elements based on theory and operation of "non-ideal" low-pass, high-pass and band-pass filter sections and to the comparison between characteristics of non-ideal and ideal sections.

LOW-PASS NON-IDEAL SECTION

Consider a proto-type symmetrical T-section in which the total impedance in series arm $Z_1 = R + j\omega L$ and total impedance in the shunt arm $Z_2 = R' - j/\omega C$.

(a) *Characteristic impedance.*—From general equation for T-section,

$$Z_0 = \left[\left(\frac{L}{C} + \frac{R^2}{4} + RR' - \frac{\omega^2 L^2}{4}\right) + j\left(\omega LR' - R/\omega C + \frac{\omega LR}{2}\right)\right]. \qquad \ldots \quad (1)$$

It will be seen from (1) that Z_0 will be in general an impedance containing both resistance and reactance components for all frequencies except for the two shown in (2*b*) and (2*c*).

Z_0 reduces to the value given for ideal T-type filters when $R = 0$ and $R' = 0$.

$$\text{When } \omega = \frac{2}{\sqrt{LC}}, \quad Z_0 = \left[\left(RR' + \frac{R^2}{4}\right) + j\sqrt{\frac{L}{C}}\left(2R' + \frac{R}{2}\right)\right]^{\frac{1}{2}}. \qquad \ldots \quad (2a)$$

$$\text{When } \omega = \frac{1}{\sqrt{LC\left(\frac{R'}{R} + \frac{1}{2}\right)}}, \quad Z_0 = \left[\frac{L}{C} + \frac{R^2}{4} + RR' - \frac{LR}{2C(R + 2R')}\right]^{\frac{1}{2}}. \qquad \ldots \quad (2b)$$

$$= \text{a pure resistance.}$$

$$\text{When } \omega = 2\sqrt{\frac{1}{LC} + \frac{R^2}{4L^2} + \frac{RR'}{L^2}},$$

$$Z_0 = \left[j\left\{2L\left(\frac{1}{LC} + \frac{R^2}{4L^2} + \frac{RR'}{L^2}\right)^{\frac{1}{2}}\left(R' + \frac{R}{2}\right) - \frac{R}{2C}\left(\frac{1}{LC} + \frac{R^2}{4L^2} + \frac{RR'}{L^2}\right)^{-\frac{1}{2}}\right\}\right]^{\frac{1}{2}}$$

$$= \text{a pure resistance.} \qquad \ldots \quad (2c)$$

If R_0 and X_0 be the resistance and reactance components of Z_0 in equation (1), then

$$Z_0 = R_0 + jX_0. \qquad \ldots \quad (3)$$

From (1) and (3)

$$R_0 = \left[\frac{1}{2}\left\{\sqrt{\left(\frac{L}{C} + \frac{R^2}{4} + RR' - \frac{\omega^2 L^2}{4}\right)^2 + \left(\omega LR' - \frac{R}{\omega C} + \frac{\omega LR}{2}\right)^2} + \left(\frac{R^2}{4} + RR' + \frac{L}{C} - \frac{\omega^2 L^2}{4}\right)\right\}\right]^{\frac{1}{2}} \qquad \ldots \quad (4)$$

$$X_0 = \left[\frac{1}{2}\left\{\sqrt{\left(\frac{L}{C} + \frac{R^2}{4} + RR - \frac{\omega^2 L^2}{4}\right)^2 + \left(\omega LR' - \frac{R}{\omega C} + \frac{\omega LR}{2}\right)^2} - \left(\frac{R^2}{4} + RR' + \frac{L}{C} - \frac{\omega^2 L^2}{4}\right)\right\}\right]^{\frac{1}{2}}. \qquad \ldots \quad (5)$$

(*b*) *Attenuation and phase constant.*—If the ratio of 'sending-end current' (I_1) to 'receiving-end current' (I_2) when the section is terminated by its proper characteristic impedance be I_1/I_2,

then
$$\frac{I_1}{I_2} = 1 + \frac{R + j\omega L}{2(R' - j/\omega C)} + \frac{R_0 + jX_0}{R' - j/\omega C}. \qquad \ldots \quad (6)$$

If the propagation constant 'P' $= \log_e (I_1/I_2) = \alpha + j\beta$ (where α = attenuation constant and β = phase constant), then

$$\alpha = \log_e \left[\left\{ 1 + \frac{RR' - L/C + 2(R_0R' - X_0/\omega C}{2(R'^2 + 1/\omega^2C^2)} \right\}^2 + \left\{ \frac{\omega LR' + R/\omega C + 2(X_0R' + R_0/\omega C}{2(R'^2 + 1/\omega^2C^2)} \right\}^2 \right]^{\frac{1}{2}} \qquad \ldots \quad (7)$$

$$\beta = \tan^{-1} \frac{\omega LR' + R/\omega C + 2(X_0R' + R_0/\omega C)}{2R'^2 + 2/\omega^2C^2 + RR' - L/C + 2(R_0R' - X_0/\omega C)}. \qquad \ldots \quad (8)$$

(*c*) *Cut-off frequencies and sharpness of cut-off.*—In case of non-ideal sections, the cut-off frequencies cannot be calculated from the relations $Z_1/Z_2 = 0$ and $Z_1/Z_2 = -4$ as in case of ideal sections. The above values of Z_1/Z_2 are the *limiting* values between which the characteristic impedance of the ideal section is pure resistance (that is, they give the limits of transmission band), and consequently are inapplicable to case where the characteristic impedance of the section is in general an impedance having both resistance and reactance components in the transmisssion band.

The calculation of cut-off frequencies in this case is derived from equation (7). $d\alpha/d\omega$ can be determined from (7). Then the real and admissible value of ω for which $d\alpha/d\omega$ is maximum or, say, at least of the order of 40 *db* in 1000 *c/s* gives the cut-off frequency. Graphical determination is more convenient.

Experiments have been carried out on a non-ideal section in which

$$L/2 = 10.575 \text{ mH}; \quad R = 20\Omega \text{ at } 800 \sim \text{ to } 28.25\Omega \text{ at } 6500 \sim;$$

$$C = 0.1\mu F, \text{ and } R' = 1.5\Omega \text{ at } 800 \sim \text{ to } 0.2\Omega \text{ at } 6500 \sim.$$

The characteristic impedance and attenuation constants were measured according to standard practice. For measurement of phase constant, an arrangement similar to that used by Messrs. Hinton Rendall and White in their paper have been adopted.[5]

Fig. 1 shows the values of R_0 and X_0 components of Z_0 at various frequencies calculated from (4) and (5), and the measured values of $|Z_0|$ over the same range, for the non-ideal section. It further shows the calculated values of R'_0 and X'_0 components of the characteristic impedance of the same section when the elements are purely reactive (that is, of the ideal section).

Fig. 2 shows the attenuation—frequency characteristics of non-ideal section both measured and calculated from (7) as well as that of the ideal section.

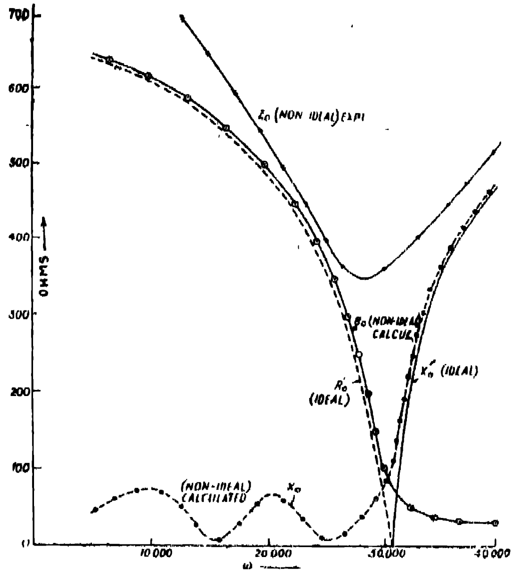

FIG. 1

Fig. 2 also shows the phase-shift—frequency characteristics of non-ideal section both measured and calculated from (8) as well as that of the ideal section.

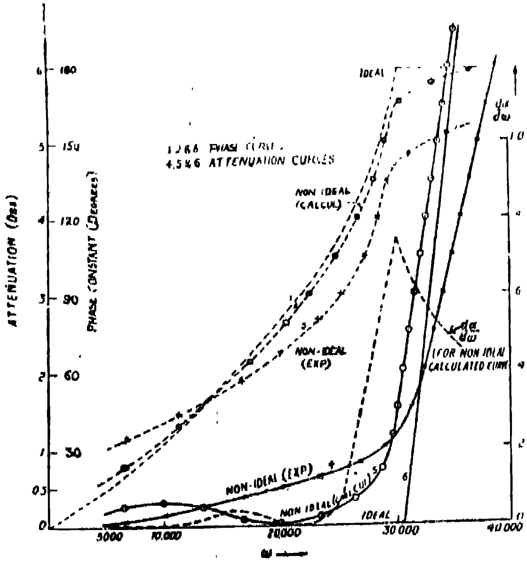

FIG. 2

In Fig. 2, $d\alpha/d\omega$ obtained from the calculated attenuation—frequency characteristic of the non-ideal section is plotted against frequency. From this curve the cut-off frequency of the non-ideal section is found to be 4·8 *kc/s*.

HIGH-PASS NON-IDEAL SECTION

Consider a proto-type symmetrical T-section, in which the total impedance in the series arm $Z_1 = R' - j/\omega C$ and total impedance in the shunt arm $Z_2 = R + j\omega L$.

(*a*) *Characteristic impedance.*—

$$Z_0 = \left[\left(RR' + \frac{R'^2}{4} + \frac{L}{C} - \frac{1}{4\omega^2C^2}\right) + j\left(\omega R'L - \frac{R}{\omega C} - \frac{R'}{2\omega C}\right)\right]^{\frac{1}{2}} \quad \ldots \quad (9)$$

which reduces to the value given for ideal section when $R' = 0$ and $R = 0$.

When $\omega = \frac{1}{2\sqrt{LC}}$, $Z_0 = \left[\left(RR' + \frac{R'^2}{4}\right) - j\sqrt{\frac{L}{C}}\left(\frac{R'}{2} + 2R\right)\right]^{\frac{1}{2}}$. ... (10)

When $\omega = \sqrt{\frac{1}{LC}\left(\frac{R}{R'} + \frac{1}{2}\right)}$, Z_0 is a pure resistance.

When $\omega = \sqrt{\frac{1}{C(4CRR' + CR'^2 + 4L)}}$, Z_0 is a pure reactance.

If R_0 and X_0 are resistance and reactance components respectively of Z_0, then

$$R_0 = \left[\frac{1}{2}\left\{\sqrt{\left(RR' + \frac{R'^2}{4} + \frac{L}{C} - \frac{1}{4\omega^2C^2}\right)^2 + \left(\omega R'L - \frac{R}{\omega C} - \frac{R'}{2\omega C}\right)^2} + \left(RR' + \frac{R'^2}{4} + \frac{L}{C} - \frac{1}{4\omega^2C^2}\right)\right\}\right]^{\frac{1}{2}} \quad \ldots \quad (11)$$

$$X_0 = \left[\frac{1}{2}\left\{\sqrt{\left(RR' + \frac{R'^2}{4} + \frac{L}{C} - \frac{1}{4\omega^2C^2}\right)^2 + \left(\omega R'L - \frac{R}{\omega C} - \frac{R'}{2\omega C}\right)^2} - \left(RR' + \frac{R'^2}{4} + \frac{L}{C} - \frac{1}{4\omega^2C^2}\right)\right\}\right]^{\frac{1}{2}} \quad \ldots \quad (12)$$

(*b*) *Attenuation and phase constants.*—

$$\frac{I_1}{I_2} = \left[1 + \frac{RR' - L/C + 2(R'R_0 + X_0\omega L)}{2(R^2 + \omega^2L^2)}\right] - j\left[\frac{\omega R'L + R/\omega C + 2(R_0\omega L - RX_0)}{2(R^2 + \omega^2L^2)}\right]$$

so that

$$\alpha = \log_e \sqrt{A^2 + B^2} \quad \ldots \quad (13)$$

and

$$\beta = \tan^{-1}\frac{B}{A} \quad \ldots \quad (14)$$

where

$$A = 1 + \frac{RR' - L/C + 2(R'R_0 + X_0\omega L)}{2(R^2 + \omega^2L^2)}$$

and

$$B = \frac{\omega R'L + R/\omega c + 2(R_0\omega L - RX_0)}{2(R^2 + \omega^2L^2)}.$$

(*c*) *Cut-off frequencies and sharpness of cut off.*—As in the previous section $d\alpha/d\omega$ can be determined from (13), and the real and admissible value of ω for which $d\alpha/d\omega$ is maximum or at least of the order of 40 db in 1000 c.p.s. determines the cut-off frequency.

Experiment have been carried out on a non-ideal section in which

$$2C = 0.3\mu F \, ; \quad \frac{R'}{2} = 10.8\Omega \text{ at } 800\sim \text{ to } 0.2 \text{ at } 5000\sim \, ; .$$

$$L = 50 mH \text{ and } R = 13.55\Omega \text{ at } 800\sim \text{ to } 18.10\Omega \text{ at } 5000\sim .$$

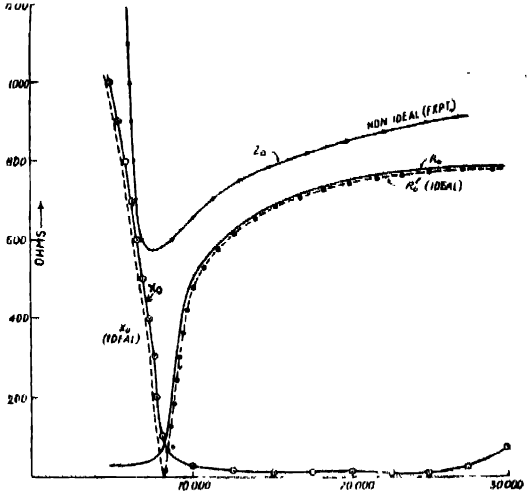

FIG. 3

Fig. 3 shows the values of R_0 and X_0 components of Z_0 calculated from (11) and (12) and the measured value of $|Z_0|$ over the frequency range. The R'_0 and X'_0 components for the ideal section over the same range is also shown.

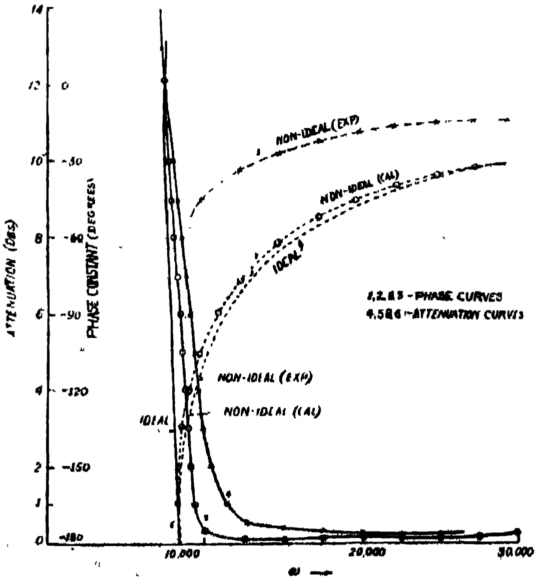

FIG. 4

Fig. 4 shows the attenuation—frequency characteristics of non-ideal section both measured and calculated from (13) as well as that of the ideal section. Fig. 4 also shows the phase-shift—frequency characteristics of non-ideal section both measured and calculated from (14) as well as that of the ideal section.

BAND-PASS NON-IDEAL SECTION

Consider a symmetrical T-section in which the total impedance in the series arm $Z_1 = R_1 + j\left(\omega L_1 - \frac{1}{\omega C_1}\right)$ and total impedance in the shunt arm $Z_2 = R_2 + j\left(\omega L_2 - \frac{1}{\omega C_2}\right)$; R_1 and R_2 include resistances in inductive as well as capacitative elements.

(*a*) *Characteristic impedance.*—

$$Z_0 = \left[\left\{R_1 R_2 - \left(\omega L_1 - \frac{1}{\omega C_1}\right)\left(\omega L_2 - \frac{1}{\omega C_2}\right) + \frac{R_1^2}{4} - \frac{1}{4}\left(\omega L_1 - \frac{1}{\omega C_1}\right)^2\right\} + j\left\{R_1\left(\omega L_2 - \frac{1}{\omega C_2}\right) + R_2\left(\omega L_1 - \frac{1}{\omega C_1}\right) + \frac{R_1}{2}\left(\omega L_1 - \frac{1}{\omega C_1}\right)\right\}\right]^{\frac{1}{2}} \quad \ldots \quad (15)$$

which reduces to that of the ideal case when $R_1 = 0$ and $R_2 = 0$.

If R_0 and X_0 are the resistance and reactance components respectively of Z_0, then

$$R_0 = \left[\frac{\sqrt{a^2 + b^2} + a}{2}\right]^{\frac{1}{2}} \quad \ldots \quad (16)$$

$$X_0 = \left[\frac{\sqrt{a^2 + b^2} - a}{2}\right]^{\frac{1}{2}} \quad \ldots \quad (17)$$

where $a = R_1\left(R_2 + \frac{R_1}{4}\right) - \left(\omega L_1 - \frac{1}{\omega C_1}\right)\left\{\left(\omega L_2 - \frac{1}{\omega C_2}\right) + \frac{1}{4}\left(\omega L_1 - \frac{1}{\omega C_1}\right)\right\}$

and $b = R_1\left(\omega L_2 - \frac{1}{\omega C_2}\right) + \left(R_2 + \frac{R_1}{2}\right)\left(\omega L_1 - \frac{1}{\omega C_1}\right)$.

(*b*) *Attenuation and phase constants.*—

$$\frac{I_1}{I_2} = \left[1 + \frac{R_1 R_2 + \left(\omega L_1 - \frac{1}{\omega C_1}\right)\left(\omega L_2 - \frac{1}{\omega C_2}\right) + 2\left\{R_0 R_2 + X_0\left(\omega L_2 - \frac{1}{\omega C_2}\right)\right\}}{2\left\{R_2^2 + \left(\omega L_2 - \frac{1}{\omega C_2}\right)^2\right\}}\right] + j\left[\frac{R_2\left(\omega L_1 - \frac{1}{\omega C_1}\right) - R_1\left(\omega L_2 - \frac{1}{\omega C_2}\right) + 2\left\{R_2 X_0 - R_0\left(\omega L_2 - \frac{1}{\omega C_2}\right)\right\}}{2\left\{R_2^2 + \left(\omega L_2 - \frac{1}{\omega C_2}\right)^2\right\}}\right]$$

Then $$\alpha = \log_e \sqrt{p^2 + q^2} \quad \ldots \quad (18)$$

and
$$\beta = \tan^{-1}\frac{q}{p} \qquad \ldots \quad (19)$$

where
$$p = 1 + \frac{R_1R_2 + \left(\omega L_1 - \frac{1}{\omega C_1}\right)\left(\omega L_2 - \frac{1}{\omega C_2}\right) + 2\left\{R_0R_2 + X_0\left(\omega L_2 - \frac{1}{\omega C_2}\right)\right\}}{2\left\{R_2^2 + \left(\omega L_2 - \frac{1}{\omega C_2}\right)^2\right\}}$$

$$q = \frac{R_2\left(\omega L_1 - \frac{1}{\omega C_1}\right) - R_1\left(\omega L_2 - \frac{1}{\omega C_2}\right) + 2\left\{R_2X_0 - R_0\left(\omega L_2 - \frac{1}{\omega C_2}\right)\right\}}{2\left\{R_2^2 + \left(\omega L_2 - \frac{1}{\omega C_2}\right)^2\right\}}.$$

(*c*) *Cut-off frequencies.*—As in the previous sections $d\alpha/d\omega$ can be determined from (18), and the real and admissible values of ω for which $d\alpha/d\omega$ is maximum or at least of the order of 40 db in 1000 c.p.s. give the cut-off frequencies of the section.

Experiments have been carried out on a non-ideal section having the following elements :—

$2C_1 = 0.15\mu F$; $L_1/2 = 19.4 mH$; $R_1/2$ (total) $= 19.3\Omega$ at 800~ to 12.1Ω at 6500~ ; $L_2 = 48.6 mH$; $C_2 = 0.0183\mu F$ and R_2(total) $= 254.3\Omega$ at 800~ to 50Ω at 6500~ ;

Fig. 5 shows the values of R_0 and X_0 components of Z_0 calculated from (16) and (17) as well as the measured and calculated values of $|Z_0|$ over the range.

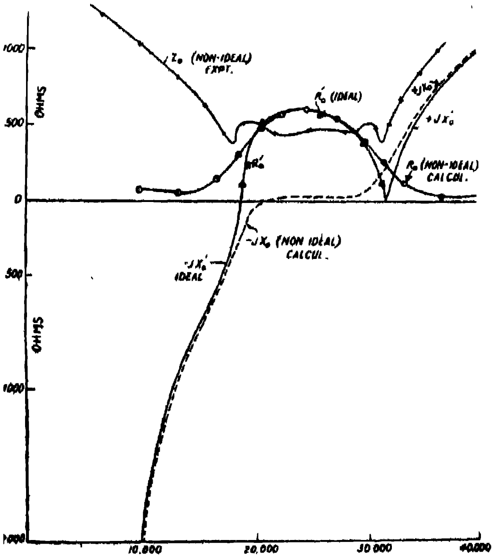

FIG. 5

Fig. 6 shows the attenuation—frequency characteristics of non-ideal section both measured and calculated from (18) as well as that of the ideal section.

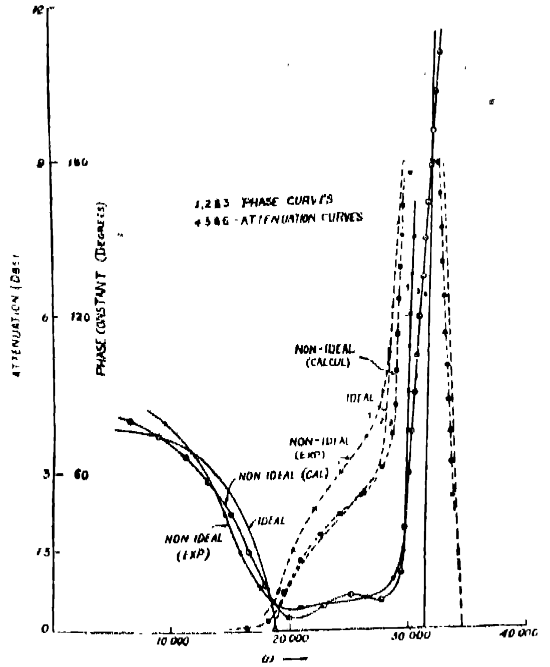

FIG. 6

Fig. 6 also shows the phase-shift—frequency characteristics of non-ideal section both measured and calculated from (19) as well as that of the ideal section.

CONCLUSIONS

The following conclusions have been arrived at :—

(1) The characteristic impedance of "non-ideal" filter section (low-pass, high-pass or band-pass type) will be an impedance containing both resistance and reactance components for frequency components in transmission as well as in attenuation band.

The resistance component of the characteristic impedance within the transmission band is more or less the same in magnitude as the non-reactive characteristic impedance of the ideal section, whereas the reactance component of characteristic impedance in the attenuation band is the same in magnitude as the reactive characteristic impedance of the ideal section in the same range.

(2) The characteristic impedance has been found to be pure resistance and pure reactance only at two particular frequencies respectively.

(3) The attenuation constant within the transmission band varies with frequency and may be from 0.2 to 1.0 db per section with typical values of resistance components in the elements.

(4) The cut-off frequencies of non-ideal sections cannot be obtained from the usual relations $\frac{Z_1}{Z_2} = 0$ and $\frac{Z_1}{Z_2} = -4$ as in the case of ideal filter-sections, since the above relations are the limiting values between which the characteristic impedance of ideal section is pure resistance.

The cut-off frequency or frequencies in this case will be the real and admissible value or values of ω for which $\frac{d\alpha}{d\omega}$ is maximum or at least of the order of 40 db in 1000 c.p.s.

(5) The values of phase constant for ideal and non-ideal sections are observed to be roughly the same.

ACKNOWLEDGMENTS

The whole of the experimental and theoretical work was carried at the Kanodia Electrical Communication Engineering Laboratories of the Department of Applied Physics, Calcutta University. The author desires to thank Mr. S. P. Chakravarti, M.I.R.E., A.M.I.E.E., for suggesting the problem, guiding the experimental and theoretical work and going through the paper in final form. My grateful thanks are also due to revered Prof. P. N. Ghosh, M.A., Ph.D., Sc.D., F.Inst.P., for his constant encouragement and assistance for research work.

REFERENCES

[1] Speed and Elman, *Trans. A.I.E.E.*, **40** (1921).

[2] Fortescue, *J.I.E.E.*, 933 (1923).

[3] Butterworth, *Wireless Engineer*; April, May, July and August (1926).

[4] Shackleton and Barber, *Trans. A.I.E.E.*, **17** (1928).

[5] Hinton, Rendall and White, *Electrical Communication*, **8** (1929).

[6] Schneider, *Wireless Engineer*, April (1933).

ON THE THERMAL CONDUCTIVITY OF INDIGENOUS INSULATING SUBSTANCES

By K. C. NIYOGI

AND

J. R. BASU MALLIK

(Received for publication, February 10, 1942)

ABSTRACT. The present communication reports on the measurement of thermal conductivities of substances like Glass, Mica, Tintex, Masonite, Beaver, Plywood, Asbestos, Saw-dust, Straw, Husk, Jute, Cocoanut-fibre, Kapok, etc., with the aid of a handy apparatus constructed on the well-known principle of " wall " method.

INTRODUCTION

At the present time India is greatly interested in the refrigeration industry for its application to home, both in household refrigerating machines and in comfort cooling, and also in other applications of air-conditioning, *viz.*, in auditoriums, industries, cold storage ware-houses, etc. With this development of comfort cooling the refrigerating engineer has to face with problems arising out of losses due to heat leakage. Let us take, for example, the case of food preservation. The refrigeration of food consists mainly of removing heat from the food and keeping the outside heat away from it. Foods which have been cooled by refrigeration will absorb heat again unless care is taken to keep heat away from coming in contact with them. This action takes place because heat flows from places of higher temperature to places of lower temperature. Thus heat is constantly passing into a refrigerated compartment from the outside. The refrigerating unit must have enough capacity to remove this heat leakage along with the heat that is admitted when the doors are opened and closed and the heat that is brought in with the warm foods.

Extended tests on household cabinets indicate that the total cooling load on the condensing unit may be apportioned as follows :

Opening or closing doors	5%
Cooling the foods and liquids	18%
Leakage through insulation, frames and joints	77%

It is evident from this that the proper insulation of a cabinet is an important item in keeping down operating costs to a reasonable figure. And, in fact, no insulation exists which can keep out all the heat ; but there are certain kinds of insulating materials which are more effective than others. The present report gives the results of an investigation of the thermal conductivity of indigenous Indian materials that may be suitably used as heat-insulating bodies. The apparatus designed and constructed is a handy one and with its aid the thermal conductivity of any substance can be determined within 4 hours.

DESCRIPTION

We now describe the technique developed for testing a large number of materials of low conductivity, of which relatively small samples can fairly be taken as representative of the parent material. The apparatus designed is a modification of the 'plate' or 'wall' method to which the standard equation defining the conductivity, 'k,' shown by the relation

$$Q = kAt\,\theta_1 - \theta_2$$

is directly applicable. Here, 'Q' is the quantity of heat which, when the steady state is reached, passes normally in time 't' through a material of cross-section 'A' and thickness 'd,' the faces of which are maintained at temperatures θ_1 and θ_2.

The hot face is a copper block and is heated electrically. The cold face is a similar copper block and the material to be tested is sandwiched between these two faces. The heater is made by winding Constantan wire (No. 32 S. W. G.) of total length 100 inches on a mica sheet. This is placed between two copper blocks, each 4 in. sq. and 0.22 in. thick, the blocks being insulated from the heater by two mica sheets. The sample to be tested (when available in slab form) is cut to the same size and of suitable thickness and is placed by the side of one of these two copper blocks. Another similar copper block is placed on the other side of the sample. The exposed surfaces of this whole arrangement are varnished so as to give them the same emissivity. This assemblage is then held as a compact body with their surfaces in vertical position and housed in a wooden box with the lower surfaces resting on two wooden knife edges covered with asbestos. Three holes are drilled right up to the centre of all the three blocks from their top-edges for the insertion of the thermo-couple junctions required for the measurement of their temperatures. The arrangement is shown in Fig. 1.

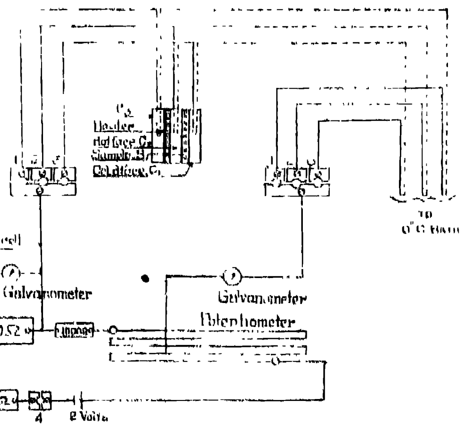

FIG. 1

EXPERIMENT

The experiment is started with the sample kept as described above. To ascertain the temperatures of the copper blocks directly, the thermo-couples are calibrated in degrees-centigrade with the help of a potentiometer by usual methods. The reference junctions are kept at 0°C. To ensure good thermal contact of the other junctions with the copper blocks mercury is poured into the three holes. Electric current is now passed into the heating grid and the electrical energy spent in heating the heater is obtained by measuring the current with an ammeter reading .0.02 amp. per scale division and the potential drop across the heating coil with a voltmeter reading 0.5 volts per scale division. The steady state can be attained in times from 90 to 100 minutes and often 2 hours.

The measurement of the surfaces and edges of the blocks as well as the sample presents no difficulty. But some difficulty arises regarding the measurement of the thickness *d* in case of compressible materials like fabrics, saw-dust etc. and for these the following device has been adopted.

Thermal conductivity of plywood is first determined carefully. It is then cut as shown below (see Fig. 2) and is pasted between the hot and cold faces with Duco cement.

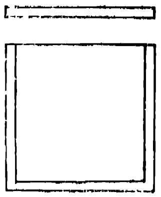

FIG. 2

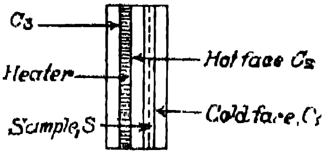

FIG. 3

The sample to be studied is placed in the hollow space left within. The quantity of heat flowing through the sample is equal to the heat lost from the exposed surface of the block C_1 (Fig. 3) minus the heat flowing through the plywood. Knowing the difference of temperature, area, thickness and conductivity of the plywood frame, the heat flowing through the plywood frame is calculated. In this way the thickness, *d*, of such samples is made fixed and the conductivity for a definite density of packing is known.

THEORETICAL CALCULATION

A simple sketch of the arrangement is given here (see Fig. 3).

Let H = rate of energy supplied to the heating coil.

h = heat loss per sq. cm. for 1°C. excess of temperature of the blocks over that of the surrounding.

$\theta_{1,2,3}$ = the excess of temperatures of C_1, C_2 and C_3 over that of the surrounding.

d = thickness of the substance S.

$A_{1,2,3,s}$ = areas of the copper blocks as well as of the substance across which heat is flowing.

$a_{1,2,3,s}$ = areas of the edges of C_1, C_2, C_3 and of substance S.

Now heat that is received per second by the block C_1 and given up to the air is

$$(A_1+a_1)h\theta_1 \qquad \cdots \quad (1)$$

and the heat that is received per second by the sample S and given up to the air from its edges and passed on to C_1 is

$$(A_1+a_1)h\theta_1+ash\frac{\theta_1+\theta_2}{2}. \qquad \cdots \quad (2)$$

If k is the thermal conductivity of the sample S, then the heat flowing through this per second is

$$Ask\frac{\theta_2-\theta_1}{d}. \qquad \cdots \quad (3)$$

Assuming that the heat flowing through the substance S is the mean of the quantities of heat flowing in and out of the substance, *i.e.*, the mean of the equations (1) and (2), it is evident that

$$Ask\frac{\theta_2-\theta_1}{d}=(A_1+a_1)h\theta_1+ash\frac{\theta_1+\theta_2}{4} \qquad \cdots \quad (4)$$

giving a relation between k and h.

Further the total heat imparted to the system must equal that given up to the surrounding air from all the exposed surfaces. Hence

$$H=(A_1+a_1)h\theta_1+ash\frac{\theta_1+\theta_2}{2}+a_2h\theta_2+(A_3+a_3)h\theta_3. \qquad \cdots \quad (5)$$

Thus (5) determines h and so, from (4), k can be obtained, as all other quantities in (4) are measured experimentally.

The actual values for the conductivity of certain insulating materials as obtained by the above calculation are given in the table.

CONCLUDING REMARKS

The problem of maintaining efficiently the desired low temperatures in refrigeration units requires a careful study of the available insulating materials. The investigation so far carried out is only a part of this study. Besides the property of thermal conductivity of different materials, the following other properties must also be studied for the selection of an insulator :—

(1) *The structural strength.*—Some insulating materials lend themselves readily to various types of construction and are easily handled under all circumstances. This strength is generally obtained by the use of wood or steel framework to hold or contain the insulation. And the slab forms of insulation provide a stronger, more sturdy and economical type of construction than the powdered

TABLE

Conductivity of some insulating materials

No	Sample	Nature of sample	Density in lbs /c.ft.	Humidity	Thermal conductivity in $(\text{B.T.U.})\,(\text{in.})\,(\text{ft.})^{-2}\,(\text{hr.})^{-1}\,(^{\circ}\text{F.})^{-1}$
1	Glass	Crown glass in slab form of thickness 0.197″	164.2	85%	7.54/162°F.
2	Mica	In the form of sheet of thickness 0.0085″ to 0·03″	...	72%	Varying from 2.82 to 4.05/145°F
3	Tintex	Trade product in board form, 0.511″ thick	19.2	96%	0.63*/167°F.
4	Masonite	Trade product in board form, 0.523″ thick	18.2	70%	0.65*/161°F.
5	Beaver	Trade product in board form, 0.503″ thick	18.7	66%	0.64*/161°F.
6	Plywood	Three pieces compressed into board shape of thickness 0.165″	44.4	83%	1.12/136°F.
7	Asbestos	Fibres compressed into board form, 0.157″ thick	52.4	83%	0.81/174°F.
8	Saw-dust	Obtained from Teak-wood, finely grained and packed in the form of a slab, 0.165″ thick	27.1	84%	0.66/158°F.
9	Straw	Cut into small pieces of average length—5/8″ and packed in the form of a slab, 0.165″ thick	7.8	73%	0.24/165°F.
10	Husk	Coarsely powdered and packed in the form of a slab, 0.165″ thick	17.6	93%	0.31/143°F.
11	Jute	Fibrous structure, loosely packed in the form of a slab of thickness 0.165″	9.0	80%	0.25/154°F.
12	Cocoanut fibre	The fibres are packed loosely in the form of a slab of thickness 0.165″	8.0	70%	0.28/154°F.
13	Kapok	Fine tubular fibres obtained from sundried pods of *Simul* trees growing in the country and loosely packed in the form of a slab of thickness 0.165″	3.0	88%	0.17/170°F.

---

* These are commercial products and the thermal conductivity values we have obtained for them are higher than the values given by their manufacturers. These higher values may partly be due to the fact that the experiment is carried out in an atmosphere where the percentage of humidity is sufficiently large.

forms. So, investigation is necessary for transforming these powdered samples into cake forms with the minimum change in their k values.

(2) *The weight.*—This becomes a deciding factor when the application of insulation to railroad refrigerator cars, marine works, etc., is considered.

(3) *Selection of different insulators.*—Insulators derived from vegetable and animal sources are always subject to decomposition in course of time resulting in the development of odours. Odours are also developed on account of the growth of mould which takes place when the insulation is affected by the presence of moisture. There are many articles of food which absorb odours when exposed to them and this is really unsanitary. Hence the development of odours must be avoided.

(4) *The resistance to vermin.*—Several forms of vermin regard insulators of vegetable origin as their food and in a tropical country like that of ours the presence of various forms of vermin is not uncommon. Hence these insulators are to be specially protected.

(5) *Resistance to the absorption of moisture.*—Moisture in an insulation not only increases the thermal conductivity of it but also has a destructive effect. Changes in temperature between the interior and exterior surfaces of the insulation have a breathing action resulting in the condensation of moisture inside and even on the exterior in very humid climates. This causes dripping and odours, thus allowing the formation of mould. So, the insulation must be properly sealed against moisture.

(6) *Resistance to fire.*—This is not a deciding factor in the choice of an insulator, but in some applications, such as for fire-proof ware-houses, this characteristic is important.

It is evident from what has been said so far that the insulation cannot be chosen on the basis of only one desirable characteristic. On the other hand, preference should be given to that insulation which has the greater number of desirable qualities with respect to some particular application. And unless all these properties of the materials which have been investigated so far are studied carefully, we cannot be definite about the right selection of insulation which is so essential for the efficient production of household refrigerating units and installation of self-contained air-conditioning plants.

In fine, the authors have great pleasure in thanking B.S.I.R. for scholarship, grant for apparatus and the necessary permission for publication, and also Prof. M. N. Saha, F.R.S., and Mr. K. N. Ghosh for their kind interest and valuable advice in the work.

PALIT LABORATORY OF PHYSICS,
CALCUTTA UNIVERSITY.

REFERENCES

1 E. Griffiths, *J. Sci. Inst.*, **15**, 117 (1938).

2 E. Griffiths and W. C. Kaye, *Nat. Ph. Lab*, Collected Researches, Vol. 19 (1926)

3 E. Griffiths, *J. Inst. Heat. Vent. Engngrs.*, **5**, 21 (1937).

4 C. Dannatt, *Engineering*, **144**, 385 (1937).

5 Nagaoka, Watanabe & Yasiro, *Sc. Pap. Inst. Phy. Chem. Res.*, Tokyo, **824**, 1034 (1938).

6 Van Dusen, *J. Am. Soc. Heat. Vent. Engng.*, **26**, 625 (1920)

7 Van Dusen, *Bureau of Standards Journal of Research*, **5**, 385 (1930).

8 Glazebrooke, *Dict. Appld. Phys.*, Vol. 1.

9 *Proc. Roy. Soc.*, **104A**, 71 (1923).

ERRATA

Study of Electrolytic Dissociation in Iodic Acid by Raman Effect—By N. Rajeswara Rao :—

In Plate V (facing page 76), *for* 1N *read* 6N ; *for* 6N, *read* 1N.

Propagation of Sound in Liquids and Viscosity—By G. Suryan :—

Page 77, eqn. (2) *for* $\log_{10} = [\log_{10}(\eta \times 10^5)]1.2$

read $\log_{10} v = [\log_{10}(\eta \times 10^5)]1.2$

Page 78, line 19, *for* 113 (2,3) *read* 1113 (23).

THE THERMAL CONDUCTIVITY OF LAC AND LAC MOULDING COMPOSITIONS

By G. N. BHATTACHARYA

(Received for Publication, April 30, 1942)

ABSTRACT. The thermal conductivity of lac and lac moulding compositions has been determined at different temperatures by the double-disc method of Lees as modified by the National Physical Laboratory. It has been observed that for certain materials 'aqua-dag' may conveniently be used instead of mercury on the plane faces of heater and cold bars, the advantage being that the former does not interfere with any soldering in the heater or cold bars whereas the latter does. The thermal conductivity of lac moulding compositions is generally of the same order of magnitude as that of phenol-formaldehyde compositions. Water immersion for 24 hours has very little effect on the thermal conductivity of lac, shellac-urea-formaldehyde and shellac-melamine formaldehyde resins, but it affects most of the shellac moulding compositions to an extent dependent upon the nature of the filler. The variation of incumbent pressure on the shellac moulded specimens has no effect on the conductivity.

INTRODUCTION

A knowledge of the thermal conductivity of electrical insulating materials is of utmost importance since the power rating and the behaviour of electrical machineries depend largely on the temperature rise of these materials and the rise of temperature is dependent upon the rate at which heat generated in the electrical and magnetic circuits can be conducted away or dissipated by the cooling medium through these insulating materials. Unfortunately, however, these electrical insulating materials are poor conductors of heat and often a large difference of temperature is necessary between the inner and outer sides of these dielectrics before heat generated in the machineries can pass into the cooling medium outside. The rating of such machineries can therefore be increased by employing dielectrics of greater thermal conductivity or such as can stand a higher temperature rise without their insulating properties being affected. A study of the thermal conductivity of electrical insulating materials is therefore of considerable practical importance.

For a long time shellac has been known to the electrical industry as an insulating material of quality and a considerable percentage of the world's output is consumed annually by this industry in various forms.

The thermal conductivity of lac was measured by Lee[1] as early as 1892 employing the classical method of Lodge[2] and later in 1898 he again repeated the work by a modification[3] of the method used by him previously. A summary of the previous work relating to this property of lac has been given by Verman.[4] The purpose of the present investigation was to determine the heat conductivity of lac, modified lac and various lac moulding compositions which have been evolved at this Institute and are being used now by some moulding and electrical industries in this country and elsewhere. The object was also to study the effect of temperature and the influence of water on the heat conductivity of these materials, as water and water-vapour have been found to play an important role in the behaviour of lac and some other natural resins regarding some of their physico-chemical properties.

THEORY OF THE METHOD

It is known[5] that when a thin flat disc type electrical heater is enclosed on both sides by two similar discs of a material, the amount of heat generated in the heater flows equally through its two faces when a steady state is reached, if we neglect the very small amount of heat lost radially. The conductivity of the material in such a case is given by

$$k = \frac{Q.t}{2A(\theta_1 - \theta_2)}$$

where k = the conductivity in c.g.s. units,
if Q = the amount of heat in calories supplied per second,
t = the thickness of the material in cms.,
A = the area of one of the discs of the material in sq. cms.,
and θ_1, θ_2 = the temperatures in degrees centrigrade on the two faces of the material.

The amount of heat, Q, generated in the heater may be ascertained from the electrical input energy and the temperatures, θ_1 and θ_2, may be determined by thermo-couples. Hence from the known dimensions of the test-sample of the material, its conductivity, k, may be calculated.

In electrical engineering practice it is sometimes convenient to express heat transference with reference to thermal resistivity instead of thermal conductivity. In such a case, the resistivity

$$K = \frac{0.24}{k},$$

where K is expressed in degrees centigrade to cause an energy transfer at the rate of 1 watt instead of 1 calorie, and k is the conductivity in c.g.s. units.

EXPERIMENTAL

Apparatus.—The method used for carrying out these measurements was the 'double disc' method of Lees as modified by the National Physical Laboratory for the experimental investigations on the thermal resistivity of dielectrics.[6] A diagrammatic sketch of the apparatus used has been shown in Figure 1(A).

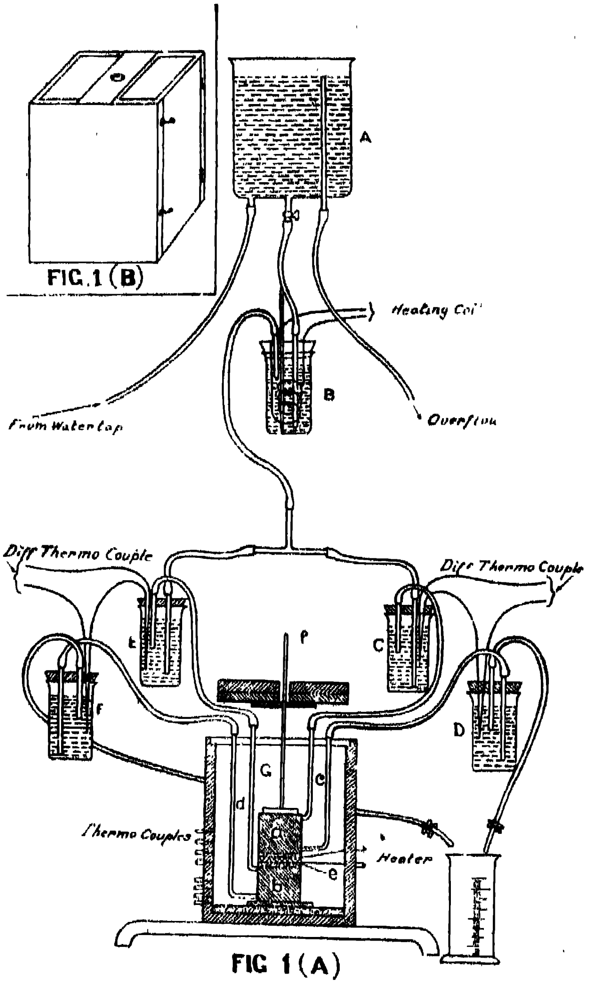

FIG. 1

A was a vessel for supplying water at a constant head and B, a tube which contained a heating coil for regulating the temperature of this water. From B this water was led into two channels by means of a T-piece and each stream passed through another vessel (C and E) just before entering the box G, which contained the main apparatus. On coming out, these streams similarly passed through the vessels D and F before being led out. These vessels C, D, E and F contained differential thermo-couples for measuring very accurately the rise of temperature of the flowing water. The rate of water-flow could be regulated by means of screw-clips.

The main apparatus assembly has been shown inside the box G, where *a* and *b* were two solid copper cylindrical bars kept cold by a steady stream of cold water circulated through two copper spirals (*c*, *d*) which surrounded the outer surface of these two bars and were fixed to them for intimate contact by soldering. *e* was the electrical heater in the form of a disc of the same diameter as that of the copper bars and it consisted of a heating coil of about 8 ohms enclosed between two sheets of mica and encased in a flat copper container. Two exactly similar test samples of each material were employed, one on either surface of the heater, and cold copper bars were placed on the other surface of these specimens as shown in the figure. The surfaces of the copper bars as well as of the heater disc were ground plane in order that there might be good contact between these surfaces and the specimens under test. A copper-constantan thermo-junction was soldered at the centre of the surface of each of these copper bars and connecting leads were taken out through a hole on the sides. Two other thermo-junctions were similarly fixed, one on each surface of the heater. The leads of all these junctions as well as of the heating coil were brought out and fixed with binding terminals on the sides of the wooden box G, the leads of copper and constantan being fixed with terminals of the same material. This box had a hinged door on one side so as to facilitate the assembling of the heater, cold blocks and the specimens. The top of the box was open and a flat steel plate with a central hole, through which an iron rod, *f*, could pass, was fixed on the sides as shown in Fig. 1(B). The rod *f* had a circular steel plate attached to it to carry weights for applying pressure on the samples. The rod rested on an ebonite disc placed on the top of the copper bar in order to isolate it thermally from the main apparatus. The lower copper bar similarly rested on an ebonite and a cork slab. The wooden box G could be filled with cork powder before carrying out an experiment.

The electrical connections for the thermo-couples were made and arranged on a distribution board as described in the E. R. A. Technical Report, Ref. L/T 41, so that either the temperatures of the faces of the test-specimen or their difference could be measured directly on a potentiometer at will. The temperature rise of the inlet and outlet water could also be measured from the same distribution board.

Method of Measurement.—Test samples of a material were first prepared by moulding to a disc of 4 cm. diameter and about 1 mm. thickness. The same thickness of two specimens was obtained by putting into the mould weighed quantity of the material. These samples were then kept in a desiccator for drying.

In assembling the apparatus each time care was taken to see that the axes of copper blocks, heater and test-samples were in line. Though the surfaces of the cold bars and the heater were ground plane as much as possible, it was found that the copper surfaces in contact with the specimens when amalgamated gave a slightly higher value of conductivity showing thereby a more intimate contact. Subsequently it was found, however, that 'aqua-dag' (colloidal graphite) when diluted to about three times its original volume could be used instead of mercury and the results were practically the same. The advantage of using aqua-dag over mercury was that the latter was found to interfere with any soldering on the copper surfaces, whereas the former had no such disadvantage. For substances which absorb moisture readily, aqua-dag cannot be used. The results of test on the same pair of samples using aqua-dag as well as mercury have been shown in Table I. A small correction for the thermal resistance of aqua-dag or mercury film was determined by blank experiments with thin steel sheets and this was subsequently used in other determinations.

TABLE I

The effect of using mercury or aqua-dag

Pressure = 20 lbs./sq. inch

Sample	With mercury		With aqua-dag	
	Mean Temp. in °C.	Conductivity $k \times 10^5$	Mean Temp. in °C.	Conductivity $k \times 10^5$
Shellac moulding composition No. 91	22.1	25	22.0	25
	33.5	28	33.6	29
	51.0	32	51.4	32
,, ,, ,, ,, 54	23.5	90	23.5	89
	32.7	92	32.9	92
	52.5	93	52.5	94

The effect of applying variable pressure had very little effect as may be seen from the results given in Table II. This may be expected as the materials were all hard enough not to yield under pressure at ordinary temperatures. A dead weight of 40 lbs. equivalent to about 20 lbs. per square inch was then applied constantly on the specimen. The determination was made at different temperatures by regulating the temperature of the inlet water. A set of five copper-constantan thermo-couples used as a differential one and giving 200 microvolts per degree was used for the determination of the temperature-rise of water. Measurements were first made on a Cambridge potentiometer and subsequently on a Tinsley one, both being capable of reading 2μv. The current was supplied from a battery of large-capacity accumulators and the input energy was carefully measured by means of a voltmeter and an ammeter. The rate of water-flow through the copper spirals was regulated in such a way that the temperature-rise of the outlet water could be conveniently measured on the potentiometer. When a steady state was reached, readings were taken on the potentiometer for different points on the distribution board. The output energy could also be determined from the rate of flow of water and its temperature rise. The input and output energies usually agreed within a few per cent everywhere. It may be pointed out here that the calculation of the output energy from the temperature-rise and the rate of flow of water only served as a check on the measurement of input energy. This did not enter into the actual calculation of conductivity.

TABLE II

The effect of pressure on the samples

Sample	Mean Temp in °C.	Total pressure in lbs.	Conductivity $k \times 10^5$
Kusum shellac	27.3	10	59
		20	60
		40	60
		60	60
	33.0	10	61
		20	61
		40	60
		60	61
Shellac moulding composition No. 72	25.3	10	72
		20	72
		40	72
		60	72
	53.5	10	84
		20	84
		40	82
		60	83

TABLE III

Particulars of shellac moulding compositions used

Shellac moulding composition No.	Resin	Filler	Percentage of		
			Resin	Filler	Dye and mould lubricant
22	Shellac-urea-formaldehyde	Slate dust	30	69	1
23	,,	Fine asbestos	30	69	1
25	,,	Kaolin	30	69	1
54	,,	Fibre asbestos	23	76	1
68	,,	Paddy straw	45	52	3
72	,,	Mica dust	30	69	1
91	,,	Wood flour (1st quality)	48	49	3
179	,,	Wood flour finely ground (2nd quality)	45	52	3
49 S	Shellac-melamine-formaldehyde	Wood flour (1st quality)	45	52	3

RESULTS

The results of test have been shown in different tables. The particulars of composition of shellac moulding powders which were taken for this work have been shown in Table III. The effect of temperature on the thermal conductivity has been shown in Table IV. The study was confined up to a maximum of 60°C., as it was considered unnecessary to extend it beyond this range for the simple reason that the above temperature might be considered to be the limit for most of the applications to which these materials may be used and as also it was apprehended that the specimens might yield slightly under a heavy load above that temperature. For this reason, thickness measurements were repeated for each specimen after conductivity test in order to see whether any deformation took place at the elevated temperatures. Table V shows the results of thermal conductivity measurements at different temperatures after the specimens were immersed in water for 24 hours. This gives an idea of the effect of water on thermal conductivity of shellac-moulded articles.

Accuracy.—The power input could be measured to an accuracy of 0.5% and the measurements of thickness which were done with a micrometer screw gauge were correct within 2%. Special copper and constantan wires for thermocouple purposes were used and the calibration done up to about 100°C. was found to be in good agreement with the data given in the International Critical Tables. Temperature measurements might, therefore, be thought to be accurate to within 2% for worst cases and within 1% for most cases. The overall accuracy, therefore, may be considered to be within 5%.

DISCUSSION

The value obtained by Lees for shellac at a temperature of 35°C. is practically the same as found here for Kusum shellac. The slight discrepancy is well within experimental error or even this may be attributed to the difference in the samples. The specimen of shellac used in these experiments was a genuine Kusum one manufactured at the experimental factory of this Institute but nothing unfortunately is known about the purity of the sample of shellac used by Lees. The agreement of the two values, however, is quite good. The value for shellac given in this paper confirms the figure obtained in a very recent work carried out in America.[7] It may be seen from Tables IV and V that no change in the thermal conductivity of Kusum shellac takes place even after immersion in water for 24 hours. Therefore, it may be assumed that atmospheric humidity will have practically no effect on the thermal conductivity of shellac. Commercial dewaxed lac, however, shows slight increase in conductivity after water immersion. On the other hand, the conductivity of pure lac resin increases to a greater extent on immersion in water. It is difficult to explain this increase in conductivity, since hard resin is not known to absorb more

TABLE IV

Thermal conductivity of desiccated materials at different temperatures

Materials	Thickness in cm.	Temp. of hot face in °C.	Temp. of cold face in °C.	Mean Temp in °C.	Conductivity $k \times 10^6$	Resistivity K
Kusum shellac	0.176	41.0	25.0	33.0	61	394
		28.8	25.9	27.3	60	400
Dewaxed lac (lemon)	0.170	43.0	26.9	35.2	56	429
		32.8	26.6	29.7	56	429
		29.3	26.5	27.9	56	429
Pure lac resin (ether extracted)	0.121	44.1	30.3	37.2	49	490
		32.7	27.5	30.1	47	511
		30.4	27.7	29.0	47	511
Shellac-urea-formaldehyde resin	0.155	41.5	26.7	34.1	57	421
		32.6	27.1	29.9	56	429
		29.6	26.8	28.2	56	429
Shellac-melamine-formaldehyde resin	0.128	40.7	25.9	33.3	48	500
		31.5	25.7	28.6	46	522
		28.8	26.2	27.5	45	533
Shellac moulding composition No. 22	0.164	33.0	22.0	27.5	83	289
		45.5	40.3	42.9	104	231
		58.5	50.2	54.4	106	226
		34.7	31.7	33.2	101	237
		33.3	22.3	27.8	83	289
Shellac moulding composition No. 23	0.082	28.0	24.0	26.0	96	250
		28.7	25.0	27.4	94	255
		30.0	25.3	27.7	94	255
		52.4	49.0	50.7	101	237
Shellac moulding composition No. 25	0.090	29.3	21.9	25.6	75	320
		36.0	33.8	34.9	89	269
		59.6	53.6	56.6	92	261
Shellac moulding composition No. 54	0.086	26.3	20.7	23.5	89	269
		33.8	32.0	32.9	92	261
		55.1	50.0	52.5	94	255
Shellac moulding composition No. 68	0.210	39.2	21.2	30.2	58	414
		41.9	23.1	32.5	59	407
		47.6	36.8	42.2	61	394
		59.3	42.8	51.1	64	375
Shellac moulding composition No. 72	0.093	28.3	22.3	25.3	72	333
		56.2	50.8	53.5	84	285
Shellac moulding composition No 91	0.042	23.7	20.3	22.0	25	960
		35.1	32.1	33.6	29	827
		54.4	48.5	51.4	32	750
Shellac moulding composition No. 179	0.055	26.7	20.7	23.7	47	511
		33.4	31.3	32.4	48	500
		53.5	47.7	50.6	49	489
Shellac moulding composition No. 498	0.065	26.0	20.5	23.3	56	429
		31.3	29.2	30.3	56	429
		52.3	47.4	49.8	58	414

TABLE V

Thermal conductivity of materials at different temperatures after immersion in water for 24 hours

Materials	Thickness in cm.	Temp. of hot face in °C.	Temp. of cold face in °C.	Mean Temp. in °C.	Conductivity $k \times 10^5$	Resistivity K
Kusum shellac	0.176	43.5	27.9	35.8	61	394
		28.6	25.6	27.1	61	394
Dewaxed lac (lemon)	0.170	44.3	27.9	36.1	58	414
		28.8	26.0	27.4	57	421
Pure lac resin (ether extracted)	0.121	38.0	27.0	32.5	60	400
		30.6	26.7	28.6	62	387
Shellac-urea-formaldehyde resin	0.155	41.8	28.9	35.0	60	400
		33.8	28.8	31.3	62	387
		31.1	28.8	29.9	60	400
Shellac-melamine-formaldehyde resin	0.128	41.8	29.1	35.5	55	438
		34.0	29.0	31.5	52	461
		31.25	29.0	30.2	50	480
Shellac moulding composition No. 22	0.164	28.5	22.4	24.2	126	190
		47.1	41.4	44.2	135	178
Shellac moulding composition No. 23	0.082	44.8	41.7	43.3	123	195
		22.9	19.3	21.1	106	226
Shellac moulding composition No. 25	0.090	24.2	20.3	22.2	116	207
		32.9	31.6	32.3	126	190
		52.6	48.3	50.5	124	193
Shellac moulding composition No. 54	0.086	24.4	20.9	22.6	168	143
		31.9	30.9	31.4	171	140
		51.3	48.5	49.9	168	143
Shellac moulding composition No. 68	0.210	35.3	20.5	27.9	67	358
		58.5	44.6	51.5	70	343
		41.0	34.7	37.8	68	353
Shellac moulding composition No. 72	0.093	24.4	20.3	22.3	104	231
		32.5	30.9	31.7	124	193
		49.8	45.9	47.8	111	216
Shellac moulding composition No. 91	0.042	25.0	19.3	22.2	41	585
		28.6	26.5	27.6	41	585
		54.1	48.5	51.3	41	585
Shellac moulding composition No. 179	0.055	23.0	20.0	21.5	63	380
		32.6	30.8	31.7	61	394
		50.1	45.8	48.0	58	414
Shellac moulding composition No. 49 S	0.065	23.0	18.3	20.7	84	285
		30.0	28.1	29.0	81	296
		54.4	49.6	52.0	82	292

moisture than shellac. In the form of films rather this resin is said to be more water-resistant than shellac in the sense that it is 'nonblushing' whereas shellac films 'blush' in contact with water. Properties of resins in the form of moulded disc or cast otherwise by melting, however, differ fundamentally from those of their varnish films obtained from solutions. Even the properties of films in different solvents vary widely. The moulded disc of Kusum or dewaxed lac (thickness about 1 mm.) was found, for example, not to blush even after 96 hours' water immersion, although their films made from alcoholic solution are known to blush after a few hours' immersion in water. The water absorption data of pure lac resin-moulded disc did not show such a value that so much difference in conductivity after water immersion might be accounted for. The explanation may be that there were very fine cracks in the desiccated pure lac specimens and the apparent low value of conductivity owing to their presence was made good by the absorbed water, however small. Aldis[8] has shown how cracks develop in the desiccated lac samples. It might be said in this connection that water, although a bad thermal conductor itself, may be considered to be a better conductor when compared with substances like lac, ebonite, etc., and the absorption of water, therefore, resulted in an increase in their conductivity.

The shellac-urea-formaldehyde and shellac-melamine-formaldehyde resins (*i.e.*, without any filler) were found to be affected by water but slightly, but most of the shellac moulding compositions were affected by it to a greater extent. Undoubtedly the fillers were responsible for this. This may be seen from the values for compositions Nos. 23 and 54. In both these powders asbestos was used as filler but the latter contained a greater percentage of it and the change of its conductivity was also higher after water absorption. The mineral fillers, in general, gave greater thermal conductivity than organic fillers. Wood flour when used as filler decreased the conductivity of the shellac-urea-formaldehyde resins. But when used with shellac-melamine-formaldehyde resin it showed a slight increase in conductivity. This may be explained on the ground that other ingredients such as dyes, mould-lubricants, etc., are also present in moulding powders and that they also affect the heat conductivity of such compositions to a small extent. Moreover, wood flour itself has different grades and their conductivity was found to be different. This may be seen from the values of composition Nos. 91 and 179.

Comparing the values of other insulating materials it may be seen that thermal conductivity of shellac mouldings is of the same order of magnitude as those of pressboard, varnished cloth, treated silk, ebonite, phenol-formaldehyde resin compositions, and paraffin. As mica has a slightly higher value of thermal conductivity, the shellac moulding composition containing mica dust has yielded a comparatively high value. It was expected, therefore, that compositions containing mica dust as filler would have better thermal as well as dielectric properties. This expectation has subsequently been found to be true." But unfortunately the mechanical strength of such a composition is inferior.

The variation of thermal conductivity with the temperature of materials tested before and after immersion in water shows a marked difference. In most cases the temperature had very little effect on conductivity after immersion in water. The explanation may be that at higher temperatures moisture is eliminated from the specimen which has absorbed water and the consequent fall in the value of its conductivity annuls the increase due to the temperature rise. This view is substantiated from the figures of composition No. 23 in Table V, where measurement at the higher temperature was done first. Here the increase in conductivity at the higher temperature has been obtained. The results of test obtained after the samples were immersed in water and recorded in Table V are, therefore, not so accurate. They indicate, however, how these composition are affected by water.

ACKNOWLEDGMENT

The author is grateful to Dr. H. K. Sen, the Director of this Institute, for his kind interest in this work and to Professors P. N. Ghosh and J. N. Mukherjee of the University College of Science, Calcutta, and Professor H. E. Watson of the University College, London, for some suggestions and helpful criticisms. Thanks are also due to Mr. A. R. Dunton of Messrs. Metropolitan-Vickers Electrical Company Limited, Manchester, for kindly bringing to the notice of the author the results of a recent work carried out in America which seem to confirm some of the figures given in this paper.

INDIAN LAC RESEARCH INSTITUTE,
RANCHI.

REFERENCES

[1] Lee, C. H., *Phil. Trans. Roy. Soc. (Lond.)*, **A. 183**, 481 (1892).
[2] Lodge, O. J., *Phil. Mag.*, **5**, 110 (1878).
[3] Lee, C. H., *Phil. Trans. Roy. Soc. (Lond.)*, **A. 191**, 399 (1898).
[4] Verman, L. C., *Tech. Paper of Lond. Shel Res Bur.*, **4**, 3 (1935).
[5] Saha, M. N., and Srivastava, B. N., *A Treatise on Heat*, 338, 363 (1935).
[6] *E.R.A. Technical Report Ref. L/T*, **41**, 9 (1931) and *I.E.E. Journal*, **68**, 1313 (1930).
[7] *International G E. Data Folder* 71241.
[8] Aldis, R. W., *Bull. Ind. Lac. Res. Inst.*, **5**, 3 (1932).
[9] Unpublished information from Research Dept., Metropolitan-Vickers Electrical Co Ltd., Manchester, England.

THE EFFECT OF SURROUNDING MEDIUM ON THE DIELECTRIC STRENGTH OF LAC AND LAC-MOULDED MATERIALS

By G. N. BHATTACHARYA

(Received for publication, May 2, 1949)

Plate VIII

ABSTRACT. The dielectric strength of lac and different lac moulding compositions have been determined using a brass sphere and a plate electrode. Six different liquid media, *viz.*, transformer oil, xylol, kerosene, turpentine, castor oil and a mixture of xylol and acetone have been used successively in the test jar. It has been found from the results of the experiment that the specific resistance and not the dielectric constant of the liquid media is effective in making a difference in the breakdown voltage values. The effect of thickness of specimens on the dielectric strength has also been studied in each of the above liquid media and it has been observed that the general logarithmic law between the thickness and the breakdown voltage values also holds good for lac as well as other moulded lac specimens. The constants for such a law have been evaluated for these materials in different surrounding media. The nature of breakdown has been discussed and has been shown in a few photomicrographs

INTRODUCTION

Data on the dielectric strength of insulating materials are of utmost practical utility, although it is still a disputable point whether the dielectric strength of a material is a physical constant of the material or is only an effect resulting from the method of measurement. Whatever it may be, the value of the dielectric strength of a material under actual operating conditions is of extreme importance in designing electrical machineries. There are so many uncertain factors associated with the mechanism of failure of electrical insulating materials, especially solid dielectrics, that the fundamental information regarding the breakdown of solid materials is still lacking. A large amount of data has, however, been collected by different workers on various materials owing principally to their practical utility. Whitehead[1] has presented these data in a systematic manner whilst Peek[2] and Schwaiger[3] have also dealt with this important subject in order to find out a satisfactory theory regarding the breakdown by analysis of previous data. The importance of the elimination of 'edge-effect' in determining the electric strength of materials was first shown by Moscicki[4], and a great advance has been made by Inge and his collaborators[5] since then, towards a better understanding of the problem.

The effect of surrounding medium on the breakdown of solid dielectrics has also been the subject of much speculation Littleton and Shaver[6] reported their results of test on insulators under oils containing different amounts of moisture. Inge and Walther[7], however, used liquids of known properties and they found that the specific resistance of the medium is only effective in making a difference in dielectric strength measurements.

The present paper presents the results of test on shellac and shellac-urea-formaldehyde-wood-flour-filled moulded discs in different liquid media.

EXPERIMENTAL

The test-specimens were all moulded discs of 4″ diameter, but of different thickness. Pure Kusum shellac was used for making shellac specimens. The moulding technique has already been described by Karim[8] and the same procedure was adopted except that tin foils were not used since it was found that these were not necessary when the mould was polished with french chalk powder after each operation. These discs were all desiccated for more than a week in a vacuum desiccator before they were tested. Electrodes were a sphere and a flat plate made of brass, the lower electrode being the plate. Six liquids, *viz.*, transformer oil, xylol, kerosene, turpentine, castor oil and a mixture of xylol and acetone were used successively in the test jar and discs of different thickness were employed in order to find out the effect of thickness on the breakdown voltage in each liquid medium. The rate of application of voltage was approximately 0.5 KV. per second. The voltage was measured by means of a Starke-Schroeder electrostatic voltmeter on the secondary side of the H.T. transformer, the primary of which was fed from a 50-cycle sine-wave alternator. The control was in the field of the alternator. The thickness measurements were made near the point of breakdown by means of a micrometer screw-gauge.

RESULTS

The results are given in Tables I and II.

TABLE I

Material—Kusum shellac

Surrounding medium	Thickness of specimen in mm.	Breakdown voltage in KV.	Dielectric strength in KV./mm.	Remark
Castor oil	1.22	25.2	20.6	
	1.48	29.0	19.6	
	1.62	30.0	18.4	
	2.05	34.8	17.0	
	2.45	38.2	15.6	Mean of 2 readings
	2.53	37.8	14.9	
	3.06	41.0	13.4	Mean of 2 readings

TABLE I (*contd.*)

Surrounding medium	Thickness of specimen in mm.	Breakdown voltage in KV.	Dielectric strength in KV./mm	Remark
Transformer oil	1.03	26.4	25.7	Mean of 2 readings
	1.63	32.8	20.1	
	1.88	35.2	18.7	
	1.98	36.0	18.2	
	2.50	40.8	16.3	Mean of 3 readings
	2.91	45.2	15.5	
	3.01	44.0	14.6	
Kerosene oil	0.91	26.0	28.6	
	1.06	28.0	26.4	
	1.43	30.9	22.9	
	1.62	34.8	21.1	
	1.85	37.0	20.0	
	2.02	39.6	19.7	Mean of 3 readings
	2.52	42.4	16.8	Mean of 2 readings
	3.02	46.8	15.4	
Xylol	1.18	31.0	26.0	
	1.25	31.8	25.4	
	1.45	34.0	23.4	
	2.00	40.5	20.2	
	2.49	45.1	18.3	
	2.95	52.5	17.6	
	3.02	49.4	16.3	
Turpentine	1.18	28.6	24.2	
	1.40	34.0	24.3	
	1.45	33.2	22.9	
	1.63	41.0	25.1	
	1.99	40.0	20.1	
	2.08	41.0	19.7	Mean of 2 readings
	2.10	39.8	19.3	
	2.40	48.0	20.0	
	2.85	53.0	18.6	
Xylol + 12% Acetone	0.98	51.0	52.0	
	1.05	59.0	56.2	
	1.07	58.0	54.2	
	1.46	64.0	43.8	
	1.50	62.8	41.8	
	1.52	72.0	47.3	
	1.95	82.0	42.0	
	2.03	84.0	41.4	
	2.38	95.0	40.0	
	2.45	98.0	40.0	
	2.54	96.0	38.8	

DISCUSSIONS

Choice of electrodes.—Experiments carried out for the British Electrical and Allied Industries Research Association have yielded results on the basis of minute test such that for good dielectrics, such as ebonite, etc., a sphere and plate electrode generally gave higher values than two discs. Particularly for thick specimens the disc electrodes gave lower values of B.D.V. than the sphere and plate owing probably to more flux-concentration at the edges of the

TABLE II

Material—Shellac-urea-formaldehyde-wood-flour composition

Surrounding medium	Thickness of specimen in mm	Breakdown voltage in KV.	Dielectric strength in KV./mm.	Remark
Castor oil	0.54	16.0	29.7	
	0.76	18.8	24.9	
	0.80	19.6	24.5	
	0.87	21.0	24.1	Mean of 2 readings
	1.60	28.0	17.5	
	1.67	28.0	16.8	
	1.71	26.2	15.3	
	1.76	26.0	14.8	
	1.88	30.0	16.0	
	2.10	30.0	14.3	
	2.13	30.6	14.5	
	2.88	34.8	12.1	
	3.02	34.8	11.5	
Transformer oil	0.59	20.0	33.9	
	0.70	20.8	29.7	
	0.73	19.8	27.2	
	0.96	23.4	24.4	Mean of 2 readings
	1.32	27.0	20.4	
	1.40	28.2	20.2	
	1.62	30.4	18.9	
	1.74	28.8	16.6	
	1.92	35.0	18.2	
	2.04	34.0	16.8	
	2.48	36.8	14.8	
	2.75	40.2	14.6	
	2.90	39.6	13.7	
	2.97	38.6	13.1	
	3.02	38.0	12.6	
Kerosene oil	0.61	19.0	31.2	
	0.64	20.0	31.2	
	0.82	22.0	26.9	
	1.14	25.8	22.6	
	1.39	29.8	21.4	
	1.72	32.8	19.1	
	1.95	34.0	17.4	
	2.13	36.0	16.9	
	2.37	40.2	17.0	
	2.45	39.4	16.1	
	2.47	41.0	16.6	
	2.55	42.4	16.7	
	2.96	45.4	15.4	
	3.03	47.2	15.6	
	3.08	46.8	15.2	
	3.12	49.0	15.7	
Xylol	0.55	21.2	38.6	
	0.73	24.2	33.2	
	0.83	26.8	32.3	
	0.88	29.0	32.9	
	0.96	28.0	29.2	
	1.21	30.8	25.5	
	1.30	33.0	25.4	
	1.61	38.2	23.7	
	1.86	41.4	22.2	
	2.01	44.0	21.9	
	2.12	45.0	21.3	
	2.46	48.8	19.9	
	2.96	58.0	19.6	
	3.14	56.4	18.0	

TABLE II (*contd.*)

Surrounding medium	Thickness of specimen in mm.	Breakdown voltage in KV	Dielectric strength in KV./mm	Remark
Turpentine	0.76	30.0	39.5	
	0.88	35.0	39.8	
	0.93	35.0	37.7	
	1.00	36.0	36.0	
	1.42	43.6	30.7	
	1.63	43.0	26.4	
	1.80	45.6	25.3	Mean of 3 readings
	2.11	52.8	25.1	
	2.14	49.8	23.3	
	2.22	51.8	23.4	
	2.90	60.0	20.7	
	3.02	64.0	21.0	
	3.11	62.0	20.0	
Xylol + 12% Acetone	0.62	27.0	43.6	
	0.72	26.0	36.1	
	0.85	30.0	35.3	
	0.92	37.8	41.0	
	0.98	34.0	34.7	
	1.32	47.0	35.6	Mean of 2 readings
	1.50	50.0	33.3	
	1.52	48.4	31.8	
	1.83	62.0	33.8	
	2.12	62.0	29.2	
	2.30	67.0	29.1	
	2.45	69.2	28.2	
	2.56	71.0	27.7	
	2.58	72.6	28.2	

former. We know that the electrostatic field between a sphere and a plate is similar to that between two equal spheres, and is practically uniform if the distance between them is small compared to the radius of the sphere. When it is intended to see the effect of the surrounding medium on the breakdown voltage, the sphere should simply be pressed on the specimen instead of having been imbedded in the material. For, in that case the results will, to a certain extent, depend upon the medium, as a layer of this medium will always surround the electrodes except at the centre. In these experiments, therefore, the choice was made of a sphere and plate electrode.

The Variation of Dielectric Strength with Thickness.—The variation of the breakdown voltage with the thickness of lac as well as of shellac-urea-formaldehyde-wood-floor composition has been shown graphically in Figs. 1 and 4. For most of the insulating materials the dielectric strength decreases with increasing thickness according to some function of the thickness. The most generally accepted formula for this function is given by

$$V = At^n,$$

where V = the breakdown voltage,
t = the thickness of the specimen,
A and n are constants, the value of n being less than unity.

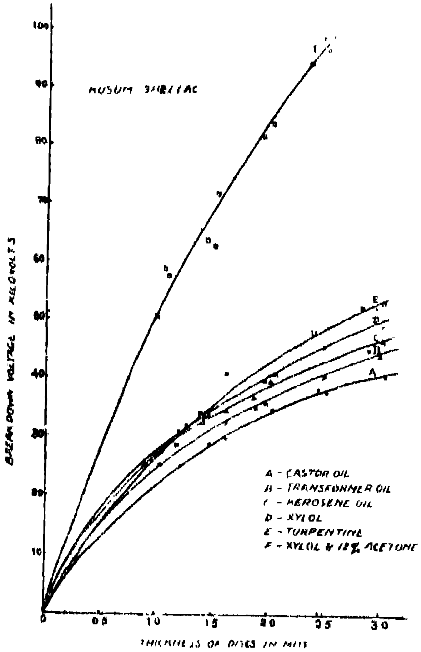

Fig. 1

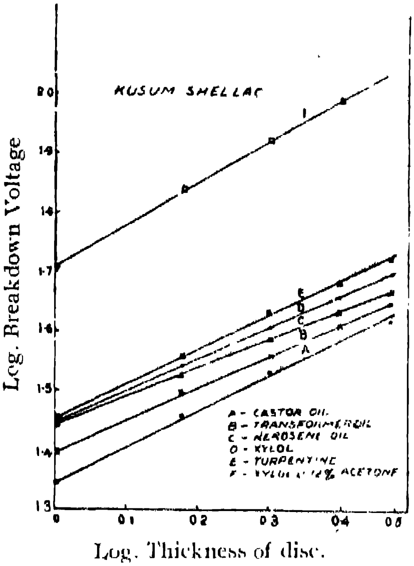

Fig. 2

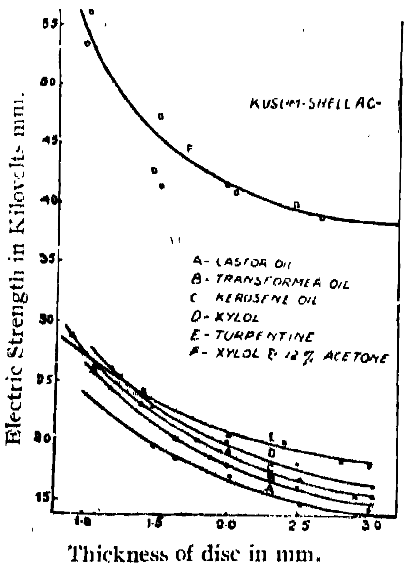

Fig 3.

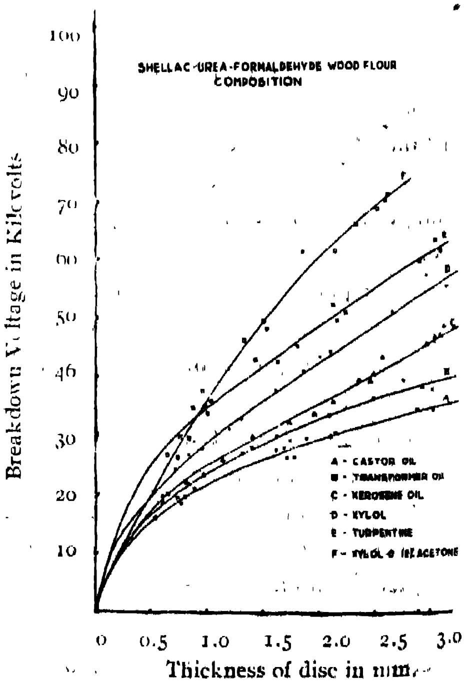

Fig. 4

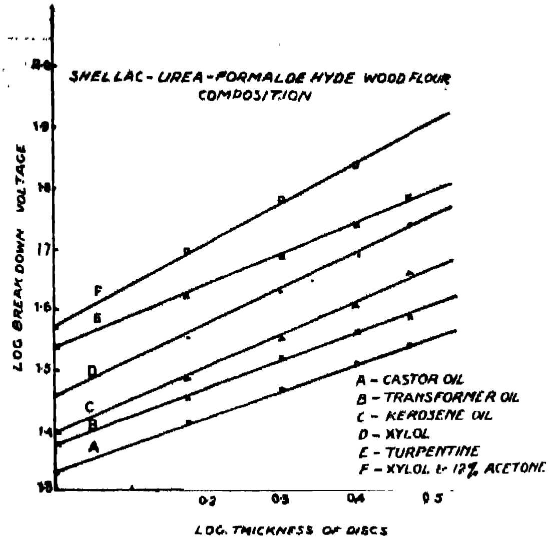

FIG. 5

For lac as well as shellac moulded materials this formula has been found to be applicable. The straight lines obtained by the plot of logarithm of breakdown voltage against logarithm of thickness have been shown in Figs. 2 and 5. The values of the constants A and n have been evaluated from these straight lines by the method of selected points." The variation of dielectric strength with thickness in the case of lac has been shown in Fig. 3. The curves are hyperbolic in nature and these may obviously be explained from the general equation obtaining between the breakdown voltage and thickness of lac materials, *viz.*, $V = At^n$, where n is less than unity.

Since we have, $$V = At^n$$

$$\frac{V}{t} = At^{n-1}$$

or, $$v = At^{n-1} = At^{-(1-n)} = At^{-n'}$$

where v = dielectric strength and n' is a positive quantity.

The last equation is of the general form of a hyperbolic curve. The value of n' can also be obtained from n, since $n' = 1 - n$, the same value of A being applicable for both the equations. The values of these constants A, n and n' for both Kusum shellac and shellac-urea-formaldehyde-wood-flour composition have been included in Table III. Here the breakdown voltage, V, or the dielectric strength, v, is expressed in kilo-volts and the thickness, t, in millimetres.

The effect of medium.—It may be seen from the curves in Figs. 1 and 4 that the castor oil gave the lowest dielectric strength values among the liquids used for shellac as well as shellac-urea-formaldehyde-wood-flour composition. The liquid

TABLE III

Surrounding medium	Kusum shellac			Shellac-urea-formaldehyde-wood-flour composition		
	A	n	n'	A	n	n'
Castor oil	22.10	0.608	0.392	21.50	0.450	0.550
Transformer oil	24.87	0.542	0.458	23.90	0.467	0.533
Kerosene oil	27.66	0.483	0.517	25.10	0.538	0.462
Xylol	27.92	0.542	0.458	28.45	0.608	0.392
Turpentine	28.41	0.585	0.415	34.67	0.525	0.475
Xylol + 12% acetone	50.90	0.708	0.292	37.87	0.667	0.333

TABLE IV

Surrounding liquid medium	Specific resistance	Dielectric constant
Castor oil	2×10^{13}	4.58
Transformer oil	7×10^{12}	2.20
Kerosene oil	5×10^{11}	2.10
Xylol	6×10^{10}	2.36
Spt. of turpentine	7×10^{8}	2.23
Xylol + 12% acetone	1×10^{8}	3.12

media when arranged in ascending order of dielectric strength of lac will be castor oil, transformer oil, kerosene oil, xylol, spt. of turpentine, and a mixture of xylol and 12% acetone. These liquids were chosen since they have varying specific resistance and different dielectric constant values. The data regarding their specific resistance and dielectric constant are shown in Table IV. The order of curves of dielectric strength in different liquid media naturally shows that it is the specific resistance and not the dielectric constant which is effective in making a difference in the breakdown voltage values. It may be quite possible, however, that the values of dielectric constant and specific resistance measured at low voltages are quite different from those obtained at very high voltages, especially near the point of discharge or breakdown. It is very difficult to determine the conditions of the surrounding medium under very high voltage stress nearing breakdown. In any case the relation between the gradually decreasing value of specific resistance of the liquid media measured at low voltages and the increasing dielectric strength values of the lac is striking. Similar results were also noticed by Inge and Walther[7] in the case of glass. They found that the specific resistance of the medium was responsible for eliminating preliminary failure of the surrounding

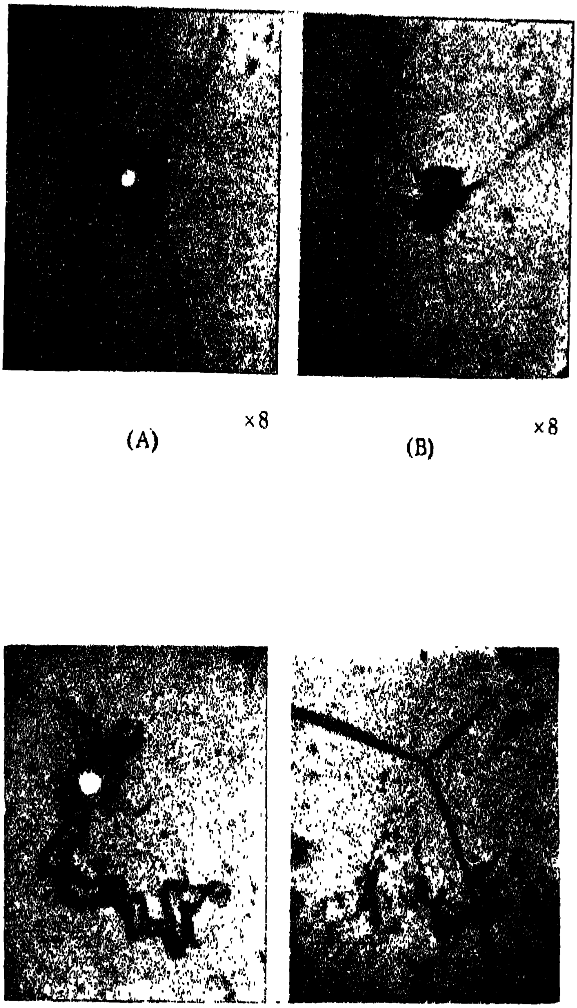

(A) ×8

(B) ×8

(C) ×8

(D) ×8

Photomicrographs of puncture

dielectric, thus making a wide difference in the results of test on the same insulator. The dielectric constants of shellac-urea-formaldehyde-wood-flour composition and castor oil may be considered to be approximately identical at low voltages, but the relation between the breakdown voltage and the thickness of the former in the medium of the latter was not even approximately linear. Naturally, it is not due to the non-homogeneity of the electric field that the relation is non-linear. The explanation is certainly to be sought somewhere else, at least in the case of shellac-moulded articles. It may be due to purely thermal effects owing to the very low thermal conductivity of these materials or to any thermal-electric effect as proposed by Rogowski in his thermal-electric theory.

The nature of breakdown.—The nature of breakdown in shellac discs has been shown in a few photomicrographs (Plate VIII). The puncture is almost invariably associated with a small crater formed by the melting of the resin on the upper side of the disc, *i.e.*, the side on which rested the sphere electrode. Sometimes this puncture is also accompanied by side-cracks. Various patterns for such cracks have been obtained, but mostly they are short crack lines emanating from the puncture-hole. Small indentations around the crater have also been noticed probably owing to collision of ions moving with high velocity in the intense electric field. The crater is indicated in the plate in (A) and (C) by the black enclosure around a white spot, which is the puncture pin-hole, and in (B) by the black spider-like picture at the centre, from which start three crack-lines. The two crack-lines in plate (A) emanating from the crater may also be seen. The puncture-hole in (B) cannot be seen, since it was inclined to the surface of the specimen, and so in the photomicrography light could not pass straightway and fall in the field of view.

It was noticed that for lac specimens puncture almost invariably occurred some distance away from the centre. In the work for the British Electrical and Allied Industries Research Association also a similar effect was noticed for high-grade dielectrics. A theoretical treatment for this effect has been given by Whitehead[10] and he has shown that this distance should increase with the thickness of the specimen as well as with the radius of the sphere, but measurement of this distance gave no definite conclusions in the case of shellac-urea-formaldehyde-wood-flour composition, since abnormal variations were found from sample to sample. Naturally other factors were present. For pure shellac specimens, however, the variation was small, but still the distance of puncture from the axis of the centre electrode, even for specimens of the same thickness, was not always the same. This only suggests the presence of some weak spots or conducting filaments through which the main current is concentrated and ultimately results in breakdown as proposed by Wagner in his Local Instability theory.

The cracks that have been observed to develop near the puncture-hole seem to be due to thermal effects. Probably they are caused by the sudden cooling of the lac disc after it has been melted by the heavy current at the point of puncture, or even they may result from sudden heating at the weak spot at the time of puncture. In one instance, however, three crack lines (Plate, D) were observed to originate from a point which was situated at a distance of about 8 mm. from the puncture-hole. A serpent-like pattern on the surface of the disc was also noticed to emanate from the puncture-hole in this case, and heading towards the point from which started the three crack-lines. The explanation probably is that there were two weak filaments of about the same conductivity on the part of the material covered by the uniform field of the electrodes. On gradually increasing the voltage stress, instability started at a certain instant of time through the two weak filaments. At the next instant, as the voltage was raised still more, the higher voltage stress was sufficient to cause a puncture through the nearer weak filament. The breakdown through this filament may either be due to its slightly higher conductivity or to the slightly more intense field, the filament being situated near the axis of the sphere electrode. Just before breakdown, however, comparatively heavy current was passing through both these weak spots and the pattern is only an automatic record of a spark or current-path through the other filament. This recording was made possible by slight melting of the resin owing to intense heat of the spark. Cracks, however, developed at the other filament due to thermal effect only. The puncture did not occur at the second spot since the stress was lessened due to breakdown having occurred through the nearer weak spot at the previous moment.

ACKNOWLEDGMENT

The author acknowledges his indebtedness to Dr. H. K. Sen, the Director of this Institute, for his encouragement and advice.

Indian Lac Research Institute,
Namkum, Ranchi.

REFERENCES

[1] Whitehead, S , *Dielectric Phenomena III—Breakdown of Solid Dielectrics* (E. Benn, Ltd), 1932.

[2] Peek. F W , *Dielectric Phenomena in High Voltage Engineering* (McGraw-Hill Book Company, Inc), 1929.

[3] Schwaiger, A , *Theory of Dielectrics* (J. Wiley & Sons, Inc.), 1932.

[4] Moscicki, J., *Elektrotech Zeit.*, **25**, 527 (1904).

[5] Inge, L., and Walther, A., *Arch. Elektrotech.*, **19**, 257 (1928); *Ibid* , **21**, 209 (1928); *ibid.*, **24**, 88 (1930); Inge, L., and Weel. B., *ibid.*, **25**, 597 (1931).

[6] Littleton, J. T., and Shaver, W. W , *Elec. World*, **91**, 759 (1928).

[7] Inge, L , and Walther, A., *Arch. Elektrotech* , **19**, 257 (1928).

[8] Karim, A., *A Study of the Mechanical and Electrical Properties of some Commercial Standard Lacs*, p. 10 (I.L R I. publication), 1937.

[9] Lipka, J., *Graphical and Mechanical Computation* (J Wiley & Sons, Inc.), p. 128, 1935.

[10] Whitehead, S , *Dielectric Phenomena III—Breakdown of Solid Dielectrics* (E. Benn, Ltd), p.110, 1932.

A NOTE ON THE PRINCIPLE OF ADIABATIC INVARIANCE*

BY P. L. BHATNAGAR
AND
D. S. KOTHARI

(Received for publication, May 2, 1942)

The principle of adiabatic invariance[1] first formulated by Boltzmann, in connection with his studies on the Kinetic Theory of gases, acquired added importance when Ehrenfest incorporated it in the old quantum theory. It is usual[2] in discussing the principle, to illustrate it with the help of some simple examples of classical mechanics. The illustration of the simple pendulum, due to Einstein, has almost become historic. Andrade[3] has also considered the case of a conical-pendulum where for E/ν to be adiabatically invariant, it is no longer necessary to confine to small angles, a restriction which has to be imposed for a simple pendulum. In the above relation E represents the energy and ν the pulsatance of vibration, where the pulsatance is defined as 2π times the frequency.

Because of its importance and many applications, it is of some interest to have other simple illustrations of the principle of adiabatic invariance (besides those referred to above).

The examples of (*i*) a compound pendulum, (*ii*) an oscillating magnet[4]† and (*iii*) an electric oscillating circuit are given below. The case of simple pendulum is treated in §1, that of compound pendulum in §2, an elementary general treatment in §3 and the magnetic and electric cases are given in §4.

§1. *Simple pendulum.*—We consider a simple pendulum, its string passing through a ring which may be moved vertically up and down to change the point of suspension [Fig. 1 (*a*)]. If l be the length of the pendulum, ν is given by

$$\nu = \sqrt{\frac{g}{l}} \quad \text{and} \quad \frac{d\nu}{\nu} = -\frac{1}{2}\frac{dl}{l}.$$

The tension T in the string is

$$T = ml\dot{\theta}^2 + mg\cos\theta,$$

and the vibrational energy E is

$$E = \tfrac{1}{2} mgl\,\theta_0^2,$$

where θ_0 is the amplitude of the vibration

$$\theta = \theta_0 \sin \nu t.$$

---

* Communicated by the Indian Physical Society.

† Darwin (1940) has referred to a very interesting application of this case.

The reaction R of the string on the ring will be $2T \sin \theta/2$ and it will be inclined at an angle $(\pi/2 - \theta/2)$ to the vertical.

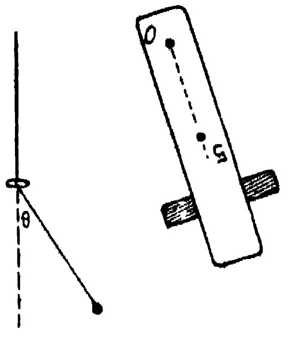

(a) (b)

FIG. 1

When the ring is displaced upwards, slowly and continuously, through a vertical height dl, the vertical component of R does work and the loss of energy of the system is equal to

$$R \sin \frac{\theta}{2} dl = \tfrac{1}{2} T\theta^2 dl = \tfrac{1}{2} mg\, \theta^2 dl,$$

neglecting terms higher than θ^2.

Therefore* the average loss of energy $d\bar{E}$ becomes

$$\tfrac{1}{2} mg\, \overline{\theta^2}\, dl = \tfrac{1}{4} mg\, \theta_0^2\, dl.$$

Hence
$$\frac{d\bar{E}}{\bar{E}} = -\tfrac{1}{2}\frac{dl}{l} = \frac{d\nu}{\nu}$$

or
$$\frac{\bar{E}}{} = \text{constant}.$$

An alteration in the length of the simple pendulum may be brought about in two ways: (i) by moving the ring as discussed above, and (ii) by suddenly clamping the string a little below the original point of suspension and then repeating this procedure of successively clamping at lower and lower points (the displacement of the pendulum remaining the same during the clamping). It is interesting to note that in the second case it is not $\bar{E}/\nu$, but $\bar{E}\nu$, that is, an adiabatic invariant.

Suppose that when the pendulum has a displacement θ, the string is suddenly clamped at a displacement dl from the initial point of suspension. The kinetic energy will remain the same during the process but the potential energy of vibration will be altered by

$$d\{mgl(1-\cos\theta)\} = \tfrac{1}{2} mg\, \theta^2\, dl,$$

and, therefore, the average change will be

$$\tfrac{1}{4} mg\, \theta_0^2\, dl = \tfrac{1}{2} \bar{E}\, dl/l,$$

and hence
$$\bar{E}\nu = \text{constant}.$$

---

* If the displacement of the ring did not take place slowly and continuously, but say at the instant when $\theta = \theta_0$, the loss of energy would be $\tfrac{1}{2} mg\, \theta_0^2\, dl$ and on the other hand, if the displacements take place when $\theta = 0$, the energy loss would be zero.

§ 2. *Compound-pendulum.*—Consider a compound pendulum. The pulsatance of small oscillation is given by

$$\nu=\sqrt{\frac{gh}{k^2}} \quad \text{and} \quad \frac{d\nu}{\nu}=-\frac{dk}{k}+\frac{1}{2}\frac{dh}{h},$$

where k is the radius of gyration about the axis of suspension and h the distance between the centre of gravity and the axis. The pendulum carries a sliding mass, whose motion alters the position of the centre of gravity along the line OG [Fig. I(b)].

The vibrational energy of the pendulum is

$$E=\tfrac{1}{2}mk^2\dot{\theta}_0^2=\tfrac{1}{2}mgh\theta_0^2.$$

At the instant when the angular displacement of the pendulum is θ, let a motion of the sliding weight lower the centre of gravity by a small amount dh, the change in the angle θ during this alteration of the position of c.g. being supposed to be negligible. As the angular momentum of the pendulum will remain constant during the above process, we have

$$mk^2\dot{\theta}=\text{constant},$$

and as the kinetic energy T is

$$T=\frac{1}{2}\frac{(mk^2\,\dot{\theta})^2}{mk^2}.$$

we have

$$\frac{dT}{T}=-\frac{2dk}{k},$$

or

$$d\overline{T}=-2\frac{dk}{k}\,(\tfrac{1}{2}mk^2\overline{\dot{\theta}^2})$$

$$=-\frac{dk}{k}\,(\tfrac{1}{2}mk^2\dot{\theta}_0^2).$$

Hence we have

$$\frac{d\overline{T}}{E}=-\frac{dk}{k}.$$

The potential energy of the pendulum in the position θ is

$$mgh(1-\cos\theta)=mgh\frac{\theta^2}{2},$$

and the increase dh in h increases the potential energy by

$$dV=\tfrac{1}{2}mg\,\theta^2dh,$$

and therefore

$$d\overline{V}=\tfrac{1}{2}mg\,\overline{\theta^2}\,dh=\tfrac{1}{4}mg\,\theta_0^2\,dh$$

or

$$\frac{dV}{E}=\frac{1}{2}\frac{dh}{h}.$$

Therefore
$$\frac{dE}{E}=-\frac{dk}{k}+\frac{1}{2}\frac{dh}{h}=\frac{d\nu}{\nu}$$

or
$$\frac{E}{\nu}=\text{constant}.$$

§ 3. *An elementary general treatment* :—Consider any simple harmonic motion defined by
$$m\frac{d^2x}{dt^2}=-\lambda x$$

and
$$\nu=\sqrt{\frac{\lambda}{m}}.$$

The energy of vibration E is given by
$$E=\tfrac{1}{2}\lambda a^2,$$

where a is the amplitude. When the displacement is x, let λ change to $\lambda+d\lambda$; then the increase in the restoring force is $xd\lambda$, and the energy of vibration is increased by
$$\int_0^x d\lambda . x\, dx=\tfrac{1}{2}d\lambda\, x^2$$

and averaging we have
$$\overline{dE}=\tfrac{1}{4}d\lambda a^2$$

and
$$\frac{dE}{E}=\frac{1}{2}\frac{d\lambda}{\lambda}=\frac{d\nu}{\nu}$$

or
$$\frac{E}{\nu}=\text{constant}.$$

§ 4 (*a*). *Small magnet* :—Consider a magnet of moment M oscillating in a field of strength H. When the deflection is θ, let H change to $H+dH$, then the increase in the restoring couple is $M\theta dH$ and, therefore, the increase in the vibrational energy will be
$$\int^{\theta}\theta M dH\, d\theta=\tfrac{1}{2}M\theta^2 dH$$

and averaging we have
$$dE=\tfrac{1}{4}M\theta_0^2 dH.$$

As the energy of vibration is
$$E=\tfrac{1}{2}MH\theta_0^2$$

and
$$\nu=\sqrt{\frac{MH}{I}},$$

where I is the moment of inertia of the magnet about the axis of vibration.

We have
$$\frac{dE}{E}=\frac{\frac{1}{4}M\theta_0^2\,dH}{\frac{1}{2}M\theta_0^2\,H}=\frac{1}{2}\frac{dH}{H}=\frac{d\nu}{\nu}.$$

Therefore
$$\frac{E}{\nu}=\text{constant}.$$

(*b*) *Electric oscillating circuit* :—We consider an electric circuit consisting of a capacity c and a self-inductance l, then

$$\nu=\sqrt{\frac{1}{lc}}\quad\text{and}\quad\frac{d\nu}{\nu}=-\frac{1}{2}\frac{dc}{c}.$$

Let q be the charge on the condenser at instant t, then

$$q=q_0\sin\nu t.$$

The electrostatic energy at this instant is $\frac{1}{2}\frac{q^2}{c}$, and the total energy of the circuit E is

$$E=\frac{1}{2}\frac{q_0^2}{c}.$$

When the charge on the condenser is q, let its capacity be suddenly changed from c to $c+dc$, then the potential difference of the condenser will be changed by

$$dV=-\frac{q}{c^2}dc$$

and, therefore, the change in the energy will be

$$dE=\frac{1}{2}\,q\,dV=-\frac{1}{2}\frac{q^2}{c^2}dc.$$

The average change of energy is

$$dE=-\frac{1}{4}\frac{q_0^2}{c^2}dc,$$

and hence we have

$$\frac{dE}{E}=-\frac{1}{2}\frac{dc}{c}=\frac{d\nu}{\nu}$$

or
$$\frac{E}{\nu}=\text{constant}.$$

UNIVERSITY OF DELHI.

REFERENCES

[1] Jeans, J. H., *Dynamical Theory of Gases*, 410, *et seq* (1925).

[2] Born, M., *Mechanics of the Atom*, 52 *et seq* (1927).

[3] Andrade, E. N. Da C., *Structure of the Atom*, 198 (1934).

[4] Darwin, C. H., *Nature*, **146**, 956 (1940).

THE MOTION OF GASES IN THE SUN'S ATMOSPHERE
PART IV

ON THE OCCURRENCE OF HIGHLY STRIPPED ATOMS IN THE CORONA

BY A. K. DAS

AND

Y. P. RAO

(Received for publication, May 2, 1942)

ABSTRACT. It has recently been announced by Edlen that the hitherto unexplained emission lines in the coronal spectrum are due to forbidden transitions in very highly stripped iron, nickel and calcium atoms The conditions of temperature and pressure in the corona are insufficient to ionise these atoms to such a great degree. The idea developed in the earlier papers of this series, that the material of the solar atmosphere is coming from the core of the sun, is applied to the coronal problems also. Eddington has shown in another connection that material in convection will not attain the equilibrium ionisation of the layer through which it is passing, if the convective velocity exceeds a critical value. The critical velocity for the breakdown of convective equilibrium in a region (26,000 km. below the photosphere) where iron atoms are stripped of the first fourteen outer electrons is computed as 300 km /sec. approximately From the available observational evidence it is shown that matter responsible for the coronal emission lines can have a velocity exceeding 300 km./sec at a depth of 26,000 km. in the interior. This explains how the ionised atoms reach the corona retaining the ionisation acquired in the interior.

INTRODUCTION

Although the chromosphere and the prominences had been visually observed for only a little over a century and the existence of the corona as an aureole of light around the sun during total eclipses had been known from antiquity, when the method of spectrum analysis was discovered it was applied first to the prominences instead of the corona. It was in 1868 that the spectroscope was for the first time employed for the study of the corona. During the total eclipse which happened in that year, only one observer, Tennant, pointed his spectroscope towards the corona, but he saw nothing more than a continuous spectrum. A year later during the eclipse of August 7, 1869, three famous solar observers, Young, Harkness and Lockyer, observed a single bright line in the green (superpoeed upon a continuous background) in the spectrum of the solar corona. This was the beginning of the study of the nature and composition of the corona. During the seventy odd years that have elapsed since the discovery of the green coronal line, eclipse observers have not let slip a single opportunity of studying the outer atmosphere of the eclipsed sun ; but the total time that has been available for the necessary observations is little over an hour. The surprising thing is not that the problem of the corona is still very far from solution, but that a great deal of observational data of varied types has been collected about the corona. The coronagraph invented and perfected by Lyot during the last few years will no doubt increase rapidly our knowledge about the lower parts of the corona ; but for gathering information about the finer details of structure of the outer corona and about the spectral composition of its light we shall still have to depend upon the rare and precious moments of the total solar eclipse.

THE BRIGHT-LINE SPECTRUM OF THE CORONA

The emission line λ 5303 being the brightest coronal line and being situated in a region of the spectrum to which the human eye is most sensitive was naturally the first line to be observed. In later years through the persistent efforts of some of the greatest solar observers and by the use of varied types of spectroscopes and spectrographs, with slit and without slit, many more lines have been discovered in the bright-line spectrum of the corona extending from the near infra-red to well into the ultra-violet. In 1918 Campbell and Moore summarised all the information gathered from about half a century of eclipse observation. They listed forty lines observed by various authorities during totality as possibly of coronal origin. More than half of these have since been expunged from the coronal list as they are now known to belong to the chromosphere. After the 1930 eclipse Mitchell catalogued the wave-lengths and intensities of lines which were then believed to be truly coronal in origin ; there are, in all, nineteen lines in Mitchell's list which is reproduced below, but Mitchell thinks that one or two lines of this list may still be suspicious.

TABLE I

Wave-length in A.U.	Intensity	Wave-length in A.U.	Intensity	Wave-length in A.U.	Intensity
3328.00	8	4086.29	6	5302.91	20
3387.96	20	4231.40	8	5536.00	1
3454.13	8	4311.00	2	6374.28	12
3600.97	10	4359.00	4	6704.00	2
3642.87	3	4567.00	4	6776.00	8
3800.77	3	4586.00	2	—	—
3986.88	8	5117.00	2	—	—

The above list has been supplemented in later years by the discovery of new lines. Particularly noteworthy are the following infra-red lines discovered by Lyot by his new method of observing the corona without a solar eclipse (see Table II). Some observers have contended also that a few lines previously believed to be of chromospheric origin really belong to the corona. For instance, Righini[1] considers that the emission line at λ 5354.2 previously attributed to the chromosphere is a truly coronal line. Similarly, Sekiguti[2] argues that his and Tanaka's observations during the 1936 eclipse require that the line at λ 4725.3, which had been rejected from the coronal list as being insufficiently supported should be restored. He points out further that this line and several other lines observed in the emission spectrum of the corona by the Japanese observers are close to, if not identical with, certain lines in the spectra of nebulae and novae now known to be forbidden lines in the spectrum of N II. But mere coincidence between certain coronal lines and certain N II lines can scarcely be regarded as proof of the existence of nitrogen in the solar corona. In fact, astronomical literature abounds in instances in which astronomers have been temporarily misled by coincidences in wave-lengths into believing that certain substances have been identified in astronomical bodies. Many have been the attempts at identification of the coronal emission lines and several workers have found remarkable coincidences between these lines and certain lines of familiar elements, but in the long run such coincidences and identifications based on them have proved to be illusory. Fresh hopes were, however, raised when in 1927 Bowen made his great discovery that the so-called "nebulium" lines were caused by certain forbidden transitions of the oxygen and nitrogen atoms; and numerous attempts were made to identify the coronal lines as originating in similar forbidden transitions of known atoms, in neutral and ionised conditions, but all these efforts were singularly unsuccessful and the old riddle of the "coronium" remained unsolved.

TABLE II

Wave-length in A U.	Intensity
7059.62	4
7891.94	20
8024.21	13
10746.80	240
10797 95	150

EDLEN'S IDENTIFICATION OF CORONAL LINES

In the afore-mentioned attempts at identification of the coronal lines only the possible forbidden transitions of neutral atoms or of atoms which had lost at most three or four of the outer electrons were considered. But very recently Edlen of Uppsala, who has been studying the ultra-violet and X-ray spectra of highly stripped atoms, has advanced strong reasons justifying the conclusion that most of the prominent coronal lines arise from forbidden transitions of iron, nickel and calcium atoms from which a large number of electrons have been torn off. No copy of Edlen's original publication is available to us, but we understand that his identifications have been accepted by the astronomical spectroscopists of Harvard and by H. N. Russell whose authority in such matters must be regarded as deserving of the highest respect. In *Scientific American*, August, 1941, Russell specifically mentions the following identifications :

TABLE III

Wave-length of coronal line (in A U.)	Origin
5303	Fe XIV
10798, 10747, 3388	Fe XIII
7892	Fe XI
6374	Fe X
3601	Ni XVI

Several other observed lines can also be accounted for by iron, nickel and calcium ; but some predicted accessible lines of potassium, chromium, manganese and cobalt are not observed. It is to be noted in this connection that a little while ago D. N. Kundu[3] suggested that the line at λ 4359 may be due to Co^{+14}. Edlen's identifications of the coronal lines are not based on actual observation of the lines of Fe XVI and Ni XVI in laboratory spectra, but upon an extrapolation from some ions earlier in the sequence. The method is, however, regarded as highly satisfactory ; it was used some time ago in the successful identification of nine forbidden lines of Fe VII in the spectrum of Nova Pictoris.

ORIGIN OF HIGHLY STRIPPED ATOMS

If the identifications proposed by Edlen are correct, then the most important question, which requires an answer before anything else, is "How do such highly stripped atoms originate in the solar corona ?" In Edlen's scheme the energies of ionisation involved amount to hundreds of volts. If the extreme state of ionisation of the coronal atoms were due to the temperature of the corona, then the corona would have to be some twenty times as hot as the photosphere. The temperature of the inner corona is however believed, for very good reasons, to be of the order of only 3000°. An equally paradoxical situation arises if one tries to associate the temperature of the corona with the widths of the three prominent lines λ5303, λ6384, λ6704 which, according to Edlen, are due to iron. The equivalent widths of these lines as measured by Lyot[4] are 0.80 A, 0.97 A, and 1.07 A respectively: if these widths are taken to be due to Doppler effect arising from the random motion of the emitting particles, then the average velocity of the particles works out to be 32 km. per second. Now, if we identify this velocity with the mean square velocity of thermal agitation, then a very simple calculation shows that the temperature of the corona must be of the order of 2.3 million degrees, which is inconceivable. The only conclusion to be drawn from these paradoxes is therefore that here we have nothing to do with the temperature of the corona. One might imagine that the observed widths of the lines might arise from the mutual collisions (*i.e.*, pressure effect of the particles of the corona, but that would require the density of coronal matter to be absurdly high and quite inconsistent with the low-pressure criterion of the production of forbidden lines. The unquestionably low density of coronal matter also precludes the possibility of the broadening of the spectral lines arising out of Stark effect due to intense electrical fields. The simplest, and the most probable, explanation of the observed breadths of the coronal lines is therefore that the emitting particles are actually endowed with an average velocity of the order of 30 km /sec., but this velocity is quite unconnected with the temperature and the electrical state of the corona. This points to the source of the highly stripped atoms of the corona being located somewhere other than the corona itself; but we do not get from this any idea of the process responsible for producing the extreme state of ionisation of the atoms. Evidently one can imagine more than one process capable of meeting the situation. For instance, M. N. Saha[5] has suggested that "it is quite possible that stripped iron and nickel atoms are produced in the chromosphere or somewhat lower as a result of some type of nuclear reaction, analogous to uranium fission, and are projected upwards with energies amounting to millions of electron-volts." We do not know how far this view harmonises with the facts of solar observation; but in private correspondence Prof. Saha has told one of us that he is preparing a paper in which he is giving a detailed working out of the above idea. A. K. Das[6] on the other hand has suggested, from entirely different considerations, an alternative process which is also capable of accounting for the presence of highly stripped atoms in the solar corona. While awaiting the details of Saha's investigation and without claiming that Das's suggestion is in any way better than the view-point advocated by Saha, we work out in the present paper some details of the former suggestion. The process here considered is roughly as follows: The highly stripped atoms of the corona which are responsible for its bright-line spectrum originally formed part of the deep interior of the sun where the conditions of temperature, pressure and density are such that most of the outer electrons of atoms like iron, nickel, cobalt, calcium, etc., are torn off. Probably through local rises in radiation pressure these highly ionised atoms are ejected outwards and eventually reach different levels of the solar envelope depending upon their velocity of ejection. So long as the velocity of outward travel remains below a certain *critical velocity*, the state of ionisation of the atoms is determined at each level by the local thermodynamical conditions. But as soon as the outward velocity of the atoms exceeds the critical velocity, the ionisation of the ejected atoms departs materially from what would be expected from convective and thermodynamical equilibrium. It is postulated that at some level in the interior of the sun this is precisely what happens and thereafter the atoms capture no more electrons, so that they finish their journey in some level of the outer envelope in a state of ionisation quite inconsistent with the physical conditions of the layer where they are observed. It is to be expected, of course, that the critical level will be different for different elements. We now proceed to see how far this picture is supported by quantitative calculations in the case of iron, which we take as a typical case.

ESTIMATION OF CRITICAL VELOCITY

In the ordinary theory the state of ionisation of stellar material is calculated under equilibrium conditions. The ionisation equilibrium is however reached rather slowly, so that the state of ionisation of convecting matter must depend very greatly upon the speed of convection. This point has been clearly brought out in a recent paper by Sir A. S. Eddington[7] who has shown that for quite small speeds of convection the state of ionisation fails to keep pace with the changing pressure and temperature of the material. In our calculation of the critical velocity at which ionisation equilibrium in the case of the highly stripped iron atoms ejected from the deep interior of the sun breaks down, we have followed Eddington's method: we give below an outline of the method.

Consider two layers, A and B, in the interior of the sun, the latter being the deeper. A particular type of atom with a critical ionisation frequency ν loses $p-1$ electrons at A and p electrons at B. T_a and T_b are the temperatures and P_a and P_b are the pressures in the two layers. The ionisation in the column of material comprised between the two layers is regarded as being produced (directly or indirectly) by the photons entering at the base of the column; so that an increase in the degree of ionisation can only be produced by a difference between the number of competent photons entering and leaving. By Planck's law the numbers of photons n, with frequency equal to or greater than ν, contained in a cubic centimetre of radiation at the temperatures T_a and T_b are calculated. Then, under equilibrium conditions, $\frac{1}{4}n_a c$ and $\frac{1}{4}n_b c$ ionising photons per sq. cm. and per sec. will pass outwards across the layers A and B respectively,

c being the velocity of light. Therefore the number of ionising photons available per sec. for a column of unit cross-section bounded by the two layers will be $\frac{1}{4}c\,(n_b - n_a)$. The total number of atoms in the column is estimated from the difference in pressure between the two layers by making some reasonable assumption with regard to the relative abundance of the elements. If this number is N, then the time necessary for ionisation equilibrium to be established is $N/\frac{1}{4}c\,(n_b - n_a)$ and the critical velocity is $d/N.\frac{1}{4}c\,(n_b - n_a)$, where d is the distance between the layers.

In principle, the above procedure can be used for calculating the critical velocity of convecting matter at which ionisation equilibrium breaks down in any region in the interior of the sun, although the result, on account of the neglect of collision excitation and ionisation, should be regarded only as approximate. It has been found in the earlier papers of this series that many of the important features of prominences, dark markings, the chromosphere, the reversing layer, etc., can be quantitatively understood on the assumption that the matter taking part in these phenomena is supplied continually from the core which roughly corresponds to a sphere of $\frac{1}{3}$ of the radius of the sun. We therefore assume that the material of the corona also is derived from the same source. It is of particular interest to judge first in what state of ionisation atoms of iron would be if they came from the core and reached the corona without losing their ionisation.

On the basis of the theory of polytropic gas spheres, the temperature, pressure and density at the centre of the sun are 39×10^6, 124.8×10^{15} dynes/cm.^{2} and 76.7 respectively, taking the polytrope index $n = 3$, $\mu = 2.1$ and $\beta = 0.9501$ (the notation adopted is the same as that in Eddington's *Internal Constitution of Stars*). At a point distant $R_\odot/3.45$ from the centre, the temperature, pressure and density (derived with the help of Emden's tables) are respectively 23×10^6, 14.4×10^{15} dynes/cm^2 and 15.19. The ionisation of iron atoms in this layer computed from the formula

$$\log \frac{1-x}{x} = \frac{0.4343\psi}{RT} + \log \frac{\rho}{\mu T^{3/2}} + 8.3925 \quad \ldots \quad (1)$$

is presented in Table IV. $\frac{1-x}{x}$ is the ratio of the number of atoms with $p-1$ electrons missing to the number with p electrons missing, ψ is the ionisation potential of the pth electron, ρ and T are the density and temperature in the layer, and R is the Boltzmann constant. The mean atomic weight, μ, is taken to be 2.1 in all these computations.

It is clear from Table IV that 95% of the iron atoms in the layer under consideration have lost 24 or more of the outer electrons. If some of these stripped atoms are ejected with velocities high enough to bring about a complete break-down of ionisation equilibrium in the expelled mass of atoms, then the

TABLE IV

p	Ionisation potential expressed as critical wave-length, λ	$\frac{1-x}{x}$	Ratio of atoms with p electrons missing	% of atoms with p electrons missing
26	1.35	1.5	351	18.24
25	1.43	1.0	526	27.34
24	6.15	0.045	1000	51.98
23	6.57	0.042	45	2.34
22	7.15	—	2	0.10

Note —The ionisation potentials given here are different from the potentials for removing K, L etc. electrons as obtained from X-ray experiments, which refer to the case of knocking out the particular electron from a complete atom. The potentials given here refer to an ion from which the outer electrons have already been removed

corona may be expected to contain iron atoms which have only one or two of the normal 26 outer electrons. The fact that so highly ionised iron atoms are not detected in the corona would of course be no proof of their non-existence, because their spectrum lines are quite inaccessible to astronomical spectroscopy. But we think that iron atoms in such extreme states of ionisation really do not exist in the corona, and for reasons which will be apparent from the following considerations. If we calculate the critical velocity for the layer about R⊙/3 away from the centre of the sun, we get a value of the order of 10^5 km./sec., which is far too great to be exceeded by the actual velocity with which atoms may be ejected, so that in reality there will be no break-down of ionisation equilibrium. We have calculated the critical velocity for other layers progressively farther away from the centre of the sun and have obtained similar results. Then we have tried a region where the 14th electron of the iron atom is torn off : the boundaries chosen are at distances of $\frac{6.63}{6.90}$R⊙ and $\frac{6.68}{6.90}$R⊙ from the centre. The corresponding pressures, temperatures and densities are given in Table V. The states of ionisation at the two boundaries have been calculated with the help of equation (1) and presented in Table VI.

TABLE V

Boundary	Temperature*	Pressure	Density
$\frac{6.63}{6.90}$R⊙	4.7×10^6	2.59×10^9	0.0001325
$\frac{6.68}{6.90}$R⊙	3.9×10^6	1.25×10^9	0.0000767

TABLE VI

p	Ionisation potential in critical wave-lengths	% of atoms with p electrons missing	
		Upper boundary	Lower boundary
16	25.8	—	3.3
15	28.4	0.7	19.4
14	31.7	10.2	41.3
13	35.3	36.5	28.5
12	41.1	40.5	7.4
11	44.1	10.5	..
10	49.5	1.5	—

On account of the closeness of the ionisation potentials for successive electrons it is not possible to find a sharp boundary with a characteristic degree of ionisation. The difference in ionisation between the two boundaries can be summed up as follows: 31% of the iron atoms which have lost 12 electrons at the upper boundary lose the 13th and the 14th electrons at the lower boundary; 8% which have lost 13 electrons lose also the 14th and the 15th; 10% which have lost 11 electrons lose the 12th, 13th, 14th and 15th electrons.

The difference in pressure between the two boundaries is 1.34×10^9 dynes./cm.^{2}. Taking the mean value of gravity to be 2.929×10^4 cm /sec.^{2}, the mass of a column of unit cross-section enclosed between the two boundaries is 4.5×10^4 gm. The whole of this mass is, however, not due to iron. According to ideas underlying the present series of papers the material of the solar envelope is derived from the interior of the sun, so that there is no special reason to suppose that the material of the interior is essentially different in composition from the material of the envelope. We therefore take the composition of the envelope as given by Russell to be valid for the interior. From Russell's mixture we get the proportion of metals to the total mass as 32 : 132 and the ratio of iron to the metals by weight as 1000 : 4184. The mass of iron in the column under consideration is 2.65×10^3 gm. and the number of iron atoms in the column is therefore 2.86×10^{25}.

Now by Planck's law the density of radiation in a thermodynamical enclosure at temperature T is $\frac{8\pi h\nu^3}{c^3} \cdot \frac{1}{e^{h\nu/kT} - 1}$. For the very short wave-lengths under consideration this may be written as $\frac{8\pi h\nu^3}{c^3} . e^{-h\nu/kT}$. The density (*i.e.*, number/cm.^{3}) of photons of frequency equal to ν or greater than ν is therefore given by

$$\int_\nu^\infty 8\pi\frac{\nu^2}{c^3}\, e^{-h\nu/kT}\, d\nu = \frac{8\pi}{c^3} e^{-h\nu/kT}\left[\nu^2\frac{kT}{h} + 2\left(\frac{kT}{h}\right)^2 \nu + 2\left(\frac{kT}{h}\right)^3\right]$$

Consequently,

$$\frac{1}{4}\, nc = \frac{2\pi}{c^2} e^{-h\nu/kT}\left[\nu^2\frac{kT}{h} + 2\left(\frac{kT}{h}\right)^2 \nu + 2\left(\frac{kT}{h}\right)^3\right]. \qquad \ldots \quad (2)$$

From (2) we get for the value of $\frac{1}{4}\, nc$ for the lower and upper boundaries 2.985×10^{26} and 5.428×10^{25} respectively for wave-lengths shorter than 41.1A. Hence the number of photons available per second for ionising the column is 2.44×10^{26}.

From Table VI it will be seen that the critical ionisation wave-lengths for the different stages of ionisation vary between 28.4 A for the 15th electron and 41.1 A for the 12th electron. For wave-lengths below 28.4 A the value of log ($\frac{1}{4}\, nc$) at the lower boundary is 25.3278, while for $\lambda = 41.1$ A, it is 26.4749 ; the margin of variation is more than ten times. The absorption of photons by the iron atoms to attain equilibrium ionisation is as follows :

18% absorb below 28.4 A
49% absorb below 31.7 A
41% absorb below 35.3 A
10% absorb below 41.1 A

Thus the absorption is greater below $\lambda = 31.7$. To allow for this we take the total number of effective photons to be one-fifth of the value for $\lambda = 41.1$ A. Before proceeding to the estimation of the critical velocity, another important factor has to be considered. So far it has been tacitly assumed that all the photons are available for the ionisation of iron atoms ; this assumption is certainly not justified. In the layer under consideration the ionisation of most elements (other than hydrogen and helium) is incomplete, so that the atoms of these elements will naturally use up some of the available ionising photons. It may reasonably be assumed that the photons will be distributed among the different elements in accordance with their relative abundance. According to Russell's estimate the proportion of metallic atoms to all atoms (except H and He) is 1.14 : 3.14 and the ratio of iron atoms (atomic weight 55.84) to the metallic atoms (mean atomic weight 28) is $\frac{\cdot 100}{55.84} \cdot \frac{418}{28}$ or 1.791 ; 14.930. The proportion of ionising photons available to the iron atoms is therefore 0.04355, and accordingly the total number of photons available for ionising the iron atoms in the column under consideration is $2.44 \times 10^{26} \times 0.2 \times 0.04355$ or 21.25×10^{23}. The total number of photons required for equilibrium ionisation of the iron atoms is $\frac{2.86 \times 10^{25} \times 118}{100}$ or 3.37×10^{25}. Now the number of photons available per second is 21.25×10^{23}. Therefore the time required for ionisation equilibrium is 15.86 seconds. The distance between the two boundaries is 5039 km., and consequently the critical velocity for the break-down of ionisation equilibrium is 318 km./sec. This means that iron atoms travelling outwards with a velocity of the order of 300 km./sec. at a depth of about 26000 km. below the photosphere will have a good chance of reaching the corona with 11 to 15 of their outer electrons missing. We may note here that 300 km./sec. is quite a moderate speed compared to the scale of velocities sometimes observed even on the surface of the sun.

DISCUSSION AND CONCLUSIONS

Now the question is : " Is there any evidence to justify the conclusion that particles ejected from the interior of the sun actually travel with velocities of the order of 300 km./sec. or more at a depth of about 26000 km. below the photosphere?" Naturally there can be no direct evidence, but the evidence available, though indirect, appears to be decidedly in favour of this conclusion. The spectrum of the corona shows the Fraunhofer lines in addition to the emission lines superposed upon a faint continuous background. This Fraunhofer spectrum of the corona can only be the result of scattering of the disc spectrum by the particles in the higher reaches of the corona. From measurements of the plates secured during the 1922 and 1932 eclipses, Moore[8] comes to the conclusion that the scattering particles have an outward velocity of the order of 15 to 25 km./sec. Of course this velocity cannot be regarded as very accurate, but it may be taken to represent the right order of magnitude. There seems to be some doubt as to the identity of the scattering particles. According to a view expressed by Grotrian[9] which seems at present to be rather widely accepted, they must be considerably larger than ordinary molecules. If Grotrian's view is correct, these particles could not have come as such from the interior, and therefore they would have acquired their outward velocity through bombardment by other particles coming from below the corona. If we identify these latter with the particles ejected from the interior of the sun, then we must expect them to possess, when they reach the corona, a velocity considerably higher than 15 to 25 km./sec. When one considers the retarding forces which must operate upon particles travelling from the depth of some 26000 km. below the photosphere to a height of 10′ to 20′ above the limb (where the above velocity has been measured), a diminution of the initial velocity by a factor of 10 or more seems entirely probable. Thus the depleted Fe atoms ejected from the deep interior of the sun may very well have a velocity of 300 km./sec. or higher during their outward travel through the

26000 km. level. Of course, on account of the nature of the data available for the calculations, the position of the critical level should be regarded only as a rough estimate, but the significant point is that the calculations indicate the existence of such a level for the Fe^{+13} and Fe^{+12} atoms.

The boundary at which ionisation equilibrium fails will be different for different atoms depending upon the ionisation potentials, the atomic weights and the abundances of the different species. The ionisation potentials for the 14th electron of Fe, the 15th electron of Co and the 16th electron of Ni are as 29 : 32 : 36. These are so close to each other that ionisation equilibrium for all these three atoms will break down in a fairly thin layer not very far from the 26000 km. level calculated above. This helps us to understand to some extent at least why the lines of these atoms appear prominently in the coronal spectrum. Another point which looks favourable to the process imagined in the present paper is that the lines identified by Edlen as being due to Fe^{+13} and Fe^{+12} are stronger than those which arise from less highly ionised iron atoms. The intensity of any emission line in the corona will depend upon the abundance of the appropriately ionised atoms and the probability of the transition which gives rise to the line. If ionisation equilibrium breaks down in the region considered above, then the number of Fe^{+10} and Fe^{+9} atoms in the corona will be much less than the number of Fe^{+13} and Fe^{+12} atoms. This may partly explain the greater intensity of the Fe^{+13} and Fe^{+12} lines over the Fe^{+10} and Fe^{+9}.

The outer parts of the corona which scatter the Fraunhofer spectrum are believed to consist of particles much larger than ordinary molecules. In fact, according to Grotrian, the sun is surrounded by a dust-cloud (perhaps of meteoric origin) which is composed of particles having about 3 times the size of an ordinary molecule. Observational data show that the Fraunhofer lines of the corona are displaced with respect to those of the disc spectrum in a way which shows that the dust-cloud is moving outwards with a velocity of 15 to 25 km./sec.; also the coronal Fraunhofer lines are not wider than the ordinary Fraunhofer lines, showing that the scattering particles are not endowed with any extraordinary random motion. At the same time the widths of the emission lines $\lambda 5303$, $\lambda 6374$ and $\lambda 6704$ show that the emitting Fe atoms have a random velocity of the order of 32 km./sec. These observational facts are just what one would expect from the process imagined in the present paper as will be seen from the following considerations. The particles coming from the interior would have to possess a velocity of 50 km./sec. or more outside the photosphere in order that they may reach the outer corona; this follows from a rough calculation based on the equations of motion derived in the earlier parts of this series of papers. These particles will, through impact, impart an outward velocity to the heavier particles of the dust-cloud which will therefore show an expansive velocity of a smaller magnitude than the velocity of the particles coming from the interior. The impinging particles will, on the other hand, be slowed down and deflected through collisions ; this will appear as an average random velocity which will show itself as a broadening of the emission lines.

Finally, we may also mention the general correspondence which exists between solar activity as judged from sunspots, prominences, eruptive phenomena, etc., and the intensity of the coronal emission lines. Solar activity is admittedly due to some deep-seated variations in the interior of the sun, and therefore the above correspondence points to the interior as the probable place of origin of the highly stripped atoms of the corona. The same indication is given by the fact that some of the prominent coronal lines are observed also in certain novæ.

Note added in proof

Soon after the present paper was sent out for publication Prof. Saha's paper entitled "On a physical theory of the solar corona" appeared in the *Proc. Nat. Inst. of Sc. of India*, Vol. VIII, pp. 99-126. The standpoints of the two papers are so fundamentally different from each other that it does not seem profitable yet to compare them. Both theories require to be developed much further and given greater definiteness before it can be possible to form a reliable judgment in favour of one to the exclusion of the other.

SOLAR PHYSICS OBSERVATORY,
KODAIKANAL, SOUTH INDIA.

REFERENCES

[1] Abetti, *The Sun*, p. 253 (1938).
[2] Sekiguti, *Nature*, **140**, 724 (1937)
[3] Kundu, *Science and Culture*, **7**, 364 (1942).
[4] Lyot, *Bull. Sc. Astr. de France*, **51**, 203 (1937).
[5] Saha, *Science and Culture*, **7**, 251 (1941)
[6] Das, *Science and Culture*, **7**, 357 (1942).
[7] Eddington, *M.N R.A.S.*, **101**, 177 (1941).
[8] Moore, *P.A S.P.*, **35**, 333 (1923).
[9] Grotrian, *Zeit. f. Astrophys.*, **8**, 124 (1934).

THE STRUCTURE OF ATOMIC NUCLEI

By M. F. SOONAWALA

(*Received for publication, May 6, 1942*)

ABSTRACT. · The possibility of atomic nuclei consisting of smaller nuclei of comparable masses is discussed. The depth and width of the potential holes corresponding to the nuclear energy are calculated for some nuclei. The expected masses and charges of the exchange particles holding the nuclei together are calculated for some cases. The nuclear spins of some of the rare gases are derived by comparison.

The study of the properties of the atomic nucleus has received much attention in recent years both from the theoretical and the experimental standpoints. Prominent among these has been the work of Bohr who has considered in detail a model of the nucleus, now familiar as the liquid drop model. On the other hand, the essence of a theory propounded by the present writer some years ago[1] is to consider the nucleus as resembling a binary or multiple stellar system in which there are a few components of comparable masses. A few simple assumptions led to a unified scheme of arrangement of the different elements, which fell into naturally related groups. The components of the nucleus were assumed to be provided by the rare gas nuclei and the protons. Considering only the binary systems composed of two components, a satisfactory picture was obtained of the building up of chemically similar nuclei. On making a second assumption of positron emission (the newer version of electronic absorption), whole series of chemically similar elements take up their places in a natural way in a new kind of periodic table, which is reproduced here as Table I. The fundamental particles have since increased in number following the discovery of the neutron, the positron, the mesotron, and possibly the neutrino and the antineutrino. A large number of new isotopes has also been discovered, and the laws of interaction have been investigated. The inherent consistency of the original scheme makes it worth our while to revise and re-assess it in the light of these new discoveries.

The large number of isotopes which have been discovered during the past few years fit in well into the scheme for two nuclei made up of two components. A very complete list of the lighter isotopes up to mass 40 has been given by Barkas.[2] The isotopes of Na, Mg, K and Ca, and most of Cl, fit in quite well, isotope by isotope, as constituted of Ne, A and He nuclei and protons. The existence of a number of isotopes of Ba has come to light and these find places in the nuclei originating from X.

TABLE I

	H	He	Ne			A			Kr						X									Rn
			(18-27)			(35-40)																		
	1	4	20	21	22	36	38	40	78	80	82	83	84	86	124	126	128	129	130	131	132	134	136	222
H	—	—	—	—	Na	Cl	K	K	Br	Br	—	—	Rb	Rb	—	I	—	—	--	—	Cs	—	—	—
			Na(20-29)			Cl(32—40) K(36—40)																		
He	—	—	Mg	Mg	Mg	Ca	Ca	Ca	Se	Sr	Sr	Sr	Sr	Zr	Te	Te	—	--	Ba	Ba	Ba	Ba	Ce	Ra
			Mg 22-31			Ca(38—45)																		
Ne	—	—	—			Atc wts: 56-62 (53-67) Atc No.: 28 and less Ni, Fe, Co: Wt: 54-62 Nos: 26, 27, 28.			Atc. wts.: 98-108 (96—113) Atc. Nos.: 46 and less. Ru, Rh, Pd, Mo, Ma: Atc. wts: 96-108: Atc Nos: 42, 43, 44, 45, 46.						Atc. wts 144-158 (142-163); Atc. Nos.: 68 and less. Atc. wts. of Group I of rare earths, La to Gd: 139—158 Atc. Nos. of Group I of rare earths: 57-64.									—
A	—	—	—			—			Atc wts.: 114-126 (113-126) Atc Nos: 54 and less. Cd, In, Sn, Sb, Te: Atc. wts.: 106-124; Atc. Nos: 48-52.						Atc wts: 160-176 (159—176); Atc Nos: 72 and less. Group II of rare earths: Tb to Hf: Atc. wts: 159-176: Atc. Nos.: 65-72.									—
Kr	—	—	—			—			—						Atc wts: 202—222; Atc. Nos. 90 and less. Radioactive elements: Atc. wts: 206—238: Atc. Nos: 92 and less									—
X	—	—	—			—			—						—									—

This table primarily includes the commoner isotopes[4]. Figures in brackets indicate inclusion of all the isotopes of Ne, A and the synthesised elements about whose existence there is any evidence

Coming to the question of the interaction forces holding the nucleus together, we cannot do better than follow the lead of the well-determined investigations into the structure of the deuteron. The nature of the force there found is of the exchange type, first introduced by Majorana. We may imagine the deuteron nucleus as composed of two neutrons with a positron moving between them, attaching itself to the neutrons alternately. During the period of such an attachment the neutron becomes a proton, and the nucleus consists of a neutron and a proton. When the positron disengages itself from the proton and goes over to the neutron, the nucleus once again consists of a proton and a neutron, with their positions virtually interchanged. This mechanism may or may not correspond to reality in nature; but the force derived from this idea of the interchange of positions of the constituents of the nucleus has been shown to be sufficient to hold the deuteron nucleus together. The potential function is found to be of the form $Ve^{-\lambda r}/r$, where $1/\lambda$ defines the range of the internuclear force and is given by

$$\lambda = \frac{2\pi Mc}{h},$$

where M is the mass of the exchange particle.[3] This range is taken extremely small, the exchange force being effective for values smaller than this and virtually disappearing at greater distances. The depth, V, of the potential hole, and its breadth have been investigated for certain representative forms of the function.[4] To calculate the approximate values of the depth and breadth of the potential hole of the deuteron nucleus, we follow the general procedure adopted by Bethe and Bacher.[5] The wave equation for a nucleus made up of two nuclei of masses M_1 and M_2 can be written down as

$$\frac{1}{M_1}\left(\frac{\partial^2\psi}{\partial x_1^2}+\frac{\partial^2\psi}{\partial y_1^2}+\frac{\partial^2\psi}{\partial z_1^2}\right)+\frac{1}{M_2}\left(\frac{\partial^2\psi}{\partial x_2^2}+\frac{\partial^2\psi}{\partial y_2^2}+\frac{\partial^2\psi}{\partial z_2^2}\right)+\frac{8\pi^2}{h^2}E_0\psi$$
$$=\frac{8\pi^2}{h^2}.J(r).[\psi]. \qquad (1)$$

Here ψ signifies a function of the co-ordinates, as

$$\psi \equiv \psi(x_1, y_1, z_1, s_1\ ;\ x_2, y_2, z_2, s_2)\ ; \qquad \dots \quad (2a)$$

and $[\psi]$ the same function with positional co-ordinates interchanged, as

$$[\psi] \equiv \psi(x_2, y_2, z_2, s_1\ ;\ x_1, y_1, z_1, s_2). \qquad \dots \quad (2b)$$

Here x_1, y_1, z_1, s_1 denote the co-ordinates of position and the spin of M_1, and x_2, y_2, z_2, s_2, similar quantities for M_2. The equation indicates an exchange force of the Majorana type, only the spatial co-ordinates of M_1 and M_2 being interchanged without their spins being affected. The condition for this is that

$$\psi(x_2, y_2, z_2, s_1\ ;\ x_1, y_1, z_1, s_2) = F_1(x_2, y_2, z_2\ ;\ x_1, y_1, z_1).F_2(s\ , s_2) \qquad \dots \quad (3)$$

and

$$\psi(x_1, y_1, z_1, s_1\ ;\ x_2, y_2, z_2, s_2) = F_1(x_1, y_1, z_1\ ;\ x_2, y_2, z_2).F_2(s_1, s_2). \qquad \dots \quad (4)$$

This reduces (1) to

$$\frac{1}{M_1}\Delta_{x_1}F_1(x_1, x_2)+\frac{1}{M_2}\Delta_{x_2}F_1(x_1, x_2)+\frac{8\pi^2}{h^2}E_0F_1(x_1, x_2)$$

$$=\frac{8\pi^2}{h^2}J(r)\,F_1(x_2, x_1). \quad \dots \quad (5)$$

Here x_1 and x_2 denote, in short, all the co-ordinates x_1, y_1, z_1, and x_2, y_2, z_2. $J(r)$ is the potential energy. We introduce new variables x, y, z, describing the motion of the centre of mass of the system, and r, θ, ϕ, the polar co-ordinates of M_2 relative to M_1. The relation between the different co-ordinates is given by

$$x=\frac{M_1x_1+M_2x_2}{M_1+M_2}, \quad \dots \quad (6)$$

$$y=\frac{M_1y_1+M_2y_2}{M_1+M_2}; \quad \dots \quad (7)$$

$$z=\frac{M_1z_1+M_2z_2}{M_1+M_2}; \quad \dots \quad (8)$$

$$r\sin\theta\cos\phi=x_2-x_1; \quad \dots \quad (9)$$

$$r\sin\theta\sin\phi=y_2-y_1; \quad \dots \quad (10)$$

$$r\cos\theta=z_2-z_1. \quad \dots \quad (11)$$

The introduction of these co-ordinates reduces (5) to

$$\frac{1}{M_1+M_2}\left(\frac{\partial^2F_1}{\partial x^2}+\frac{\partial^2F_1}{\partial y^2}+\frac{\partial^2F_1}{\partial z^2}\right)+\frac{2}{M}\left\{\frac{1}{r^2}\cdot\frac{\partial}{\partial r}\left(r^2\frac{\partial F_1}{\partial r}\right)+\frac{1}{r^2\sin^2\theta}\cdot\frac{\partial^2F_1}{\partial\phi^2}\right.$$

$$\left.+\frac{1}{r^2\sin\theta}\cdot\frac{\partial}{\partial\theta}\left(\sin\theta.\frac{\partial F_1}{\partial\theta}\right)\right\}+\frac{8\pi^2}{h^2}E_0\psi=\frac{8\pi^2}{h^2}.J(r).F_1(x, y, z, -r) \quad \dots \quad (12)$$

Here M/2 is the reduced mass of the system given by

$$M=\frac{2M_1M_2}{M_1+M_2}. \quad \dots \quad (13)$$

We separate the equations by expressing F_1 as the product of a function of x, y, z, and a function of r, θ, ϕ.

$$F_1(x, y, z, r, \theta, \phi)=F(x, y, z).U(r, \theta, \phi). \quad \dots \quad (14)$$

Introducing this in (12), it separates out into the two equations

$$\frac{\partial^2F}{\partial x^2}+\frac{\partial^2F}{\partial y^2}+\frac{\partial^2F}{\partial z^2}+\frac{8\pi^2}{h^2}(M_1+M_2)E_1.F=0, \quad \dots \quad (15)$$

and $$\frac{1}{r^2}\cdot\frac{\partial}{\partial r}\left(r^2\frac{\partial U}{\partial r}\right)+\frac{1}{r^2\sin^2\theta}\frac{\partial^2U}{\partial\phi^2}+\frac{1}{r^2\sin\theta}\cdot\frac{\partial}{\partial\theta}\left(\sin\theta.\frac{\partial U}{\partial\theta}\right)$$

$$+\frac{4\pi^2M}{h^2}E.\ U(r)=\frac{4\pi^2}{h^2}M.\ J(r).\ U(-r)=0; \quad \dots \quad (16)$$

with
$$E_1+E=E_0. \qquad \ldots \quad (17)$$
The equation (16) can be expressed as

$$\frac{h^2}{4\pi^2 M}.\Delta U(r)+E.\,U(r)=J(r).\,U(-r). \qquad \ldots \quad (18)$$

Here

$$-E=\epsilon, \qquad \ldots \quad (19)$$

the binding energy of M_1 and M_2.

Assuming the potential energy to be spherically symmetrical, we can separate (18) into the polar coordinates; as

$$U(r)=\frac{U_l(r)}{r}\,.\,P_{lm}(\theta).e^{im\phi} \qquad \ldots \quad (20)$$

P_{lm} being a spherical harmonic duly normalized. Now, if the polar coordinates of a point x, y, z, are r, θ, ϕ, those of the point $-x, -y, -z$, will be r, $\pi-\theta$, $\pi+\phi$. Also,

$$P_{lm}(\pi-\theta)e^{im(\pi+\phi)}=(-1)^l.P_{lm}(\theta)e^{im\phi}\,. \qquad (21)$$

The wave-equation for u becomes

$$\frac{h^2}{4\pi^2 M}\left(\frac{\partial^2 u_l}{\partial r^2}-\frac{l(l+1)}{r^2}u_l\right)+Eu_l=(-1)^l.\,J(r).u_l. \qquad (22)$$

For the ground state, $l=0$, and assuming J to be negative,

$$-\frac{h^2}{4\pi^2 M}\frac{d^2u}{dr^2}=\{J(r)-E\}.u, \qquad (23)$$

u is not to become infinite for large values of r, and is to vanish as r for small values of r. $J(r)$ has the essential character of an exchange force, being effective within a range a, say, and becoming negligible in comparison with E for $r>a$.

We have assumed the exchange interaction potential to be of the form

$J(r)=-V.\frac{e^{-\lambda r}}{r}$, the range $\frac{1}{\lambda}$ being defined by

$$\lambda=\frac{2\pi M'c}{h}, \qquad \ldots \quad (24)$$

M' being the mass of the exchange particle. With

$$J(r)=-V.\frac{e^{-\lambda r}}{r}, \qquad \ldots \quad (25)$$

equation (23) becomes

$$\frac{d^2u}{dr^2}=\frac{4\pi^2 M}{h^2}\left(-V.\frac{e^{-\lambda r}}{r}-E\right)u. \qquad \ldots \quad (26)$$

If we put

$$x=\lambda r, \qquad \dots (27)$$

then,

$$\lambda=\frac{dx}{dr}$$

and

$$\frac{d}{dr}\left(\frac{du}{dr}\right)=\frac{d}{dr}\left(\frac{dx}{dr}\,\frac{du}{dx}\right)=\frac{dx}{dr}\cdot\frac{d}{dx}\left(\frac{dx}{dr}\,\frac{du}{dx}\right)=\lambda^2\frac{d^2u}{dx^2}. \qquad \dots (28)$$

Equation (26) becomes

$$\lambda^2\frac{d^2u}{dx^2}=-\frac{4\pi^2M}{h^2}\left(\lambda . V\frac{e^{-x}}{x}+E\right)u. \qquad \dots (29)$$

Or,

$$\frac{d^2u}{dx^2}+\frac{4\pi^2MV}{h^2\lambda}\cdot\frac{e^{-x}}{x}\cdot u-\frac{4\pi^2M\epsilon}{h^2\lambda^2}u=0 \qquad \dots (30)$$

This can be put in the form

$$\frac{d^2u}{dx^2}+a\left(\frac{e^{-x}}{x}-b\right)u=0 \qquad \dots (31)$$

with

$$a=\frac{4\pi^2MV}{h^2\lambda}, \qquad \dots (32)$$

and

$$b=\frac{\epsilon}{V\lambda}. \qquad \dots (33)$$

At $x=0$, (31) assumes the form

$$\frac{d^2u_0}{dx^2}+\frac{a}{x}.u_0=0. \qquad \dots (34)$$

The function,

$$u_0=A.x.e^{-\frac{a}{2}x} \qquad \dots (35)$$

satisfies this relation, because

$$\frac{d^2u_0}{dx^2}=-\frac{au_0}{x}+\frac{a^2}{4}u_0\,; \qquad \dots (36)$$

which, for $x\longrightarrow 0$, becomes

$$\frac{d^2u_0}{dx^2}+\frac{au_0}{x}=0. \qquad \dots (37)$$

Following the procedure adopted in similar cases,[6] we put the solution to be

$$u=u_0v \qquad \dots (38)$$

where v is developable in a series. On substituting in (31),

$$v'' + v'\left(\frac{2}{x} - a\right) + av\left(\frac{e^{-x}}{x} - \frac{1}{x} + \frac{a}{4} - b\right) = 0 \qquad \text{.. (39)}$$

or

$$v'' + v'\left(\frac{2}{x} - a\right) + av\left(\frac{a}{4} - b - 1 + \frac{x}{2\,!} - \frac{x^2}{3\,!} + \ldots\ldots\right)$$

$$\equiv v'' + p(x).v' + q(x)v$$

$$= 0\,; \qquad \text{... (40)}$$

where $p(x)$ and $q(x)$ are the coefficients of v' and v. Here $p(x)$ has a pole of the first order at $x=0$, and $q(x)$ has no pole of an order higher than the second. We put[7]

$$L(v) \equiv x^2 v'' + x(2 - ax)v' + v\left(\frac{a^2}{4}x^2 - abx^2 - ax^2 + \frac{ax^3}{2\,!} - \frac{ax^4}{3\,!} + \ldots\ldots\right)$$

$$\equiv x^2 v'' + v'P_1(x) + vP_2(x)$$

$$= 0. \qquad \text{... (41)}$$

Here, let

$$P_1(x) = \alpha_0 + \alpha_1 x + \alpha_2 x^2 + \ldots \qquad \text{... (42)}$$

and

$$P_2(x) = \beta_0 + \beta_1 x + \beta_2 x^2 + \ldots \qquad \text{... (43)}$$

Comparing (42) and (43) with (41),

$$\alpha_0 = 2,$$

$$\alpha_1 = -a,$$

and

$$\alpha_n = 0 \qquad (\text{for } n > 1) \qquad \text{... (44)}$$

and

$$\beta_0 = 0,$$

$$\beta_1 = 0,$$

$$\beta_2 = \frac{a^2}{4} - ab - a,$$

$$\beta_3 = \frac{a}{2\,!}$$

$$\beta_4 = -\frac{a}{3\,!}, \text{ etc.} \qquad \text{.. (45)}$$

We express v as the series

$$v = x^p(c_0 + c_1 x + c_2 x^2 + \ldots). \qquad \text{.. (46)}$$

In general, with

$$L(x) = x^p(f_0 + f_1.x + f_2.x^2 + \ldots) \qquad \text{... (47)}$$

the coefficients c's are obtained by making the individual coefficients in (47) vanish ; when we get

$$f_0(\rho)=\rho(\rho-1)+\rho.\alpha_0+\beta_0,$$

$$f_1(\rho)=\rho.\alpha_1+\beta_1$$

$$f_n(\rho)=\rho.\alpha_n+\beta_n. \qquad \dots \quad (48)$$

In our case

$$f_0(\rho)=\rho(\rho-1)+2\rho$$

$$f_1(\rho)=-a\rho$$

$$f_2(\rho)=a\left(\frac{a}{4}-b-1\right)$$

$$f_3(\rho)=\frac{a}{2\,!}$$

$$f_4(\rho)=-\frac{a}{3\,!}, \text{ etc.} \qquad \dots \quad (49)$$

The coefficients c's satisfy the equations

$$c_0.f_0(\rho)=0, \qquad \dots \quad (50)$$

$$c_1.f_0(\rho+1)+c_0.f_1(\rho)=0, \qquad \dots \quad (51)$$

$$c_2.f_0(\rho+2)+c_1.f_1(\rho+1)+c_0.f_2(\rho)=0, \qquad \dots \quad (52)$$

etc.

The first of these gives the indicial equation ; for,

$$\rho(\rho-1)+2\rho=0 \qquad \dots \quad (53)$$

giving the values

$$\rho=0$$

and

$$\rho=-1.$$

For $\rho=0$, (51) gives

$$c_1=0\,; \qquad \dots \quad (54)$$

$$c_2=-\frac{1}{6}a\mathrm{B}\,; \qquad \dots \quad (55)$$

where

$$\mathrm{B}=\frac{a}{4}-b-1\,; \qquad \dots \quad (56)$$

$$c_3=-\frac{1}{12}c_0.a\left(\frac{a\mathrm{B}}{3}+\frac{1}{2}\right); \qquad \dots \quad (57)$$

$$c_4=\frac{c_0.a}{120}\left\{1+a\mathrm{B}^2-\frac{a^2\mathrm{B}}{2}-\frac{3a}{4}\right\}, \qquad \dots \quad (58)$$

etc.

For $\rho=-1$, we get identical coefficients for the series in v, which is to be expected as the two values of ρ differ by unity. A second solution would be of the form

$$v = g.v_1(x).\log x + v_2(x), \qquad \dots (59)$$

where
$$v_1 = c_0 + c_1x + c_2x^2 + \dots \qquad \dots (60)$$

and
$$v_2 = c'_0 + c'_1x + c'_2x^2 + \dots \qquad \dots (61)$$

The solution (59) contains the term $\log x$; and, therefore, it is of no interest to us.[6]

Thus we take

$$v = A.v_1(x). \qquad \dots (62)$$

From this,

$$u = A.x.e^{-\frac{ax}{2}}.v = A.x.e^{-\frac{ax}{2}}(c_0 + c_2x^2 + c_3x^3 + \dots) \qquad \dots (63)$$

and
$$u' = A.e^{-\frac{ax}{2}}(c_0 + c_2x^2 + c_3x^3 + \dots) - \frac{A.a}{2}x\,e^{-\frac{ax}{2}}(c_0 + c_2x^2 + c_3x^2 + \quad)$$

$$+ A.x.e^{-\frac{ax}{2}}(2c_2x + 3c_3x^3 + 4c_4x^3 + \dots)$$

$$= A.x.e^{-\frac{ax}{2}}\left\{\frac{c_0}{x} - \frac{ac_0}{2} + 3c_2x + \left(4c_3 - \frac{ac_2}{2}\right)x^2 + \left(5c_4 - \frac{ac_3}{2}\right)x^3 + \dots \right. \quad (64)$$

Putting u and u' in the form

$$u = A.c_0.x.e^{-\frac{ax}{2}}(1 + b_1x + b_2x^2 + \dots) \qquad \dots (65)$$

and
$$u' = A.c_0.x.e^{-\frac{ax}{2}}\left(\frac{1}{x} - a_0 + a_1x - a_2x^2 + \dots\right), \qquad \dots (66)$$

$$\frac{u'}{u} = \frac{1}{x} - a_0 + (a_1 - b_2)x + (a_0b_2 - a_2)x^2 + \dots$$

$$= \frac{1}{x} - \frac{a}{2} + \frac{ax}{3}\left(1 + b - \frac{a}{4}\right) + \frac{ax^2}{3}\left(-\frac{a^2}{12} + \frac{ab}{3} + \frac{a}{3} - \frac{1}{2}\right) + \dots \qquad \dots (67)$$

Following Bethe and Backer, we can derive some useful information from (67). For, J(r) or V can be assumed to be negligible for $r > 1/\lambda$; *i.e.*, $x > 1$. Then (30) reduces to

$$\frac{d^2u}{dx^2} = \frac{4\pi^2 M\epsilon}{h^2\lambda^2}.x. \qquad \dots (68)$$

Or
$$u = c.e^{-\frac{2\pi\sqrt{M\epsilon}}{h\lambda}.x} \qquad \dots (69)$$

and
$$u' = -\frac{2\pi c\sqrt{M\epsilon}}{h\lambda}.e^{-\frac{2\pi\sqrt{M\epsilon}}{h\lambda}.x}. \qquad \dots (70)$$

so that
$$\frac{u'}{u} = -\frac{2\pi\sqrt{M\epsilon}}{h\lambda}. \qquad \dots (71)$$

The shape of the u—x curve is as shown in Fig. 1.

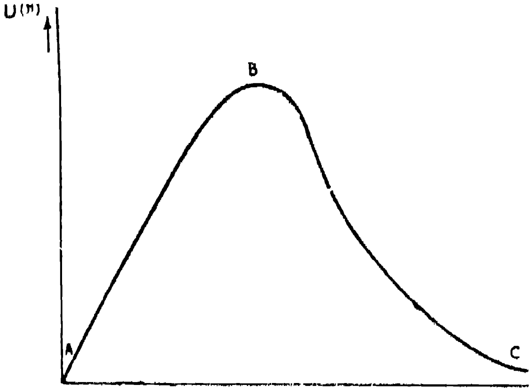

Fig. 1

If we evaluate u'/u for any point, and if it is found to be positive, the point must lie on the ascending part of the curve, AB. Similarly, a point for which u'/u is negative lies on the descending part BC of the u—x curve. The former condition holds for too low a value of $J(r)$ and indicates instability; while, on the other hand, the latter condition denotes stability. We may suppose the values of u'/u calculated for $x > 1$ and for $x < 1$ to join up smoothly at $x = 1$.

To a first approximation, from (67)

$$\frac{u'}{u} = 1 - \frac{a}{2}. \qquad \ldots (72)$$

Equating this to (71)

$$1 - \frac{a}{2} = -\frac{2\pi\sqrt{M\epsilon}}{h\lambda}. \qquad \ldots (73)$$

Substituting the values $M = 1.67 \times 10^{-24}$ gm., $\epsilon = 3.42 \times 10^{-6}$ erg., $M' = 130 \times$ the electronic mass, we find for the deuteron nucleus,

$$\frac{2\pi\sqrt{M\epsilon}}{h\lambda} = 0.68. \qquad \ldots (74)$$

This gives

$$a = 3.36. \qquad \ldots (75)$$

Retaining terms including x in (67), we get the second approximation,

$$1 - \frac{a}{2} - \frac{a^2}{12} + \frac{ab}{3} + \frac{a}{3} = -0.68. \qquad \ldots (76)$$

From (32) and (33)

$$ab = \frac{4\pi^2 M\epsilon}{h^2\lambda^2} = 0.46. \qquad \ldots (77)$$

This gives

$$a = 3.8. \qquad \ldots (78)$$

Retaining terms up to x^2 in (67), we get the further approximation

$$\frac{u'}{u} = 1 + \frac{ab}{3} - \frac{a}{3} + \frac{a}{9} \times ab + \frac{a^2}{36} - \frac{a^3}{36} = -0.68. \qquad \ldots \quad (79)$$

This cubic equation is satisfied for the value

$$a = 3.5. \qquad \ldots \quad (80)$$

Adopting this value of a, (32) gives

$$V = \frac{ah^2\lambda}{4\pi^2 M} = 7.7 \times 10^{-18}. \qquad \ldots \quad (81)$$

From (81) and (24),

$$\lambda . V . = 2.60 \times 10^{-5} \text{ erg} = 16.4 \text{ million electron-volts.} \qquad \ldots \quad (82)$$

The essence of the exchange theory is that two of the constituent particles of the nucleus virtually exchange their positions, and this is effected by the exchange particle transferring itself periodically from one of them to the other. The aid of a similar mechanism can be invoked to form a basis of the hypothesis advanced here that the rare gas nuclei form the principal constituents of the other nuclei. Thus a nucleus will consist of two equal particles of equal mass at equal distances and in line with a residual particle of the remainder of the mass of the nucleus. If this residual particle be taken at the centre of the co-ordinates, the co-ordinates of the two equal particles will be taken to be x and $-x$ respectively. According to our view, each of these equal terminal particles will be one of the rare gas nuclei composing the nucleus. Thus, Na^{23} nucleus will consist of two particles of protonic mass with a residual particle of mass 21 between them (Fig. 2).

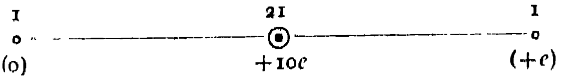

FIG. 2

The exchange particle will be a heavy positive electron oscillating between the extreme particles and converting each of them in turn from proton to neutron and back to proton, exactly as in deuteron. The central particle will then carry a charge $+10e$. Similarly the structure of Mg^{26} nucleus would be represented by Fig. 3.

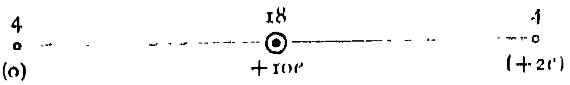

FIG. 3

The moments of inertia of some nuclei are known. For example,[8] the moment of inertia of B^{10} is 1.2×10^{-48}; of Mg^{26}, 6.25×10^{-48}; and of AcX^{228}, 2.2×10^{-46}. If I represents the moment of inertia and A the atomic number, then, the relation between log I and log A is very truly linear for the above three values, indicating the relation $I = 2.53 \times 10^{-50} \times A^{1.676}$. Thus, for Ba^{138},

$I = 1.0 \times 10^{-46}$. Presuming the structure of the Ba^{138} nucleus to be represented by Fig. 4, the distance between the extreme particles would be given by 1.0×10^{-46}

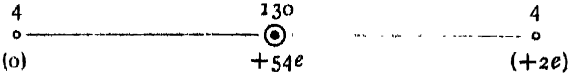

FIG. 4

$= 8 \times 1.67 \times 10^{-24} \times r^2$; or, $2r = 5.47 \times 10^{-12}$ cm. Similarly, for, Mg^{26}, $2r = 1.37 \times 10^{-12}$ cm. Taking these distances as the range, $1/\lambda$, of the interaction forces, we can calculate the mass, M, of the exchange particle from

$$M = \frac{h\lambda}{2\pi c}.$$

For Ba^{138}, $M = 6.35 \times 10^{-27}$ gm. $= 7.01 \times m$, and for Mg^{26}, $M = 2.535 \times 10^{-26}$ gm. $= 28.05 \times m$, where m is the electronic mass. We may, therefore, expect to find particles of masses $7 \times m$ and $28 \times m$ and of charge $+2e$ in any process involving the disintegration of the Mg^{26} and Ba^{138} nuclei.

We have assumed the constituents of the Mg^{26} nucleus to be Ne^{22} and He^4; and, therefore, the binding energy of Mg^{26} would be given by the mass defect of the constituent particles, and would amount to 1.91×10^{-5} erg. Applying as in (79), with $M = 6.68 \times 10^{-24}$ gm., $ab = 220.2$, and $a = 31.7$. Then, (32) would give $V = 3.8 \times 10^{-18}$. Similarly, for Ba^{138}, $a = 129$, and $V = 3.8 \times 10^{-18}$. Table II shows similar calculations for some other nuclei.

TABLE II

	$E \times 10^5$ ergs	$1/\lambda \times 10^{12}$ cm.	$I \times 10^{48}$ gm. cm.^{2}	M	e
Na^{23}	1.003	2.41	4.85	15.9	1
K^{39}	1.115	3.75	11.72	10.25	1
Cs^{133}	0.601	10.48	91.67	3.66	1
Mg^{24}	1.545	1.248	5.20	30.8	2
Mg^{25}	1.467	1.29	5.56	29.05	2
Mg^{26}	1.912	1.368	6.25	28.05	2
Ca^{40}	1.184	1.913	12.2	20.08	2
Ba^{138}	2.254	5.47	100.0	7.01	2
Cl^{35}	2.65	3.443	9.91	11.16	1
Cl^{37}	1.236	3.58	10.72	10.72	1
Br^{79}	0.75	3.30	38.3	5.67	1
Br^{81}	1.212	6.90	39.8	5.56	1
I^{127}	0.301	10.1	84.9	3.80	1
Ni^{58}	4.32	1.17	22.8	26.08	10
D	0.3421[11]	0.3833	—	130	1

The mass M of the exchange particle is represented in the above table in terms of the electronic mass as the unit.

E is calculated from the isotopic masses as given by Barkas[12] and by Aston.[13]

e is the charge upon the exchange particle in terms of the electronic charge as the unit.

The artificially activated fission of the uranium nucleus presents a problem bearing very directly on the view put forward here.[9] The products of this fission are known to be X, Kr ; Ba, Te ; Cs, I ; Br, Rb, Sr, Se ; La, Y ; Mo; Ma ; Sb, and, perhaps, Ag. It is of extreme interest to note that, excepting the doubtful product Ag, all the above-mentioned products of the fission are represented in the scheme of Table I as made up of either X or Kr as one of the components with the addition of a proton or He or Ne nucleus ; while the structure ascribed to the U nucleus is X plus Kr. Thus, Ba and Te are products from X and He nuclei ; I and Cs from X and H nuclei ; La and Y from X and Ne nuclei ; Br and Rb from Kr and H nuclei ; Se and Sr from Kr and He nuclei ; and Mo and Ma from Kr and Ne nuclei ; and Sb from Kr and A nuclei. This would indicate that the products of the fission are X, Kr, Ne, He, and protons, in addition to neutrons which have been observed experimentally. If we consider the U nucleus to be a binary system whose component are X and Kr, then, the lighter nuclei, He. Ne, and H, would have to be traced to the disruption of one or other of the X and Kr nuclei. The fission of uranium seems to provide a convincing demonstration of the fact that the constituents of the atomic nuclei are of comparable masses, and that these constituents are provided by the nuclei of the rare gases as outlined here.

For the time being, we can only speculate on the nature of the exact mechanism by which the incident neutrons loosen the bonds between the constituent particles sufficiently enough by disturbing the exchange forces to cause these constituents to fall asunder. It is probable that some kind of resonance is set up in the nucleus at the entry of the neutron into it.

Another aspect of our theory is the change in the isotopic number which would give a family of similar elements. In the original exposition, this was provided for on the assumption that, after the formation of the binary or multiple nucleus, the isotopic number was changing by absorption of negative electrons. For example, the synthesis of X and A produces nuclei of the second group of the rare earths, whose number is further increased by absorption of one or more electrons. We would then have elements ranging in atomic weights between 160 and 176, and ranging in atomic numbers from 72 downwards. This shows a fair agreement with facts, the atomic weights of the second group of the rare earths from Tb to Hf lying between 159 and 176 and the atomic numbers between 72 and 65. A better understanding of the phenomena leads us to believe that it is extremely improbable that electrons hold a free existence in nuclei. We have, on the other hand, abundant evidence to support the view that it is protons and neutrons that exist in the nuclei as their ultimate constituents. We can, therefore, replace the above assumption of the absorption of electrons by one of emission of positrons. That this is possible can be concluded from a comparison of the masses of the several primary particles involved in the process.[10] The masses of proton, neutron and electron are, respectively, 1.00812, 1.00893 and

0.00055 mass units. If we consider the neutron as the primary particle, then the proton consists of a neutron plus a positron, and its binding energy will be given by the mass defect

$$1.00893 + 0.00055 - 1.00812 = 0.00136 \text{ mass units.}$$

Evidently, this is not possible on the view that it is the proton that is the primary particle, and that the neutron is composed of a proton plus an electron. For, the binding energy would have to be

$$1.00812 + 0.00055 - 1.00893 = -0.00026 \text{ mass units,}$$

which is a negative quantity. Thus, there arises a probability of the proton disrupting into a neutron and a positron. The exact circumstances under which this would be possible cannot be understood ; but we have a similar case of positron emission in artificial radioactivity. Similarly induced instability in neuclei of binary or multiple character would change the isotopic number to yield the various elements of a group.

TABLE III

Isotope and their nuclear spins, I
Those for the rare gases are derived from the values of the others

Isotope and components	I
$Na^{23} = Ne^{22} + H$	3/2
$K^{39, 41} = A^{38, 40} + H$	3/2
$Br^{79} = Kr^{78} + H$	3/2
$Br^{81} = Kr^{80} + H$	3/2
$Rb^{85} = Kr^{84} + H$	5/2
$Rb^{87} = Kr^{86} + H$	3/2
$Cs^{133} = X^{129} + He$	7/2
$Eu^{151} = X^{(129, 131)} + Ne^{(22, 20)}$	5/2
H	1/2
He	0
$Ne^{22\ (20)}$	1
A^{38}	1
A^{40}	1
$Kr^{78, 80, 84, 86}$	1/2
$X^{129, (131)}$	7/2

We may be justified in assuming that the spin of a nucleus is the algebraic sum of the spins of its constituents. In Table III are listed some of the values of nuclear spins that are known with any degree of certainty. From these we can surmise the values of the spins of the constituents, which are also included in the table.

DEPARTMENT OF PHYSICS.
MAHARAJA'S COLLEGE, JAIPUR (RAJPUTANA).

REFERENCES

[1] Soonawala, M. F., *Ind. J. Phys.*, **3**, 489 (1929).

[2] Barkas, W. H., *Phys. Rev.*, **55**, 691 (1939).

[3] Frohlich, H, Heitler, W., and Kammer, N., *Proc. Roy. Soc.*, (*A*), **166**, 154 (1938); Bhabha, H. J., *Proc. Roy. Soc.* (*A*) **166**, 501 (1938).

[4] Bethe, H. A., and Bacher, R. F., *Rev. Mod. Phys.*, **8**, 110 (1936).

[5] *Ibid.*, **8**, 105 (1936).

[6] *Cf.* Sommerfeld, *Wellenmechanischer Erganzungsband* (1929); Kp. I, § 1 and 3.

[7] *Cf. Handbuch der Physik*, B. III, Kp. IX, § 17.

[8] Guggenheim, K. M, *Nature*, **145**, 104 (1940).

[9] Turner, L. A, *Rev. Mod. Phys.*, **12**, 1 (1940). This is a full report with all references up to December (1939).

[10] There is a discussion on similar lines in Millikan's *Electrons, Protons, Photons, Neutrons and Cosmic Rays* pp 377, 378.

[11] Bethe, H. A. and Bacher, R. F., *Rev. Mod. Phys*, **8** (1936).

[12] Barkas, W. H, *l.c.*

[13] Aston, F. W., *Mass Spectra and Isotopes*, p. 235.

[14] Bethe, H. A., and Bacher R. F., *Rev. Mod. Phys.*, **8**, 215 (1936).

PROPAGATION OF SUPERSONIC WAVES IN LIQUID MIXTURES AND INTERMOLECULAR FORCES: ETHER AND ACETONE IN CHLOROFORM—III

By RAM PARSHAD

(*Received for publication, May 6, 1942*)

INTRODUCTION

ABSTRACT. Ultrasonic velocities and adiabatic compressibilities have been determined of the solutions, ether-chloroform and acetone-chloroform. The compressibility-concentration curves lie below and above the straight lines for ideal mixtures in ether-chloroform and acetone-chloroform respectively. It is the first case, where ether and acetone have behaved oppositely with respect to chloroform. Previous work on these solutions in various other fields is sketched and combining the findings in these with the results on compressibilities, it is shown how in these solutions both hydrogen bonds and dipole associations are present, and how compressibility-determination is a method for finding which of the combinations, hydrogen bond or dipole association preponderates. In acetone-chloroform hydrogen bonds preponderate, while in ether-chloroform, dipole associations preponderate.

This paper is the third of the series on liquid mixtures.[1,2] The experimental technique and the basic considerations have been described in the first paper and will not be repeated here.

Ethers and ketones are known to form abnormal solutions with chloroform, with respect to solubility, heat of solution,[3] viscosity, dielectric polarisation, vapour pressure, volume contraction, etc. Both ethers and ketones behave similarly in respect of the above properties in chloroform and some sort of close relationship is supposed to be formed in the solution.

In our experiments, they behave absolutely in the opposite way, as will be evident from the graphs. In acetone-chloroform the compressibility-concentration curve lies above the straight line for the ideal case, and in the case of ether chloroform it lies appreciably below. This means that the intermolecular or inter-group forces in ether chloroform are enhanced while those in the other decreased as compared to the ideal case. This is a unique observation in that ethers and ketones have been observed to behave oppositely in chloroform.

EXPERIMENTAL RESULTS

The experimental technique and basic considerations relating compressibility to molecular interaction have been given in the first paper and will not be repeated here. The following are the results:

MIXTURE : ETHER-CHLOROFORM

Temp. = 27°.2C.

No.	Mole-fraction of ether	Density gm./cc.	Velocity m /s.	Compressibility (adiabtic) × 10^{-6} in bar^{-1}
1	0	1.466	984.7	70.3
2	.0665	1.429	981.5	72.6
3	.0792	1.398	977.4	75.0
4	.249	1.255	947.5	83.9
5	.328	1.181	975.2	89.0
6	.436	1.109	976.1	94.8
7	590	.996	978.1	105.0
8	.644	.955	976.8	109.7
9	.875	.795	980.0	131.0
10	1	7025	980.9	148.0

The velocity-concentration and compressibility-concentration curves are plotted in Fig. 1.

The velocity curve shows a well-defined minimum at mole-fraction of ether of .25.

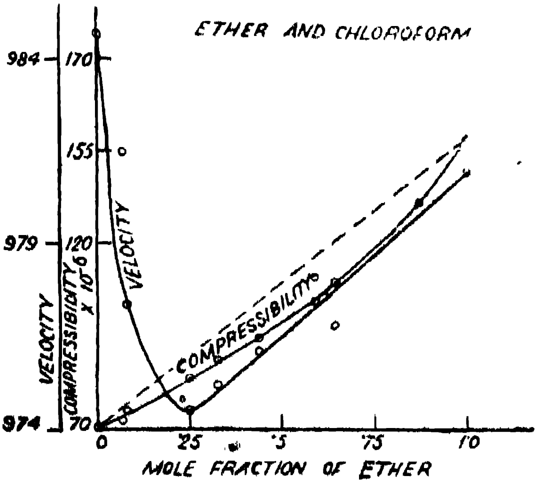

FIGURE 1

The compressibility curve always remains below the straight line corresponding to the ideal case.

MIXTURE : ACETONE-CHLOROFORM

Temp. = 27°.5C.

No.	Mole-fraction of acetone	Density gm./cc.	Velocity m /s.	Compressibility (adiabatic) $\times 10^{-6}$ in bar^{-1}
1	0	1.472	989	69.5
2	.109	1.403	994	72.2
3	.321	1.268	1009	77.5
4	.524	1.131	1037	82.2
5	.720	.991	1077	86.9
6	.909	.856	1139	90.1
7	1	.788	1183	90.7

The velocity-concentration and compressibility-concentration graphs are shown in Fig. 2.

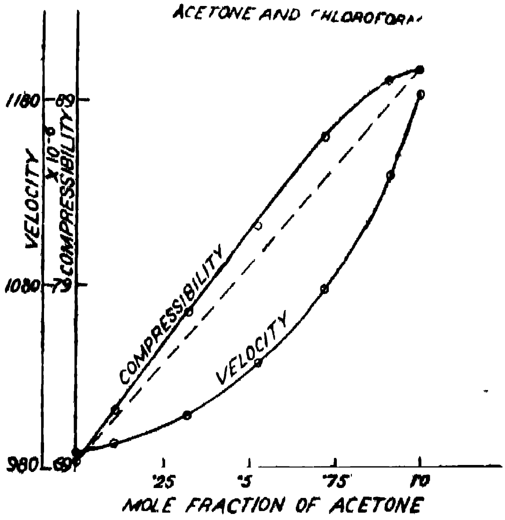

FIGURE 2

The velocity-curve remains below the straight line and compressibility-curve above the straight line corresponding to the ideal case.

From Figs. 1, 2, we gather the important fact that ether and acetone behave oppositely in chloroform with regard to compressibility of the solutions. In ether-chloroform the compressibility is less than that for the ideal case, and in acetone-chloroform the compressibility is greater than that for the ideal case.

It will be our purpose in the following to discuss and explain this opposite behaviour of ether and acetone.

Since this is the first case when acetone and ether behave oppositely in chloroform as against the numerous other properties where they act in the same way, we must go deep into the subject requiring full discussion.

DISCUSSION

The structure of molecules.—Acetone, 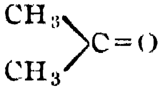 $(CH_3)_2C{=}O$ and ether₂ 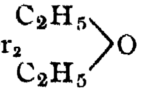 $(C_2H_5)_2O$ have the peculiarity, as is evident from the structural formulae, that the negative end of their dipoles, *i.e.*, O atoms are on the outside of the molecules while the positive ends are embedded inside or distributed. The forces of cohesion arising from dispersion, induction and dipole action are very short range forces, varying inversely as the sixth power of the distance. Further, the effectiveness of the contribution depends not so much upon the magnitude of the dipole moment as on its actual position with respect to the remaining part of the molecule. Dipoles, well-embedded in the molecule or distributed, have little action as compared to those on the outside. In the case of acetone and ether, the positive end being well-embedded inside, there will not be much dipole interaction energy between two molecules as compared to, say, the dispersion energy. For this reason, these liquids will be absolutely unassociated. This has been confirmed experimentally also, for example, by measuring their dielectric polarisation as a function of concentration when they are dissolved in some inert solvent like benzene or carbon tetrachloride.

Chloroform.—Chloroform, 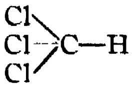 $Cl_3C{-}H$ has the dipole C—H and the three negative atoms Cl that are known for their electronegativity, *i.e.*, electron-attracting or proton-repelling power. Also these Cl atoms due to their polarisability polarise the C—H dipole. Now in the molecule of chloroform, as is evident from the structural formula the positive end H of the dipole is open to the surface.

Now, when acetone or ether is mixed with chloroform, the conditions become ideal for dipole action, the negative end O and positive end H, of dipoles of different molecules being on the surface. For this reason, the unlike molecules will be attracted to each other strongly and many abnormalities will arise in the properties of the solution as compared to the ideal case. Some sort of complex is supposed to be formed between the unlike molecules to explain the abnormalities. The question that has not been settled well, yet, is what is the exact nature of intermolecular relationship. Our compressibility data seem to decide the nature of the relationship.

In order to appreciate the light thrown by our compressibility data on the mode of behaviour of the solutions, it will be necessary to give experimental evidences of the existence of strong similar intermolecular action and the attempts that have been made in forming a suitable intermolecular picture on the basis of these data.

PREVIOUS EXPERIMENTAL EVIDENCES

Heat of mixing.—Macleod and Wilson studied the heat evolved when ether is mixed with chloroform in varying concentrations. The maximum heat is evolved at or very close to equimolecular proportions. This indicates that any complex formed might be having one molecule of ether and one of chloroform.

By applying the law of mass action, it was deduced that 14 to 20 per cent. of the molecules are mutually attached at 15°C. The method, however, lacks precision. A similar abnormal heat of solution is found in acetone-chloroform.

Partial pressures.—The solutions show large negative deviations from Raolt's law.[4,5] This shows that molecules are held together strongly in a complex, of whatever nature it may be, so that it is more difficult for molecules to evaporate in this state, than from an ideal solution. Dolezalek[7] concludes from the study of vapour pressures of ether and chloroform mixtures that at 19°C. about 24% of the molecules are combined. This is a slightly higher percentage than that deduced by Macleod and Wilson from heat of mixing.

Volume contraction on mixing.—There is a volume contraction of 1.25% for an equimolecular mixture of ether and chloroform. On the other hand, the volume contraction for acetone-chloroform is only .19%.[7] The wide difference between the two values is significant and will be discussed afterwards.

Solubility.—Zellhoefer, Copley and Marvel[8] measured the solubility of chloroform in ketones and ethers and found that ethers and ketones are highly soluble in chloroform, indicating strong intermolecular action. They investigated the effect of different forms of R_2O and R_2CO in CHX_3 on solubility, where R and X denote any radicals.

Dielectric polarisation.—Glasstone[9] observed that ethers and ketones have abnormal polarisation in tri-halogenomethanes. The abnormal polarisation must be attributed to the fact that the dipole moment of each constituent was greater than its usual value as a result of association with the other.

Infra-red absorption spectra.—Gordy[10] has observed the absorption spectra in solutions of chloroform and bromoform in various solvents including ketones, esters, ethers and amines. In the region of 4μ, a band has been observed which apparently is not characteristic of the spectrum of either the solute or the solvent. Because of the intensity of the band, it is thought to be a fundamental. Gordy thinks that the most reasonable interpretation is that it is an NH or OH vibration resulting from intermolecular hydrogen bond formation between the CH of chloroform and an N or O of the solvent. The band for the bromoform is weaker than that for the corresponding chloroform solutions.

Gordy[11] again remarks that although the spectra indicate the formation of hydrogen bonds in the manner suggested above, it is not absolutely necessary that they must combine in order to produce the absorption actually found. The dielectric constant of the solution and other factors can probably also produce the results, the magnitude of which is extremely small.

DISCUSSION OF INTERMOLECULAR ACTION

From the above list of experimental evidence, there seems no doubt that there is strong intermolecular action, and now we wish to investigate the exact nature of the intermolecular process taking place.

Two probable pictures of intermolecular action have been proposed to account for the abnormal properties of the mixtures, and there has been a lot of discussion as to which of the two is in fact taking place. The two processes are as follows :

(*i*) Hydrogen bond formation
(*ii*) Dipole association.

Hydrogen bond.—The O of acetone or ether is supposed to donate two electrons to the H of chloroform, as is represented in the figure

$$CH_3CO \rightarrow HCCl_3.$$

Due to quantum mechanical consideration, there will be in fact a resonance as shown

$$(CH_3\overset{+}{C}O \rightarrow H\overset{-}{C}Cl_3) \rightleftharpoons (CH_3COH—CCl_3).$$

Dipole association.—In this case the H and O are attracted under their mutual fields, but there is no actual donation of the electrons. The dipole association may be represented in the figures as

$$\left(CH_3\overset{+\rightarrow}{CO} \quad \overset{+\rightarrow}{H\text{-}C}Cl_3 \right).$$

Glasstone[9] was the first to put forward the hypothesis of hydrogen bond formation from his studies on dielectric constants. There is a long discussion about hydrogen bond *versus* dipole association in his paper to which the reader may refer for greater details. Zellhoeffer, Copley and Marvel have discussed the problem from the solubility considerations to which also reference may be made.

Up till now the situation is that the experimental facts listed above can be explained on both the hypotheses, for both assume a great mutual attractive force between the unlike molecules through their different mechanisms. The usual tests of the hypotheses have been made by introducing electron-repelling or electron-attracting groups in the two molecules of chloroform, and of acetone or ether and then investigating the change in their mode of interaction.

On the hydrogen bond theory they are explained as due to their attraction or repulsion on the two electrons, thus affecting the tendency for donation, while the same results are explained equally well on the dipole association theory by involving the polarising action of those groups on the electrons in question. These groups will alter the electron distribution of the respective bonds of chloroform and acetone in a way leading to a greater or less attraction between the unlike atoms, and thereby producing the observed effects.

There has been thus, so far, no critical criterion or observation which would show unambiguously the presence of one form of interaction or the other.

Now we shall show that our compressibility data are incomparably better in deciding for the mode of interaction. In the following we shall discuss the effect of hydrogen bond formation or dipole association on compressibility.

HYDROGEN BONDS AND COMPRESSIBILITY

The compressibility will increase on hydrogen bond formation and may be shown to be as follows:

As shown by Keesom and London,[1,12] the average cohesive energy over all positions between two dipoles of moments μ_1 and μ_2 at a distance R is

$$U = -\frac{2}{3} \cdot \frac{\mu_1^2 \mu_2^2}{R^6} \cdot \frac{1}{kT}$$

(k is Boltzmann's constant ; T, absolute temperature).

It has been shown[1] that compressibility behaves in the inverse way to the cohesive energy. In the to and fro motion in the liquid under ultrasonic waves, it is not one molecule which is the unit, but a whole associated structure, which may be composed of more than one molecule. Of course, when the molecules are free individuals, they singly form the units in the oscillating motion.

Now when the two unlike dipoles are at a distance from each other, there is cohesive energy among them as given by the above formula. The cohesive energy will increase rapidly as the distance still decreases. But when it becomes so little that the two molecules become a single unit through the hydrogen bond or otherwise, the cohesive energy between them, though very strong, gets ruled out from contributing to the decrease of compressibility concerned in the problem of sound propagation. Now it will be the cohesive energy between two such separate units, that we must consider for sound propagation.

As a hydrogen bond is formed, making two molecules as one close unit, the distance among the separate units will become greater than the distance that would have been between two free molecules in the absence of hydrogen bonds. As is clear from the above formula, the cohesive energy is very sensitive to distance, falling off as inverse of the sixth power of the distance. Hence this increase of distance on the formation of hydrogen bonds will lead to the increase of compressibility.

Besides, the dipoles in hydrogen bond will become effectively shielded for wielding any cohesive effect upon other units or molecules. It has already been shown how shielding of dipoles reduces the intermolecular activity of dipoles.

It has been found that compressibility of water decreases as its temperature rises, although the distance among the molecules is increasing due to thermal expansion. This is, no doubt, due to the breaking up of hydrogen bonds, which fact has been amply confirmed by infra-red and Raman spectra. Again in the mixture of water and alcohols, it has been shown that the decrease of compressibility from the ideal case is due to the breaking up of hydrogen bonds.

In a solution, therefore, the occurrence of hydrogen bonds will decrease the cohesive energy below the ideal value, or in other words, the compressibility curve will lie above the straight line corresponding to the ideal case (see acetone, chloroform).

COMPRESSIBILITY AND DIPOLE ASSOCIATION

In dipole association, there is no actual donation of electrons. The distance between the two molecules in dipole association is obviously greater than that when a hydrogen bond is formed, and the molecules vibrate as separate units in sound oscillations. This means that the strong cohesive energy between them is directly concerned in sound propagation, and the compressibility will therefore be much decreased. Again, in dipole association, there will not be a similar shielding as in the case of hydrogen bonds and the dipole activity will be present at all times as contrasted to the case of hydrogen bond. All these will lead to a lower value of compressibility than in the case of hydrogen bonds.

THE MIXTURE

In ether-chloroform, the compressibility is below the ideal value, while in acetone-chloroform, it is above the ideal value. The conclusions to be derived from the compressibility data, with regard to hydrogen bond *versus* dipole association theory, becomes self-evident in the light of what has been said before. They may be repeated as (1) in acetone-chloroform, hydrogen bonds are formed and (2) in ether chloroform, dipole associations are formed.

By examining the structure of acetone and ether molecules, it is quite easy to see why one type should prefer one way of coupling to the other. In acetone the C=O dipole has its 'O' absolutely unshielded by the rest of the molecule and its dipole moment is quite high (2 D). Both these factors are favourable for hydrogen bond formation. In ether on the other hand, the 'O' atom–is relatively more shielded and the dipole moment is less (1.5 D). These may be taken as strong reasons why in acetone-chloroform hydrogen bonds are prevalent, while in ether-chloroform, the dipole associations.

Volume contraction.—The data on volume contraction on mixing support our findings. In ether-chloroform there is a larger contraction (1.25%) while in acetone-chloroform, a comparatively much smaller one.

In ether-chloroform, dipole associations being prevalent, there is high cohesional energy leading to this contraction, while in acetone-chloroform due to the formation of hydrogen bonds, forces among units whether in the form of free molecules or bonded molecules, are much reduced; this will explain the experimental findings.

Vapour-pressure.—The data on vapour-pressure deviations can be explained quite easily on our views since in ether-chloroform mixture the escaping molecule has to overcome the attraction of its neighbouring dipole or dipoles, associated or free, while in the acetone-chloroform solution, it has to overcome the bond energy of its partner.

However, while keeping our main conclusions intact, we may accept a modified picture as well.

It can be seen that there is really no difference of kind but only of degree between hydrogen bonds and dipole association. When the H of chloroform and O of ether or acetone approach very near together under the action of electrostatic forces and random heat motion, conditions become favourable for the transfer of two electrons from the O atom, and a hydrogen bond may thereby be formed. When the two unlike molecules, on the other hand, are at a greater distance, it may not be possible for the transfer of electrons, but still it is a dipole association. Hence it seems that both dipole associations and hydrogen bonds are present, their relative preponderance depending upon the circumstances of the case.

So, in our actual case, we are led to the plausible conclusion that (1) Hydrogen bonds are preponderating in chloroform-acetone solution; (2) Dipole associations are preponderating in chloroform-ether solution.

Thus the determination of compressibilities is a new method of determining the nature of preponderance of the combinations between dipole associations or hydrogen bonds.

In the end it is my great pleasure to thank Prof. D. M. Bose for his keen interest in my work. I tender my hearty thanks to Dr. A. K. Dutta for his unfailing help and suggestions during the investigation.

BOSE INSTITUTE,
CALCUTTA.

REFERENCES

[1] R Parshad, *Ind. J. Phys.*, **15**, 323 (1941).
[2] „ „ **16**, 1 (1942).
[3] Macleod and Wilson, *Trans. of Farad. Soc.*, **31**, 596 (1935).
[4] Kohnstramm and Balfsen, *Proc. Akad. Wel.*, **29**, 156 (1901).
[5] Zanvidiski, *Z. Physik. Chem.*, **35**, 129 (1900).
[6] Dolezalek, *Z. Physik. Chem*, **71**, 191 (1910).
[7] Hubbard, *Z. Physik Chem.*, **35**, 129 (1900)
[8] Zellhoeffer, Capley and Marvel, *Am. J. Chem. Soc.*, **60**, 1337 (1938).
[9] Glasstone, *Trans. of Farad. Soc.*, **33**, 200 (1937).
[10] Gordy, *J. Chem. Phys.*, **7**, 163 (1939).
[11] Gordy, *Am. Jour. of Chem. Soc.*, **60**, 605 (1938).
[12] London, *Trans. of Farad. Soc.*, **33**, 8 (1937).

ON THE IDENTIFICATION OF LINES IN THE SOLAR CORONA*

BY D. N. KUNDU

(*Received for publication, May 13, 1942*)

ABSTRACT. The elements claimed as being present in the solar corona have been examined from a spectroscopist's standpoint. The possibility according to Saha's theory of the solar corona, of the presence of other elements in the neighbourhood of Fe has been studied and the reasons of the absence of many of them have been explained. The presence of Co has been suspected in the corona.

I. INTRODUCTION

The identification of the lines in the solar corona which had long defied the attempts of physicists and astronomers appears at last to have been possible by the brilliant discovery of Grotrian and Edlen that the most intense coronal lines may be ascribed to forbidden transitions of highly stripped iron, nickel and calcium atoms. The details of the identification as far as known at present is given below (Table I).

TABLE I

Lines in the Solar Corona

Wavelength λ	Frequency cm^{-1}	Intensity	Origin	Remarks
3328	30039.46	2.8	—	—
(3359)	29762.24	—	—	—
3388 10	29506.62	44.4	Fe^{+12} ... $3p^2\ {}^3P_2-{}^1D_2$	Identified by Edlen
3454 13	28942.59	5.6	—	—
(3461)	28885.14	—	—	—
(3505)	28522.54	—	—	—
(3534)	28288.49	—	—	—
3601.00	27762.17	4.4	Ni^{+16} ... $3p\ {}^2P_{\frac{1}{2}}-{}^1P_{\frac{3}{2}}$	Identified by Edlen
(3626)	27570.76	—	—	—
(3641)	27457.18	—	—	—
3642·9	27442.86	—	—	—
(3648)	27404.50	—	—	—
(3651)	27381.98	—	—	—
3800·8	26302.81	—	—	—

---

* Communicated by Prof. M. N. Saha.

TABLE I (*contd.*)

Wavelength λ	Frequency cm⁻¹	Intensity	Origin	Remarks
3865	25865 91	—	Fe^{+10} ... $3p^4\ {}^3P_1-{}^1D_2$	Bowen obtains a line at λ3871 9, and assigns it to the transition given here.
(3891)	25693.08	—	Fe^{+4} ... $3d^4\ {}^5D_4-{}^3F_4$	(?) *Vide* Text
3986.9	25075.07	.8	—	—
4086.3	24465.13	1.2	—	—
(4130)	24206.27	—	—	—
(4131 4)	24298.06	—	—	—
4231.4	23626.21	3.2	—	—
(4244 8)	23551.62	—	—	—
4311 0	23189.97	—	Ni^{+11} ... $3p^5\ {}^2P_{\frac{3}{2}}-{}^2P_{\frac{1}{2}}$	(?) *Vide* Text
4359.0	22934.61	< .8	Co^{+14} ... $3p\ {}^2P_{\frac{1}{2}}-{}^2P_{\frac{3}{2}}$	Identified by D. Kundu (1941)
(4398)	22731.24	...	—	—
(4533.4)	22054 28	—	—	—
4567.0	21890.09	1.2	—	—
4586	21799.40	—	—	—
(4722)	21171.56	—	—	—
(4725)	21158.12	—	—	—
(4779)	20919.04	—	—	—
(5073)	19706.72	—	—	—
5116 03	19540.98	4.8	—	—
5302.86	18852.52	110	Fe^{+13} ... $3p\ {}^2P_{\frac{1}{2}}-{}^2P_{\frac{3}{2}}$	Discovered in 1868 by Harkness and Young. See further.
5536	18058.58	—	—	—
(5694.0)	17557.48	—	—	—
6374.51	15683.15	28	Fe^{+9} ... $3p^5\ {}^2P_{\frac{3}{2}}-{}^2P_{\frac{1}{2}}$	Discovered in 1914. Identification due to Grotrian.
6704 83	14910.51	3.3	—	Discovered in 1929 by Grotrian.
7059.6	14161 21	4	—	—
7891.94	12676.68	29	Fe^{+10} ... $3p^4\ {}^3P_2-{}^3P_1$	Identified by Grotrian.
8024 2	12458.88	1.3	—	—
10746.8	9314.4	240	Fe^{+12} ... $3p^2\ {}^3P_0-{}^3P_1$	Discovered by Lyot (1934) by means of the Coronagraph. Identified by Edlen.
10797.9	9261.0	150	Fe^{+12} ... $3p^2\ {}^3P_1-{}^3P_2$	,,

The table is taken from Saha[1] with slight modifications. The number of lines in the corona whose existence is admitted by all workers is 22, but, from time to time, other lines have been claimed by various workers. Such lines are shown in round brackets. The intensities are calculated in units of 10^{-6} of the intensity at the same wavelength of the photospheric emission comprised within 1 Å.

The exact physical conditions in the solar corona which give rise to these highly stripped atoms have not yet been satisfactorily solved. Attempts were first made by Russell[2] to explain them on a meteor-shower hypothesis but certain experimental facts, for example, the broadening of the lines towards the reversing layer, did not fit in with it. The subject was taken up in more details in an extensive paper by Saha who after a critical review of the whole problem came to the conclusion that some nuclear reaction like uranium fission might be going on in the reversing layer, and the theory worked out on this assumption agrees very well with most of the observed facts. Without concerning ourselves with the explanation of the origin of these highly ionised atoms, we propose to discuss the problem of identification of the coronal lines, which, though partly solved, still needs further elucidation.

2. HOW THE DISCOVERY WAS MADE

From Edlen's data on the spectra of highly stripped atoms, Grotrian noted that the line λ 6374 was given by the difference $^2P_{3/2} - {}^2P_{1/2}$ of the fundamental $2p^5$-state of Fe^{+9} and λ 7892 was given by the difference $^3P_2 - {}^3P_1$ of Fe^{+10} ... $3p^4$. With this clue, Edlen tried to trace the origin of the other coronal lines. From his data on lines of stripped Fe-atoms, he identified the other lines as shown above. Russell states that Edlen has been able to ascribe certain other lines to highly stripped atoms of Ni and Ca, but as Edien's paper has not been available, this has not been shown.

Russell says that 15 out of the 22 well-established lines appear to be due to highly ionised atoms of Fe, Ni and Ca. Apparently none of the other elements Cr, Mn, Co, etc., has been found . From the fact that these elements are prominent also in iron meteorites, Russell appears to throw the suggestion that the coronal lines might be due to large scale meteoric flashes in the outermost atmosphere of the sun, though the subject has not been further pursued.

But spectroscopists are well aware that the absence of the lines of an element may be due to many other causes and mere absence of certain lines does not always indicate the absence of the element in the sources, for the corresponding lines may fall outside the observable region. No one can, thus, make a positive assertion without a critical discussion. For this purpose, a systematic examination of all the available data for tracing out the corresponding lines of neighbouring elements has been undertaken. The results of this investigation are shown in Table II.

TABLE II

Electron configuration ↓	Elements → Difference ↓	Zn	Cu	Ni	Co	Fe	Mn	Cr	V	Ti	Sc	Ca	K
$3p^1$	$^2P_{\frac{1}{2}}-{}^2P_{\frac{3}{2}}$	λ 2546·3	λ 3017	λ 3601	λ 4359	λ 5303	λ 6527	λ 8148	λ 10318	7530 cm^{-1}	5748 cm^{-1}	4307 cm^{-1}	3123 cm^{-1}
$3p^2$	$^3P_1-{}^1D_2$	—	—	—	—	—	—	—	—	—	—	λ 4938.6	λ 5603
	$^3P_2-{}^1D_2$	—	—	—	—	λ 3388.10	—	—	—	—	—	—	—
	$^3P_0-{}^3P_1$	—	—	—	—	λ 10746.8	—	—	—	—	—	—	—
	$^3P_1-{}^3P_2$	—	—	—	—	λ 10797·9	—	—	—	—	—	—	—
$3p^3$	$^4S_{\frac{3}{2}}-{}^2D_{\frac{3}{2}}$	—	—	—	—	—	—	—	—	—	—	λ 3702.6	λ 4165.4
	$^2P_{\frac{1}{2}}-{}^2D_{\frac{5}{2}}$	—	—	—	—	—	—	—	—	—	—	λ 5587	λ 6316
	$^2D_{\frac{3}{2}}-{}^2P_{\frac{3}{2}}$	—	—	—	—	—	—	—	—	—	—	λ 5459·7	λ 6423
	$^4S_{\frac{3}{2}}-{}^2D_{\frac{5}{2}}$	—	—	—	—	—	—	—	—	—	—	λ 3646.3	λ 4124.5
$3p^4$	$^3P_2-{}^1D_2$	—	—	—	—	λ 2596.6	λ 2918 8	λ 3273	λ 3686	λ 4144 6	λ 4672	λ 5309	λ 6101
	$^3P_1-{}^1D_2$	—	—	—	—	λ 3872	λ 4122.4	λ 4407·9	λ 4733	λ 5105 8	λ 5539.4	λ 6085 8	λ 6794.8
	$^3P_2-{}^3P_1$	λ 3862	λ 4424	λ 5234	λ 6335	λ 7892	λ 9997	7860 cm^{-1}	6000 cm^{-1}	4540 cm^{-1}	3350 cm^{-1}	2404 cm^{-1}	1673 cm^{-1}
	$^3P_1-{}^3P_0$	—	—	—	—	1760 cm^{-1}	1740 cm^{-1}	1740 cm^{-1}	1580 cm^{-1}	1360 cm^{-1}	1126 cm^{-1}	862 cm^{-1}	641 cm^{-1}
$3p^5$	$^2P_{\frac{3}{2}}-{}^2P_{\frac{1}{2}}$	λ 3104.6	λ 3662	λ 4314	λ 5185	λ 6374	λ 7949	λ 10053	7657 cm^{-1}	5825 cm^{-1}	4328 cm^{-1}	3124 cm^{-1}	2165 cm^{-1}

3. METHOD OF CALCULATION

The $3p[^2P_{1/2}-{}^2P_{3/2}]$ *lines.*

The elements range from Zn^{+17} to K^{+6} having Al-like structure. The data for these isoelectronic elements were available for Al, Si^{+1}, P^{+2}, ... Sc^{+8} from various workers, a valuable guide in this search being provided by the extensive bibliography given by Boyce[3] on atomic spectra in the vacuum ultra-violet. The values for Fe and Ni were taken on the assumption that Edlen's identification of the line λ 5302.86 from Fe^{+13} and λ 3601.00 from Ni^{+15} was valid. We know that

$$\Delta\nu[3p^2P_{\frac{1}{2}}-3p^2P_{\frac{3}{2}}]=\frac{R\alpha^2(Z-\sigma)^4}{n^3l(l+1)}$$

where

R = Rydberg constant,
α = Sommerfeld's fine-structure constant,
Z = atomic number,
σ = screening factor,
n = principal quantum number,
and l = azimuthal quantum number.

The screening factor σ was calculated for the known atoms by using the above formula (Table III). The values of σ were plotted against atomic number (Graph 1) and σ for the unknown elements Zn, Cu, Co, Mn, Cr, V, and Ti found

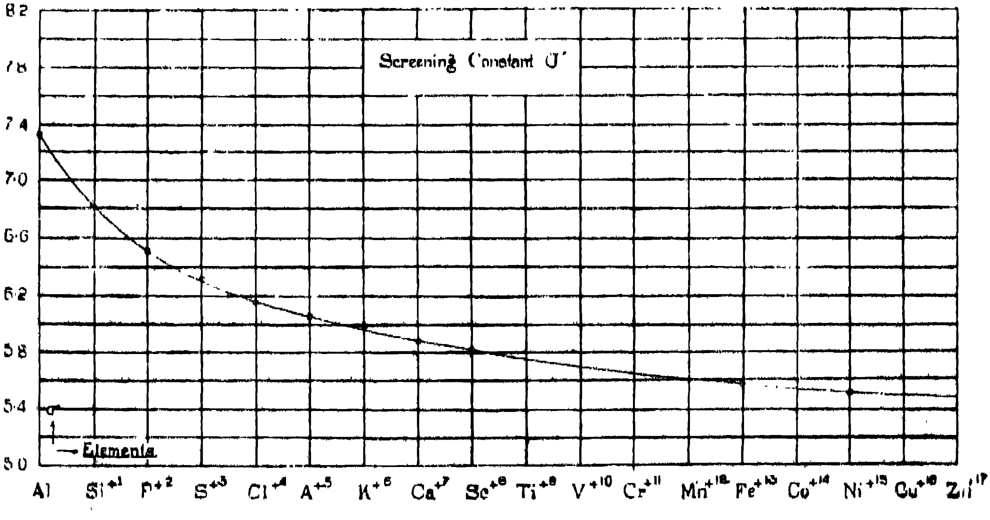

FIGURE 1 (Graph 1)

from the curve by interpolation and extrapolation. The $\Delta\nu$'s were then calculated by using the above relation.

The $3p^2$-lines.

The elements included are from Zn^{+16} to K^{+5}. The data for these Si-like atoms were available only up to K^{+5} and Ca^{+6} (Robinson[4]). So no extrapolation was attempted as this leads to large error when the elements are very far removed from each other.

TABLE III

$\Delta\nu[3p^2P_{\frac{1}{2}} - 3p^2P_{\frac{3}{2}}]$ and Screening factor σ

Element $1s^2.2s^2.2p^6.3s^2\,3p$.	$\Delta\nu$ (obs.)	σ (calc.)	Reference
Al	112.07	7·326	Saha, *Mod. Phys.*, 1, 571.
Si^{+1}	287	6.82	,,
P^{+2}	559.5	6.519	,,
S^{+3}	950.2	6.318	,,
Cl^{+4}	1500	6.147	,,
A^{+5}	2210	6.05	Parker & Phillips, *Phys. Rev.*, **58**, 93, (1940).
K^{+6}	3123	5·97	Whitford, *Phys. Rev.*, **46**, 793, (1934).
Ca^{+7}	4307	5·87	,,
Sc^{+8}	5748	5·82	Kruger & Phillips, *Phys. Rev.*, **52**, 97 (1937).
Ti^{+9}	—	—	
V^{+10}	—	—	
Cr^{+11}	—	—	
Mn^{+12}	—	—	
Fe^{+13}	18853	5·57	Edlen
Co^{+14}	—	—	
Ni^{+15}	27762.4	5·50	Edlen

The $3p^3$-configuration.

The elements run from Zn^{+15} to K^{+4} and have P-like structure. The data are available only up to K^{+4} and Ca^{+5} (Bowen[5]). So extrapolation was not practicable. Now, it will be found from Table I that iron atoms having $3p$, $3p^2$, $3p^4$ and $3p^5$ electronic structure have all been found in the corona but no $3p^3$-lines. But this cannot be used as an argument that Fe^{+12} is absent in the corona, for since Fe^{+11} and Fe^{+13} are present, Fe^{+12} must be present. The data for the $3p^3$-atoms being insufficient, an attempt was made to study how

$$^4S_{3/2}-{}^2D_{3/2},\ {}^2P_{3/2}-{}^2D_{5/2},\ldots$$

differences progress from element to element with $2p^3$-configuration. But there too the available data were too meagre for the purpose.

$3p^4$-configuration.

The elements range from Zn^{+14} to K^{+3}. Reliable data were available up to Fe^{+10} (Table IV). On tabulating the data, it was found that the lines for the $^3P_2-{}^1D_2$ and $^3P_1-{}^1D_2$ differences had already become so short that it was not necessary to extrapolate up to Zn for them. The $^3P_1-{}^3P_0$ differences again would give lines too far in the infra-red. The lines for the $^3P_2-{}^3P_1$ differences alone were in the observable region. The log $\Delta\nu$'s for these S-like elements

TABLE IV

$3p^4$ – lines

Ion $1s^2.2s^2.2p^6.3s^2.3p^4$	$^3P_2-{}^3P_1$	$^1D_2-{}^3P_1$	$^3P_2-{}^1D_2$	$^3P_1-{}^3P_0$	Reference
S	398	—	—	—	Bacher & Goudsmit, *At. Energy States*, p. 397.
Cl^{+1}	694	—	—	—	,, p. 140.
A^{+2}	1112 4	12888	—	—	Boyce, *Phys. Rev.*, **48**, 096.
K^{+3}	1673	14713	16386	641	Bowen, *Phys. Rev.*, **46**, 791.
Ca^{+4}	2404	16427	18831	862	,,
Sc^{+5}	3350	18047	21397	1126	Kruger & Pattin, *Phys. Rev.*, **52**, 621.
Ti^{+6}	4540	19580	24120	1360	Edlen, *Z. fur Phys.*, **204**, 190.
V^{+7}	6000	21120	27120	1580	,,
Cr^{+8}	7860	22680	30540	1740	,,
Mn^{+9}	10.000	24250	34250	1700	,,
Fe^{+10}	12680	25820	38500	1760	,,

up to Fe^{+10} were plotted against the atomic numbers and the wavelengths for Co, Ni, Cu, and Zn were obtained by extrapolation (Graph 2).

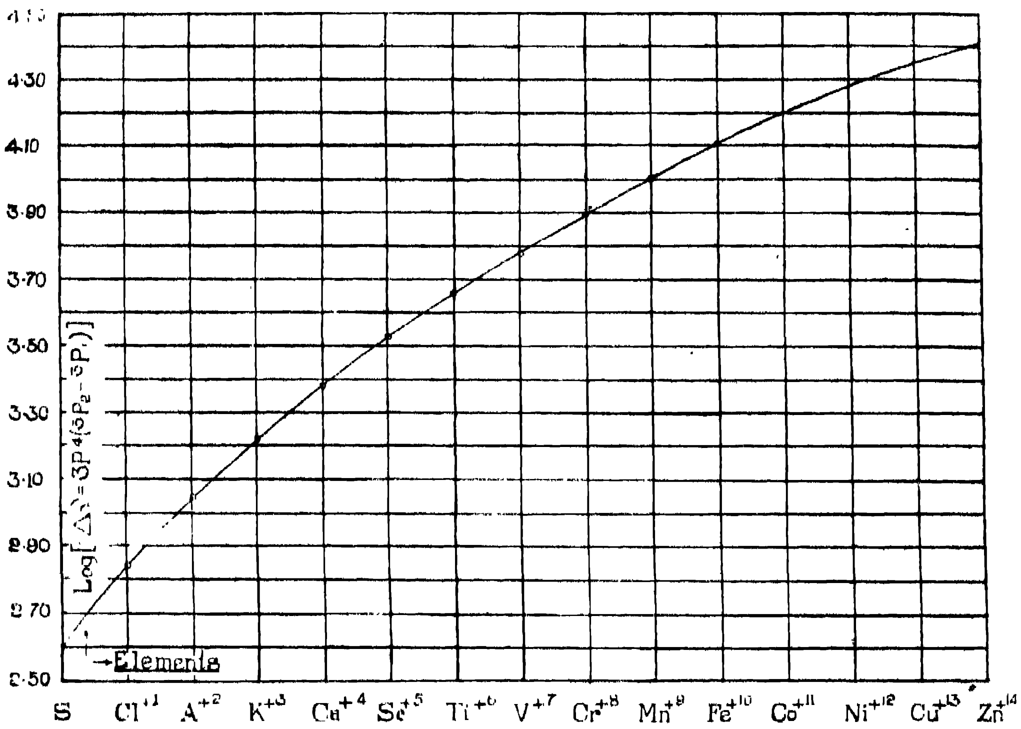

FIGURE 2 (Graph 2)

The $3p^5[{}^2P_{\frac{1}{2}} - {}^2P_{\frac{3}{2}}]$ *lines.*

The elements run from Zn^{+13} to K^{+2}. These elements are isoelectronic with Cl. Data were available up to Co (Table V). The lines for Ni, Cu and Zn

TABLE V

$3p^5$ – lines

Ion $1s^2.2s^2\ 2p^6.3s^2.3p^5$	${}^2P_{3/2} - {}^2P_{1/2}$ ν	Reference
Cl	883	Bowen, *Phys. Rev*, **31**, 497.
A^{+1}	1433	,,
K^{+2}	2165	,,
Ca^{+3}	3124	,,
Sc^{+4}	4328	Kruger & Phillips, *Phys. Rev.*, **51**, 1087.
Ti^{+5}	5825	,,
V^{+6}	7657	,,
Cr^{+7}	9947	,,
Mn^{+8}	12576	,,
Fe^{+9}	15690	Edlen, *Z. fur Phys.* **104**, 407.
Co^{+10}	19280	,,

were obtained by plotting log $\Delta\nu$ against atomic number as before and extrapolating the curve (Graph 3).

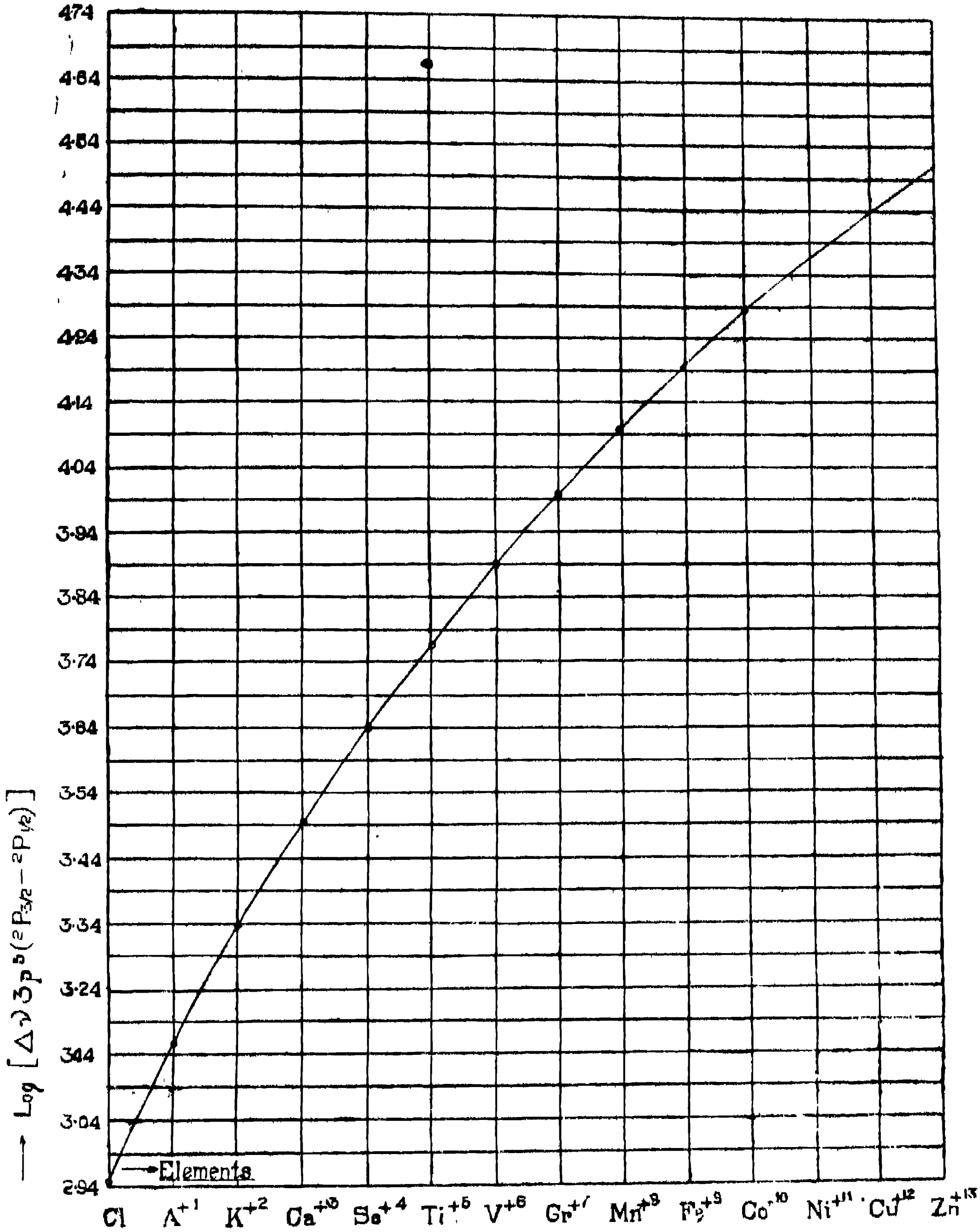

FIGURE 3 (Graph 3)

4. DISCUSSION

The lines identified by Grotrian and Edlen are mostly due to $3p^x$-combinations of Fe and Ni and two lines due to $2p^x$-combinations of Ca. The data for the $2p^x$-sequence being insufficient for extrapolation up to Ca, we have studied only the $3p^x$-configurations of elements in the neighbourhood of Fe.

As has already been pointed out, the $3p$, $3p^2$, $3p^4$ and $3p^5$ lines of Fe have been observed in the corona. The absence of $3p^3$ which on Saha's theory, must also be occurring, is easily seen to be due to the fact that the wave-lengths diminish very rapidly for the $3p^3$-combinations and for Fe and Ni the lines would be too short to be observed. The line λ 3872 is interesting in that Bowen[6] has observed that this single line due to $3p^4\ {}^3P_2 - {}^3P_1$ comes in the spectra of nebulae N G C 7027, 7662. The coronal line λ 3865 whose wave-length is very uncertain may be due to this transition.

Presence of other elements.

Since the exact theory of a three-fold fission of the type assumed by Prof. Saha has not yet been rigorously worked out, we do not know exactly the masses of the fragmentary nuclei. Assuming, therefore, that the theory is substantially correct, one may justifiably look for the presence of elements close to Fe and Ni, for example, Cu, Co, Mn, Cr, V, Ti,...etc. If they occur, the strongest lines will be due to $3p\ {}^2P_{1/2} - {}^2P_{3/2}$, $3p^5\ {}^2P_{3/2} - {}^2P_{1/2}$. The probable position of these lines is shown in Table II. We find that the $3p\ {}^2P_{1/2} - {}^2P_{3/2}$ -combination gives us lines which cannot be traced beyond Ni, as they lie in the short wave-length side of λ 3000 (for Cu it is λ 3017). For Co we have a line λ 4359 tentatively identified by the author [7]. If Co occurs at all, this line would come first as in the case of the line λ 5303 of Fe. The Mn-line is λ 6527 and we do not have yet any such line in the corona. The lines for Cr^{+11}, λ 8148 and V^{+10}, λ 10318 may be looked for in the infra-red. Though Lyot[8], by his excellant coronagraph, has succeeded in photographing the coronal lines in board day-light up to λ 10800, yet by this method only the intense lines can be studied. The investigation of this region during total eclipses is thus still an useful work for settling the problem of the corona. Ti, Sc.......are too far in the infra-red.

Turning to the $3p^5\ {}^2P_{3/2} - {}^2P_{1/2}$ lines, we cannot go beyond Cu. The copper line is λ 3662 and there is a number of doubtful lines here, *e.g.*, λ 3648 and λ 3651. The accuracy in the measurement of the wave-lengths of the faint coronal lines is very small for, owing to the short duration of the totality of the eclipse, the spectrographs have necessarily to be of low dispersion and high light-gathering power so as to enable the fainter lines to be photographed. The line λ 5185 for Co^{+10} appears to be absent on the strength of Edlen's data. The case of Ni is more favourable in that Ni^{+11} gives the line λ 4314 which agrees fairly well with λ 4311 in the corona. The method followed was not capable of a greater accuracy. The Mn-line is at λ 7949 and the Cr-line at λ 10053 for which search may be made. The line of Zn provisionally put at λ 3105 is more uncertain. We see, therefore, that no other element than Co possesses for its identification such advantages as are enjoyed by Fe and Ni.

5. OTHER ELECTRONIC CONFIGURATIONS OF Fe

If the theory of Prof. Saha be correct, then not only atoms having np^x configurations will be found in the corona but also atoms having nd^x, etc., electron-structures ; for the highly stripped atom after being formed will in course of its upward flight go on capturing electrons one after another and provided the ion originated at a sufficiently low level, we shall get all the electronic configurations until we get a neutral atom. The data for the other elements Ni, Co, and Ca found in the corona being insufficient, and iron being by far the most important element traced in the corona, we confine ourselves to the latter only and examine its other configurations.

Fe^{+x}, for $x = 1$ to 6, all have metastable states and their forbidden lines have been found to occur in many novae and stars, *e.g.*, Fe^{+1} in η-Carinæ[8], Fe^{+5} in Nova Pictoris, Fe^{+4}...Fe^{+6} in nebulae N G C 7027, 7662 [6]. $x = 1$ to 3 ($3d^6 4s$, $3d^6$, $3d^5$) have not yet been found in the corona. The case of Fe^{+4} is interesting that it is found in nebulae N G C 7027 and 7662[6], and almost all of the lines which are strongest in these nebulae appear to be present in the corona as very weak lines, as will be evident from a comparison of Table I with Bowen's chart[6] for $Fe^{+4}...3d^4$ atom. The line λ 3891 [$Fe^{+4}...3d^4\ {}^5D_1 - {}^3F_4$] which is very strong in the nebulae appears to be definitely present in the corona as a faint line. $Fe^{+15}...3d^3$ and $Fe^{+6}...3d^2$ are found to be absent. $Fe^{+7}...3d$ has no metastable state. The $3p^x$, $x = 1, .. , 6$ have all been found with the exception of $x = 3$, in which case though there are four metastable states, yet the transitions give lines too far in the ultra-violet to be observed in the corona. $Fe^{+14}...3s^2$, $Fe^{+15}...3s$, $Fe^{+16}...2p^6$ have no metastable states. The higher ionised atoms have not yet been spectroscopically studied.

6. CONCLUSION

Considering the inaccuracy in the measurement of the coronal lines except the strongest ones, it is very difficult to try to identify the lines and trace them to known ions. If according to Prof. Saha's ideas, Fe or some other neighbouring atoms are produced, an examination of Table II will show that many of these atoms will remain undetected by virtue of their spectra falling outside the accessible range of wave-lengths. The extrapolation method is at best only tentative, no exact prediction being possible until these ions are experimentally investigated. Even in the latter case there is the unavoidable error involved in calculating visible lines from data in the X-ray region.

My grateful thanks are due to Prof M. N. Saha, D.Sc., F R.S., for his kindly checking the extrapolation curves and for his kind interest and helpful discussions.

PALIT LABORATORY OF PHYSICS,
UNIVERSITY COLLEGE OF SCIENCE,
CALCUTTA.

REFERENCES

[1] Saha, M. N., *Proc. Nat. Inst. Sc. India*, **8**, 99 (1942).
[2] Russell *Scien. American*, August (1941).
[3] Boyce, J. C., *Rev. Mod. Phys.*, **13**, 1 (1941).
[4] Robinson *Phys. Rev.*, **52**, 724 (1937).
[5] Bowen, *Phys. Rev.*, **46**, 793 (1934).
[6] Bowen, I. S., *Lick Observatory Bull.*, No. 495.
[7] Kundu, D. N., *Science and Culture*, **7**, 364 (1942)
[8] Merrill, P. W., *Astro.Phys. Jour.*, **67**, 391 (1928).
[9] Jones, H. G., *M. N. R. A. S.*, **92**, 728 (1932).

VOLUME RECTIFICATION OF CRYSTALS

By B. K. SEN, M.Sc.

(*Received for publication, May 26, 1942*)

ABSTRACT. Experiments have been performed to show that the volume rectification effect is not confined to crystals like carborundum, zincite and silicon alone, which have no centres of symmetry, but that it is also exhibited by crystals like galena, iron-pyrites and pyrolusite possessing centres of symmetry. From the results of these experiments it is suggested that the so called volume rectification may not take place within the body of the crystal, but may be due to the differential effect of the surface rectification occurring at the two large contacts of the crystal with the electrodes.

INTRODUCTION

The rectifying action of crystals has usually been divided into two classes—(*a*) one is associated with a point contact at one end of the crystal and a large electrode at the other, (*b*) the other is obtained when the crystal has large contacts at both the ends, *e.g.*, when the crystal is placed between two mercury electrodes. The former kind of rectification has been called point or surface rectification and the latter kind, volume rectification. It has been thought that this volume rectification takes place within the body of the crystal, and following Krönig,[1] this effect has been attributed to the asymmetry in the crystal structure. The experiments of Khastgir and Dasgupta[2] have shown that crystals like carborundum (SiC), zincite (ZnO) and silicon, which have no centres of symmetry, give volume rectification when placed between mercury electrodes, whereas with symmetrical crystals, *e.g.*, galena (PbS), iron-pyrites (FeS_2), pyrolusite (MnO_2), etc., no trace of such rectifying effect was obtained by passing low-frequency alternating current through the crystals similarly placed between two mercury electrodes of large contact areas.

Natural Cu_2O crystals, which show the Dember effect, exhibit rectifying properties when illuminated. In this case, however, it has been shown[3] that the action does not occur at the electrodes but takes place in the body of the crystal. It is to be noted here that artificial Cu_2O crystal, in which the Dember effect is absent, does not show any rectifying effect.

In course of the investigation on the effects of heat and ultra-violet light on crystal rectification[4] the present author noticed that besides carborundum, zincite and silicon, crystals of iron-pyrites, galena and pyrolusite exhibited pronounced rectifying properties when placed between mercury electrodes. It was, therefore, felt desirable to further study this phenomenon of volume rectification and the preliminary results obtained were reported in a short note.[5] The details of some experiments are, however, given in the present paper.

EXPERIMENTAL

The method of mounting the crystals was practically the same as that adopted by Khastgir and Dasgupta in their study of volume rectification,[6] with an additional arrangement for slowly moving the glass tube, carrying the crystal vertically up and down. For this purpose the stand of a travelling microscope was utilised. The glass tube with the crystal was kept vertical by passing it through a hole in a cork which was fitted to the microscope stand in the position of the microscope, so that the crystal holder could be moved up and down as required with the associated slow-motion attachments. With this arrangement the contact-area between the crystal and the mercury at the lower end could be conveniently altered, that at the upper electrode remaining constant, and the effect of the change of contact area at one of the electrodes could be studied. The source of low-frequency alternating voltage was a 1000-cycle audio-oscillator. For the measurement of the rectified current a milli-ammeter was generally used which was, however, sometimes replaced by a shunted galvanometer.

The following symmetrical crystals were tested, both with low-frequency and high-frequency alternating currents, for volume rectification and in each case prominent rectified current was obtained, the nature of which is given below in detail. Characteristic curves have also been obtained in all cases by applying direct voltage in the usual way.

Low-frequency Test.

(1) Galena: When the alternating current is passed through a good crystal of galena put between mercury electrodes, there is a pronounced rectified current as indicated by the shunted galvanometer placed in the circuit. Next, keeping the upper contact-area constant, as the lower contact-area is gradually altered the following changes, as regards direction and magnitude, are noticed in the rectified current: When the lower end of the crystal just touches the mercury surface, the rectified current flows upwards, the magnitude being nearly 1 milli-ampere. But this current is rather unsteady and occasionally goes downwards. When the lower contact area is made sufficiently large, the rectified current remains steady. The current now flows upwards and its strength is 1.25 milli-amps. On further

increasing the contact-area gradually the rectified current first increases a little, then diminishes, becomes zero and finally changes direction and flows downwards. This result has been reproduced several times during the experiments.

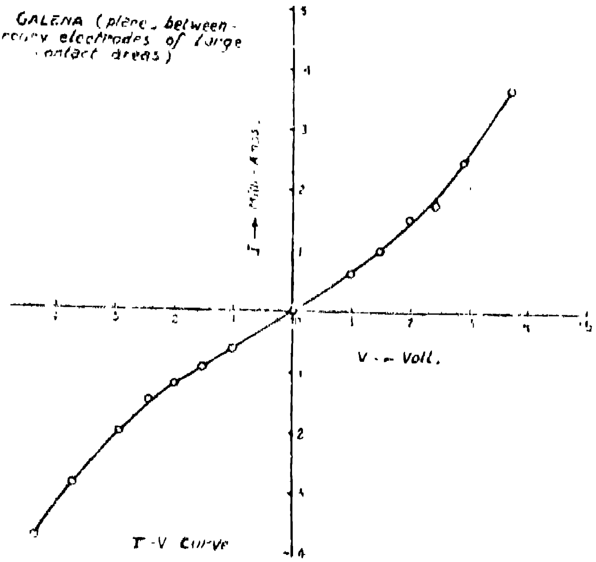

FIGURE 1

Characteristic curve is next drawn with both ends of the crystal well within mercury. The data given in Table I and the curve in Fig. 1 clearly show that under the given arrangement the crystal produces good rectificition.

(2) Iron-pyrites : Alternating voltage is applied to the crystal placed between mercury electrodes. A steady rectified current flows up when there are large contact-areas at the electrodes at both ends of the crystal. The upper contact-area is kept constant and the lower one is changed when the following results are obtained : (a) For a small area of contact the rectified current flows upwards, (b) for increasingly large contact-area the rectified current diminishes gradually, reaches a minimum value and then changes direction, i.e., flows downwards through the crystal. The experimental results obtained with direct voltage applied to the crystal are given in Table I and in Fig. 2. In this case characteristic curves have been obtained under two different adjustments. For the first, the rectified current flows upwards through the crystal and for the second it flows downwards. The curves reveal marked asymmetry and it is evident that the crystal should give good rectification effect under both the adjustments.

(3) Pyrolusite : In the case of the pyrolusite crystal the rectified current is highly prominent and as in the previous two cases it also changes direction under

suitable adjustments of the contact-areas at the electrodes. The results of D. C. test for this crystal are given in Table I and Fig. 3. The characteristic curve here also indicates the existence of a strong rectification effect with the crystal placed between mercury electrodes.

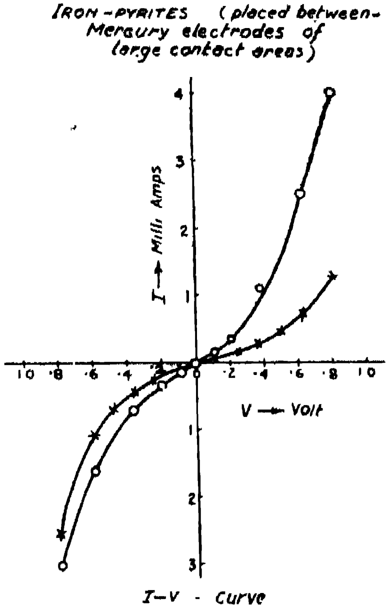

FIGURE 2

o—o—o—o for rectified current flowing upwards
×—×—×—×— ,, ,, ,, flowing downwards

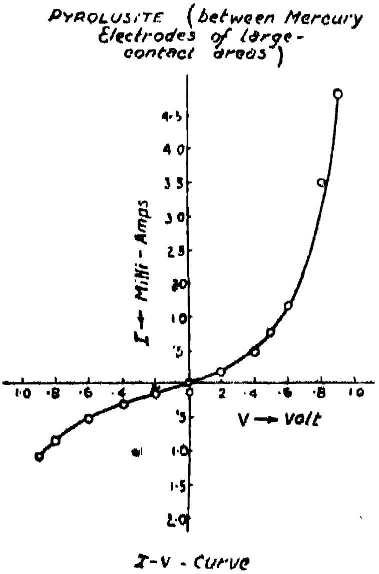

FIGURE 3

TABLE I

Voltage (volt)	Current (milli-amps)		Voltage (volt)	Current (milli-amps)	
	Up	Down		Up	Down
			Iron-pyrites		
Galena			(*a*)		
.10	.64	.62	.10	.15	.13
.15	1.00	.92	.20	.40	.30
.20	1.50	1.20	.38	1.10	.70
24	1.80	1.49	.62	2.50	1 60
29	2.50	2 00	.82	4.00	3.00
.37	3.75	2.85	(*b*)		
.43	4.80	3.70	.10	.05	.05
Pyrolusite			.24	.16	20
.2	.18	.15	.38	.30	38
.4	.50	.30	.50	.45	.60
.6	1.15	.50	.62	.70	1 00
.8	3.00	.90	.82	1.30	2.50
.9	4 30	1.10			

(*a*) For rectified current flowing upwards.
(*b*) For rectified current flowing downwards.

High-frequency A. C. test.

All the crystals are next tested with high-frequency alternating voltage obtained from a valve oscillator. In every case there is a pronounced rectified current so that it is definite that volume rectification is exhibited by these crystals, also with high-frequency current, when placed between mercury electrodes.

Crystals tested for the Dember effect.

To be sure that the volume rectification, so far obtained with the crystals in the above experiments, is not due to any Dember-effect produced by the diffused sun-light, experiments are repeated after cutting off the light from the crystal surfaces. Good rectification effect was, under this condition, obtained in all the cases by passing alternating current through the crystals.

DISCUSSION

In point-rectification it is an admitted fact that different parts of the surface of a crystal possess rectifying properties to quite different degrees. It may also be noted here that parts which have good rectifying properties exhibit very poor conductivity, whereas parts having good conductivity show very little rectifying action. Moreover, the rectification effects at different parts are also of different sense, *i.e.*, at some points the rectified current flows from crystal to whisker while at others it flows from whisker to crystal. The results of the experiments reported in the present paper, combined with the facts stated above, point to the conclusion that the volume rectification in crystals is due to the differential or the average effect of point or surface rectification occurring at the two electrodes. For, the surface of a crystal may be divided into a large number of rectifying regions of varying efficiency and giving rectification in opposite directions. At any particular electrode these regions, having varying degrees of rectification and revealing the effect in opposite directions, will produce a net rectified current whose magnitude and direction at that electrode will be determined by the predominance of the total effect in one direction (*i.e.*, of one sign) over that in the other. When we take into account the effects at both the electrodes, the final resultant direction of the rectified current through the crystal, for any particular adjustment of the contact areas of the electrodes, will be determined by the combined effects at the two surfaces of the crystal in contact with the electrodes. For instance, if the net rectification effect at one electrode A produces current from, say, crystal to electrode and that at the other contact B gives current from electrode to crystal, then the combined effect will be a very strong rectified current flowing through the crystal in the direction B-A. If, on the other hand, rectification effect at the end A produces current from crystal to electrode and that at the other end B also sends the current from the crystal to the electrode, then the resultant direction and magnitude of the rectified current will be determined solely by the strength or rather the difference of the strengths of the rectified currents produced at the two electrodes. Thus there is no distinction between point-rectification and the so-called volume-rectification of crystals, as regards the mechanism by which the effects take place. Both must be due to the same cause. The only difference between the two lies in the contact area at one of the electrodes. As a matter of fact the end of the whisker, in point-rectification, has never such an extremely small area as to lie on a single rectifying region but it would possibly rest on a number of rectifying regions generally of varying efficiency and different signs. It is thus quite possible for all crystals, exhibiting point-rectification, to give the effect—

the so-called volume-rectification—when placed between large electrodes on both sides.

PHYSICS LABORATORY,
RAJSHAHI COLLEGE,
RAJSHAHI.

REFERENCES

1 Krönig, *Nature*, **123**, March 2 (1929).
2 Khastgir and Das Gupta, *Ind. J. Phys.* **9**, 259-60 (1935).
3 Groetzinger and Lichtschim, *Phys. Zeit*, **38**, 202 (1937).
4 Sen, *Ind. J. Phys.* **10** 91-102 (1936).
5 Sen, *Nature*, **140**, 1102 (1937).
6 Khastgir and Das Gupta, *Ind J. Phys.*, **9**, 259 (1935)

ERRATA

In the paper '*On effect of resistance component in wave filter elements and performance of non-ideal filter sections*' by Waquar Ahmed (August, 1942, p. 231), in equation (2c), instead of " =a pure resistance," read "a reactive impedance" and in equation (5), instead of RR in first term under radical sign, read RR′.

SHUNT EXCITED BROADCASTING ANTENNA*

By S. S. BANERJEE

AND

S. Y. TIWARI

(*Received for publication, June 26, 1942*)

ABSTRACT. A theoretical study has been made of the effect on the intensity of the field radiated from a shunt excited antenna when the point of excitation is gradually altered. From the knowledge of the distribution of current in the upper and in the lower parts of the antenna, mathematical equations have been obtained for calculating the intensity of the field radiated from it Field strengths for quarter, half and full wave long antennae have been calculated at a ground distance of one wave-length from the base and suitable points for excitation have been indicated.

INTRODUCTION

The shunt excited antenna recently developed by Morrison and Smith[1, 2] has very closely drawn the attention of radio engineers due to its various advantages. Such an antenna offers a high economy in the cost of erection, owing to the elimination of base insulators and tower lightning chokes which are always associated with the insulated tower antenna so widely used for commercial broadcasting purposes. The shunt excited antenna is essentially a vertical antenna efficiently grounded and excited at a suitable point on it above the ground. It may be mentioned that this type of antenna is of recent origin and much work has not been done as yet with it. Baudoux[3] has lately studied theoretically the radiation, resistance and space radiation characteristics of such an antenna. It has been incidentally observed by the previous workers that the situation of the excitation point changes the field characteristics of such an antenna, though detailed and systematic results are still lacking.

In view of the importance of such an antenna, it has been felt necessary to study the various aspects of this in a more elaborate manner. The present communication deals with the effect on the intensity of the field radiated from a shunt excited antenna when the excitation point is gradually altered. Considering the distribution of current in the lower and upper parts of the antenna, the portion of it above the excitation point is assumed to behave like an insulated system. Equations have been obtained for the computation of the radiated energy

---

* Communicated by the Indian Physical Society.

following the method of Carter[4] and subsequently developed by Banerjee.[5] The present method possesses the advantage of being able to calculate the field strength for antenna of any length and for the excitation point being situated at any point above the ground. The field strengths due to quarter, half and full wave antennae at a distance of one wave-length on the ground have been calculated and their variation with the alteration of feeding point has been graphically shown. It may be noted that in the case of a quarter wave antenna the radiated field strength is not affected by changing the excitation point as the current distribution along the antenna remains unaltered by a change of the feeding point.

METHOD OF CALCULATION

Let AB in Fig. 1 be an antenna of length l grounded at its base B. Let it be excited at a point C in it which is at a height h_0 above the ground.

If I donotes the maximum amplitude of the current and i the instantaneous current at an arbitrary point on the antenna at a vertical distance h from the ground, it can be shown that the instantaneous current i_u at a point in the upper part of the antenna AC is given by,

$$i_u = \mathrm{I} \sin m\,(l-h)\, e^{j\omega t}$$

where $m = 2\pi/\lambda$,

and $\omega =$ the angular frequency of the wave.

Similar current, i_l at a point in the lower part of the antenna, BC, is given by

$$i_l = \mathrm{I}' \cos mh\; e^{j\omega t}$$

where $\mathrm{I}' = \mathrm{I} \cos m\,(l-h_0)/\sin mh_0.$

In view of the above distribution of current, the field strength at any point P in space can be calculated from the resultant of the fields radiated by the part AC of the antenna which may be treated as insulated and by the part BC which is a grounded antenna.

We shall first find out the field strength due to the lower part BC of the antenna in which the distribution of the current is given by

$$i = \mathrm{I}' e^{j\omega t} \cos mh \qquad \dots (1)$$

If ρ denotes the charge density at any point on the antenna and i the current at the same point, both in the electrostatic units, then according to the law of continuity we may write,

$$\frac{\partial \rho}{\partial t} = -\frac{\partial i}{\partial h},$$

from which we get $\rho = -j\, \dfrac{\mathrm{I}'}{c} e^{j\omega t} \sin mh, \qquad \dots (2)$

where c = velocity of light.

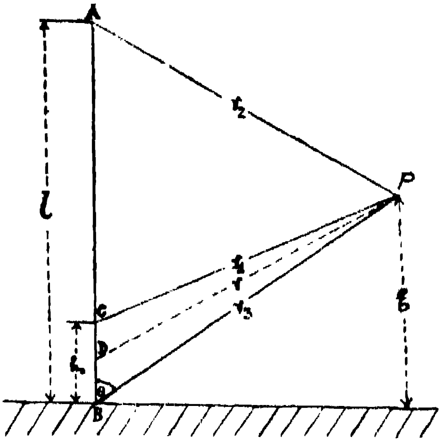

FIGURE 1

The electric force E_z at P (Fig. 1) parallel to the length of the antenna and due to the length BC may be determined from the retarded vector and scalar potentials V and A respectively from the relation,

$$E_z = -\text{grad}_z\, V - \frac{1}{c}\frac{\partial A}{\partial t} \qquad \ldots \quad (3)$$

where

$$V = \int_0^{h_0} \frac{[\rho]_{t-\frac{r}{c}}}{r}\, dh \qquad \ldots \quad (4)$$

and

$$A = \int_0^{h_0} \frac{[i]_{t-\frac{r}{c}}}{r}\, dh \qquad \ldots \quad (5)$$

From equations (1), (2), (4) and (5), after putting sin mh in the exponential form, we get,

$$V = -\frac{I'}{2c} e^{j\omega t} \int_0^{h_0} \left[\frac{e^{-jm(r-h)}}{r} + \frac{e^{-jm(r+h)}}{r} \right] dh \qquad \ldots \quad (6)$$

and

$$A = -\frac{I'}{2c} e^{j\omega t} \int_0^{h_0} \frac{\partial}{\partial z} \left[\frac{e^{-jm(r-h)}}{r} - \frac{e^{-jm(r+h)}}{r} \right] dh \qquad \ldots \quad (7)$$

It can be shown from Fig. 1 that $\frac{dr}{dz} = -\frac{dr}{dh}$.

Using this relation, it can be shown after integration that

$$E_z = -j\frac{I'}{c} e^{j\omega t}\, \frac{e^{-jmr_1}}{r_1} \sin mh_0$$

As the part BC of the antenna is grounded, the actual field strength will be given by

$$E_z = -2j\frac{I'}{c}e^{j\omega t}\frac{e^{-jmr_1}}{r_1}\sin mh_0 \qquad \ldots \quad (8)$$

The distribution of current in the upper portion AC, which may be treated as insulated, is given by

$$i = Ie^{j\omega t}\sin m(l-h).$$

Proceeding in the same manner as above, it can be shown that field strength due to this part will be given by

$$E_z = j\frac{I}{c}e^{j\omega t}\left[\frac{e^{-jmr_1}}{r_1}\cos m(l-h_0) - \frac{e^{-jmr_2}}{r_2}\right]. \qquad \ldots \quad (9)$$

Assuming the feeder lines to be non-radiating, the total field strength at P due to the shunt excited antenna AB may be written from equations (8) and (9) as

$$E_z = j\frac{I}{c}\left[\frac{e^{-jmr_1}}{r_1}\cos m(l-h_0) - \frac{e^{-jmr_2}}{r_2} - \frac{2e^{-jmr_1}}{r_1}\cdot\frac{\cos m(l-h_0)}{\sin mh_0}\cdot\sin mh_0\right]. \qquad \ldots \quad (10)$$

Taking only the real parts, equation (10) may be written as

$$E_z = -\frac{I}{c}e^{j\omega t}\left[\frac{\sin mr_1}{r_1}\cos m(l-h_0) + \frac{\sin mr_2}{r_2}\right] \qquad \ldots \quad (11)$$

For the sake of convenience of calculation, we may express the lengths involved in the above equation in terms of the wave length and thus we may write

$l = M\lambda$, $h_0 = N\lambda$ and $r_3 = K\lambda$, where M, N and K are some constants.

Therefore, $r_2 = \lambda\sqrt{K^2 + M^2 - 2KM\cos\theta}$

and $r_1 = \lambda\sqrt{K^2 + N^2 - 2KN\cos\theta}$

Equation (11) may then be written as

$$E_z = -A\left[\frac{\sin 2\pi\sqrt{K^2+N^2-2KN\cos\theta}}{\sqrt{K^2+N^2-2KN\cos\theta}}\cos 2\pi(M-N) + \frac{\sin 2\pi\sqrt{K^2+M^2-2KM\cos\theta}}{\sqrt{K^2+M^2-2KM\cos\theta}}\right] \qquad \ldots \quad (12)$$

where $A = \frac{I}{c}e^{j\omega t}$.

It should be mentioned that when the length of the shunt excited antenna is $\lambda/4$, the distribution of the current in both the parts is given by $i = I \cos mh$, and therefore the entire length of the antenna may be treated as one quarter wave earthed antenna The field strength due to such an antenna will then be given by

$$E_t = -2\frac{I}{c}.e^{j\omega t}\ \frac{\sin mr_2}{r_2} \cos ml$$

and this is independent of the excitation point.

CALCULATED RESULTS

Fields radiated from antennae having half and full wave-lengths at a radial distance of λ from the base of them have been calculated by equation (12) for different excitation points. Tables I and II below show the results for half wave and full wave antennae resepectively. In order to compare the radiation from shunt excited antenna with that from the base insulated one of the same length, the intensities of the fields emitted from the latter type have been calculated. These values are shown at the bottom of the tables for the corresponding lengths of the antennae.

TABLE I

Half wave antenna

Height of excitation point from the ground in fractions of λ	Field strength in fractions of Λ
1/32	−.6046
1/24	−.5989
1/16	−.5930
1/8	−.0331
1/4	−.6046
1/3	−.7678
—	—
—	—
—	—
—	—
Insulated	−.6046

TABLE II

Full wave antenna

Height of excitation point from the ground in fractions of λ	Field strength in fractions of Λ
1/32	−.3639
1/24	−.3693
1/16	−.3753
1/8	−.3992
1/4	−.3639
1/3	−.2007
2/5	−.0145
1/2	+.2407
2/3	+.0326
3/4	−.3639
Insulated	−.3639

The variation of the field strength with the change of excitation point for the above antennae has been depicted graphically in Fig. 2, neglecting the direction of the field indicated in the tables. The continuous curve represents the field intensities for half wave antenna and that with the broken lines represents the same for full wave antenna.

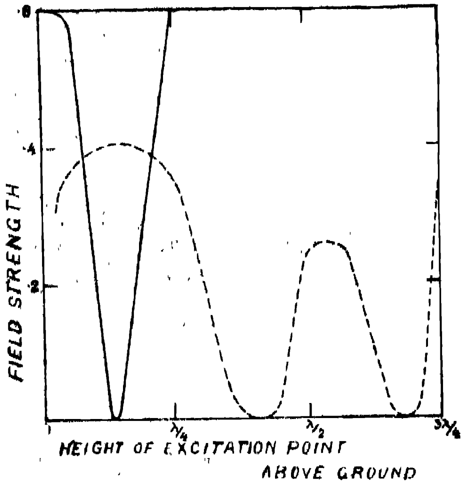

FIGURE 2

It will be observed from these curves that the radiated field strength from the half wave shunt excited antenna very rapidly falls when the point of excitation is lifted beyond the height of $\lambda/4$ from the ground. This kind of rapid fall, however, is not observed in the case of full wave antenna. Comparing the intensity of the fields radiated from a shunt excited antenna with that radiated from the insulated one of the same length, it may be concluded that the profitable point of excitation for the half wave antenna would be below $\lambda/16$ and above $\lambda/4$. Such points for the full wave antenna should be above the height of a quarter wave from the ground.

WIRELESS SECTION,
PHYSICS LABORATORY,
BENARES HINDU UNIVERSITY.

REFERENCES

[1] J. F. Morrison and P. H. Smith, *Proc Inst. Rad. Eng.*, **24**, 685 (1936).
[2] J. F. Morrison and P. H. Smith, *Proc. Inst. Rad. Eng*, **25**, 673 (1937).
[3] P. Baudoux, *Proc. Inst. Rad. Eng.*, **28**, 271 (1940).
[4] P. S. Carter, *Proc. Inst., Rad. Eng.*, **20**, 1004 (1937).
[5] S. S. Banerjee, *Phil. Mag.*, **19**, 787 (1935).

STRUCTURE OF THE ELECTRONIC BANDS OF THE OD MOLECULE—PART VI (ISOTOPIC SHIFT)

By M. G. SASTRY

ABSTRACT. From the constants of the OH molecule, the vibrational and rotational isotope shift in the OH and OD band heads have been calculated In estimating the rotational shift, a direct method of using Hill and Van Vleck's theoretical expression for the rotational energy for doublet electronic states representing any stage of coupling, has been adopted. When the total calculated shifts are compared with the observed shifts obtained directly from experiment, large discrepancies are found. No electronic shift could be postulated and, if it exists, it is estimated to be less than a unit of wave number.

INTRODUCTION

It was pointed out in Part I of this series of papers that OH and OD form an interesting pair of isotopic molecules, the band structure of which yields valuable information on the isotopic effect in band spectra. Apart from the conventional treatment of the isotopic effect in molecular spectra, Johnston and Dawson[1] considered from unpublished data the isotope effect on the spacings of the spin components and the Λ-coupling electronic isotopic effect associated with the $^2\pi$ components of the OH and OD molecules. These considerations have been dealt with by the author in the earlier parts.

In a short note, Johnston and Dawson[2] reported at first the presence of a large electronic isotope shift, amounting approximately to about 10 cms^{-1} in the lines at the head of the (1,0) band. Later, they considered the isotopic displacements of three of the heads, (2,0), (1,0) and (0,1).[3] In deriving the total displacements, they have calculated the vibrational, rotational and spin coupling effect separately and indicated that there is agreement between the calculated and observed displacements if, instead of postulating a large electronic shift, the spin coupling effect is taken into account. It must be pointed out, however, that according to their own calculations, the agreement is close only in the case of the (2,0) band and perhaps also of the (1,0) band, but in the (0,1) band there is a difference as large as about 10 cms^{-1}.

In H^1H^1 and H^1H^2 band systems, a large electronic shift, as high as 136 units was observed by Jeppesen[4], Dieke[5], and Dieke and Lewis[6], from a study of the H_2, HD, D_2 band systems observed that these electronic shifts could be accounted for by taking correction terms arising from the interaction between the electronic motion and the rotation and vibration in the case of diatomic molecules. These correction terms, discussed by Van Vleck[7], become very important in the case of such light isotopic molecules as H_2, HD, etc.

In view of the theoretical importance of the determination of the isotope shifts in bands where H and D are involved, a detailed study of the isotope effect in OH and OD bands has been attempted by the author. In this paper the shifts of the heads of the various bands are considered, as was done by Johnston and Dawson, but following a more direct method in the evaluation of the shift. In a later paper, the method will be applied for studying the displacements of the various lines in the individual bands. A very direct and appropriate method[8] of investigating the isotope effect would be to determine with *a high degree of precision* the constants of both the molecules of OH and OD and to determine therefrom the values of the first, second and third powers of the mass factor and to compare these with the corresponding values from mass spectra data. For this purpose, experiments must be carried out with mixtures of ordinary and heavy water, obtaining thus the band systems of both the molecules without any relative mechanical shifts. Such a method is found practicable if the study is made on the (2,0) and (3,1) bands of these molecules ; the results will be published in the next part of these papers.

CALCULATION OF THE ISOTOPE SHIFT

Vibrational shift.—The vibrational isotope displacement of the (v', v'') band can be directly determined from the equation (Jevons' Report, p. 213):

$$\nu_v^i - \nu_v = (\rho - 1)\left\{\omega'_e\left(v'+\tfrac{1}{2}\right) - \omega''_e\left(v''+\tfrac{1}{2}\right)\right\} - (\rho^2 - 1)\left\{x'_e\omega'_e\left(v'+\tfrac{1}{2}\right)^2 - x''_e\omega''_e\left(v''+\tfrac{1}{2}\right)^2\right\} + (\rho^3 - 1)\{-\} \text{ etc.} \quad \ldots \quad (1)$$

The values of the constants used in this and the succeeding equations are listed in Table II at the end. For the (1,0) band the shift is obtained as −697.64 units.

Rotational shift.—The rotational isotopic displacement of a band line is given by the expression (Jevons' Report, p. 216):

$$\nu_r^i - \nu_r = (\rho^2 - 1)\{B'_eN'^2 - B''_eN''^2\} - (\rho^3 - 1)\{\alpha'U'N'^2 - \alpha''U''N''^2\} + (\rho^4 - 1)\{D'_eN'^4 - D''_eN''^4\} + \text{ etc.} \quad \ldots \quad (2)$$

negecting higher terms.

In estimating the proper values of N′ and N″ in equation (2), use is made of general expression for the rotational energy derived by Hill and Van Vleck (Jevons' Report, p. 124) for doublet electronic states representing any intermediate stage of coupling between Hund's Case (*a*) and Case (*b*).

$$F(J) = B_v\left[(J+\tfrac{1}{2})^2 - \Lambda^2 \pm \sqrt{\left\{(J+\tfrac{1}{2})^2 - \frac{\Lambda^2 A}{B_v}\left(1 - \frac{A}{4B_v}\right)\right\}}\right] \quad (3)$$

neglecting the small term involving γ and the term in D_v.

The following illustration shows the calculation for the (1,0) band :

(*a*) The band lines are expressed by the formula

$$\nu = \nu_0 + (B'+B'')M + (B'-B''+D'-D'')M^2 + 2(D'+D'')M^3. \quad \ldots \quad (4)$$

By differentiation,

$$(d\nu/dM) = (B' + B'') + 2M(B' - B'' + D' - D'') + 6M^2(D' + D''). \qquad \ldots \quad (5)$$

Equating this to zero we get the value of M corresponding to the head. In general this value is not integral. Hence in choosing the proper value, that particular nearest integer is adopted for which the value of ν is maximum. This procedure is considered to be justifiable as the band is degraded to the red. Perhaps the experimental value of M might be preferred to that derived from equation[4] in the above manner but it is to be noticed that even the experimental value is not unique, the head of the band often being assigned two or more values of J, for want of adequate resolution.

Substituting the values of the rotational constants shown in Table II at the end, we obtain $M = 6.58$. The proper integer chosen is $M = 7$; the head of the band (1,0) then corresponds to $J' = 7$, and $J'' = 6$.

(2) Hence for the initial state, from equation (3) $N'^2 = 48.75$ and for the final state $N''^2 = 34.25$.

(3) Substituting these values of N' and N'' in equation (2) we obtain,

$$\nu_r^i - \nu_r = \delta\nu_r = -59.67.$$

The results obtained in the case of all the bands in the above manner have been collected in Table I. In the fifth column of this table are given the shifts directly obtained from the measurements on the plates in which the OH and OD bands are obtained in juxtaposition on either side of the standard Fe arc spectrum.

TABLE I*

Isotope shifts

Band (v', v'')	Vibrational	Rotational	Total calculated shift	Observed shift	Obs.-Calc.
(0, 0)	+ 76.7	− 90.1	− 13.4	− 12 4	+ 1.0
(1, 0)	− 697 6	− 59.7	− 757 3	− 749.3	+ 8.0
(2, 0)	−1380.2	− 46 8	−1427.0	−1414.8	+12.2
(3, 0)	−1971 2	− 39.7	−2010.9	−1994.5	+16.4
(0. 1)	+1014.8	−140 4	+ 874 4	+ 860.6	−13.8
(1, 1)	+ 240.6	− 75.3	+ 165.3	+ 166 7	+ 1.4
(2, 1)	− 442.0	− 52.8	− 494.8	− 486.7	+ 8.1
(3, 1)	−1033.1	− 40.7	−1073.8	−1061 8	+12.0
(2, 2)	+ 418.7	− 63 5	+ 355.2	+ 358.6	+ 3.4
(3, 2)	− 172.3	− 45.8	− 218.1	− 200.1	+18.0

* The values quoted in the above table are a revision of those published in Current Science (Vol. X, No. 8, 1941 pp. 362-63). In the note

(1) in estimating the vibrational shifts the third term in y', w', has been omitted,

(2) in estimating the rotational shifts from the general expression the value of M, is directly substituted for N, hence the difference.

The last column in the table shows rather large discrepancies between the observed and the calculated values, the differences showing an increase with increasing values of v'. It is possible that they may be due partly to the uncertainity in the choice of M, but on calculation with different integral values of M a change of only 2 to 3 units in the final values of the rotational shift is obtained.

A definite electronic isotope shift cannot be postulated ; and, if at all there is one, it must be less than a unit as the observed *minus* calculated values for the (0,0) and (1,1) bands are only of this order. It would seem therefore that the differences are to be ascribed either to the inadequacy of or the approximations made in the theoretical expression used for the rotational energy; for instance, in neglecting the terms $D_v J^2(J+1)^2$, and the small term involving γ ; it must be emphasised also that the errors in the evaluation of the various constants for the OH molecule adopted in obtaining the shifts cannot be negligible.

TABLE II

Values of the Constants[9]

$H^1 = 1.00778$; $\rho - 1 = -0.271931$; $\rho^3 - 1 = -0.614062$.

$H^2 = 2.01363$; $\rho^2 - 1 = -0.469915$; $\rho^4 - 1 = -0.719011$.

$O = 16.000$

$\omega'_e = 3184.1$; $x'_e \omega'_e = 97.7$

$\omega''_e = 3734.9$; $x''_e \omega''_e = 82.6$

$B'_e = 17.375$	$B''_e = 19.009$	$D'_e = -2.07.10^{-3}$	$D''_e = -1.97.10^{-3}$
$B'_0 = 16.954$	$B''_0 = 18.663$	$\alpha' = 0.838$	$\alpha'' = 0.686$
$B'_1 = 16.101$	$B''_1 = 17.952$	$\beta' = 4.3.10^{-5}$	$\beta' = 5.0.10^{-5}$
$B'_2 = 15.233$	$B''_2 = 17.216$	$\gamma'_e = -0.0075$	$\gamma''_e = -0.0125$
$B'_3 = 14.350^{\dagger}$	$A = 141.0$		

The author is indebted to Dr. K. R. Rao and to Dr. R. K. Asundi for helpful advice in the preparation of this paper. His thanks are also due to the Andhra University for the award of a Fellowship.

ANDHRA UNIVERSITY,
GUNTUR.

REFERENCES

[1] *Phys. Rev.*, **46**, 79 (1934).
[2] *Naturwiss.*, **21**, 495 (1933).
[3] Quoted by Urey and Teal, *Rev. Mod. Phys.*, **7**, 83 (1934).
[4] *Phys. Rev.*, **46**, 480 (1934).
[5] *Phys. Rev.*, **47**, 661 (1935)
[6] *Phys. Rev.*, **52**, 100 (1937).
[7] *Journ. Chem. Phys.*, **4**, 327 (1936).
[8] (*a*) Babcock and Birge, *Phys. Rev.*, **37**, 233 (1931) ; (*b*) Jenkins and McKellar, *Phys. Rev.*, **42**, 464 (1932) ; (*c*) McKellar, *Phys. Rev*, **44**, 155 (1933) ; (*d*) Dieke and Lewis, *loc. cit.*
[9] For the isotopic masses : Bainbridge, *Phys. Rev.*, **41**, 115 (1932) ; For the vibrational and rotational constants of OH : Johnston, Dawson and Walker, *Phys. Rev.*, **43**, 480 (1933).

† Extrapolated value.

MEASUREMENT OF THE ANGLE OF ARRIVAL OF DOWNCOMING WAVES FROM INDIAN REGIONAL SHORT-WAVE STATIONS

By M. R. RAO

(Received for publication, June 29, 1942)

Plates IX and X

ABSTRACT. Results of the measurements of downcoming angles carried out at Delhi on signals radiated from the Bombay and Madras broadcasting stations of All-India Radio are given and discussed. Close agreement has been found between the experimental and the theoretical values. Use of pulse signals radiated from these stations made it possible to resolve the downcoming waves into their component waves and to determine the downcoming angles of each. The results provide an interesting study of the importance of the various parameters which may control propagation under given conditions. The role of the intervening ionized strata such as the E-layer is also analysed and discussed.

INTRODUCTION

The importance of a knowledge of the angle of arrival of short-waves propagated *via* the ionosphere has been pointed out in an earlier paper.[1] The present programme of work was undertaken to analyse the propagation conditions that prevail in the case of transmissions from the regional short-wave transmitters of All-India Radio. As will be apparent from a study of the results presented in the text, use of pulse signals not only helped to overcome the difficulty experienced in connection with the agitation and haphazard rotation of the patterns appearing on the cathode-ray oscillograph screen, but also helped to resolve the downcoming waves into their various components, thus providing direct information regarding the extent and importance of the various modes of propagation prevailing at any time. The use of pulse signals for downcoming angle measurements is therefore a very potent and vigorous method of attack for obtaining information on short-wave propagation.

HISTORICAL

Various methods of measurement have been adopted by previous workers in this field of downcoming angle measurements, some of the notable workers among them being Friis,[2] Eckersley,[3] Hollingworth,[4] Friis, Feldman and Sharpless,[5] Wilkins,[6] Crone, Kruger, Goubau and Zenneck,[7] Eyfrig,[8] Edwards,[9] and Chamanlal.[1] Here the various methods are described briefly. Friis used two vertical aerials spaced one-third of a wavelength apart to collect the signal and used a C.R.O. for measuring the phase difference. The method employed by Hollingworth consisted in recording simultaneously the signals picked up on a vertical aerial and a loop aerial with its plane in the plane of propagation. It can be shown that ratio of the e.m.f. developed in the vertical aerial to that in the loop is proportional to the cosine of the angle of incidence measured to the horizontal. Also instead of recording signal strengths, he employed two amplifiers the gains of which were adjusted to give a null on a galvanometer when connected differentially to the outputs of the amplifiers. The ratio of the outputs of the amplifiers would then give the cosine of the angle of incidence. Eckersley used another development of the vertical and loop aerial. Wilkins, and recently Chamanlal employed the method developed by the Radio Research Board of England. It consists essentially in measuring the phase difference set up in two similar and parallel horizontal aerials with their centres in the great circle path of the transmitter and with their axes at right angles to it. A C.R.O. is used for measuring the phase difference. Friis, Feldman and Sharpless employed primarily two methods known as (*i*) the Differential output method, and (*ii* the Phase method. In the differential output method, they employed two horizontal aerials with different heights above the ground to give a contrasting directional pattern in the vertical plane and the outputs were recorded simultaneously on integrating field-strength recorders and the ratio of the output was the measure of the downcoming angle. In the phase method, two vertical aerials spaced apart in the great circle path between transmitter and receiver were used and the difference in phase set up was either measured by inserting a calibrated phase adjuster in one of the limbs and adjusting for balance or measured on the C.R.O. in the usual way. Edwards and Jansky used the very elaborate musa system with an array of rhombic antennae.

The present method is the same as used by Chamanlal [1] in the determination of the downcoming angles of foreign short-wave stations. This method is adopted for two reasons. It is easy to set up, and it works admirably well on pulse signals. With the help of a C.R.O., it is possible to resolve the wave into its component rays and to measure their downcoming angles simultaneously.

THEORY

The basic principle underlying the method is illustrated in Fig. 1.

A and B are two parallel horizontal aerials and EA is the direction of the downcoming ray making an angle θ to the horizontal. The phase difference set up as a result of the path difference AF is given by :

$$\varphi = \frac{2\pi d}{\lambda} \cos\theta \cos\psi \text{ radians,}$$

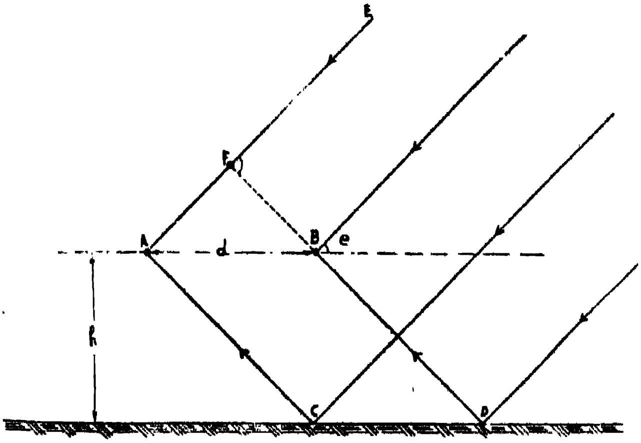

FIG. 1

where d = Spacing in metres between the two parallel aerials.

λ = The wave-length in metres of the wave under investigation.

θ = The downcoming angle of the incident wave measured to the horizontal.

ψ = The angle between the direction of the transmitting station and the line joining the centres of the aerials.

It can be shown that in a homogeneous field the effect of the ground will be similar for both the aerials. Though it might affect the signal strength, it does not alter the phase relationship. θ, the downcoming angle, can be calculated if ϕ is measured.

The requisite part of the experiment is the correct measurement of this phase difference. When the e.m.f.'s of the aerials are fed to the opposite pairs of plates of the C.R.O., an ellipse is formed. If the two e.m.f.'s are equal, the major axis of the ellipse will be inclined at an angle of 45° to the axes of the C.R.O. screen and the eccentricity of the ellipse is dependent upon the phase difference between the two e.m.f.'s. However the aerial outputs are to be considerably amplified before a suitable deflection can be obtained on the C.R.O. For this purpose amplifiers are used.

THE EXPERIMENTAL SET-UP

The set-up is essentially the same as was used by Chamanlal[1] in his earlier work. Therein the set-up and the technique of measurement are dealt with in detail. Here only a brief description need be given.

Two horizontal doublet aerials 12 feet high, cut for the proper wave-length and spaced suitably, are used as signal collectors. The outputs are taken through twisted flex feeders on to a 'Receiving hut.' In the hut, are housed the shielded aerial switching panel and the amplifier assembly. The amplifier assembly consists of two commercial receivers, each receiver consisting of two stages of R.F. amplification and five stages of I.F. amplification. The local oscillators in the receivers are made inactive. An external oscillator replaces them and feeds both the receivers similarly and in the same phase. This ensures that the same phase relationship is passed on from the R.F. to I.F. stages. The outputs of the final I.F. amplifiers are fed to the opposite pairs of the plates of the C.R.O. The aerial switching panel consists of two shielded double-pole double-throw switches connected in such a way that any one of the two receivers can be connected to any of the two aerials separately or together.

PROCEDURE

The desired station is tuned in by means of the heterodyning oscillator and by setting the receivers approximately to the desired station. The same aerial is connected to both the receivers. Then the finer tuning is made by the help of the C.R.O. for maximum deflection. By slight adjustment of the tuning condenser and R.F. gain controls of the receivers, the trace on the C.R.O. is made into a line inclined at 45° to the horizontal and vertical axes. In this condition the receivers will have the same gain and zero phase difference. All that is then necessary is to put the two receivers on independent aerials and record the resultant ellipse. The resultant ellipse should not change its size or shape by interchanging the aerials. It however does change under improper conditions.

The improper conditions arise due to the input impedance conditions not remaining the same when the two receivers are connected in parallel to the same aerial as when they are connected independently to two separate aerials. In this case when the two receivers are connected in parallel and adjusted for zero phase and then changed over to independent aerials, the change in input impedance introduces a certain error which manifests itself as an extra phase difference. This extra phase difference adds up in one case and subtracts in the other from the incoming phase, when the aerials are interchanged. The change of shape of the ellipse noticed is due to this. It is obvious that the correct phase difference is the mean of the two. If, however, the extra phase introduced is large, the results become complicated. Taking for instance a case where the phase difference set up between the aerials is only 10° while the impedance error is say 20°, the eccentricity of the ellipses appearing on the C.R.O. will be $10° \pm 20°$, *i.e.*, $-10°$ and $30°$. An ellipse of a phase difference $-10°$ means the same as the one of $10°$. Thus the ellipses are of 10° and 30° eccentricity and the mean of the two gives a value of 20° which is erroneous. With a view to correct this, the input circuits in the earlier work [1] were made resistive by connecting very low value resistances across the inputs. This, however, reduces the gains considerably. In the present set-up the problem is solved slightly differently. The two receivers, particularly their input circuits, are aligned very carefully by means of a sweep frequency oscillator. This alignment is carried out right on the working band itself to ensure absolute identity. It was found by this that no extra phase error is introduced because the two input circuits being identical are affected equally. Any slight error that may creep in will be accounted for by taking the mean of the two values. This improvement over the previous method gave greater sensitivity to the receivers and better definition to the ellipses.

BEHAVIOUR AND INTERPRETATION OF THE ELLIPSES APPEARING ON THE C.R.O. SCREEN

Under actual working conditions it was observed that the two regional stations, Bombay and Madras, seldom gave ellipses that were sufficiently steady for downcoming angle measurements. The ellipses were often found to rotate, and change their size and shape in a haphazard manner. It was the worst in the mornings and the nights when multiple reflections were many. During the noon and early evening they were steadier. Mention is to be made of Madras signals in the early evenings. When Madras was working on 60 metres the signals were extremely steady though poor and the ellipse on the C.R.O. hardly changed its eccentricity. The pulse transmission at this time gave a single return indicating single ray transmission.

USE OF PULSE SIGNALS

This unsteady nature of the ellipse is known to every worker in this field and is correctly ascribed to energy being received in more than one direction in the vertical plane. (Friis, Feldman and Sharpless are probably the first to bring into use the pulse signals for downcoming angle measurements.) If the transmitter sends out short duration pulses instead of a steady carrier, the incident wave could be resolved into component rays. Each pulse signal sent out, travelling by several different paths or different numbers of reflections, would arrive at the receiving end as a succession of pulses, each characterised by its time-delay and by its angle of arrival. These characteristics are made use of to study the component rays separately.

In the present case pulses were radiated at a rate of 50 per second, each occupying about ·0004 second. The pulse signals are received in the same way as the carrier, with this difference that the receiving equipment is suitably modified. Pulse reception calls for wide-band receivers. This was achieved by modifying the equipment by introducing resistances in the tuned circuits of the I.F. stages, thus flattening out their response characteristics.

Typical patterns of the succession of pulses received at Delhi from Bombay and Madras broadcasting stations are given in plates IX and X. They give information on the time-delays suffered by each ray and they also show the energy distribution in the component rays of an incident wave. This will be dealt with more fully later. Such patterns are obtained by tuning in the pulse signals on one of the dual-receivers and applying the amplified signals to the vertical deflecting plates of the C.R.O., to the horizontal deflecting plates of which is applied a linear time base of 50 cycles per second and synchronized with the pulse frequency. If, however, to the horizontal plates, the signals from the other receiver are applied instead of the linear time base, ellipse patterns such as the ones shown in plate X are obtained. The ellipses formed will be equal in number to the number of component pulses, the size and eccentricity of each depending upon the amplitude and downcoming angle respectively of the component pulses.

The pulse-pattern and the ellipse-pattern combined give all the necessary information.

In practice, the method adopted for recording the pulse and ellipse-patterns is to take a series of photographs of each by means of a camera. The pulse-patterns could be switched over to the ellipse pattern by operating a switch.

The calculation of the downcoming angle from the eccentricity of the ellipse is then a simple matter. This was discussed fully in the earlier paper referred to before.

RESULTS

The results cover a period of eight months from 27th February, 1941, to 12th November, 1941. They are presented in a tabular form (Table I) giving the most common downcoming angles obtained during the period of measurements for the various transmissions. The actual mode of propagation

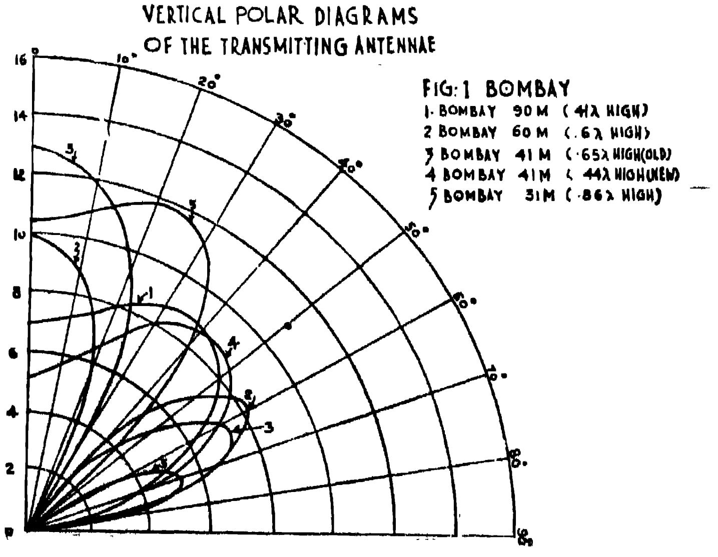

FIG. 2

TABLE I

Transmission No.	Transmission between—	Working wave-length in metres	Height of transmitting antenna	Period of measurements	Time of measurements	Average downcoming angle (measured) to the horizontal	Order of hop	Strongest hop	Layer governing the transmission
III Part—II	Bombay and Delhi	90	.41λ	March—April '41	Night	44° 56°	2nd hop 3rd hop	3rd hop	F - Layer
”	”	60	.6λ	April '41	”	27° 46°	1st hop 2nd hop	1st hop	F—Layer
III Part—I	”	60	6λ	March—April '41	Early evening	8° 19°	1st hop 2nd hop	2nd hop in March 1st hop in April	E—Layer
”	”	41	.65λ	April '41	”	46°	2nd hop	2nd hop	F—Layer
II	”	31	.86λ	May '41	Noon	22°	2nd hop	2nd hop	E—Layer
”	”	41	.44λ	Oct.—Nov. '41	”	21° 40° 47° 59°	1st hop 2nd hop 3rd hop 4th hop	2nd hop	F2—Layer
Trans. I	”	41	.65λ and .44λ	August—Nov. '41	Morning	21° 38° 53° 63°	1st hop 2nd hop 3rd hop 4th hop	1st & 2nd hops with the higher antenna, and 2nd & 3rd hops with the lower antenna.	F—Layer
Trans. III (Part—II)	Madras and Delhi	90	.49λ	March—April '41	Night	30° 45°	2nd hop 3rd hop	2nd & 3rd hops	F—Layer
	”	60	.71λ	April '41	”	17½° 45° 52° 56°	1st hop 3rd hop 4th hop 5th hop	1st hop	F—Layer

TABLE I (*contd.*)

Transmission No.	Transmission between—	Working wave-length in metres	Height of transmitting antenna	Period of measurements	Time of measurements	Average down-coming angle (measured) to the horizontal	Order of hop	Strongest hop	Layer governing the transmission
Trans. III (Part—I)	Madras and Delhi	60	.71λ	March—April '41	Early evening	9°.75 19°	2nd hop 3rd hop	2nd hop in April 3rd hop in March	E—Layer
	,,	41	.56λ	April '41	,,	35° 46°	2nd hop 3rd hop	2nd hop	F$_2$—Layer
Trans. I	,,	41	.56λ .44λ	August—Nov. '41	Morning 7-30 A.M.	8° 24° 35° 45° 56°	1st hop 2nd hop 3rd hop 4th hop 5th hop	3rd hop	F—Layer
					Morning 9 A.M.	8° 22° 44° 55°	1st hop 2nd hop 3rd hop 4th hop	3rd hop	F$_1$—Layer F$_2$—Layer

TABLE II*

Station	Transmission I		Transmission II		Transmission III				Period of operation
					Part I		Part II		
	Wave-length in metres	Duration	Wave-length in metres	Duration	Wave-length	Duration	Wave-length	Duration	
		I. S. T.		I. S. T.	Metres	I. S. T.	Metres	I. S. T.	
Bombay	41.44	0800-1000	31.4λ	1230-1425	61.48	1700-1915	89.15	1930-2245	1st November, 1940 to 15th April, 1941.
	,,	0730-0930	,,	,,	41.44	,,	61.48	,,	16th April, 1941 to 15th May, 1941.
	,,	,,	41.44λ	,,	,,	,,	,,	,,	16th May, 1941 to 15th October, 1941.
	,,	0800-1000	,,	,,	61.48	1615-1915	89.15	,,	16th October, 1941 to date
Madras	41.27	0730-0900	31.35λ	1330-1500	60.98	1600-1845	87.34	1900-2230	1st November, 1940 to 15th April, 1941
	,,	,,	,,	,,	41.27	,,	60.98	,,	16th April, 1941 to 15th May, 1941.
	,,	,,	41.27λ	,,	,,	,,	,,	,,	16th May, 1941 to 15th October, 1941
	,,	,,	,,	1300-1500	60.98	,,	87.34	,,	16th October, 1941 to date.

---

* Please note that the I.S.T. referred to is 5½ hours ahead of G.M.T.

and the downcoming ray of maximum energy are also indicated in this table. As mentioned earlier, these measurements were mostly on pulse signals. Special pulse transmissions were radiated for about 15 minutes' duration before the commencement of and soon after the close of any particular transmission. Table II gives the details of the transmission hours and the wave-lengths in the case of Bombay and Madras stations of All-India Radio on which the measurements were conducted. From the results arrived at on the pulse transmissions that were radiated just before and just after a particular transmission, the mode of propagation that prevailed during the actual transmission is deduced.

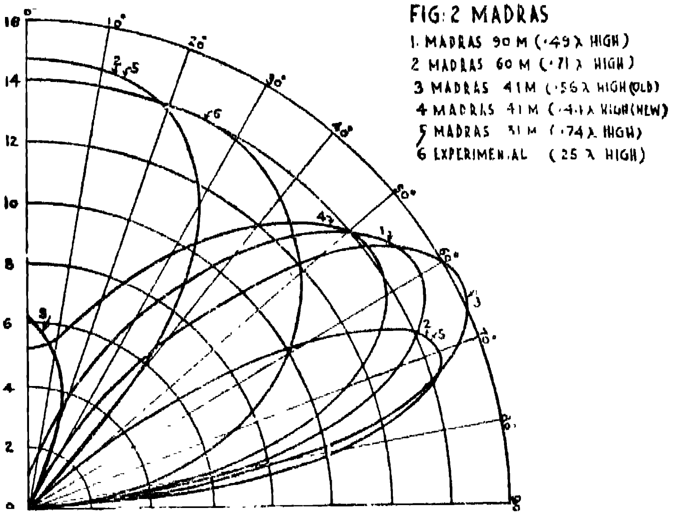
FIG: 2 MADRAS
1. MADRAS 90 M (·49 λ HIGH)
2 MADRAS 60 M (·71 λ HIGH)
3 MADRAS 41 M (·56 λ HIGH(OLD)
4 MADRAS 41 M (·44 λ HIGH(NEW)
5 MADRAS 31 M (·74 λ HIGH)
6 EXPERIMENTAL (25 λ HIGH)
16
14
12
10
8
6
4
2
0
0°
10°
20°
30°
40°
50°
60°
70°
80°
90°
2, 5
6
4
1
3
2, 5
5

Fig. 3

In considering propagation between any two points, it is very necessary to know the state of the ionosphere, such as the ionic densities and the layer heights, the distance between the two places, the transmitting and receiving antennae characteristics and the working wave-lengths. The working wave-lengths are given in Table II. Table III gives the details of the transmitting antennae. The transmitting antenna in all cases is a horizontal dipole aerial at different heights above the ground. The vertical polar diagrams of these aerials as calculated and drawn for the Delhi bearing are given in Figs. 2 and 3. The distance between Bombay and Delhi is 1,145 kms. and between Madras and Delhi is 1,971 kms. on the great-circle path. Such of the ionosphere data that are available are given in the form of graphs III, IV, V and VI (Figs. 6 and 7).

For facilitation of discussion, the results for each transmission are taken up separately. Thus the results fall under 4 parts: (*i*) Transmission I (morning); (*ii*) Transmission II (noon); (*iii*) Transmission III, part 1 (early evening); and (*iv*) Transmission III, part 2 (night).

In order to follow the sequence of the measurements made, the results for the night transmission are presented first.

TRANSMISSION III (PART 2)

As would be expected, the propagation at this time is *via* the F-layer.

The two stations, Bombay and Madras, on which the measurements were conducted, were operating in the 90 metre band for the winter of 1940-41 and in the 60 metre band for the summer of 1941. The details of the change-over appear in Table II.

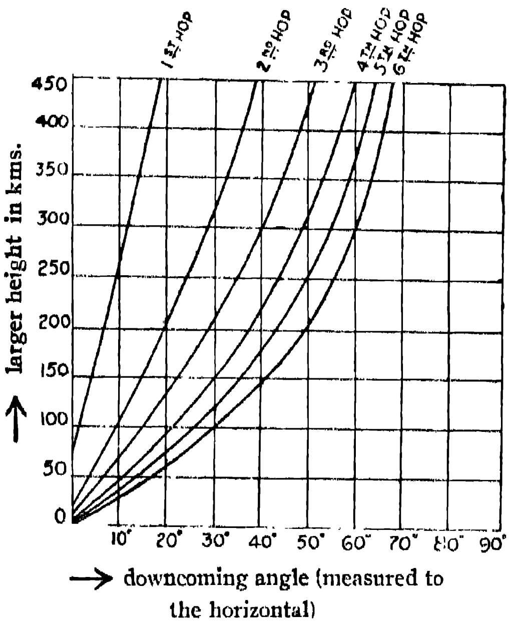

FIG. 4

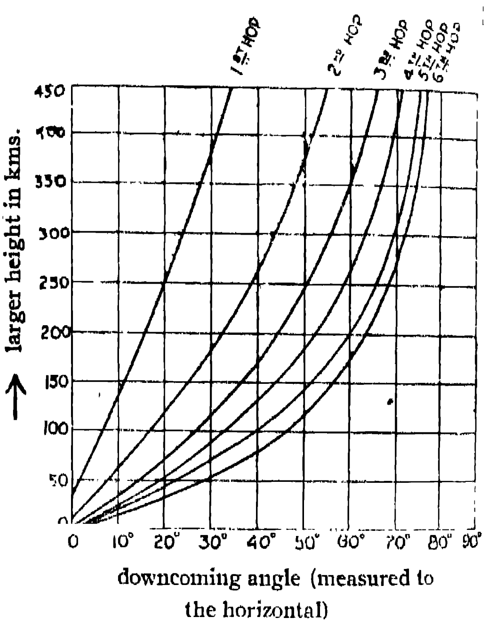

FIG. 5

TABLE III

Station	Wave-length	Height of transmitting antenna in terms of λ	Bearing of transmitting antenna	Bearing of the station from Delhi	Angle between the directions of antenna and Delhi
Bombay	31.4 m.	.86λ	North-South	203°.27 E of N.	23°.27
	41.44 m.	.65λ (old)	,,	,,	,,
	,,	.44λ (new)	,,	,,	,,
	61.48 m.	·6λ	,,	,,	,,
	89.15 m.	.41λ	,,	,,	,,
Madras	31.35 m.	.74λ	75° E of N.	168°.85 E of N.	86°.15
	41.27 m.	.56λ (old)	,,	,,	,,
	,,	.44λ (new)	,,	,,	,,
	60.98 m.	.71λ	,,	,,	,,
	87.34 m.	.49λ	,,	,,	,,

During 90 metre operation, a typical pulse pattern obtained in the case of Bombay is to be seen in pattern No. 1, plate IX, and the case of Madras is to be seen in pattern No. 1, plate X. It will be seen that there are several component pulses, or 'returns,' in each case. They represent successive multiple reflections from the F-layer. The downcoming angles for each of these returns were obtained. On a reference to Table I, it will be seen that in the case of Bombay, the second return was giving an angle of 44° to the horizontal while the third return gave an angle of 56°. In order to know the layer height from these angles, reference is to be made to graph I (Fig. 4), which is drawn to show the downcoming angle against the virtual height for the first, second, third, fourth, fifth and sixth hop transmission between Bombay and Delhi. The virtual height of the layer comes out to be of the order of 290 km. In the case of Madras, the downcoming angles obtained were 33° and 45° corresponding to the second, and third returns in the pulse-pattern. On a reference to graph II (Fig. 5) drawn, for transmission between Madras and Delhi, the layer height comes out to be 350 km. An idea of the nature of the F-layer height is to be obtained from that recorded at this time at Madras and Delhi working on 90 metre wave. This is given in graph III (Fig. 6). The average layer height at Delhi is nearly 300 km. while at Madras it is of the order of 350 km.

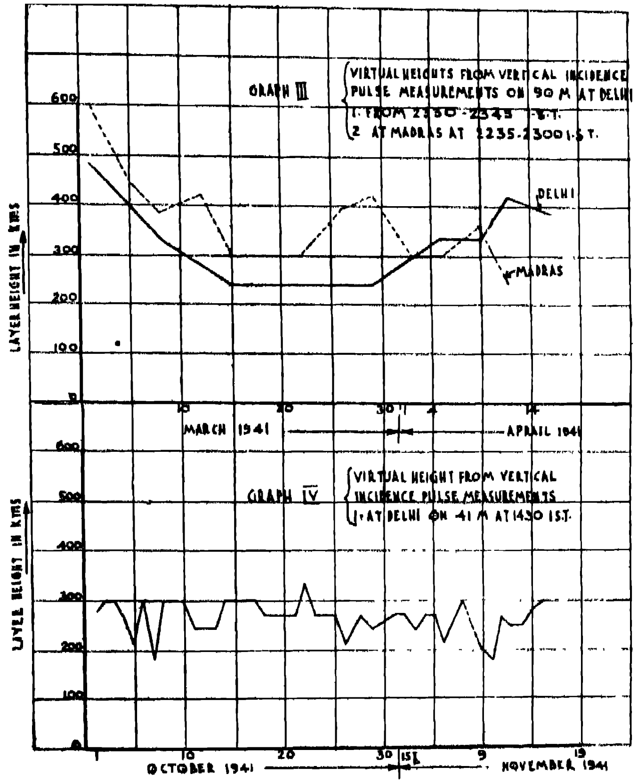

FIG. 6

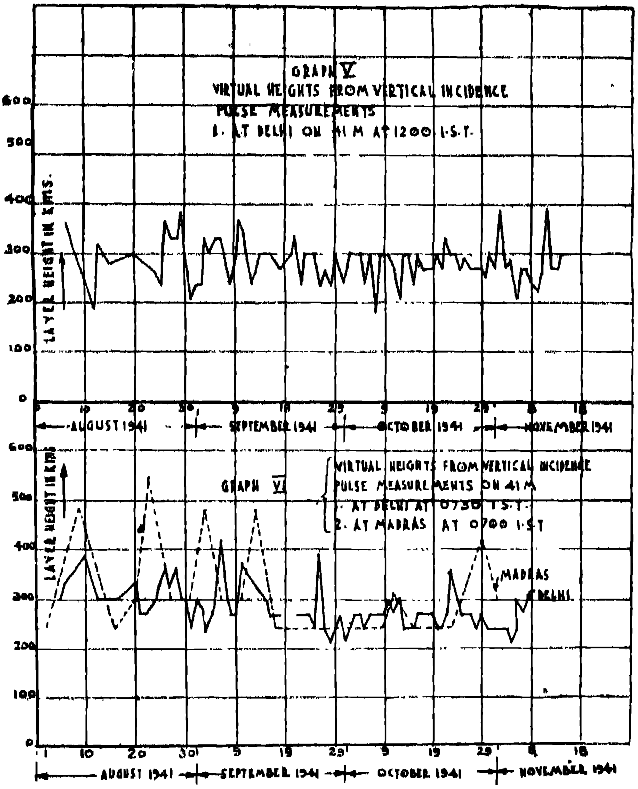

FIG 7

On a study of the pulse patterns it will be seen that in the cases of Bombay and Madras, the third hop is the strongest. During the several observations made, it was found that it was either the second hop or the third hop that was the strongest. It may be remembered that the amplitudes of these returns were subject to 'fading.' They would vary considerably and irregularly. Seldom was the 1st hop strong. The reason for this is not far to seek. It is due to the characteristics of the transmitting and the receiving antennae used. The transmitting antenna is not radiating at the angle required for 1st hop propagation and the receiving aerial is not picking up so well at the 1st hop angle as at the 2nd and 3rd hop angles. The result observed is the product of the both.

In the case of Bombay for F-layer transmission the downcoming angles are 24°.5 for 1st hop, 44° for the 2nd hop and 56° for 3rd hop. These are read off from graph I (Fig. 4) for a virtual height of 300 km. The relative radiation amplitudes for the transmitting antenna given in Fig. 2 are 5.3 for 1st hop, 8.7 for the 2nd hop, and 9 for the 3rd hop, while the pick-up figures of the receiving aerial are 5, 8.2 and 9.8, respectively. As a result of these, the received signal amplitudes, being proportional to the products of these, are 26.5, 71.3 and 88.2 for 1st, 2nd and 3rd hops respectively. Allowing for the correction to be made for

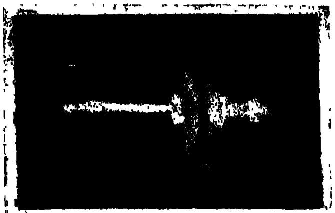

NO: 1.
BOMBAY ([illegible] m) ON 15 3 1941
AT 2250 I.S.T.

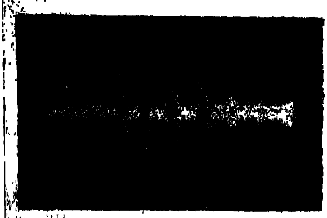

NO: 2.
BOMBAY (50.15 m) ON 10.4.1941
AT 2250 I.S.T (RETARDATION EFFECT)

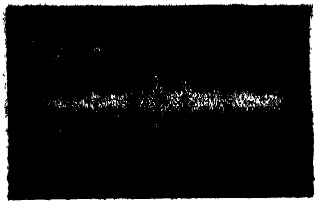

NO: 3
BOMBAY (61.48 m) ON 20.4.1941
AT. 2255 I.S.T

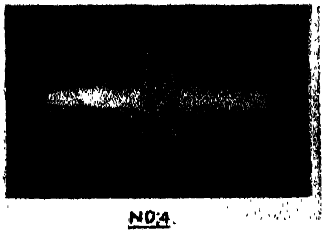

NO: 4.
BOMBAY (61.48 m) ON 2.4.1941
AT 1845 I.S.T.

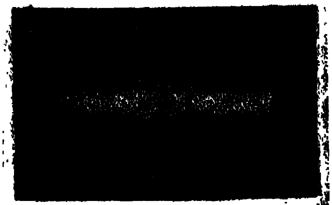

NO: 5.
BOMBAY (41.44 m) ON 28.4.41
AT 1845 I.S.T.

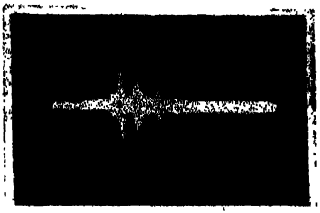

NO: 6.
BOMBAY (31.4 m) ON 28.4.1941.
AT 1215 I.S.T.

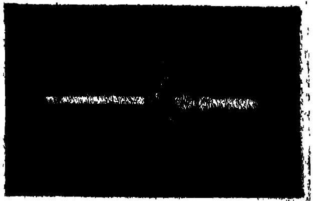

NO: 7.
BOMBAY (41.44 m) ON 14.10.1941
AT 1215 I.S.T

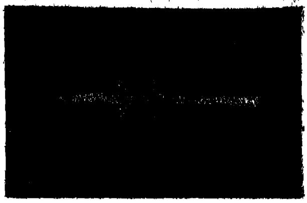

NO: 8.
BOMBAY (41.44 m) ON 14.10.1941
AT 1430 I.S.T

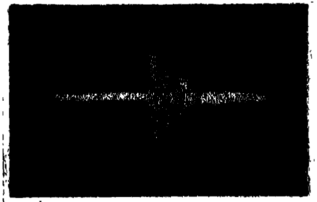

NO: 9
BOMBAY (41.44 m.) ON 2.9.1941
AT 0715 I.S.T. (OLD ANTENNA)

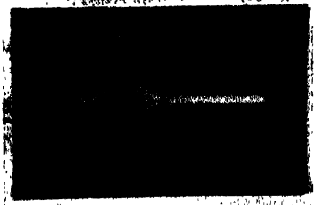

NO: 10
BOMBAY (41.44 m) ON 14.10.1941
AT 0745 I.S.T (NEW ANTENNA)

Typical pulse-pattern photographs

spreading and attenuation (the latter however being usually negligible at the time when these measurements are made) it can be shown that the 1st hop would be considerably weaker than the 2nd and 3rd hops.

Similarly in the case of Madras (Fig. 3), the resultant amplitudes work out to be 17.6, 70.5 and 92.4 for 1st, 2nd and 3rd hops respectively. From this it is clear why 2nd and 3rd hops are stronger in the cases of both Bombay and Madras.

The vital part the antenna plays is brought out in the following results: Aerial change-over tests were carried out at the Madras transmitter using a high and a low aerial alternately. The test was carried out during the pulse transmission. When the higher aerial (.49λ high) was used the maximum energy was received at an angle of 30° to the horizontal and it corresponded to the 2nd hop from the F-layer, while with the lower aerial (.25λ high) the maximum energy received was at 58° and corresponded to 5th hop from F. Turning to the polar diagrams of the two transmitting aerials, it will be seen that in the case of higher aerial, maximum radiation is at about 34° to the horizontal, while with the lower aerial, the maximum radiation is at a much higher angle.

When Madras and Bombay started operating on 60 m. band for the summer of 1941, the same 90 m. aerial was used, thus raising the height of the transmitting antenna in terms of λ (wave-length), and favouring low angle radiation. It was then predicted that 1st hop should be the strongest and, as will be seen later, this was the case. When Madras and Bombay stations lowered the height of their transmitting antenna on 41 m. to .44λ in the day transmission, the immediate effect was the weakening or disappearance of the first hop.

There are a few interesting observations to be noted here. On the 4th of March, 1941, at 2230 I.S.T. Bombay 90 m. carrier was observed to be fading as a rapid flutter. This was unusual, but the downcoming angle was all the time very steady, indicating a single-ray transmission. The angle was 32° and represents 1st hop from F, the virtual height being 407 km. The 4th of March, 1941, happens to be a magnetically disturbed day, though reported to be of slight intensity. The low ionization density and high layer height would tend to decrease maximum usable frequency. This may explain why the 2nd and 3rd hops which are usually the strongest were absent on this date. The agitation of the signal observed is probably due to a similar state of agitation of the ionosphere to be expected on a magnetically disturbed day.

THE VIRTUAL HEIGHT PARADOX

In a multi-hop transmission, the virtual height of the layer from which reflections take place would increase as the order of the hop increases, as shown in Fig. 8. The results on Bombay and Madras stations working in the 90 m. band usually conformed to this. However, at the beginning of April, an unusual phenomenon was observed on Bombay pulse-patterns. Fig. 2, plate IX, gives such a type of pattern. It will be seen that as against Fig. 1, plate IX, which is the usual pulse-pattern, the returns are very much separated, indicating greater

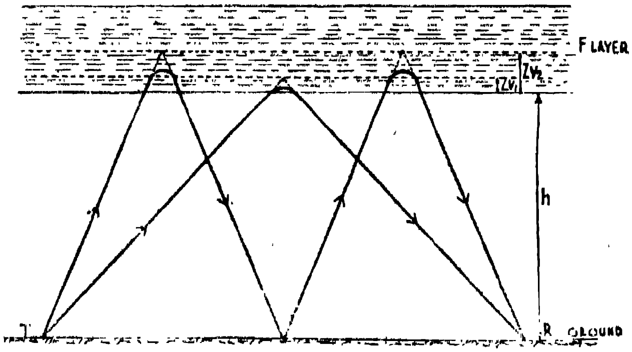

Indicating the increase of virtual height with the increase in the order of the hop

FIG. 8

time delays. The downcoming angles obtained for such returns showed that the virtual height decreases as the order of hop increases. For instance, the results on the 10th April, 1941, showed that the 1st hop is reflected from a virtual height of 500 km., the 2nd hop from 440 km. and 3rd hop from 393 km. This is in variance with the established notions. As an explanation it is suggested that a deflecting layer in the transmission path, such as the residual E-layer that could have been present at the time of measurement, would be responsible for such a phenomenon. In Fig. 9 the transmission path and the virtual height are diagrammatically shown based upon the equivalence theorem for the plane earth. It will be seen from the diagram that the virtual height for the 2nd hop is actually lower than that for the 1st hop. In the presence of a deflecting layer in the transmission path, the amount of deviation produced is dependent upon the angle of incidence of the ray. A vertically incident ray does not suffer

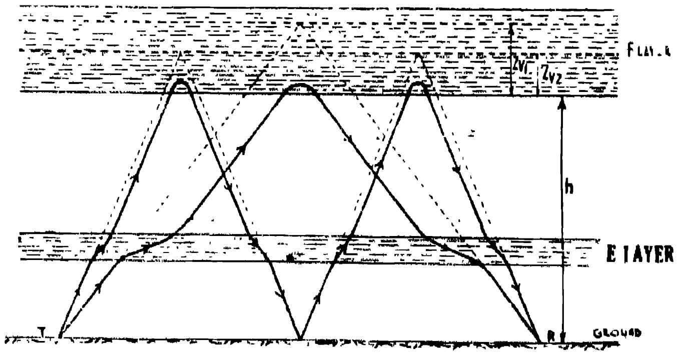

Indicating decrease in the virtual height with increase in the order of hop in the presence of an intervening ionised layer

FIG. 9

any deviation, whereas the greater the obliquity of the incident ray the greater will be the deviation. The greater the deviation the greater is the virtual height. Thus the 1st hop is affected more than the 2nd hop which in turn is affected more than the 3rd hop.

Another effect of the intervening layer is its effect on the energy distribution in the various component rays. Referring to the pulse-pattern No. 2, plate IX, again, it will be noted that the first four hops are of the same order of amplitude. The first hop which on normal days was very much weaker than the second and third hops, is now equal in amplitude. It was shown earlier that the amplitudes are in the ratio of 21, 71 and 88 on an assumption of no attenuation being experienced. However, with the presence of the intervening E-layer, this factor cannot be ignored. The attenuation suffered will be greater, the greater the number of hops. This tends to equalize the relative amplitudes. Thus it will be seen that the effects of intervening ionized strata are felt in the time-delays, in the energy distribution, and in the values of the downcoming angles of the component waves. Here the effects are only mentioned. It allows a study on a quantitative basis.

On the 16th of April, 1941, Bombay and Madras changed over to the 60 metre band. As entered in Table I, the results show that the propagation is taking place by multiple reflections from the F-layer. In the case of Bombay the downcoming angles were 27° for the first hop and 46° for the 2nd hop. These give virtual heights of 335 km. and 317 km. respectively. The lowering of the virtual height as the order of the hop increases is again due to intervening E-layer. In the case of Madras the angles are 17°.5, 45°, 52°, 56° for the first, third, fourth and fifth hops respectively, giving virtual heights of 410 km., 357 km., 337 km. and 315 km., respectively. This marked progessive lowering of the virtual height is once again the effect of the E-layer.

As the pulse-patterns reveal (No. 3, plate IX, and No. 2, plate X), in either case it is the first hop which gives the maximum energy. The reason, as was predicted earlier, was due to the transmitting antennae favouring low-angle radiation.

TRANSMISSION III, PART I (EARLY EVENING)

The two reference stations were operating on the 60 metre band during the winter of 1940-41, and on the 41 metre band during the summer of 1941.

During winter, a typical pulse-pattern obtained on pulse-signals radiated from Bombay just before the commencement of the actual transmission is given in pattern No. 4, plate IX. Two returns were usually present. They are the first and the second hops from the E-layer. The first hop gave an angle of 8° while the second gave an angle of 19°. The virtual heights work out to be 103 km., in either case.

The question which now arises is whether E-layer transmission between Bombay and Delhi is possible at this time (5 p.m.) and whether the transmitting antenna gives appreciable radiation at such low angles. Although no experimental data for E-layer critical frequencies are available for this period, fairly reliable computation can be made by the use of Chapman's formula

$$\frac{f_{E_1}}{f_{E_2}} = \left(\frac{\cos Z_1}{\cos Z_2}\right)^{\frac{1}{4}}$$

(where Z_1 and Z_2 are the Sun's zenithal angles) and the Washington critical frequency data available for this period. Calculated maximum usable frequencies for the months of March and April, 1941, work out to be 9.1, 5 and 3.8 Mc/s for the first, second and third hop propagation during the month of March and 9.6, 5.3 and 4 Mc/s, respectively for the month of April, 1941. Thus the first and the second hop transmission *via* the E-layer may be possible. There is a certain amount of radiation at these angles, but the radiation is low. This would suggest that the signals are to be expected to be poor, which was actually the case. Radiation at higher angles was useless as far as the particular receiving point was concerned, as such signals would be badly attenuated on their passage through the E-layer.

In March, the second hop was observed to be the stronger while in April the first hop was the stronger. The pulse-pattern given in plate IX is for April. There are two factors to be considered in this connection. One is the radiation at these angles and the other is the attenuation in the lower regions such as the D region. The radiation at the second hop angle is greater, but so are the attenuation losses. As the attenuation losses would be greater in April it would appear that the balance is in favour of second hop in March and first hop in April.

The results presented above refer only to the propagation conditions prevailing at the beginning of the transmission. There is unfortunately insufficient interval between part I and part II of transmission III for special pulse transmission in order to study the propagation conditions at the end of part I of transmission III.

In the case of Madras, there was usually a solitary return present, as will be seen from pulse-pattern No. 3, plate X. The carrier was found to be exceedingly steady and the ellipse on the C.R.O. showed a steady angle all the time. Such an ellipse is illustrated in pattern No. 8, plate X. The transmission is evidently by a single ray. The downcoming angle was measured to be 19° in March, 1941, which is probably E-layer transmission.

Though no experimental data for E-layer critical frequencies are available for this period, on computation it was found that the first, second and the third hop propagation *via* the E-layer was possible. Added to this possibility, is the suitability of the transmitting aerial. The transmitting aerial was 0.71λ high, giving fairly low-angle radiation. Referring to Fig. 5, the downcoming angles for propagation *via* the E-layer come out to be 1°.2 for 1st hop, 9°.1 for 2nd hop

PLATE X

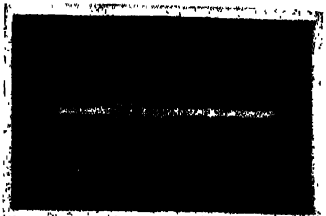

NO: 1.
MADRAS ([illegible]) ON [illegible].1941
AT [illegible] I.S.T.

NO: 2.
MADRAS ([illegible]) ON [illegible].1941
AT [illegible] I.S.T.

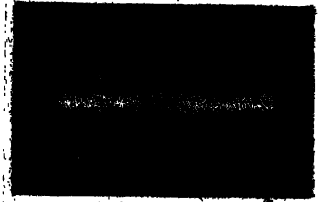

NO: 3.
MADRAS ([illegible]) ON [illegible].1941
AT [illegible] I.S.T.

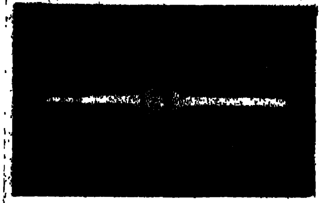

NO:4
MADRAS (41.27 m.) ON 14.8.1941
AT 1545 I.S.T.

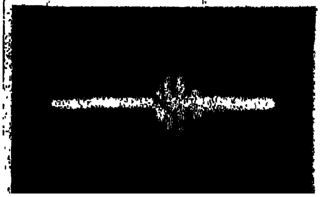

NO:5
MADRAS (41.27 m.) ON [illegible].1941
AT 0715 ([illegible] ANTENNA)

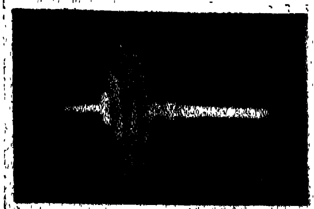

NO. 6.
MADRAS (41.27 m.) ON 15.10.41
AT [illegible] (NEW ANTENNA)

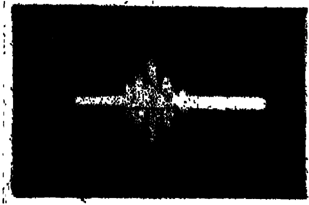

NO: 7.
MADRAS (41.27 m.) ON 1.11.1941
AT [illegible] I.S.T.

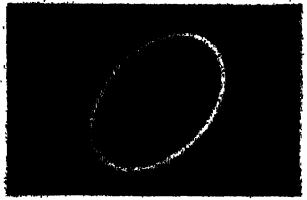

NO: 8
MADRAS (60.98 m.)
CARRIER ON [illegible].1941 AT 1800 I.S.T

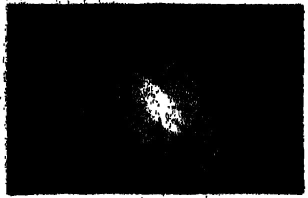

NO: 9
MADRAS ([illegible].34 m.)
ELLIPSE-PATTERNS ON 9.4.1941
AT 2255 I.S.T

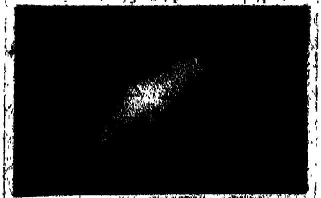

NO: 10
BOMBAY ([illegible].27 m.)
ELLIPSE-PATTERNS ON [illegible].1941
AT [illegible] I.S.T.

Typical pulse-pattern photographs

and 15°.1 for 3rd hop. The relative intensities in these directions, as read from the polar diagram in Fig. 3, are nil, 10.6 and 14.4, respectively. Transmission by 1st hop being ruled out, transmission by either 2nd or 3rd hop is possible.

Supporting the E-layer transmission, there is a certain amount of practical evidence too. Strong echoes from E-layer were observed on vertical incidence pulse measurements carried out on the 60 m. band at Delhi on the 2nd April and at Madras on the 9th April, 1941, at the time of these measurements. They were not of sporadic nature but they were strong and persistent echoes—which would suggest a probability of transmission by E-layer on these two days. The same characteristics of the received signal, *i.e.*, steady though poor, were observed on those two days as on other days, indicating no difference in the mode of propagation. It is, therefore, deduced that the transmission on all the days is probably by E.

As stated above, the downcoming angle in March, 1941, was 19°. This works out to be 3rd hop from E. In April, the conditions were not as steady as in March. The downcoming angle came out to be 9°.75 which works out to be 2nd hop from the E-layer. Here again the two factors, the radiation and the attenuation, seemed to have come into consideration.

As in the case of Bombay, these results presented above refer only to the beginning of the evening transmission. Later in the transmission, the steady ellipses on carrier slowly gave place to more unsteady ones and by the close of the transmission, the ellipses were found to be highly unsteady, indicating the presence of two or more component waves. It is to be expected that the E-layer propagation gave way to the F-layer propagation.

On the 16th of April, 1941, both Bombay and Madras changed over to the 41 metre band for the summer.

Madras begins its transmission at 4 p.m. The signal on the pulses was found to be extremely poor. In general the pulse-patterns were composed of 3 groups of returns well separated as seen in pattern No. IV, plate X. Generally the 2nd group was found to be the strongest. The downcoming angle came out to be 35°. On these days when the 2nd group was found to be the strongest in the pulse pattern measurements made on the carrier soon afterwards, when full power was put on for the actual transmission, the angle came out to be 34°. The angle for the 3rd group was also obtained and it came out to be 46°. Thus we have a pattern of three returns, the 2nd giving an angle of 34° and the 3rd an angle of 46° ; 34° corresponds to 2nd hop from a layer height of 370 km. and 46° corresponds to 3rd hop from a virtual layer height of 370 km. again. On this basis we may assume that the three returns observed in the pulse pattern are the 1st, 2nd and 3rd hops from F_2 layer. These returns instead of being in the form of single pulses are in the form of groups. The groups are formed due to the angular spread in the vertical plane, which may be due to scattering or irregular reflections in the ionized layer. Theoretical considerations show a possibility of 2nd hop propagation *via* the E-layer. No results were obtained to confirm this.

Bombay starts its transmission at 5 p.m. The special pulse transmission, preceding this, usually gave a pulse-pattern of four returns out of which the 2nd was observed to be the strongest (No. 5, plate IX). The angle corresponding to this comes out to be 46° as shown in table I, and fits in as 2nd hop from a layer of a virtual height of 317 km. The delays between the successive returns appear to show that they are the successive hops from F-layer. The maximum usable frequencies for transmission *via* the E-layer show that that only one hop transmission would be possible. However, there is no radiation from the transmitting antenna at this angle as can be seen from the polar diagram. As at 5 p.m. it is difficult to show clear demarcation between F1- and F2-layers, we may say that the transmission is by F-layer.

Summarising the results for the beginning of transmission III, it would appear that propagation on 60 metres is *via* E-layer, while in the case of 41 metre transmissions, it is probably *via* F2 in the case of Madras and F in the case of Bombay.

TRANSMISSION II (NOON)

In the winter months of 1940-41, and till the 15th May, 1941, Bombay and Madras were working on 31 metres and changed over to 41 metres on the 16th May, 1941.

The pulse transmissions from Bombay, preceding and succeeding the actual transmission, gave three returns as seen in pulse-pattern No. 6 in plate IX. The second was always the strongest. It was usually several times stronger than either the 1st or 3rd. The average downcoming angle for the 2nd return came out to be 22° to the horizontal, which represents 2nd hop transmission from E at a height of 125 km. The time-delays between the first two returns in the pulse-pattern also go to show that the transmission is by E-layer.

The theoretical considerations based on critical frequencies show that one hop and two hop transmission *via* the E-layer is the most probable mode of propagation.

It was stated above that the 2nd hop giving an angle of 22° was several times stronger than either the 1st or the 3rd. The reason lies in the characteristics of the transmitting antenna. The polar diagram given in Fig. 2 shows that most of the energy is transmitted at very high angles. But for a small lobe there is no energy until we reach 50° to the horizontal. The small lobe gives a maximum at 20° to the horizontal which was nearly the angle that was obtained for the second return. All the high-angle radiation was useless as far as the receiving point was concerned. Such high-angle radiation could be received as a 7th or 8th hop from E or 3rd or 4th hop from F_2. Neither of these would, however, reach the receiving place, for they would be attenuated away.

No definite results could be obtained on Madras during transmission II due to the poor signal strength.

After the introduction of 41 metres for noon transmission, results were obtained in the case of Bombay during the months of October and November, 1941. The pulse transmission preceding and succeeding the actual transmission usually gave four returns (pulse-pattern Nos. 7 and 8, plate IX). The average downcoming angles obtained were 21°, 40°, 47° and 59° corresponding to the first four returns. They work out to be 1st, 2nd, 3rd and 4th hop from F_2 layer at a virtual height of nearly 250 km. E-layer transmission by one hop could be possible, but for little energy being radiated by the transmitting antenna at this angle. Data are available from the vertical incidence pulse measurements carried out at Delhi before the commencement and after the end of noon transmission that give an average layer height of about 280 km at 12.00 noon and 270 km. at 14.30 hrs. The day-to-day variations in height are shown in graphs IV and V (Figs. 6 and 7). For oblique incidence the layer height as expected was obtained to be lower than for vertical incidence.

Summarising the results for the noon transmission, we find that the transmission between Bombay and Delhi on 31 metres is *via* the E-layer in May, 1941, and by F2-layer in October, 1941, when the working wave-length was 41 metres. Taking all the factors into consideration we find once again that the practical and theoretical modes agree.

TRANSMISSION I (MORNING)

Bombay and Madras operated on 41 metres during transmission I for the entire period under review. The results in the case of Bombay, both before and after the transmission, work out to be multiple hops from F-layer. They fairly closely follow mirror-like reflections. The average downcoming angles were 21°, 38°, 53° and 63° for the 1st, 2nd, 3rd and 4th hops respectively. The virtual height is nearly 250 km. Vertical incidence pulse measurements carried out before the commencement of transmission show considerable variations in the virtual heights recorded as can be seen from graph VI (Fig. 7). These variations are due to the working frequency being close to the critical frequency. The average layer height in the month of August to the middle of September is approximately of the order of 300 km., and from the middle of September till the middle of November is of the order of 260 km. Thus once again the layer heights obtained by the oblique incidence measurements are lower. Bombay was originally using a transmitting aerial 0.65λ above ground and changed over to an aerial 0.44λ above ground on the 8th of October, 1941. A simultaneous change was noticed. First hop, which was quite strong, became considerably weaker. Fig. 9, plate IX, shows the pulse-pattern observed before the aerial change-over and Fig. 10, plate IX, shows the pulse-pattern after the change-over. The polar diagram for the old and new transmitting antennae (Figs. 2 and 3) bear out the results that were obtained. When the higher aerial was used, the 1st and 2nd hops were observed to be quite strong and the 3rd hop was considerably weak. With the lower aerial 1st hop was weak and the 2nd and the 3rd hops were strong.

In the case of Madras, multiple reflections from F-layer during the pulse transmission preceding the morning transmission were observed. The downcoming angles measured were 8°, 24°, 35°, 45° and 56° for the first five hops. The virtual heights came out to be 220, 247, 250, 260 and 310 km. respectively. The ascending order in the virtual heights is to be expected. As the working frequency approaches the maximum usable frequency, the virtual height increases. It was observed that usually the 3rd hop was the strongest, both in the case of the old and new antennae. Typical pulse-patterns obtained are given in plate X, Nos. 5 and 6. The transmitting aerial was originally 0.56λ above ground and it was changed over to 0.44λ on the 5th October, 1941. After the change-over the 1st hop almost disappeared. Polar diagrams of the old and new antennae are given in Figs. 2 and 3, which show that the new aerial hardly gives any radiation at the 1st hop angle

The pulse transmission following soon after the close of the morning transmission usually gave five returns. The first two reflections are close together while the 3rd and the 4th are well separated. The downcoming angles obtained are 8° and 22° for the 1st and 2ndreturns. The 3rd return gave a downcoming angle of 44° while the 4th gave an angle of 55°. They correspond to 1st hop from 220 km., 2nd hop from 220 km., 3rd hop from 350 km., and 4th hop from 375 km. A sudden jump in the virtual height for the 3rd and 4th hops is to be noticed. These measurements were taken at about 9 A.M. The results appear to show that the first two returns observed are the 1st and 2nd hops from F1 layer while the 3rd and 4th returns are the 3rd and 4th hops from the F2-layer. The basis for such a transmission is this : At 9 A.M. in October, 1941, the F1-layer critical frequency is such that only one-hop and two-hop transmission between Madras and Delhi is possible. Radiation at higher angles will penetrate the F1-layer and will be reflected from the F2-layer. It seems that the transmission between Madras and Delhi is by both F1- and F2-layers. The lower angles are reflected from F1-layer while higher angles are reflected from F2-layer.

Summarising the results for the morning transmission, we find that the multiple reflections from F-layer observed are in agreement with the theory. The results in the case of Madras for the end of the transmission suggest propagation both *via* F1- and F2-layers.

CONCLUSIONS

A few general conclusions that may be drawn from the present study are as follows :—

(1) Multiple reflection phenomenon is involved in the type of wireless propagation that was investigated.

(2) Presence of the E-layer and other intervening absorbing strata has the effect of reducing the number and strength of the components that comprise a downcoming wave. Such strata also introduce large deviations in the ray path, as a result of which the downcoming angles are enhanced.

(3) In the absence of any intervening layers, as for instance in the early mornings and nights, the downcoming angles agree fairly with the values calculated on the basis of simple mirror-like reflections

(4) Under the conditions, as postulated in (3) above, a knowledge of the state of the ionisation of the ionosphere, the working wave-length, the characteristics of the transmitting and receiving antennae, etc., could be used for making reliable predictions of the type of propagation that may prevail in the case of short-distance short-wave propagation.

ACKNOWLEDGMENTS

The author wishes to acknowledge his sincere thanks to Mr. C. W. Goyder, Chief Engineer, All-India Radio, for the personal interest he has taken in the problem and for his many useful suggestions, to Mr. Chamanlal, Research Engineer, All-India Radio, under whose immediate guidance the author pursued the work and to his colleagues in the Department who had given considerable help throughout Thanks are also due to the Engineers of the Bombay and Madras Broadcasting stations of the All-India Radio who had so readily co-operated in arranging the test schedules.

RESEARCH DEPARTMENT,
ALL INDIA RADIO,
DELHI

REFERENCES

[1] Chamanlal, *Ind. J. of Phys.*, **15**, 289 (1940)
[2] Friis, H. T., *Proc. I. R. E.*, **16**, 658 (1928).
[3] Eckersley, T. L., *Jour. I. E. E.*, **65**, 607 (1927)
[4] Holingworth, J., *Jour. I. E. E.*, **72**, 236 (1933).
[5] Friis, H. T., Feldman, C. B , and Sharpless, W. M., *Proc. I. R. E.*, **22**, 47
[6] Wilkins, A. F., *Jour. I. E. E.*, **74**, 582
[7] Crome, W., Krüger, K., Goubau, G., and Zenneck, J., *Hochf. Tech. u. Elek. akus.* **48**, No. 1, 1-7.
[8] R. Eyfrig, *Hochf. Tech. u. Elek. akus.*, Dec. (1940).
[9] Edwards, C. F., and Jansky, Karl G., *Proc. I. R. E.*, **29**, 322.

DIPOLE MOMENTS OF PALMITIC ACID, ALEURITIC ACID AND ALKYL ESTERS OF ALEURITIC ACID

By G. N. BHATTACHARYA

(Received for publication, August 21, 1942)

ABSTRACT. Dipole moments of palmitic acid, aleuritic acid (9, 10, 16 trihydroxypalmitic acid) and methyl and ethyl esters of aleuritic acid have been determined from their dilute solutions in 1, 4 dioxane. The temperature of measurement was 25°C. for all but aleuritic acid for which the temperature 40°C. was used due to the latter's limited solubility in the above solvent at the lower temperature. The values obtained for palmitic acid, aleuritic acid, methyl aleuritate and ethyl aleuritate are 1.75, 4.28, 4.27 and 4.31 Debye units respectively. The cause of anomalous solubility of aleuritic acid or its esters in polar solvents or when some polar helper is added to the solvent has been discussed with reference to solvation and dissolution owing to the highly polar nature of these substances.

INTRODUCTION

Although the anomalous solubility of some natural resins in organic solvents was the subject of much speculation for a long time, no satisfactory explanation of the same came forth till very recently.[1] Some very interesting observations were made in this connection in that many of the non-solvents for such resins may be rendered good solvents for the same by the addition of small quantities of some 'polar-helpers' to these non-solvents. The effect of such polar-helpers has also been observed and recognised in many other fields.[2] The current conceptions[3] regarding solvation of large molecules and the consequent dissolution process may explain the rôle which these polar-helpers play in such non-solvents.

There are reasons to believe from what has been stated above that either the molecules of natural resins, such as shellac, pontianak or copal, are themselves polar in nature or the different constituent groups which make up such molecules behave as polar bodies towards different solvents, and consequent solvation and dissolution take place. It has been thought desirable, therefore, to study the dielectric properties of such resins and their constituent bodies in different solvents in order to throw light on the nature of their molecules from this point of view. The present paper only embodies the results of dipole measurement on aleuritic acid, the only acid isolated from shellac whose constitution has been definitely established[4] and the alkyl esters of this acid.

Since aleuritic acid is a hydroxy palmitic acid, it was also thought necessary to determine the dipole moment of palmitic acid from its dilute solutions in dioxane as it is related to the above acid in structure. Its value in benzene although available[5,6] cannot be taken as its actual moment for single molecules owing to their association in that solvent. Wilson and Wenzke[7] have, however, shown that fatty acids have practically no complex solvent-solute interaction in 1, 4 dioxane and so their dipole moments determined from dilute solutions in the above solvent conform to the values of single molecules in the gaseous state. The evaluation of electric moment of palmitic acid from dioxane solutions was therefore undertaken, as no value of moment of this acid seemed to be available from this solvent. The limited solubility of aleuritic acid in dioxane also necessitated measurements on its methyl and ethyl esters, which are soluble in the above solvent.

PREPARATION OF MATERIALS

Dioxane.—American dioxane bottled by A. Boake Roberts & Co., Ltd., of England was allowed to stand over sodium wire for several days, distilled and the middle fraction boiling constantly at a fixed temperature collected. This fraction was further purified by refluxing over sodium for 8-10 hours and then again distilling. The main fraction distilling between 98°.0C. and 98°.1C. under 693 mm. of mercury* was collected by means of an efficient fractionating column. It was noticed that the sodium wires assumed the form of silver-white balls during refluxing and they retained their lustre in the liquid as reported by Eigenberger.[8]

F. P. = 11°.6C., $n^{25} = 1.4198$, $d^{25} = 1.0282$, $\epsilon^{25} = 2.2024$

Benzene.—A sample of pure crystallisable benzene was dried over sodium wire for some days and refluxed over it for 8-10 hours. It was distilled and the main fraction boiling between 79°.5C. and 79°.6C. collected. This was then fractionally crystallised twice and the solid residue taken. This portion when molten was allowed to stand over fresh sodium wire which retained its lustre in the liquid. It was again fractionated by means of an efficient column and the main fraction used.

F. P. = 5°.5C., $n^{25} = 1.4985$, $d^{25} = 0.8738$, $\epsilon^{25} = 2.2725$

Aleuritic acid.—The crude aleuritic acid, prepared from dewaxed lac according to the method of Nagel,[9] was freed from ether-soluble impurities by extraction with ether in a Soxhlet apparatus. This product was then refluxed with pure ethyl acetate and decolourising charcoal for six hours, filtered hot and then the solution allowed to crystallise. The first crop of crystals was separated from the mother-liquor and subsequently twice recrystallised from a mixture of alcohol and ethyl acetate. It was finally washed with pure and dry ether and dried in a vacuum oven. M. P. 99°.8C.

* The altitude of Namkum (Ranchi) being 2300 ft. above sea-level, its normal barometric height is about 700 mm

Methyl aleuritate.—A portion of the pure aleuritic acid thus obtained was refluxed with chemically pure methyl alcohol and a few c.cs. of pure concentrated sulphuric acid for 6 hours. The methyl ester was then obtained by precipitation from a large volume of water. This ester was dissolved in ether, the ethereal solution filtered and allowed to crystallise. These crystals were further purified by recrystallisation from dilute methyl alcohol and then dried in a vacuum-oven. M. P. 69°C.

Ethyl aleuritate.—Another portion of the pure aleuritic acid was similarly refluxed with absolute ethyl alcohol and a little of concentrated sulphuric acid for about 10 hours. The ethyl ester was obtained as before by precipitation from water. It was dissolved in ether, filtered and the solution allowed to crystallise. The final crystallisation was done from dilute ethyl alcohol, and the drying was carried in a vacuum-oven. M. P. 58°C.

Palmitic acid.—Merck's product was twice recrystallised from hot alcohol. M. P 62.4°C

EXPERIMENTAL

Apparatus.—The substitution method of measurement was used employing General Radio type 516-C radio-frequency bridge[10] and a calibrated 1100 μμF General Radio variable air condenser. Another 25 μμF General Radio variable condenser having 1 μμF graduations was fitted with a precision slow-motion dial so that readings could be taken to 0.05 μμF. This was used in connection with the main condenser and the instrument calibrated in position. The oscillator employed was a General Radio Type 684-A modulated oscillator[11] which could give power over a wide range of frequency from 10 kilocycles to 30 megacycles. From this oscillator a current of 50-kilocycles modulated at 1000-cycles at about 15 volts was used for the bridge. The detector was a pair of high sensitivity headphones used in conjunction with a high gain amplifier specially built for this purpose. The sensitivity of the apparatus was very good and the frequency of 50-kilocycles was used in order to have the most sensitive arrangement in conjunction with the amplifier-detector.

The experimental cell was constructed of pyrex glass according to the design of Sayce and Briscoe and fully described by Le Fèvre.[12] The silvering of this cell was done according to the directions given by Sugden.[13] The cell could be placed inside a big thermos which served as a water thermostat. The temperature was kept constant within 0°.05C. The thermostat-water was earthed and the outer silver coating of the experimental cell was connected with the grounded terminal of the standard condenser. Screened cables were used for connecting the oscillator and the amplifier to the bridge, and the oscillator and the amplifier were kept at a distance from each other to avoid direct interference.

The apparatus was calibrated with pure and dry benzene and the capacity of the leads, etc., was found out from the 'zero capacity' of the experimental cell. This was obtained from the relation

$$C_0 = \frac{\epsilon . C_A - C_B}{\epsilon - 1}$$

where C_0 = 'zero capacity' of the cell,
C_A = air capacity of the same,
C_B = capacity of the cell filled with benzene,
and ϵ = dielectric constant of benzene.

With the value of C_0 thus obtained the dielectric constant of a solution or any other liquid was determined from

$$\epsilon_s = \frac{C_S - C_0}{C_A - C_0}$$

where C_S = the capacity of the cell when filled with the solution,
and ϵ_S = the dielectric constant of the solution.

The best condition of silence in the headphones was obtained by adjusting the power-factor knob of the radio frequency bridge in order that the headphones were actually connected to points which were not only at the same potential but also at the same phase.

Density measurements were carried out with a pyknometer of 25 c.c. capacity and the results may be considered to be accurate to 0.01%. Dielectric constant values are probably accurate to 0.03%.

Glass-stoppered Erlenmeyer flasks were used in making up solutions by weight. All measurements were made at 25°C. except for aleuritic acid for which the temperature 40°C. was used, since aleuritic acid was not sufficiently soluble in dry dioxane at 25°C. to permit accurate determination of its electric moment.

CALCULATIONS AND RESULTS

Polarisations were calculated using Sugden's formula[14] for specific polarisation in place of molar polarisation,

$$P = \frac{\epsilon - 1}{\epsilon + 2} \cdot \frac{1}{d},$$

in which p is the specific polarisation, C, the dielectric constant, and d, the density of the liquid.

The total polarisation according to the above relation is

$$P_1 = M_1\left(P_2 + \frac{P_{12} - P_2}{w}\right)$$

in which P_{12} and P_2 are the specific polarisations of the mixture and the solvent respectively and w is the weight fraction of the solute of molecular weight M_1.

TABLE I

Dielectric constants, densities and polarisations. Solvent—Dioxane

Palmitic Acid (25°C.)				*Aleuritic Acid* (40°C.)				*Methyl aleuritate* (25°C.)				*Ethyl aleuritate* (25°C.)			
w	d	ϵ	P_1	w	d	ϵ	P_1	w	d	ϵ	P_1	w	d	ϵ	P_1
0 000000	1.0281	2 2024	—	0 000000	1 0112	2.1759	—	0.000000	1.0281	2.2024	—	0.000000	1.0281	2.2024	—
0.002121	1.0278	2.2052	140 0	0 002332	1.0112	2 1919	138.0	0 002252	1.0282	2 2186	463 3	0.002652	1.0281	2.2208	475 5
0.005033	1.0273	2.2094	142 4	0 002487	1.0113	2.1933	142 7	0 004258	1 0284	2.2346	479.6	0.004756	1 0283	2 2350	473 5
0.007605	1.0269	2.2129	141 6	0.004153	1.0113	2 2046	438.2	0.008750	1 0287	2.2654	476.2	0.007944	1.0285	2.2580	467.7
0.009479	1.0265	2.2151	140.4	0 004904	1.0114	2.2104	441 6	0 008850	1 0287	2.2668	456 3	0.014277	1 0291	2.3017	459.8
0.016231	1 0252	2.2248	142.3	0.006029	1.0114	2.2188	445.0	0.014500	1 0291	2.3056	448 0	0 020500	1.0294	2.3386	439 7
0.021806	1.0241	2 2330	143.5					0 020102	1.0295	2.3346	418.0				
0.027103	1.0229	2.2404	143 8												
0 032414	1.0218	2.2484	144.7												

TABLE II

Molar Refractions, Polarisations and Dipole Moments

Substance	MR_D	P_∞	$\mu \times 10^{18}$
Palmitic Acid	77.7	141.7	1.75
Aleuritic Acid	82.0	444.5	4.28
Methyl aleuritate	86.6	466 6	4.27
Ethyl aleuritate	91.2	478.4	4.31

Polarisations at infinite dilutions, P_∞, were calculated by means of equations suggested by Le Fèvre and Vine[15] involving specific polarisations and which are similar to Hedestrand's formula.[16] For the sake of comparison, the graphical extrapolation method suggested by Sugden[17] in extrapolating total polarisation—volume polarisability graph to the point $\epsilon = \epsilon_2$, where ϵ_2 is the dielectric constant of the solvent, was also used. The difference between the two P_∞ values obtained by these two methods was very small in the case of acids, but as the esters showed some difference, the graphical extrapolation method using P_1-w curves was employed for them.

Molar refractions were calculated as the sum of the atomic refractions[18] for the sodium D-line. The contributions of the atomic polarisations to polarisations at infinite dilutions were neglected. The dipole moments were calculated from the equations

$$\mu = 0.0127 \times 10^{-18} \sqrt{(P_\infty - MR_D)T} \ ,$$

where T is the temperature of measurement in absolute scale.

DISCUSSIONS

The electric moment of palmitic acid in dilute benzene solutions has been found to be 0.72 Debye units by Smith[5] and 0.77D by Paranjpe and Deshpande.[6] Probably these values are for double molecules of the acid, since most of the fatty acids, especially the lower members of this group, are known to form double molecules in benzene due to association. Zahn[19] and Piekara[20] measured the moments of the first few members of the fatty acid group and found these moments to vary with temperature. They explained this variation as due to changing degree of association. Wilson and Wenzke,[7] however, found that the oxygenated solvent dioxane gave dipole moments of fatty acids quite in agreement with those determined by Zahn[21] for the gaseous state of their molecules, thus showing no effect of association. They gave the value 2.07D for formic acid and 1.74D for acetic acid, and observed that the lengthening of the carbon chain had practically no effect on the latter value of the moment. This they proved by obtaining the same value of moment for stearic acid, too, *viz.*, 1.74D. The value of the moment 1.75D for palmitic acid found here is therefore quite in agreement with their results and corroborates the above statement of these authors that the moment remains the same for all monobasic fatty acids after the first member of this group. This fact was also observed by Smith[5] independently from benzene solutions.*

It is generally believed from many observations of the type stated above that the electric doublet is located at the carboxylic head of these acid molecules, but unfortunately the moment assigned to the carboxyl group or the exact nature of the binding forces inside the group has not yet been finally settled. Williams[22] found this group to have a moment of 0.9×10^{-18} e.s. units, but this value is usually considered to be too low considering the moments of single molecules of monobasic fatty acids in general. Eucken and Meyer[23] have calculated the limiting values of moment of the carboxyl group by considering the effect of rotation about the C-O bond in fatty acids and they gave 1.1D and 3.4D for its minimum and maximum values. The tendency of the acid hydrogen to be attracted towards the oxygen of the carboxyl would, according to these authors, accounts for moments of monobasic fatty acids to be nearer the minimum value of the carboxyl rather than the maximum. Very recently Brooks and Hobbs[24] have calculated from the observed moment of para-chlorobenzoic acid that the carboxyl makes an angle of 74° with the C-C line. But the calculated angle (from the accepted bond moments for C=O, C−O and O−H and assuming the valence angle at the oxygen atom to be 110° and that at the carbonation 125°) is 85°. The discrepancy is quite large and has been explained by them as due to resonance.

The constitution of aleuritic acid has been definitely established[4] as 9, 10, 16 trihydroxypalmitic acid. The structure may be written, therefore, as $CH_2OH.(CH_2)_5CHOH.CHOH(CH_2)_7.COOH$. The high value of moment can only be expected because the molecule contains three hydroxyl groups attached to the hydrocarbon chain of palmitic acid. It is useless, however, to try to calculate the dipole moment of aleuritic acid at the present state of our knowledge from the known bond moments of C=O, C−O and O−H, since rotation around the C−O bond brings in complexities and other unknown factors, such as induction and resonance, are also present.

The dipole moments of both the methyl and the ethyl esters of aleuritic acid are practically the same as that of the acid itself. From a knowledge of the moments of most of the fatty acid esters[25] this is to be expected.

It may now be understood that the highly polar nature of aleuritic acid or its esters may lead to the formation of solvates in polar solvents or when some polar helper is added to the solvent. It should be remembered, however, that polarity in itself cannot be the only criterion for solvation unless the substances differ in the character of their dipoles, *i.e.*, positive and negative, to have the affinity for the formation of solvates. For dissolution process it is recognised[26] now that polarity of the solvent is one of the most important factors for the organophillic compounds, such as cellulose, rubber, etc., probably because they contain heterogeneous polar groups, and the solvates present such a structure that they can then be easily dissolved by the solvent.

ACKNOWLEDGMENT

The author wishes to express his gratitude to Professor P. N. Ghosh of the University College of Science, Calcutta, for the loan of his standard variable-air condenser for the purpose of calibration and to Dr. H. Rakshit of the same college, for the design and construction of the amplifier-detector

used in this investigation. It is also a pleasure to acknowledge indebtedness to Dr. H. K. Sen, D.Sc., F.N.I., the Director of this Institute, for his kind interest in this work.

PHYSICAL AND PHYSICO-CHEMICAL LABORATORIES,
INDIAN LAC RESEARCH INSTITUTE, NAMKUM, RANCHI.

REFERENCES

[1] Palit, S. R., *Jour. Ind. Chem. Soc.*, **27**, 308 (1940).

[2] Holmes, H. N., and Maxson, R. N., *Colloid Symposium Monograph*, **5**, 287 (1928). Faensteiner, *Holme's Introductory Colloid Chemistry*, 100 (1934); Eirich, F., *Annual Reports on the Progress of Physics*, **7**, 329 (1940); Heymann, E., *Trans. Farad. Soc.*, **31**, 846 (1935), and *Ibid.*, **34**, 689 (1938).

[3] Hildebrand, J. H., *Solubility* (Reihnold), 77-122 (1936).
Sheppard, S. E., Carver, E. K., and Houck, R. C., *Colloid Symposium Monograph*, **5**, 243 (1928).

[4] Harries, C., and Nagel, W., *Ber. der Deut. Chem. Ges.*, **60**, 605 (1927)

[5] Smith, J. W., *Jour. Chem. Soc.*, 1567 (1933).

[6] Paranjpe, G. R., and Deshpande, P. Y., *Jour. Univ. Bombay*, **9**, 24 (1940).

[7] Wilson, C. J., and Wenzke, H. H., *Jour. Chem. Phys.*, **2**, 546 (1934).

[8] Eigenberger, J., *Jour. Prakt. Chem.*, **130**, 78 (1931).

[9] Harries, C., and Nagel, W., *Ber. der Deut. Chem. Ges.*, **55**, 3833 (1922); *Chem. Umschau.*, **29**, 135 (1922).

[10] General Radio Catalogue K., 78 (1939).

[11] *Ibid.*, 104 (1939).

[12] Le Fevre, R. J. W., *Dipole Moments* (Methuen), 32 (1938)

[13] Sugden, S., *Jour. Chem. Soc.*, 770 (1933).

[14] Sugden, S., *Trans. Farad. Soc.*, **30**, 720 (1934).

[15] Le Fevre, R. J. W., and Vine, H., *Jour. Chem. Soc.*, 1805 (1937).

[16] Hedestrand, S., *Zeit. Physikal, Chem.* **B2**, 428 (1929).

[17] Sugden, S., *Nature*, **133**, 415 (1934).

[18] Getman, F. H., *Outlines of Theoretical Chemistry*, 86 (1937); Swietoslawski, *Jour Amer. Chem. Soc.*, **42**, 1945 (1920).

[19] Zahn, C. T., *Phys. Rev.*, **35**, 1047 (1930).

[20] Piekara, A. and Piekara, B., *Compt. Rend.*, **198**, 1018 (1934).

[21] Zahn, C. T., *Phys. Rev.*, **37**, 1516 (1931).

[22] Williams, J. W., *Jour. Amer. Chem. Soc.*, **50**, 2350 (1928).

[23] Eucken, A., and Meyer, L., *Phys. Zeit*, **30**, 397 (1929).

[24] Brooks, C. S., and Hobbs, M. E., *Jour. Amer. Chem. Soc.*, **62**, 2851 (1940).

[25] Lewis, G. L., and Smyth, C. P., *Jour. Amer. Chem. Soc.*, **62**, 1529 (1940); Smyth, C. P., and Walls, W. S., *Jour. Amer. Chem. Soc.*, **53**, 527 (1931).

[26] Whitby, G. S., *Colloid Symposium Monograph*, **4**, 203 (1926); Whitby, G. S., McNally, J. G., and Gally, W., *Ibid.*, **6**, 225 (1928).

PRODUCTION OF BURSTS BY MESON AND ITS DEPENDENCE ON THE MESON SPIN

By S. K. CHAKRABARTY

(Received for publication, August 5, 1942)

ABSTRACT. An analytic expression has been derived for the calculation of the frequency of bursts containing N particles or more than N particles produced by a meson. Three different values for the meson spin, *viz.*, 0, ½ and 1, have been taken into consideration and the results thus obtained have been compared with the experimental results of Schein and Gill. It is observed that for a meson, spin 0 or ½ is not a possibility, whereas spin 1 is quite probable, provided the effect of the radiation damping be taken into consideration in processes involving mesons. The reasons for arriving at a conclusion just opposite to that of Christy and Kusaka have been discussed. It has also been shown from general considerations that for large bursts the radiation process is the predominant one, when the knock-on process produces only an insignificant contribution.

The production of large bursts under thick layers of a material has been observed and their frequency has been estimated by various authors. Bhabha[1] (1938) tried to explain these as a consequence of a knock-on collision, in which a meson while passing through a thick layer of a material makes a very close collision with an atomic electron and knocks out the electron, which subsequently produces a large number of particles by the ordinary cascade process. His calculations are based on the assumption that the meson has a spin of half a unit and thus can be described by the Dirac equation. Later on, Bhabha, Carmichael and Chou[2] (1939) have modified these calculations on the assumption that the mesons have a spin of one unit and are described by the equations given by Proca[3] (1936). Large bursts are naturally produced by high-energy mesons, and bursts containing more than 100 particles can only be produced by mesons having energies more than 10^{10} e.v. But in this energy range, the cross-sections for the production by a meson of a secondary knock-on electron is different for different spins, and consequently it is believed that a comparison of the theoretical results on the frequency of the burst production, containing a large number of particles, will provide a good test of the meson theory. High-energy mesons have also a large probability of radiating high-energy quanta, while passing the electric field of the nucleus (*Bremsstrahlung*), which again will produce showers by the ordinary cascade process. Bhabha[1] (1938) has shown that if the meson has a spin of half a unit, the number of electrons produced through the radiation process, for a meson of mass 100 times or more than that of an electron, is negligible in comparison with that produced by the knock-on process, but similar calculations were not extended when the meson has a spin of one unit. Moreover, as will be evident in the following section, such a conclusion is not valid for large bursts. Christy and Kusaka[4] (1941) have made these calculations, both for the knock-on process and the radiation process, and taking for the meson various possible spins, *viz.*, zero, half and one unit. Finally they have compared their results with the experimental results of Schein and Gill[5] (1939) and have derived the conclusion that mesons, at least those observed in cosmic rays, cannot have spin 1, but may have a spin zero or half, and preferably zero.

The most serious uncertainty in these calculations is the lack of knowledge of the fluctuations. Christy and Kusaka have assumed Furry's fluctuation formula while Bhabha and others have taken the Poisson distribution. But it is well known that Furry's fluctuation formula is justified only for very small thickness of the material traversed, and is not valid for large thicknesses. But for small thicknesses Furry's formula deviates but little from the Poisson formula. Consequently in large thickness of the material, which is more important in the burst production, it is doubtful whether Furry's fluctuation formula can be used. Another uncertainty in these calculations of the burst frequency arises due to the rough approximations usually made in the Cascade theory, since in the production of the bursts cascade multiplication plays in the end a decisive part. Christy and Kusaka have taken, for the average number of particles produced in the cascade process, an approximate form which very roughly fits with the results of Serber's[6] (1938) calculations. But this expression for the average is in error for various reasons.* Moreover for reasons already pointed out (Chakrabarty[7], 1942) the result of Serber is seriously open to doubts. As the conclusion derived from the results obtained by Christy and Kusaka has far reaching effects, it is desirable to see how far these approximations may affect their final result.

In the present paper we shall calculate the frequency of bursts produced by a meson in a thick layer of a material, assuming that the fluctuation around the average obey a Poisson distribution and using the accurate results of the Cascade theory obtained previously.[8] A comparison of the results of calculations of the present paper with the experimental results of Schein and Gill[5] (1939) will also be made at the end.

---

* The expression for S_{AV} giving the average number of particles produced by a primary of energy E at a depth x (in shower units of length), as taken by Christy and Kusaka, has always a maximum at $x=7$ and the corresponding maximum value of S_{AV} is $E/9\beta$, whatever the value of E may be. Apart from the fact that the position of the maximum for S_{AV} will change with the change of E, the value of S_{AV} at the maximum is in excess by a factor ranging from 1.5 to 2.1 as E increases from 10^{10} e.v. to 10^{12} e.v., when compared with the accurate figures for S_{AV} obtained by us (Bhabha and Chakrabarty, 1942)[8]. This is primarily due to the defects in the analysis of Serber, as has already been shown in a previous paper. These considerations show that neither in the position nor in the height of the maximum the approximation is valid, and it is difficult to estimate how much these approximations will affect the final results.

To investigate the production of showers by heavy particles, two distinct processes are to be considered. (1) The meson may produce a very fast secondary electron by direct collision which will subsequently produce a shower by cascade multiplication. (2) The meson may radiate a high-energy quantum which ultimately produces the shower. The cross-sections for these processes, taking different spins and magnetic moments, have been given by various authors [Bhabha[1] (1938), Massey and Corben[9] (1939), Corben and Schwinger[10] (1940), Christy and Kusaka[4] (1941), Bothe and Wilson[11] (1940), Wilson[12] (1941)].

The differential effective cross-section $Q(W, E_0)dE_0$ for the production by a meson of energy W, of a secondary electron or a quantum, by either of the two processes mentioned above, and having energies lying between E_0 and E_0+dE_0, are given by the following expressions, depending on the spin of the meson. Since we are concerned with large bursts and consequently with highly energetic mesons, we can take $W \gg Mc^2$, where M is the mass of the meson. With this approximation we have for the knock-on process; and

(*i*) Spin 0, magnetic moment 0

$$Q_c(W,E_0)dE_0 = 2\pi r_0^2 mc^2 Z[1 - E_0/E_{0m}]E_0^{-2}dE_0, \qquad \dots \quad (1a)$$

(*ii*) Spin ½, magnetic moment $e\hbar/2Mc$,*

$$Q_c(W,E_0)dE_0 = 2\pi r_0^2 mc^2 Z[1 - (E_0/E_{0m}) + \tfrac{1}{2}(E_0^2/W^2)]E_0^{-2}dE_0, \quad \dots \quad (1b)$$

(*iii*) Spin 1, magnetic moment $e\hbar/2Mc$,

$$Q_c(W,E_0)dE_0 = 2\pi r_0^2 mc^2 Z\left[1 - \frac{E_0}{E_{0m}} + \frac{1}{3}\frac{E_0^2}{W^2} + \frac{1}{3}\frac{mE_0}{M^2c^2}\left(1 - \frac{E_0}{E_{0m}} + \frac{1}{2}\frac{E_0^2}{W^2}\right)\right]\frac{dE_0}{E_0^2}, \quad \dots \quad (1c)$$

where $r_0 = e^2/mc^2$ and E_{0m} is the maximum energy which can be communicated to an electron in a free collision, and is given by

$$E_{0m} = W[1 + Mc^2/(2mW)]^{-1}. \qquad \dots \quad (2)$$

Similarly the expressions for $Q(W,E_0)dE_0$ for the radiation process are given by the following expressions.

(*i*) Spin 0, magnetic moment 0,

$$Q_r(W,E_0)dE_0 = \frac{16}{3}\cdot\frac{Z^2r_0^2}{137}\left(\frac{m}{M}\right)^2\left(\frac{W-E_0}{E_0}\right)\left[\log\frac{2W(W-E_0)}{Mc^2E_0} - \frac{1}{2}\right]\frac{dE_0}{W}, \qquad (3a)$$

(*ii*) Spin ½, magnetic moment $e\hbar/2Mc$,

$$Q_r(W, E_0)dE_0 = \frac{16}{3}\cdot\frac{Z^2r_0^2}{137}\left(\frac{m}{M}\right)^2\left[\frac{W-E_0}{E_0} + \frac{3}{4}\frac{E_0}{W}\right] \times \left[\log\frac{2W(W-E_0)}{Mc^2E_0} - \frac{1}{2}\right]\frac{dE_0}{W}, \qquad \dots \quad (3b)$$

when the screening of the atomic nuclei is neglected, and

---

* $\hbar$ denotes Planck's constant divided by 2π.

$$Q_r(W, E_0)dE_0 = \frac{16}{3}\cdot\frac{Z^2 r_0^2}{137}\left(\frac{m}{M}\right)^2 \log\left(183\frac{M}{m}Z^{-\frac{1}{3}}\right)\left[\frac{W-E_0}{E_0}+\frac{3}{4}\frac{E_0}{W}\right]\frac{dE_0}{W}, \quad (3c)$$

when the screening is complete.

(*iii*) Spin 1,* magnetic moment $c\bar{h}/2Mc$,

$$Q_r(W, E_0)dE_0 = \frac{1}{12}\cdot\frac{Z^2 r_0^2}{137}\left(\frac{m}{M}\right)^2 \frac{W}{Mc^2}\left[2-2\frac{E_0}{W}+7\frac{E_0^2}{W^2}\right]\frac{dE_0}{W}, \quad \ldots \quad (3d)$$

when the effect of radiation damping is neglected. If the effect of radiation damping be taken into consideration, then as given by Wilson[12] (1941) we have for spin 1,

$$Q_r\ W, E_0)dE_0 = \frac{\pi}{6}\cdot\left(3^{-\frac{7}{6}}a^{-\frac{2}{3}}\right)\cdot\frac{Z^2 r_0^2}{137}\left(\frac{m}{M}\right)^2 \log\left(137\frac{M}{m}Z^{-\frac{1}{3}}\right)$$

$$\times\left[2-2\frac{E_0}{W}+7\frac{E_0^2}{W^2}\right]\frac{dE_0}{W}. \quad \ldots \quad (3c)$$

We shall first calculate the probability $P(N)$, of a meson being accompanied by N electrons and positrons after passing through a layer of some substance of thickness l and of atomic number Z. If $N(y_0, t)$ be the average number of particles produced at a depth t in characteristic units, defined previously,[8] produced by a primary particle or quantum of energy β exp. y_0, then as shown by Bhabha and Heitler[14] (1937) the probability of N particles appearing instead of N by a fluctuation is given by

$$\exp.(-\bar{N}).\bar{N}^N/\Gamma(N+1). \quad \ldots \quad (4)$$

Following Bhabha if we neglect the small variation in the energy of the heavy particle, we get

$$P(N) = l\sigma\int_0^{\epsilon} Q(W, E_0)J_N(y_0)dE_0, \quad \ldots \quad (5)$$

where

$$J_N(y_0) = \int_0^{\epsilon} dt'\exp.(-\bar{N})\{\bar{N}(y_0, t')\}^N/\Gamma(N+1), \quad \ldots \quad (6)$$

where $Q(W, E_0)$ is the cross-section given by equations (1) or (3), according as one considers the knock-on process or the radiation process, for which the values of ϵ will be E_{0m} or W respectively. σ represents the number of atoms per cubic centimetre of the substance, and

$$y_0 = \log_e(E_0/\beta), \quad \ldots \quad (7)$$

---

* The expression given by Christy and Kusaka, differs from that given by Booth and Wilson in having an additional factor $\pi/(5Mc^2Z^{\frac{1}{3}})$ and also in having further terms varying as log W. These differences arise due to the difference in the nature of the approximations made in the limits of the impact parameter. The logarithmic terms will, however, have no appreciable effect in the calculations of the burst frequency.

where β is the critical energy (or the mean collision loss in the characteristic unit) for the substance of the material and has been defined in a previous paper.[8] Following Bhabha, the upper limits of the integral in (6) can be extended to ∞ when we are concerned with large thickness of the material. We therefore have

$$J_N(y_0) \simeq \int_0^\infty dt \, \exp.(-\bar{N}) \, \bar{N}^N / \Gamma(N+1). \qquad \dots \quad (6a)$$

From the results of the cascade theory (Bhabha and Chakrabarty, 1942)[8] we can easily calculate the values of $\bar{N}$ for different values of y_0 and t. When $\bar{N}(y_0, t)$ for any given y_0 is plotted against t it is observed that the curves are of the skew type of a Gaussian curve. It is observed that $\bar{N}$ can be obtained empirically by the process of curve fitting and the best fit is given by the following equations:

$$\bar{N} = N_m \exp.\{-a_1 t_m (1 - t/t_m)^2\}, \qquad \text{when} \quad t \leq t_m \qquad \dots \quad (8a)$$

$$\bar{N} = N_m \exp.\{-a_2 t_m (t/t_m - 1)^2\}, \qquad \text{when} \quad t \geq t_m \qquad \dots \quad (8b)$$

where N_m is the maximum value of $\bar{N}$ and t_m the value of t at this point for a given y_0 and were deduced accurately in a previous paper.[8] They are given by*

$$t_m = 1.01 y_0 - 1.92 \qquad \dots \quad (9a)$$

and

$$N_m = 0.169 (y_0 - 1.90)^{-\frac{1}{2}} \exp. y_0 \simeq 0.169 \, t_m^{-\frac{1}{2}}. \exp. y_0, \qquad \dots \quad (9b)$$

with $a_1 = 0.70$ and $a_2 = 0.17$.

Except for very small values of t (~ 1) and again when $t >> t_m$ the fit of the empirical curves with the actual curves is very good, and in any case even for small values of t, the error introduced in taking (8) is well within the limits of error already existing in the calculations of the Cascade theory.

From (6a) and (8) we thus have,

$$J_N(y_0) = \int_0^\infty dt \, e^{-\bar{N}} \, \bar{N}^N / \Gamma(N+1)$$

$$= \frac{N_m^N \, t_m}{\Gamma(N+1)} \cdot \int_0^\infty \sum_{r=0}^{\infty} (-1)^r \cdot \frac{N_m}{\Gamma(r+1)}$$

$$\times [\exp.\{-(N+r) a_1 t_m z^2\} + \exp.\{-(N+r) a_2 t_m z^2\}] dz$$

$$= \tfrac{1}{2} \sqrt{\pi} \left(a_1^{-\frac{1}{2}} + a_2^{-\frac{1}{2}} \right) \left(N_m^N \, t_m^{\frac{1}{2}} / \Gamma(N+1) \right) \sum_0^\infty (-1)^r . N_m^r / \{\Gamma(r+1)(N+r)^{\frac{1}{2}}\},$$

$$= 3.21 \, t_m^{\frac{1}{2}} . \frac{1}{2\pi i} \int_{c-i\infty}^{c+i\infty} \frac{\Gamma(z) N_m^{N-z}}{\Gamma(N+1) \sqrt{(N-z)}} . dz, \qquad \dots \quad (10)$$

---

* These values are slightly modified when the variations of the cross-sections for radiation and pair-creation processes with energy and also with the nature of the material is considered in the Cascade theory. This has been shown in a different paper.

where c is any real number greater than zero. The integral in (10) can be evaluated by the saddle point method. It can easily be shown that so long as $N_m < N$, the saddle point lies in the neighbourhood of N_m and the corresponding value of $J_N(y_0)$ tends to zero, but when $N_m > N$ the saddle point lies in the neighbourhood of N, but is always less than N and in that case the corresponding values of $J_N(y_0)$ is finite, has a maximum when N_m is slightly greater than N, and for larger values of N_m (*i.e.*, of y_0) the values of $J_N(y_0)$ slowly diminishes. This behaviour of $J_N(y_0)$ will be apparent from Fig. 1, in which the values of $J_N(y_0)$ for different values of N have been plotted against y_0. Bhabha[1] (1938) has also explained such a behaviour of $J_N(y_0)$ from geometrical considerations. Consequently, as has already been mentioned by Bhabha, it is now clear that for a rough estimate one can assume that for a given y_0, $J_N(y_0)$ is zero when $N > N_m$ and remains constant when $N \leq N_m$, where N_m is the maximum number of particles produced by a particle or quanta of energy β exp. y_0. Hence the largest shower which occurs with any probability, produced by a meson of energy W contains N particles, where

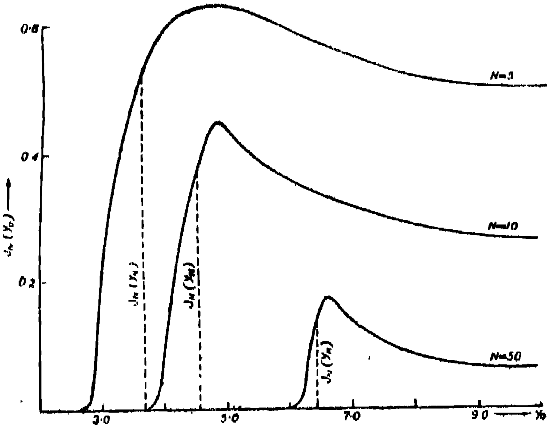

FIG. 1

$$N = N_m(y_0) = 0.169(y_0 - 1.90)^{-\frac{1}{2}}.\text{exp}.\, y_0 \qquad \dots \quad (11)$$

and $y_0 = \log(E_{om}/\beta)$ or $\log(W/\beta)$, depending on whether the shower is produced through a knock-on process or a radiation process respectively. A similar expression has also been obtained by Bhabha, where he has considered only those particles in the shower having energies greater than the critical energy. Lovell[13] (1939) tried to obtain a similar expression, taking into consideration the particles having energies less than the critical energy. But his values are too large, roughly by a factor four.

From (5) and (10) we can now proceed to calculate the values of P(N) for different values of N using for $Q(W, E_0)$ different expressions given by (1) and (3). All the integrations occurring cannot be evaluated analytically, and we have to calculate them numerically. But this is not the quantity which is of direct physical interest, and in order to compare the theoretical results with experiments we have to integrate this probability over the spectrum of the meson which is incident on the layer of material under consideration. This can be done as in the next section. But to determine only the order of P(N) one can follow Bhabha, and take $J_N(y_0)=0$ when $y_0 < y_N$ and $J_N(y_0)=J_N(y_N)$ when $y_0 \geqq y_N$ where y_N is that value of y_0 which makes $N_m=N$.* A comparison of the values of $J_N(y_0)$ derived in the present paper with the corresponding values obtained by Bhabha shows that the values of $J_N(y_0)$ taken by him are nearly twice those of the values obtained in the present paper. Bhabha has introduced a factor c to explain the behaviour of $J_N(y_0)$ which he initially stated to be of the order of unity. The argument given above shows that it can be taken to be unity. This probably explains why the values calculated by Bhabha for Σ NP(N) were roughly twice the calculated average number of particles accompanying the heavy particles. Consequently, the value of c will be 1 and not 2 as has been finally suggested by Bhabha. Lovell has taken $c=0.25$ which naturally makes his result too large by a factor four.

To compare with the experimental results of Schein and Gill and others and also with the theoretical results of Christy and Kusaka it is necessary to calculate the probability of a meson producing *more than* N particles. Bhabha and Heitler[11] (1937) have shown that if the fluctuation obeys the Poisson law, then the probability of getting *more than* N particles in a shower, when the average is $\bar{N}$ is $W(N+1, \bar{N})$,

where
$$W(N+1, N)=\frac{N^{N+}}{\Gamma(N+1)} \cdot \int_0^1 z^N \exp.(-\bar{N}z)dz.$$

Consequently, the probability $P(N_>, W)$ of a meson of energy W emerging accompanied by a shower containing *more than* N particles from an infinitely thick layer of a substance is given by

$$P(N_>, W)=l\sigma\int_0^{\epsilon} Q(W,E_0)J_{N>}(y_0)dE_0, \qquad \ldots \quad (12)$$

where
$$J_{N>}(y_0) = \frac{1}{\Gamma(N+1)}\int_0^{\infty} \bar{N}^{N+1}\, dt\int_0^1 z^N \exp.(-\bar{N}z)dz. \qquad \ldots \quad (13)$$

Substituting the values of $\bar{N}$ from equation (8) and interchanging the order of integration in (13) we have

$$J_{N>}(y_0)=\frac{N_m{}^{N+1}}{\Gamma(N+1)} \cdot \tfrac{1}{4}\sqrt{\pi}\,(a_1{}^{-\frac{1}{2}}+a_2{}^{-\frac{1}{2}})t_m{}^{\frac{1}{2}} \sum_0^{\infty}(-1)^r N_m^r, \{\Gamma(r+1), (N+r+1)^{+\frac{3}{2}}\}.$$

$$=3.21 \cdot \frac{1}{2\pi i}\int_{c-i\infty}^{c+i\infty} \frac{\Gamma(z)N_m{}^{N-z+1}\, t_m{}^{\frac{1}{2}}}{\Gamma(N+1)(N-z+1)^{\frac{3}{2}}}\, dz. \qquad \ldots \quad (14)$$

---

* This approximation is no longer necessary, since the analytical expression for $J_N(y_0)$ as given by (10) can now be used for the calculations of P(N).

If $S(W)dW$ be the number of mesons, having energies between W and $W+dW$, incident on the layer of the material under consideration, then the total probability of getting a shower containing *more than* N particles below an "infinitely thick"* layer of the material is given by

$$B(N)=l\sigma\int_0^\infty S(W)dW\int_0^\epsilon Q(W{\cdot}E_0)J_{N>}(y_0)dE_0$$

$$=3.21\ l\sigma.\frac{1}{2\pi i}\int_{c-i\infty}^{c+i\infty}\frac{\Gamma(z)(.169)^{N-z+1}}{\Gamma(N+1)(N-z+1)^{\frac{3}{2}}}dz\int_0^\infty S(W)dW$$

$$\times\int_0^\epsilon Q(W,E_0)(y_0-\zeta)^{-\frac{1}{2}(N-z)}\exp.(N-z+1)y_0.dE_0 \quad \ldots \quad (15)$$

where $\zeta=1.90$

As in the case of $J_N(y_0)$ it can also be shown here that for all values of y_0 for which $N_m<N$, $J_{N>}(y_0)\simeq 0$, and for other values of y_0, $J_{N>}(y_0)$ gradually increases as y_0 increases. Consequently the lower limit of the E_0 integration and hence also of the W integration can be taken to be E_N or any other value less than E_N whichever is convenient, where E_N is that value of E_0, corresponding to which $N_m=N$. For convenience in the evaluation of the integrals in (15) we shall henceforth take the lower limit of the E_0 integration as β exp. ζ. This is justified so long as the value of N is greater than 3.

Following Euler and Heisenberg[15] (1938) we have assumed that

$$S(W)dW=\delta I_0\frac{(2\times10^9.e.v)^\delta}{(\epsilon T+W)^{\delta+1}}dW, \quad \ldots \quad (16)$$

where $\delta=1.87$ and $\epsilon T=2.10^9$ e.v. at sea-level. Also from the analysis of Street and Woodward[16] (1934) and Blackett[17] (1938) we assume that the total meson intensity at sea-level is 0.01 per cm.^{2} per sec. per unit solid angle. Hence from equations (1), (3), (15) and (16) we can now calculate the number of bursts of size *greater than* N per cm.^{2} per sec. due to any particular cross-section. This is what Christy and Kusaka has calculated but with a different expression for $\bar{N}$ and a different form for fluctuation.

We shall first consider those bursts produced by a meson radiating a hard quantum which ultimately produce the burst through the usual cascade process and so take for $Q(W, E_0)$ its values given by equations (3). We therefore have

$$B(N)=\delta I_0(2\times10^9\ e.v.)^\delta.(3.21\ l\sigma).\frac{1}{2\pi i}\int_{c-i\infty}^{c+i\infty}\frac{\Gamma(z)(0.169)^{N-z+1}}{\Gamma(N+1)(N-z+1)^{\frac{3}{2}}}dz$$

$$\times\int_{\beta e^{\zeta}}^{\infty}\frac{\exp.(N-z+1)y_0}{(y_0-\zeta)^{\frac{1}{2}(N-z)}}dE_0\int_{E_0}^{\infty}Q(W,E_0).\frac{dW}{(\epsilon T+W)^{\delta+1}}. \quad \ldots \quad (17)$$

---

* In the sense used by Bhabha (1938).

For the caculations of large bursts for which $N \geq 100$ it is necessary to consider only those mesons for which $W > E_N$ ($\approx \beta e^7$). So that as long as $N \geq 100$, for convenience in integration we can in (17) take $W^{-(\delta+1)}$ instead of $(\epsilon T + W)^{-(\delta+1)}$, since the error thus introduced will be negligible. It may be noted here that as the number of incident mesons decreases rapidly as W increases (when $W > \epsilon T$), and on the other hand $P(N_{\blacktriangleright}, W)$ tends to zero when $W < E_N$ and is finite and gradually increases as W increases, the combined effect of S(W) and $P(N_{\blacktriangleright}, W)$ will show that the major part of B(N) is contributed by the values of W in the neighbourhood of E_N. This has also been shown graphically by Lovell. Consequently, any error either in the value of S(W) or $P(N_{\blacktriangleright}, W)$ in the neighbourhood of $W = E_N$ will produce an appreciable effect in the calculations of B(N).

It will be shown in the appendix, that the values of B(N) for different values of $Q(W, E_0)$ as given by (3) can be written in the following form :—

(*i*) Spin 0,

$$B(N) = A \exp.(-\delta\zeta).\{(K_0 + \zeta L_0)f_1(N, \delta) + L_0 f_2(N, \delta)\}. \quad \dots \quad (18a)$$

(*ii*) Spin half (screening neglected),

$$B(N) = A \exp.(-\delta\zeta).\{(K_{\frac{1}{2}} + \zeta L_{\frac{1}{2}})f_1(N, \delta) + L_{\frac{1}{2}} f_2(N, \delta)\}. \quad \dots \quad (18b)$$

(*iii*) Spin half (screening complete),

$$B(N) = AK'_{\frac{1}{2}} \exp.(-\delta\zeta).f_1(N, \delta). \quad \dots \quad (18c)$$

(*iv*) Spin 1 (neglecting radiation damping),

$$B(N) = AK_1 \exp.(-\delta\zeta).\exp.\zeta.f_3(N, \delta). \quad \dots \quad (18d)$$

(*v*) Spin 1 (considering the effect of radiation damping),

$$B(N) = AK'_1 \exp.(-\delta\zeta).f_1(N, \delta), \quad \dots \quad (18e)$$

where

$$A = \delta I_0(3.21 l\sigma)\frac{Z^2 r_0^2}{137}\left(\frac{m}{M}\right)^2\left(\frac{2 \times 10^9 . \text{e.v.}}{\beta}\right)^\delta. \quad \dots \quad (19a)$$

$$K_0 = L_0\left[\{\log(2\beta/Mc^2) - \tfrac{1}{2}\} + 2\delta^{-1}(\delta+1)^{-1}(2\delta+1) + \delta\psi(\delta+2) - (\delta+1)\psi(\delta+1) - \gamma\right], \quad \dots \quad (19b)$$

$$L_0 = \frac{16}{3}\delta^{-1}(\delta+1)^{-1}, \quad \dots \quad (19c)$$

$$K_{\frac{1}{2}} = K_0 + 4\left[(\delta+1)^{-1}\{\log(2\beta/Mc^2) - \tfrac{1}{2}\} + 2(\delta+2)^{-2} - (\delta+2)^{-1}\{\psi(\delta+3) + \gamma\}\right], \quad (19d)$$

$$L_{\frac{1}{2}} = L_0 + 4(\delta+1)^{-1}, \quad \dots \quad (19e)$$

where $\psi(\delta) = \dfrac{d}{d\delta}\log_e\Gamma(\delta)$ and γ is the Euler-Mascheroni constant.

$$K'_{\frac{1}{2}} = \frac{16}{3}\log\left(183\frac{M}{m}Z^{-\frac{1}{3}}\right)\left[\delta^{-1}(\delta+1)^{-1} + \frac{3}{4}(\delta+2)^{-1}\right], \quad \dots \quad (19f)$$

$$K_1 = \frac{1}{12}.\frac{\beta}{Mc^2}\left[2\delta^{-1}(\delta+1)^{-1} + 7(\delta+2)^{-1}\right], \quad \dots \quad (19g)$$

$$K'_1 = \frac{\pi}{6} \cdot \left(3^{-\frac{7}{6}} a^{-\frac{2}{3}} \right) \log \left(137 \frac{M}{m} Z^{-\frac{1}{3}} \right) \left| 2(\delta+1)^{-1}(\delta+2)^{-1} + 7(\delta+3)^{-1} \right|, \tag{19h}$$

and

$$f_1(N, \delta) = \frac{1}{2\pi i} \int_{c-i\infty}^{c+i\infty} \phi(N.z).\Gamma \left(1 - \frac{N-z}{2} \right) (\delta + z - N - 1)^{-\frac{1}{2}(2-N+z)} dz, \tag{20a}$$

$$f_2(N, \delta) = \frac{1}{2\pi i} \int_{c-i\infty}^{c+i\infty} \phi(N, z)\Gamma \left(2 - \frac{N-z}{2} \right) (\delta + z - N - 2)^{-\frac{1}{2}(4-N+z)} dz, \tag{20b}$$

$$f_3(N, \delta) = \frac{1}{2\pi i} \int_{c-i\infty}^{c+i\infty} \phi(N, z)\Gamma \left(1 - \frac{N-z}{2} \right) (\delta + z - N - 2)^{-\frac{1}{2}(2-N+z)} dz, \tag{20c}$$

where

$$\phi(N, z) = \frac{\Gamma(z)(0.160 \exp. \delta)^{N-z+1}}{\Gamma(N+1)\ (N-z+1)^{\frac{3}{2}}}.$$

The values of $f_1(N, \delta)$, $f_2(N, \delta)$, $f_3(N, \delta)$ are to be evaluated by the saddle point method. The accuracy of the saddle point method of integration is well within 2%, as has been tested by the method already mentioned in a previous paper.[7] Taking $\delta = 1.87$, we have evaluated the values of f_1, f_2, f_3 for different values of N, and the values thus obtained are given in Table I. The values of K_0, L_0, $K_{\frac{1}{2}}$, etc., depend also on Z and the ratio (M/m). At the present moment a certain amount of uncertainty exists as to the value of (M/m). Several experiments seem to suggest that it lies between 150 and 200. Following Bethe[18] (1940) we shall take $(M/m) = 177$. For a given material it is therefore no longer difficult to calculate the values of K_0, L_0, $K_{\frac{1}{2}}$, etc., and also of A. With these values and the values of f_1, f_2, f_3 as given in Table I, the values of B(N), for different values of N and for the different cases mentioned before, can be easily calculated. The results thus obtained have been given in Table II. The figures in the table show that even for N = 1600, the value of B(N) for a spin half meson, when the screening is neglected is less than those when screening is complete. It is therefore clear that even for N = 1600, the meson energy is not high enough for screening to be complete.*

TABLE I

Values of f_1 (N, δ), f_2 (N, δ), f_3 (N, δ) with $\delta = 1.87$.

N	100	200	400	600	800	1000	1200	1600
$f_1 \times 10^6$	62.99	15.96	4.084	1.876	1.073	.6860	.4890	.2782
$f_2 \times 10^6$	299.8	86.35	24.86	12.02	7.210	4.710	3.393	2.017
$f_3 \times 10^3$		19.05	10.60	7.416	5.840	4.661	4.056	3.117

---

* I am indebted to Dr. Bhabha for drawing my attention to this point in a private communication.

TABLE II

Values of $B(N) \times 10^9$, for different values of N

N→ Spin ↓	100	200	400	600	800	1000	1200	1600
0	47.02	13.41	3.816	1.838	1.144	.7166	.5158	.3057
½ (Screening neglected)	86.66	25.55	7.461	3.631	2.191	1.435	1.035	.6183
½ (Screening complete)	162·1	41.08	10.51	4.829	2.702	1·766	1.259	.7161
1 (Radiation damping neglected)	...	255.5	142.1	99·45	78.31	62·50	54.39	41.80
1 (Radiation damping considered)	478.7	121.3	31.04	14.26	8.155	5.214	3.710	2.114

The frequency of bursts produced through the knock-on process can be similarly calculated. For small bursts these have been obtained by Bhabha, and Bhabha, Carmichael and Chou. For large bursts the knock-on process gives an insignificant contribution to the burst production which can be shown by the following considerations. Let us estimate the relative probability of a shower being produced by the radiation process and the collision (knock-on) process which amounts to estimating the *ratio* R (say) of the chance of a meson emitting a quantum of energy greater than E to the chance of its producing by direct collision an electron of energy greater than the same amount. The cross-sections for these processes have been given in equations (1) and (3). The required ratio is thus given by

$$R = \frac{\int_E^W Q_r(W, E_0)\,dE_0}{\int_E^{E_{0m}} Q_c(W, E_0)\,dE_0} = \frac{I(\text{rad.})}{I(\text{coll.})} \qquad \ldots \quad (21)$$

The values of I(rad.) and I(coll.) can be obtained by easy calculations for different spins.

For given values of W and E the values of R can thus be easily calculated. The values of R thus obtained, for different values of W and E, have been given in Table III. The lowest value of E required for a given N is easily obtained from (11) and these values have also been shown in the table III. It shows that as N increases R also increases and for N $\geq$ 100, R is much greater than 1,

TABLE III

Values of R for different values of W and E

$R_{\frac{1}{2}} \rightarrow$ spin half and screening complete, $R_1 \rightarrow$ spin 1, neglecting the effects of radiation damping, $R_1' \rightarrow$ spin 1, considering the effect of radiation damping.

W/Mc²	E/Mc²	1.0	5.0	10.0	50.0	100.0
	N$\sim$	3	7	12	50	100
10^2	$R_{\frac{1}{2}}$	.1124	.4457	.8760	—	—
	R'_1	0649	.4109	1.064	—	—
	R_1	1.626	10.29	26.64	—	—
10^3	$R_{\frac{1}{2}}$	.1622	.6183	1.082	3.834	6.576
	R'_1	0595	.2948	.5858	2.879	5.827
	R_1	1622	6183	1.082	3.834	6.576
10^4	$R_{\frac{1}{2}}$	2199	8966	1.620	6.165	10.77
	R'_1	.0588	.2817	.5385	2.129	3.469
	R_1	1.473×10^2	7.050×10^2	1.348×10^3	5.329×10^3	8.681×10^4

and gradually increases as N increases.* On the other hand for small values of N we get $R < 1$, which shows that for small showers the knock-on process predominates while for large bursts the radiation process gives nearly the whole contribution and the knock-on process only producing an insignificant effect. The results obtained by Christy and Kusaka also show this behaviour. The calculations of Bhabha, Charmichael and Chou, in which they considered only the knock-on process, give a good fit with their experiments, since the experiments do not involve sufficiently high energy and the results were obtained in the region where the knock-on process is the predominant one or at least the two processes give equivalent contributions (*i.e.*, $R \sim 1$).

The values of B(N) as obtained from equations (17) to (20) can therefore be considered as giving the *total burst frequency* when $N \geq 100$. In Fig. 2, B(N) has been plotted as a function of N, on a log-log scale and it is observed that all the cases give practically straight lines. It is observed that the experimental values of Schein and Gill fit very well with the case of *spin* 1, *when the effect of the radiation damping is considered*. The burst frequencies calculated either with spin 0 or half are very much less than the experimental values. The difference is certainly much more than the possible range of experimental error. The case of spin 1 when the effect of radiation damping is neglected is certainly

---

* This conclusion is altered if the radiation damping is neglected in the case of collision cross-section for spin 1. It appears that when $E \geq 10^{11}$ e.v., the value of R for spin 1 begins to decrease and will ultimately be less than 1. This shows that the radiation damping will also produce important effect on the collision cross-sections, but this effect is perceptible only at very high energies. The values of $R_{\frac{1}{2}}$ when the screening is neglected and also that of R_0 have not been calculated, but their order can easily be obtained from the values of $R_{\frac{1}{2}}$ when the screening is complete. In these cases also the above conclusions hold good.

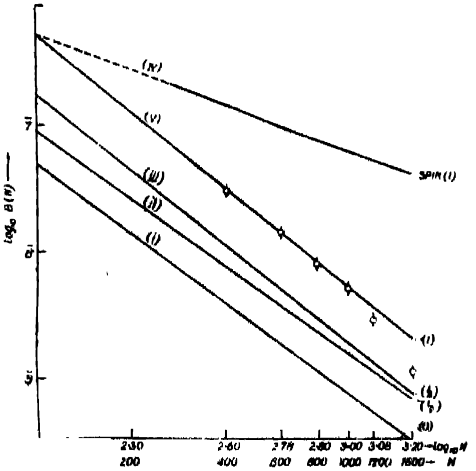

Calculated and observed size frequency distribution for large bursts. Numbers (*i*,—(*v*) refer to the different cases given by equations (18), and (φ) represents the experimental points of Schein and Gill.

FIG. 2

not a possibility, since both the intensity as well as the slope of the curve in this case is very different from the experimental curve. The experimental point at N = 200 is probably in error since it is possible that some small bursts have escaped detection. For very large bursts again, the statistical errors become very considerable, and the discrepancy at large values of N, say N ≧ 1200, is probably due to this.

The only source of uncertainty in the above calculations is the nature of the fluctuations. Unless the actual form for the fluctuation differs considerably from a Poisson's distribution, the results deduced above can be considered to be fairly accurate. The reasons for getting results which are so much different from those of Christy and Kusaka, and consequently leading to just an opposite conclusion are mainly, (*i*) the difference in the form of the fluctuation assumed, (*ii*) the very rough approximation made by them for $\bar{N}$, the average number of particles produced in a cascade shower by an energetic particle or quantum, and (*iii*) the consideration of the effect of radiation damping for spin 1. The consequence of these effects on the calculations will be clear when we compare the values of $J_{N\rightharpoondown}(y_0)$ as given by (14) with the corresponding expression obtained by Christy and Kusaka,* for various values of N. It may be noted that the validity of the expressions for the cross section for the different processes for very high energies is open to serious doubts as have been pointed out by Oppenheimer,

---

* The corresponding expression of Christy and Kusaka is $7(E_0/9\beta N)^{\frac{1}{2}}$ exp.$(-9\beta N/E_0)$ although they have finally modified it and have taken $13.5(E_0/15\beta N)^{\frac{1}{2}}$ exp.$(-15\beta N/E_0$ in the subsequent calculations.

Snyder and Serber (1940).[19] But similar extension of the range of validity of the quantum-mechanical expressions have been made in many other problems of Cosmic ray phenomena. While making the calculations for the knock-on process, and spin 1, the effect of the radiation damping on this cross-section was not considered. To my knowledge no one has as yet given the form of this cross-section after taking into account the effect of radiation damping, but it appears that this will largely modify the last term in (1c), which gives the spin dependence of the cross-section. But this will not materially affect the conclusions made before, since this term is of importance only for very high energy ($\sim 10^{11}$ e.v.) of the meson, when the total contribution of the knock-on process to the burst production is itself negligible.

We thus see that the frequency-size curve for large bursts provides evidence that the meson cannot have spin 0 or half. The case of spin 1 is a possibility or even a probability only when the effect of radiation damping is taken into consideration. *The meson has therefore a spin of one unit* in agreement with what is believed from nuclear considerations and the above calculations lend further support to the fact that the effect of radiation damping plays an important rôle in the processes involving mesons and the expression given by Wilson for the radiation cross-section is a much more reasonable one than those calculated previously wherein radiation damping was ignored.

APPENDIX

For the case of spin 0, we have from (3*a*) and (17),

$$\int_{E_0}^{\infty} Q(W, E_0) W^{-(\delta+1)} dW = \frac{16}{3} \cdot \frac{Z^2 r_0^2}{137} \cdot \left(\frac{m}{M}\right)^2$$

$$\times \int_{E_0}^{\infty} \left(\frac{W-E_0}{E_0}\right) \left[\log \frac{2W(W-E_0)}{Mc^2 E_0} - \tfrac{1}{2}\right] W^{-(\delta+2)} dW$$

$$= \frac{16}{3} \frac{Z^2 r_0^2}{137} \cdot \left(\frac{m}{M}\right)^2 E_0^{-(\delta+1)} \left[\delta^{-1}(\delta+1)^{-1} \left\{ \log \frac{2E_0}{Mc^2} - \tfrac{1}{2} \right\} - \int_0^1 (1-x) x^{\delta-1} \left\{ \log \frac{x^2}{1-x} \right\} dx \right]$$

$$= \frac{Z^2 r_0^2}{137} \cdot \left(\frac{m}{M}\right)^2 E_0^{-(\delta+1)} \left[K_0 + L_0 \log \frac{E_0}{\beta} \right].$$

$$\therefore \int_{\beta_c \zeta}^{\infty} (y_0 - \zeta)^{-\frac{1}{2}(N-z)} \exp.(N-z+1) y_0 \, dE_0 \int_{E_0}^{\infty} Q(W, E_0) W^{-(\delta+1)} dW$$

$$= \frac{Z^2 r_0^2}{137}\left(\frac{m}{M}\right)^2 \beta^{-\delta} \ \exp.(N-\delta-z-1)\zeta \int_0^\infty x^{-\frac{1}{2}(N-z)} \exp.(N-\delta-z+1)x$$

$$\times \{K_0 + L_0\zeta + L_0 x\} dx$$

$$= \frac{Z^2 r_0^2}{137}\left(\frac{m}{M}\right)^2 \beta^{-\delta} \exp.(N-\delta-z-1)\zeta \left[\frac{(K_0+L_0\zeta)\,\Gamma(1-(N-z)/2)}{(\delta+z-N-1)^{(1-(N-z)/2)}} \right.$$

$$\left. + L_0 \frac{\Gamma(2-(N-z)/2)}{(\delta-N+z-1)^{(2-(N-z)/2)}} \right]$$

$$\therefore \quad B(N) = A(K_0+\zeta L_0)\exp.(-\delta\zeta)\,.\frac{1}{2\pi i}\int_{c-i\infty}^{c+i\infty} \phi(N,z)\,\Gamma(1-(N-z)/2)$$

$$\times (\delta-N+z-1)^{-(1-(N-z)/2)}.\,dz.$$

$$+ AL_0 \exp.(-\delta\zeta).\,\frac{1}{2\pi i}\int_{c-i\infty}^{c+i\infty} \phi(N,z)\,\Gamma(2-(N-z)/2)$$

$$\times (\delta-N+z-1)^{-(2-(N-z)/2)}.\,dz.$$

For the case of spin 1, and neglecting the effect of radiation damping,

$$\int_{E_0}^{\infty} Q(W, E_0)\, W^{-(\delta+1)} dW = \frac{1}{12}.\,\frac{Z^2 r_0^2}{137}\left(\frac{m}{M}\right)^2 .\,\frac{E_0^{-\delta}}{Mc^2}\,.$$

$$\times \{2\delta^{-1}(\delta+1)^{-1} + 7(\delta+2)^{-1}\}.$$

$$\therefore \int_{\beta e^\zeta}^{\infty} \frac{\exp.(N-z+1)y_0}{(y_0-\zeta)^{\frac{1}{2}(N-z)}}\, dE_0\,.\int_{E_0}^{\infty} Q(W, E_0) W^{-(\delta+1)} dW$$

$$= \frac{1}{12}.\,\frac{Z^2 r_0^2}{137}\left(\frac{m}{M}\right)^2 .\,\frac{\beta^{-(\delta-1)}}{Mc^2}\{2\delta^{-1}(\delta+1)^{-1} + 7(\delta+2)^{-1}\}.\exp.\{-(\delta+z-N-2)\zeta\}$$

$$\times \Gamma(1-(N-z)/2)(\delta+z-N-2)^{-(1-(N-z)/2)}$$

$$\therefore \quad B(N) = AK_1 \exp.-(\delta-1)\zeta.\,\frac{1}{2\pi i}.\int_{c-i\infty}^{c+i\infty} \phi(N,z),$$

$$\times \Gamma(1-(N-z)/2)\ (\delta+z-N-2)^{-(1-(N-z)/2)}.\,dz.$$

With other values of $Q(W, E_0)$ the integrals occurring in (17) may be similarly evaluated and we get the results given in equations (18)—(20).

DEPARTMENT OF APPLIED MATHEMATICS,
CALCUTTA UNIVERSITY.

REFERENCES

[1] Bhabha, H. J., *Proc. Roy. Soc. A.*, **164**, 257 (1938).
[2] Bhabha, H. J., Carmichael, H., and Chou, C. N., *Proc. Ind. Aca. Sc. A.*, **10**, 221 (1939).
[3] Proca, *J. Phys. Radium*, **7**, 347 (1936).
[4] Christy, R. F., and Kusaka, S., *Phys. Rev.*, **59**, 405, 414 (1941).
[5] Schein, M., and Gill, P. S., *Rev. Mod. Phys.*, **11**, 267 (1939).
[6] Serber, R., *Phys. Rev.*, **54**, 317 (1938).
[7] Chakrabarty, S. K., *Proc. Nat. Inst. Sc. Ind.*, **8**, 331 (1942).
[8] Bhabha, H. J., and Chakrabarty, S. K., *Proc. Ind. Aca. Sc. A.*, **15**, 464 (1942).
[9] Massey, H. S. W., and Corben, H. C., *Proc. Camb. Phil. Soc.*, **35**, 463 (1939).
[10] Corben, H. C., and Schwinger, J., *Phys. Rev.*, **58**, 953 (1940).
[11] Booth, F., and Wilson, A. H., *Proc. Roy. Soc. A.*, **175**, 483 (1940).
[12] Wilson, A. H., *Proc. Camb. Phil. Soc.*, **37**, 301 (1941).
[13] Lovell, A. B. C., *Proc. Roy Soc. A.*, **172**, 568 (1939).
[14] Bhabha, H. J., and Heitler, W., *Proc. Roy. Soc. A.*, **159**, 432 (1937)
[15] Euler, H., and Heisenberg, W., *Ergeb. exakt. Naturwiss.*, **17** (1938).
[16] Street, J. C., and Woodward, R. H., *Phys. Rev.*, **46**, 1029 (1934).
[17] Blackett, P. M. S., *Proc. Roy. Soc. A.*, **165**, 11 (1938).
[18] Bethe, H. A., *Phys. Rev.*, **57**, 261 (1940).
[19] Oppenheimer, J. R., Snyder, H., and Serber, R., *Phys. Rev.*, **57**, 75 (1940).

VISIBLE ABSORPTION BANDS OF MERCURY HALIDES HgCl, HgBr AND HgI

By A. L. SUNDARA RAO

(Received for publication, August 10, 1942)

Plate XI

ABSTRACT. The absorption bands of HgCl, HgBr and HgI have been obtained by heating the substance in an open steel tube to a temperature of 1100°C. In HgCl and HgBr the band systems have been measured and a vibrational analysis is suggested. From the values of the constants, the heats of dissociation of these molecules in the upper and lower electronic states have been determined.

INTRODUCTION

The importance of the study of absorption spectra is well known. In the case of atoms and molecules, in the former of which lines and in the latter band absorption is obtained, the ground state of absorption is known to be the normal state. In certain molecules, *e.g.*, oxygen and the halogens,[1] converging progressions of absorption bands are obtained from which their heats of dissociation, could be directly determined. In other molecules, such as sulphur and phosphorous,[2] the absorption bands show diffuseness of the heads or their sudden absence abruptly in a sequence, indicating what is known as the phenomenon of pre-dissociation. In all cases the absorption spectra are considered to be providing valuable data concerning the molecules involved. The author has therefore undertaken the investigation of the absorption spectra of the halides of various elements, particularly those of high atomic weight, the ground states of which have either not been determined at all or have not been determined from the study of absorption. In the course of such an investigation with the halides of mercury, absorption bands have been obtained characteristic of the molecules, lying in the visible region, which do not appear to have been recorded till now. It is the purpose of the present paper to give details of these results, a short report of which has appeared in Current Science.[3]

EXPERIMENTAL

The procedure adopted in obtaining the absorption spectra consists in heating the substance in a seamless steel tube about 50 cms. long and 5 cms. in diameter, open at both ends. In the first experiments a similar tube closed at both ends by glass or quartz windows protected by water-cooled jackets was used. The tube was exhausted continuously by a Cenco Hyvac pump and the substance was heated. But, in spite of the protecting water jackets, the substance got deposited on the windows almost instantaneously and prevented all further examination. The open tube was found very useful and extremely simple to operate.

Different temperatures had to be tried before any absorption bands were observed. Two furnaces were employed—an electrical furnace capable of heating the tube up to 800°C and a specially constructed coke furnace, through which a powerful blast of air from a motor blower could be steadily maintained. By replenishing the coke at intervals, temperatures of the order of 1200°C could be easily attained. An exact measurement of the temperatures was made by the use of a standardised direct-reading optical pyrometer. At the temperature of the electrical furnace (about 800°C) no bands were observed. Using the coke furnace the characteristic bands made their appearance. There was observed also that an optimum temperature was necessary for the excitation of the bands—determined by the pyrometer to be about 1000-1100°C. Due to the need of replenishing the substance every two or three minutes, it was not found practicable to use a spectrograph of very high dispersion. The instrument used was of the Fuess type of large light-gathering power giving a dispersion of about 20 Å per mm. at λ4400. Effective exposures of about ten minutes were given: larger exposures often obliterated the appearance of the bands, due probably to the above condition of an optimum temperature for the excitation of the bands. The source of continuous spectrum was a hundred-watt projector lamp. Ilford Special Rapid panchromatic plates were used and the spectra were measured by a Hilger comparator using iron standards and a simple Hartmann dispersion formula.

Absorption spectra of various other salts of mercury were also photographed to make sure that the reported bands could be ascribed, from an experimental basis, as due to the particular halide, chloride, bromide or iodide that was worked with. Bands were obtained only with the above three halides and with none of the other salts tried—*e.g.*, the fluoride, sulphide, oxide and the nitrate—all of which were attempted, under identical experimental conditions.

RESULTS AND DISCUSSION

Mercuric Chloride.—In emission, the band systems of HgCl have been previously investigated chiefly by three workers. Wieland[4] divided the characteristic bands into three classes—Class III occurring in the visible region and the other classes in the ultra-violet. He reported the analysis of Class I system. Cornell[5] and more fully Sastry,[6] investigated the Class II system and reported a complete vibrational analysis. The visible bands are yet to be measured accurately before an analysis can be attempted. The absorption bands obtained in the present work lie in the region from λ4900 to λ4100 which is a portion of the extended region in which the visible emission system is reported to lie.

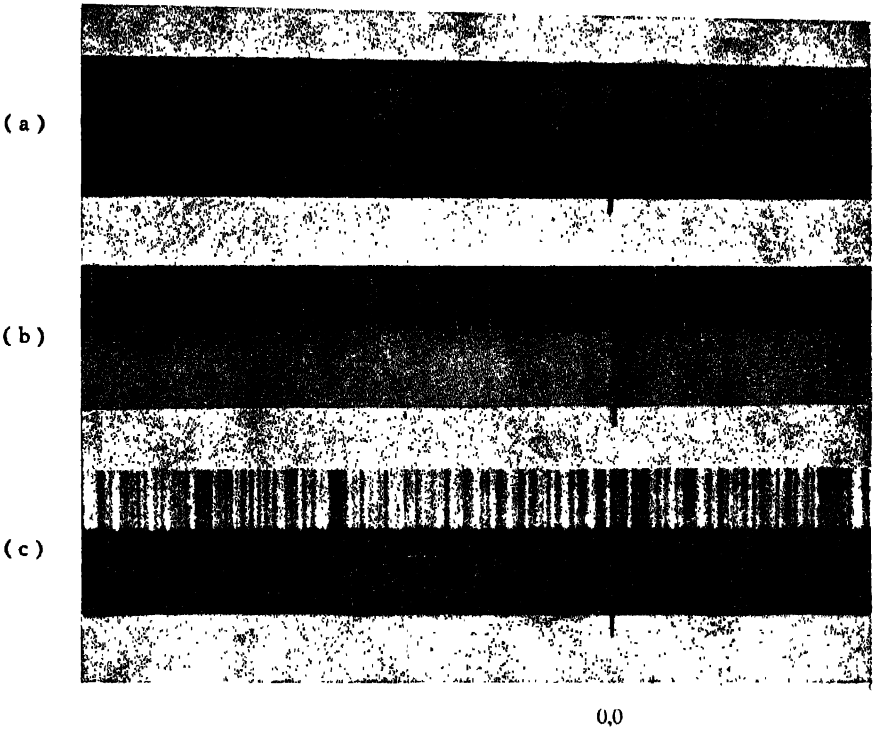

Absorption bands of mercury halides.

(a) HgCl, high temperature.

(b) ,, low temperature.

(c) HgBr

The latter system was also reported to be very complex and diffuse and for that reason perhaps could not be analysed. The writer believes that the absorption bands recorded in this paper are part of the emission system, involving the lower vibration quantum numbers. In general appearance they resemble the Class II system analysed by Cornell and Sastry. They consist of sequences of distinct doublet bands. Three of these sequences $\Delta v = 0, \pm 1$ in the region λ4500 to λ4250 are well developed. The very disposition of the heads, as can be seen from the reproduction (plate XI), suggest that they ought to form long sequences giving a narrow Condon parabola. They are thus ascribed to the diatomic molecule HgCl. Table I contains the wave-lengths of all the band heads measured on the plate and are given only correct to the nearest Angstrom unit. The doublet at λ4876, λ4842 could be measured with difficulty. The wave numbers are found from Kayser's Scwingungzahlen and the intensities are visual estimates. The various heads could be arranged in a diagonal array, the most intense of the heads being assumed as the (0,0) band. The quantum numbers assigned to each head are shown in the last column of the table. It will be seen that the bands consist of doublet heads, the two components having been designated as the Q_1 and Q_2, the doublet interval having an average value of about 120 units of wave number. The other alternative of assigning one of the component heads as due to isotope Cl^{35} and the other component to the isotope Cl^{37} cannot be possible on account of the relative intensities of the component heads. If they are due to the isotopes, the intensities of the heads should be in the ratio of 3 : 1, the abundance ratio of the two isotopes of chlorine. The failure to detect the isotopic head might be due, as in the Class II system of HgCl studied by Cornell and Sastry, to its overlapping with the next or the previous band head in the sequence.

Of particular interest to the chemist is the estimate of the heats of dissociation of molecules. For this purpose an approximate formula has been found to fit the band heads contained in Table I. It must be stated, however, that owing to the small dispersion used, there are large discrepancies in the intervals of the vibrational levels and hence the formula must be considered approximate. For the Q_1 heads the formula is

$$\nu = 22978 + [399(v'+\tfrac{1}{2}) - 4(v'+\tfrac{1}{2})^2] - [436(v''+\tfrac{1}{2}) - 7(v''+\tfrac{1}{2})^2]$$

the coefficients of $(v'+\frac{1}{2})$ and $(v''+\frac{1}{2})^2$ in the above equation, according to the usual relation

$$D' = \frac{\omega'^2_e}{4x'_e\omega'_e \times 8106}$$

give the value of D′, the energy of dissociation of the initial electronic state of the molecule. Similarly D″, the energy of dissociation corresponding to the lower electronic state can be obtained. The values, expressed in electron volts, are

$$D' = 1.1 \qquad D'' = 0.8.$$

Mercury Bromide.—The absorption bands obtained in the case of mercury bromide, extend between λ5000 and λ4000. About fifty heads have altogether been measured. These have been arranged into five sequences, $\Delta v = 0, \pm 1, \pm 2$. Another sequence is also indicated, a few bands remain unclassified. A catalogue of the wave-lengths, wave numbers and intensities of the band heads is shown in Table II in which the last column gives the classification. Here again, in deriving the vibrational assignments, the strongest band is assumed to be first

TABLE I

Absorption Bands of HgCl

Wave-length A. U.	Int.	Wave number	Classification v', v''	
4870	0	20503	0, 6	Q_1
4842	0	20647	0, 6	Q_2
	0	20142	0, 2	Q_1
4493	1	22251	0, 2	Q_2
4447	1	22481	4, 5	Q_1
4443	2	22501	3, 4	
4439	1	22521	2, 3	
4437	3	22531	1, 2	
4434	3	22547	0, 1	
4418	1	22628	3, 4	Q_2
4416	2	22639	2, 3	
4415	2	22644	1, 2	
4412	3	22659	0, 1	
4371	1	22872	4, 4	Q_1
4368	1	22887	3, 3	
4365	1	22914	2, 2	
4359	2	22935	1, 1	
4355	3	22955		
4354	5	22961	0, 0	
4346	1h	23003	5, 5	Q_2
4344	1h	23014	4, 4	
4342	1h	23024	3, 3	
4340	1h	23035	2, 2	
4337	1h	23051	1, 1	
4334	4	23067	0, 0	
4301	2	23244	5, 4	Q_1
4296	3	23271	4, 3	
4292	3	23293	3, 2	
4287	4	23320	2, 1	
4281	3	23352	1, 0	
4264	1	23445	4, 3	Q_2
4262	2	23456	3, 2	
4261	2	23462	2, 1	
4259	3	23473	1, 0	
4211	1	23741	2, 0	Q_1
4191	1	23854	3, 1	Q_2
4187	1	23877	2, 0	

h means hazy

TABLE II

Absorption Bands of HgBr

Wave-length A. U.	Int.	Wave number	Classification v', v''
4957	1	20168	--
4880	1	20486	--
4816	1	20748	—
4491	2	22260	5, 7
4484	2	22295	4, 6
4479	2	22320	3, 5
4473	2	22350	2, 4
4467	2	22380	1, 3
4462	2	22405	0, 2
4420	3	22618	3, 4
4413	3	22654	2, 3
4408	3	22679	1, 2
4401	3	22716	0, 1
4381	1	22819	—
4379	1	22830	6, 6
4373	1	22862	5, 5
4366	1	22898	4, 4
4361	1	22924	3, 3
4355	2	22956	2, 2
4346	3	23003	1, 1
4341	5	23030	0, 0
4321	3	23136	—
4309	4	23200	4, 3
4301	4	23244	3, 2
4295	4	23276	2, 1
4289	4	23309	1, 0
4273	2	23396	—
4263	2	23451	-
4256	2	23490	5, 3
4251	2	23517	4, 2
4246	2	23545	3, 1
4239	2	23584	2, 0
4230	1	23634	—
4220	1	23690	—
4210	1	23746	6, 3
4204	1	23780	5, 2
4197	1	23820	4, 1
4165	1	24002	—
4162	1	24020	—
4160	1	24032	—
4112	1	24312	—
4081	1	24497	—
4066	1	24587	—

member of the $\Delta v = 0$ sequence. The following formula has been obtained for the band heads; as in HgCl, this too must be considered as an approximate one.

$$\nu = 23057 + [267(v'+\tfrac{1}{2}) - 1(v'+\tfrac{1}{2})^2] - [324(v''+\tfrac{1}{2}) - 5(v''+\tfrac{1}{2})^2].$$

The values for D′ and D″ are obtained to be

$$D' = 2.2 \text{ volts}$$

$$D'' = 0.7 \text{ volts.}$$

Mercury Iodide :—With this substance in the tube the absorption bands of iodine in the red have been obtained intensely; in addition to these only a few band heads about a dozen have been obtained in the region $\lambda 4600-\lambda 4100$. They are however feebly developed and the system is thus only incompletely photographed. Further investigation of the bands is necessary. The wave-length data of the bands are, hence, not reported in this paper.

The author is deeply indebted to Dr. K. R. Rao for his interest in the work and to Mr. M. G. Sastry for considerable help in arriving at the analysis of the bands and the estimation of the constants involved.

ANDHRA UNIVERSITY,
WALTAIR.

REFERENCES

1 Jevons, *Report on Molecular Spectra.*
2 Jevons and Herzberg, *Ann. d. Phys.*, **15**, 077 (1932).
3 Sundara Rao, *Curr. Sci.*, **10**, 669 (1941).
4 Wieland, *Helv. Acta. Phys.*, **2**, 46, 77 (1929).
5 Cornell, *Phys. Rev.*, **54**, 341 (1938).
6 Sastry, *Proc. Nat. Inst. Sci* (India), in press; *Curr. Sci.*, **10**, 669 (1941).

INVESTIGATIONS ON ATMOSPHERICS IN HIGH-FREQUENCY CHANNELS*

BY S. R. KHASTGIR

AND

MD. INNAS ALI

(Received for publication, September 16, 1942)

ABSTRACT. The results of investigations on atmospherics carried out at Dacca during the monsoon time of 1940 on a range of frequencies from 2 Mc. to 20 Mc. are given in this paper. The peak method of measurements was employed and experiments were carried out along the following lines :

I. Determinations of the numbers of atmospherics from different directions in different frequency channels at different times of the day, with special reference to the sunrise and the sunset periods.

II. Measurements of the field-strengths of the atmospherics from the east-west direction (and occasionally from the north-south) in different frequency channels at different times of the day with special reference to the sunrise and the sunset periods.

Usually one and occasionally two maxima, some minutes *before* the ground sunrise were observed in both sets of experiments. Soon after the maximum, the field-strength and also the number decreased very rapidly and continued diminishing till some time after the sunrise. There was a subsequent rise indicating a maximum an hour or two after the ground sunrise. The field-strength as well as number were found to be minimum from about 12 to 2 in the day. One maximum both in number and field-strength was observed some minutes *after* the ground sunset. In some observations, a maximum appeared about the time of ground sunset.

A general explanation has been given of the observed maximum *before* the ground sunrise and *after* the ground sunset in terms of the changes in the ionospheric conditions during the transition period. The two maxima observed could be associated with the E- and the F-layers. According to this view, it has been possible to locate the source of the distant atmospherics from the observed position of the maximum in relation to the ground sunset or sunrise. The basic idea in this explanation has been verified by observing the position of the field-strength maximum for short-wave signals from the Calcutta station during and after the sunset time.

III. The frequency distribution of the atmospherics from the east-west direction was studied in two different ranges of frequencies, *viz.*, 2 Mc.—5 Mc. (60 m—150 m) and 10 Mc.—20Mc. (15 m—30 m) under the following heads:

(*a*) Measurements of field-strengths of *distant* atmospherics during *day* and *night*.

(*b*) Measurements of field-strengths of the atmospherics of *near* origin during local thunderstorms.

---

* Communicated by Indian Physical Society

(c) Measurements of field-strengths of the "rain-statics," when there was continuous drizzle with slight flashes but with no thunder.

All the experimental results on the frequency distribution of the atmospherics in the different cases have been satisfactorily explained.

IV. The average values of the daily maximum peak-strength of the atmospherics on 5 Mc. and 10 Mc. during the usual morning, afternoon and night programme hours for the monsoon months were determined and an estimate of the signal-strength values for good reception about this time at Dacca on these frequencies has been made from these averages.

INTRODUCTION

The study of atmospherics in India is of extreme importance in order to determine the best conditions for radio communication. Every radio-listner knows that except for a few months in the year there are all sorts of atmospheric disturbances. In fact during the monsoon time in India the field-strengths of the atmospherics could be as high as 100 times or even more than the corresponding values in the temperate countries. Systematic investigations on the subject under tropical conditions had, therefore, been felt necessary for the past few years when several broadcasting stations were opened in India by the All-India Radio. It was increasingly evident that a better understanding of the atmospheric noise over a wide range of broadcast frequencies was desirable. Recently some measurements were carried out at the Kanodia Electrical Communication Engineering Laboratories, University of Calcutta, on wave-lengths from 50 metres to 500 metres (*i.e.*, from 0.6 to 6 megacycles), by S. P. Chakravarti, P. B. Ghosh, and H. Ghosh.[1] Some work on very long wave-lengths had also been previously reported by Chakravarty and Paranjpye[2] on the atmospherics at Bangalore during the polar year 1932-33. Some investigations were also made in this laboratory by Khastgir and Rao[3] on medium wave-bands from 150 metres to 1200 metres (*i.e.*, from 250 Kc. to 2000 Kc.) on the atmospherics at Dacca following the 'warbler' method of noise measurements. The frequency distribution of the atmospherics was studied and the diurnal characteristics of the atmospherics were investigated with special reference to the sun-rise and sunset times. Similar studies were also made by Khastgir and Ray[4] following the peak-method of measurements over a range of medium wave-lengths 150 metres to 800 metres (*i.e.*, from 375 Kc. to 2000 Kc.). In the present investigation these measurements were extended to still shorter wave-lengths. Experiments were carried out on wave-lengths from 15 metres to 150 metres (*i.e.*, from 2 Mc. to 20 Mc.) which cover practically all the broadcasting short and shorter medium wave-bands. All measurements were made during the monsoon months of 1940.

It should be mentioned here that similar noise measurements were carried out by Espenschied, Anderson and Bailey[5] on long wave-lengths from 5,300 metres to 20,000 metres (*i.e.*, from 15 Kc. to 55 Kc.) following the warbler method in several receiving centres in England. They studied the diurnal and seasonal characteristics of the noise and also the frequency distribution of the atmospherics within their range of frequencies during the day and the night. An elaborate investigation on similar lines was later made by Potter [6] in the range of short wave-lengths from 15 m. to 60 m. (*i.e.*, from 5 Mc. to 20 Mc.). Mention should also be made of the recent work done on similar lines by Schafer and Goodall[7] on a wave-length of 2 metres (150 Mc.).

METHOD OF MEASUREMENT AND EQUIPMENT

In measuring the intensity of the received atmospherics, the peak-method of measurement, as followed by Potter,[6] was employed in the investigation. In obtaining the field-strength values, only the peak crashes were considered during the period of observations. The measurements were made on a specially constructed 3-valve receiver with a balanced galvanometer in the anode circuit of the last valve of the receiver. The major deflections were noted over a period of 2 or 3 minutes. *The deflections greater than a third of the maximum deflection were only considered and the arithmetic mean of these larger deflections was taken as the equivalent signal deflection in the calculation of the field-strength of the atmospherics.* This arithmetical mean was expressed as micro-volts per metre.

The diagram of the receiving set is shown in Fig. 1. The anode current of the detector valve was balanced as shown in the diagram.

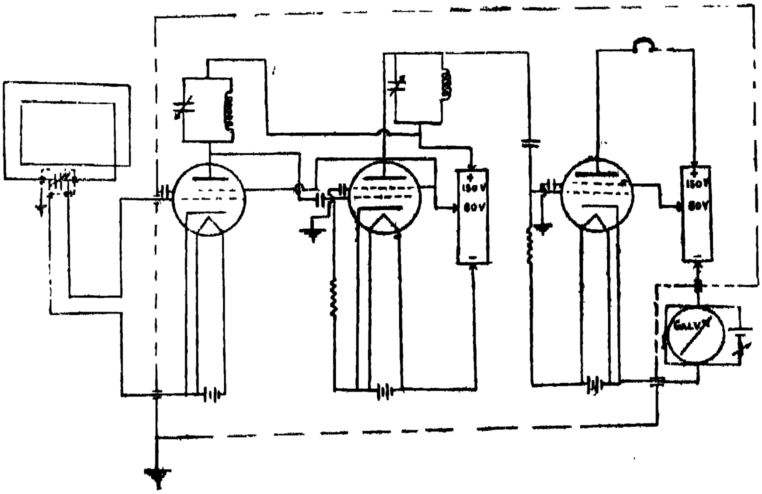

FIG. 1

The receiving set with batteries was placed inside a shielded cabinet. A frame aerial having a few turns of thick copper wire was employed with a tuning condenser in parallel. In counting the number of atmospherics on higher frequencies, a L.F. amplifier of conventional design was sometimes used.

EXPERIMENTAL RESULTS

A. *Total number of atmospherics per minute for different directions at different hours of the day on some specified frequencies*

The numbers of atmospherics within a short interval of time were counted usually in two specified directions, north-south and east-west, on different frequencies, *viz.*, 3 Mc., 5 Mc., 10 Mc. and 20 Mc. (*i.e.*, 100 m., 60 m., 30 m. and 15 m). In the case of 3 Mc., observations were also taken in the direction 45° between N. and E.

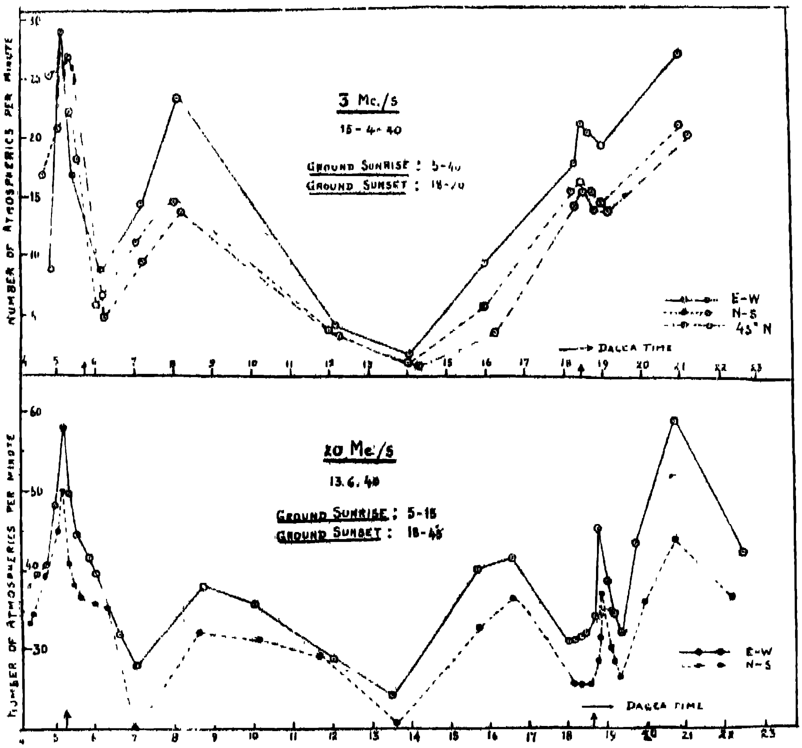

FIG. 2(*a*)

Some typical curves are shown in Fig. 2. These curves reveal certain general features in the diurnal characteristics of the atmospherics. The general features in these atmospherics counts can be summarised as follows :

(1) The number of atmospherics per min. from any direction usually showed *a maximum* some minutes *before the ground sunrise.* The number then decreased sharply about the ground sunrise time. In some observations *two distinct maxima,* one after another, *both before the ground sunrise* were observed.

(2) The minimum number of atmospherics occurred between 12 and 2 during the day.

(3) The number of atmospherics increased in the afternoon.

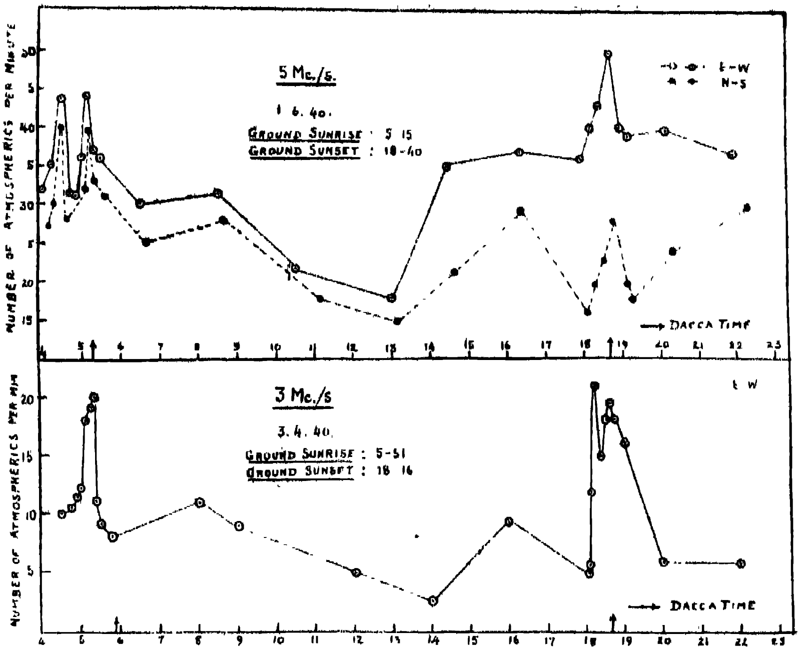

FIG. 2(*b*)

(4) Usually there was a *maximum*, some minutes *after the ground sunset.* In some observations there was a maximum about the ground sunset time.

In Fig. 3 are shown a few more sunrise curves. During the sunrise and the sunset times, observations were usually taken at intervals of 5 min. and averaged over 2 minutes.

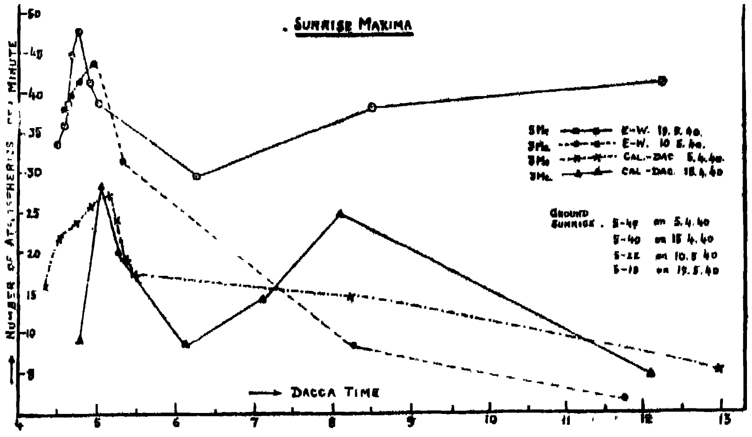

FIG. 3

B. *Peak Field-strengths of the atmospherics at different hours of the day on some specified frequencies*

The diurnal variations of the peak field-strength of atmospherics from the E-W direction (and occasionally from the north-south) were studied from about

4 A.M. to about 11 P.M. on three different frequencies : 5 Mc., 10 Mc. and 20 Mc. (*i.e.*, 60 m., 30 m. and 15 m.). The following types of results were usually obtained :

(*i*) *One maximum* some minutes *before* the ground sunrise time and *another maximum* some minutes *after* the ground sunset were observed.

(*ii*) *Two maxima* which were close together were sometimes observed *before* the ground sunrise and *only one maximum definitely after* the ground sunset was observed.

(*iii*) Occasionally *a maximum* was observed at the ground sunset time.

It should be noted that the field-strength variations were found almost similar to the variations of the numbers of atmospherics from hour to hour.

Some typical experimental results on 5 Mc. are shown in Fig. 4.

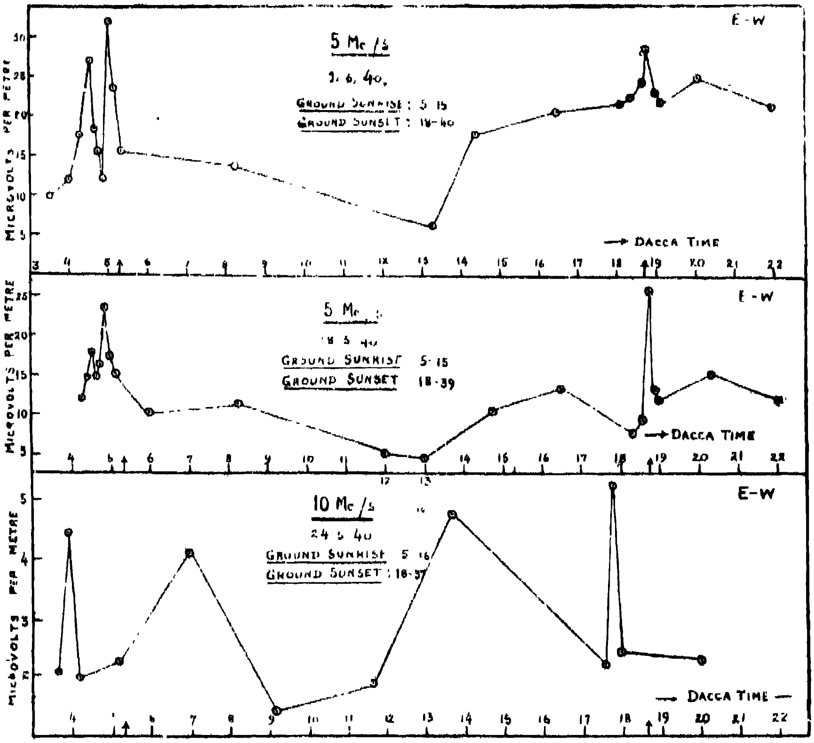

FIG. 4

THEORY OF THE SUNRISE AND THE SUNSET MAXIMA

Years ago the sunrise and the sunset effects had been observed by Eccles and others.[4] These effects had been later observed by Espenschied, Anderson and Bailey[5] and also by Potter.[6]

Potter attempted a general explanation of the effects observed and also of the double peak which was at times observed by him, but in view of the present knowledge of the ionosphere, such an explanation does not seem to be at all feasible. For very long waves Namba[11] suggested an explanation of the sunset and sunrise phenomena. According to his view, the reflection at the ionized layer is *metallic* before sunset and *dielectric* after sunset and the sunrise and the sunset effects are due to this transition in the reflection characteristics of the layer.

We offer here an explanation of the phenomena in the light of our experimental results in the following manner :—

(a) *A General Explanation of the Sunrise and the Sunset Effects*

A lightning stroke gives rise to damped electromagnetic pulses and each such pulse can be regarded as consisting of all the frequencies in the Fourier series. When lightning takes place at some distance from the receiving point, the electromagnetic pulse may arrive at the receiver after reflection from the ionospheric layer.

It is now well-known that the E-layer ionization gradually falls during the night and attains a minimum value in the small hours of the morning. The ionization then begins to increase and the increase is rather rapid during the sunrise period. During the sunset period too, the ionization is found to fall rather abruptly. The minimum ionization in early morning can be associated with the maximum observed before sunrise in the field-strength of the atmospherics. Before the ionization minimum is attained, it is evident that there will be a gradual decrease in attenuation due to gradually decreasing electron collision frequency in the layer causing thereby a gradual increase in intensity of the downcoming waves till there is a peak when the E-layer ionization is minimum. After the minimum, as the collision frequency considerably increases the attenuation rapidly increases. This causes a rapid fall in the intensity of the downcoming wave. The gradual formation of an absorbing layer, the D-layer, after sunrise would also increase the attenuation. This explains ina general way the sunrise maximum both in numbers and field-strengths of the atmospherics received in a particular frequency channel. It is however evident that when the observed field-strength is greater, the greater would be the numbers of atmospherics recorded ; because with greater or less intensities, larger or smaller numbers of the atmospherics could be distinguished.

The explanation of the sunset maximum is also somewhat similar. Before the sunset period it is known that there is a gradual decrease in the E-layer ionization. It is therefore expected that there would be a gradual rise in the intensity of downcoming waves due to a continuous fall in ionospheric absorption or attenuation. At the sunset time, when the ionizing solar rays are suddenly withdrawn, there is a sudden and a perceptible decrease in electron-concentration, so that the downcoming waves, originally coming from the distant source of atmospherics would be much less deviated and would fail to reach the receiving point. Thus at this point of the withdrawal of the solar rays, the intensity would fall, although attenuation would be less. Subsequently, however, the gradually decreasing attenuation would assert itself and the intensity would increase. The subsequent increase in intensity would also be partly due to the gradual disappearance of the D-layer after sunset.

The double peaks which were usually observed before the ground sunrise can be explained in terms of the two layers E and F. It is, however, known that the F-layer ionization also indicates a rapid increase in value about the sunrise (in the layer) and also a sharp fall about the sunset time (in the layer).

(b) *The Positions of the Sunrise and Sunset Maxima*

The work on the early morning increase of the E-layer ionization by Mitra[10] and his associates has shown that the ionization begins to increase *not* when the early morning solar rays strike the E-layer by grazing the surface of the earth *but* when the rays strike the layer by grazing the top of the ozonosphere at a height of 35 Km. from the earth's surface. The sun's rays in order to produce ionization in the E-layer should evidently pass over the ozone region so as not to have its shorter wave-lengths absorbed by ozone. Let the source of the atmospheric disturbance and the receiving point be represented in the *East-West plane* by S and R respectively on the earth's surface. Then the pulse of the atmospherics which contains all the frequencies of the Fourier series would reach the receiving point after reflection at A in the ionospheric layer. It will be evident from the diagram (Fig. 5) that the ionization in this region A would begin to increase only when the sun's rays would pass over the tangent from A to the top of the ozone layer OO. The ground sunrise or sunset at the receiving point is of course easily determined by drawing a tangent plane to the earth at the receiving site. We shall consider first the case of sunrise. Let us draw a tangent from A touching the ozone layer at G and let the tangent to the earth at the receiving point cut the straight lines joining the centre C of the earth and the point A where the ionospheric reflection takes place at the point P. If the

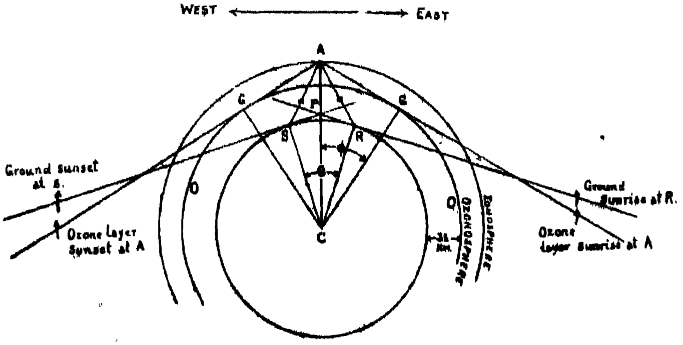

FIG. 5

angular distance between the noise source and the receiving point be denoted by θ, then the angle PCR would be $\theta/2$. Denoting the angle ACG by ϕ, it can be easily seen that the instant when the sun's rays would begin to produce ionization in the region A by grazing the top of the ozone layer would be earlier or later than the ground-sunrise at R, according as $\phi >$ or $< \theta/2$. Thus if the receiving point R is to the east of the noise source the difference between the instant of ground sunrise at the receiving point and the instant when the ionization begins to increase in the region A would be given by :—

$$\Delta T = 4(\phi - \theta/2) = (4\phi - 2\theta) \text{ minutes.}$$

On the other hand, if the receiving point R is to the west of the noise source S, the ionization at the reflection point in the ionosphere would begin to increase invariably before the ground sunrise at the receiving point. (This can be easily understood if we suppose that the locations of S and R are interchanged, and that the reflection point A remains in the same position.) In this case the time-difference would be given by $(4\phi + 2\theta)$ minutes.

From these considerations and in view of the nature of variation of the E-layer ionization during the small hours of the morning, it can thus be said that a maximum would be observed $(4\phi + 2\theta)$ min. before the ground sunrise, if the receiving point is to the west of the noise source, and if the receiving point is to the east of the noise source, the maximum would be expected at $(4\phi - 2\theta)$ min. before, provided $\phi > \theta/2$. Similar arguments would apply to the case of the sunset. It should be noted that the sunset maximum would appear *after* the ground sunset, provided $\phi > \theta/2$; whereas under the same condition, the sunrise maximum would appear *before* the ground sunrise.

With short waves when there is reflection from the F-layer also, another maximum is also expected $(4\phi' \mp 2\theta)$ min. before the ground sunrise, where ϕ' for the F-layer corresponds to the angle ϕ in the case of the E-layer. We are assuming here that the F-layer ionization begins to increase when the sun's rays grazing the ozonosphere reach the region in the F-layer where the reflection is taking place. Measurements of the F-layer ionization do not, however, give definite information on the point.[11] Sometimes the increase in ionization takes place some minutes *after* the sunrise time in the F-layer and sometimes *before*. It is significant, however, that the ionization does not begin to fall till about 1½ hours after the sunset in the F-layer.[12] This perhaps accounts for the absence of the sunset maximum which could be associated with F-layer.

Occasionally however, a maximum was observed about the ground sunset time. It is possible that a sudden fall in temperature and electrical conductivity of the atmosphere, a rise in humidity and a change in the other meteorological conditions during the sunset period can account for a maximum intensity of a distant thunderstorm field.[13]

EXPERIMENTAL TEST OF THE THEORY OF THE SUNRISE AND THE SUNSET MAXIMA

According to the suggested theory of the sunrise and the sunset maxima in the variation of the field-strengths of the atmospherics, we would expect similar effects in the signal-strength observations of a distant transmitter at times of ground sunrise and sunset. In Fig. 6 typical curves showing signal-strength variations of the Calcutta short-wave station (4840 Kc., $\lambda = 61.98$ m.) are given for three different days. A distinct maximum is evident in all the three cases. In table 1 are given the times of occurrence of the maximum after the ground sunset for the three days :

TABLE I

No.	Dates of observation	Times of occurrence of signal maximum after ground sunset	Ground sunset time
1	3.2.41	20 min. 27 sec.	17h. 43′33″
2	4.2.41	21 min. 32 sec.	17h. 44′13″
3	17.3.41	23 min. 19 sec.	18h. 5′11″

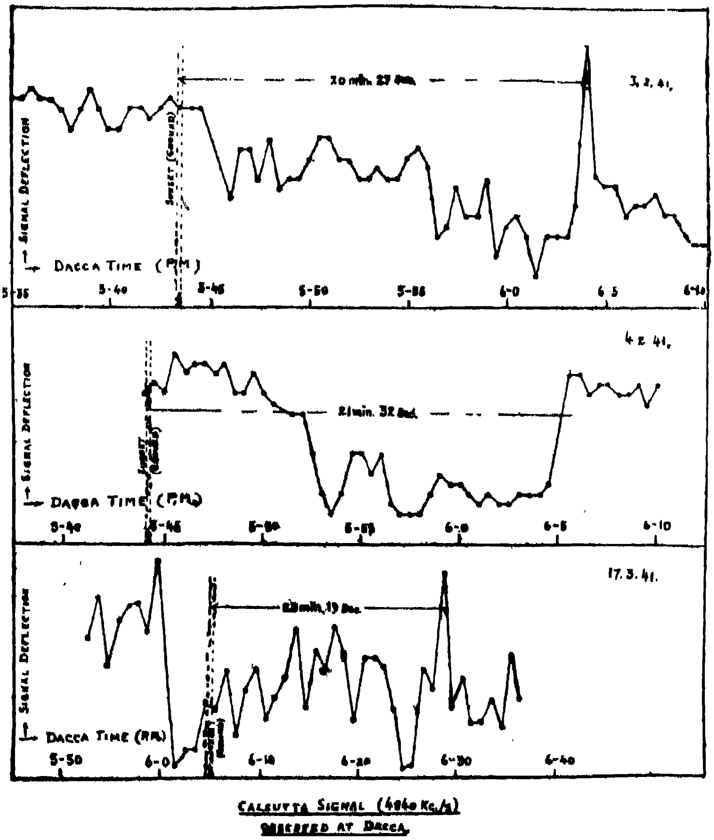

FIG. 6

The time of occurrence of the sunset maximum can also be computed from the following data :—

Radius of the earth = 6371 Km.

Reflection height in the E-layer before sunset = 80 Km.

Top of the ozone layer = 35 Km. With these values $\phi = 6^\circ.9$

Since the difference between Calcutta and Dacca local times = 8 minutes,

$$\therefore \qquad \theta = 2^\circ.$$

The signal maximum is therefore expected at $(4\phi - 2\theta)$ min., *i.e.*, 23 min. 36 sec. after ground sunset. The time calculated on the basis of our explanation is thus in good agreement with the observed time of occurrence of the sunset maximum.

EXAMINATION OF THE EXPERIMENTAL RESULTS ON THE SUNRISE AND THE SUNSET MAXIMA

According to the theory of the sunrise and sunset maxima, the position of the maximum in respect of time would give an indication of the location of the source of atmospherics. If the time of occurrence of the maximum is less than 4ϕ min. before ground sunrise or after ground sunset, it is evident that the disturbance is coming from the west and if the time of occurrence is more than 4ϕ min. before ground sunrise or after ground sunset, the disturbance may either come from the east or from the west. It is possible to draw a curve showing the position of the maximum with reference to the ground sunrise or the sunset and the approximate location of the atmospheric disturbance in miles. Taking the E-layer reflection height to be 80 Km. and the top of the ozone layer 35 Km., the distance of the source of the received atmospherics was found to lie between 50 miles and 750 miles, either in the east or in the west of the receiving point.

If the double sunrise peak is to be associated with the E-layer and the F-layer reflections respectively, it is possible also to calculate approximately the separation in time between the two intensity maxima. The observed values of this time

TABLE II

Frequency channel	Observed time difference between two peaks (in minutes)	Theoretical values of ΔT (in minutes) H⟶Reflection height in F-layer
5 Mc.	21.0	24.0 (H = 200 Km.)
5 Mc.	29.0	31 (H = 250 Km.)
20 Mc.	15.0	16 (H = 150 Km.) 24 (H = 200 Km.)
800 Kc.	19.0	16 (H = 150 Km.)
800 Kc.	15.0	16 (H = 150 Km.)

difference for some typical cases are given in table II. The theoretical values which would give approximate agreement for suitable values of the reflection height are also shown in the table. The results of similar experiments with R. G. Basak on 800 Kc. (*vide* Current Science, Oct. 1942) are also incorporated in this table.

Considering the uncertainty in the actual reflection height the agreement can be regarded as satisfactory.

FREQUENCY DISTRIBUTION OF THE ATMOSPHERICS

The measurements of the atmospheric field-strengths as a function of frequency were undertaken for two frequency ranges, *viz.* (1) from 2 to 5 megacycles (60 m.—150 m.) and (2) from 10 to 20 megacycles (15 m.—60 m.). The following experiments on the frequency distribution of the field-strengths of the atmospherics were performed *both during the day time and the night*:

EXPERIMENTAL RESULTS

(i) *Experiments on distant Atmospherics during the Day*

Some typical experimental results for the frequency ranges 2 Mc.—5 Mc. and 10 Mc.—20 Mc. are shown in Fig. 7.

It is to be observed that during the day, the field-strength of the distant atmospherics when plotted against $\frac{1}{f^2}$ gave an approximate straight line only in one case. In the other cases, the $E-\frac{1}{f^2}$ curve was found to be straight over a limited range only.

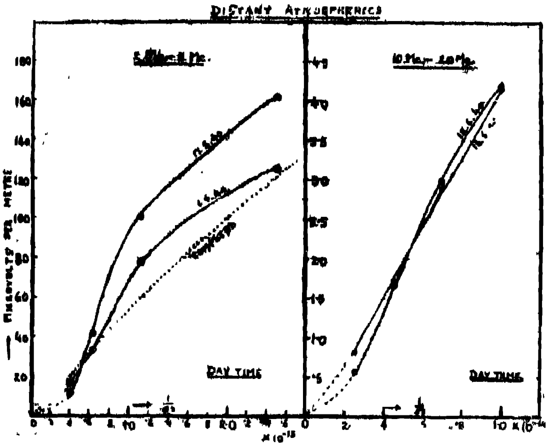

FIG. 7

(*ii*) *Experiments on distant atmospherics during the night when the sky-waves were predominant*

Some typical results are illustrated in Fig. 8.

In both the frequency ranges, it was found that during the night the field-strength of the distant atmospherics decreased exponentially with the increase of frequency.

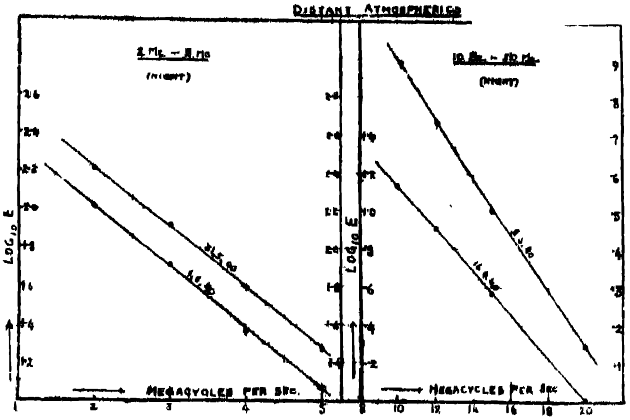

FIG. 8

(*iii*) *Atmospherics due to local thunderstorms*

The experimental results are illustrated in Fig. 9. It can be seen that the field-strength, when plotted against the reciprocal of frequency gave a straight line in each set of observations. The relation between field-strength and frequency was of the form : $E = A + \frac{B}{f}$, where A and B are constants.

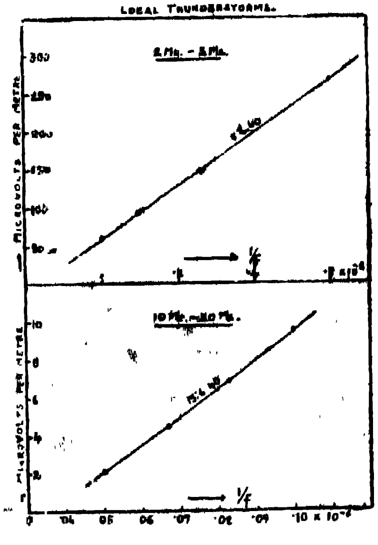

FIG. 9

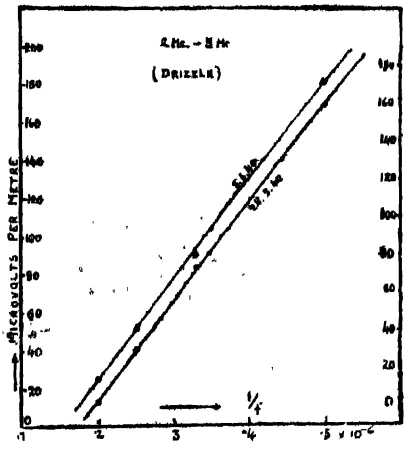

FIG. 10

(iv) *Observations on "Rain statics"*

On certain days when there was continuous drizzle for hours together with slight flashes but with no thunder, some experiments were performed to study the frequency distribution of the received atmospherics. Two sets of experimental results are illustrated in Fig. 10. It should be noticed that in these experiments also, as in the case of experiments during local thunderstorms, the relation between the measured field-strength and the frequency was of the same form, *viz.*, $E = A + \frac{B}{f}$, where A and B are constants.

THEORETICAL CONSIDERATIONS IN THE STUDY OF THE FREQUENCY DISTRIBUTION OF ATMOSPHERICS

I. *Distant Atmospherics*

Let us suppose that the source of atmospherics gives rise to damped sinuous waves. It can be seen from Burch and Bloesma's'[4] Fourier analysis of such waves that for frequencies much higher than the frequency of the received atmospherics, the amplitude of the particular term involving the frequency to which the receiver is tuned is inversely proportional to the square of that frequency. Hence the Fourier co-efficient of the particular component involving the high frequency f is given by

$$B_f = \frac{A}{f^2} \qquad \dots \quad (1)$$

where A is some constant.

Now neglecting any kind of attenuation, we know that the field-strength at distance r from a dipole aerial radiating sinuous waves is obtained from

$$E = f.\left[\frac{37.28 \times 2\pi(hI)}{rc}\right],$$

where hI is the metre-amperage of the transmitter and c the velocity of light. Thus at a particular distance r we have $E = K.\,f$, where K is constant.

Considering now the particular Fourier component of frequency f, we can write

$$E = \frac{A}{f^2}.K.f \quad \text{or} \quad \frac{A.K}{f}.$$

We shall here take the following cases :

(*a*) *When the ground waves alone are present.*—In this case the field-strength of the atmospherics received in frequency channel f is given by

$$E = \frac{A.K}{f}.A_1$$

where A_1 is the ground-attenuation factor.

According to Norton[15] the ground-wave attenuation factor is given by

$$A_1 = \left| 1 + i\sqrt{\pi p_1}\, e^{-p_1} .\ \operatorname{erfc}(-i\sqrt{p_1}) \right| \quad \ldots \quad (3)$$

where

$$p_1 = p e^{ib} \quad \ldots \quad (4)$$

$$p = \frac{\pi}{x} . \frac{r}{\lambda} . \cos b$$

$$= \frac{\pi}{\epsilon+1} \frac{r}{\lambda} \sin b \quad \ldots \quad (5)$$

$$\tan b = \frac{\epsilon+1}{x} = \left\{ \frac{\epsilon+1}{2\sigma} \right\} f \quad \ldots \quad (6)$$

$$x = \frac{2\sigma}{f} \ (\sigma \text{ in e.s.u.}) \quad \ldots \quad (7)$$

$r =$ actual distance from the source
$p =$ numerical distance
and $\lambda =$ wave-length.

It can be shown that for $p > 20$

$$A_1 = \frac{1}{2p} \quad \ldots \quad (8)$$

Now, putting $\frac{\epsilon+1}{2\sigma} = a$, we have $\tan b = a.f.$

On putting again $\frac{c(\epsilon+1)}{2\pi r} = B$, we can show

$$A_1 = \frac{B}{f} \left\{ 1 + \frac{1}{a^2 f^2} \right\}^{\frac{1}{2}} \quad \ldots \quad (9)$$

so that

$$E = \frac{A.K}{f} . A_1 = \frac{A.K.B}{f^2} \left(1 + \frac{1}{a^2 f^2} \right)^{\frac{1}{2}} . \quad \ldots \quad (10)$$

For the shorter waves, we can neglect $1/af$,

so that

$$E \simeq \frac{A.K.B}{f^2} \propto \frac{1}{f^2} . \quad \ldots \quad (11)$$

Moullin[16] also obtained a somewhat similar expression.

(*b*) *When the Sky Waves alone are present.*—In the case of the sky waves which are returned from the ionosphere, the constant K in (1) should be multiplied by $\sin i_0$, since the sky path would be $r/\sin i_0$, where i_0 = angle of incidence at the ionized layer. Thus without considering attenuation, we have in this case

$$E = \frac{A.K}{f} \sin i_0 \quad (12)$$

This should be multiplied by the relevent attenuation factor to get the actual field-strength of the sky waves.

Long Waves

For low-frequency waves (100 Kc. or below), the ionosphere behaves as a good reflecting surface. According to Namba's[9] calculations, for values of the angle of incidence corresponding to fairly long distances the reflected intensity is usually larger at night than during the day. During the night, however, the reflection is practically independent of wave-length. Hence for the night-time observations

$$E=\frac{A.K.\sin i_0}{f}A_2$$

where A_2=attenuation constant which is independent of frequency.

Thus $$E=\frac{\text{constant}}{f}. \qquad \dots \quad (13)$$

Dellinger's[17] report on radio propagation data mentions this simple inverse relationship in the case of night atmospherics.

Medium Waves

When the frequency of the wave is below the critical penetration frequency, the wave is sufficiently refracted in the E-layer and gets returned to the surface of the earth. During the day, there is no appreciable amount of downcoming wave. During the night, the sky wave intensity may be considerable.

Assuming an exponential gradient for electron concentration in the ionized layer, (*viz.*, electron density $N=pe^{qz_0}$, where z_0 is the reflection height above the boundary of the layer and p and q are constants), it has been shown by Namba[9] that the total attenuation along the curved path, when the wave gets bent and returns to the earth will be given by

$$A_2=\frac{2\nu}{cq}\left[\cos^2 i_0+\frac{2z}{r_0}\right] \qquad \dots \quad (14)$$

where ν=electron-collision frequency, r_0 the radius of the earth and c the velocity of light. Here the collision frequency could be taken proportional to frequency,[18] *i.e.*, $\nu=k.f$, where k is constant. Since the height z of the ionized layer above the ground is much smaller than the radius of the earth, we can approximately write :

$$A_2=a.f, \qquad \dots \quad (15)$$

where $$a=\frac{2k}{cq}\cos^2 i_0=\text{constant},$$

when the source of the atmospherics and the receiving point are fixed.

Hence the field-strength of the particular Fourier component of frequency f as returned from the E-layer will be

$$E=\frac{A.K.\sin i_0}{f}.\quad A_2=\frac{A.K.\sin i_0}{f}.e^{-af}$$

or

$$E=\frac{\text{const.}}{f}.e^{-af} \qquad \dots \quad (16)$$

i.e.,

$$\log E+\log f=\text{constant}-af.$$

The frequency here is of a high order, so that the variation of $\log f$ with f is rather small in the limited range of frequencies. Thus we can write

$$\text{Log } E=\text{const.}-af. \qquad \dots \quad (17)$$

In most cases, our experimental results *during the night* in the medium and high frequency ranges were found in accordance with this exponential law of decrease of field-strength with frequency.

Short Waves

High-frequency waves which are of frequencies higher than the critical penetration frequency penetrate through the E-layer and reach the F-layer. They are subsequently returned from the higher layer, when the maximum electron density of that layer is sufficient for the bending of such waves. With these waves, we have to consider attenuation during transmission through the E-layer and attenuation along the curved path in the F-layer while getting bent and returning to the earth's surface. The first attenuation can be taken as inversely proportional to the frequency and the second one can be taken as varying with frequency in accordance with (14) or (15). Thus the field-strength of such downcoming waves can be written as

$$E=\frac{M}{f}.\ \frac{e^{-m}}{f^2}.\ e^{-af} \qquad \dots \quad (18),$$

where M and m are constants. Usually at night $m/f^2 << 1$,

so that $$E=\frac{M}{f}\left(1-\frac{m}{f^2}\right)e^{-af}\simeq\frac{M}{f}e^{-af},$$ which is similar to (16).

(*c*) *When Ground Waves and Sky Waves are both present.*—Let n_g and n_s be the fractions representing the two portions reaching the receiver by the ground path and sky path, so that $n_g+n_s=1$. The field-strength at the receiving point will then be given by

$$E=\sqrt{\left(\frac{A.K.B.}{f^2}\right)^2 n_g^2 \pm\left(\frac{A.K.\sin i_0}{f}\right)^2 n_s^2 e^{-2af}}$$

$$=\frac{D}{f^2}\left[1+b.f.^2e^{-2af}\right]^{\frac{1}{2}} \qquad \ldots \quad (19)$$

where $D=n_g.$ A.K.B and $b=\frac{n_s^2}{n_g^2}\cdot\frac{\sin^2 i_0}{B^2}$, $\left[\text{Here} \quad B=\frac{c(\epsilon+1)}{2\pi r}.\right]$

Putting $\Delta=D(1+bf^2e^{-2af})^{\frac{1}{2}}$,

we get $E=\frac{\Delta}{f^2}$.

The slope of the curve showing E against $1/f^2$ would be given by Δ. It is evident from (19) that for values of $af>1$, the slope would increase with the increase of $1/f^2$ and after attaining a maximum value when $af=1$, the slope would decrease for $af<1$ with the increasing value of $1/f^2$; the curvature would change sign when $af=1$.

Our day observations in the two frequency ranges 2 Mc.—5 Mc. and 10 Mc.—20 Mc. showed that the field-strength E, when plotted against $1/f^2$, gave a straight line *only in very few cases.* In these few cases, we may suppose that the ground waves were predominant, so that $\frac{n_s}{n_g}=0$ and we get $E=\frac{D}{f^2}$. In most cases, however, the sky waves were not negligible and the curve $E-\frac{1}{f^2}$ was straight only over a limited range. The experimental curves could be explained according to (19).

We have drawn an approximate theoretical curve for the range 2 Mc —5 Mc. taking

r = distance between the source of atmospherics and the receiving point = 250 Km.

$i_0=40°$

ϵ = Effective dielectric constant of the earth = 10 e.s.u.

and $n_s=n_g$.

The theoretical curve is shown in Fig. 7, where the experimental curves are also shown.

II. *Atmospherics due to local Thunderstorms*

In the case of local thunderstorms, the source of the atmospherics is near the receiving point. The ground attenuation or the ionospheric attenuation is not to be considered in this case. If we suppose now that the lightning discharge gives rise to damped sinuous waves, the field-strength of the received atmospherics on a high frequency f would be given by (1), *viz.*,

$$E=\frac{\text{A.K.}}{f}=\frac{\text{const}^{\text{t}}}{f}$$

It is, however, known that the electrical discharges in thunderstorms would often consist of disturbances in the nature of sharp impulses. Let us represent this impulse by $f(t) = -f(-t)$, which tends to zero sufficiently rapidly for large values of the time t. Let us also suppose that near $t = 0$ the function tends to have very large values. The Fourier coefficient of angular frequency ω for such a function is then given by

$$
\begin{aligned}
B_f &= \int_{-\infty}^{\infty} f(t).\, e^{i\omega t}\, dt = \int_{0}^{\infty} f(t).\, e^{i\omega t}\, dt + \int_{\infty}^{0} f(t).\, e^{i\omega t}\, dt \\
&= \int_{0}^{\infty} f(t).\, e^{i\omega t}\, dt + \int_{0}^{\infty} f(-t).\, e^{-i\omega t}\, dt \\
&= 2i \int_{0}^{\infty} f(t) \sin \omega t.\, dt.
\end{aligned}
$$

Now if $f(t) \int \frac{1}{e^{2\pi\lambda t} - 1}$ where λ determines the rapidity with which the function tends to zero with the increase of time t, then the Fourier coefficient of angular frequency ω will be $\int_{0}^{\infty} \frac{\sin \omega t}{e^{2\pi\lambda t} - 1}\, dt$. Putting $\tau = \lambda t$, we have[19]

$$
B_f = \frac{1}{\lambda} \int_{0}^{\infty} \frac{\sin \omega/\lambda d\tau}{e^{2\pi\tau} - 1} = \frac{1}{\lambda} \left[\frac{1}{4} \, \frac{e^{\omega/\lambda} + 1}{e^{\omega/\lambda} - 1} - \frac{\lambda}{2\omega} \right]. \quad \ldots \quad (20)
$$

For large values of ω, this is reduced to $\left(\frac{1}{4\lambda} - \frac{1}{\omega} \right)$, so that for large values of λ when the function comes down sufficiently to zero, the Fourier coefficient will be varying as $\frac{1}{\omega}$, *i.e.*, $B_f = \frac{\text{const.}}{f}$. To obtain the field-strength at the receiving point, we have to multiply this by f, so that $E = \frac{\text{const.}}{f} f = \text{const.}$

If we suppose that the lightning discharges give rise to damped sinuous waves and also impulses of short duration, it is easily seen that the field-strength of the atmospherics in local thunderstorm centres will be of the form: $E = A + \frac{B}{f}$, where A and B are constants. Our experimental results are in agreement with this relation.

III. "*Rain-statics*"

The observed field-strength of the atmospherics received during continuous drizzle in the day varied with the frequency in the same way as the field-strength of the atmospherics from local thunderstorm centres. It can therefore be conjectured that the source of the disturbance was near the receiving point and that its nature was similar to that of the lightning discharges. It is known, however, that when many thousands of charged particles of water vapour coalesce to form a rain drop, there is a great and sudden increase in the electric field resulting in disruptive discharges or 'flashes.' It is also known that the highest charge whether positive or negative is carried by light rain. It is therefore expected that during such drizzle there would be sources of atmospherics in the disruptive discharges or 'flashes' near the receiving point.

ESTIMATION OF THE SIGNAL-STRENGTH VALUES FOR GOOD RECEPTION AT DACCA ON 5 Mc. AND 10 Mc.

The average values of the daily maxima of the peak field-strengths of the atmospherics from the east-west direction on 5Mc. and 10Mc. were determined for May-June during the usual morning, afternoon and the night programme hours. In table III are given these averages :—

TABLE III

Field-strengths in Microvolts per metre.

10 Mc.			5 Mc.		
Morning	Afternoon	Night	Morning	Afternoon	Night
8—12 A.M.	1—5 P.M.	7—11 P.M.	8—12 A.M.	1—5 P.M.	7—11 P.M.
5.83	7.20	7.50	22.03	26.21	27.25

In table IV are given the signal-strength values which will be 20 db above the averages of the peak field-strengths of the atmospherics on 5 Mc. and 10 Mc. Such signal-strengths can be regarded as standard values for good reception.

TABLE IV

Periods (May-June)	Signal-strength which is 20 db above the peak strength of the atmospherics	
	10 Mc.	5 Mc.
(1) Morning 8 to 12 A.M.	58 microvolts/metre	220 microvolts/metre
(2) Afternoon 1 to 5 P.M.	72 „	262 „
(3) Night 7 to 11 P.M.	75 „	273 „

ACKNOWLEDGMENTS

Our sincere and grateful thanks are due to Prof. S. N. Bose for his unfailing interest and many helpful suggestions. For the signal observations of the Calcutta short-wave station during the sunset period, we are indebted to Mr. S. C. Majumdar, M.Sc.

Finally we would like to place on record our deep sense of gratitude to the Indian Meteorological Dept., for supplying us with some meteorological data.

REFERENCES

1 Chakravarty, S. P., Ghosh, P. B., and Ghosh, H., *Proc. I.R.E.*, **67**, p. 780 (1939); Chakravarty, S. P., *L'on de Elec.*, **18**, No. 207, p. 99, March (1939).

2 Chakravarty, S. P., and Paranjpye, B. H., *Jour. Ind. Inst. Science (Bangalore)*, **17 B** 1 (1934).

3 Khastgir, S. R., and Rao, Kameswar, *Proc. I.R.E.*, **28**, 511 (1940).

4 Khastgir, S. R., and Ray, *Science and Culture*, **5**, 772 (1940).

5 Espenschied, Anderson and Bailey, *Proc. I. R. E.*, **14**, 7 (1926).

6 Potter, *Proc. I. R. E.*, **19**, 1731, Oct. (1931), and **20**, 1512, Sept. (1932).

7 Schafer and Goodall, *Proc. I. R. E.*, **27**, 202 (1939).

8 Eccles, *Handbook of Wireless Telegraphy and Telephony*, p. 176 (1918).

9 Namba, *Proc. I. R. E.*, **21**, 238 (1933).

10 Mitra, *Science and Culture*, **3**, 496 (1938).

11 Mathur, *Proc. Nat. Acad. Sciences* (India), **7**, 222 (1937); Bajpai and Pant, *Ind. J. Phys*, **12**, 211 (1938); Ghosh, *Ind. J. Phys.*, **14**, 101 (1940).

12 Bajpai and Pant, *Ind. J. Phys.*, **12**, 211 (1938).

13 A. Venkat Rao Telang, *Proc. Ind.*, Science Congress, Paper No. 20 (1941).

14 Burch, C. R., and Bloesma, J., *Phil. Mag.*, **49**, 480 (1925).

15 Norton, K. A., *Proc. I. R. E.*, **24**, 1367 (1936).

16 Moullin, *Jour. I. E. E.*, **62** (1924).

17 Dellinger's Report on Radio Propagation Data, *Proc. I. R. E.*, **21**, 1419 (1933).

18 Appleton and Booohariwala, *Proc. Phys. Soc.* (Lond.), **47**, 1074 (1935).

19 *See* Whittaker's Modern Analysis, Chap. VI, Theory of Residue.